LA-8000-C
Conference

C.4

Proceedings of the Impact Fusion Workshop

National Security and Resources Study Center

Los Alamos Scientific Laboratory

Los Alamos, New Mexico

July 10—12, 1979

LOS ALAMOS SCIENTIFIC LABORATORY
Post Office Box 1663 Los Alamos, New Mexico 87545

This report was not edited by the Technical Information staff.

UNITED STATES
DEPARTMENT OF ENERGY
CONTRACT W-7405-ENG. 36

LA-8000-C
Conference
UC-21
Issued: August 1979

Proceedings of the

Impact Fusion Workshop

National Security & Resources Study Center
Los Alamos Scientific Laboratory
Los Alamos, New Mexico
July 10-12, 1979

Compiled by
A.T. Peaslee, Jr.

Sponsored by the
Office of Research Policy
U.S.Department of Energy

Preface

The Impact Fusion Workshop was held at the National Security and Resources Study Center of the Los Alamos Scientific Laboratory (LASL), Los Alamos, New Mexico, on July 10-12, 1979. Following this open Workshop, classified sessions were held on July 13, 1979.

The Divisions of Research Assessment and of Advanced Technology Projects of the Office of Research Policy of the U.S.Department of Energy's (DoE) Office of Research jointly sponsored the Workshop. Dr. R.N.Kostoff was the DoE Project Manager.

The Workshop was planned and carried out as part of Field Tasks for the Evaluation of Impact Fusion Concepts at the University of Washington with Dr. F.L.Ribe as Principal Investigator and at the LASL with Dr. J.M.Williams as Contract Task Monitor. Dr. Ribe was the Technical Director of the Workshop.

The purposes of the Workshop were to provide a forum for the exchange of ideas among those scientists and engineers who have expertise relevant to impact fusion and to arrive at a state-of-the-art description. The results of the Workshop will form the basis for generating technical criteria to be used by the DoE in the assessment of impact fusion proposals.

The Impact Fusion Workshop did not uncover any fatal flaws that rule out impact fusion. But neither did the Workshop discover any path of research and development that would definitely lead to impact fusion power generation.

The Workshop determined the minimum projectile requirements for impact fusion to include a velocity of 200 km/sec with a kinetic energy of about 10 megajoules. The classified sessions of the Workshop did not alter these minimum projectile requirements.

The Workshop started with overview presentations of three major topics: Target Dynamics, Reactor Systems, and Accelerator Systems. The overview presentations were followed by two days of detailed presentations, that reported theoretical and experimental work in progress, as well as conceptual presentations, that reported new ideas covering all three topics. Since there were no parallel sessions, an opportunity was provided for healthy interaction between participants whose interests covered more than one of the topics.

These presentations were followed by Working Group Sessions for each of the three topics. The conclusions of the Working Groups follow.

Target Interactions: In order to obtain a reasonable thermonuclear gain, one needs a plasma temperature of about 10 kilovolts, a plasma pressure of about 1000 megabars, and an ion density of about 3×10^{22} ions $/cm^3$. A characteristic thickness of the macroparticle and plasma cavity might be a few millimeters, and the time scale of the thermonuclear burn might be 5 to 10 nanoseconds. A one half gram macroparticle with a velocity of 200 km/sec, or 10 MJ of kinetic energy, may be able to provide these conditions. A major problem is to convert the linear kinetic energy into a three dimensional compression without energy losses that negate the efficiency advantages of three dimensional over one dimensional compressions. Calculations estimate an energy gain of more than 100 would require kinetic energy inputs of 10 megajoules for three dimensional compresssions and 50 megajoules for one dimensional compressions. The corresponding projectile velocities are 130 and 500 km/sec. An accelerator to drive a laser pellet must provide a velocity of 300 km/sec.

Reactor Systems: A reactor system with an energy per pulse of up to 100 gigajoules might be feasible with a fluid wall containment vessel with a radius of up to 10 meters. Duty cycles as short as one pulse every ten seconds may also be feasible. There are many problems, such as trajectory control and targeting, for which no solutions have been posed. Much more information on the basic performance requirements, such as target gain values for a range of target input energies, is neeeded before a system evaluation can be attempted. An overall system engineering gain of four or five is needed before impact fusion will be competitive with other forms of energy generation.

Accelerator Systems: Four conceivable accelerator systems that might meet the minimum projectile requirements are the rail gun accelerator, the travelling magnetic wave accelerator, the ablative accelerator, and the plasma impulse accelerator:

Accelerator Type	Efficiency[1]	Size[2]	Present Capability
Rail Gun	~20-50 %	140 meters[3]	3 gm @ 6 km/sec
Travelling Magnetic Wave	~10-75 %	5 kilometers[4]	Tens of kgs @ low velocities
Laser Driven Ablative	~5-10 %	140 meters[3]	Theoretical
Plasma Impulse	$\lesssim$ 20%	140 meters[3]	Theoretical

[1] Projectile kinetic energy / accelerator input energy.

[2] For minimum projectile requirements.

[3] Length determined by restricting the force on the projectile to below the elastic limit.

[4] A proposed toroidal travelling magnetic wave accelerator might be much smaller.

Considerable further evaluation of the last three accelerators is needed before proceeding with experiments. The two stage gas gun and the electrostatic accelerator systems very probably can not meet the minimum projectile velocity requirements.

One hundred and nineteen scientists and engineers participated in the Impact Fusion Workshop. Fifty five represented fifteen States, the District of Columbia, and the United Kingdom. The remaining participants were from the LASL.

A.T.Peaslee, Jr.
LASL

Table of Contents

PROCEEDINGS OF THE IMPACT FUSION WORKSHOP
National Security and Resources Study Center
Los Alamos Scientific Laboratory
Los Alamos, New Mexico
July 10--12, 1979

Compiled by

A. T. Peaslee, Jr.

ABSTRACT

The workshop began with overviews of Target Dynamics, Reactor Systems, and Accelerator Systems. Next were two days of detailed presentations, reporting theoretical and experimental work, as well as new ideas. Working group sessions made conclusions concerning target interactions, reactor systems, and accelerator systems.

The 119 scientists and engineers attending the conference comprised 55 delegates from 15 states, the District of Columbia, and the United Kingdom; the remaining participants were from the Los Alamos Scientific Laboratory.

The results of the Workshop will form the basis for generating technical criteria to be used by the US Department of Energy in the assessment of impact fusion proposals.

SCOPE OF IMPACT FUSION AND REVIEW OF MACROPARTICLE ACCELERATORS

F.L. Ribe and G.C. Vlases
University of Washington
Seattle, WA 98195

The problems of Impact Fusion involve macroparticle (projectile) acceleration, target dynamics and thermonuclear burn, and conceptual power reactors for converting the repeated fusion explosions to useful electrical power. As compared to other types of inertial fusion, impact fusion may have significant advantages. A set of accelerator and projectile parameters can be defined approximately on the basis of the fluid dynamics and plasma energy losses during the initial shock and isentropic compression following the projectile impact on the DT target assembly. In this overview paper we review the published and preprint literature on various types of macroparticle accelerators for orientation of the conference participants.

I. SCOPE OF IMPACT FUSION

In the present workshop we have a representative group of scientists whose work covers the main topics of Impact Fusion. "Impact Fusion" refers to the transformation of the kinetic energy of an accelerated moving mass (macroparticle) to thermal energy of deuterium-tritium (DT) plasma in order to produce fusion energy. The energy recirculated to the macroparticle accelerator from the fusion power plant which is energized by the fusion explosions must be a small fraction of the plant output. Therefore, we can identify the following major topics which are the subject of this workshop:

a. Acceleration of macroparticles (projectiles)
b. Conversion of macroparticle energy to fusion energy (target dynamics and thermonuclear burn)

c. Conceptual power-reactors for converting the fusion energy to econimical power output.

It is natural to compare this form of inertial fusion to more conventional approaches based on lasers and accelerated electron and ion beams. It may be possible to derive power more simply or economically from impact fusion because of the following possible advantages:

a. Simple transport of small macroparticles through smaller penetrations in the reactor containment vessel
b. The availability of an accelerator art which may be more simply and economically extendable to fusion conditions
c. More efficient conversion of particle energy to fusion plasma energy
d. More efficient conversion of accelerator input energy to particle energy

Regarding acceleration of macroparticles, we shall hear from a number of proponents and practitioners of rail-gun, traveling magnetic-wave, ablative, and plasma-impulse techniques. Winterberg,[1] Harrison[2] and Maisonnier[3] provided early proposals and reviews of macroparticle accelerators.

Conversion of macroparticle energy to fusion energy has been considered by Winterberg[1] and others as a process of shock heating of the DT fluid by the macroparticle impact, followed by further isentropic compression in the presence of electron thermal conduction and radiation (Bremsstrahlung) losses. For reasonable thermonuclear gain the following conditions are necessary: macroparticle energy $\approx$ 10 MJ, macroparticle velocity $\approx$ 200 km/s, macroparticle mass $\approx$ 0.5 g, target plasma temperature $\approx$ 10 keV, plasma pressure $\approx 10^3$ megabar, ion density $\approx 3\times10^{22}\,cm^{-3}$ A characteristic thickness of the macroparticle and plasma cavity might be a few mm and the burn time approximately 5 to 10 ns. Present macroparticle accelerators achieve maximum velocities of approximately 5-10 km/s; accelerator techniques must therefore be considerably extended. A major object of this workshop is to exchange information on this possibility.

Previous impact-burn calculations have not taken account of magnetic insulation of the plasma to reduce thermal conduction to the cavity walls. Provided suitable configurations can be found to produce the necessary initial plasma currents for preheat and insulation, this could result in longer burn times, smaller densities and smaller macroparticle velocities, more easily attainable by present accelerator techniques. Here the subject of impact fusion overlaps that of fast-liner fusion.[4]

From a reactor point of view the problem of containment of repeated 1 to 10 GJ explosions in the thermal-conversion cavity is a central one. The tolerable limits are reasonably well understood and will be discussed by L. Booth, I. Bohachavsky, R. Krakowski, et al. Energy-balance considerations place limits on the product of acceleration efficiency and macroparticle-to-plasma energy conversion efficiency. The economics of power production limits the capital cost of the plant and of each macroparticle, as will be discussed by J. Williams, L. Booth and R. Krakowski.

In this first orientation paper of the workshop, we limit our further discussion to an overview of present and proposed accelerator concepts. The speakers who follow will address the topics of macroparticle-to-fusion energy conversion and power reactor concepts before we hear the more detailed technical papers.

The overview papers summarize the field as we know it from published and preprint information for orientation of the conference participants. New information for use in evaluating the field will come from the more detailed papers of the conference.

II. MACROPARTICLE ACCELERATOR CONCEPTS

A number of papers have identified the principal methods of macropartile acceleration.

a. Two-stage light gas guns
b. Rail-gun accelerators
c. Traveling magnetic-wave accelerators
d. Plasma-impulse accelerators
e. Ablative accelerators
f. Electrostatic accelerators

In order to scale the problem, we consider the simplest case of a right cylindrical pellet of base area A, length ℓ, and density ρ being accelerated along its axis by a constant force pA on its base. The particle will acquire an energy E in a distance z given by $E = \frac{1}{2}\rho A\ell v^2 = pAz$. The maximum pressure that can be applied is on the order of the yield stress, which we take to be 7 kbar (7×10^8 Pa) as a typical value. We assume the final velocity is also specified, which fixes the total mass, and the mass per unit area, $\rho\ell$, according to $\rho\ell = 2E/Av^2$, and the acceleration time is $\tau = v\rho\ell/p$.

Table I lists values of z, τ, and $\rho\ell$ for two values of E, v, and A, and also gives ℓ for densities of 2.7 g/cm^3 (Al) and 8 g/cm^3 (Cu). From this table it is seen that a distance of 143 to 1430 m is required to reach E = 10^7J, without exceeding p = 7 kbar, depending on A, with times ranging from 143 μsec to 1.43 ms. (These scalings do not apply strictly to ablative techniques, for which p ≈ const, but the mass, and hence acceleration, change continuously.)

E (MJ)	1				10			
v (cm/s)	5×10^6		2×10^7		5×10^6		2×10^7	
m (g)	.8		.05		8		.5	
A (cm^2)	1	.1	1	.1	1	.1	1	.1
z (m)	14.3	143	14.3	143	143	1430	143	1430
$\rho\ell$ (g/cm^2)	0.8	8	0.05	5	8	80	0.5	5
ℓ (cu) (cm)	0.1	1	0.0063	0.063	1	10	0.063	0.63
ℓ (Aℓ) (cm)	0.3	3	0.019	0.19	3	30	0.19	1.9
τ (ms)	0.057	0.57	0.014	0.143	0.57	5.7	0.143	1.43

Table 1. Characteristic Scaling for Constant Force Acceleration (p = 7 kbar)

1. Light-Gas Guns. Two-stage devices in which explosively driven pistons (artillery projectiles) compress hydrogen or helium to high temperature for acceleration of the final projectile are presently used to obtain velocities of ~ 7 km/s. The projectiles produce pressures of ~ 5 megabars (Mb) upon impact, providing high-pressure equation-of-state data. Here the maximum velocity for a projectile of vanishing mass is $2/(\gamma-1)$ times the speed of sound in the high-temperature gas, leading to a limitation on projectile velocity for hydrogen given by[5] $v = 380\ [T(H_2)]^{\frac{1}{2}}$ m/s. For $T(H_2) \leq 10^4$ K the velocities are not in the impact-fusion range.

2. Rail-Gun Accelerators. In a rail gun a conducting projectile (which may be a solid or a plasma or a combination of the two) completes the current connection between two conducting rails (Fig. 1) connected to a source of current. The current I produces magnetic induction B between the rails of width w and height h parallel to B, and the magnetic pressure $B^2/2\mu$ drives the projectile with a force over its area hw given by $F = L'I^2/2$. The inductance per unit length $L' \approx \mu w/h$ is approximately 0.42 μH/m for "square" rail geometry, w = h.

A. Experimental Results. There are three well-defined experimental results from rail-gun experiments: (a) Marshall, Barber and coworkers,[5][6][7] using the 500-MJ Canberra Homopolar Generator as a current source, produced velocities of 6 km/s in a 12.7 mm cube of polycarbonate plastic (mass ≈ 3g) driven by an arc in a 5-m gun whose copper rails were 19.1 x 3.2 mm copper strips. Their experimental arrangement[7] is shown in Fig. 2. A current of 360 kA from the homopolar generator (HPG) energizes the 22-μH storage inductor which is shorted from the HPG by the clamp switch, accelerating the switching slug in the rail switching gun. As the switching slug passes the breech of the rail gun, the current from the inductor is diverted to the projectile. The explosively driven post-clamp switch closes after projectile acceleration to dissipate remaining storage-inductor energy and suppress an arc at the gun muzzle. The initial connection across the gun rails behind the projectile consists of a copper fuse which initiates the driving arc. (b) Brast and Sawle[8][9] used a 28-kJ, 142-μF capacitor bank to accelerate arc-driven nylon macroparticles with masses between 2.4 and 31 mg to velocities as large as 6 km/s. The rails were 10 mm x 1 mm in cross section, had lengths of 7 to 20 cm and carried about 150 kA. Melting of the rails occured, leading to considerable swept-up rail material with the projectile. (c) Chapman, Harms and Sorenson[10] used high-explosive compression of magnetic flux into the breech of a rail gun to accelerate 0.21 g to 9.5 km/s, using accelerating magnetic fields in the range of 200 T. Approximately 500 g of explosive (~2.4 MJ) produced the $\sim 10^4$ J of projectile kinetic energy.

B. Rail-Gun Parameters. The most efficient method of projectile acceleration is at constant acceleration or constant current I. For the parameters of our nominal impact-fusion case (E = 10 MJ, m = 0.5 g, v = 200 km/s) the equation $\frac{1}{2}mv^2 = \frac{1}{2}L'xI^2$ gives the following relation between accelerator length and current (L' = 0.42 μH/m):

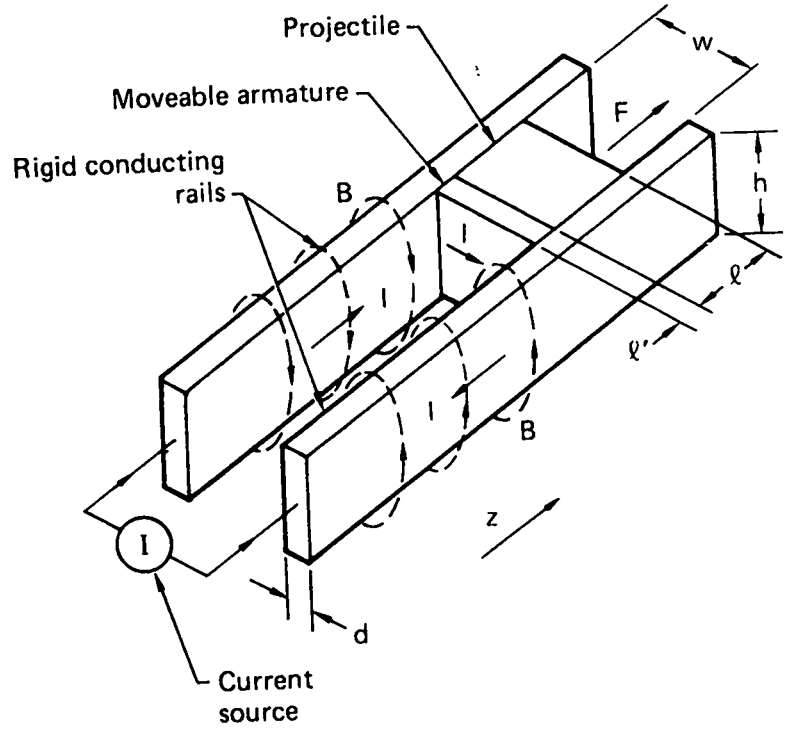

Fig. 1 Schematic diagram of a rail gun[11]

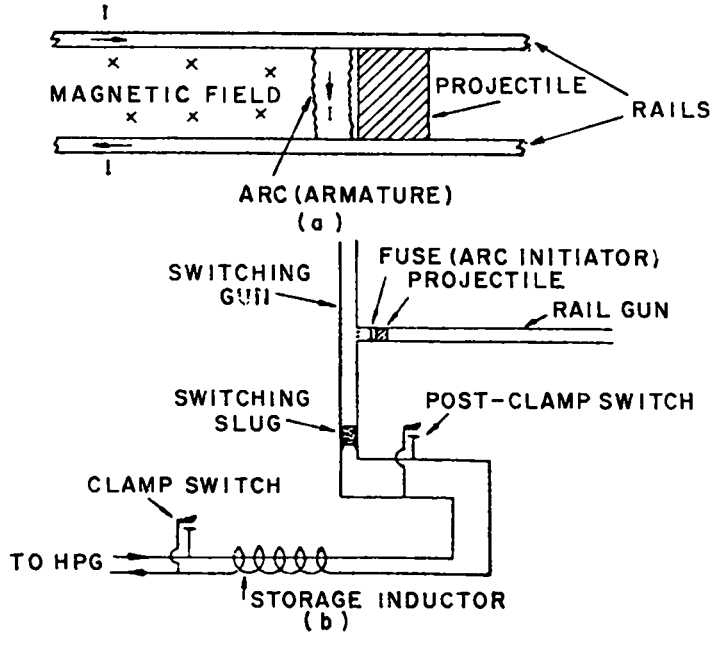

Fig. 2 The Canberra rail-gun arrangement[7]

$$I^2 z = 5 \times 10^{13} v^2 m. \quad (1)$$

For a maximum current of 0.2 MA (see below) this corresponds to a length $z \approx 1250$ m.

Hawke and Scudder[11] and Barber[5] discuss a number of limitations on rail-gun performance:

C. Magnetic Energy Stored Between Rails. In the example being studied at least 10 MJ must be stored in the inductor L of Fig. 2. For $I = 2 \times 10^5$ A its value must be 500 μH. The fraction of magnetic energy stored between the rails is $L'z/L$. For the parameters under study this fraction would be about 100%, leading to a magnetic efficiency of zero if the rail energy were dissipated. To achieve a magnetic efficiency of 90% it would be necessary to store 10 times the projectile energy in L (perhaps as ten 500-μH sections, each driving 125 meters) allowing only 5% "droop" in the current. If extra stored energy is recovered between shots, the large $L/L'z$ is not necessary.

D. Resistive Rail Losses. The energy loss $W_R = I^2R$ from a single pair of rails and power supply is of the same order of magnitude as the projectile energy[5][11] for the rail-gun parameters under discussion. Hawke and Scudder[11] suggest reducing W_R by dividing the length into $N \approx 100$ sections. The resistive loss is then divided by $N^{1/2}$ since each rail section is activated only when the projectile is in residence, incurring resistive-power losses only then.

E. Rail Melting and Strength Limits. For copper rails Barber[5] showed that melting and yield failure because of the $B^2/2\mu$ energy density limits the current to $I \approx 4 \times 10^7 h$. For a practical dimension $h \approx 1$ cm, the previously chosen value of 0.2 MA is safe. The average magnetic field between the "square" rails is $B \approx 0.5\mu_o I/h = 12$ T, and $B^2/2\mu_o \approx 6 \times 10^7$ Pa. This is about the same as the limiting magnetic pressure Hawke and Scudder estimate in the insulating and confining dielectric for similar rail spacing.

Brast and Sawle[8] estimate that the voltage drop in a current-carrying arc is 200 V. In our example, the acceleration time is $t = 2z/v = 12$ ms. The arc energy dissipation (0.2×10^6A $\times$ 200V $\times$ $12 \times 10^{-3} = 0.5$ MJ) is negligible. They also show that the arc will deposit heat in the rails equal to its energy density $B^2/2\mu_o$. For B = 12T this is 6×10^7 J/m^3; copper melts starting from room temperature at an energy deposition of 6×10^9 J/m^3, again providing a margin of safety.

F. Projectile Stress. The acceleration inertial force must not exceed the yield stress, σ_y times the projectile area hw. This limits the maximum accelerating

current (for w = h) to the value $I \approx (2\sigma_y/L')^{\frac{1}{2}} h$. For a plastic projectile $\sigma_y \approx 1.4 \times 10^9$ Pa, giving a limiting I ≈ 0.7 MA.

G. Projectile-Rail Drag and Friction. Assuming that the projectile does not exceed its elastic limit, Hawke and Scudder[11] discuss drag from liquid and gaseous layers between the projectile and rails, showing it to be negligible for the accelerations and dimensions under discussion in this example. However, drag effects are sufficiently varied and unpredictable as to provide a serious uncertainty, requiring experimental research for its resolution.

H. Rail Gun Power Supplies. For impact fusion we have estimated a possible total energy of 100 MJ over 0.012 s, or 8000 MW of power. This can be derived from storage inductors energized either from capacitors or homopolar generators (electromechanical capacitors), with charging times of the order of one second (power ≈ MW). At these values of energy storage the latter are probably more economical.

I. Conclusions. A segmented rail gun can produce impact-fusion projectile parameters at conditions involving feasible extensions of technology and at efficiencies exceeding 50%, provided the rails can be divided into many sections and that drag losses do not greatly exceed present theoretical estimates.

3. Traveling-Wave Accelerators. The idea of accelerating particles having induced or permanent dipole moments M by a traveling wave without material contact to the current-carrying drive conductors has been advanced by Winterberg, et al,[12,13,14] O'Neil and Kolm, et al,[15,16,17] Garwin, et al,[18] and Chen, et al[19]. Such a linear accelerator is shown in Fig. 3, where each drive magnet coil is excited by a charged capacitor C. For a traveling wave[12,13,14] the left-hand switch may be used to initiate current propagation with the other switches replaced by shorts. In a synchronous arrangement[18,19] each coil is excited by a separate switch actuated by the approach of the magnetized projectile. If $H_z(z,t)$ is the component of magnetic field along the axis, the accelerating force is

$$F_z = M_z \, \partial H_z/\partial z \qquad (2)$$

Fig. 4 shows schematically the field lines, as well as H_z and $\partial H_z/\partial z$ as functions of accelerator length z. In regions D a diamagnetic projectile loop carrying current I_D with magnetic moment M_D will be accelerated to the right as it "leads" the driven coil. In regions P a paramagnetic projectile with magnetic moment M_p will be

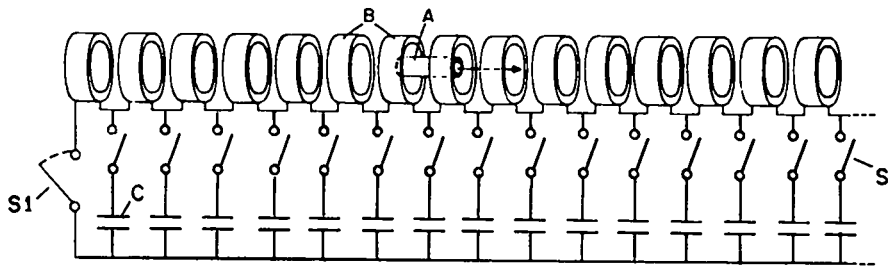

Fig. 3 Schematic diagram of a traveling-wave accelerator[12]

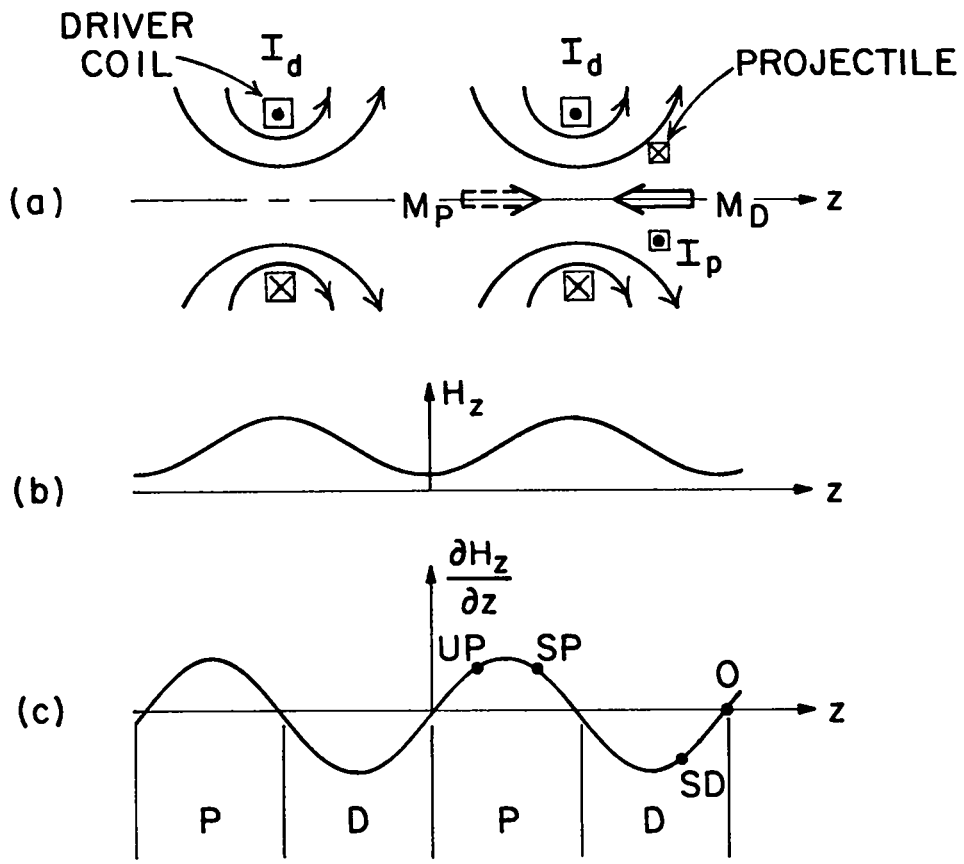

Fig. 4 Illustrating the magnetic fields and magnetic-moment M of driving coils(d) and superconducting projectile in a traveling-wave accelerator.

accelerated to the right as it "trails" the driven coil. If the driver current I_D oscillates in time and changes direction M_D will then accelerate in the trailing regions. Kolm, et al[16] suggest a synchronous accelerator based on this principle whereby the particle (bucket) gets a double impulse in the coil region whose current reverses in time during the traversal from P to D.

There are various physical choices for magnetized macroparticles:

A. Diamagnetic normal conducting cylinders will have a dipole moment M_D induced because of eddy currents j_θ which prevent the penetration of H_z. However, the joule heating $j_\theta^2 \eta$ is prohibitive. Barber[5] gives the following relation between attainable velocity and temperature rise from the eddy currents:

$$v \approx (\Delta T/0.3\mu\rho)^{\frac{1}{2}}, \tag{3}$$

where ρ is the density of the projectile material. For copper $\Delta T \approx 800K$ at $v \approx 0.5$ km/s.

B. Superconducting cylinders with induced diamagnetic moments suffer from insufficient acceleration. Type I superconductors with complete Meissner skin effect go normal at fields which are too small to provide interesting velocities. Type II superconductors are subject to large hysteresis losses from time-changing currents which will necessarily be present when the traveling magnetic field induces the diamagnetic currents.

C. Ferromagnetic cylinders produce paramagnetic M values and are not necessarily subject to eddy currents. However, the saturation values of their magnetic polarization are too low for achieving velocities in the 200 km/s range.

D. Persistently magnetized superconducting cylinders can be produced with large M values (diamagnetic or paramagnetic)[12] using cylinders wound with Type-II superconductor wire (NbTi or Nb_3Sn) which have high critical fields and currents. Kolm[15] suggests adding thermal inertia in the form of Woods-metal impregnation. Winterberg[12] estimates the length z of an accelerator to achieve velocity v with a superconducting cylinder of critical field H_0, density ρ and length $\ell \approx 10^{-3}$ m) as

$$z = 10^{-5}\, \rho \ell (v/H_0)^2. \tag{4}$$

For $H_0 = 20$ T, $\rho = 5 \times 10^3$ kg/m^3, $v = 2 \times 10^2$ km/s we find $z \approx 5$ km. This is perhaps not an excessive length in view of the fact that present more complex proton and electron accelerators have comparable lengths.

E. Stability of the acceleration: Provided the diamagnetic projectile rides to the right of point SD of Fig. 4C (but not past point O), it will be stably "levitated" against its own "gravitational" force - md^2z/dt^2 in the moving frame of the particle. If it moves to the right (left) of SD it feels less (more) force and is restored in phase; i.e., it has phase stability. Similarly a paramagnetic projectile is phase stable at SP. However, both of these projectiles are unstable to radial displacement, and there is a necessary apposition of phase stability (instability) and radial instability (stability). Chen, et al[19] propose to use the phase unstable point UP for paramagnetic projectiles, where radial motion is stable. They propose feedback stabilization of the longitudinal motion, whereby the field is applied in response to a signal which measures particle position. Kolm[15,16] points out that radial motion might be stabilized by a normal conductor near the superconducting projectile whose eddy currents, induced by the changing dipole field on the projectile's radial excursions, will restore it to the axis.

F. Acceleration efficiency: A given driver coil need only be energized when the projectile is in its vicinity. After that the energy can be withdrawn with little resistive loss and restored to the local capacitor. This leads to high efficiency for this type of accelerator, without the possible drag losses of the segmented rail gun.

G. A set of possible parameters has been estimated by Garwin, et al.[18] as follows:

mass, length of projectile	0.1 g, 1.4 mm
velocity, energy of projectile	1.5×10^5 m/s, 1.1 MJ
driver loop radius, number of turns	0.005 m, 1 turn
driver loop inductance, current	9 nH, 80 kA
driver magnetic field, energy	10 T, 30 J
driver capacitance, voltage	0.5 μF, 10 kV
accelerator length	2 km

They also estimate the vacuum requirement along the acceleration path from the heat imparted to the projectile (of area A) by a gas of density ρ_g: $Q = \rho_g v^2 Az$. For a superconductor moving in a 10^{-6} torr vacuum $Q \approx 1$ J. A heat shield would be required, or else 10^{-10} torr vacuum, to preserve the superconducting state. Kolm points out that such small projectile dimensions would be difficult to achieve with practical superconducting wire whose bulk at a composite current density of 25 kA/cm^2 for NbTi requires a minimum dimension of the order of a few cm.

H. A synchronous accelerator model has been operated by Kolm, et al, at the MIT National Magnet Laboratory. It has 20 drive coils spaced along its 2 meter length, each driven by a 200-joule, 450-V electrolytic capacitor. The number of turns per coil is graduated along the length z, decreasing from 99 turns to 16 turns in order to match the transit time from SP to SD of Fig. 4C to the quarter period of the LC combination. The projectiles are aluminum loops of mass 305 g, inductance 0.087 μH which derive their excitation current from sliding contact with a bus bar. The driver and projectile radii are 8.6 and 4.5 cm. The acceleration is ~10^3 m/s^2(10^2 g), imparting 1.3 kJ to a bucket

4. Plasma-Impulse Accelerator. Tidman and Goldstein[20] have proposed an accelerator based on repeated impulses from "z-pinches" of plasma as shown in Fig. 5. The high-voltage sources (capacitors) HV are triggered by the approach of the conical projectile as sensed by the light beams and generate current between their adjacent annular conducting plates, imploding plasma sheaths inward. These plasmas impinge on the projectile, enveloping it and partially transforming radial plasma momentum into longitudinal projectile monentum. If U, M and θ are the projectile velocity, mass and half angle, and m_g is the mass of filling gas (or gas adsorbed on the electrodes) swept up with velocity V_r, then

$$U = m_g V_r \sin 2\theta / M. \qquad (5)$$

This type of driver would have much in common with a segmented rail gun which uses a plasma arc to drive the projectile. The ambiant filling gas might impose large heating on the projectile according to paragraph G above. The pinch might also spill over the nose of the projectile as in a dense plasma focus device, detracting from the acceleration.

5. Acceleration by Laser Ablation. When a strong laser pulse is incident upon the base of a projectile in vacuum, ablation products are ejected at high velocity, producing a reaction force which accelerates the non-ablated mass in the manner of a rocket. The absorbed laser energy produces an enthalpy increase in the ablation products similar to the situation in chemical rockets. If we consider the case of constant exhaust velocity relative to the projectile, the total system momentum remains constant (neglecting the momentum of the photon beam [radiation pressure]), or

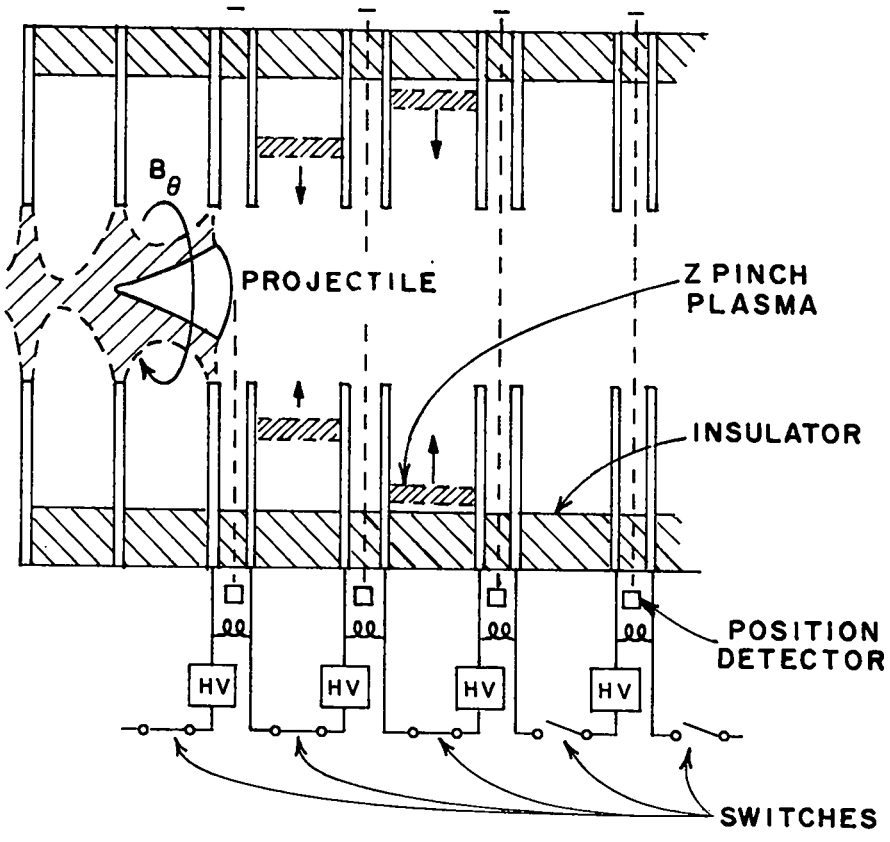

Fig. 5 Schematic diagram of a plasma-impulse accelerator[20]

$$\frac{d}{dt}\left\{(m_o - \dot{m}t)\, v + \dot{m}\int_0^t v\, d\tau - \dot{m}\, u_e t\right\} = 0, \tag{6}$$

from which one obtains the "simple rocket equation,"

$$v(t) = u_e \ln \frac{m_o}{m(t)} = u_e \ln \frac{1}{(1-t/\tau)}, \tag{7}$$

where v is the projectile velocity, m_o the initial mass, $\dot{m}$ the (constant) ablation rate, u_e the (constant) exhaust velocity relative to the projectile, and τ the characteristic ablative time given by $m_o/\dot{m}$.

The distance travelled is

$$z = \int v dt = \frac{u_e m_o}{\dot{m}}\left[1 + \frac{m}{m_o}\left(\ell n \frac{m}{m_o} - 1\right)\right] \rightarrow \frac{u_e m_o}{\dot{m}} \text{ as } \frac{m}{m_o} \rightarrow 0. \tag{8}$$

From equation (7) it is seen immediately that the projectile velocity can exceed the exhaust velocity by an arbitrary amount, but the projectile mass becomes very small for $v >> u_e$.

The ratio of projectile energy to exhaust kinetic energy in this simple rocket model (which ignores exhaust thermal energy) is given by[2]

$$\eta \equiv \frac{\frac{1}{2}mv^2}{\frac{1}{2}(m_o - m)u_e^2} = \frac{1}{x-1}(\ell n x)^2, \tag{9}$$

where $x = m_o/m$. The efficiency rises to a peak of about 0.65 at $x \simeq 5$, at which point the projectile has acquired about 40% of the total system energy (absorbed laser energy).

In order to calculate the exhaust velocity u_e and the ablation rate $\dot{m}$, one must consider the details of the laser-projectile interaction. This has been done in the present context by several authors, including Raiser[29] Bobin[21], McCann and deGroot[22] and Felber[23,24]. The details of this interaction will be given in subsequent papers in this workshop and will only be summarized here. The laser energy is absorbed primarily in the neighborhood of the critical surface ($\omega_{laser} = \omega_{Pe}$; $n_{ec} = 10^{19}\ cm^{-3}$ for CO_2 radiation), and transported into the higher density region by electron heat conduction. For the intensities of interest, $I = 10^8 - 10^{12}$ watts/cm^2, the process can be analytically modeled as a deflagration zone, where "fluid" elements increase in temperature and kinetic energy and decrease in density in passing through the interaction region from the solid to the exhaust. Because of the nonlinear heat conductivity ($K \propto T^{5/2}$), the diffusion of heat becomes wave-like (finite signal speed), and Felber[23] has shown that the deflagration can be modeled in steady state in the accelerated frame of the

ablation surface. In a Chapman-Jouget deflagration[25], the fluid exits at the local sound speed. Simple estimates than give $I_a \approx n_c(kT)_c v_{ex}$, where "c" denotes the critical surface and I_a is the absorbed laser intensity. Since $v_{ex} \propto (kT_c)^{1/2}$ (C-J condition), then $I_a \propto n_c(kT)^{3/2}$, or $(kT)_c \propto (I/n_c)^{2/3}$, and the ablation pressure

$$p \propto \rho_c v_{ex}^2 \propto n_c(kT_c) \propto n_c^{1/3} I^{2/3}, \tag{10}$$

a scaling law developed by several authors. McCann and deGroot[22] have applied the LASNEX (laser implosion) code to this problem and find that the inclusion of radiation losses and hydrodynamic effects weakens the dependence of T on I to give

$$(kT)_c \propto (I/n_c)^{1/2}, \tag{11}$$

and

$$p \propto n_c^{1/2} I^{1/2}. \tag{12}$$

They give an example of a pellet of SiO_2, m_o = 8 g, subjected to a laser pulse rising linearly in time to 2×10^{10} watts/cm^2 in 1 ms. At that time, the final values were m = 0.16 g, v = 1.3×10^7 cm/sec, and E = 1.35 MJ. The final projectile energy was about 12% of the incident laser energy, which agrees with other estimates in the literature of 10-20%, and the acceleration length was approximately 50m. The peak pressure reached was about 6.5 kbar. The authors further state that the results are quite insensitive to the time dependence of the laser pulse, and that a constant intensity pulse, for which $u_{ex} \sim$ constant and the simple rocket model applies, may be close to optimum.

This example is encouraging in that it indicates that the projectile energies and velocities needed for impact fusion are in principle attainable. There are several effects left out of this one dimensional model, of course, which reduce the propulsion efficiency. Principal among these are refraction of the beam around the target by the ablation tail, and radial components of the blowoff which reduce the axial force. In addition, the problem of maintaining the required spot size (3 mm - 1 cm) over a distance of >100 m is non-trivial.

Perhaps the most serious objection to acceleration by laser ablation, however, is that of relatively low "propulsion efficiency." If 10-MJ projectile energy is required, then the laser energy must exceed 50 MJ, and it may turn out that 100 MJ is more realistic. The energy of the ablation products would not appear to be

readily recoverable. On the other hand, if the projectile energy can be as low as 1 MJ, the required laser energy drops into a quite reasonable range. For CO_2 lasers, for example, the "long-pulse" efficiency, where all the rotational CO_2 lines contribute fully, has been demonstrated to be as high as 25%, or about an order of magnitude higher than with nanosecond pulses. An Antares-size system[26], for example, would produce about 1 MJ, and the long pulse lengths desired could be achieved by sequentially firing the amplifier modules. An even higher efficiency, greater than 50%, has been demonstrated for CO lasers ($\lambda = 5\mu$), but very large devices have not yet been built.

Finally, we note that the laser could in principle be replaced by a beam of relativistic electrons or light ions, provided that beam-transport, focussing, and pulse-length problems could be solved. In this case, however, the collisions may become primarily elastic due to electrostatic charge build-up on the projectile. The propelling force would then be primarily by momentum transfer rather than energy deposition and subsequent ablation. Simple models for this process have been advanced by Harrison[2] and, from a different viewpoint by Winterberg[27], both of whom conclude that the technique is promising. Up to now, however, the models appear to be too simple to permit critical evaluation, and further work remains to be done.

6. Electrostatic Accelerators: Electrostatic acceleration of macroscopic particles has been considered by many authors; three of the most recent papers are References 2,3 and 29. It is generally agreed that acceleration of particles of radius much greater than a few microns to velocities $>10^7$ cm/sec requires prohibitively long lengths (or equivalent, high potentials). This can easily be shown. The equation of motion is

$$m \frac{dv}{dt} = q\mathcal{E} \tag{13}$$

where $\mathcal{E}$ is the accelerating field, and the charge q is related to the surface field by $q = 4\pi\varepsilon_0 r^2 \mathcal{E}_0$. The value of $\mathcal{E}_0$ is limited to 10^9 V/m for negatively charged particles by field emission, and up to 10^{10} V/m for positive charges by tensile strength.[2]

From Eq. (13) we find immediately, for constant acceleration over a distance z in a field $\mathcal{E}$,

$$E = \tfrac{1}{2}mv^2 = 4\pi r_0^2 \varepsilon_0 \mathcal{E}_0 \mathcal{E} z \tag{14}$$

and $v = [6\epsilon_o \mathcal{E}_o \mathcal{E} z/\rho_o r_o]^{1/2} = [6\epsilon_o \mathcal{E}_o \mathcal{E} z/(\frac{m}{4\pi})^{1/3} \rho_o^{2/3}]^{1/2}$. (15)

Thus, large pellet energies can be obtained ($E \propto r_o^2$), but large velocities cannot. For example, to obtain $E = 10^7$ J we require $M = \frac{1}{2}$g, which even for light material ($\rho = 1$ g/cm^3, $r_o \approx 0.5$ cm) yields $z = 3.76 \times 10^4$ m for $v = 2 \times 10^5$ m/s. The physical reason for this limit is clear. Since, for $(\mathcal{E}_o)_{max}$ fixed, the force on the particle goes as $q \propto r_o^2$, while the mass $\propto r_o^3$, the acceleration decreases as $1/r_o$ and is orders of magnitude too small to reach the high velocities. Therefore, since velocity is of key importance in impact fusion (see the paper by Christiansen & Marshall, this workshop), electrostatic acceleration of single charged macroscopic particles to the required velocity and energy is not feasible.

Several authors [2,28] have suggested using beams of small (micron-sized) particles electrostatically accelerated to $v \sim 10^5$ m/sec; the interaction of such "macro-beams" with DT targets is not within the scope of this review.

REFERENCES

1. F. Winterberg, On the Attainability of Fusion Temperatures Under High Densities by Impact Shock Waves of Small Solid Particles Accelerated to Hyper-velocities, Z. Naturforsch. 19, 232 (1964).
2. E.R. Harrison, The Problem of Producing Energetic Macrons (Macroscopic Particles), Plasma Physics 9, 183 (1967).
3. C. Maisonnier, Macroparticle Accelerators and Thermonuclear Fusion, Il Nuovo Cimento 42b, 332 (1966).
4. R.A. Gerwin and R.C. Malone, Adiabatic Plasma Heating and Fusion-Energy Production by a Compressible Fast Liner. Nucl. Fusion 19, 155 (1979).
5. J.P. Barber, The Acceleration of Macroparticles and Hypervelocity Electromagnetic Accelerator. The Australian National University Research School of Physical Sciences, Report EP-TR12, March 1972.
6. R.A. Marshall, The Rail Gun Installation. Presentation at the Seminar on High Energy, High Power Pulses, Production and Applications, Research School of Physical Sciences, Australian National University, Canberra, Australia, November 1977.
7. S.C. Rashleigh and R.A. Marshall, Electromagnetic Acceleration of Macroparticles to High Velocities, J. Appl. Phys. 49, 2540 (1978).
8. D.E. Brast and D.R. Sawle, Feasibility Study for Development of a Hypervelocity Gun. NASA-CR-60119 (1964).
9. D.E. Brast and D.R. Sawle, Study of a Rail-Type MHD Hypervelocity Projectile Accelerator, Proc. Seventh Hypervelocity Impact Symposium, Tampa, Florida, 1964. Vol. I, p. 187.
10. R.L. Chapman, D.E. Harms and G.P. Sorenson,The Magnetohydrodynamic Hypervelocity Gun, in Proc. Sixth Symposium on Hypervelocity Impact, Cleveland, 1963. Vol. 1.
11. R.S. Hawke and J.K. Scudder, Magnetic Propulsion Railguns: Their Design and Capabilities. Lawrence Livermore Report Preprint UCRL-82677 (1979).
12. F. Winterberg, Magnetic Acceleration of a Superconducting Solenoid to Hypervelocities, J. Nucl. Energy, Part C, 8, 541 (1966).
13. F. Winterberg, Nuclear Fusion by Magnetic Acceleration of a Superconducting Solenoid, Nucl Fusion 6, 152 (1966).
14. D. Anderson, S. Claflin and F. Winterberg, On the Acceleration of a Superconducting Macroparticle in a Magnetic Traveling Wave Accelerator, Z.F. Naturforsch 26, 1415 (1971).

15. G.K. O'Neill and H.H. Kolm, Mass Driver for Lunar Transport and as a Reaction Engine, J. Astro. Sciences 25, 349 (1977).
16. H.H. Kolm, Basic Coaxial Mass Driver Reference Design, AIAA Paper No. 77-534, 1977. Princeton/NASA/ERDA/GE Conference on Space Manufacturing. AIAA, New York, 1977.
17. H. Kolm, K. Fine, P. Mongeau and F. Williams, Electromagnetic Propulsion Alternatives, 1979 Princeton Conference on Space Manufacturing, AIAA New York (1979).
18. R.L. Garwin, H. Muller and B. Richter, Magnetic-Gun Igniter for Controlled Thermonuclear Fusion, JASON Report JSN-77-20 (1978). SRI International Project 7593.
19. K.W. Chen, R.W. Hartung, E. Lehman and S.D. Mahanti, Design of a Magnetic Linear Accelerator (MACLAC) as Driver for Impact Fusion (IF), Proc. 1979 Particle Accelerator Conference, San Francisco, CA, March 12-14, 1979.
20. D.A. Tidman and S.A. Goldstein, Mass Accelerator for Producing Hypervelocity Particles Using a Series of Imploded Annular Discharges, Jaycor Tech. Note 350-79-004 (1979).
21. J.L. Bobin, Phys. Fluids 14, 2341 (1971).
22. T.E. McCann and J.S. deGroot, Lawrence Livermore Laboratory Preprint UCRL-79732 (1977).
23. F.S. Felber, Phys. Rev. Letters 39, 84 (1977).
24. F.S. Felber, General Atomics Report GA-A14944 (1979).
25. R. Courant and K.O. Friedrichs, Supersonic Flow and Shock Waves, Interscience, N.Y. (1948).
26. Antares is the 100-kJ CO_2 laser system under construction at the Los Alamos Scientific Laboratory.
27. F. Winterberg, to appear in Lettere Al Nuovo Cimento.
28. F. Winterberg, Z. Naturforsch. 19a, 231 (1967).
29. Yu. P. Raiser, Sov. Phys. JETP 21, 1009 (1965).

TARGET DYNAMICS AND THERMONUCLEAR BURN
PART I

J. Marshall
Los Alamos Scientific Laboratory*
Los Alamos, NM 87545

Introduction

Impact fusion appears at first sight to make possible a very attractive fusion reactor system. An accelerator, capable of many repetitive shots, drives projectiles at high velocity into a reactor volume where they hit targets placed there before each shot. Fusion fuel is heated by the impact to thermonuclear temperature and contained inertially to produce fusion energy greater than the energy required to accelerate the projectile by a factor q. The accelerator can stand off at a large distance from the reactor volume so that it is not exposed to blast and radiation from the fusion reaction. The reactor volume contains no complicated structures, but is simply a blast container with tritium breeding blanket and heat store.

When we look at details, we find a number of problems with impact fusion that may interfere with its realization. Projectiles must be accelerated to very high velocities, tens to hundreds of times the present state-of-the-art. The accelerator must be efficient and durable. Suitable projectile-target systems must be developed capable of producing a high q. I intend here to concentrate on projectile-target problems rather than those of the accelerator. We must keep in mind, however, that there are serious accelerator problems so that systems requiring modest projectile velocities and energies are highly desirable. Also, we would like to avoid systems requiring large fusion yield per shot because of the economic cost of large blast containment.

*Work performed under the auspices of U.S. Department of Energy.

Shock Waves

Shock waves are frequently visualized as being generated in a hard-walled cylinder filled with unshocked material. A piston is driven into the cylinder from one end accumulating material ahead of it. The velocity of the piston is v_p.

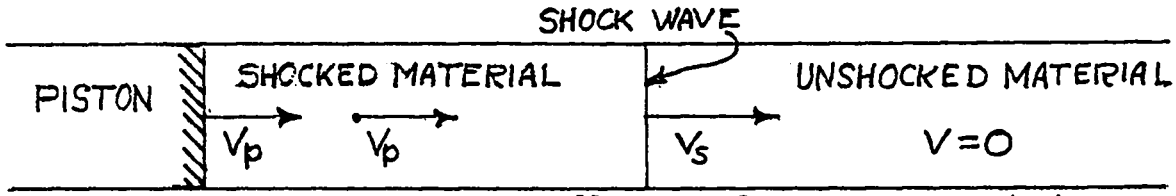

The unshocked material, we shall assume for our purposes to have

pressure = 0

density = ρ_0

velocity = 0

A shock wave moves ahead of the piston into unshocked material at velocity

velocity = $v_s > v_p$

Material that has passed through the shock has

pressure = p_s

density = ρ_s

velocity = v_p

The shocked material has the same velocity as the piston. Using conservation of material and a pressure vs. rate of change of momentum equation, we can derive

$$p_s = \rho_0 v_p v_s$$

$$\rho_s = \rho_0 \left(\frac{v_s}{v_s - v_p} \right)$$

If the shock is energetic enough that the energy required to ionize the material can be neglected, and if the resulting electron plus ion plasma obeys the perfect monatomic gas law, with $\gamma = 5/3$, i.e., the internal energy per unit volume is 3/2 times the pressure, then the density of the shocked material is 4 times the unshocked density.

$$\rho_s = 4\rho_o$$

With a $\gamma = 5/3$ gas, the shock velocity is given by

$$v_s = 4/3\ v_p$$

and the pressure by

$$p_s = 4/3\ \rho_o v_p^2 .$$

These gas shock formulae would be be modified somewhat for $\gamma \neq 5/3$. For instance, if γ were 1.4, approximately the value for weak shocks in air, the density ratio would be 6 instead of 4.

We might inquire as to the reason for being interested in the behavior of a monatomic perfect gas when the problems we face concern shock waves in solid materials, solid frozen DT and various metals. The case of solid DT with a density

$$\rho_0 = 0.2\ \text{gm/cm}^3$$
$$n_0 = 4.82 \times 10^{22}/\text{cm}^3$$

is particularly easy to justify. The energy required to dissociate and ionize a hydrogen molecule is 29.5 eV. Once it is ionized, it has become 4 particles instead of 1 particle, 2 electrons and 2 ions. The dissociation plus ionization energy per particle is then about 7.4 eV. We are interested in shocks producing temperatures of at least several hundred eV. As an example, a temperature of 400 eV would imply a thermal energy of 3/2 kT for each electron and ion or 600 eV, 80 times the dissociation-ionization energy, which would thus appear to be negligible.

Impact Against an Immovable Wall

A simple coordinate transformation on the shock wave diagram given above, namely subtracting v_p from every velocity, puts the shock in a system in which the piston does not move. In other words, it describes a system in which the material streams from the right at velocity v_p, accumulating as a lengthening cylinder of shocked material against an immovable wall.

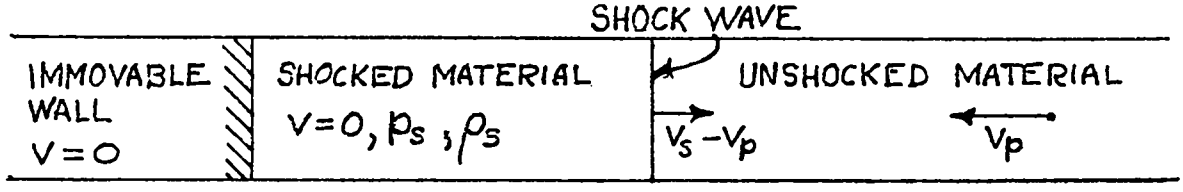

The equations applicable to the moving piston case apply equally here. In addition, in this system it is particularly easy to calculate the temperature of DT. Assume a cylinder of DT, containing N D+T atoms, impacts at velocity v_p against a hard wall. The initial kenetic energy is

$$U = 1/2\ NMv_p^2$$

where M is the DT ion mass

$$M = 2.5 \text{ atomic mass units}$$
$$= 4.15 \times 10^{-24} \text{ gm}$$

A shock wave moves through the DT cylinder until, when it reaches its back surface, the velocity is zero everywhere and all of the kinetic energy has been turned into thermal energy,

$$1/2\ NM\ v_p^2 = 3\ N\ kT$$

3 instead of 3/2 because there are now 2N particles, including electrons. From this we get

$$kT = 1/6\ Mv^2$$

Putting numbers into this

$$T = 4.32 \times 10^{-13}\ v_p^2 \text{ (T in eV, } v_p \text{ in cm/sec)}$$

To achieve a shock temperature of 10 keV in DT, we need a relative velocity between DT and an immovable wall of

$$v_p = 1.52 \times 10^8 \text{ cm/sec.}$$

Impact Between Two Different Materials

If disks of two materials collide with each other with relative velocity normal to their surfaces, a plane impact surface is formed with a shock wave moving away from it into each material. The shocked material is at rest with respect to the impact surface, and the pressures of the two shocked materials are equal. If we examine this system in the frame of the impact surface, we see that it can be described by the following diagram.

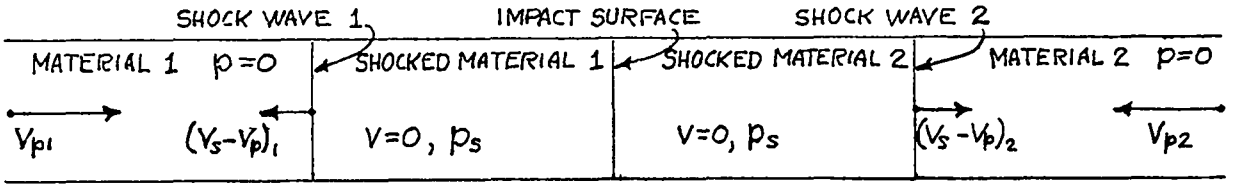

To get the relative velocity between the two materials, we add the streaming velocity (v_p) in one material, required to produce the pressure p_s against an immovable wall to the v_p in the other material, required to produce the same pressure. For example, if the impact is between DT and DT, the required relative velocity is twice the velocity required in DT collision against an immovable wall. The velocity required of a projectile striking a stationary target is just the relative velocity between the two materials. Clearly, we would like to minimize that velocity, and to do that we need an impact between DT and some material capable of producing the required shock pressure at much smaller velocity.

Extensive investigations of pressure and density in strong shocks have been carried out, using explosives to produce the necessary high pressures. Pressures up to 2 megabars (Mb) have been studied at LASL, while the work of Al'tshuler, et al., in the USSR has gone as high as 10 Mb. The experimental results are summarized in LLL report UCRL 50108 (1977), "Compendium of Shock Wave Data." The results are mostly displayed as "Hugoniots," plots of shock velocity or pressure vs. particle velocity. In Fig. 1 we have plotted pressure Hugoniots for a number of substances as log p_s vs. log v_p. The substances cover the range of densities from that of uranium to that of gaseous DT and cover pressures over 6 orders of magnitude from 100 kb. All pressures covered are above the strength of materials. The substances are U, Cu, Al, CH_2 (polyethylene) Li and DT, solid and gas. The sections of the curves in the lower left corner, where individual points are plotted, are the results of experiment. They are confined to pressures less than 10 Mb and particle velocities less than 10^6 cm/sec. Some of the points represent individual experiments and some are taken from smoothed curves. The straight lines in the upper right are Hugoniots calculated on the assumption that the shocked materials behave like $\gamma = 5/3$ gases.

$$p_s = 4/3 \rho_0 v_p^2$$

The dashed sections in between are sketched in by eye.

Chemical effects on the Hugoniots are limited to velocities less than a few times 10^6. It is obvious that the overriding effects on pressure are density and velocity. Above $v_p = 10^7$ cm/sec, all shocked materials behave like monatomic gases, for instance having a shock compression ratio of 4.

If we read from the Hugoniots, the particle velocities required in 2 materials to produce some given pressure, and if we then add those 2 velocities, we get the relative velocity in a head-on impact between the materials required to produce the pressure. For example, to produce 1000 Mb (10^{15} dynes/cm^2) shock pressure in the impact between solid DT and U, the uranium velocity is 6.2×10^6 cm/sec, while the DT velocity is 6.3×10^7 cm/sec. The relative velocity is then the sum of these velocities or 6.9×10^7 cm/sec. We could use either a DT projectile of this velocity striking a heavy target or vice versa.

Burn After Shock Heating

We have been discussing heating by plane shock waves in DT. The burn to be expected after this depends on how long the temperature remains high enough and how long before the DT compressed to 4 times its original density decompresses to low density. Heat is lost from the hot plasma by bremsstrahlung and by thermal conduction. Expansion will take place through the sides of a slab of DT and by rarefaction waves after the shock wave reaches the surface of the DT. Expansion through the sides can be reduced either by heavy materials there or simply by making the slab wide relative to its thickness. The burn can take place either through ignition or simply because of the high temperature produced by the shock. Ignition is the condition where the 3.6 MeV alpha particles, produced in the fusion reaction, return their energy to the plasma so as to maintain or increase the reaction rate. It depends on the hot DT plasma being thick enough so that the range of the alphas is smaller than or comparable to the thickness. This problem does not normally arise in

magnetic fusion where the alphas are assumed to be contained with the plasma by the magnetic field. The range depends on the electron temperature of the plasma, being larger at high temperature, but the rate of reaction, and thus the alpha particle power, also increases with temperature. The necessary thickness for alpha particle heating to be effective is usually taken to be from 0.2 to 1.0 gm/cm^2, and is referred to as the $\rho\ell$ of the system. For a simple shock system in a wide slab, the disassembly time might be estimated to be the time for the shock wave to traverse the slab once. To shock heat to 10 keV, we need a particle velocity in the DT shock of

$$v_p = 1.52 \times 10^8 \text{ cm/sec}$$

or a shock velocity

$$v_s = 4/3\ v_p = 2.02 \times 10^8 \text{ cm/sec.}$$

If the slab, before compression, is 1-cm thick, the disassembly time would then be $1/v_s$ or 5×10^{-9} sec. At 4 times solid DT density, this would give an $n\tau$ Lawson parameter of 9.6×10^{14}. This would be marginal for nonignition burn, and it appears to be roughly marginal for ignition.

Loss of energy by bremsstrahlung can be compensated by alpha heating. In the absence of effective heating, the bremsstrahlung cooling time is

$$\tau_{br} = 9.04 \times 10^{14} \frac{T_e^{1/2}}{n} \qquad (T_e \text{ in keV})$$

$$= 1.48 \times 10^{-8} s \qquad (10 \text{ keV, } 4 \text{ x solid density})$$

This is somewhat longer than the disassembly time in our example, but not by a large factor.

To get ignition in a target such as we have been discussing here, would require a large target and a very fast, energetic projectile.

The result would be a technically difficult, expensive accelerator and an enormous explosive yield on every shot. Altogether, it appears that simple one-dimensional shock heating is unsuitable for fusion power production.

Compression After Shock Heating

An obvious improvement to simple shock heating is shock heating to some lower temperature, followed by further compression. In a one-dimensional situation, we can imagine a high-density projectile moving normal to its surface, colliding with a DT layer, backed up by another high-density slab. Initial heating would be identical to what we have discussed above, except that the velocities and temperatures would be smaller; however, the DT would not start to disassemble when the shock wave reached its rear surface, but would be further compressed by a second shock reflecting from the high-density slab. The temperature would be further elevated by the reflected shock, and compression and heating would continue by shocks and isentropic compression once the sound velocity becomes larger than the relative velocities of the high-density slabs. This subject will be discussed in other papers by Christiansen, Jarboe, and Krakowski so I shall not attempt to cover it here. Suffice it to say that in order to achieve energy gains (q's) large enough to make an impact fusion reactor practical, ignition or near-ignition conditions appear to be necessary and in plane slab systems, this implies large amounts of DT, perhaps one gram or greater and very large explosive yields. A one gram, DT burn produces nearly 400 GJ of energy. Not all of this energy must produce explosive yield, but still the explosion might be equivalent to 50 tons of TNT and would require a very massive containment vessel.

Three-dimensional compression of thermonuclear fuel has the advantage that because of convergence, large effective thickness of fuel can be achieved with modest amounts of DT. A 1-mm radius sphere of solid DT has a mass before compression of 0.84 mg, and after compression by a factor 10 in radius, would have a ρr of 2 gm/cm^2, comfortably above the ρr requirement for ignition. There

have been suggestions of ways in which linear motion of a projectile can be turned into strong three-dimensional compression. One method has been published in the open literature by a Polish group under Kaliski. They have done experiments in which linear motion, produced by explosives, has resulted in conical compression of D_2 after shock heating, leading to appreciable neutron yields. This work will be discussed in a later session.

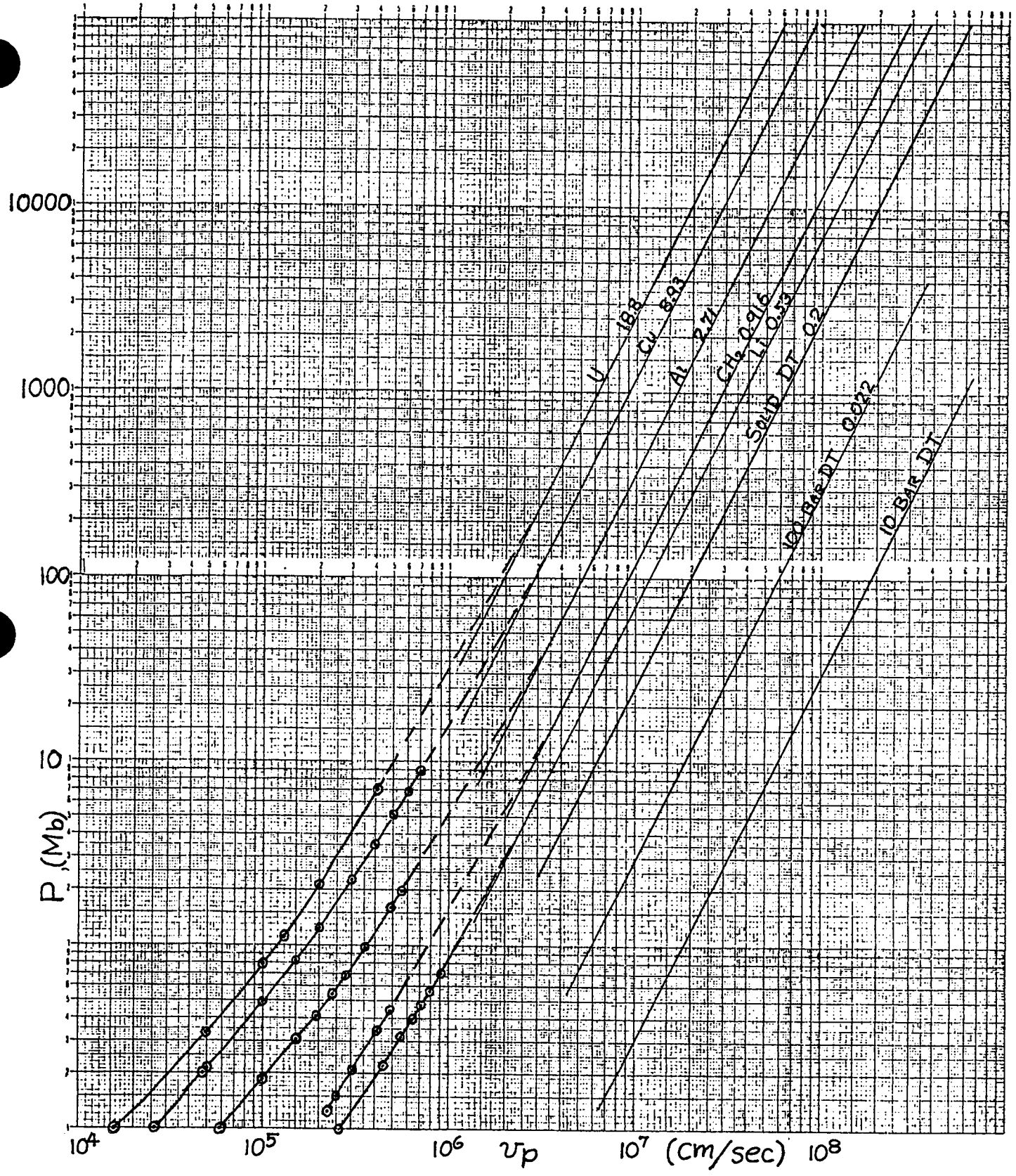

Fig. 1. Pressure vs. particle velocity Hugoniots for representative materials. Hugoniots are experimental below 10^6 cm/sec and 10 Mb. Straight lines at high velocity and pressure assume $\gamma = 5/3$ gas law behavior.

TARGET DYNAMICS AND THERMONUCLEAR BURN
Part 2

Walter Christiansen
University of Washington

Adiabatic Compression Following Initial Shock Heating

Additional heating and compression may occur on subsequent wave reflection within the target material. We can easily envision this process for the simple plane 1-D case, in which we ignore all losses at present. Imagine a heavy projectile made from U striking DT. In order to avoid movement of the target, also imagine an infinitely rigid wall backing the thermonuclear fuel. (This can be arranged in principle by a symmetrical strike of two equal mass particles.) The resulting wave and fluid motion is schematically illustrated for the target only in the following x-t diagram. The wave system within the projectile has not been shown for the sake of simplicity. When the projectile strikes DT, a strong shock is generated which reflects off the rigid wall and then repeatedly interacts as the projectile approaches the wall. The greatly rising pressure decelerates the particle which in turn transfers its energy to the DT plasma. Conditions marked 1, 2, 3 and 4 represent the initial conditions, post primary shock state, first reflected shock state, and peak compression state. States 2 and 3 may be easily related to state 1 using the conservation equations described in the preceding part and assuming a perfect gas. Since the incident shock is very strong, we have

$$\frac{\rho_2}{\rho_1} = \frac{\gamma+1}{\gamma-1}, \; p_2 = \frac{\gamma+1}{2}\rho_1 U_2^2, \; T_2 = \frac{\gamma-1}{4}\frac{u_2^2}{k/\bar{m}_i}, \; M_2 = \sqrt{\frac{2}{\gamma(\gamma-1)}} = \frac{U_2}{a_2} \quad . \qquad (1)$$

The relation between U_2 and U_{p1} may be obtained using the results indicated in Part 1.

The wave is not so strong on reflecting from the wall as the speed of sound in 2 is much larger than 1. But in the strong incident shock limit, there results for state 3 for $\gamma = 5/3$

$$\frac{\rho_3}{\rho_2} = \frac{\gamma}{\gamma-1} = 2.5, \; \frac{T_3}{T_2} = \frac{3\gamma-1}{\gamma} = 2.4, \; \frac{p_3}{p_2} = \frac{3\gamma-1}{\gamma-1} = 6.0 \quad . \qquad (2)$$

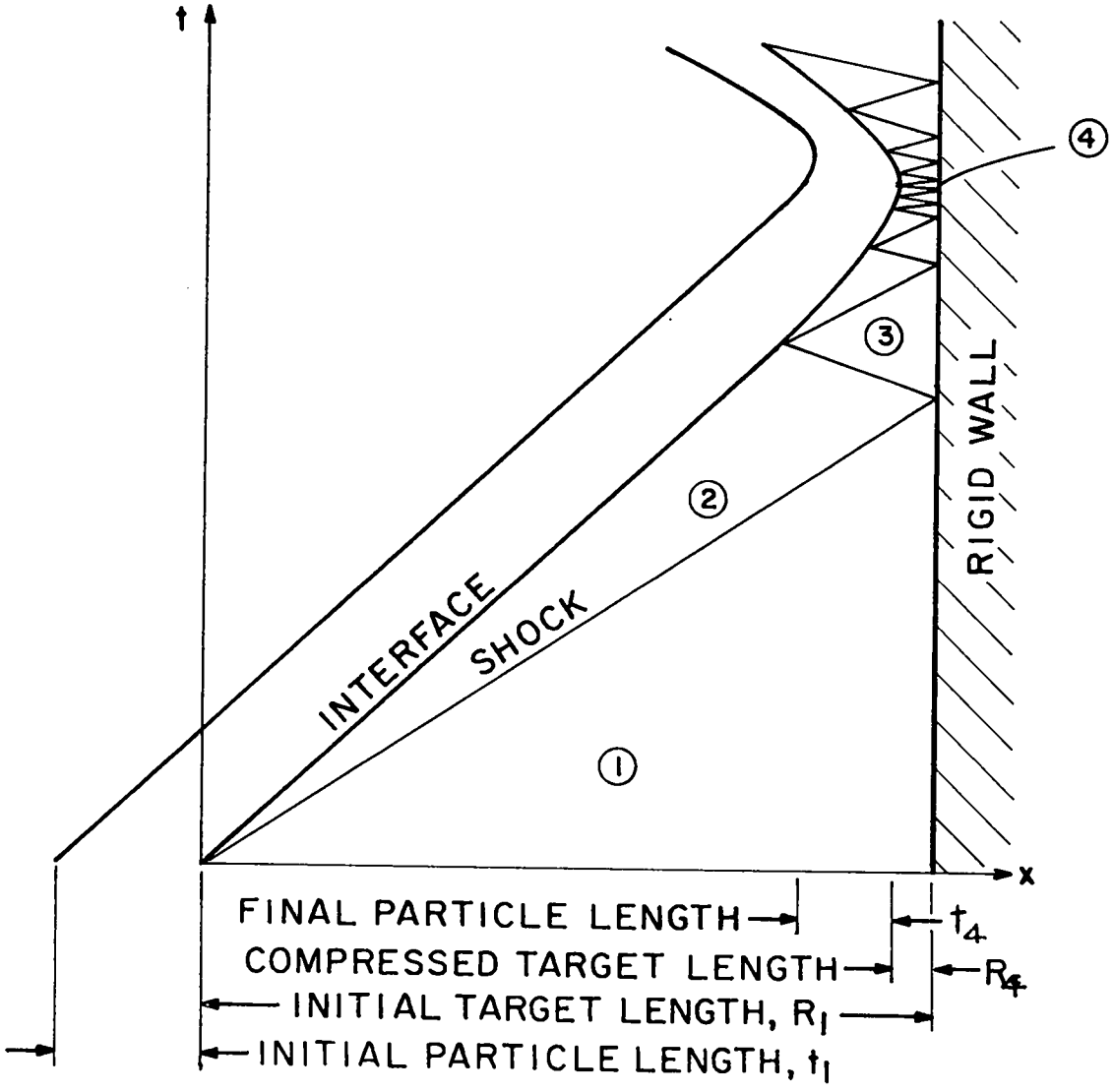

Figure 1. x-t Diagram of Wave Motion in Target.

It may be noted that the projectile is slowing down after this phase while the plasma is heating up. The ratio of U_p/a is being continually reduced which means the subsequent waves are rapidly approaching the weak wave limit, in which they are isentropic. A cursory estimate for the case of U_p = 200 km/sec shows that $\Delta S/R \approx 11.8$ for the first shock, $\Delta S/R = 0.39$ for the second, $\Delta S/R \sim 0.16$ for the third, etc. Thus, it makes sense to treat the subsequent wave action after state 3 as if it were isentropic. Furthermore, since a is becoming very large, the wave speeds are increasing even though they are weakening in strength. As such, we may ideally treat the complicated region near 4 using simple isentropic laws with no pressure or temperature gradients. In this way, the implosion is much like a fast liner compression, except for the shock preheat solution.

(a) <u>The Incompressible Projectile ($a_p \to \infty$, vertical Hugoniot)</u>

This case is extremely easy to analyze and quickly shows some of the features of the compression. We must be on guard, though, as sometimes the results are overly optimistic, if not even incorrect.

Neglecting losses for the moment, the relation between projectile energy and plasma energy may be written as

$$E_3 + \frac{m_p U_{p_2}^2}{2} = E_c + E_{KE} + E \qquad (3)$$

$\frac{m_p U_{p_2}^2}{2}$: projectile energy in region 2

E_c: compression energy of projectile

E_{KE}: kinetic energy of projectile

E: plasma energy

At 4, $E_{KE} = E_C = 0$ because the projectile is incompressible and is not moving, hence

$$\frac{m_p U_{p_2}^2}{2} = 2N_i \frac{3}{2} k(T_4 - T_3) \qquad (4)$$

Further,

$$\frac{T_4}{T_3} = \left(\frac{\rho_4}{\rho_3}\right)^{\gamma-1} = \left(\frac{\rho_4}{\rho_3}\right)^{2/3} \qquad (5)$$

Consider a sample case in which a U projectile is moving at an initial speed of 200 km/sec and strikes DT gas at a pressure of 10 Bar under standard conditions. Substitution of the quantities into the appropriate equations shows that ($U_{p_1} \sim U_{p_2} = 200$ km/sec).

$p_1 = 10$ Bar	$p_2 = 1.12$ Mb	$p_3 = 6.7$ Mb	$p_4 = 3400$ Mb
$T_1 = 300°K$	$T_2 = 173$ ev	$T_3 = 415$ ev	$T_4 = 5000$ ev
$\rho_1/\rho_\ell = 0.01$	$\rho_2/\rho_\ell = 0.04$	$\rho_3/\rho_\ell = 0.10$	$\rho_4/\rho_\ell = 4.2$

$\rho_\ell = 0.213$ gm/cm^3 = cryogenic density

Here we have chosen $T_4 = 5$ kev to approximate the requirement for TN burn. To get to the final state we must have sufficient mass of the projectile for a given mass of DT. Solving Eqn.(4) for a unit cross sectional area gives

$$\rho_{p_1} t_1 = \frac{n_1 R_1 6k(T_4 - T_3)}{U_2^2} \tag{6}$$

where R and t represents the thickness of the DT and projectile respectively. On substitution of values and taking $R_1 = 1$ cm, we find $\rho_{p_1} t_1 = 0.052$ g/cm^2. For U, $\rho_{p_1} = 18.8$ g/cm^3 and this gives $t_1 = 2.7\ (10^{-3})$ cm. It may be noted that $R_4 = 2.3(10^{-3})$ cm for this case. The energy/area of the particle $\frac{(m_{p_1} U_{p_1}^2)}{2A_p}$ is 1.04 MJ/cm^2. At these speeds a 1 cm x 1 cm cross section should be sufficient so that edge losses are negligible (i.e., 0.1 cm/a_4 > times of interest).

An estimate of the time scale of the peak compression may be obtained using using momentum, that is,

$$\int pAdt = \bar{p} A \tau_e = 2 m_p U_{p_2} = 2 \rho_{p_1} A t_1 U_{p_2} \ . \tag{7}$$

Choosing $\bar{p} = p_4$ to be conservative, we find the time for the piston to rebound as

$$\tau_e = \frac{2\rho_{p_1} t_1 U_{p_2}}{p_4} \qquad (8)$$

which equals 6.2 (10^{-10}) sec for the preceding example. The important nuclear parameters for this case are:

$$n_4\tau_e = 1.2\ (10^{14})\ \text{sec/cm}^3,\ T_4 = 5\ \text{kev}.$$

The yield, Y, of the TN reaction is calculated by

$$Y = \int \frac{n^2}{4}\langle\sigma v\rangle q_T V dt = \frac{(nV)\langle\sigma v\rangle q_T}{4kT^2}\int pTdt\ .$$

Note that $\frac{\langle\sigma v\rangle}{T^2}$ ~ constant in the range of interest.

Treating $\int pTdt = \overline{pT}\tau_e \approx p_4 T_4 \tau_e$, we find that

$$Y \approx \frac{N\langle\sigma v\rangle_4 q_T (n_4\tau_e)}{4} = 0.42\ \text{MJ}\ .$$

Thus, the gain $Q = Y/E_{KE_1} = 0.4$ which is not a useful value. On the other hand, we probably underestimated τ_e somewhat using $p_4 = \bar{p}$ and thus Q. However, one can see from the simplified equations the changes to be made to increase Q substantially.

(b) The Compressible Projectile

If the projectile is compressible, the preceding problem is considerably more difficult as both wave action and internal energy of the projectile must be taken into account. That is, energy partitioning becomes an important issue as $E_c \neq E_{KE} \neq 0$ now. Obviously, additional energy is required to achieve the final state as some energy may reside in the projectile as kinetic or internal energy (cf. Ref. 1). It is important to realize that there are essential differences in the way the projectile rebounds, too, due to finite wave speeds in the projectile.

Consider extreme cases, for example, in which the initial DT density is larger (than previously calculated) or the projectile velocity is smaller. A considerable increase in the mass of the projectile (thicker projectile) is

needed to achieve T = 5 kev on the basis of simple energy arguments. In particular, for the lower speed case, smaller shock preheat requires large post shock compression and subsequent pressure rise. In the case of a thick compressible projectile the leading edge may be coming to rest while the trailing edge is continuing with unchanged momentum because of the finite wave speed in the projectile. Thus, only part of the projectile energy is being used to energize the plasma and only part of the momentum of the projectile is being used to compress the plasma.

As the final compression and deceleration of the projectile is very rapid, one may estimate the peak pressure using wave arguments in the projectile. (Note that if the metal stays relatively cool, as it should due to only weak initial waves in it, then $a_p << a_4$.) Assume the waves which slow the projectile down act in the limit as nothing more than a shock wave impulsively bringing the projectile matter to rest. Fig. 2 shows the projectile path and shock wave which is used to stop the projectile and compress it. Even if the compressive wave action is not discrete, the result would nearly be the same as compression waves normally tend to focus. Thus, as in part 1,

$$p_4 = \rho_{p_2} D u_{p_2}$$

where D is the wave speed relative to the fluid. Assuming a Gruniesen coefficient of 2 (refs. 2,3) for the metal and little initial compression gives

$$p_4 \doteq 2\rho_{p_1} U_{p_2}^2 . \qquad (9)$$

If the metal is vaporized to a perfect gas of $\gamma = 5/3$, then $p_4 = 4/3\ \rho_{p_1} U_{p_2}^2$ which is not much different from Eqn.(9). If the isentropic compression requirements exceed the value predicted by Eqn.(9), they can't be obtained on the basis of increased projectile mass! They can only be obtained by increased speeds or increased particle density (an unlikely prospect when U is used as the example). Thus, slow initial projectile speeds (<100 km/sec) seem very doubtful for TN burn. Low speeds are inappropriate (even in the absence of losses) because they give smaller shock preheat (see Eqn.(1)) and then require larger isentropic compression to increase the temperature to the necessary values. This requires very large increases in pressure in the isentropic com-

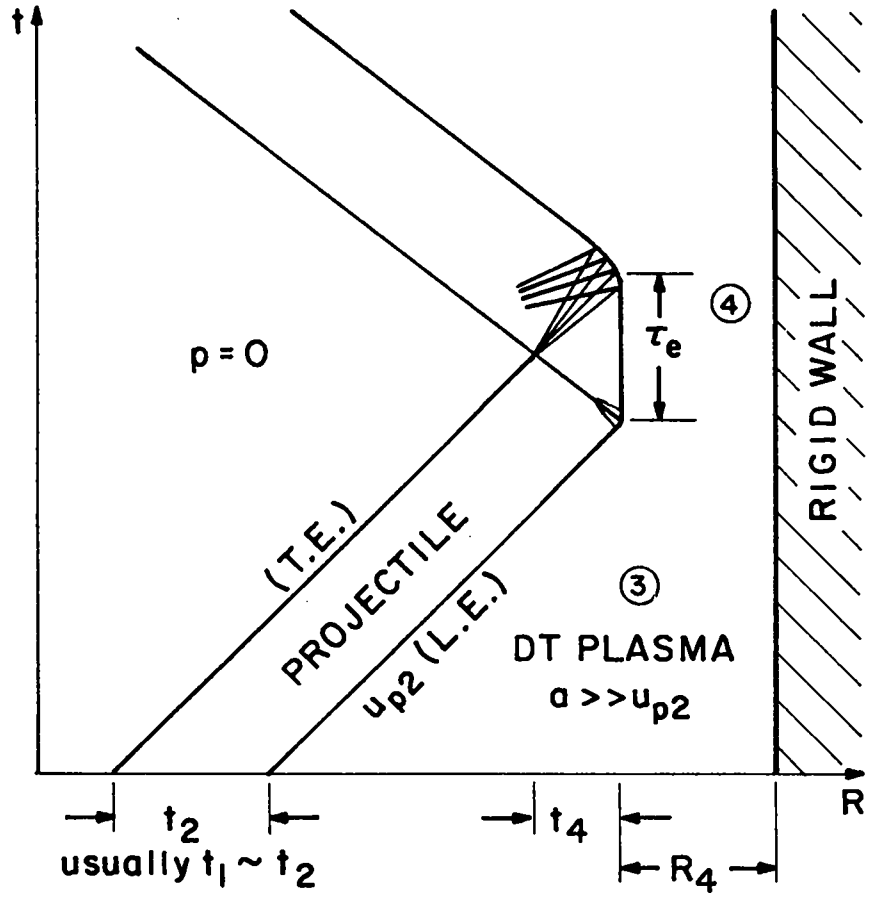

Figure 2. Idealized Projectile Motion.

pression stage, which cannot be obtained as U_{p_2} is now too small. If lower speeds are to be contemplated, some form of preheat other than shock heating will be necessary. Even if it were possible to do this without violating the maximum p predicted by Eqn.(9), very thick projectiles will likely be inefficient. Gerwin and Malone, in their studies of compressible fast liners, have shown that a liner thickness, much in excess of R_4, is inefficient.

Thick projectiles, however, are useful in increasing the duration of the implosion. The shock wave on reaching the trailing edge of the projectile is now reflected as an expansion wave pattern in order to match the pressure at the rear surface which equals 0. Thus, the duration, τ_e, is a measure of the round trip wave transit time in the projectile. As an estimate, $\tau_e \simeq 2t4/a_p$, where the projectile speed of sound should be evaluated at some mean value of the material state. One should expect that this sound speed is considerably less than in the plasma. A more accurate analysis shows for a strong shock in a perfect gas of $\gamma = 5/3$ that τ_e may be related to the projectile speed, U_{p_2}. This result is

$$\tau_e \doteq \frac{4.3t_4}{U_{p_2}} = \frac{1.1t_1}{U_{p_2}} \quad . \tag{10}$$

(At the high pressures required for isentropic compression of the target material, the shock is strong. The Hugoniots shown in Part 1 indicate $\gamma = 5/3$ are a satisfactory description of the material.) This result is in fair agreement with Ref. 1 for optimal conditions using other methods and a more accurate description of the equation of state of the projectile medium. If the projectile is much thinner than the final plasma thickness, momentum calculations as done in Section (a) probably give better results for τ_e because of the complicated wave picture.

Energy Requirements

The minimum energy requirement of a projectile is something in excess of the plasma energy content at maximum compression, i.e.,

$$\frac{m_p U_{p_1}^2}{2} > n_4 V_4 2(\tfrac{3}{2}kT_4) = \rho_4 V_4 \frac{3kT_4}{m_i} \tag{11}$$

It is known that ρR represents a grouping that is important in determining α particle trapping and burn fraction (c.f. Ribe). Suppose we take $\rho_4 R_4 = \lambda$ as a desired number. Then

$$E \propto \rho_4 R_4^m T_4 = \rho_4 \frac{\lambda^m}{\rho_4^m} T_4 = \frac{\lambda^m T_4}{\rho^{m-1}}$$

where m = 1, 2 or 3 for plane, cylindrical, and spherical cases. Obviously, less energy is required if the density is made large (high p). From earlier remarks in Part 1, the best geometrical situation is a spherical one (m=3), with $\rho_1 R_1^3 = \rho_4 R_4^3$. Assuming that the linear motion of a projectile may be converted into one which is spherical in nature (a question that must be satisfactorily answered by further work), we have

$$E/\text{sphere} = 4\pi \frac{\lambda^3 k T_4}{\rho_4^2 m_i} .$$

Suppose $\lambda = 0.1$ g/cm^2 which is considerably smaller than that required to trap α particles (Ref. 4); we get the following results for $T_4 = 10$ kev.

E(MJ)	$3(10^6)$	300	$3(10^{-2})$
ρ_4/ρ_ℓ	$6(10^{-3})$	0.6	60
p_4(Mb)	10	10^3	10^5
R_4(cm)	78	0.78	$7.8(10^{-3})$

$\rho_\ell = 0.213$ g/cm^3
$\rho_4 R_4 = 0.1$ g/cm^2
spherical case

Obviously we must be interested in DT densities greater than 0.127 g/cm^3 if reasonable energies are to be required even for spherical cases. Of course, following the earlier arguments for simple ID motion, this requires high particle speeds.

An estimate of the burn fraction vs. $\rho_4 R_4$ may be made. From Ribe the burn fraction f is

$$f = \frac{\tau_e/2\tau_r}{1+\tau_e/2\tau_r} \tag{12}$$

where τ_r is the reaction burn time $= \dfrac{1}{\rho\frac{\langle\sigma v\rangle}{m_i}} \approx \left.\dfrac{4.2(10^{-8})}{}\right|_{10\text{ kev}}$

Normally the confinement time, τ_e, for inertially confined systems is of the order of the acoustic transit time across the plasma radius. However, for an inertially tamped plasma, it is more correct to take the round trip transit speed across the projectile. Using Eq.(10) and using the Gerwin and Malone result (Ref. 1) that showed under optimal conditions the order of $t_4 = R_4$, we have approximately

$$\frac{\tau_e}{2\tau_r} = 4.3\frac{R_4}{U_{p_2}}\frac{\rho_4}{2(4.2)10^{-8}} = \frac{51(10^6)\rho_4 R_4}{U_{p_2}}$$

so estimating $U_{p_2} \simeq 200$ km/sec,

$$f\Big|_{10\text{ kev}} = \frac{\rho_4 R_4}{\rho_4 R_4 + 0.4} \Rightarrow 0.20 \text{ at } \rho_4 R_4 = 0.1$$

Because of containment by a heavy projectile and the fact that the sound speed in the projectile is considerably less than in the very hot plasma, appreciable burn fractions may occur even with relatively low values of ρR.

Dynamic Processes

If the linear motion of the projectile can be turned into a cylindrical or spherical implosion, there is a possibility that ignition could be achieved if a strong wave collapses onto the origin (r=0) of the target material. Some laser pellet designs are of this type. By wave focussing, a relatively low energy density (low speeds) of the boundary can be very concentrated at the center of the target resulting in large densities and temperatures. Since only a small portion of DT in the center is highly compressed and heated to ignition temperatures, and if propagation occurs, such an approach has the potential of very high gain. In such a case the plasma is far from isobaric and isothermal. However, spherical or cylindrically collapsing waves tend to be unstable during

the implosion phase (a loss of strengthening) and probably are very sensitive to perturbations.

One suggested scheme for approaching a spherical implosion with a projectile is to devise a conical target with high density tamping material. That is

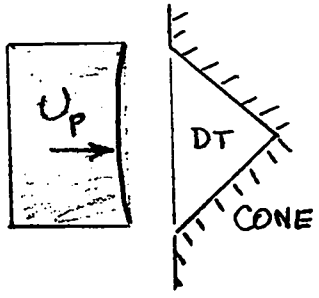

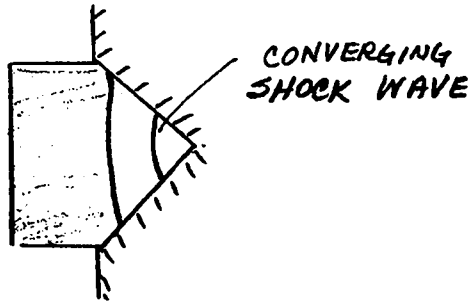

As the cone is part of a sphere, we have a segment of a spherical implosion. However, unless the wave is uniformly initiated, the wave will not focus as illustrated above. It tends to break up and behave as if it were plane with shock reflections at the walls, as shown on the left.

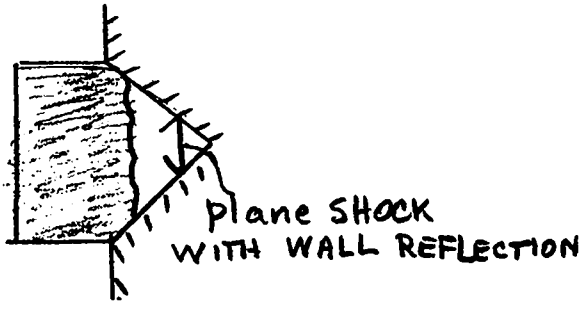

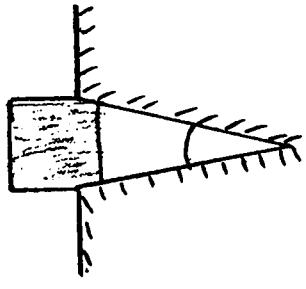

A situation which is probably less sensitive to the initial conditions is shown on the right with a smaller cone angle. However, such a situation has poorer surface to volume characteristics and thus increased losses.

Even if shock focussing was not used as part of the overall process and the cone was only used to shape the volume, there would be difficulties. The temper can't withstand the imposed stresses and so is only inertially confined. The shape of the cone would change under load due to compressibility which will lead to important geometrical alterations and changes in performance. However, detailed calculations should be done to quantitatively predict the detailed effect of a conical geometry.

Losses

The preceding description of DT heating and compression has ignored a number of phenomena that can only have undesirable effects on the outcome of TN burn. Among these are:

(1) Bremsstrahlung losses
(2) Heat conduction losses
(3) Contamination of DT by projectile material
(4) Rayleigh Taylor instabilities of the interface.

As time is short, we will discuss only the first two.

Following the ideas of Winterberg (Ref. 5), Rioux and Jablon (Ref. 6), and others, the equations for the relatively slow ($U_p << 4$) implosion of a plasma without TN reactions are

$$\frac{d\rho}{dt} + \rho\nabla\cdot\underline{v} = 0 \qquad \frac{d}{dt} = \text{total derivative following a fluid element}$$

$$\frac{dv}{dt} = 0 \qquad \text{as } \nabla p = 0,\ p(t) \neq 0 \tag{13}$$

$$\rho C_v \frac{dT}{dt} = \nabla\cdot(K\nabla T) - p\nabla\cdot\underline{v} - C_v a\rho^2 T^{\frac{1}{2}}$$

$$\text{where } a = 8.2(10^{11})\ \frac{{}^\circ K^{\frac{1}{2}} cm^3}{sec\ gm}$$

Consider the case of Bremsstrahlung only; then

$$\rho C_v \frac{dT}{dt} = -p\nabla\cdot\underline{v} - C_v a\rho^2 T^{\frac{1}{2}} = \frac{\rho RT}{\rho}\frac{d\rho}{dt} - C_v a\rho^2 T^{\frac{1}{2}}$$

or (14)

$$\frac{1}{T}\frac{dT}{dt} = \frac{2}{3}\frac{1}{\rho}\frac{d\rho}{dt} - \frac{a\rho}{T^{\frac{1}{2}}} \ .$$

Imagine $\rho \neq \rho(x)$. (This is possible as conduction is zero and $\nabla p = 0$.) Note also $\rho = \rho_1 R_1^m/R^m$ and $m = 1, 2, 3$ for plane, cylindrical, and spherical case. We find then $\frac{1}{\rho}\frac{d\rho}{dt} = -\frac{m}{R}\left(\frac{dR}{dt}\right)$ where $\frac{dR}{dt}$ = speed of the projectile. Consider a Consider a stationery point, i.e., $\frac{1}{T}\frac{dT}{dt} = 0$; then

$$\frac{dR}{dt} = -\frac{3}{2}\frac{a(\rho R)}{m\sqrt{T}} = -\frac{3}{2}\frac{a}{m\sqrt{T}}(\rho_1 R_1)\left(\frac{R_1}{R}\right)^{m-1} \tag{15}$$

Values of $\dot{R}$ less than this result in plasma cooling, whereas R greater than this results in plasma heating. The parameter ρR is also an important element. Large values of ρR require large values of $\dot{R}$. Further, the spherical implosion

scheme reduces $\dot{R}$ requirements by 3 over that of a plane implosion.

Equation (15) also shows the advantages of a spherical implosion through the factor m. For a plane explosion m = 1 and ρR is a constant throughout the compression stage. At low T the relative losses by Bremsstrahlung are very important, especially since $\rho_1 R_1$ must be preset to a significant value. But in the spherical case ρR stays low when T is low until the last moment. Evaluating Eq.(15) for T = 10 kev and $\rho R = 0.1$ g/cm^2 shows

$$U_{p_2} = \dot{R}\left(\frac{km}{sec}\right) > 1141 \frac{\rho R(g/cm^2)}{m} = 38 \frac{km}{sec} \text{ for } \rho R = 0.1 \text{ g/cm}^2 \text{ and } m = 3.$$

Thus, it would appear with the large velocities (on the order of 100-200 km/sec) needed for shock preheat that Bremsstrahlung is not an important effect, at least for moderate values of ρR.

Now consider conduction effects only. The equations are much more difficult to work with in this case because of the presence of spatial gradients. Consider for simplicity's sake dimensional arguments and imagine a case of no convection so that diffusion is dominant. The characteristic time scale for diffusion is known to be

$$\tau_d = \frac{R^2 \rho C_p}{K} \quad . \tag{16}$$

Defining $R/\dot{R} = \tau$ (time scale of compression), we desire $\tau_d > \tau$ or solving for $\dot{R}$ we get

$$U_{p_2} = \dot{R} \geq \frac{K^e}{(\rho R)C_p} \text{ where } K^e = 1.2(10^{12})T^{5/2}(\text{kev}) \frac{\text{erg/sec}}{^\circ\text{K cm}} \text{ (ref. 7).}$$

Notice that in contrast to Bremsstrahlung, large values of ρR are useful to reduce the time scale requirements. Evaluating (16) at $\rho_4 R_4 = 0.1$ and T = 10 kev shows $\dot{R} > 235$ km/sec. Of course, $\dot{R}$ at state 4 is zero but the order of magnitude for U_{p_2} should be correct. Comparison with Winterberg's analytic results (Ref. 5) for this problem show reasonable agreement with dimensional arguments. However, he studied the infinitely massive incompressible projectile trajectory ($\dot{R}$ = const) which, of course, overestimates the speed at bounce. Presumably larger values of U_{p_2} are needed for an actual piston path. Although

heat conduction will be smaller in the early stages of compression, it is obvious that electron heat conduction must be suppressed by the use of B fields of appropriate geometry and strength to reduce the velocity requirement. There is no need to reduce heat losses (by electronic or ionic conductivity) below that of the Bremsstrahlung losses which are not affected by B. A minimum reduction of K^e by 10 is required for the example. The classical conduction coefficient (across B field lines) is

$$K^e = \frac{K^e(B=0)}{1+(\omega\tau)^2} \; ; \quad \omega\tau = \frac{1.9(10^{21})B(\text{tesla})T^{3/2}(\text{kev})}{n(\text{cm}^{-3})\ln\Lambda}$$

To reduce K^e by 10 requires $\omega\tau \approx 3$ and $B_4 = 1$ M gauss for $\rho/\rho_\ell = 4.3$. Larger values of B probably would be needed because of analomous effects. If the field is imbedded and frozen in the plasma before compression, B/n = const and B_1 = 2400 gauss. This is a modest field and represents a low β plasma so that compression of the magnetic field requires little energy requirement.

Summary

High speeds in excess of 100 km/sec are probably needed to get satisfactory shock preheat and high density compressions (high pressures too). Furthermore, speeds only somewhat less than this are required to avoid large losses in the plasma, if a magnetic field is suitably imposed. Spherical implosions are a definite advantage over plane ones, but there is a difficulty in constructing such a geometry with impact fusion. Energy requirements on the order of 10 MJ or greater are probably required in the plasma, inferring even larger energy requirements from the accelerator.

References

1. R.A. Gerwin and R.C. Malone, Nucl. Fusion 19, 155 (1979).
2. Y. Zeldovich and Y. Raizer, "Physics of Shock Waves and High Temperature Hydrodynamic Phenomena," Vol. II, Academic Press (1967).
3. L.V. Al'tshuler, Sov. Phys. Uspekii 8, 52 (1965).
4. F.L. Ribe, Rev. Mod. Phys. 47, 7 (1975).
5. F. Winterberg, Plasma Phys. 10, 55 (1968).
6. C. Rioux and C. Jablon, Nucl. Fusion 15, 425 (1979).
7. S. Braginskii, Rev. Plasma Phys., Vol. I (1965).

OVERVIEW OF

SYSTEMS REQUIREMENTS

FOR

IMPACT FUSION POWER

J. M. Williams, L. A. Booth, R. A. Krakowski

A. PURPOSE

The DOE is considering funding research on the impact fusion concept. The University of Washington and the Los Alamos Scientific Laboratory have been asked to evaluate impact fusion and to develop a set of criteria for assessing the potential of impact fusion for power production. The purpose of this paper is to outline key areas in which the impact fusion concept must prove feasibility.

Little research has been devoted toward developing impact fusion as a potential power-producing technology. Many uncertainties will need resolution before this concept can have practical value. When certain key subsystems of a conceptual impact fusion reactor are taken separately, the development of a viable solution to technophysical problems may seem possible. However, to reach the practical goal of economic power production, an integrated power system must be economically feasible from the practical engineering standpoint.

At this time the scientific feasibility of impact fusion is the primary question. For the purposes of this paper scientific feasibility is defined as the condition in which the thermonuclear energy yield from impact fusion is equal to or greater than the energy in the incident

projectile. The main purpose of this workshop is to investigate if any concepts or approaches are sufficiently promising to conclude that an appropriate experimental program could prove the scientific feasibility of impact fusion. Even if the physics concept appears scientifically feasible, numerous technical/economic questions must be addressed. How does this physics concept compare to others such as laser fusion and particle beam fusion, etc.? Is research and development easier and/or less costly? What are the engineering problems of establishing a net energy balance? Can one attain an average power level at which significantly more power is produced than is required for accelerating projectiles? Is it possible to operate an impact fusion reactor reliably in a pulsed mode for a long period of time -- weeks, months, years? Is there any feasible target-projectile combination which can be economically produced?

These and numerous other questions are the topic of this paper. The primary interest is to provide a perspective on problems of engineering feasibility which, although too early to solve now, could ultimately negate or enhance any practical solution for Impact Fusion power. Considering the state-of-the-art of Impact Fusion, any attempt to define "Systems Requirements for Impact Fusion" is pretty risky business. Thus, the material presented here is elementary and conjecture, and is primarily intended to stimulate discussion in this workshop; to prepare a definitive statement at this point is premature.

B. DESCRIPTION OF AN IMPACT FUSION POWER SYSTEM

An impact fusion power system exhibits many of the characteristics of inertial confinement concepts. It must drive a D-T implosion of some suitable target, achieve sizable gains of ~ 30 or greater and subsequently contain and convert the energetic particles and debris to useful power. Since impact fusion is by nature a pulsed system, all components, power supplies, accelerator, vacuum system, containment system and thermal hydraulic systems must be designed to tolerate cyclic loads for many millions of cycles per year during their useful lifetime. The energy efficiency of these components must be sufficiently high to assure a cost-effective, net energy balance.

Figure 1 shows the key components in an impact fusion power system. Key subsystems and their functions are described below.

1. Power Conversion and Conditioning

The power conversion and conditioning system will be required to utilize electrical energy from the power generation system and convert it into the proper pulse shape, current and voltages required to power the accelerator system. This function will probably require energy storage systems (e.g., capacitors and/or homopolar generators) and appropriate high-voltage switching gear. This equipment will have to operate in a pulsed mode at repetition rates in the range of 0.1 to 10 pulses per second. The total amount of energy to be provided to power conditioning systems in each pulse will probably range from 10 MJ to 1 GJ. Depending upon the time scale of the pulse characteristics from the power supply, there will be major requirements for development of hardware to satisfy this need. Much of the power conditioning hardware required for beam-driven fusion may be applicable here, but will probably require considerably more energy per pulse.

2. Projectile/target Production

The purpose of this subsystem will be to produce complete projectile/target assemblies at a rate of at least one assembly every 10 s during the operating lifetime of this facility. This requirement would amount to approximately 2.5 million assemblies per year, if they are consumed at the rate of one every 10 seconds at an 80% duty factor. It is quite likely that these assemblies will require exotic materials, such as superconductors and high density refractories, which will have to be fabricated to close dimensional tolerances. In addition, the assembly that suspends the target in place will have to be partially replaced because it, in all likelihood, would be destroyed during each explosion. If the total energy yield from a single explosion is 10 GJ, then the value of an equivalent amount of electric energy produced at 3 ¢/kWe hour at the busbar would be approximately $25. Maybe 1/5 to 1/3 ($5-$8) of this revenue would be available for production of target projectile assemblies. This facility will have to be highly automated in order

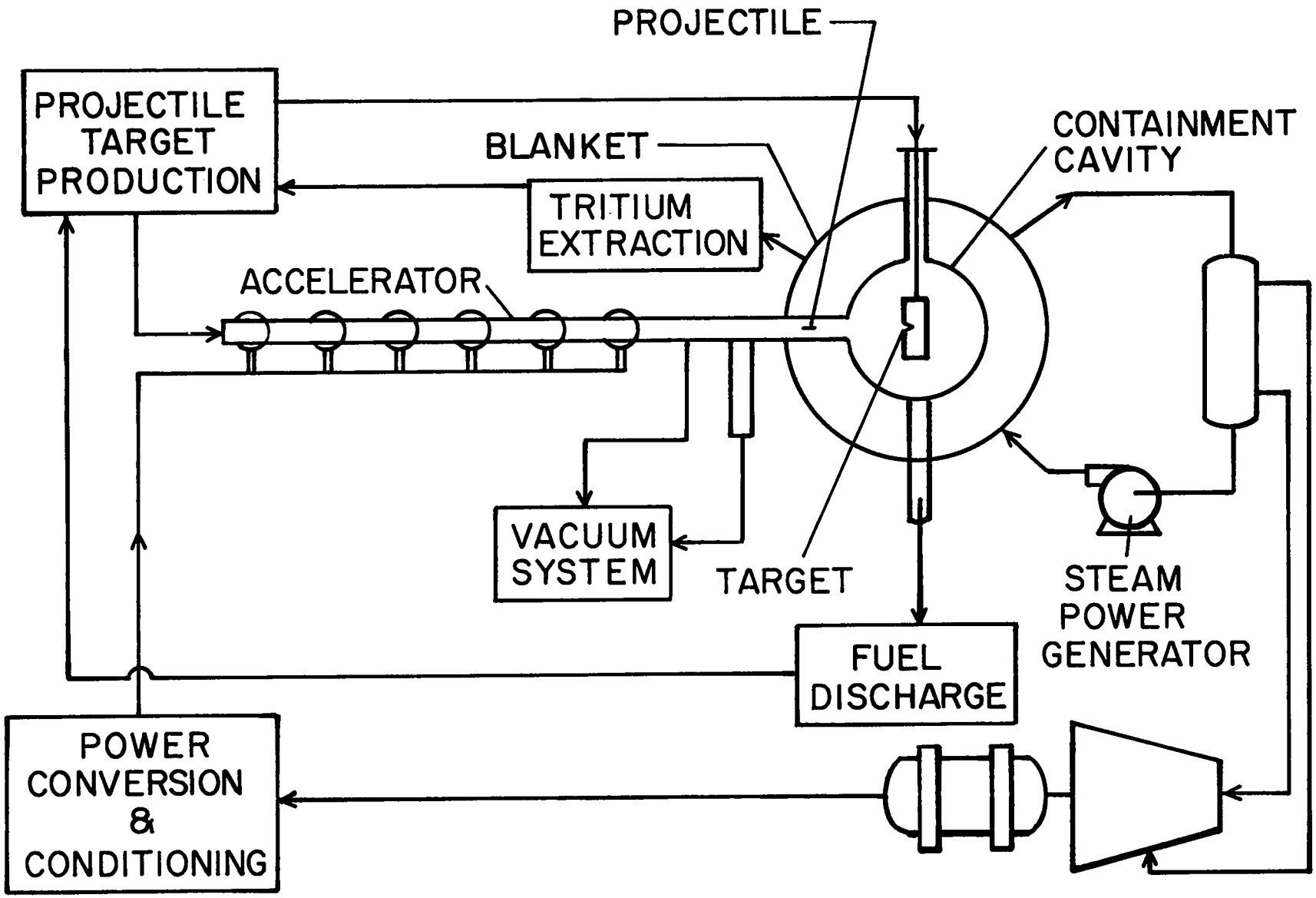

KEY IMPACT FUSION COMPONENTS & SUBSYSTEMS

Fig. 1

achieve the required production rates. Possibly through proper economies of scale, it might be possible to produce reasonable cost assemblies. By degree, there is no counterpart to this system in beam-driven fusion although similar problems are encountered in the imploding liner in the magnetic fusion program.

3. Accelerator

The primary function of the accelerator will be to accelerate macroparticles or projectiles to velocities exceeding 10^7 cm/s. These projectiles may range in mass from 0.1 gm to as high as 1 kg. The accelerator will have to operate with reasonable conversion efficiencies for the conversion of electric to kinetic energy and must maintain a very stable trajectory targeted within close tolerances to impact on the target. This is probably one of the most challenging hardware development components in impact fusion. There are a number of accelerator concepts which may be promising; this workshop will evaluate each of them. There is no comparable technology currently under development in other fusion programs.

4. Containment Cavity

The primary purpose of the containment cavity is to provide an environment in which the target can receive the high velocity projectile and convert resulting fusion energy into useful thermal energy. The cavity must be capable of evacuation to an acceptable pressure such that the projectile does not overheat in traversing from the accelerator through a drift tube and across the radius of the cavity. The cavity must also be capable of absorbing the radiation and energetic particles that impact on the cavity first wall as well as thermalizing the energy deposited by 14-MeV neutrons in the coolant and structure of the blanket. Impact fusion containment concepts may be required to handle energy releases (in the form of x rays and ion debris) of up to 50 GJ. This energy is higher than for laser or magnetic fusion concepts. Containment technology has been studied extensively in the inertial confinement program and also in the fast-liner reactor studies. A number of conceptual approaches to energy containment will be discussed in greater detail in subsequent workshop papers.

5. Vacuum Systen: Cavity/Accelerator

Vacuum systems will be required to maintain the low pressure in both the accelerator and the containment cavity. This system will probably require high pumping speeds in order to minimize the debris that diffuses into the accelerator, and to prepare, on a short time scale (1-10 s), the cavity for the next explosion. Fast acting valves may be needed to separate the accelerator from the containment cavity between pulses. Vacuum system pumping capacity could be the primary limiting factor on the pulse repetition rate in the cavity. In view of the large quantity of debris from target projectile and supporting structure, the handling capacity of the vacuum system may be a severe engineering limitation.

Significant effort has been devoted to evaluation of vacuum system problems in both inertial confinement and magnetic fusion programs. From this work, it is clear that vacuum requirements can indirectly be a significant contributor to power system costs.

6. Blanket and Energy Conversion System

The blanket and energy conversion system serves the purpose of transferring radiation and particulate energies from the first wall to the coolant and accepting the energy from slowing down of 14-MeV neutrons in the coolant and structure to drive eventually the steam-generating system. The primary function of the blanket and energy conversion system is to convert the pulsed energy into steady state thermal power. This function requires a relatively large thermal sink to assure that thermal transients do not occur at the steam/electric generation system. The blanket design interacts closely with the containment cavity and must provide for effective containment, tritium breeding and cooling. Although this technology is unproven, various concepts have been under continuous study in the inertial and magnetic confinement programs for some time. Some concepts propose the combination of blast-containment, thermal-cooling, and tritium-breeding functions into a single system.

7. Tritium Breeding, Extraction and Recycle

Assuming that deuterium and tritium are the most likely fusion constituents, lithium will have to be used to generate tritium for maintaining the fusion fuel cycle. The blanket system must incorporate sufficient lithium in the system to breed net tritium for recycle. This function is normally done through use of lithium in the blanket and as a coolant; and is probably a reasonable way to proceed for impact fusion. Neutron economy for tritium breeding will be important, particularly if the target mass results in significant neutron degradation. Systems for extraction and recycle tritium have been adequately conceptualized and designed by other fusion programs, and this aspect is not a major technological problem for impact fusion.

8. Steam Power Generator

The steam power generator system serves the purpose of converting energy from the high-temperature lithium (or other) coolant into steam, which eventually drives a turbo-electric generator. This technology is well developed for other major systems applications and needs little additional discussion here.

C. CONCEPTUAL DESIGN PROBLEMS

Many of the subsystems discussed above appear conceptually feasible and significant development programs are underway in the magnetic and inertial fusion programs to solve these problems. The most crucial conceptual design problems for impact fusion are discussed below.

1. Accelerator Design and Performance

The accelerator must be designed to accelerate efficiently a complicated projectile to velocities of 10^7-10^8 cm/s. Two promising concepts for accomplishing this macroparticle velocity are the rail gun concept, which has demonstrated approximately 6×10^5 cm/s, and the traveling magnetic wave accelerator. Crucial system design parameters for the accelerator will be the power consumption per unit length, the total length of the accelerator, accelerator efficiency, and the stability of the traveling force front which drives the projectile.

It is desirable to design an accelerator of minimum length. A number of key accelerator-related questions can be formulated: design factors that limit the accelerator length; forces, stresses and heat loads on the projectile; maximum achievable magnetic field gradient; and spacing of driver coils around high-velocity end of accelerator.

Another aspect of accelerator system design is the question of proper projectile injection systems and (trajectory/energy) control systems to assure projectile stability during acceleration. It may be necessary to utilize pointing and tracking systems to assure that the target is properly positioned for impact. Other problems or system requirements may emerge as a result of further evaluations. Reasonable ranges for some of the design parameters might be as follows: accelerator efficiency, 30-90%; minimum projectile velocity, 10^7 cm/s; accelerator length, 2-3 km.

2. Accelerator/Projectile Coupling Constraints

Depending upon the accelerator concept proposed, the coupling of the accelerating force to the projectile will place major constraints on the overall system design. For example, in the case of the traveling magnetic wave accelerator, either a superconducting or ferromagnetic projectile is proposed. The projectile must have some minimum length in order to interact effectively with the accelerating magnetic field gradient. The total force on the projectile must not exceed stress limits in the projectile. Projectile heating or degradation of superconducting properties, resulting from electrical or magnetic effects, must also be minimized.

In addition to projectile/accelerator coupling constraints, consideration must be given to stability, oscillations of the magnetic field and eddy current heating of the projectile. The consequences of a projectile inadvertently running off course, particularly at the high energy end of the accelerator, presents another potential problem. Conceptual solutions to these problems are necessary in order to enhance the overall credibility of this concept.

3. Projectile Design and Performance

In addition to the projectile/accelerator/target coupling problems, the question arises of how a projectile can be designed to couple effectively with the accelerating field while at the same time being constructed in such a shape that its hydrodynamic interaction with the target makes maximum efficient use of the energy in the projectile. These two conflicting design constraints may be a very difficult problem for impact fusion.

It appears that minimum projectile velocities of 10^7 cm/s will be required when coupled with the more sophisticated target designs. At this velocity threshold complicated, expensive projectile target designs are likely to be necessary. If projectile velocities of 10^8 cm/s or greater are achievable, however, it appears that significantly simpler projectile/target designs may be possible at more acceptable costs.

Parameter values for this system might be as follows: projectile mass, 0.1 to 1000 gm; projectile energy, $> 10^7$ cm/s; and projectile/target cost, 30% net revenues.

4. Projectile/Target Coupling

Probably the most crucial question on the feasibility of impact fusion is associated with the means by which the linear kinetic energy in a projectile can be converted into implosive energy in an appropriate target. The simplest situation would be a planar shock and subsequent compression on a "fixed surface." Maximum shock compressions achievable is a factor of ~ 4 over normal D-T densities. Under these conditions the possibility of attaining sufficiently high values (fusion energy divided by projectile energy) before the compressed density is reduced below fusion conditions implies unacceptably high yields. Other techniques, such as pre-heating prior to compression, compression in cylindrical or spherical geometry, are probably necessary to achieve acceptable system gain factors at acceptable project velocities.

Many questions can be formulated on projectile/target design. How does linear kinetic energy transform into cylindrical or spherical implosive energy? How much kinetic energy is wasted?

Of course, these are the difficult, but important questions for this workshop. Numerous factors will affect the answers. Geometric matching is one factor that varies widely with design concept. The accuracy with which the projectile and target must match on impact to assure efficient implosive energy coupling may present stringent requirements. The target must be carefully positioned, and the projectile must be carefully guided and targeted. In some concepts, mismatches on the axis of impact and in the yaw of either target or projectile may have to be less than a micrometer of axis and a fraction of a degree in yaw in order to minimize energy dissipation and assure acceptable fusion yields and gains. Less sensitive designs may be possible at the expense of increased projectile velocity and/or energy.

The efficiency of coupling the projectile energy to implosive energy will probably have to be 5% or greater. This requirement, of course, depends upon overall energy balance considerations, but below 5% coupling efficiency D-T gain (Q) requirements rise rapidly.

Projectile/target design will also be a major factor in determining the quantity and complexity of materials destroyed by each blast. The integrated system design will need to remove and possibly reclaim these materials. Lastly, one must answer the question of what happens if the projectile misses the target? It would likely pass through the containment vessel wall.

5. Target Design and Performance

It may not be unreasonable to consider one vs two-sided impacts. Each approach has advantages and disadvantages. A two-sided impact has the primary advantage of being more symmetric and possibly easier accelerator and target design. However, accuracy requirements (particularly arrival time) for the increased trajectory are greater, two accelerators are needed, and the system becomes longer. Thus, there appears to exist a preference for a one-sided impact.

If the impact projectile comes from one side, then the target will have to be designed to assure that, in case of misfire, the linearly directed energy from the projectile does not damage the cavity. Other design considerations are important. What will be the final compressed geometry? How will this affect energy release and the distribution of energy in neutrons, alpha particles and

debris? These uncertainties are important to assure tritium breeding and to evaluate blast effects on containment.

Other important design parameters are target mass, structure/geometry and degree of shock vs compressional heating. These parameters will all affect the cost of the projectile target assembly. The estimated budget for the complete assembly destroyed each shot will be a strong function of the overall energy balance parameters.

The system required for rapid target positioning and replacement will be important to overall system performance. To achieve maximum average power, the pulse repetition rate in each cavity must approach one to ten seconds per pulse for yields in the range of 10 GJ.

The main differences from other fusion concepts are that impact fusion will probably require higher yields per pulse and will produce large quantities of activated debris. These large quantities of materials will be circulated through the cavity, producing a large ex-reactor irradiated materials handling load.

6. Target/Containment Coupling

Although very important, this problem is possibly the least crucial to impact fusion feasibility of the problems that have been analyzed. Target/containment coupling is well understood in the magnetic fusion and inertial confinement applications at energy releases up to 10 GJ. Methods for minimizing detrimental blast effects of containment, such as wetted walls, lithium waterfalls, liquid-metal rains/sprays, etc., may provide adequate solutions to this problem. It should be noted, however, that an economical, viable, and integrated system must provide energy containment for millions of cycles per year in a radiation environment comprised of high energy neutrons, energetic alpha particles, γ rays and relatively massive debris. After each energy release the containment must attain a quiescent atmosphere into which the target and projectile can subsequently be injected within 1-10 s.

D. ENERGY BALANCES

Compared to other energy systems, fusion requires substantial investments in high quality energy to release net energy from the nuclear fusion reaction. The efficiency with which this high quality energy is handled therefore becomes one of the crucial analyses of fusion systems. A typical energy balance diagram is shown in Fig. 2. Analysis of the energy flows depicted in this diagram allows comparison of the key parameters in the energy balance. The key energy balance parameters for impact fusion which require understanding and significant development are:

- The energy gain curve (Q versus projectile energy W_K) for the envelope of projectile/target designs, which includes understanding the mechanism for efficient conversion of projectile energy into implosion energy in an impact fusion target.
- The efficiency of converting electrical energy into accelerated projectile energy.

For the energy flow diagram (Fig. 2) the following energy balance relation can be derived:

$$Q_E = \frac{1}{\varepsilon} = \frac{\eta_P \, \eta_{ACC} \, \eta_{TH}(1+Q)}{1 + f_{AUX} \, \eta_P \, \eta_{ACC} \, \eta_{TH}(1+Q)}$$

where, referring to Fig. 2:

Q_E Engineering gain of system, W_{ET}/W_C

ε Circulating power fraction W_C/W_{ET}

η_{ACC} Acceleration efficiency

η_{TH} Thermal-to-electric conversion efficiency

Q Target/projectile gain

f_{AUX} Fraction of auxiliary energy

η_P Power conditioning efficiency

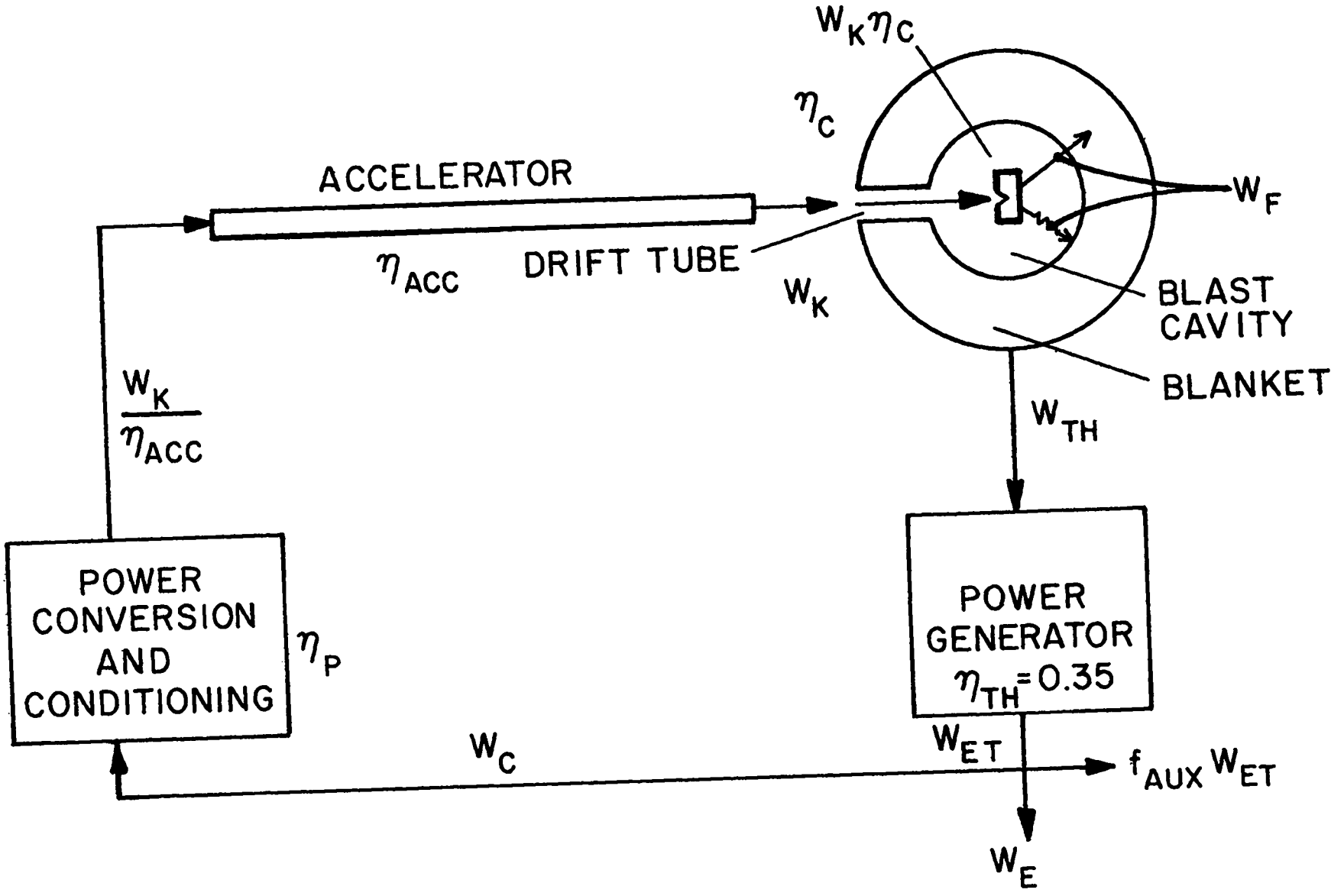

ENERGY BALANCE DIAGRAM

Fig.2

Setting nominal values of $\eta_{TH} = 0.35$, $\eta_P = 1.0$, and $f_{AUX} = 0$, the functional relation between the accelerator efficiency, η_{ACC}, and system gain, Q, with circulating power, ε, as a parameter, can be determined. Figure 3 illustrates this relation. For a circulating power fraction greater than 0.3, the fraction of total capital cost that must be devoted to (parasitic) circulating power becomes large and the achievement of an economical system becomes increasingly more difficult.

For example, if the accelerator efficiency is 50%, the circulating power fraction is 0.2, a system gain factor of > 30 would be needed. On the other hand, if the accelerator efficiency is 0.5 and the circulating power fraction is 0.2, then the required system gain is > 70. If a smaller circulating power fraction is desirable or lower accelerator efficiencies more likely, the required target gain rises rapidly.

The consequences of a high-Q requirement on the overall system design/feasibility cannot be quantified until the gain curve (Q versus W_K) is known. The gain curve for a range of projectile/target configurations represents the most crucial unknown for impact fusion today, in that the requirements of both the accelerator and blast cavity are directly determined by this relationship between Q and W_K.

E. KEY SYSTEMS PARAMETERS

At this early state of our knowledge of impact fusion systems, it is useful to try to quantify key systems design parameters which will bound the region of acceptable conceptual design solutions. Five constraining parameters can be identified: minimum system gain, Q; maximum yield for practical containment, maximum practical projectile energy and velocity, minimum economical yield, $W_E = Q_{WK}$; and minimum acceptable projectile energy and velocity. The following is a rough rationale for how these parameters might be set. It is emphasized that the following development is intuitive and judgmental, and the conclusions and/or indications that follow from this development should be treated in this light.

1. Minimum System Gain

The minimum system gain is set by the energy balance just discussed. If we choose the following parameters: $\eta_{TH} = 0.35$, $\eta_P = 1.0$, $\eta_{ACC} = 0.5$, $1/Q_E = \varepsilon = 0.2$, and $f_{AUX} = 0.0$; it can be seen (Fig. 3)

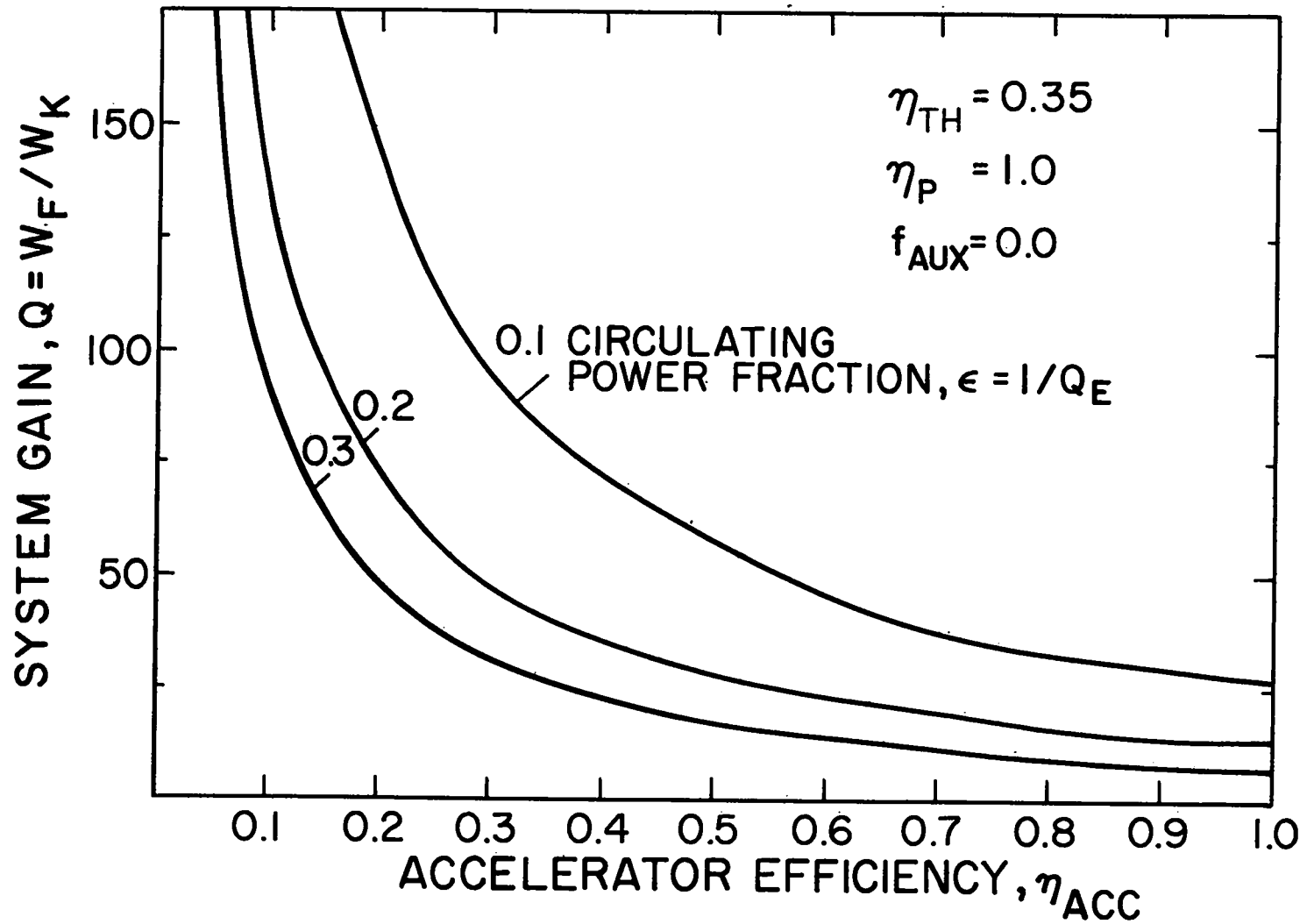

ACCELERATOR EFFICIENCY vs SYSTEM GAIN TRADEOFF

Fig.3

that a gain of 30 is required. A minimum system gain of 30 is, therefore, chosen.

2. Maximum Yield for Practical Containment

Although it is a subjective conclusion at this point, experience in reactor design for inertial confinement and imploding liners provides a background for assessing practical limits on maximum containable yield. Conceptually there is some maximum limit on the radius of a practical containment vessel. This limit is set by the ability to construct large structures and to transport components or modules of that structure to the construction site. In addition, the reactor containment vessel must be capable of supporting itself while providing an evacuated volume where energy release takes place. Structural engineering considerations of such a vessel will set practical limits on size. The containment vessel must also be designed to accept energy pulses at the rate of once every 1 to 10 seconds for a lifetime as long as 10 to 30 years. Based on these considerations and more detailed analyses to be discussed (Krakowski, Booth and Bohachevsky), it seems optimistic to choose a maximum yield of $W_F \sim 100$ GJ, (~ 25 tonnes of TNT). Approximately 20-50% of this total fusion yield will contribute to the blast energy, depending upon the projectile/target interaction and design.

However, it is emphasized that cavity diameters are determined by both the wall protection method (bare metal walls would require uneconomically large diameters) and the energy form of pellet x ray and debris output, i.e., yield fractions, spectra, and temporal pulse widths. Furthermore, in all concepts except thick lithium fluidized walls, pulsed neutron damage may also be a major constraint in determining cavity diameter. Although an optimistic maximum yield of 100 GJ has been chosen, these considerations would result in significantly lower maximum yield, dependent upon wall protection method and pellet output characteristics unknown at this time.

3. Maximum Practical Projectile Energy

The maximum practical projectile energy is set by the capability of the accelerator to achieve a maximum velocity for a given projectile configuration and mass. If the minimum gain of 30 and the

maximum yield of 100 GJ is accepted, then the maximum acceptable projectile energy is approximately 3.3 GJ (Fig. 4). If larger gains are achieved within the maximum acceptable yield of 100 GJ, then the maximum projectile energy will be reduced. Therefore, a maximum projectile energy in the range of 1 GJ has been specified.

4. Minimum Economical Yield

The minimum economical yield is set by considerations of reasonable revenues resulting from power production and minimum reasonable power production rate of the reactor system. If the maximum pulse rate for an impact fusion reactor system is approximately 1 pulse every 10 seconds at a yield of 1 GJ per pulse, an equivalent average power level of 35 MW(e) will be produced by a single cavity. Multiple cavities for a single accelerator do not appear conceptually feasible at this time. Thirty-five megawatts of electrical energy would result in a revenue, at a busbar power cost of 3¢ a kWh, of 29¢ per second, or $2.90 per shot. The annual revenue at this rate is approximately $6.9 M per year. At a fixed charge rate of 15% per year, this would support a capital investment, neglecting fuel costs, of $50 M. If we allow $1 per shot for fuel production and for other operating and maintenance expenses, this $50 M reduces to an apportionment to capital investment of approximately $35 M. This is approximately equivalent to $1000/kW of installed capacity and compares favorably with current estimates for advanced electrical power systems.

Thus, the question becomes, "at what cost can each projectile/target assembly be manufactured?" If the fabrication and production problems of complex targets and projectiles are considered, as well as the insertion and positioning hardware which will all be destroyed each shot, it seems reasonable that the target/projectile assembly would easily cost $1 each. Thus, $\sim$ 1 GJ yield represents a reasonable estimate of minimum economical yield. Clearly, if more economical assemblies could be manufactured, the minimum economic yield would be reduced.

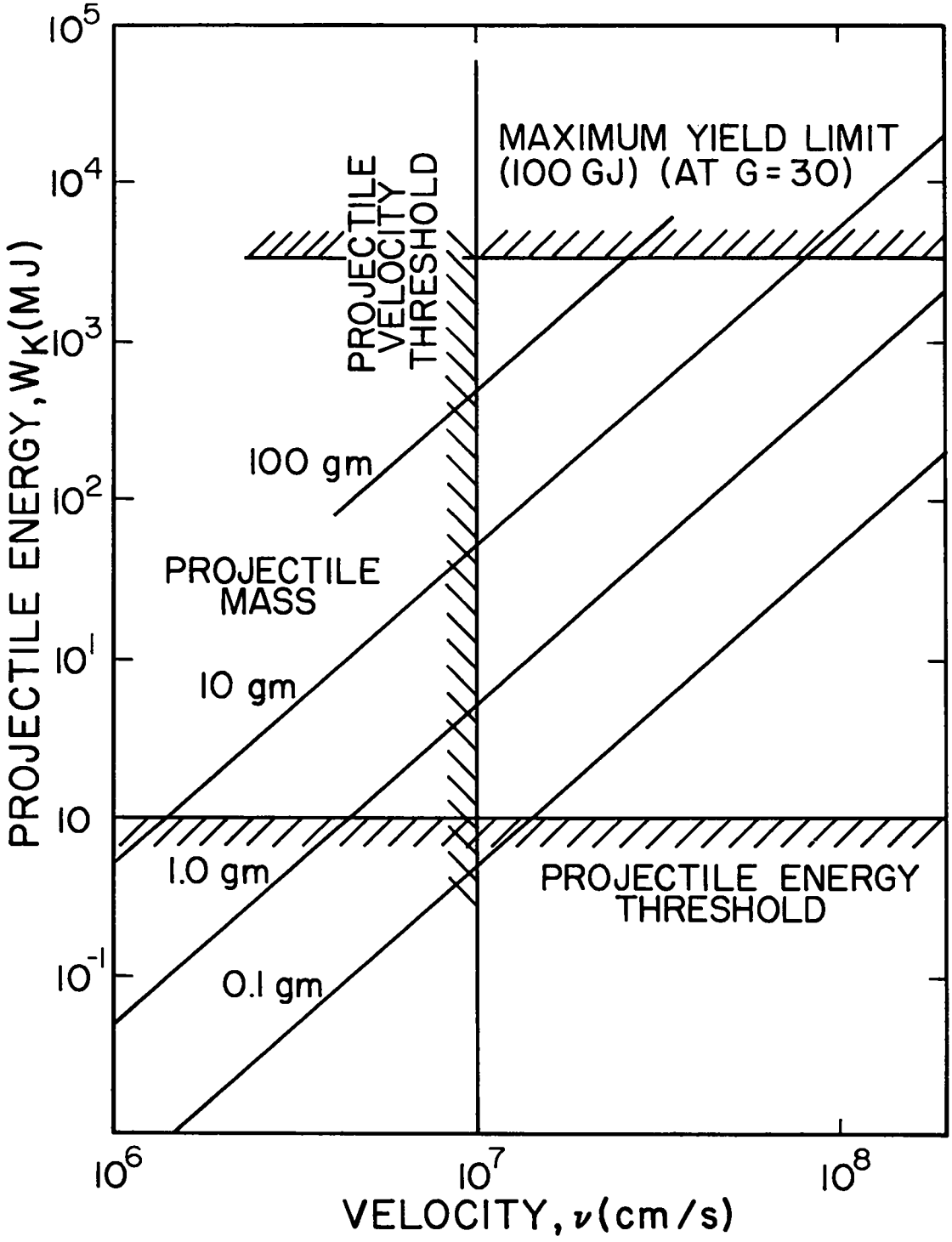

PROJECTILE ENERGY, MASS, VELOCITY RELATIONS

Fig. 4

5. Minimum Projectile Energy

The minimum projectile energy will be set by the minimum acceptable velocity for impact fusion and the minimum mass which can be economically fabricated and efficiently accelerated. Consideration of the simplest target/projectile design led to the conclusion that a minimum velocity of 10^7 cm/s will be necessary. Numerous papers in this workshop will address that subject. At 10^7 cm/s, the projectile mass is slightly less than 0.2 gram for a 1 MJ projectile. The handling and manufacturing of millions of complex projectiles to high quality control specs which have a mass less than 0.2 of a gram may be very difficult. In addition, projectile energies less than a MJ are probably not likely to initiate significant fusion reactions via impact fusion approaches. Although these reasons are somewhat simple and specious, we have chosen 1 MG as a minimum reasonable projectile energy.

6. Summary of Key System Parameters

The following summarizes key systems parameters which bound the solutions:

Minimum System Gain	30
Maximum Yield for Practical Containment	100 GJ
Minimum Economical Yield	100 MJ
Maximum Practical Projectile Energy	1 GJ
Minimum Projectile Energy	1 MJ

If we accept these parameters, although, clearly, better values may be developed later as a result of more thorough analysis, the results can be presented as shown in Fig. 5 in terms of a Q versus W_K phase space. Figure 5 shows a set of three hypothetical gain curves which might result from different target projectile designs. Upon this gain curve we have superimposed the above-determined upper and lower bounds. From this visual representation, some insight can be gained into the required combination of systems performance parameters that must be achieved in order to obtain an "acceptable" solution to the impact fusion power concept.

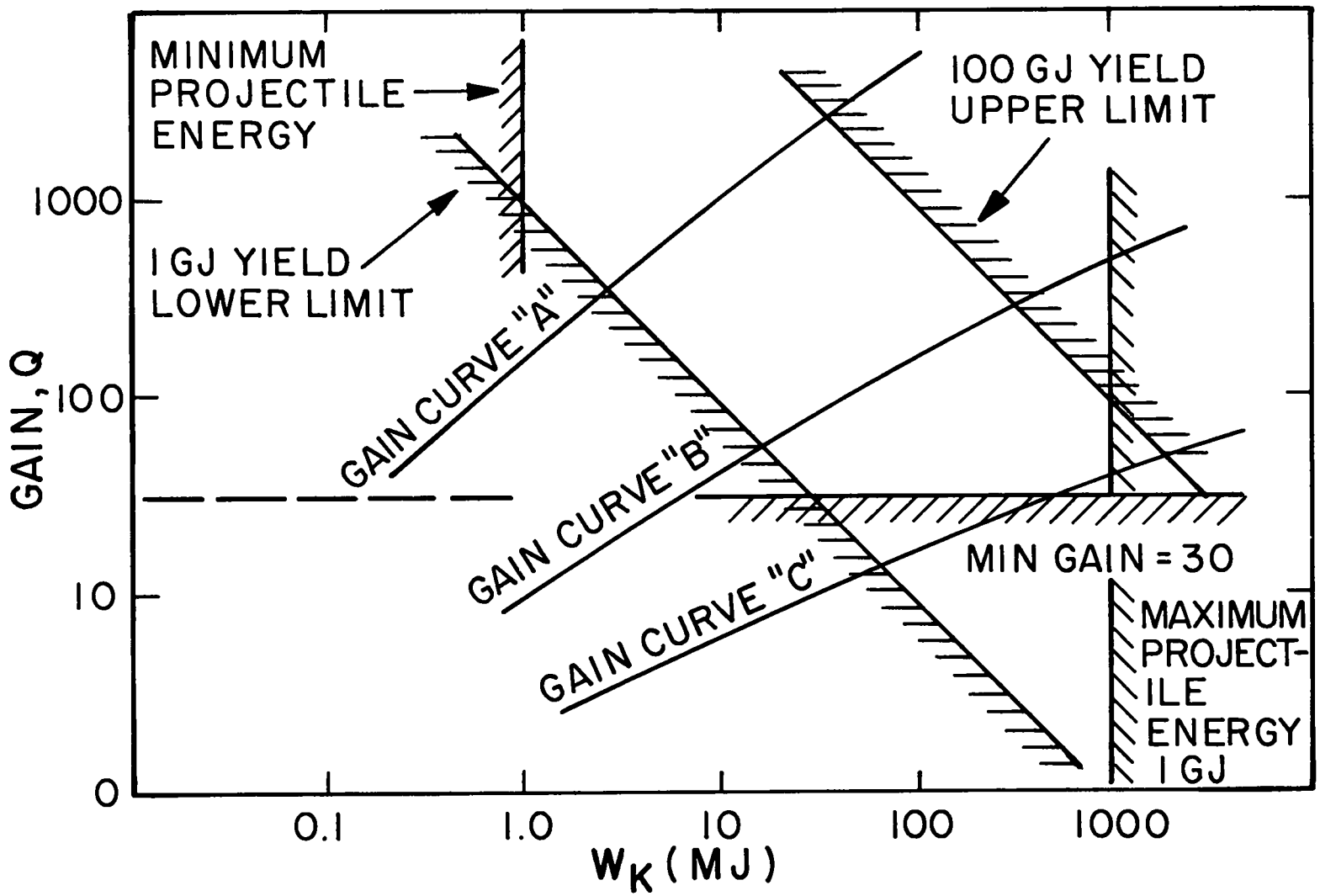

ENERGY IN PROJECTILE

LIMITING PARAMETERS FOR IMPACT FUSION

Fig.5

F. CONCLUSIONS

The development of impact fusion power reactor concepts is very limited at this time. Key systems factors in arriving at practical concepts will be conception of credible systems and subsystems which promise an acceptable overall energy balance and development of target/projectile designs and gain versus projectile energy curves which allow system design tradeoffs to be accomplished. Important system parameters will be subsystem efficiencies (particularly the accelerator), target/projectile gain as a function of target design, circulating power fraction or engineering gain, system pulse repetition rate, size/cost scaling of components, containment cavity design limits, maximum yield, minimum economical yield, minimum projectile velocity and energy, and overall economics. When more detailed conceptual designs are available, then system tradeoffs and performance optimization will be possible.

REACTOR DESIGN CONSIDERATIONS FOR INERTIAL CONFINEMENT FUSION

by

Lawrence A. Booth
Los Alamos Scientific Laboratory
Los Alamos, NM 87545

INTRODUCTION

Inertial-confinement fusion is characterized by compressing and heating thermonuclear fuel contained in a minute pellet by inertial forces. These forces can be generated during interaction of an intense, pulsed beam energy source with the pellet or, as proposed for this workshop, by accelerating the pellet to very high velocities ($> 10^7$ cm/s) and converting its kinetic energy to useful work for compression upon collision with a stationary target or another high-velocity pellet. The fusion pellet contains a stoichiometric mixture of deuterium and tritium (D+T), either in cryogenic solid or gaseous form, usually encapsulated in structures of higher-Z materials, serving as a pusher during the compression process. For beam-driven pellets, the outer region consists of an absorber-ablator material in which energy from the beam source is deposited. This material is blown off, thereby creating a recoil impulse which, together with the plasma pressure, heats and compresses the (D+T) core. Thermonuclear ignition occurs at the center of the compressed core and propagates radially outward in a time that is short compared to the time required for the pellet core to disassemble, resulting in fusion of an appreciable fraction of the (D+T) fuel.

The fusion of a deuterium and a tritium atom results in the release of 17.6 MeV of energy, appearing as the kinetic energy of an alpha particle (3.5 MeV) and a neutron (14.1 MeV). For the thermonuclear burn to propagate from the center of the compressed pellet core, the density-times-radius product of the fuel pellet must greatly exceed the range of the 3.5-MeV alpha particles. Energy deposition by the alpha particles in the pellet core results in very high temperatures with subsequent additional thermonuclear reactions. The 14-MeV neutrons escape the pellet with only slight degradation in energy.

The energy released as photons can be as high as 20% of the thermonuclear yield; in general, larger fractional energy releases as photons are accompanied by higher photon energies. Photon energy release occurs from fusion pellets with yields of a few hundred megajoules in time intervals of a few tens of nanoseconds. The initial photon release has a blackbody spectrum, but, after initial release, most of the photons are not in equilibrium with the temperature of the outer surface of the pellet. Any degradation of the 14-MeV neutron energy by inelastic scattering interactions with the pellet structural material results in the emission of high-energy (~1 MeV) gamma rays. The thermonuclear energy not released as photons or high-energy neutrons is deposited in the pellet debris. Essentially all the debris energy is converted to kinetic energy. Debris particle arrival times at cavity wall surfaces may extend over several tens of microseconds.

REACTOR DESIGN CONSIDERATIONS

For commercial applications, fusion-pellet microexplosions must be contained in reactor cavities in a manner that prevents severe damage to reactor components, yet permits convenient recovery of the energy for conversion to electricity or to some other usable form. Reactor cavities must be surrounded by regions (blankets) containing lithium, which are designed for the breeding of tritium for the fuel cycle and for the collection and multiplication of fusion energy. It is essential that a fusion economy be self-sufficient in tritium i.e., for each fusion reaction, at least one atom of tritium must be produced by nuclear transmutation of lithium. Stresses can result from high rates of energy deposition in the blankets and structural materials. Energy deposition by x rays and particles in the pellet debris occurs at, or very near, free surfaces of incidence in structural and coolant materials; whereas the kinetic energy of 14-MeV neutrons is deposited throughout relatively large volumes.

The most challenging reactor design consideration is protection of the cavity wall from the various energy forms as released by the pellet

and as affected by the reaction-chamber phenomena. These phenomena depend on both the design and the yield of the pellet, as well as on ambient conditions in the chamber at the time of the pellet microexplosion. The effects on pellet energy-release mechanisms of various reaction chamber atmosphere options are summarized in Table I.

Other important design considerations are pellet yield and energy release forms (which determine reactor size), pellet firing repetition rate (which determines power level), and pellet gain (which generally increases with incident beam energy and has a great effect on plant economics). The minimum practical yield, determined by both physical and economic considerations, is about 100 MJ, and the minimum pellet gain for economically viable beam-driven fusion, at a minimum driver efficiency of 5%, is about 100. There are no fundamental physical constraints on maximum yield; however, economic penalties associated with the containment of very large energy releases will result in an optimum pellet yield for a given combination of the relationship between pellet gain and driver energy level, driver efficiency, and firing-pulse repetition rate. There is an incentive to maximize the pellet firing repetition rate, which would maximize the power level; however, this repetition rate may be constrained by cavity phenomena as discussed below.

The most important effect of pellet output on cavity design is energy deposition by x rays and pellet debris, which may result in evaporation and/or sputtering of material surfaces of incidence and thereby impose constraints on some reactor cavity concepts. For reactor concepts with cavity walls exposed to surface evaporation and sputtering, there are tradeoffs for minimum damage to structures between relative x-ray and debris energy yields and their energy spectra. These tradeoffs lead to different optimum fusion-pellet designs for different reactor cavity concepts.

Heating and vaporization from x-ray deposition is a complex function of fluence, x-ray energy, and temporal pulse width. In general, vaporization increases as x-ray energy decreases because the depth of penetration is less at lower x-ray energies (see Fig. 1). This means that for a given fluence, less material is heated to higher temperatures at lower

x-ray energies, resulting in higher vaporization rates. As shown in Fig. 1, at smaller temporal pulse widths, there is less time for thermal conduction into the material and, here again, less material is heated to higher temperatures resulting in higher vaporization rates. Therefore, higher surface temperatures are the result of less heat capacity caused by either decreasing x-ray penetration depth with decreasing x-ray energy or by insufficient time for thermal conduction at shorter pulse widths, e.g., 10 ns or less for carbon liners.

The effects of pellet output on sputtering erosion rates are also complex, depending on the Z-number, mass, velocity, and angle of incidence of pellet debris constituents, and on the Z-number of the target-surface material (see Fig. 2).[1] In general, erosion rates increase with increasing mass and energy yield, but may increase or decrease with the Z-number of pellet materials, depending on the kinetic energy of the particles upon incidence. Sputtering erosion decreases as the atomic number of the target surface material decreases. Results of analyses, based on well understood theory and on some experimental data, indicate that sputtering erosion is important in the design of bare-wall and sacrificial-liner first-wall concepts. For high yield pellets (~4000 MJ) with heavy metal pushers, sputtering erosion is the dominant damage mechanism on a carbon sacrificial-liner surface, accumulating to several centimeters per year at one pulse per second.

A bare cavity wall (consisting of, e.g., a bare refractory metal) would be the simplest of reaction-chamber enclosures. However, if the density of the ambient gas is low, the cavity wall will be very susceptible to evaporation from x-ray heating and debris energy deposition as well as to erosion from sputtering by high-energy plasma ions. Thus, either cavities of very large diameter will be required or an appropriate atmosphere (e.g., buffer gas) has to be placed between the pellet microexplosion and the first wall to transpose the x-ray and ion kinetic energy into different forms and to permit their efficient utilization. The SOLASE concept,[2] proposed by the University of Wisconsin, is an example of gas protection of the first wall. One might think of operating the reactor at the highest permissible chamber gas density (determined by the necessity to transmit beam energy efficiently), allowing a

spherical blast wave to develop. Steady-state operation with repeated fusion-pellet microexplosions would result in a very turbulent, hot cavity medium whose energy would be transported to the chamber walls by radiation and thermal conduction, complicating pellet injection and illumination by laser beams.

Several reactor cavity concepts employ evaporative and/or ablative materials to protect interior cavity wall surfaces. The protective material in such designs must be either renewable between pellet microexplosions or the amount of protective material evaporated and/or sputtered by each microexplosion must be small enough so that the cavity wall lifetime will be long enough for economic operation. Protection of exposed surfaces by a liquid metal such as lithium has many attractive features and is used in the wetted-wall concept proposed by LASL[3] and in the suppressed ablation concept proposed by LLL.[4]

As an alternative to liquid-metal films one could use a sacrificial, solid-state liner to protect the cavity wall. Desirable properties of the protective material are: low Z-number (sputtering yields decrease and x-ray penetration depths increase as the atomic number decreases), high thermal conductivity and heat capacity, high-temperature resistance (to maximize heat transfer and minimize evaporation during energy deposition), low cost, and ease of fabrication. These properties appear to be satisfied best by carbon, which has therefore been chosen for studies of sacrificial-liner concepts.

Cavity walls can be protected by externally applied magnetic fields in a cylindrical cavity from energy deposition and from sputtering due to impinging ionized pellet debris.[5] The pellet debris is diverted out the ends of the cylindrical cavity to energy-sink surfaces, leaving only the x-ray energy to be accomodated by the cavity wall surface.

In a totally different approach to conceptual reactor designs, a thick layer of lithium or a lithium-lead mixture is interposed between the pellet microexplosion and the reactor structure. Examples of such designs are the BLASCON proposed by the Oak Ridge National Laboratory,[6] the lithium-fall concept proposed by Lawrence Livermore Laboratory,[7] and the liquid lead-lithium fall concept proposed by the Brookhaven

National Laboratory. The region in which pellet microexplosions occur is evacuated by some dynamic process such as rotation of the protective fluid (with the formation of a vortex) or its circulation by pumps and gravity with a fluid fall inside the cavity.

A summary of the effects of pellet output energy forms on these generic classes of cavity concepts and discussion of their advantages and disadvantages is presented in Table II.

In most conceptual fusion reactor designs, circulating liquid lithium is being considered for the breeding of tritium and the removal of heat in blanket regions surrounding the reaction chambers. Lithium is a relatively good neutron moderator, has good heat-transfer properties, and is reasonably abundant. Other blanket concepts consider lithium compounds, such as Li_2O or $LiAlO_2$, and a gas coolant, such as helium.

Reactor blankets must withstand repeated stresses due to the cyclic nature of inertial fusion reactor oeration. Energy deposition on reaction-chamber interior surfaces greatly increases their temperature which, in turn, produces high thermoelastic stresses. If a protective coating is ablated (as, e.g., in the wetted-wall concept), and impulse is transmitted to the cavity structure. Neutron-energy deposition in liquid-lithium regions results in heating and expansion of the lithium. Because energy deposition in the lithium has a radial gradient, pressure waves are created that travel between structural components. For gas-cooled blankets containing solid lithium compounds, the stresses in structural components are much lower than for blankets containing liquid lithium; however, the extent to which the lithium compounds may be damaged by neutron irradiation or may sinter, resulting in difficult tritium removal, are not known.

Possible blanket structural materials include stainless steels, ferritic alloys and refractory alloys such as molybdenum. Considerations that will be important in determining final choices include: temperature limitations, corrosion resistance, fatigue strength, radiation damage effects, neutron-induced radioactivity and afterheat, and availability. Stainless steels are limited to operation below ~750 K because of limitations due to lithium corrosion; and ferritic alloys, which are less susceptible to lithium corrosion, are limited to about the same temperature

by strength properties. Molybdenum, of which there is an abundant supply in the continental United States, is also an attractive blanket structural material: It is compatible with lithium, has good high-temperature mechanical properties, is relatively impermeable to the diffusion of hydrogen isotopes, and has a large (n,2n) cross section for high-energy neutrons.

REACTOR CONCEPTS

Two laser-fusion reactor concepts conceived at LASL have been submitted to detailed engineering feasibility evaluations: the wetted-wall and the magnetically protected reactor. The wetted-wall concept is illustrated in Fig. 3. The spherical reactor cavity is surrounded by a blanket region of liquid lithium and structural components. The cavity wall is lined with a porous refractory metal through which coolant lithium flows from the blanket into the reaction chamber to form a protective coating on its inside surface. The protective lithium layer absorbs the energy of the pellet debris and part of the x-ray energy. Part of the lithium layer is evaporated and ablated in the cavity by each pellet microexplosion and is subsequently exhausted through a supersonic nozzle into a condenser. The protective layer is restored between pulses by radial inflow of lithium from the blanket. If laser beams are used to initiate pellet fusion, it may be necessary to evacuate the cavity to a lithium density of $\sim 10^{16}$ atoms/cm^3 between microexplosions for efficient penetration by the laser beams. The time required to restore the cavity to this condition after a pellet microexplosion is ~ 0.8 s. From this and other considerations it appears that 100-MJ repetition rates of about one microexplosion per second will be practical for the wetted-wall reactor concept, resulting in a minimum average thermal power level of 100 MW.

The essential features of a laser-driven magnetically protected reactor concept are shown schematically in Fig. 4. The pellet debris is diverted out the ends of the cylindrical cavity to energy-sink surfaces leaving only the x-ray energy to be accomodated by the cavity wall surface. The geometry shown in Fig. 4 permits energy sinks to be designed

with large surface areas. Fringing of the magnetic field is used to tailor the energy deposition density over the surfaces of the energy sinks. A variant of this concept uses induction-type MHD decelerators at the ends of the cylinder to extract sufficient energy from the ions for thermalization. Calculations indicate the ~ 35% of the ion energy can be converted to electricity, which results in net power production, i.e., more power generated than consumed by the magnets.[9]

The University of Wisconsin SOLASE concept is depicted in Fig. 5. The spherical cavity has a 6-m-radius, using a pellet yield of 150 MJ at a pulse rate of 20 Hz, resulting in an average neutron wall loading of 5 MW/m^2. The blanket design is a honeycomb structure of graphite fiber composite, where lithium oxide microspheres (100-200 μm diam) flow by gravity through the honeycomb passages. The cavity first wall and last optical surface are protected from ion debris by ~ 0.5 torr (300 K) neon buffer gas.

The Livermore thick lithium fall (HYLIFE) concept is shown in Fig. 6. This concept, designed for yields up to 4000 MJ, uses low alloy ferritic steels as structural materials to minimize lithium corrosion. The lithium fall configuration is a close-packed hexagonal array of 400 cylindrical jets, 10-30 cm in diameter. The jet configuration mitigates impulse loading of the first wall by dissipation of kinetic energy of blowoff lithium through the impact of colliding jets. THe first wall assembly is a perforated "basket" inside the main pressure vessel. The injector plate manifold at the top establishes the array of jets, and the collector plate is designed to prevent "splashing" of the jets at the bottom.

CONCLUSIONS

Without information concerning the target/projectile system, it is difficult to choose which of the above concepts might be applicable to Impact Fusion. However, some qualitative judgments can be made as follows:

- Target/projectile assemblies are likely to be massive and to provide higher yields compared to beam-driven targets, resulting

in larger fractional yields of ion debris. This might require larger cavity diameters for sacrificial liner concepts to provide acceptable material losses or for the wetted-wall concept to provide wall impulse loading.

- Use of buffer gas wall protection as in the SOLASE concept might be precluded because of excessive aerodynamic drag on the projectile as traverses the cavity radius.
- Because of likely high yields and large ion debris fractions, the fluidized wall (HYLIFE) or magnetic deflection concepts may be feasible choices. For the magnetic deflection concept, the projectile can be inserted along the magnetic field axis, the cavity can be maintained at any background pressure desired, and is not pusle-rate limited. The fluidized wall concept can be operated at lower lithium temperatures to reduce cavity pressure or could use lithium-lead mixtures to reduce background pressure to acceptable levels. The HYLIFE concept would have smaller than the magnetic deflection concept cavity diameters for a given yield at the expense of more complex engineering design.

REFERENCES

1. I. O. Bohachevsky and J. F. Hafer, "Sputtering Erosion of Fusion Reactor Cavity Walls," 1976 International Conference, ANS, Washington, DC (November 1976).

2. R. W. Conn, et al, "SOLASE, A Conceptual Laser Fusion Reactor Design," University of Wisconsin report UWFDM-220 (December 1977).

3. L. A. Booth (compiler), "Central Station Power Generation by Laser Driven Fusion," Los Alamos Scientific Laboratory report LA-4858-MS, Vol. I (February 1972).

4. J. Hovingh, J. Maniscalco, M. Peterson, and R. W. Werner, "The Preliminary Design of a Suppressed Ablation Laser-Induced Fusion Reactor," Proc. 1st Topical Meeting on the Technology of Controlled Nuclear Fusion, ANS, San Diego, CA (April 1974).

5. J. J. Devaney, "Magnetically Protected First Wall for a Laser-Induced Thermonuclear Reaction,: Los Alamos Scientific Laboratory report LA-5699-MS (August 1974).

6. A. P. Fraas, "The BLASCON - An Exploding Pellet Fusion Reactor,: Oak Ridge National Laboratory report TM-3231 (July 1971).

7. M. Monsler, et al, "Electric Power from Laser Fusion: The HYLIFE Concept," Proc. 13th IECEC Conf. San Diego CA (August 1978).

TABLE I

EFFECTS OF AMBIENT CAVITY CONDITIONS ON FUSION-PELLET MECHANISMS

Cavity "Atmosphere"	X rays	Neutons	Plasma Debris
Vacuum	No effect	No effect	No effect
Ambient gas	Some attenuation	No effect	Energy transfer
Vapor	Attenuation	Little effect	Energy transfer
Liquid	Absorption	Attenuation and absorption	Energy transfer
Magnetic fields	No effect	No effect	Diversion possible

TABLE II

CHARACTERISTICS OF REACTOR CAVITY CONCEPTS

Generic Class	X-Ray Heating	Sputtering Pellet Debris	Impulse from Ablated Material	Pulse Repetition Rate Limitations	Major Advantages	Major Disadvantages
Lithium Wetted wall	Soft x rays absorbed in lithium film	Prevented by lithium film	Significant but not severe. Structural requirements determined by blanket phenomena	Limited to ~1/s by requirement to evacuate cavity of ablated lithium	Small cavity size possible, surface damage to cavity wall by evaporation and sputtering eliminated	Pulse repetition rate limited, damage of last optical surface by pellet debris and contamination by lithium vapor
Magnetically protected wall	Determines minimum cavity diameter	Avoided by deflecting ions away from walls	No	Not serious. Repetition rates of 10/s probably feasible	Protection of last optical surface from energetic ions, high pulse repetition rate possible, cavity wall accessible for repair or re-replacement	Magnetic fields necessary, energy-sink replacement will increase power production costs
Gas filled	Diminished or eliminated by attenuation in gas	No, debris energy deposited in gas	No	Possibly, energy removal from cavity not well established	Surface damage to cavity wall by evaporation and sputtering eliminated	Complicated cavity phenomena, may require removal of hot cavity gas between pulses, damage and contamination of last optical surface
Bare metal wall	Determines minimum cavity diameter and cavity lifetime		Trivial	Probably not, depends on final disposition of ablated wall material	High pulse repetition rate possible, simple design	Large cavity diameter required, damage and contamination of last optical surface
Sacrificial liner	Determines minimum cavity diameter and cavity lifetime. Smaller minimum cavity diameter than for bare metal wall		Trivial	Probably not, depends on condensation and removal of ablated wall material	Relatively small cavity size possible, evaporation and sputtering confined to liner, high pulse repetition rate possible	Damage and contamination of last optical surface, liner replacement will increase power production cost
Thick lithium cavity wall	X-ray and debris energy absorbed in lithium first wall		May be very severe, total pellet yield deposited in lithium first wall	Limited by requirement to evacuate cavity of vaporized lithium	Surface damage to cavity wall by evaporation and sputtering eliminated. Radiation damage of structure essentially eliminated	Severe limits on pulse repetition rate, complicated cavity phenomena--difficult to analyze, damage and contamination of last optical surface and cavity components, pumping power required to maintain cavity configuration, limited access for beam transport

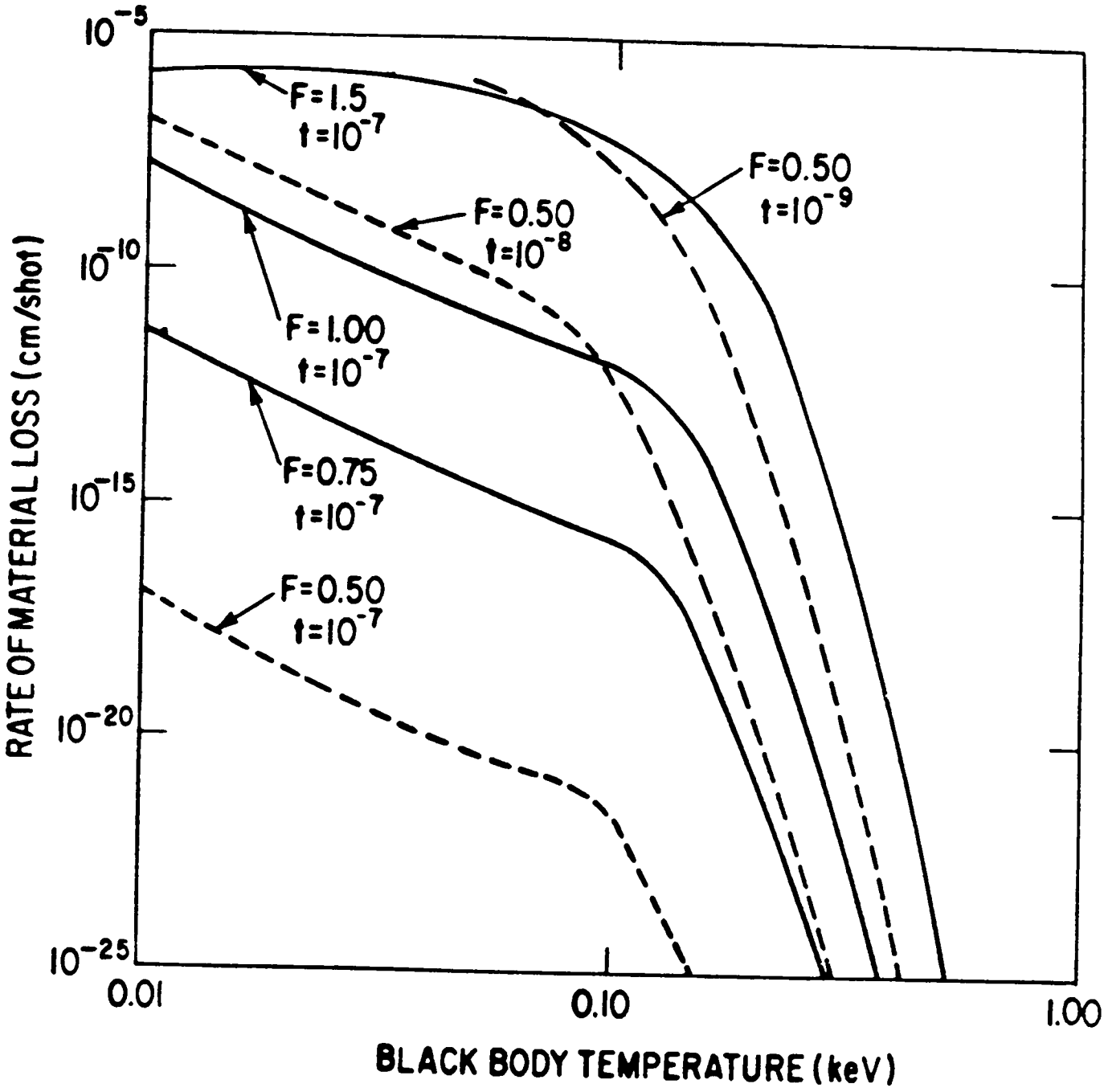

Fig. 1 Rate of material loss of carbon surface from x rays. F is fluence in J/cm2, t is pulse width in seconds.

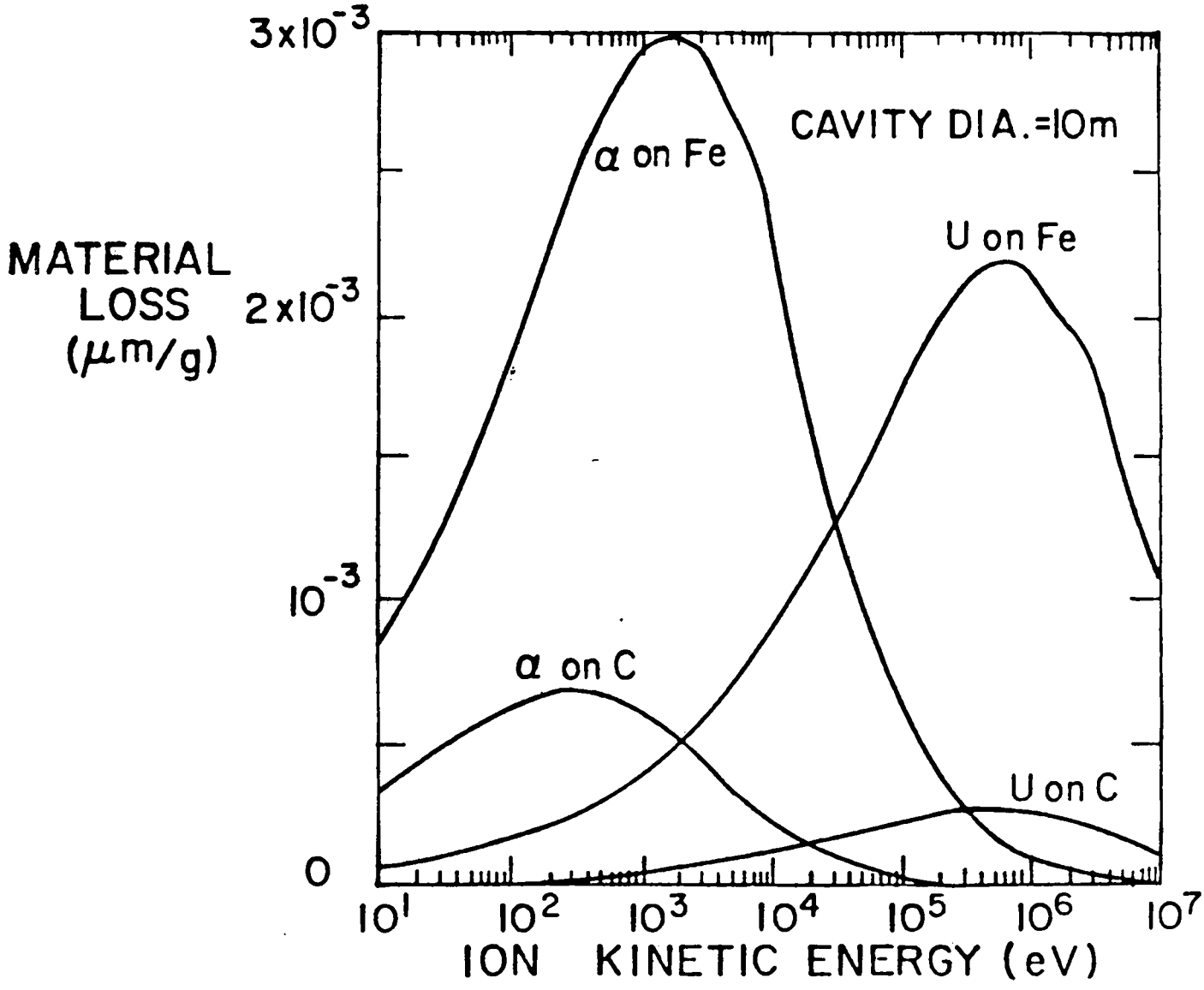

Fig. 2. Effect of ion sputtering on first wall materials. Material loss expressed per unit mass of ion species.

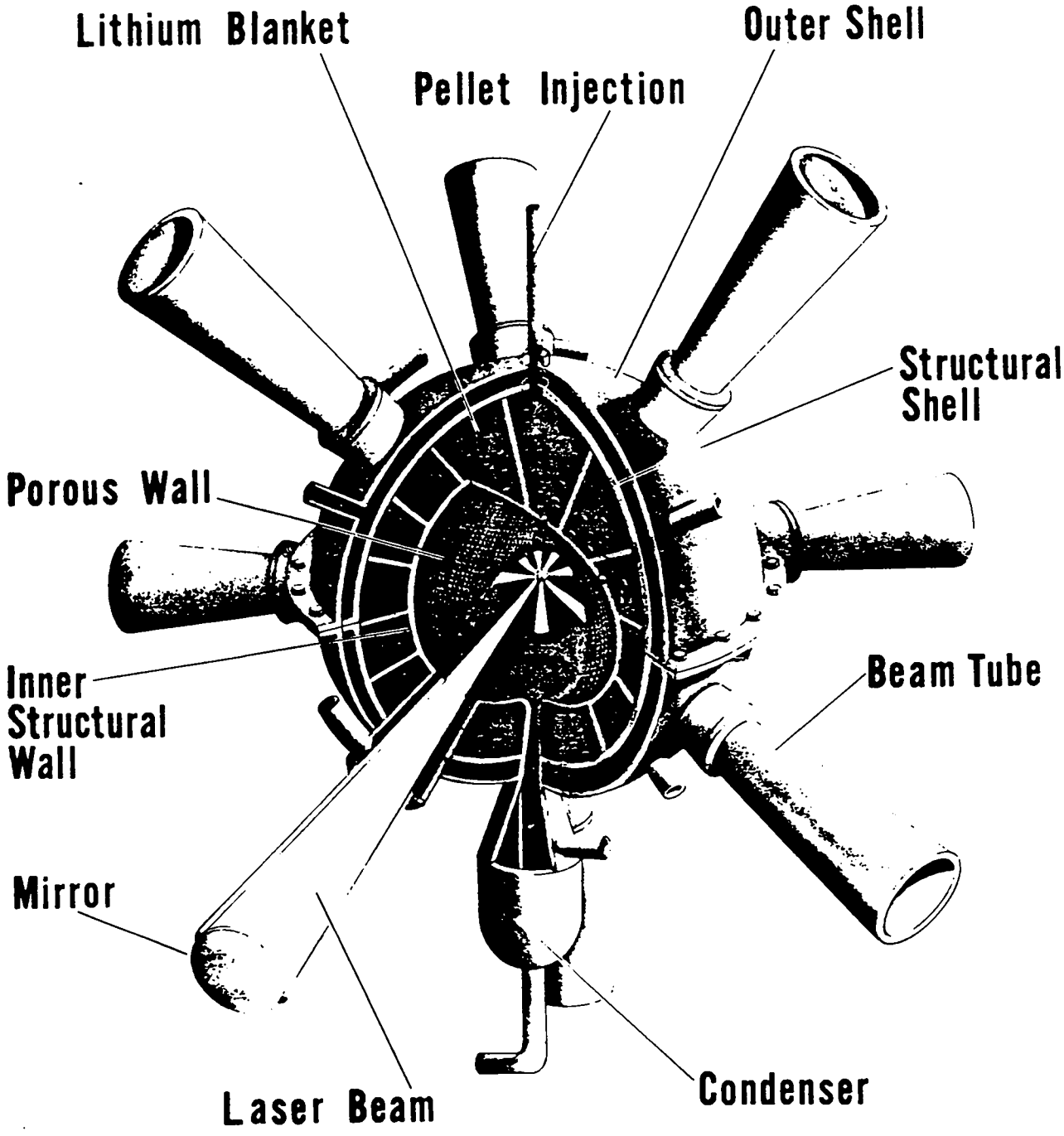

Fig. 3. The wetted-wall reactor concept

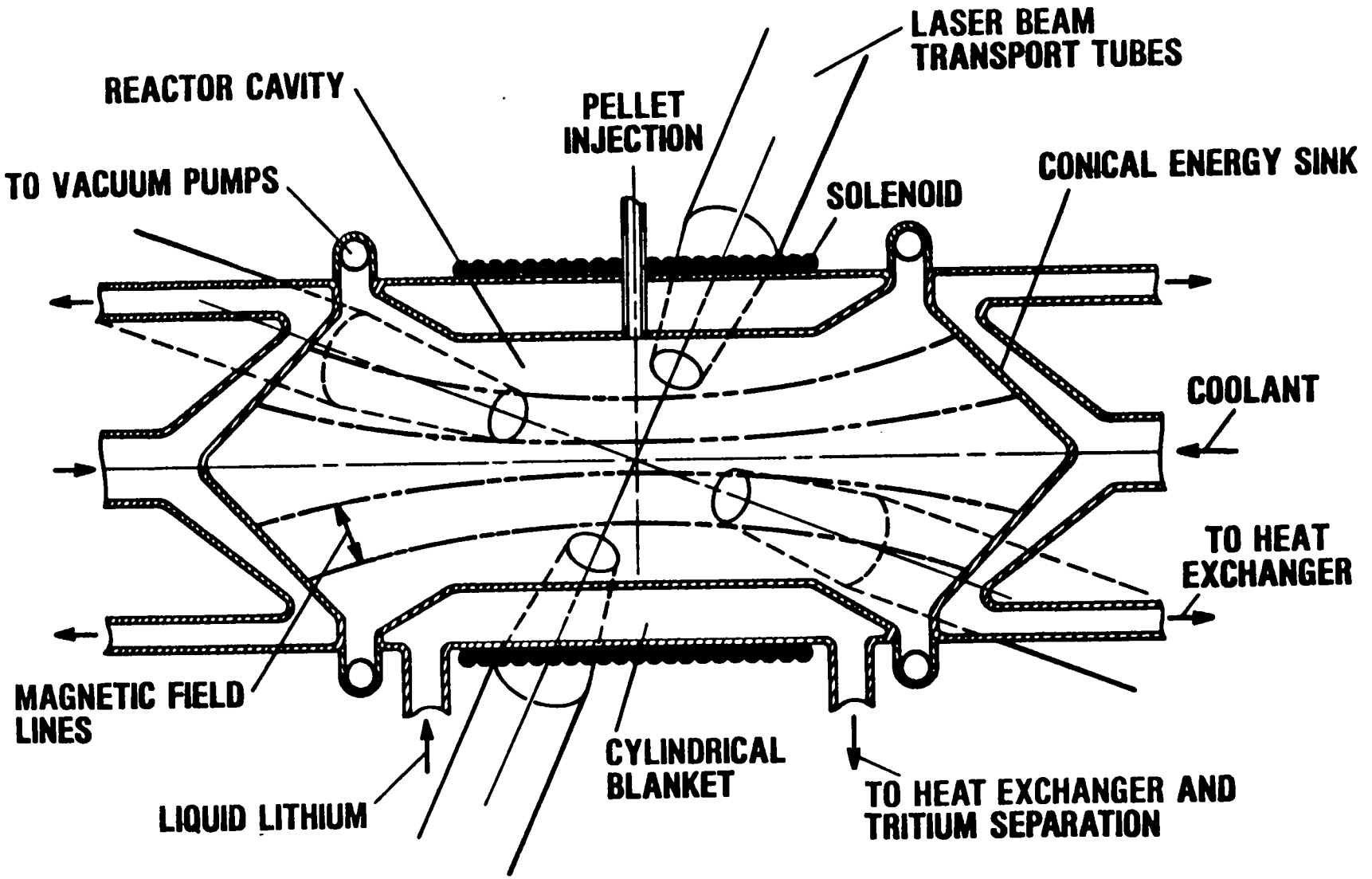

Fig. 4. The magnetically protected reactor concept.

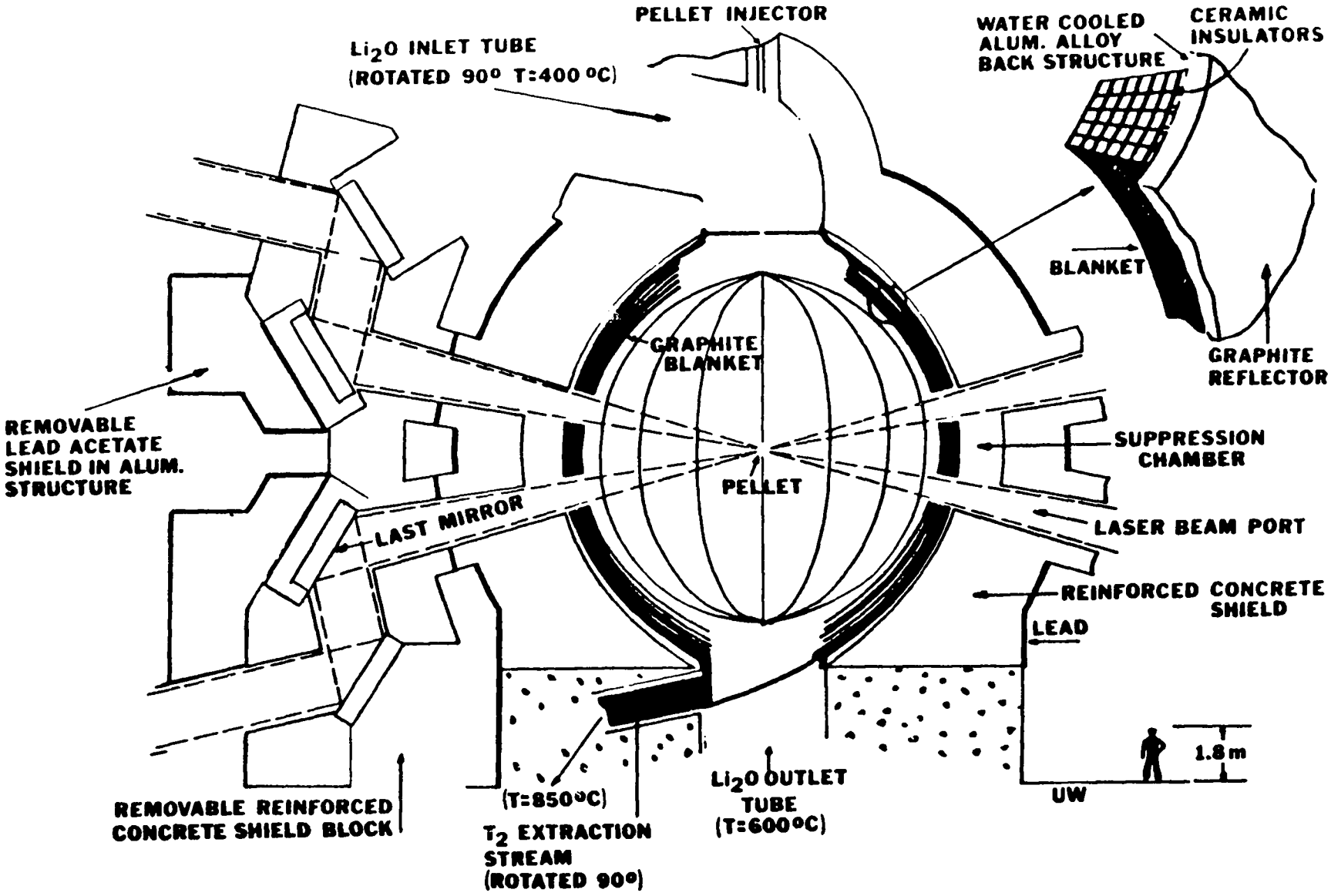

Fig. 5. The SOLASE concept.

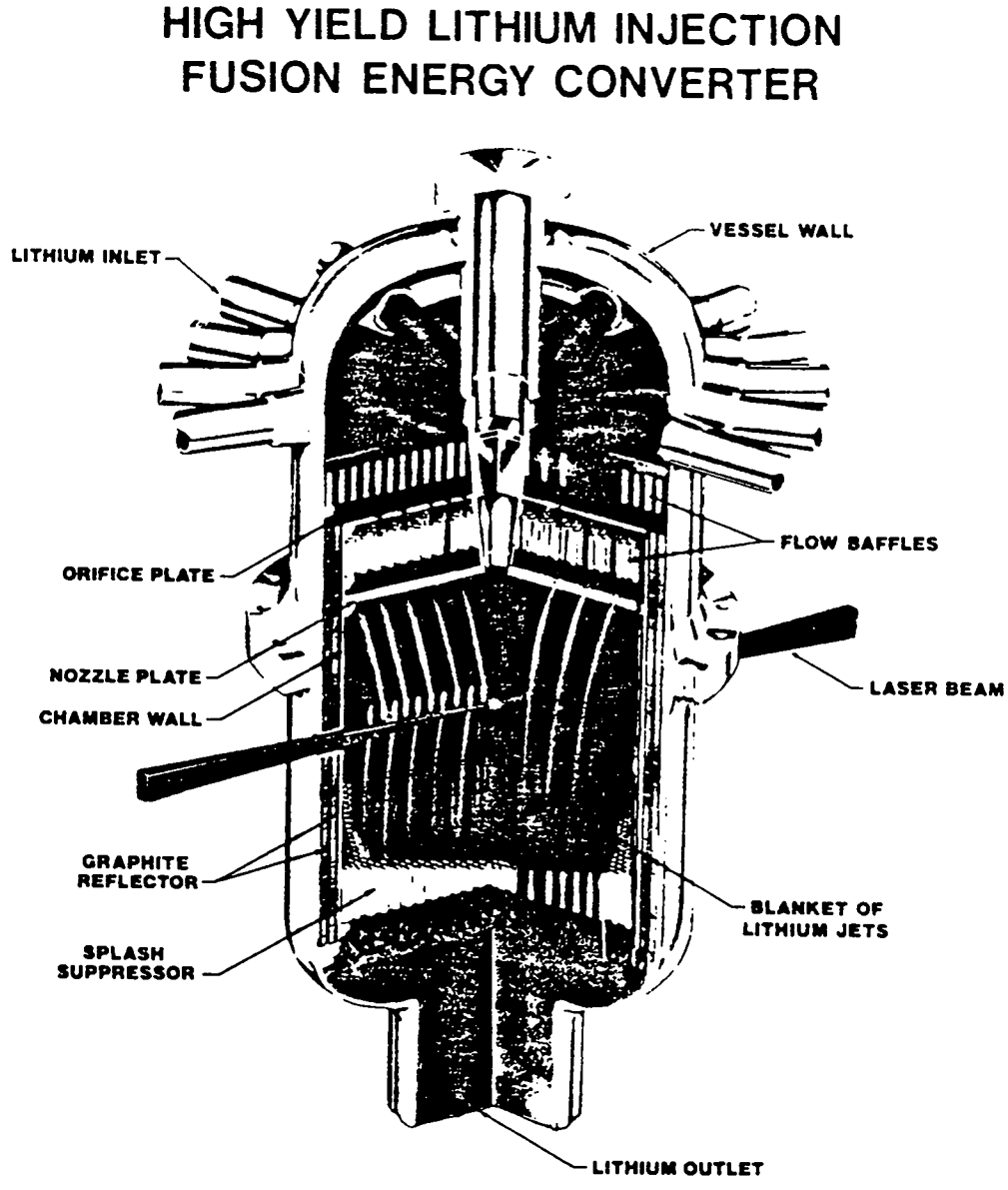

Fig. 6. The HYLIFE concept.

FUSION IMPULSE CONTAINMENT

Ihor O. Bohachevsky
Los Alamos Scientific Laboratory
Los Alamos, NM 87545

Impact Fusion Workshop, LASL, July 10-13, 1979.

PROBLEM FORMULATION

At the present time the characteristics of impact fusion energy releases are not known sufficiently well to examine in detail specific containment vessel concepts or designs. Therefore it appears appropriate to formulate the impulse containment problem in general and to derive results in the form of explicit expressions from which magnitude estimates and parametric dependencies (trends) can be inferred conveniently and rapidly. In the following presentation we carry out this task using assumptions and approximations that are required to perform the analysis.

The fusion impulse containment problem may be formulated in the following general way: for a total projectile or pellet energy release Y, the energy to be contained is (f+x)Y where (f+x) is the fraction of energy yield in debris and x rays (i.e. 1-f-x is the fraction of energy release which escapes the containment vessel as high energy neutrons). Assuming that the response of the containment vessel remains in the elastic regime (necessary for long term repetitive operation) and that its wall thickness, δ_i, is small in comparison to the radius, R_i, the elastic energy stored in the volume of the containment vessel material as two-dimensional membrane strain is given by $(4\pi R_i^2 \delta_i) \cdot \left[E\epsilon^2/2(1-\nu)\right] \cdot 2$ where E is the Young's modulus, ϵ the linear strain, and ν the Poisson's ratio. It is reasonable to postulate that there exists a functional relation between the energy contained in the cavity and the energy elastically stored in the wall material:

$$2(4\pi R_i^2 \delta_i) \frac{E\epsilon^2}{2(1-\nu)} = F\left[(f+x)Y\right]. \qquad (1)$$

In this analysis we derive the dependence F and thus obtain explicit expressions relating energy yield Y to containment vessel parameters.

The function F depends on the mechanism of energy transfer from the cavity medium into the wall material. It is clear that F, in general, is not an idetity because it is not possible to transfer the entire energy content of the cavity into the wall. This circumstance is analogous and related to the fact that in inertial confinement fusion, in general, only a small fraction (5%-50%) of the pusher kinetic energy can be transferred to the thermonuclear fuel. To determine F it is necessary to investigate a specific containment model and momentum coupling between the energy release and the vessel wall.

THE MODEL

The containment vessel model most suitable for obtaining explicit results consists of two concentric spherical shells with a layer of liquid (blanket) between them as shown in Fig. 1. To proceed with the analysis we make the following assumptions:

1. Structural shells are spherical;
2. Shell thickness, δ_i is small relative shell radius, R_i;
3. Blanket thickness, Δ, is small relative to the radius;
4. Structural shell responses remain in the elastic regime;
5. Load pulses are short relative to the period of free (elastic) shell vibrations.

The last assumption permits us to approximate loads applied to the vessel wall with Dirac delta functions; it is a very good approximation because load pulse durations in inertial confinement fusion are estimated to be in the microsecond range whereas periods of free shell vibrations are in the millisecond range for radii exceeding one meter.[1] The use of thin shell approximation in stress calculations for the containment vessel walls is justified because these walls will be thin relative to the vessel radius ($\delta_i/R_i < 0.01$) in practical (commercial) applications to avoid excessive neutron energy depositon and material cost.

To obtain conservative estimates that are valid when voids or bubbles develop in the liquid blanket or when the blanket is absent, we omit the hydrodynamic coupling term in the equation governing the elastic response of a thin shell to the impulse per unit area I and obtain the following formulation:[1]

$$\rho \frac{d^2 w_i}{dt^2} + \frac{2E}{(1-\nu)R_i^2} w_i = 0 \quad , \tag{2}$$

where w_i is the radial shell displacement related to the tensile or compressive strain, ϵ, by the geometric compatibility relation:

$$\epsilon_i = w_i / R_i \tag{3}$$

and t is time measured from impulse application.

The initial conditions for the solution $w_i(t)$ are given by:

$$w_i(0) = 0 \text{ and } \frac{dw_i(0)}{dt} = \frac{I}{\rho \delta_i}, \tag{4}$$

The effect of the hydrodynamic coupling of the shell to the liquid blanket will be discussed in a separate section.

The solution of Eq. (2) which satisfies compatibility conditions (3) and initial conditions (4) is given by:

$$\epsilon_i = \sqrt{\frac{1-\nu}{2E\rho}} \frac{I}{\delta_i} \sin \sqrt{\frac{2E}{(1-\nu)R_i^2 \rho}}\, t \tag{5}$$

and therefore the maximum strain is given by:

$$\epsilon_{im} = \sqrt{\frac{1-\nu}{2E\rho}} \frac{I}{\delta_i} \tag{6}$$

Using this result together with Eq. (1) we obtain an expression for the dependence of F on the momentum applied to the wall:

$$F = 2\pi R_i^2 \frac{I^2}{\rho \delta_i} \quad . \tag{7}$$

To complete the analysis we must now examine different mechanisms by

which the energy relased in pellet microexplosion generates impulse at the vessel wall and derive the corresponding expressions for I in terms of Y.

IMPULSE GENERATION

Thermonuclear burn of D-T fuel in inertial confinement fuel pellet releases energetic (14 MeV) neutrons, x rays, and energetic ionized pellet debris. We will not consider the possibility that parts of the projectile may remain as solid chunks of material (shapnel). Above energy forms apply impulse to the wall through:

1. Evaporation recoil
2. Debris impact
3. Blast wave reflection
4. Blanket thermal expansion

In addition to these mechanisms, excitation of stress waves in the vessel wall generates stresses different from membrane; we will analyze this phenomenon in a separate section.

Evaporation Recoil - The pulse of x rays produced in fusion microexplosion is absorbed in a thin layer of wall material, part of which may evaporate and thus generate an impulse at the wall. The magnitude of the recoil impulse per unit area, I_r, maximized with respect to the mass of material evaporated is given by:[1]

$$I_r = \frac{Yx\eta}{4\pi R_1^2 \sqrt{2H}} \quad , \tag{8}$$

where H is the heat of vaporization of the wall material, and η the effectiveness coefficient that accounts for the fact that not all vapor moves away from the wall with maximum attainable velocity. For a particular model of a Riemann wave expanding into vacuum, $\eta = 0.15$.

With this expression for the impulse, Eqs. (1) and (6) result in the following radius-yield relation:

$$R_i = \left[\frac{E}{(1-\nu)H_\rho}\right]^{1/4} \sqrt{\frac{Yx}{8\pi\sigma_m \delta_i}\eta} \tag{9}$$

in which the strain ϵ_{im} has been eliminated in favor of maximum allowable stress σ_m using:

$$\sigma = \frac{E\epsilon}{1-\nu} \quad . \tag{10}$$

Impact of Pellet Debris - The kinetic energy of the high-velocity fuel pellet debris delivers to the vessel wall an impulse per unit area, I_d, whose magnitude is given by:[1]

$$I_d = \frac{\sqrt{YfM}}{2\sqrt{2\pi R_1^2}} \quad . \tag{11}$$

Here M is the fuel pellet mass. Equation (11) is a conservative estimate because it is based on the assumption that all the kinetic energy is converted into the impulse; in practice, part of the kinetic energy will appear as heat and will produce a recoil impulse whose magnitude can be estimated from Eq. (8) with an appropriate value for the energy fraction x. The two recoil impulses, however, cannot be combined because they occur at different times.

In this case the radius increases as the fourth root of the energy yield:

$$R_i = \frac{1}{2}\sqrt{\frac{1}{\pi\sigma_m\delta_i}}\left[\frac{EMYf}{(1-\nu)\rho}\right]^{1/4} \tag{12}$$

Blast Wave Reflection - When the ambient density in the cavity exceeds about 10^{14} atoms/cm^3, the pellet microexplosion will generate a spherical blast wave. The impulse experienced by the reactor vessel wall during blast wave reflection is easily estimated as the product of the pressure at the wall behind the reflected wave, Eq. (7) of Ref. 1 , and the pulse duration, which we approximate with the transit time of a sound wave through the shock compressed layer of the ambient cavity gas. The resulting expression for the impulse per unit area, I_b, is

$$I_b = \sqrt{\frac{3\gamma-1}{8\pi}}\sqrt{\frac{Yf\rho_o}{R_i}} \quad , \tag{13}$$

where ρ_o is the ambient mass density of the cavity medium and γ is the constant ratio of specific heats in that medium. In the derivation of Eq. (13), the Taylor-Sedov similarity description[2] of the blast wave was used. The validity of this solution deteriorates as the pellet mass increases and approaches the mass of the ambient cavity medium; at that point, a modified blast wave theory[3] should be used to obtain accurate results. Unfortunately, any analysis of the blast phenomena that is more complex than the Taylor-Sedov description precludes the possibility of obtaining an analytic impulse estimate like Eq. (13).

When the above assumptions are valid, the radius is directly proportional to the yield with the proportionality constant depending on the ambient cavity density ρ_o:

$$R_i = \frac{1}{16\pi} \frac{3\gamma - 1}{1 - \nu} \frac{E\rho_o}{\rho\sigma_m^2\delta_i^2} Yf \quad . \tag{14}$$

Thermal Response of the Blanket - Lithium blankets, both liquid and solid compounds in pellet form, are designed to convert neutron kinetic energy into thermal energy and, therefore, will expand during reactor operation. The mean pressure increase caused by a confined expansion of a liquid lithium blanket is easily calculated to be:[1]

$$p = \frac{\beta b}{c_\ell \rho_\ell} \frac{Y(1 - f - x)}{V} , \tag{15}$$

where p is the pressure increase, β the adiabatic bulk modulus, b the volume coefficient of thermal expansion, c_ℓ the heat capacity of liquid lithium, ρ_ℓ the density of liquid lithium, and V the blanket volume. This estimate is based on the assumption that neutron energy deposition is sufficiently slow or uniform and does not induce dynamic imbalances in the process. Actually, neutron energy is deposited with an exponentially decreasing intensity in a time that is short relative to the hydrodynamic response time and therefore generates pressure waves in the liquid blanket. To analyze these waves and to model their effect, we solved the acoustic equations (in the plane wave

approximation) for pressure, p, and velocity, u, perturbations in a liquid medium between two concentric shells shown in Fig. 1. The medium was initially at rest with an exponentially decreasing (from the inner shell R_1 to the outer shell R_2) pressure distribution induced by a postulated instantaneous neutron energy deposition with the scale depth λ ($\lambda \approx 70$ cm for liquid lithium). The details of the solution are presented in Ref. 4 ; here we summarize the conclusions relevant to the present discussion:

(a) The mean pressure rise and the first harmonic component account for nearly 90% of the deposited energy and therefore provide an approximate description of the phenomena that is adequate for the purpose of this paper;

(b) The ratio of the amplitude of the first harmonic to the mean pressure rise increases nearly linearly with the nondimensional blanket thickness Δ/λ for values of $\Delta/\lambda < 4$, as shown in Fig. 2. At the typical value of the blanket thickness $\Delta/\lambda \approx 1.6$, that ratio is approximately 0.50. Therefore, in stress calculations the mean pressure estimate given by Eq. (15) should be multiplied by a factor of ~ 1.50 to account for the transient overpressure.

The analysis reported in Ref. 4 also verified the intuitively expected fact that the pulse duration to be used with Eq. (15) to estimate the impulse at the wall is given by $\tau = \Delta/a_\ell$ where a_ℓ is the sound speed in the blanket liquid given by $a_\ell = \sqrt{\beta/\rho_\ell}$. Using these results, the expression for the impulse delivered to the vessel wall because of confined thermal expansion of the blanket becomes:

$$I_t = \frac{1.5\ a_\ell b}{4\pi c_\ell R_i^2}\ Y(1-f-x); \qquad (16)$$

it is independent of the blanket thickness Δ.

Using this expression for the impulse with Eqs. (1) and (6) results in the following radius-yield relation:

$$R_i = \left[\frac{E\beta}{2(1-\nu)\rho\rho_\ell}\right]^{1/4} \sqrt{\frac{1.5\ b}{4\pi\delta_i c_\ell \sigma_m}\ Y(1-f-x)} \qquad (17)$$

The pressure increase in the blanket not only generates tensile and compressive stresses in the structural shells but also tends to buckle the inner shell. Assuming that the critical value of the pressure for this mode of failure is the same as that developed for a static load application and substituting an expression for it[5] into Eq. (15) we find that the radius of the vessel cancells out and the wall thickness, δ_i, required to prevent buckling increases as the square root of the yield:

$$\delta_i = \sqrt{\frac{\sqrt{3(1-\nu^2)}}{2E}}\ \sqrt{\frac{\beta\, b}{c_\ell \rho_\ell}}\ \sqrt{\frac{1.5}{4\pi\Delta}\ Y(1-f-x)}\ . \qquad (18)$$

In the derivation of this result the approximation $V = 4\pi R_i^2 \Delta$ was used.

RESULTS

The radius-yield relations developed in the previous section have been evaluated in the range of parameters applicable to laser and impact fusion and the results are presented in Figs. 3, 4, and 5. The constants used in the evaluation are listed in Table I (cgs units).

In Fig. 3 the shell thickness is δ_i = 1 cm, the pellet mass is M = 0.5 g, and the ambient density of the cavity medium is $\rho_0 = 1.5 \times 10^{-7}$ g/cm^3 which corresponds to approximately 0.1 Torr of argon at 500 K; this apparently is the highest density that may allow satisfactory propagation of the laser beam through the cavity. We see that in laser fusion, structural strength requirements for an uprotected containment vessel wall are dominated by evaporation recoil and elastic buckling and that the blast wave effects are negligible.

For higher yields, more representative of impact fusion and presented in Figs. 4 and 5, the shell thickness is δ_i = 2 cm and the ambient density $\rho_0 = 1.33 \times 10^{-6}$ g/cm^3 (1.0 Torr of argon at 500 K). Again the evaporation recoil dominates except for heavy projectiles or very high yields.

In all cases, however, the structural requirements of fusion impulse containment appear to be very mild; the radii required are less than 1 m except when the yield exceeds 1 GJ in which case they reach values of a few meters. Therefore the design of containment vessels will be determined not by the structural integrity requirement but by lifetime considerations which depend on first wall material loss and neutron damage mechanisms.

HYDRODYNAMIC COUPLING

The natural oscillations of a structural shell described by Eq. (5) are signifantly modified when the shell is surrounded by a blanket because of the transfer of kinetic energy from the shell to the liquid. This energy loss mechanism, which is much more effective than the internal damping in the shell material, will be estimated in this section.

In an unbounded fluid the pressure pulses generated by an oscillating sphere carry the energy away in the form of sound waves; in a fluid blanket of finite thickness, the pulses are reflected at the outer shell and the wave interaction pattern must be determined to obtain a complete description of the phenomena. In this section we limit the anlaysis to a time interval shorter than the time when the first reflected wave returns to the inner shell; with this restriction we explicitly model the coupling of the shell to the liquid blanket and show that the motion is overdamped. Some general remarks about complete description of the motion will be made at the end of this section.

The differential equation governing the elastic motion of a shell hydrodynamically coupled to the surrounding fluid is obtained by adding to Eq. (2) a term representing the pressure exerted by the fluid. When the fluid is inviscid and the propagation of spherical waves can be approximated with locally plane wave fronts, this term is $\rho_\ell a_\ell (dw_i/dt)$ where a_ℓ is the sound speed in the liquid an the product $\rho_\ell a_\ell$ is known as the acoustic impedance of the medium. With this addition the differential equation for the radial shell displacement is:

$$\rho \frac{d^2 w_i}{dt^2} + \frac{\rho_\ell a_\ell}{\delta_i} \frac{dw_i}{dt} + \frac{2E}{R_i^2(1-\nu)} w_i = 0 \tag{19}$$

and the boundary conditions are given by Eq. (4) supplemented with the condition of no cavitation.

The solution of this system is:

$$w_i(t) = C\left(e^{-\omega_1 t} - e^{-\omega_2 t}\right) \tag{20}$$

with the characteristic roots given by:

$$\omega_{1_1 2} = \frac{\rho_\ell a_\ell}{2\rho\delta_i} \pm \left[\left(\frac{\rho_\ell a_\ell}{2\rho\delta_i}\right)^2 - \frac{2E}{\rho R_i^2(1-\nu)}\right]^{1/2} \tag{21}$$

and the constant C by:

$$C = -\frac{I}{2\rho\delta_i} \left[\left(\frac{\rho_\ell a_\ell}{2\rho\delta_i}\right)^2 - \frac{2E}{\rho R_i^2(1-\nu)}\right]^{-1/2} \tag{22}$$

In applications of interest to laser and impact fusion investigators the inequality

$$\left(\frac{\rho_\ell a_\ell}{2\rho\delta_i}\right)^2 >> \frac{2E}{R_i^2(1-\nu)} \tag{23}$$

is usually satisfied[1] and therefore solution (20) is exponential and not oscillatory.

Solution (20), even though it is explicit, is too complex to allow convenient interpretation. To gain insight into physical meaning of different terms and thus identify parameters which determine its behavior we make use of inequality (23); it implies that the isolated shell response represented by the term $2E/\rho R_i^2(1-\nu)$ may be neglected in comparison to the hydrodynamic coupling effect $(\rho_\ell a_\ell)^2/(2\rho\delta_i)^2$ except in ω_2 where the ratio

of these terms is the dominant contribution. With this approximation and an appropriate expansion of the square root the result simplifies to:

$$\omega_1 \approx \frac{\rho_\ell a_\ell}{\rho \delta_1} \quad , \tag{24}$$

$$\omega_2 \approx \frac{\delta_i}{R_i} \frac{2E}{R_i(1-\nu)\rho_\ell a_\ell} \quad , \tag{25}$$

$$\omega_C \approx - \frac{I}{\rho_\ell a_\ell} \quad . \tag{26}$$

These terms have clear physical interpretations: ω_1 is the ratio of the hydrodynamic inpedance to the shell mass per unit area, ω_2 is the ratio of the shell elastic stiffness to the hydrodynamic impedance modified by the aspect ratio (δ_i/R_i), and C is the negative of the ratio of applied impulse to the hydrodynamic impedance.

To illustrate the behavior of the shell-blanket system we evaluated Eq. (2) for I = 183 dyne·s/cm^2, R_i = 500 cm, δ_i = 1.35 cm, (the values of the remaining parameters are listed in Table I) and plotted the result in Fig. 6. It shows that the time t_m given by:

$$t_m = \frac{\ell n(\omega_1/\omega_2)}{\omega_1 - \omega_2} \tag{27}$$

at which the strain (and stress) peaks occurs well before the return of the first pressure wave given by $t_r = 2\Delta/a_\ell$ and that the stress reaches its maximum value very rapidly in comparison to the subsequent relaxation. For the conditions of this example the maximum stress is $\sigma(t_m) = 4.17 \times 10^6$ dyne/cm^2; this value is approximately ten times smaller than the corresponding value for an isolated shell given by Eq. (6). Such result is physically obvious: the inertia of the liquid blanket inhibits shell expansion thus reducing strain and stress.

The shell relaxation time indicated by the result shown in Fig. 6 is very long in comparison to the hydrodynamic wave transit time, Δ/a_ℓ. Therefore in some investigations it may be justified to approximate the wave

motion in the blanket with reflections from stationary shells. We have determined such approximation explicitly[4] but continued the solution only past the first reflection at the outer shell. The results indicated that for physically realistic representation of the wave motion the reflection boundary conditions at each shell must be determined empirically or from exact numerical modeling of the wave reflection from an elastic wall. Preliminary numerical calculation indicates that for containment vessel shells of interest in inertial confinement fusion, the correct reflection boundary condition should provide for approximate equipartition of impulse: nearly half of the impulse carried by the hydrodynamic wave is reflected and the remainder is expended to accelerate the structural shell. We expect that, in general, the fraction of the impulse that is reflected will depend on the ratio of the shell stiffness to the acoustic impedance of the blanket medium but we have not yet determined that dependence.

STRESS WAVES

Stress waves are generated in the wall because x-ray or debris energy is deposited in a thin layer of material in a time that is short in comparison to the characteristic thermal diffusion time. Denoting the depth of energy deposition by δ and considering the effect of x rays to be specific, the corresponding temperature increase in the surface layer of depth δ is:[6]

$$\Delta T_s = \frac{Yx}{4\pi R_i^2 \delta \rho c_i} \tag{28}$$

where c_i is the heat capacity of the shell material. The denominator of Eq. (28) is the heat capacity of the spherical shell of thickness δ, and therefore this expression for surface temperature increase has the obvious physical interpretation; it is also the limit of the exact solution of the one-dimensional time-dependent heat equation as the heat pulse duration tends to zero.[6]

An instantaneous surface temperature increase ΔT_s induces a local thermal stress of magnitude[1]:

$$\sigma = \frac{E \alpha \Delta T_s}{1 - \nu} , \qquad (29)$$

where α is the linear coefficient of thermal expansion. Substituting into this equation the expression for ΔT_s from Eq. (28) will result in a relation between vessel radius R_1 and pellet yield Y if the allowable value of the stress σ_m for these conditions were known. However, because the surface temperature increase given by Eq. (28) persists for only approximately 10^{-9} s and is localized to a depth of less than a few micrometers, it is not clear that a catastrophic failure would occur if the surface material yields locally or even melts for such a short time. Clearly, theoretical and experimental investigations are needed to determine allowable values of the stress to be used in Eq. (29) for the loading characteristics indicated .

A possible approach to the determination of allowable transient thermal stress is through the analysis of stress wave propagation in the vessel wall. A surface layer of depth δ heated sufficiently rapidly to a high temperature does not have time to expand and consequently experiences a compressive stress σ_0 that is relieved with a stress wave rather than by heat conduction. This can be seen from the following simple estimates. The characteristic time to propagate the effect elastically through a distance δ is given by $t_w \approx \delta/a_i$; (a_i is the wave speed in the wall material); for steel and $\delta \approx 10^{-4}$ cm, $t_w \approx 2 \times 10^{-10}$ s. The characteristic time for heat conduction is $t_c \approx \delta^2/\kappa$; ($\kappa$ is the coefficient of thermal diffusivity);for the same material and δ, $t_c \approx 2 \times 10^{-7}$ s. Hence the effect of the thermal pulse will propagate elastically approximately a thousand times faster than by conduction.

Instead of giving a standard mathematical description of wave propagation, we summarize the characteristics of thermally excited stress waves graphically in Fig. 7. Shown schematically is the initial compressive stress σ_0 induced by the temperature increase ΔT_s in the surface layer of depth δ, the resulting stress wave during reflection from the inner face of the wall, and the same wave at the time δ/a_i when the reflection process is completed. The resulting wave propagating through the wall consists of a compression phase of length δ, followed by an equally long tensile phase, the

amplitudes of both phases being equal to $\sigma_0/2$. Clearly, this wave produces tensile and compressive stresses equal to $\sigma_0/2$ at the inner and outer faces of the wall and, therefore, its amplitude should be limited to an allowable stress level to avoid spallation.

Denoting the allowable stress by σ_m as before, and using Eq. (28) in Eq. (29) to obtain the expression for σ_0, we arrive at the following relation between the radius of the inner shell, R_1, and the pellet yield Y:

$$R_1 = \sqrt{\frac{E \alpha x Y}{8\pi(1-\nu)\delta\rho c_i \sigma_m}} \quad . \tag{30}$$

This estimate, however, may be excessively conservative because it does not account for the fact that some of the initial thermal energy may be used to melt and vaporize the surface material and that elastic waves may be damped significantly by internal friction of the material. Even though the thermoelastic coupling constant and therefore the logarithmic decrement are small, the cumulative effect is not negligible when the ratio $a_i\delta_i/2\kappa$ is very large[7], which is the case for containment vessel walls. Also, the analysis is not very useful unless the value of δ is known. To resolve uncertainties associated with this problem, we are investigating thermal generation and propagation of elastic stress waves numerically with realistic equations of state and stress-strain relations.

Exploratory calculations indicate that for energy densities of interest in inertial confinement fusion, part of the heated surface layer indeed melts and evaporates generating an impulse whose magnitude is closely approximated by Eq. (8). This impulse sends a shock into the cold solid wall with the pressure behind it approximately equal to one half of the value in the hot (plastic) part. The response to an x-ray pulse of one nanosecond duration lasts less than one microsecond and ends before any shear flow develops. These findings, supplemented with additional considerations, indicate that satisfactory determination of the shell response requires computations with an equation of state that models phase transitions between solid and liquid and between liquid and vapor and with a stress-strain relation that allows

tensile stress in the liquid phase in the absence of shear flow and surface instabilities.

REFERENCES:

1. BOHACHEVSKY, I. O., "Scaling of Reactor Cavity Wall Loads and Stresses," Los Alamos Scientific Laboratory report LA-7014-MS (November 1977)

2. KOROBEJNIKOV, V. P., Problems in the Theory of Point Explosion in Gases, Nauka, Moscow (1973).

3. FREIWALD, D. A., and AXFORD, R. A., "Approximate Spherical Blast Theory Including Source Mass." J. Appl. Phys., 46(3), 117.-1174 (1965).

4. BOHACHEVSKY, I. O., "Hydrodynamic Waves in Liquid Lithium Blanket," in "Laser Fusion Program Progress Report, July-December 1977," Los Alamos Scientific Laboratory report LA-7328-PR (December 1978).

5. ROARK, R. J. Formulas for Stress and Strain, McGraw-Hill, New York (1965).

6. FRANK, T. G., BOHACHEVKSY, I. O. BOOTH, L. A., AND PENDERGRASS, J. H., "Heat Transfer Problems Associated with Laser Fusion," AIChE Symp. Ser. 73(168), 77-85 (1977).

7. ACHENBACK, J. D. Wave Propagation in Elastic Solids, North Holland, Amsterdam (1973).

TABLE I

Quantity	Value
α	14.4×10^{-6} K^{-1}
b	1.39×10^{-4} K^{-1}
β	1.09×10^{11} dyne/cm^2
Δ	100 cm
c_ℓ	3.55×10^{7} erg/gK
E	2×10^{12} dyne/cm^2
η	0.25
γ	1.20
H	7.47×10^{10} erg/g
ρ	7.81 g/cm^3
ρ_ℓ	0.52 g/cm^3
σ_m	10^9 dyne/cm^2
ν	0.30
x	0.05
f	0.20

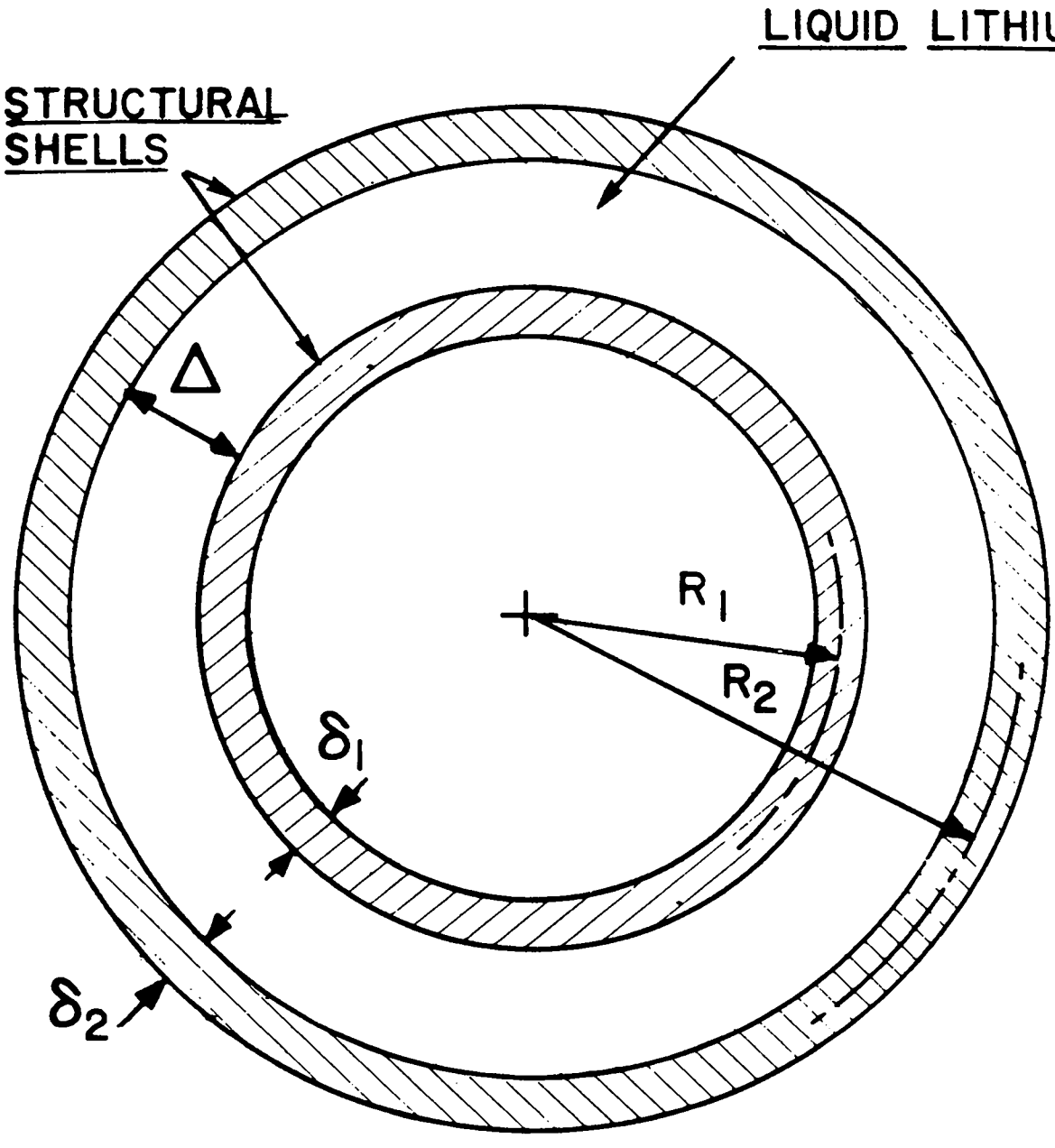

ICF REACTOR VESSEL MODEL

Fig. 1. Containment vessel model.

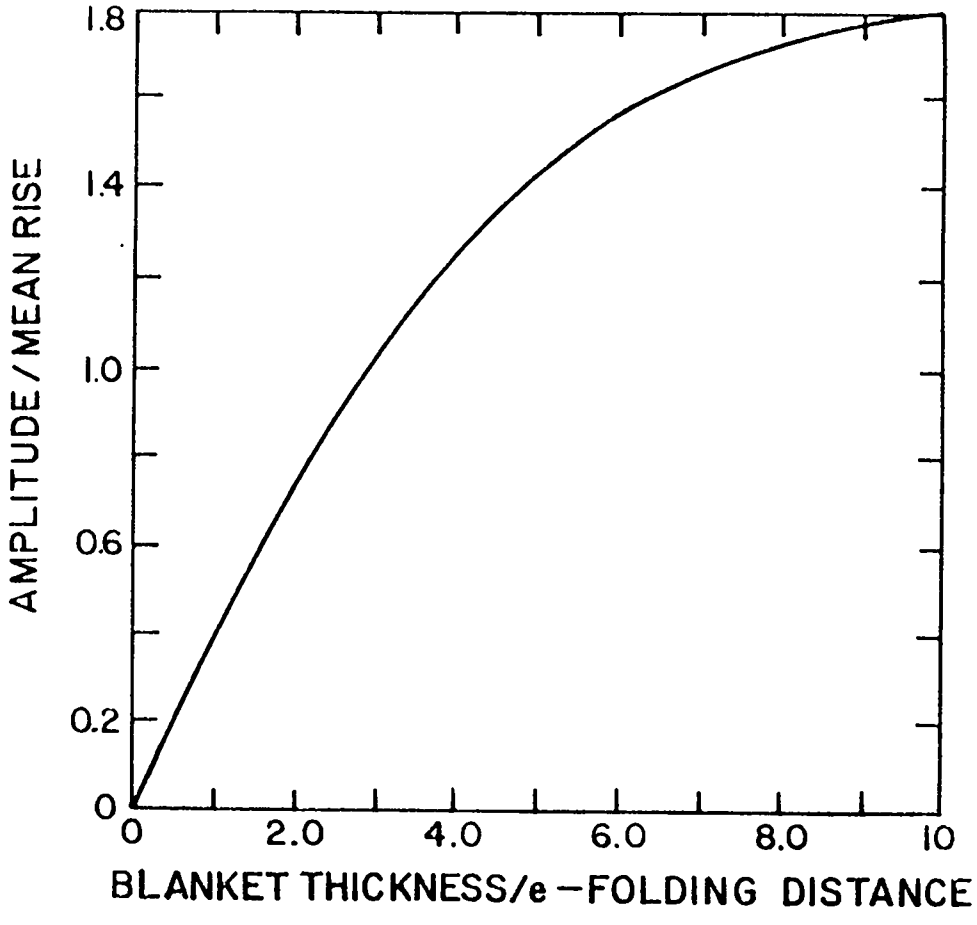

Fig. 2. Relative amplitude of the first harmonic component of the pressure wave in the blanket.

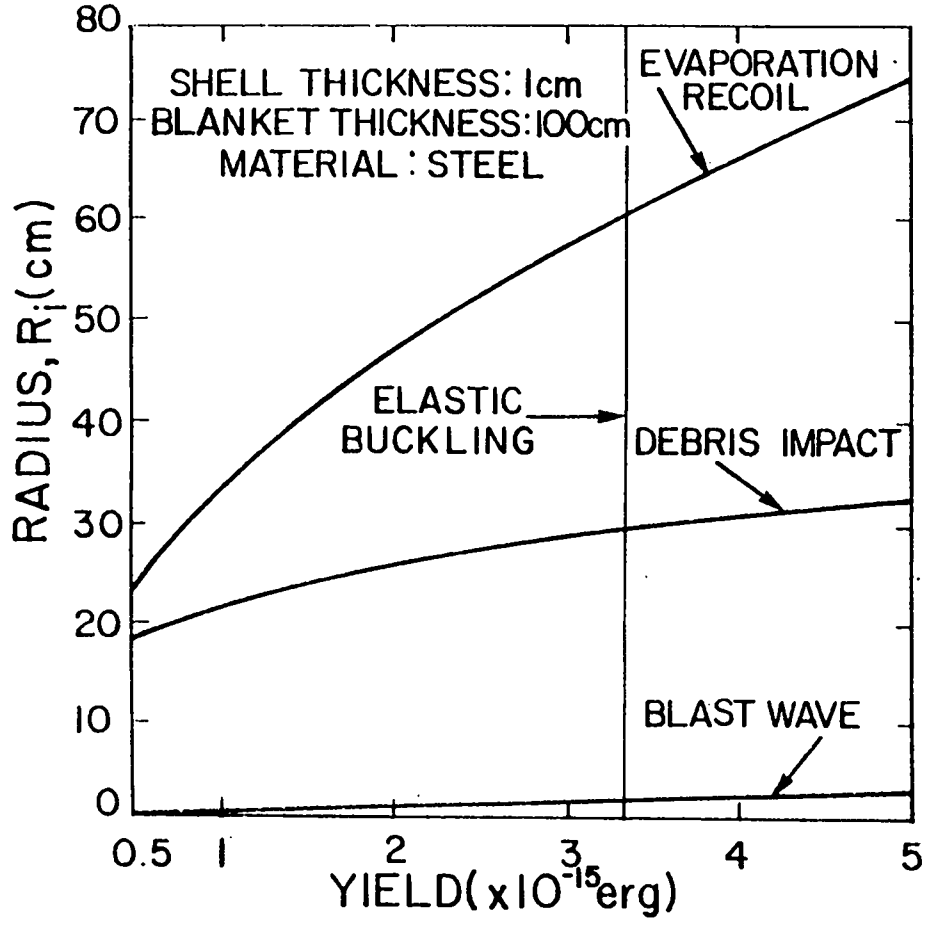

Fig. 3. Radius-yield relations for containment of anticipated laser fusion microexplosions.

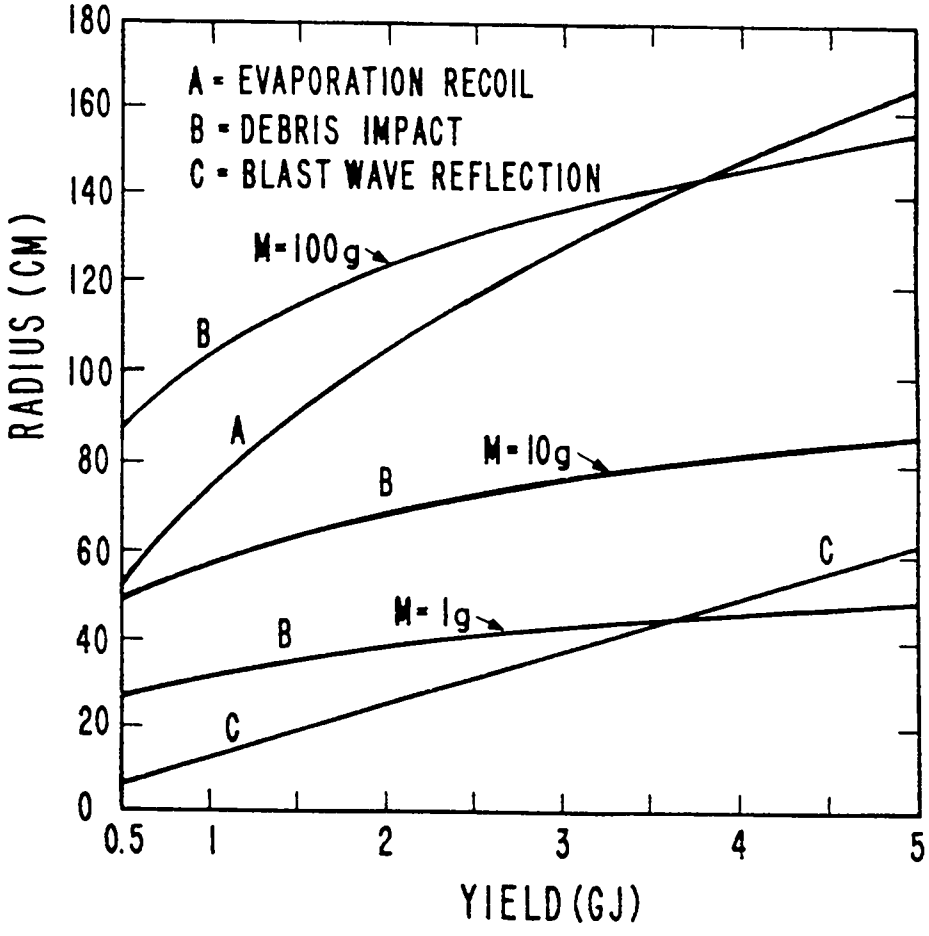

Fig. 4. Radius-yield relations for containment of fusion energy releases in the 1-5 GJ range.

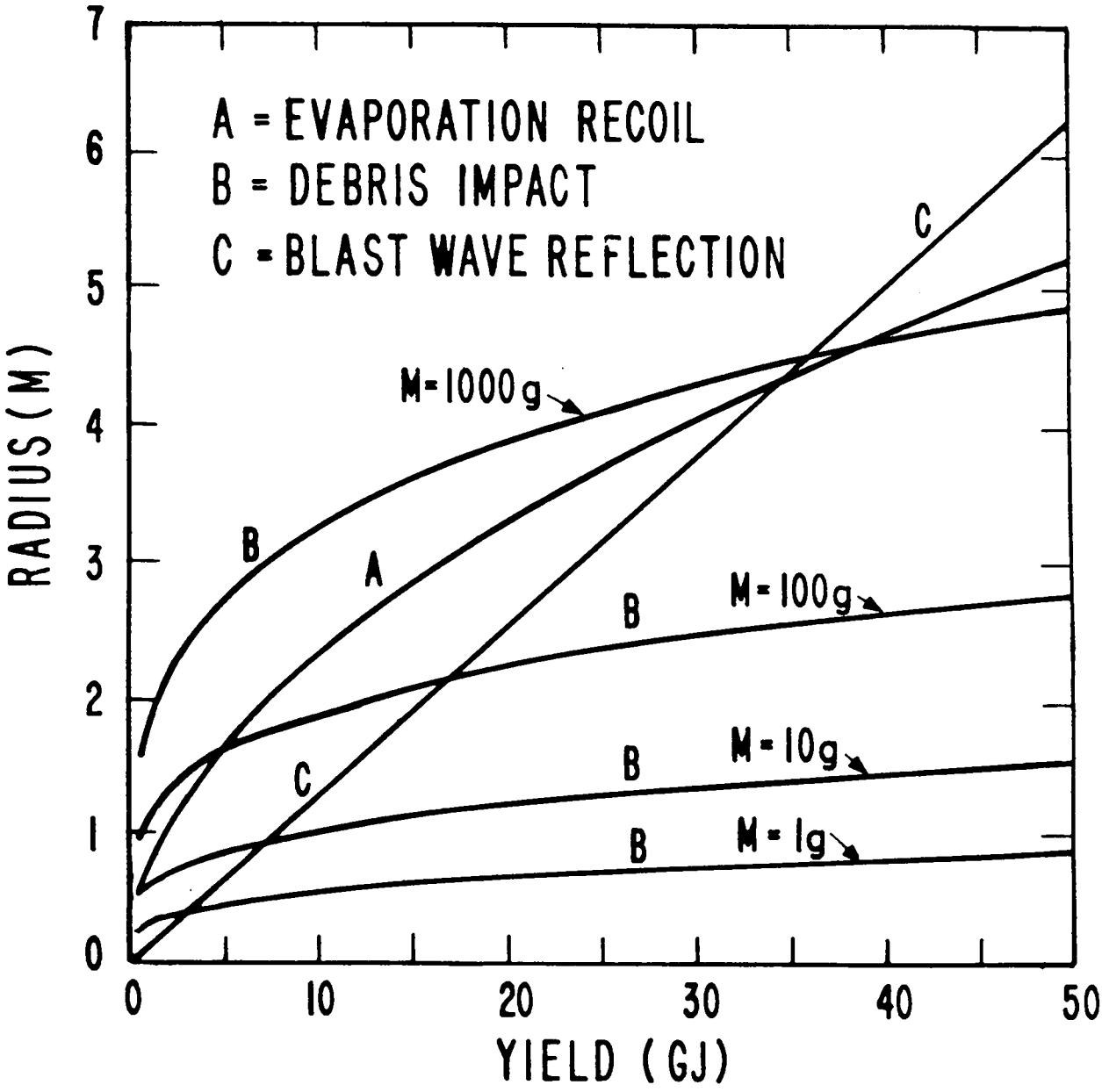

Fig. 5. Radius-yield relations for containment of fusion energy releases in the 5-50 GJ range.

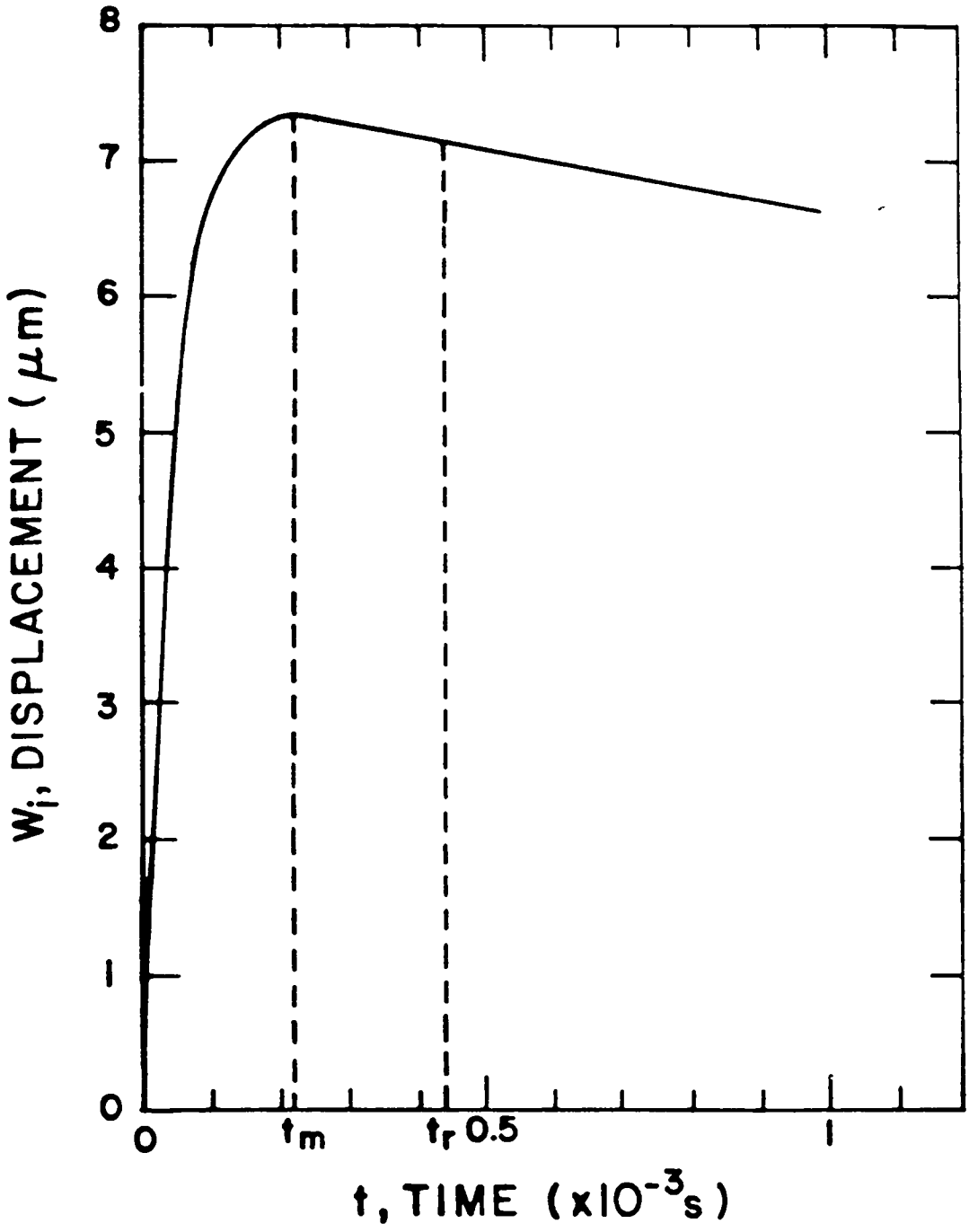

Fig. 6. Response of a structural shell in the presence of hydrodynamic coupling.

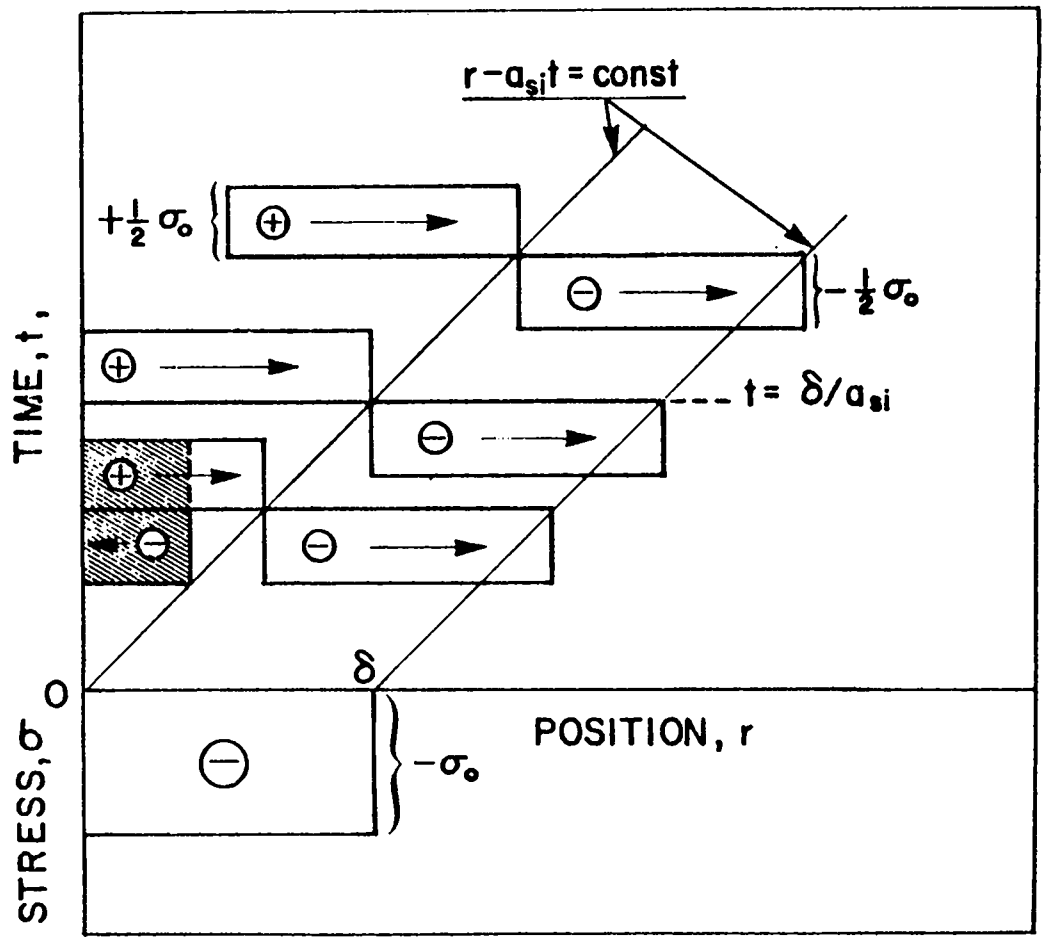

Fig. 7. Stress wave propagation (schematic) +: tensile, - compressive.

BLAST CONFINEMENT COMPUTATIONS FOR THE FAST-LINER REACTOR (FLR)

R. A. Krakowski, R. W. Moses, and J. D. Jacobson
University of California
Los Alamos Scientific Laboratory
Los Alamos, New Mexico 87545

I. INTRODUCTION

The conceptual Fast-Liner Reactor (FLR) envisages the use of magnetically-driven metallic liners for the adiabatic compression of a DT plasma to thermonuclear conditions.[1,2] The initial radius, length, and thickness of the cylindrical metal shell would be 0.2 m, 0.2 m and 3.0 mm, respectively. This shell would implode in 30 μs onto a cold and dense plasma in the presence of a thermally insulating magnetic field, causing an adiabatically-heated thermonuclear burn to occur for 1-2 μs. Detailed parametric burn calculations[1] gave optimized thermonuclear yields of 3.6 GJ for a liner energy input of 340 MJ. The plasma gain of Q = 10.7 is sufficient to predict a power plant with an overall recirculating power fraction of 0.25· higher gain systems appeared possible at the expense of additional energy input to the liner. Because of the large energy releases and the quantity of destroyed liner mass and electrical leads, blast containment was identified as an important issue for the FLR. Large fast-pulse energy releases and appreciable quantities of mass available to participate in this energy release may also be characteristic of the impact fusion approach to fusion. For this reason, the computational models and blast confinement schemes[1] investigated for the FLR are summarized; the FLR concept per se is not described here.

II. GENERAL CONSIDERATIONS FOR THE FLR BLAST-CONFINEMENT PROBLEM

As described in Ref. 1, a Li or LiPb spray or "rain"[3] would be injected around the liner to absorb a major part of the nuclear and kinetic energy release. A close coupling exists, therefore, between the requirements of radiation shielding, tritium breedion, thermal energy extraction, and blast containment/mitigation. Insofar as the latter issue is concerned, a number of coolant/blast-mitigating configurations have been considered:[1] bubble-impregnated liquid-metals, vacuum detonations, fluidized beds of blast-mitigating powders, liquid-metal first-walls, and liquid-metal sprays. Although the blast containment requirement shows a number of similarities with

beam/pellet fusion concepts,[4-6] the following significant differences are noted: a) the primary energy input to the liner is from one direction and does not require vacuum; b) the implosion time scales are considerably longer (μs versus ns); c) greater quantities of mass are disturbed and set into motion by the liner implosion; d) the possibility of large pieces of debris impacting structural components is greater for the FLR (and, possibly, for impact fusion schemes).

Approximately 20% of the fusion energy from the ~ 2-μs burn would be deposited in and near the liner by alpha particles and radiation. In addition, roughly 20% of the neutron energy is given directly to the dense, compressed liner. Lastly, approximately 1/Q of the fusion yield is retained as liner kinetic energy. Consequently, an energy equal to almost 50% of the fusion yield will appear on a ~ 2-μs time scale in the general vicinity of the liner; this potential contribution to a blast energy, W_B, corresponds to ~ 1.5 GJ for the optimized base case adopted here.[1] The remaining ~ 50% of the released thermal energy would be deposited in the lithium spray according to the neutron thermalization distribution. Although the sudden but distributed release of neutrons can lead to shocks in a liquid or liquid-gas mixture,[4] the ~ 50% release near the liner position will probably present a more serious containment problem and, consequently, has been made the focus of the blast-containment computations.

As a first step in quantifying the blast-containment problem, existing experimental data[7] have been employed in conjunction with a simple analytical model based upon the "virial theorem."[8,9] This simple approach has been used primarily to examine sudden, large energy releases in either vacuum or gas-bubble-laden liquids. For the latter case, substantial masses of liquid can be set in motion, leading to pressure amplification at the containment wall. In order to estimate this effect, a simple model of outgoing and reflected shock waves using the Hugoniot relationships[11] was developed. Lastly, a detailed time-resolution of shock spectra produced at the vessel wall was analyzed by means of a one-dimensional, Lagrangian-mesh hydrodynamics code, PAD[10] The computational models associated with and results from the "virial theorm", simple shock approximation, and the PAD hydrodynamics code approaches are described in the following sections.

III. VIRIAL THEORM APPROXIMATION FOR BLAST CONFINEMENT

As a preliminary approach to the blast-containment problem a convenient baseline for explosive containment is provided by the "virial theorem."[9] One form of this theorem[8] predicts that the mass M of a vessel needed to contain a gas or plasma of energy W must satisfy the relationship

$$M \geq 2\rho W/f\sigma \quad , \tag{1}$$

where ρ is the density of containment vessel, f is the number of stress components in the vessel wall (f = 2 for a spherical vessel of radius R and thickness ΔR), and σ is the maximum allowable stress. Taking $M = 4\pi R^2 \Delta R \rho$ and f = 2, Eq. (1) becomes

$$R\Delta R \geq (W/R)/4\pi\sigma \quad . \tag{2}$$

The relationship between tangential stress, σ, and strain, ε, for thin-walled spheres ($\Delta R << R$) is given by [12]

$$\sigma = E\varepsilon/(1-\nu) \quad , \tag{3}$$

where ν is Poisson's ratio, and E is Young's modulus. Substituting Eq. (3) into Eq. (2) gives the following expressions for the virial theorem if ε is expressed as microstrain

$$(\Delta R/R)\,\varepsilon \geq (1-\nu)\,(W/R^3)10^6/4\pi E$$

$$\geq 2.93(10)^{-7}(W/R^3) \tag{4}$$

$$\geq 1.85(M_{HE}/R^3) \quad ,$$

where $\nu = 0.3$, $E = 1.9(10)^{11}$Pa $(28(10)^6$psi), and M_{HE} has the units of

kg-equivalent high explosive (1.5 times the TNT equivalent, 4.2 MJ/kg). Equation (4) is compared to experimental data[7] in Fig. 1; these data were obtained at the inception of failure of spherical steel vessels that were subjected to gradually increased high-explosive charges up to ~ 20-kg mass. As seen from Fig. 1, the presence of blast-mitigating or shock-transmitting material within the vessel has a significant effect on the vessel response. The virial theorem shows good agreement with the vacuum case; the presence of air or other fluid media leads to shock formation, whereas the pulverization of vermiculite gives an important dissipative channel for blast energy.

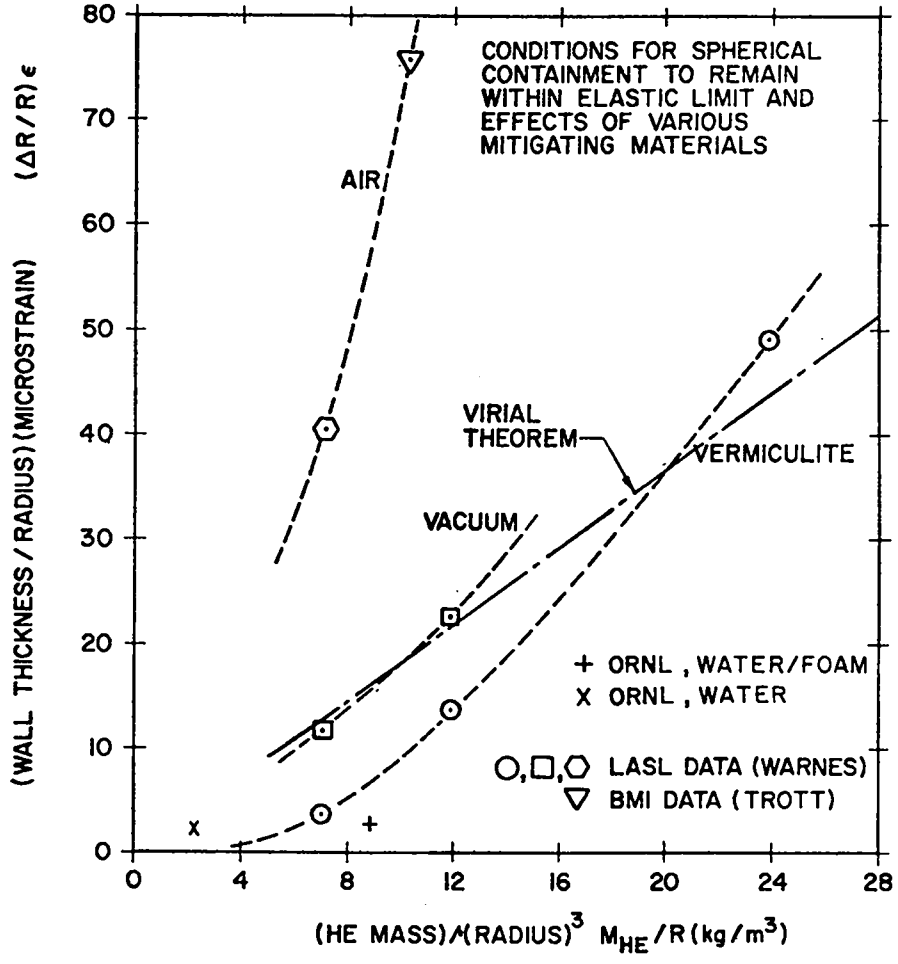

Fig. 1. Virial-theorem scaling of blast-confinement data using high-explosive detonations in spherical vessels. All data represent tests which measured only the onset of plastic deformation of the blast-containment vessel. ORNL (Ref.5), LASL (Ref.7), BMI (Ref.13).

A blast energy release of ~ 1.5 GJ (350-kg TNT, 230-kg HE) is expected for the base-case FLR design. Taking R = 2.5 m, M_{HE} = 230 kg, and ε = 3000 (failure limit for the steel vessels considered in Fig. 1, failure generally indicated by beginning of plastic deformation), the required single-shot vessel thickness would be ~ 20-25 mm for a "vacuum" or "vermiculite" response.

Although a few data points on Fig. 1 represent as many as 10 detonations of increasing magnitude, the vessels were always exposed to blast intensities that were sufficiently close to the failure threshold to preclude a serious investigation of many-cycle fatigue limits. The microstrain (ε = 3000) selected for the above evaluation of ΔR for R~2.5 m generally assures the plastic limit is not exceeded, but this microstrain is too large from the viewpoint of cyclic fatigue. The microstrain must be determined from the fatigue characteristics and desired fatigue life of the containment vessel. Coffin[14] has correlated the plastic strain, $\Delta\varepsilon_p$, and elastic strain, $\Delta\varepsilon_e$, with material properties and the number of cycles to failure, N_f, according to the following relationships

$$\Delta\varepsilon_p = C_2 \nu_c^{B(1-k)} / N_f^{\beta} \qquad (5)$$

$$\Delta\varepsilon_e = (A'/E) \nu_c^{k'} / N_f^{\beta'} \quad , \qquad (6)$$

where $\varepsilon \simeq \Delta\varepsilon_p + \Delta\varepsilon_e$, and the constraints for 304 stainless steel at 800 K and 934 K are summarized in Table I. The last two entries in Table I are the

TABLE I

SUMMARY PARAMETERS USED TO FIT ANALYTICALLY 304 STAINLESS STEEL FATIGUE DATA,[14] EQS. (5) AND (6)

CONSTANT	800 K	900 K
C_2	$0.300(10)^6$	$1.108(10)^6$
B	0.410	0.707
k	0.93	0.81
A′	$5.29(10)^{11}$	$2.26(10)^{11}$
E	$23.4(10)^6$	$21.6(10)^6$
k′	-0.02	0.089
β′	0.20	0.187
$\varepsilon[N_f = 2.5(10)^6]$	1898	823
$\varepsilon[N_f = 2.5(10)^7]$	1016	516

microstrains evaluated at the respective temperatures for failure after one year ($N_f = 2.5(10)^6$) and ten years of operation for a 10-s cycle time and an 80% plant factor. Taking the 800-K values, based upon corrosion limits, a ten-year lifetime would require $\Delta R \geq 75$ mm for the above FLR conditions ($R = 2.5$ m, $M_{HE} = 230$ kg).

The use of the virial theorem in conjunction with an idealized spherical geometry provides a lower limit for the blast-confinement problem, although the agreement with the experimental "vacuum" data on Fig. 1 lends confidence to this approach. Consideration of the vessel geometry anticipated for an actual engineering structure (i.e., stress concentration points, penetrations, acoustical responses, etc.) in conjunction with the formation of shocks will undoubtedly lead to somewhat larger vessel dimensions. The effect of shock generation in an intervening medium is examined in the following section.

IV. STRONG-SHOCK APPROXIMATION FOR BLAST CONFINEMENT

The FLR design originally envisaged the use of a He-bubble-impregnated LiPb bath to attenuate the post-implosion blast. This system is shown schematically in Fig. 2, which also shows systems that might operate in vacuum or with a fluidized bed of blast-mitigating material. For the former case the blanket must surround the vacuum vessel, whereas the fluidized bed might contain a

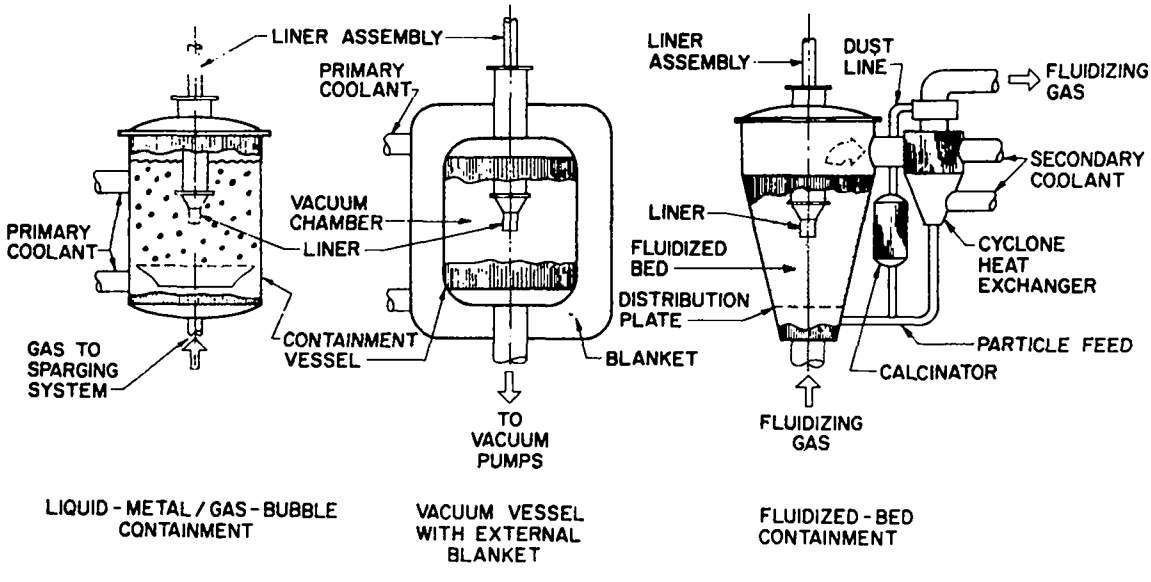

Fig. 2. Schematic diagrams of several blast containment and primary coolant schemes considered for the FLR.

lithium-bearing oxide with shock-mitigating properties similar to vermiculite (Fig. 1). The LiPb/He containment scheme is addressed here and is shown at best to respond according to the virial-theorem predictions.

A. DEVELOPMENT-OF SHOCK MODEL

A simple model was developed to consider spherical shocks in liquid-gas mixtures. Specifically, a lead-lithium mixture is considered for the primary coolant and tritium breeding, and helium bubbles are assumed to be present for shock mitigation. Dresner[4] has suggested that shock mitigation would be enhanced by creating helium bubbles in the liquid metal. The lead-lithium mixture is treated as an incompressible fluid and the helium as an ideal gas. Initially the helium occupies a fraction f_{He} of the mixture volume. For $f_{He} \ll 1$ the helium is simply considered as a fine dispersion of bubbles, and for $f_{He} \lesssim 1$ the lead-lithium is assumed to be in the form of a shower or mist of droplets; this latter case is treated more thoroughly in Sec. V.

The 14.1-MeV neutron heating will form a substantial shock in pure lithium for the fusion yields considered here, but a small fraction of helium bubbles should easily mitigate that shock.[4] Most of this neutron energy heats the liquid-metal coolant/breeder. Thermal expansion of the liquid metal is easily accomodated by the bubbles with little accompanying pressure-volume work; most of the neutron energy, therefore, remains as thermal energy in the lithium breeder. The post-burn energy in the plasma and vaporized liner debris is of primary concern; the decompression of hot gas and plasma can perform far more work than a corresponding decompression of the neutron-heated coolant.

The energy W_B is assumed to heat an ideal gas or plasma of radius r_{10} equal to the initial liner radius. For the $\ell = 0.2$-m-long cylindrical liner, this explosive energy is ≥ 1.0 GJ, and the initial fireball or blast radius is taken to be ~ 0.20 m. An adiabatic expansion of the plasma is assumed. Setting the specific-heat ratio, γ, equal to 5/3 for this hot gas and defining r_i as the time-dependent inner radius of the post-implosion cavity created in the liquid-metal, the plasma pressure P_i as a function of r_i becomes

$$P_i = P_o(r_{10}/r_i)^5, \quad P_o = W_B/2\pi r_{10}^3 . \tag{7}$$

It is further assumed that a single shock travels from r_{10} to the radius of the vessel wall, R, where a second shock is formed and returns to the plasma/liquid-metal interface. The highest pressures on the vessel wall would occur during this inward motion of the reflected shock. In order to model the shock motion, the following definitions are made.

r_s = radial postion of shock (m)
u_s = radial velocity of shock (m)
u_p = fluid velocity behind shock (m/s)
P_a = ambient pressure of LiPb-He mixture (Pa)
V_L = specific volume of liquid LiPb (m^3/kg)
V_a = specific volume of ambient LiPb-He(m^3/kg)
f_{He} = initial helium fraction = $1-V_L/V_a$
P_s = pressure directly behind shock (Pa)
V_s = specific volume behind shock (m^3/kg)
E_a = ambient specific energy (J/kg)
E_s = specific energy behind shock (J/kg)

Figure 3 depicts the geometry and associated notation.

Conservation of energy and momentum are used to derive the Hugoniot equations[11]

$$u_s = V_a \left[(P_s - P_a)/(V_a - V_s)\right]1/2 \tag{8}$$

$$u_p = u_s(1-V_s/V_a) \tag{9}$$

$$E_s - E_a = (P_a + P_s)(V_a - V_s)/2 \tag{10}$$

An equation of state (EOS) is needed to complete the relationship between properties at each side of the shock. Two significantly different EOS models are postulated and used. The first EOS model requires that the total increase in specific energy across the shock heats only the helium bubbles and is described by

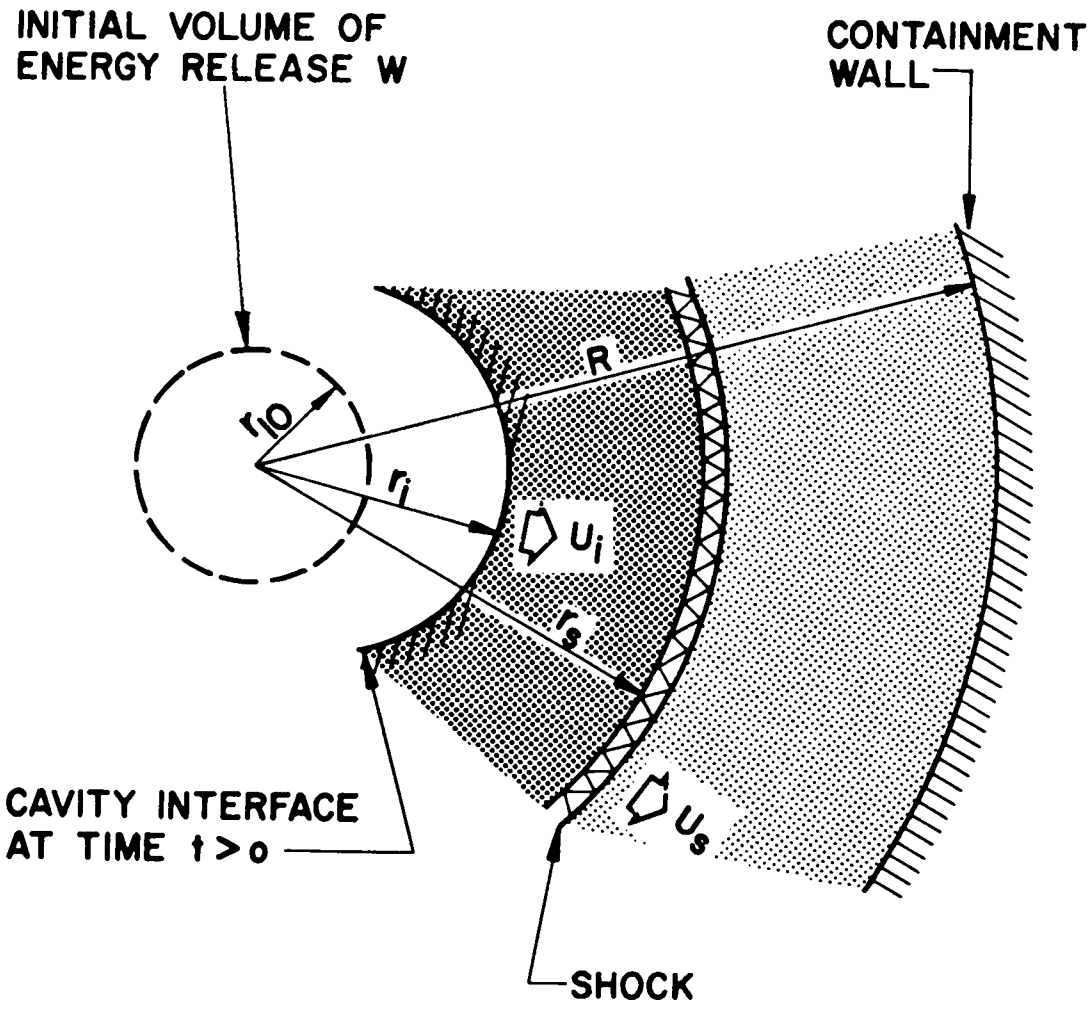

Fig. 3. Schematic diagram of simple shock model used to describe the pressure loading of a thin spherical containment shell subjected to the reflection of a coherent shock generated in a liquid/gas mixture.

$$P_s V_s^{\gamma} = P_a V_a^{\gamma} \quad . \tag{11}$$

The second EOS model assumes that the shock heats the liquid metal, and the helium bubbles are adiabatically compressed according to

$$E_s - E_a = (3/2)\left[P_s(V_s - V_L) - P_a(V_a - V_L)\right] \quad . \tag{12}$$

To complete the simple shock model the equation of motion for the shock the momentum and conservation of mass equations are introduced

$$\rho_s(du_p/dt) + \nabla P_s = 0 \tag{13}$$

$$\Delta\cdot(\rho u_p) + \partial\rho/\partial t = 0 \quad . \tag{14}$$

The simplifying assumption is made that, once a volume element is compressed by passage of the shock, the specific volume, V_s, does not change thereafter (i.e., $d\rho/dt = dV_s/dt = 0$). This assumption allows Eq. (14) to be replaced with the relation

$$r^2u_p = r'^2u_p' \quad , \tag{15}$$

where r and r′ represent any two points behind the shock. Since fluid velocities and accelerations at all points can be related to the shock position, Eq. (13) can be integrated over radius to yield an ordinary differential equation rather than a partial differential equation; this assumption greatly simplifies the numerical solution.

Undoubtedly a number of inconsistencies arise as a result of the assumption that $d\rho_s/dt = 0$ after passage of the shock. For instance, the resulting model does not apply to shocks in purely gaseous media, where compressed gas behind a shock would expand as the driving pressure decreases (Eq. (7)). When a liquid-gas mixture is shocked, such an expansion will certainly be reduced if not reversed. The hot compressed gas would lose heat to the liquid and be less able to expand as described above.

Defining the following quantities

$$G = r_s \int_{r_i}^{r_s} (\rho_s/r_s^2)dr \tag{16}$$

$$H = r_s^4 \int_{r_i}^{r_s} (\rho_s/r_s^5)dr \quad , \tag{17}$$

and combining Eqs. (8), (9), (10), (13), (16), and (17) results in the following expression for the particle velocity u_p.

$$du_p/dt = - \left[(P_s - P_i)/G + 2u_p^2(1-H/G-1/(1-V_a/V_s))\right]/r_s \qquad (18)$$

A numerical procedure combines Eqs. (7), (8), (9), (10), (11), and (18) and solves for $r_s(t)$.

The description of the reflected shock is simplified here to give an average pressure during its reverse transit across the fluid. This model is coupled with the appropriate EOS to solve for an average pressure during reflection, $\bar{P}_r$. The quantity t_{ra} is defined as the time for the outgoing shock to impact the vessel wall, and t_{rb} is defined as the time for the reflected shock to reach the inner surface of the fluid. The average specific volume of the reflected shock is $V_r = 4/3\pi\left[R^3 - r^3(t_{rb})\right]/M_L$, where M_L is the total fluid mass. It is easily shown that

$$\bar{P}_r \simeq \frac{u_p(t_{ra})\left[R^2/r^2(t_{rb}) - 1\right]}{V_r(t_{rb} - t_{ra})} \quad . \qquad (19)$$

Equation (19) is combined with Eq. (11) or Eq. (12) to solve for $\bar{P}_r$.

B. COMPUTATIONAL RESULTS

The computational results are shown in Fig. 4. The tension in the vessel wall, $T = \bar{P}_r/R$ is compared to the viral-theorem result $T_v = W/2\pi R^2$. The ratio T/T_v is equal to the ratio of respective tangential stresses σ/σ_v and in Fig. 4 is presented as a function of the helium fraction f_{He} for the following conditions: W_B = 1.13 GJ; ρ_L = 9400 kg/m^3; R = 2.3 m; and r_{10} = 0.2 m or 2 m. The two EOS models give surprisingly similar results. A shock-heated gas is compressed to no less than 25% of its original volume; however, a much greater compression occurs when a portion of the shock energy is also delivered to the liquid metal. Typically the shocked helium would then occupy only a few percent of its original volume. Even with this significant difference the results agree to within an order of magnitude for any given value of f_{He} and r_{10} = 0.2 m.

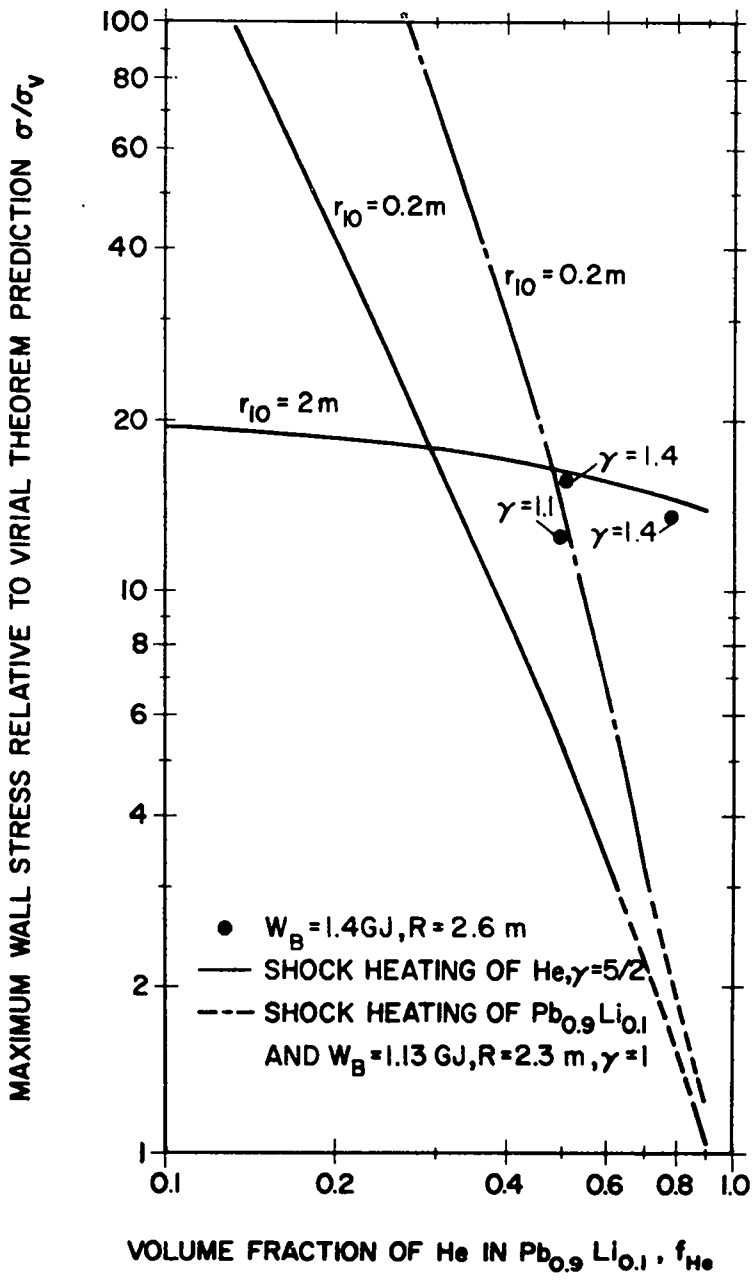

Fig. 4 Dependence of maximum wall stress relative to predictions of the virial theorem as a function of the bubble void fraction. The energy released at the center of the spherical vessel is W_B, the vessel radius is R and the specific heat ration of the gas is γ. Shown also as points are results for similar conditions from the hydrodynamic code PAD. (Ref. 10, Sec.V).

These results do not show a stress reduction such as that given by vermiculite (Fig. 1). Although these computational results show that shock heating can dissipate over 98% of the blast energy, sufficient momentum is generated in the liquid metal to produce substantial wall stresses compared to

the predicitions of the virial theorem. Two complementary phenomena appear to be in effect. When the helium is highly compressed, as for the EOS model described by Eq. (12), a larger amount of energy is dissipated in the shock. When this more dense mixture (as compared to the EOS model described by Eq. (11)) strikes the wall, the shock reversal is more sudden because of the smaller second compression that can occur.

The hydrodynamic computational results from the PAD code do not support the predictions of an increase in wall stress, corresponding to the reduction of γ. The maximum stresses computed with the PAD code for a 1.46-GJ blast with R = 2.6 m were converted in terms of σ/σ_v and incorported in Fig. 4. Since W_B and R differ slightly between the two computations, comparision is not entirely justified, but trends are indicated. The PAD results with $f_{He} = 0.5$ fall close to the $\gamma = 1$ curve of the simple shock model; however, stresses increase with γ according to the PAD model rather than decrease. Also, the PAD results do not show the sharp decrease in σ/σ_v as f_{He} approaches unity, as illustrated by the $f_{He} = 0.8$, $\gamma = 1.4$ point on Fig. 4. Most of these discrepancies probably arise because the simple shock model does not allow for expansion of shocked gas (i.e., $d\rho_s/dt = 0$).

V. HYDRODYNAMIC CODE APPROXIMATION FOR BLAST CONFINEMENT

Of primary interest to quantifying the blast-containment problem, beyond the limits of the simple models described in the previous sections, are the time-resolved shock spectra produced at the vessel wall by the equivalent blast-energy release W_B. The computer code PAD[10] was used to compute in one-dimensional (spherical) Lagrangian coordinates the motion of explosive gases and the mechanical response of the spherical container. Radiation heat transfer and thermal conduction within the ~ 1-GJ blast created at the initial liner location were not considered; asymmetry effects that may be induced by support structure were also not included. Consistent with the sample operating points, blast energies in the range 0.70 to 2.26 GJ were studied. The results of the PAD computations can be accurately scaled to other vessel sizes and energy releases by use of the following thin-shell stress/strain relationships.[12]

$$\sigma_\Theta = W_B/4\pi R^2 \Delta R \qquad (20A)$$

$$\varepsilon_\Theta = [(1-\nu)\sigma_\Theta + \nu\sigma_r]/E \qquad (20B)$$

The blast energy, W_B, is equal to 1.4 GJ for most of the PAD computations. This energy was assumed to be deposited in a sphere with the density of solid copper ($8.92(10)^3$ kg/m^3) located at the center of containment vessel. For the purposes of this analysis M is defined as the mass of destroyed structure that shares the energy W_B and contributes ultimately to the shock spectrum at the container walls. Based upon the scaling of experimental data from blasts in evacuated vessels (Sec.III), the radius R of the containment sphere is estimated to be 2.6 m if the wall thickness ΔR is 0.15 m when W_B = 1.4 GJ. The density and Young's modulus of the containment vessel are taken to be those of 304 stainless steel ($\rho = 7.86(10)^3$, kg/m^3, E = 160 GPa). The vessel was not allowed to yield in the PAD computations. When the yield stress is exceeded in a computational result, ΔR is scaled according to Eq. (20A) to reduce the stress to acceptable levels.

A. VACUUM VESSEL RESPONSES

The first PAD computations were made for W_B = 1.4 GJ released in an evacuated sphere. Two time histories of radial and circumferential stresses (σ_r and σ_Θ, respectively) are shown in Fig. 5 for blast-products masses M of 25 kg and 200 kg, respectively. The vessel oscillates at a frequency of f_v = 475 Hz that is independent of ΔR in accordance with the thin-shell approximation. The reverberating gas within the vessel oscillates at a frequency f_g that is proportional to $M^{-1/2}$. Since energy losses are not included in these computations, the radial stress asymptotically approaches the equilibrated pressure corresponding to a uniform distribution of the initial blast energy W_B.

The maximum circumferential or hoop stress, σ_Θ, is plotted as a function of M in Fig. 6. This stress is nearly constant for small values of M where $f_g >> f_v$. For this situation the gas pressure at the vessel wall, σ_r, oscillates and is ultimately damped to the pressure of a quiescent gas with energy W_B. Meanwhile, the vessel moves nearly as a harmonic oscillator from a condition of zero stress to a maximum stress. The average hoop stress will support the pressure of a quiescent gas of energy W_B (Eq. 20A)). Since the shell oscillates harmonically from zero to a maximum, the peak stress is approximately twice the average stress. This approximation fails when the explosive gas and shell come into resonance at $f_g \simeq f_v$, as seen for the M = 200-kg case in Figs. 5 and 6. In this case the maximum stress is 77% higher than the value given by the above-mentioned approximation.

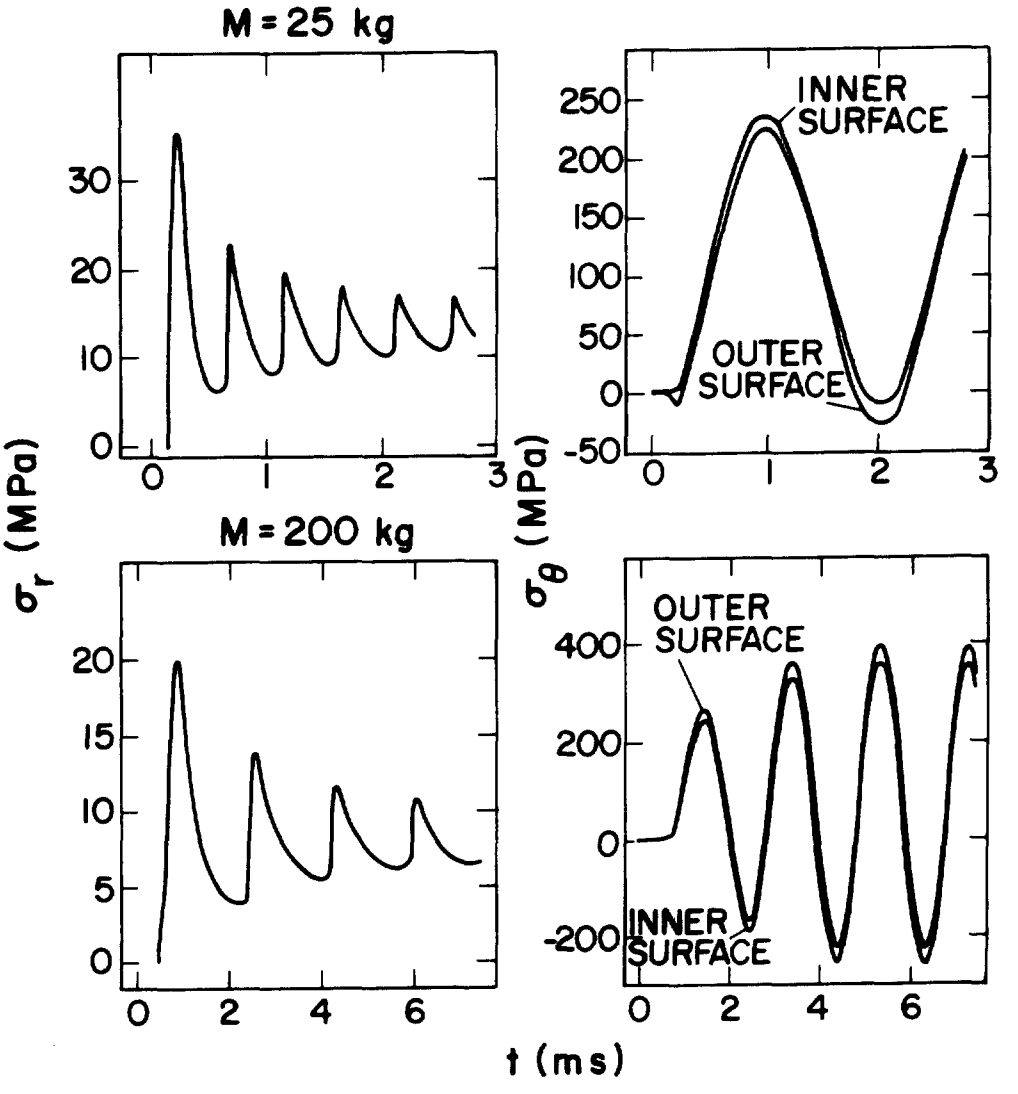

Fig. 5. Time dependence of radial (σ_r) and hoop (σ_θ) stress for a vacuum energy release of 1.4 GJ in a spherical vessel of 2.6-m radius and 0.15-m wall thickness. The mass that contains this energy is M. These results can be scaled to other vessel dimensions (R,ΔR) by Eq. (20A).

Based on fatigue data for stainless steel,[14] a peak strain of $\varepsilon_\theta = 1.016 \times 10^{-3}$ appears acceptable for a 10-yr life $(2.5(10)^7$ shots every 10 s for an 80% plant factor) at 800 K. By taking $\upsilon = 0.29$, $\sigma_r = 20$ MPa, and E = 160 GPa, Eq. (20B) is used to give the maximum acceptable circumferential stress σ_θ; the vessel wall thickness ΔR is then scaled to an appropriate value. For the M = 25 and 200-kg cases in Fig. 5 the ΔR values with acceptable fatigue strain are 0.16 and 0.27 m, respectively.

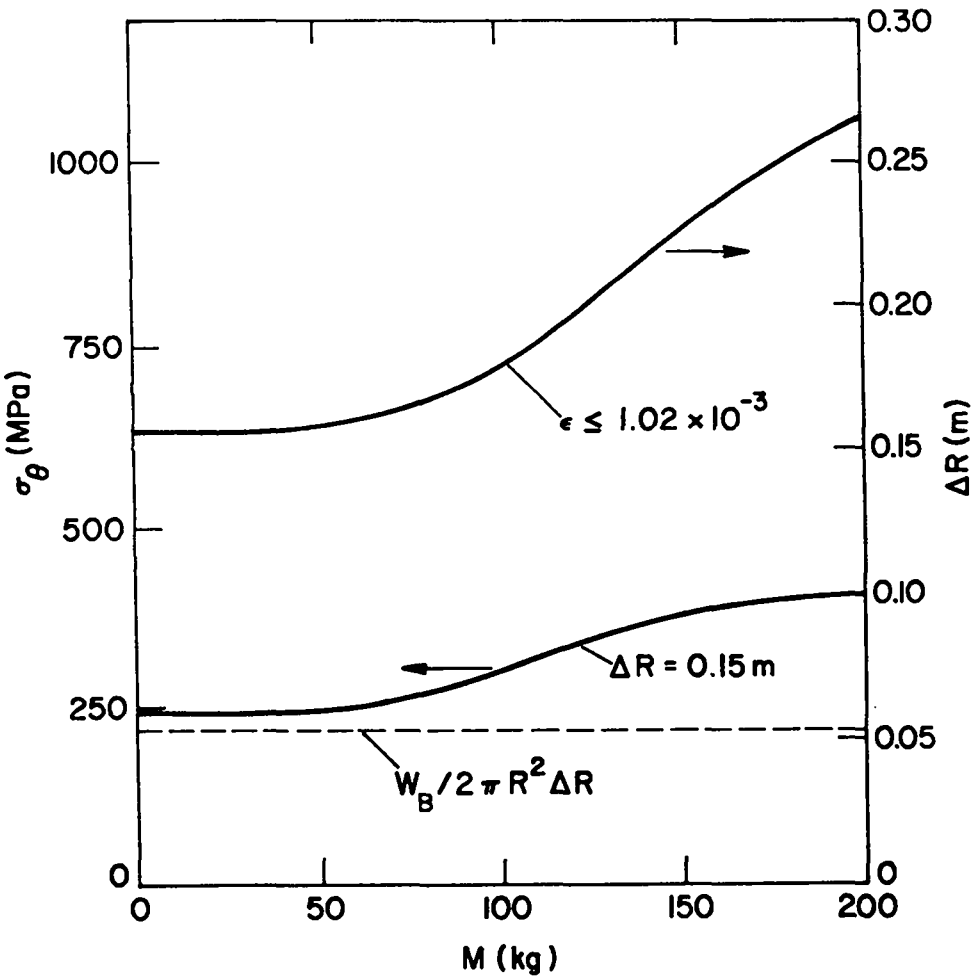

Fig. 6. Dependence of maximum hoop stress, σ_θ, on mass M assigned to a vacuum release of 1.4-GJ energy for either fixed strain, ε, or a fixed vessel thickness ΔR. The vessel radius is R = 2.6 m. Dashed line indicates virial theorem prediction, multiplied by 2 to account for shell oscillations, Eq. (20A).

B. RESPONSE OF VESSELS WITH LIQUID-GAS MIXTURES

The PAD code was also used to model blast containment in a liquid-gas mixture. Both fast liner[1] and laser[4] fusion reactor studies have proposed the use of Li (or LiPb) spray for tritium breeding and neutron moderation. If a fast liner were immersed in a purely liquid environment, the shock wave created in the liquid would present intolerable stress amplification at the containment walls (Sec.IV). On the other hand, the shock may be substantially mitigated by mixing a compressible gas with the liquid.[4] The time histories of three PAD computations are shown in Fig. 7. The blast energy is again fixed at 1.4 GJ, and the 304 stainless steel vessel dimensions are R = 2.6 m and ΔR = 0.15 m. A LiPb mixture of $9.4(10)^3$ kg/m^3 density at ~ 870 K is dispersed through the

vessel with f designated as the volume fraction. The volume fraction 1-f is filled with helium at atmospheric pressure. The liquid is assumed to be incompressible, and the helium is regarded as an ideal gas with the heat capacity ratio, γ, treated as a free parameter. Hence, when subjected to a volumetric compression, κ, the helium gas would follow the relationships: P/κ^{γ} = constant and $T/T_o = \kappa^{\gamma-1}$, where T_o is the initial (pre-shot) helium temperature. An artificial viscosity term in the PAD computation produces non-adiabatic heating across the shock fronts which traverse the LiPb/He mixture.

The radial and hoop stresses as functions of time are shown in Fig. 7 for the indicated combinations of γ and f. These results show the sensitivity of the vessel stress response to the assumed value of liquid volume fraction f and the γ values of the gas phase. For γ = 5/3 all compressive energy entering the gas-liquid mixture would ultimately heat the gas. Correspondingly, compression of the gas would be isothermal if γ = 1, which is a circumstance that simulates an immediate transfer of thermal energy to the liquid metal. The first example in Fig. 7 (γ = 1.4, f = 0.2) results in a peak hoop stress of σ_θ = 1200 MPa for ΔR = 0.15 m or a requirement that ΔR be increased to 0.9 m, according to Eq. (20B) if a 10-y fatique constraint at 800 K is imposed. Unlike the vacuum containment cases (Fig. 5), the largest wall stresses occur in a short pulse followed by smaller oscillatory stresses.

For the second case given on Fig. 20 γ is again taken to be 1.4 but the liquid volume fraction is increased to 0.5. The peak hoop stress increases to 1400 MPa for ΔR = 0.15, or a requirement of ΔR = 1.2 m results if a 10-y fatigue constraint is imposed at 800 K. Simple scaling arguments indicate that the momentum impulse at the wall, $\int \sigma_r dt$, will increase roughly as $f^{1/2}$, but the associated increase in impulse duration makes σ_θ relatively insensitive to f. This prediction is borne out by the 17% increase in σ_θ when f increases by 150%.

The third example in Fig. 7 shows the effects of a reduction in γ from 1.4 to 1.1 while f is held constant at 0.5. This model simulates the rapid transfer of shock energy to the liquid metal (i.e., the $\gamma \to 1$ limit). Since the helium temperature rise is smaller for a given compression when γ is decreased from 1.4 to 1.1, the liquid-gas mixture is more easily compressed. A somewhat smaller momentum is transferred to the liquid metal, and a reduced stress occurs at the vessel wall; this hoop stress equals 1100 MPa and corresponds to ΔR = 0.9 m to assure an acceptable stress.

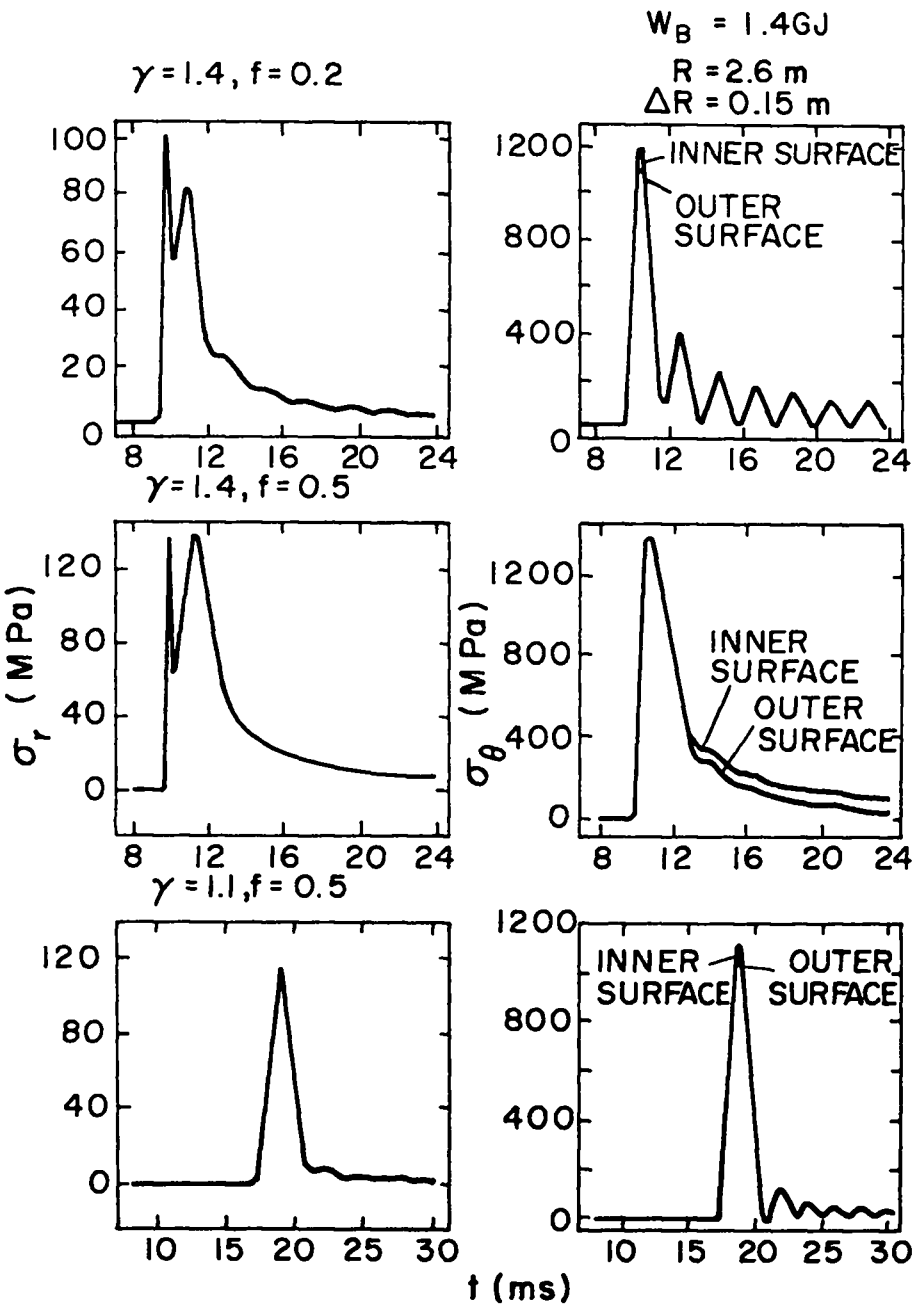

Fig. 7. Time-dependence of radial (σ_r) and hoop (σ_θ) stress for a 1.4-GJ blast energy release to a M = 25-kg mass in a gas (He)/liquid (LiPb) mixture contained in a R = 2.6-m, ΔR = 0.15-m spherical vessel that is initially pressurized to 0.1 MPa. The initial volume fraction of liquid is f, and γ is the heat capacity ratio for the gas.

All cases shown in Fig. 7 exhibit a sharp stress pulse with a duration of ~ 3 ms. This intense, initial pulse could be reduced in peak intensity and spread out in time by a blast-attenuating structure attached to the inside wall

of the containment vessel. For example, the shock velocity is ~ 100 m/s and the particle velocity is ~ 50 m/s at the time the shock impacts the structural wall. By placing rib-like structures on the inner walls that are 0.3-m high and filling 50% of the local volume, the duration of impact may be increased by a factor of ~ 2, which in turn would cause the maximum hoop stress, σ_θ, to be reduced by a comparable amount. Blast attenuators, therefore, may significantly reduce the overall structural requirements placed on the containment vessel.

VI. CONCLUSIONS

For 1.13-GJ explosive energy releases, the virial theorem predicts that the wall thickness $\Delta R \simeq 28$ mm for a containment vessel radius R = 2.0 m based upon a "single-shot" criterion (microstrain $\varepsilon = 3000$). Consideration of cyclic fatigue constraints (for 304 stainless steel) leads to a 2.5-m-radius vessel with $\Delta R = 75$-mm wall thickness (10-s cycle time for a 10-y life and an 80% plant factor). The virial theorem predicts surprisingly well experimental data from vacuum detonations in spherical steel vessels. Using the virial theorem to scale experimental data from detonations in air-filled vessels results in significantly increased vessel wall thicknesses presumably because of momentum amplification by shock propagation in the gaseous medium.

A simple shock-propagation model was developed to investigate the shock mitigation properties of He-bububble-containing lead-lithium liquid alloy. Bubble fractions could not be found that resulted in containment-vessel wall stresses that are below the predictions of the virial theorem (vacuum medium); the acceleration of the lead-lithium mass causes significant pressure amplification for all He-bubble fractions considered by this simple model for both extreme EOS models used to describe the two-phase system.

A one-dimensional hydrodynamic code (PAD) was used to model gas-liquid mitigators. Good agreement was observed between PAD and the simple shock models for equal initial volume fractions of gas and liquid, but wide discrepancies occur for small liquid fractions. Until more complete theoretical and/or empirical data are available, the most reliable results are for equal liquid-gas mixtures.

The foregoing analyses of blast containment is based on a number of simplifying assumptions. Present theoretical predictions and extrapolation of the existing data base should be treated as imprecise until experimental tests are made for much higher blast energies. The general scale of blast requirements has been quantified, however, and appears to be technologically

feasible. Generally, 2.5- to 3.0-m-radius containment vessels with 0.3- to 0.5-m-thick walls appear adequate to contain the ~ 1.5 GJ of thermal energy expected to be released every ~ 10 s; these dimensions are adequate for a ~ 10-y fatique life at 800 K for stainless steel. By proper vessel design (physical shock attenuators) and selection of blast-mitigating media, the uncertainties associated with the models used to generate these results can be counteracted. The need to build additional conservatism into the vessel design will become more apparent when the effects of long-term radiation damage and the realities of actual engineering structures (penetrations, weldments, etc.) are examined.

REFERENCES

1. R. W. Moses, R. A. Krakowski, and R. L. Miller, "A Conceptual Design of the Fast-Liner Reactor (FLR) for Fusion Power," Los Alamos Scientific Laboratory report LA-7686-MS (February 1979).

2. R. W. Moses, R. A. Krakowski and R. L. Miller, "Fast-Imploding-Liner Fusion Power," Proc. 3rd ANS Meeting on the Technology of Controlled Nuclear Fusion, CONF-780508, 1, 109, Santa Fe, NM (May 9-11, 1978).

3. C. A. Kot, "Shock and Blast Loads in Large Pulsed Inertial Confinement Fusion Reactors," Argonne National Laboratory report ANL/CTR/TM-44 (June 1975).

4. L. Dresner, "Mechanical Stress in a Pressure Vessel of a Lithium-Filled, Exploding Pellet Thermonuclear Reactor," Oak Ridge National Laboratory report ORNL-TN-4050 (1973).

5. A. P. Fraas, "The BLASCON-An Exploding Pellet Reactor," Oak Ridge National Laboratory report ORNL-TN-3231 (July 1971).

6. J. Maniscalco, J. Blink, J. Hovingh, W. Meier, M. Monsler, and P. Walker, "A Laser Fusion Power Plant Based on a Fluid Wall Reactor Concept," Proc. 3rd ANS Meeting on the Technology of Controlled Nuclear Fusion, CONF-780508, 1, 483, Santa Fe, NM, (May 9-11, 1978).

7. T. R. Neal, and R. H. Barnes, personal communication, Los Alamos Scientific Laboratory (1977)

8. R. W. Moses, "Flywheel Energy Storage," Phys. Today 15 (October 1975).

9. C. L. Longmire, Elementary Plasma Physics, Interscience Publishers, NY (1963).

10. W. Fickett, "PAD, A One-Dimensional Lagranian Hydrocode," Los Alamos Scientific Laboratory report LA-5910-MS (April 1975).

11. R. H. Rice, R. G. RcQueen, and J. R. Walsh, "Compression of Solids by Strong Shock Waves," Solid State Physics 6, 1-60 (1958).

12. S. Timoshenko, and J. N. Goodier, Theory of Elasticity, 2nd Ed., McGraw-Hill Book Co. (1951).

13. B. D. Trott, J. E. Bachofen, and J. J. White, III, "The Design, Evaluation and Delivery of a Prototype, Trailer-Mounted Chamber Capable of Complete Containment of the Blast from Forty Pounds of TNT," Final Report, Contract NOO174-74-C-0218, Battelle Memorial Institute, Columbus Laboratories, (September 1975).

14. L. F. Coffin, "Fatique at High Temperature-Predictions and Interpretation," Proc. Inter. Mechanical Engineers, (London), 188, 103 (1974).

RAILGUN OVERVIEW

R. A. Marshall
Center for Electromechanics
The University of Texas at Austin

1.0 INTRODUCTION

The rail gun work done in Canberra (1) (2) has shown that it is possible to electromagnetically accelerate solid projectiles to interesting velocities in a simple parallel rail railgun. Although the 5.9 km/s achieved (2) is modest, all indications are that higher velocities are attainable. Recent analytical work at Lawrence Livermore Laboratory (3) leads to the same conclusion.

The purpose of this paper is to present the most important factors to be kept in mind when designing railguns and railgun systems to obtain higher velocities. There are two overriding concerns. The first is that the projectile-armature-rail system must be able to withstand the electromechanical and thermal loadings imposed upon it. The second is that once the maximum allowable current is decided, the energy supply should deliver a current to the gun which is close to this value for the time required for projectile acceleration.

2.0 PROJECTILE-ARMATURE-RAIL SYSTEM

The gun arrangement found most convenient in Canberra is shown in Figure 1. The rails had to be held accurately opposite each other to minimize any vertical component of the outward forces on them during a gun firing and having the rails located in recesses in a set of spacers assured accuracy of assembly. Because the gun was dismantled after each shot to enable the rails to be examined and new rails to be installed, it was important to minimize the time taken for the operation.

2.1 Current Flow in Armature and Rails

A computer analysis made by Muttik (4) [see Figure 2(a)] showed clearly the existence of a velocity skin effect which caused the current to flow in the surface of the rails near the projectile and also in the rear corner of the armature. That this really occured was shown by two observations, the first being that the rails were banana shaped when removed from the gun after

heavy current shots. It's likely that this occurred because the inside surfaces of the rails had been preferentially heated sufficiently to cause the copper to yield longitudinally in compression. When removed from their mechanical constraint the rails then assumed a pronounced curve. The second observation was that it was clear that the rear-most leaf was taking the most current (4) when multileaf armatures were used. It was this behavior that led to the use of the "flying fuse" type armature and to the plasma armature which will be discussed later.

2.2 Velocity Limit With Metallic Armatures

A metallic armature will cease to carry current smoothly from rail to rail when it gets hot enough to lose its strength. It is of interest to note what velocity limits are set by this effect. The velocity skin effect in the armature can be overcome by arranging the armature elements as shown in Figure 2(b), with the contacts transposed fore and aft on opposite sides (5). Assuming now that in this way the current density can be made uniform over the front to back distance, z_a, of the armature and that the bore of the gun is b x b, then the current density J in the armature is $I/(bz_a)$, where I is the gun current. The time t taken for a given armature material to rise from some base temperature to its failure temperature is given by:

$$t \propto \frac{1}{J^2} \propto \frac{b^2 z_a^2}{I^2} \tag{1}$$

The driving force F on the armature is given by:

$$F \propto I^2 \tag{2}$$

The mass M of the armature is given by:

$$M \propto b^2 z_a \tag{3}$$

Thus an expression for the acceleration, a, can be found by dividing 2 above by 3, assuming that the armature is the only pay load.

$$a \propto \frac{F}{M} \propto \frac{I^2}{b^2 z_a} \tag{4}$$

Finally, by combining expressions (1) and (4), the velocity v attainable by the armature is given by:

$$v \propto at \propto \frac{I^2}{b^2 z_a} \cdot \frac{b^2 z_a^2}{I^2} \propto z_a \qquad (5)$$

showing that the attainable velocity is directly proportional to z_a regardless of the bore size of the gun, provided only that the bore ratio is fixed.

This result is of interest more particularly for low velocity railgun applications. For high velocity applications it is likely that the limiting factor for solid sliding contacts will be "gouging" (6,7) in which the slider makes tear shaped gouges in the rails. This was one of the limitations that led us to the use of a plasma armature to accelerate an electrically nonconducting projectile (8).

2.3 The Plasma Armature

Experiments using arc or plasma armatures (2) have shown two important facts. The most obvious is that the rear face of a polycarbonate projectile survives the presence of a high pressure (10,000 psi) high temperature [~50,000 °K (9)] plasma for a significant length of time (1 ms). The second is that the passage of an arc armature, carrying 300 kA on a half inch high rail, leaves only faint "chicken scratching" marks on the copper rails when the velocity is one km/s and above.

The pressure distribution on the gun axis in the plasma armature behind the projectile will be similar to that shown in Figure 3(a). The pressure will be highest on the back face and will fall to a low value a few barrel diameters further back. A similar curve would be expected for current density in the armature with the current paths being as shown in Figure 3(b). Isobars will be something like those shown in Figure 4(c). Pinch forces will tend to round them as shown and there may also be some circulation of material as indicated by the dashed arrows.

It's almost certain that the driving plasma is spread in the -z direction over at least one quarter of an inch. The evidence for this is that when the "flying fuse" (10) [Figure 3(d)] was used in the ANU gun, typically smooth

conduction (i.e., no rail damage) was obtained when the fuse faces were sliding on the rails. Similarly, after the arc had settled down after fuse-blow there was practically no rail damage, but at the point of fuse-blow there was usually a pronounced arc "splash" on the rails for an inch of travel or so, indicating that the current density in the arc after settling down was less than the current density had been in the fuse to rail contact. The length of the fuse sliding contact face was one eighth inch, thus the arc armature length in the z direction was probably greater than that.

A point worth noting is that at high speeds the current may prefer to flow in a plasma layer on the surface of the rail rather than in the rail immediately behind the armature, and this will also tend to thicken the plasma armature in the -z direction. Taking the case of 5.9 km/s ANU railgun shot, the time taken for the projectile to travel one centimeter is 1.7 μs. The half current density skin depth in room temperature copper in 1.7 μs is 0.010 cm. For a total current flowing of 300,000 A, the current density on the surface of the rails one centimeter behind the projectile is 300,000/(0.010 x 1.27) i.e., 25 MA/cm^2, giving a voltage gradient on the surface of the rail of 50 V/cm. This is getting to be a significant fraction of the observed rail to rail voltage difference behind the projectile of 160 V. If one-third of this is resistive drop in the plasma (the other two-thirds being electrode drop) then the voltage gradient in the plasma is around 40 V/cm in which case one could indeed expect the plasma to "short" the rails to some extent.

A direct indication of the thickness of the plasma armature should be obtainable from armature current pick-up coils like those shown in Figure 1. Signals similar to those shown were obtained in the ANU gun but useful information about the arc could not be deduced from them because of the unknown effect of the steel retaining tube. It would be interesting to observe the output of such coils when placed closer to the gun bore with no metal used in the gun structure except the rails themselves.

2.4 Projectile Design

Polycarbonate projectiles, backed with a layer of red electrical fiber board to take the fuse-blow shock, were found to be adequate for conditions in the ANU gun. The maximum current available was 300 kA and this gave a nominal driving pressure of 10,000 psi. The yield strength of polycarbonate

is also 10,000 psi so it is possible that some lateral flow of the plastic provided a sliding seal between projectile and gun bore. It is possible, however, that a seal in the normal sense is not required. A plasma driven railgun is different from ordinary guns in that the driving pressure is generated electrically. If plasma leaks into gaps around the projectile it may no longer be able to conduct current and may become its own seal.

It's also likely that pressures much greater than 10,000 psi can be used. For example, two stage light gas guns are thought to reach peak pressures of 200,000 psi. It will be worth considering using projectiles made of transverse laminations of reinforced resins as indicated in Figures 3(b) and (c). Simple compression tests made of candidate materials cut to projectile size would be adequate to determine suitability. An added refinement might be to make the back layer or two of some ablation resistant material.

2.5 The Meaning of L′

The driving force on the armature of a railgun may be found by computing the magnetic field strengths at all points in the armature and summing the J x B components. In practice this is tedious and it is more convenient to use the well known expression:

$$F = \frac{1}{2} L' I^2 \qquad (6)$$

where L′ is the inductance per unit length of the gun rails. However, while this removes the tedium it does not remove the effects of the uncertainties caused by lack of knowledge of where the current actually flows.

Expression 6 is derived (11) from energy considerations in a circuit of the type shown in Figure 4(a). There is no ambiguity in the result because there is no uncertainty about exactly where the current is flowing, the circuit consisting as it does of line elements. Such is not the case when the circuit elements have finite thickness and it is instructive to examine several cases.

The case which is most readily analyzed is the coaxial railgun because the azimuthal symmetry makes calculation of magnetic field strengths simple.

Consider the case shown in Figure 4(b) in which a current I is carried down to a plain transverse armature in one rail and back in the other rail. The field at points between the rails is given by

$$B = \frac{1}{2} \cdot \frac{\mu_o I}{2\pi r} \tag{7}$$

giving the force on the armature as

$$F = \int BI dr = \frac{1}{2} \cdot \frac{\mu_o}{2\pi} \ln \frac{\rho_2}{\rho_3} \cdot I^2 = \frac{1}{2} L' I^2 \tag{8}$$

where L' is the inductance per unit length of the coaxial rails, assuming that all the current flows on the inside surface of the outer conductor, and the outer surface of the inner conductor.

A similar argument will apply in the case of nonannular railguns such as that shown in Figure 4(c) in which the instantaneous current flow is indicated by the heaviness of the outlines. A reasonable approximation for L' in the case of the ANU gun was to assume the current was evenly distributed over the whole face of the rail. This gave a calculated (12) inductance of 0.49 μH/m compared with the experimentally obtained value of 0.42 μH/m.

2.6 Where the Voltages are Developed

In the case of a resistanceless railgun in which the current is constant, then the voltage measured across the muzzle is zero, i.e., the voltage from X to X in Figure 3(d) is zero. The voltage across the breech of the gun steadily rises as the speed of the projectile increases. Half the electrical energy being fed into the gun goes to increasing the kinetic energy of the projectile. The other half adds to the inductive energy stored in the gun. Thus the voltage between the rails at YY immediately behind the armature will be just half that which is required at the breech to maintain constant current, and will rise to the breech value a few gun diameters behind YY. This has practical implications for gun systems which will be discussed in the next section.

3.0 RAILGUN POWER SUPPLY SYSTEMS

3.1 The Basic Systems

The function of the power supply for a railgun is to establish the desired current flow in the gun and to keep it flowing for as along as required. This is shown in its simplest form in Figure 5(a). The idealized power supply has a voltage output which increases with time in such a way as to keep its current output constant.

There are many forms that railgun power supplies can take. The simplest of these is the inductor together with the means to charge it. In the case of the ANU gun (1), the Canberra homopolar generator was used to charge the inductor. The main complexity with this system is that the relatively low voltage of the homopolar necessitates a relatively long charging time for the inductor. Thus a diverter switch must be used to carry the current while charging. If a high voltage energy store such as a capacitor is used to charge the inductor then a diverter switch is not required because the rate of rise of current in the inductor is then great enough so that the gun may be connected directly to the inductor. The capacitor bank must be crowbarred if direct current is required in the gun.

The use of a single power supply at the breech of a railgun has two main disadvantes. One is that as higher velocities are sought (or the projectile is required to be in the gun for a longer time) then larger proportions of the input energy is lost resistively in the rails (3). The other is that the energy stored inductively in the gun at projectile exit represents a large inefficiency. A way of circumventing both these problems is to distribute the energy stores along the gun as indicated in Figure 5(c). The following analysis shows the way one such system would perform.

3.2 The Multi-energy Store Railgun

Assuming again that the current I_o through the projectile's armature is constant, then the force on the projectile is constant. Thus the energy delivered to the projectile per unit length of the gun will be constant. Assume, therefore, that n equal energy stores are distributed uniformly along a gun of length l as shown in Figure 6.

Assume that the energy stores and their leads are connected according to the following set of rules.

a) At the moment the project moves into each stage of the gun, the energy store for that stage is switched on.
b) At the same moment the power supply for the previous stage is disconnected from the gun and replaced by a short.
c) As the current drops to zero in each short, the short is open circuited.

When the projectile enters the r^{th} stage, the current in the $(r-1)^{th}$ stage is I_o, thus it has energy stored in it of W_o given by

$$W_o = \frac{1}{2}LI_o^2 = \frac{1}{2}L'\frac{\ell}{n}I_o^2. \tag{9}$$

The acceleration, a, of the projectile is constant so its velocity,v, after time, t, and travel distance, x, is given by

$$v = at = \sqrt{2ax}\ . \tag{10}$$

The voltage, V, between the rails from the breech to a few gun diameters behind the projectile is given by

$$V = I_oL'v. \tag{11}$$

(To meet this condition the energy stores will have to be quite peculiar devices. They will have to be something other than a simple homopolar-inductor or a capacitor.)

The $(r-1)^{th}$ stage will therefore see a voltage on it given by substituting v from 10 into 11 to get

$$V = I_oL'(at). \tag{12}$$

The $(r-1)^{th}$ stage will drive current into the r^{th} stage according to the equation:

$$L\dot{I} = -V$$

where I is the current in the $(r-1)^{th}$ stage. Noting that $L = L'\frac{\ell}{n}$, and substituting V from 12, we get

$$L'\frac{\ell}{n}\dot{I} = -I_o L'(at)$$

or

$$\frac{\dot{I}}{I_o} = -\frac{n}{\ell}at,$$

giving

$$\frac{I}{I_o} = -\frac{n}{\ell}\frac{at^2}{2} + K,$$

but (from 10)

$$\frac{at^2}{2} = x$$

giving

$$\frac{I}{I_o} = -\frac{n}{\ell}x + K. \qquad (13)$$

When $x = x_r$, $I = I_o$. Substituting these boundary conditions into 13 gives

$$1 = -\frac{h}{\ell}x_r + K. \qquad (14)$$

Eliminating K between 13 and 14 gives the final result,

$$\frac{I}{I_o} - 1 = \frac{n}{\ell}(x_r - x),$$

showing that I falls linearly (with x) from I_o to zero as the projectile travels from x_r to x_{r+1}.

Thus the currents will rise and fall as shown in the lower part of Figure 6.

The stage efficiency is 100%. The inductive energy from each stage is fed on to the next stage, and so on. For the whole gun, the only inefficiency is that associated with the last stage. If it is assumed that the inductive energy stored in the n^{th} stage as the projectile exits is lost then the efficiency of the gun will be given by

$$\eta = \frac{n}{n + 1}$$

In the case of a real gun with rail resistance, the resistance losses will also be reduced to around one n^{th} of those for a gun with a single energy store. While efficiency as such is not important in a research device, it would be important in a device such as an igniter for an impact fusion power plant.

4.0 CONCLUSION

There are many facets to the behavior of plasma armatures in railguns that are not understood in detail. Some careful experimentation coupled with suitable analysis in this area will be valuable. It is also indicated that study of alternative railgun-energy store systems is also likely to return dividends.

5.0 ACKNOWLEDGEMENTS

This paper was prepared with the support of the Texas Atomic Energy Research Foundation.

REFERENCES

(1). Barber, J. P., "The Acceleration of Macroparticles and a Hypervelocity Electromagnetic Accelerator," Ph.D. Thesis, Australian National University, Canberra, Australia (1972).

(2). Rashleigh, S. C., Marshall, R. A., J. Appl. Phys. 49 (1978).

(3). Hawke, R. S., Scudder, J. K., "Magnetic Propulsion Railguns: Their Design and Capabilities," presented at the Second International Conference on Megagauss Magnetic Field Generation and Related Topics, Washington, D.C. (1979).

(4). Barber, J. P., Marshall, R. A., Muttik, P., "Projectile and Current Behavior in ANU Railgun," presented at the 25th Meeting of the Aeroballistic Range Association, Naval Ordrance Laboratory, Silver Springs, MD (1974).

(5). Marshall, R. A., Nature, Vol. 221, No. 5183, pp. 852-3, March 1, 1969.

(6). Graff, K. F., Detloff, B. B., "The Gouging Phenomena between Metal Surfaces at very High Sliding Speeds," Wear, 14, pp. 87-97, 1969.

(7). Barber, J. P., "Experimental Observations on Railgun Acceleration." Presented at the 24th Meeting of the Aeroballistic Range Association (1973).

(8). Barber, J. P., Marshall, R. A., Rashleigh, S. C., "Magnetic Propulsion for a Hypervelocity Launcher." Presented at the Second International Conference on Magnetic Field Generation and Related Topics, Washington, DC (1979).

(9). McNab, I. R., p. 277, Vugraphs presented at the workshop on gun and launch applications of electromagnetic pulse power, December 5-6, 1978, Annapolis, MD.

(10). Marshall, R. A., "The "Flying Fuse" in ANU Railgun." 27th Aeroballistic Range Association Meeting, Paris, (1976).

(11). Kesselring. The Elements of Switchgear Design .

(12). Grover, F. W., Inductance Calculations: Working Formulas and Tables. Dover Publications, Inc. (1962).

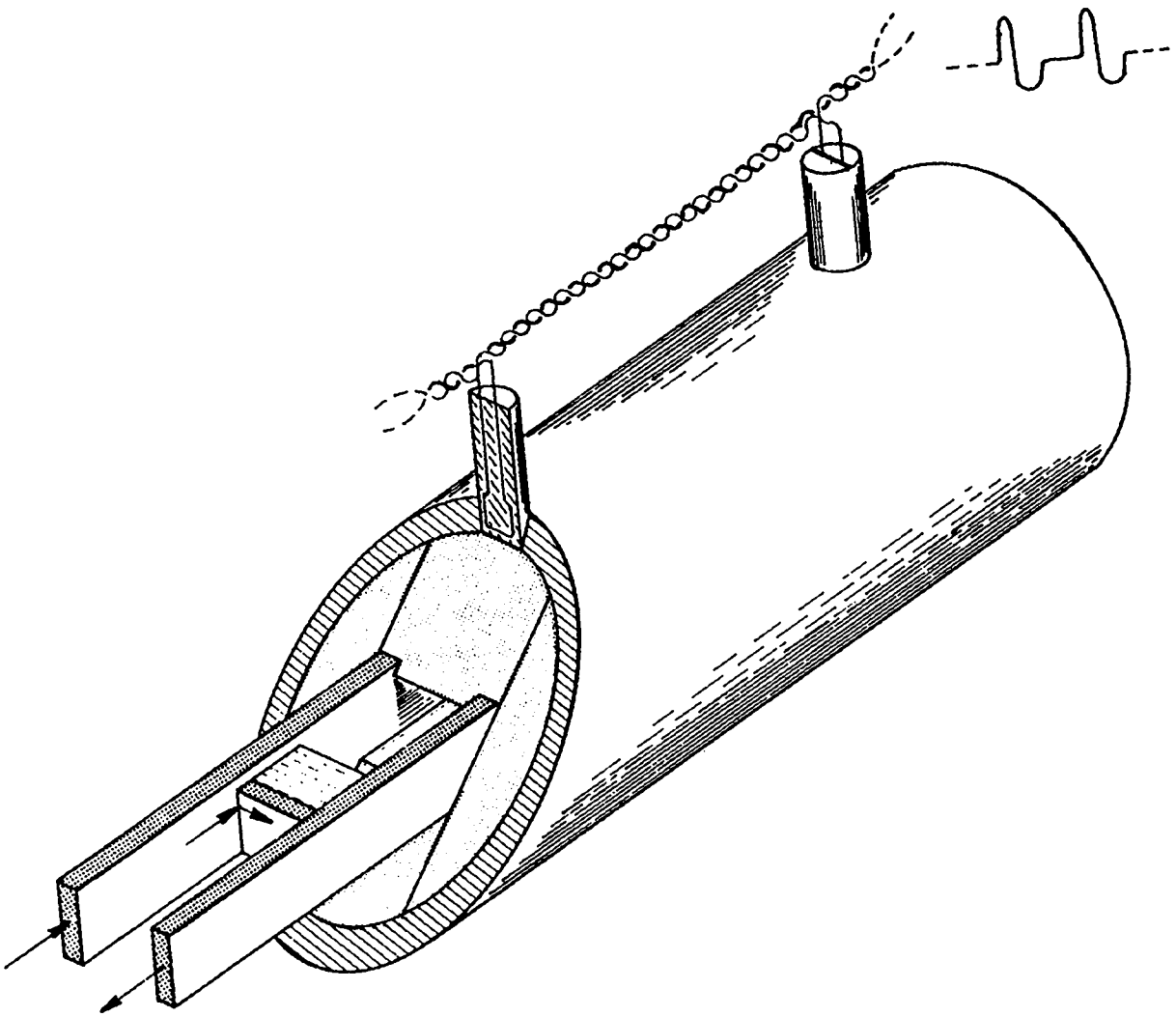

Figure 1: Cutaway view of ANU railgun showing the method of supporting the rails with insulating spacers held within a steel tube. The projectile and armature are shown schematically. Two armature current probes are indicated as well as the type of signal obtained from them.

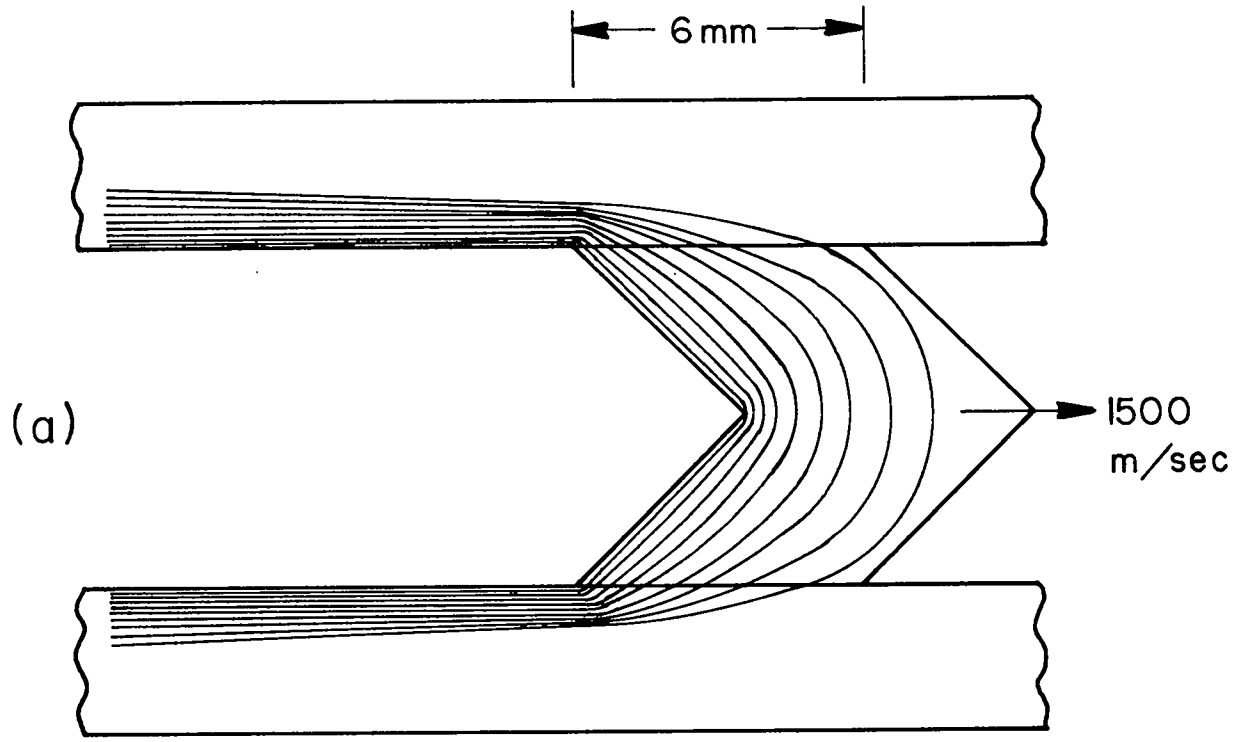

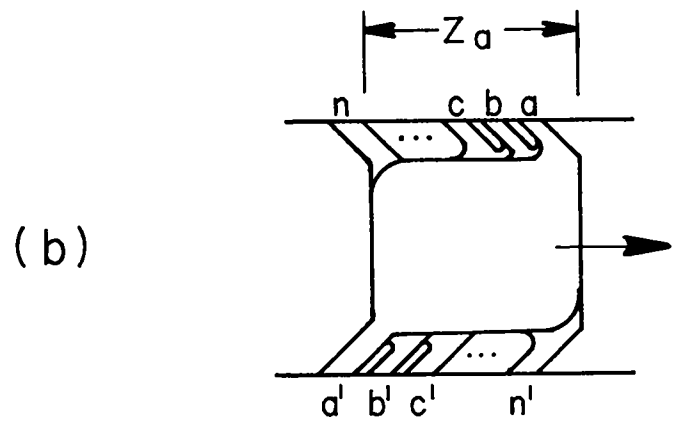

Figure 2: (a) Computer plot of current flow in a solid copper armature running between copper rails, showing velocity skin effect.

(b) Schematic of armature with transposed contacts.

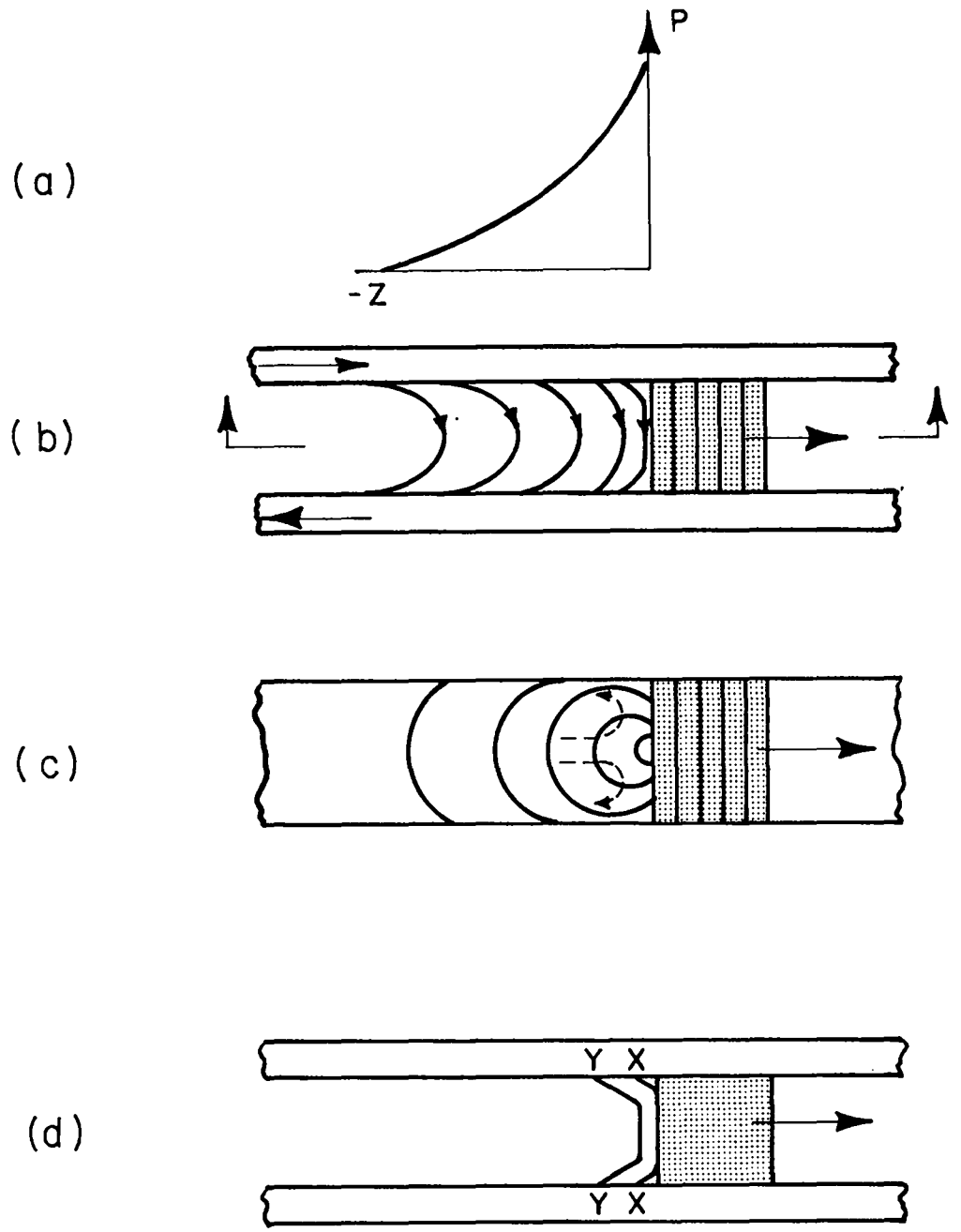

Figure 3: (a) Expected pressure on the centerline of railgun with plasma armature versus distance behind the projectile's driving face.

(b) Current flow lines in a plasma armature.

(c) Elevation on centerline of (b) indicating isobars in plasma armature.

(d) Flying fuse armature and projectile.

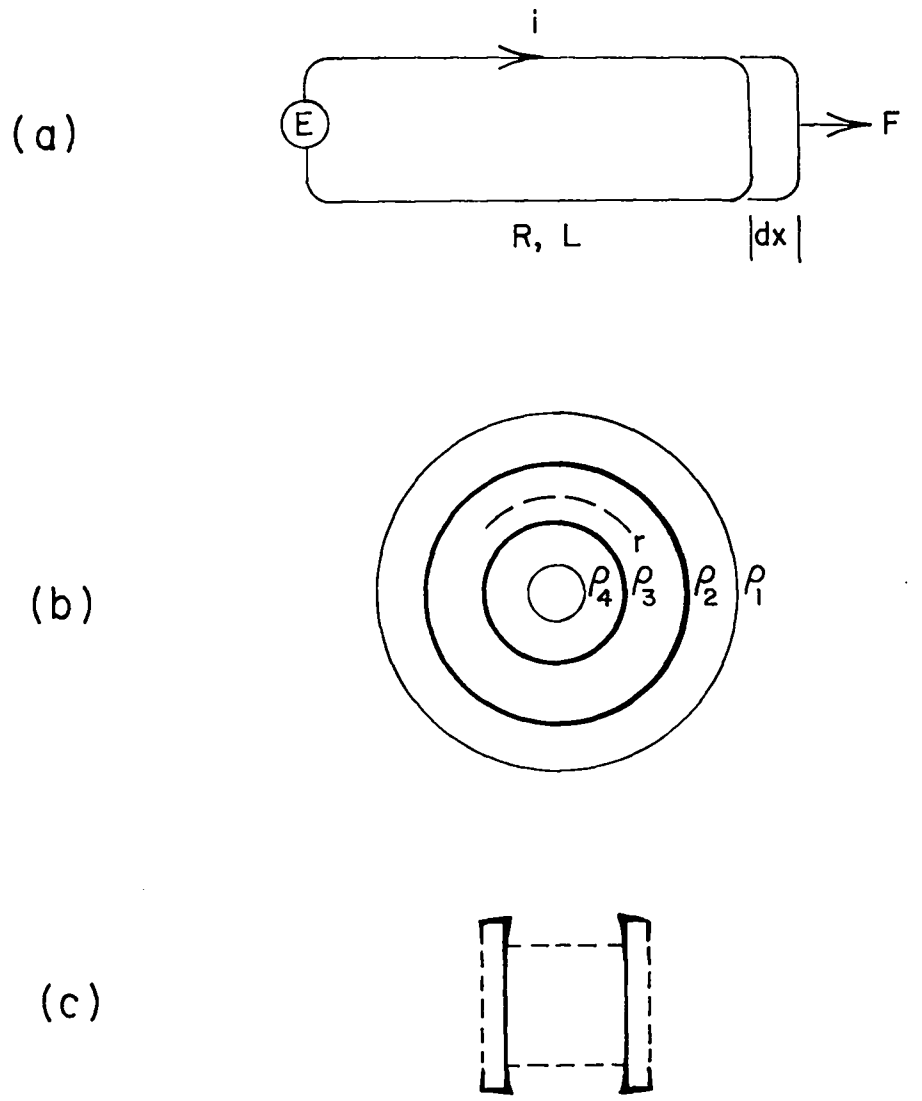

Figure 4: (a) Elementary circuit with varying inductance.

(b) Coaxial railgun geometry

(c) Square bore railgun geometry with surface current density in rails indicated by line thickness.

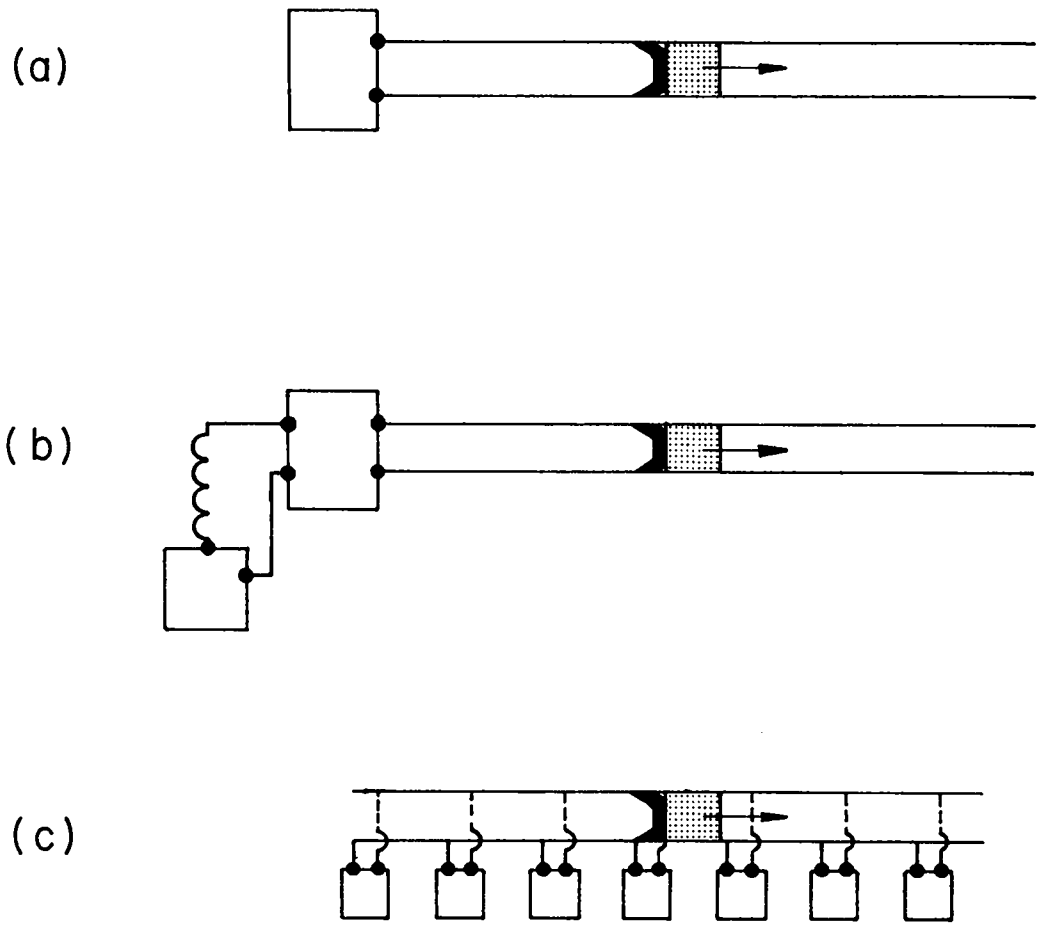

Figure 5: Schematic representations of three railgun-energy store systems with,

(a) Variable voltage store at gun breech,

(b) Inductive store,

(c) Stores distributed along the length of the gun.

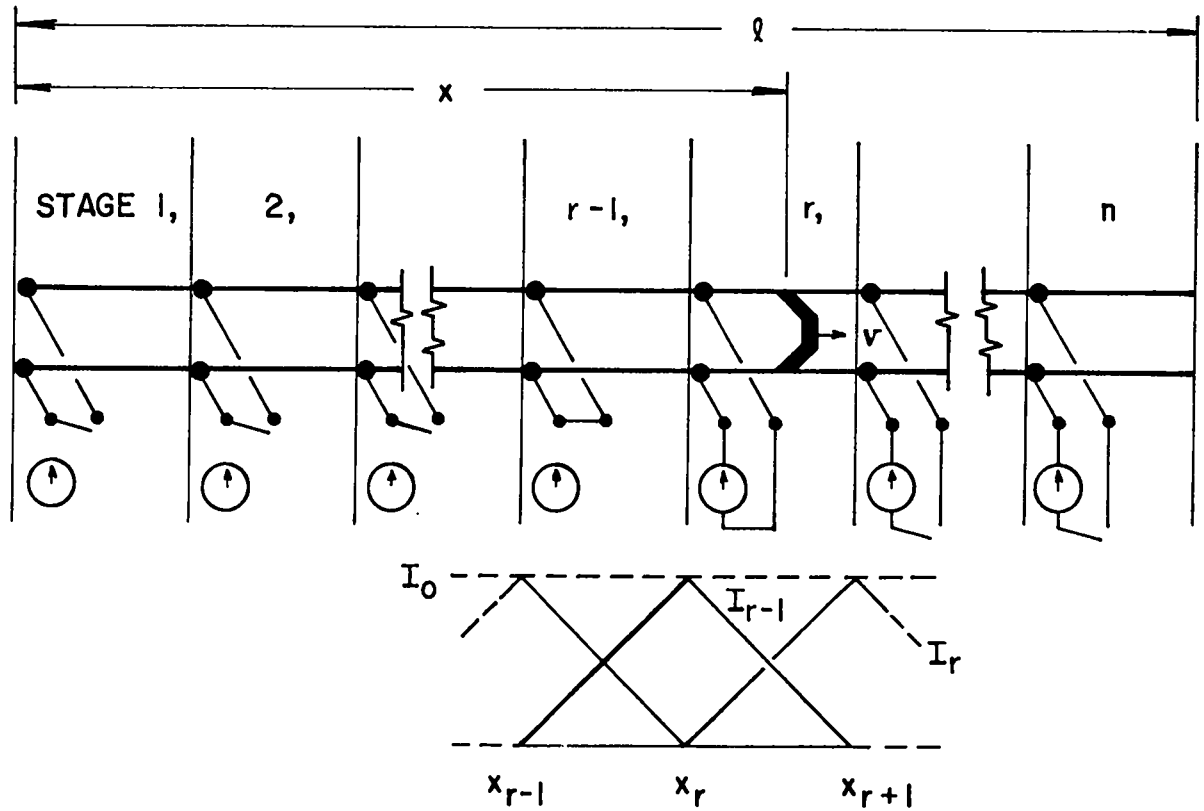

MARSHALL
UT-CEM
TAERF
7-5-79

Figure 6: Representation of a railgun of length ℓ with n energy stores uniformly distributed along it.

The lower diagram shows the current flowing in the $(r - 1)^{th}$ and r^{th} stages as a function of armature position.

MAGNETIC-GUN IGNITER FOR CONTROLLED THERMONUCLEAR FUSION*

R.L. Garwin, R.A. Muller and B. Richter

I INTRODUCTION

Major programs are underway at laboratories throughout the world attempting to ignite small pellets of deuterium and tritium (DT) to thermonuclear burn. Pellets weighing less than a gram, ignited once per second, could form the energy source for a gigawatt electric power plant. To ignite these pellets, it is generally believed to be necessary to deliver about 1 megajoule (MJ) of energy in a time period of about 10 ns into a volume of less than 1 cm^3. As of this writing, no device, other than a fission bomb, is capable of delivering this concentrated power. The future of controlled thermonuclear fusion using DT pellets depends on whether we can design and build a low-cost non-nuclear ignition system. Candidates for the igniter include lasers, electron beams and high-energy heavy-ion beams. In this paper we propose yet another igniter: a "dart" weighing about 0.1 gm, accelerated to 150 km/sec by the moving magnetic field of a delay line, a "magnetic gun."

One MJ is not a large amount of energy; it is, for example, the food energy contained in a small loaf of bread. The problem is to deliver this modest amount of energy in a very short time into a small volume, in the environment of a reactor vessel that must be designed to absorb the high power burst of the DT pellet. The delivery must be done in such a way that the apparatus will not be damaged by a blast equivalent to one ton of TNT; fragile mirrors or lenses cannot be close to the reaction region unless extremely fast and durable shutters are used. The advantage of using a

* Originally published as JASON Technical Report, JSN-77-20, SRI International, December 1978, under U.S. Department of Energy Contract EY-76-C-03-0115.

"dart" is that the energy is naturally concentrated into a small volume. If the dart moves rapidly enough to contain the energy (a 0.1 gm dart at 150 km/sec) then it is also easy to deliver the energy in the required 10 ns simply by making the dart short (a few mm). Since no focussing is required, the hole in the reactor wall need be no larger than the diameter of the dart, and the pressure inside the reactor can be high without blocking the delivery of the energy in the bullet. Space charge forces, which cause problems for charged-particle beams, are non-existent. The magnetic gun which accelerates the dart can stand far back from the reactor, and be in no danger of damage from the DT fusion blast.

Thus the potential advantages of a magnetic gun igniter are many, particularly in the simplifications that might take place in the DT reactor design. The main advantages of lasers and particle accelerators are that they are "mature" technologies. Although devices similar to the magnetic gun have been proposed for many applications, including artillery and as a means of launching satellites into space, we know of no practical use that has been made of the concept.

The magnetic gun is the only means we know of to accelerate macroscopic pieces of matter to near-relativistic velocities. Electric fields won't work in a reasonable distance, for the electric field which can apply a pressure equivalent to that of a 10^5 gauss field is 10^5 statvolts/cm = 30×10^6 volts/cm, a field that cannot be sustained with known materials. Acceleration by means of rocket propulsion (or equivalently, spallation) is too inefficient for power production unless the exhaust velocity is 20% or more of the required dart velocity of 150 km/sec. We do not, however, rule out electric or chemical acceleration for injection into the delay

line. In fact it would be quite reasonable to inject the darts into the delay lines at 1 km/sec using chemical propulsion (e.g., an ordinary or hot-gas gun). The efficiency of the injector need not be high, since most of the energy is delivered to the dart in the high velocity phase.

We will now proceed with a "conceptual design" for the magnetic gun in order to show that the various parameters required turn out to be reasonable (in an engineering sense). An engineering design will necessarily turn out to be far more complex; the purpose of the following calculations is merely to show that the basic idea* looks sufficiently good to warrant further work.

---

*Traveling wave magnetic acceleration has been described in previous publications but apparently neglected. See, for example,
F. Winterberg, Journal of Nuclear Energy C8, 541 (1966);
D. Anderson, S. Clafin, F. Winterberg, Z. Naturforch 26a 1414 (1971);
J. G. Linhart, Proceeding of International School Enrico Fermi, 151, Academic Press, N.Y. (1971).

II CONCEPTUAL DESIGN

In the magnetic gun the dart is accelerated by magnetic pressure using either ferromagnetic or superconducting material for the part of the dart on which the magnetic field pulls or pushes. If the dart has an area A from which a magnetic field B is totally excluded as the dart is accelerated over a distance D, then the dart will gain kinetic energy

$$T = A \cdot D \cdot B^2/8\pi \quad .$$

For T = 1 MJ = 10^{13} erg, A = 0.13 cm^2 (circle with radius r = 2 mm), and B = 100 kG, we find that the length of the accelerator is 2×10^5 cm = 2 km. For a ferromagnetic material the pressure would be reduced by a factor $\simeq B_{sat}/B$. For B = 100 kG, and for gadolinium which has a saturation magnetic field B_{sat} = 40 kG, D $\simeq$ 5 km. These distances are not long, considering the simplicity and low cost of the accelerator design, and the acceleration length D can always be shortened, if necessary, by going to a higher B. It should be possible to keep the dart stably centered in the transverse directions, since it need not be stable in the acceleration direction. (Since the maximum dart speed is $\leq 10^{-3}$ of the velocity of light, the phase of the accelerating wave can be adjusted by sensing the dart position in real time.)

If the mass of the dart is 0.1 gm, then the velocity of the dart is

$$v = \sqrt{2T/m} = 1.4 \times 10^7 \text{ cm/sec} = 140 \text{ km/sec}$$

which corresponds to an energy per nucleon of 100 eV. In order to deliver its energy in $\Delta t = 10$ ns, the length of the dart must be $v \cdot \Delta t = 1.4$ mm. If it is desirable to have a long precursor so that the DT pellet can be compressed adiabatically, then a thin spike can be added on the front of the dart. A typical dart might look in cross section something like that shown in Figure 1.

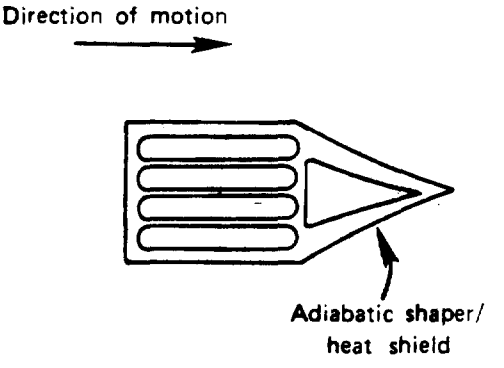

Figure 1

The simplest form of accelerator would be a lumped delay line. In order to get a rough idea of the currents, voltages, resistive losses, etc. which occur in such a machine, we make some estimates based on the simple-minded design shown schematically in Figure 2--a series of loops of radius 0.5 cm and length 1 cm, each connected to its own capacitor.

The current required for a magnetic field B at the center of a loop is

$$I \approx \frac{2Br}{\mu_o n} \quad .$$

For B = 100 kG = 10 T, r = 0.005 m, and n = 1, I will be 80,000 amps.

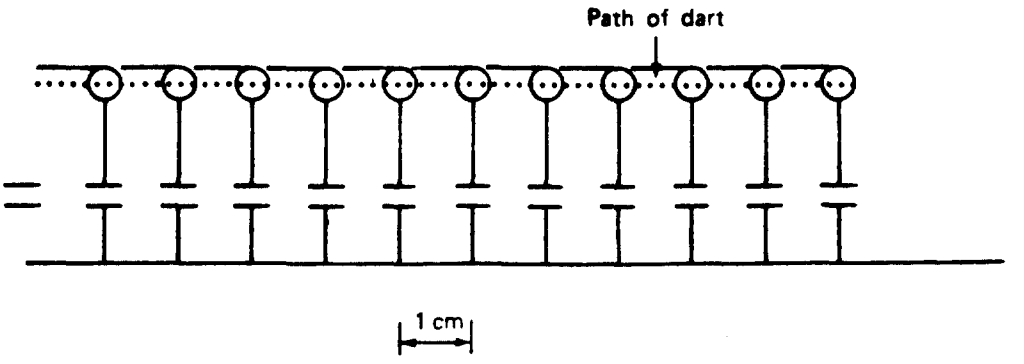

Figure 2 CONCEPTUAL DESIGN FOR THE MAGNETIC RIFLE

The inductance of each one turn loop is

$$L = \frac{\pi \mu_o r}{2} \approx 9 \times 10^{-9} \text{ henries}$$

giving a stored energy of

$$u = \tfrac{1}{2} LI^2 \approx 30 \text{ joules.}$$

The velocity of propagation down the line is

$$v = (LC)^{-\frac{1}{2}} \quad .$$

Taking $v = 1.5 \times 10^7$ cm/sec we find $C \approx 5 \times 10^{-7}$ farads. The impedance of the line is $Z = (L/C)^{\frac{1}{2}} \approx 0.13\ \Omega$, giving a peak voltage on the capacitor of about 10,000 volts.

The dart at v = 150 km/sec passes through a single loop in about 70 nanoseconds. During a time somewhat longer than this, ohmic heating

of the loop occurs, and energy is lost by this heating. The penetration depth (skin depth) of the current in the loop for the case described here is about 0.04 mm, and for a loop made of aluminum at room temperature 0.5 joule goes into heat. Since the dart gains 5 joules in passing through the loop, the heat loss is about 10% and the accelerator can be potentially very efficient even without subdividing the coil conductor, which could reduce the ohmic loss by a large factor.

It is reassuring to find such reasonable values for I, C, and V in this conceptual design, and also to find that an inexpensive coil material (solid aluminum) can be used.

In doing the delay line calculation, we have ignored the substantial loading of the dart. With only 30 joules stored in an L-C pair, and 5 joules being given to the dart at each stage, energy will have to be fed in to the system all along the path. It should be possible to do this by switching in already charged capacitors as the dart (and the pulse) passes down the line. Although such switching will initiate pulses traveling in both directions along the line, it is easy to see that most of the energy will be transformed into the pulse traveling in the original direction. Such switching should be easy to do since because of the relative slow speed of the pulse (1/2000 that of light) the position of the pellet can be used to trigger the next switch.

The cost of capacitors should be modest. At $0.10 per joule ($2 per capacitor), and assuming each L-C pair has a dedicated capacitor (i.e., the same capacitor is not reused at various points along the delay line) the cost is $400,000. Switch costs are probably higher and switch technology should be given some attention.

III VACUUM REQUIREMENTS

Vacuum is required along the beam line in order to limit the heating of the dart. For a ferromagnetic dart the temperature must remain below the Curie point during acceleration; for a superconducting dart the temperature must be kept well below the transition temperature. For a dart of area* A moving a distance D at velocity v (>>thermal velocities) through a gas of density ρ, the impact energy of the gas on the dart is

$$Q = \rho v^2 AD \quad .$$

For a pressure of 10^{-6} torr (easily obtainable), $\rho = 10^{-12}$ gm/cm^3, and the impact energy delivered to the dart is about one joule. This energy would be absorbed easily by a ferromagnetic material, but it would destroy superconductivity. If a superconductor must be used, a heat shield can be added to the front of the dart or the vacuum can be improved by the required factor $>10^4$.

---

*Strictly speaking A is the "equivalent" area, equal to a drag coefficient C_D (0.1 to 0.5) times the true area.

IV ADDITIONAL CONSIDERATIONS

Certain serious matters have been ignored in the "conceptual" design in order to keep it simple. Dispersion in the lumped delay line was neglected; in a lumped delay line the energy in a pulse will not remain confined to a region as narrow as one L-C pair, but this hardly matters since the pulse travels only a few pairs before it is regenerated. Ordinary hard superconductors may not sustain a large enough current density for this application; "artifical" hard superconductors (lead in porous Vycor) may be required. In addition, there is a hystersis loss whenever the field on a hard superconductor changes and this may impose severe requirements on field uniformity in the accelerator.

Eddy-current heating of the gadolinium dart can cause a problem if the dart is not properly laminated. Coil designs are conceivable which will provide low field ripple in the moving frame. The mass of the pellet must be kept low, and yet its effect on the magnetic field must be such as to exert a maximum pressure. These, and other remaining problems strike us as difficult, but solvable.

V CONCLUSIONS

The idea of a magnetic gun for thermonuclear ignition is not obviously absurd, and it may hold several important advantages in comparison with the particle and light-beam igniters currently being considered. Many problems remain to be solved, but we think the idea is ripe for a serious attempt at an engineering design, perhaps in conjunction with small-scale experiments to discover the most practical way to build a larger scale experiment.

IMPACT FUSION WITH A SEGMENTED RAIL GUN

R.A. Muller, R.L. Garwin and B. Richter

INTRODUCTION

The rail gun offers an attractive alternative to the traveling wave rifle for the magnetic acceleration of macroscopic (0.05 g) bullets for impact fusion. For power generation it is essential for the rail gun to be energy efficient. In this paper we review the basic rail gun equations and indicate how energy efficiency can be designed in. We set as our preliminary goal the delivery of E = 1 megajoule in dt = 10 nanoseconds, with a specific energy of 20 MJ/g (i.e. a bullet mass of 0.05 g); these values are taken from the requirements being considered for heavy-ion fusion. Using these numbers, we can solve immediately for the final particle velocity u_f from $E = 1/2\ mu_f^2$ to get $u_f = 200$ km/sec. For a delivery time of 10 nanoseconds, this velocity implies that the projectile length is about 2 mm. Impact fusion is feasible because of the coincidence that a bullet with all dimensions roughly 2 mm has the required mass.

BASIC RAIL GUN EQUATIONS

We begin by reviewing the basic equations which have been derived by J.P. Barber and others. We shall derive these equations in the simplest possible form, in order to emphasize the scaling laws and the physics contained in them. The power delivered by a current I and voltage V, ignoring losses, is:

*To be published as JASON Technical Note, JSN-79-05, SRI International, 1979, done in part under U.S. Department of Energy Contract EY-76-C-03-0115.

$$P = IV = d/dt(LI^2/2) + Fu$$

where L is the inductance, F is the force on the "armature" (i.e. the bullet), and u is the bullet velocity. Setting $V = d/dt(LI)$ and simplifying, we get the basic rail gun equation:

$$F = 1/2\ L'I^2$$

where L′ is the inductance per unit length, and is very close to L′ = 0.6 microhenries/meter for typical rail gun geometries. For simplicity we shall now assume constant acceleration, i.e. constant current I. The work done on the bullet is $E = Fz = LI^2/2$ where $L = L'z$. Note that the work done on the bullet is equal to the energy stored in the magnetic field of the rails; this inductive energy can be recovered, in principle. Note also that for fixed E and L′ the length of the rail gun "z" is proportional to I^{-2}. The required voltage can be calculated from $V = d(\text{flux})/dt = IL'u$. The values for the current, maximum voltage, and acceleration time t for two lengths of rail-gun are given in the table below:

length z =	100 meters	1 km
current =	180 kA	60 kA
maximum voltage =	23 kV + IR	7 kV + IR
time =	0.001 sec	0.01 sec

The IR term in the voltage refers to the drop from resistive losses, and is discussed below. The required current can be supplied by capacitors or by high-voltage homopolar generators (see the paper at this conference by R.L. Garwin).

EFFICIENCY

For application to impact fusion, it is essential to keep the resistive losses to a minimum. To the extent that the resistances in the rail gun are independent of velocity u, the most difficult regime is the low velocity one where the power being transferred into bullet kinetic energy $P = Fu$ is low. On the other hand, designs which are inefficient at low velocities may be considerably more efficient at high velocities, for the same reason.

The energy lost to resistive heating of the bullet or driving plasma is $Q = I^2Rt = 2ERt/L'z = 4ER/L'u_f$. The "inefficiency factor" for the bullet $Q/E = 4R/L'u_f$ is independent of accelerator length, and depends only on the final velocity to be achieved, u_f. The resistance of a copper bullet with dimensions of 2 mm will be about 10^{-5} ohm; although resistive loss is not a problem with the bullet, the copper may be heated beyond its melting point. The resistance of a driving plasma can be calculated from Spitzer's formula, and is approximately $\rho = 65\ \ln(H)/T^{3/2}$ where H depends on the temperature and density; $\ln(H) \approx 3$ for the densities and temperatures of interest. (Black body emission alone will prevent the

temperature from rising above 10^{+5} K). Substituting values, and assuming that the plasma occupies a 2 mm cube, the resistance of the plasma is $R = 3 \times 10^{-3}$ ohm, and for the plasma $Q/E = 30R = 0.1$, an acceptable value. The resistive voltage drop across the plasma will be $V = IR = (60kA)(0.003) = 180$ volts.

Resistive loss in the rails is a more serious problem, especially for the longer rail guns. The DC resistance for two 1-km rails with a cross-section of 2 mm x 2 mm is $R_{DC} = 8.5$ ohms. When the bullet is at a position z the resistance is $R_{DC}(z/z_m)$ if skin-depth effects are ignored (the true resistance will be greater). The energy lost to resistive heating in the rails during constant acceleration a is

$$Q = \int I^2 R dt = \frac{I^2 R_{DC}}{z_m} \int z dt = \frac{I^2 R_{DC} a}{2 z_m} \int t^2 dt = \frac{I^2 R_{DC} t}{3}$$

From the above result, we can define an average or effective resistance $R = R_{DC}/3 = 2.8$ ohms. We find for the rails, $Q/E = 30R = 85$, and an efficiency $E/(Q + E) = 1.2\%$. One cannot arbitrarily reduce the resistance by increasing the rail cross-section, for to do so reduces L′. A smaller L′ implies a smaller force on the bullet, and hence a longer rail gun to achieve the same terminal velocity.

To improve the efficiency, it is necessary to divide the rail into segments, with current flowing only in the segment carrying the bullet. A schematic diagram is shown in the figure:

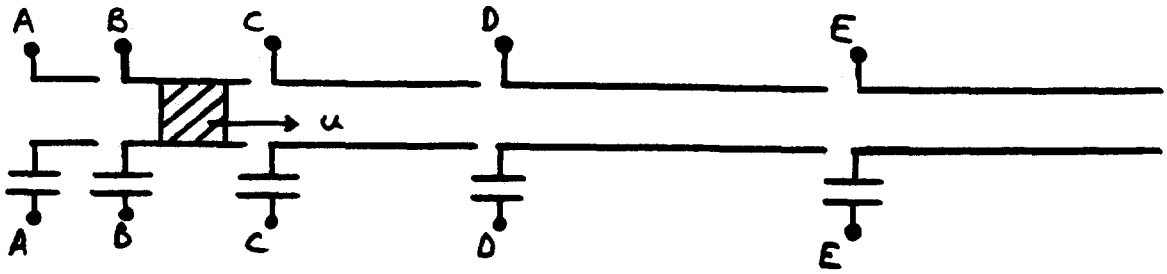

The current behind the bullet will penetrate to an average depth given by

$$s = \sqrt{\frac{\rho \Delta t}{\mu_o}} .$$

where Δt is the time since passage of the bullet, ρ is the resistivity, and μ_o is the permittivity ($= 1.3 \times 10^{-6}$ in MKS units, for non-magnetic materials). For a large number of segments N, we can assume that the skin depth s is less than the thickness of the rails, and derive the following formula (see Appendix) for the effective resistance of the segmented system:

$$R = \frac{Q}{I^2 t} = \frac{8\ell}{3h} \sqrt{\frac{\rho \mu_o}{tN}}$$

For $z = 1000$ meters, $\rho = 1.7 \times 10^{-8}$ ohm-meters (Cu), and the height of the rails $h = 2$ mm, this gives $R = 2/\sqrt{N}$ ohms. Thus for N segments, we have $Q/E \simeq 65/\sqrt{N}$. For $N = 1000$, the efficiency $e = E/(Q + E) = 30\%$. Additional

gains are possible by increasing N, the limit looking like a lumped delay line with propagation velocity matching the bullet velocity and pulse length not much longer than the bullet.

For the 1000 segment, 1 km rail gun, the maximum IR voltage drop from the resistance in the rails is 60kA x $2/\sqrt{1000}$ = 4 kV, comparable to the back EMF required of 7kV (see the table on page 2).

The segmented rail gun can be fed by power supplies along its length, represented by capacitors in the figure. No switches to close the circuit are shown, because the switching is automatically provided by the bullet. Since the resonance time of the L-C circuit is approximately equal to the transit time of the bullet, it may be possible to use the automatic switching of the bullet to open the circuit at a time of near-zero current flow.

APPENDIX

Effective Resistance of a Rail Gun Segment

Consider one element dz of segment of length ℓ_i. Let resistive heating during passage of bullet = dQ. Skin depth = $s(t) = \sqrt{\frac{t\rho}{\mu_o}}$.

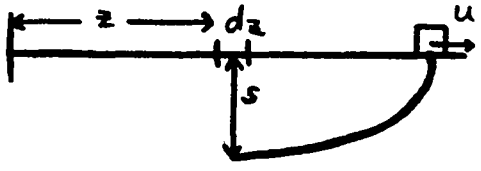

$$\frac{dQ}{dz} = \int_0^{t_2 - t_1} I^2 \frac{dR}{dz}\, dt = \frac{I^2\rho}{h}\int \frac{dt}{s} = \frac{I^2\rho}{h}\sqrt{\frac{\mu_o}{\rho}}\int_0^{\Delta t} \frac{dt}{\sqrt{t}} = \frac{2I^2}{h}\sqrt{\rho\mu_o \Delta t}$$

where h = height of rail.

Now integrate this over segment of length ℓ_i. Assume velocity u_i = constant.

$$\Delta Q_i = \frac{2I^2}{h}\sqrt{\rho\mu_o}\int\sqrt{\frac{\ell_i - z}{u_i}}\, dz = \frac{4}{3}\frac{I^2}{h}\sqrt{\frac{\rho\mu_o}{u_i}}\,\ell_i^{3/2} = \frac{4}{3}\frac{I^2\ell_i}{h}\sqrt{\rho\mu_o t_i}$$

(a) Suppose lengths are chosen such that $t_i = t/N$.

$$Q = \Sigma \Delta Q_i = \frac{4}{3} \frac{I^2 \ell}{h} \sqrt{\frac{\rho \mu_o t}{N}}$$

so

$$R = \frac{4}{3} \frac{\ell}{h} \sqrt{\frac{\rho \mu_o}{tN}}$$

For 2 rails, double this answer.

(b) Suppose lengths are chosen such that $\ell_i = \ell/N$.

$$Q = \Sigma \Delta Q_i = \frac{4}{3} \frac{I^2}{h} \sqrt{\rho \mu_o} \frac{\ell}{N} \Sigma \sqrt{t_i}$$

This sum can be done by approximating it with an integral, and the answer is the same as for (a).

COUNTER-ROTATING DISK HOMOPOLAR GENERATOR ("CRDHG")*

Richard L. Garwin

The following is a brief recap of a proposal of 1950 for a fast-discharge HPG.

1. Mechanical rotation is limited by peripheral speed v such that $1/2\ \rho v^2$ (the kinetic energy density per unit volume) is comparable with the breaking stress S in dyne/cm^2. For a set of rings, we have the well-known criterion $\rho v^2 = S$. Thus, to store a total energy E, we need a mass M such that $1/2\ v^2 M = MS/2\rho = E$, or $M = 2E\rho/S$.
For $S = 150{,}000$ psi $= 10^4$ bar $= 10^{10}$ dyne/cm^2, we need a mass M_1 per megajoule

$$M_1 = 2\rho E/S = 20 \text{ kg/Mj} .$$

2. If the mass is in the form of disks rotating at initial angular velocity ω_o, we are limited by $\omega_o R = v$, so that for no dependence on radial strength (not the only design possibility) and for uniform disk thickness, the kinetic energy stored is

$$\int_{R_i}^{R_o} (1/2)\ 2\pi R\rho H\omega^2 R^2 dR = K = \pi\rho H\omega^2 (R_o^4 - R_i^4)/4 ,$$

and per unit mass $K/M = (v^2/4)(1 + (R_i/R_o)^2)$.

3. Since the mass is already subject to an acceleration $\dot{v}_o = \omega v_o = v_o^2/R$, we can stop the rotation in one radian rotation without adding much to the stress. This is a delivery time $\tau = R/v_o = 1/\omega_o$ and

*To be published as JASON Technical Note, JSN-79-03, SRI International, 1979; done in part under U.S. Department of Energy Contract EY-76-C-03-0115.

may be 60×10^{-6} seconds for $R = 30$ cm and $v_o = 500$ m/sec , corresponding to $S = \rho v^2 = 8 \times (5 \times 10^4)^2 = 2 \times 10^{10} = 2 \times 10^4$ bar .

4. As indicated by the title, we can consider a set of annular disks, N/2 attached to an axis (perhaps loosely) and N/2 interspersed disks attached to the inside of an enclosing cylinder or rotating cage of axial bars at radius R . The N/2 disks extending from the axle and the N/2 disks extending in from the cage are counter-rotated at angular velocity $\mp \omega$. Clearly, each disk produces in the laboratory frame a voltage difference between its inner and outer rim

$$\Delta V = 10^{-8} \int v \times B dR = \omega B \times 10^{-8} \frac{R^2}{2} = \frac{BR}{2} \times 10^{-8} v_o \quad , \quad (\text{if } R_i \ll R_o) \ .$$

For $B = 10^5$ gauss , $v_o = 5 \times 10^4$ cm/sec , $R = 30$ cm , $\Delta V = 750$ volts .

A stack of 60 disks therefore gives 45 kv.

5. A cylinder of metal with a 50% packing fraction, 30 cm radius, 60 cm long, with density $\rho = 8$ g/cm^3 and $v_o = 5 \times 10^4$ cm/sec has $E = 1/2\ Mv^2 = 1/4\ Mv_o^2 = 1/4\ \rho\pi R^2 \times R \times (5 \times 10^4)^2 = 4 \times 10^{14}$ ergs = 40 Mj . The output power at $\omega = v_o/R = 5 \times 10^4/30 = 1.7 \times 10^3$ rad/sec (or 16000 rpm) is about 40 Gw.

The matched load impedance is order of magnitude Z , such that $V^2/Z = \omega E$ or $Z = N^2(\Delta V)^2/\omega E$. So for $N = 60$, $\Delta V = 750$ volts , $\omega = 1.7 \times 10^3$, $E = 4 \times 10^7$ joule , $Z = 0.03$ ohms . So that $I = 1.5 \times 10^6$ amp .

The circumferential magnetic field near a disk is then $I/10\ R = 1.5 \times 10^6/10 \times 30 = 5000$ gauss , small compared with the 100 kilogauss assumed axial field. Therefore the inductance is <u>low</u> (i.e., the internal magnetic energy is only about $E_B = \int H^2 d^3R/8\pi = I^2R/400$ ergs = 20 kj versus some 40 Mj stored kinetic energy.

Although many applications do not need the rapid delivery available from the counter-rotating disk homopolar generator, the potential of such a device should be kept in mind. Naturally, one has the problem of rapidly and synchronously making contact between adjacent rims and center rings of rotating disks, which can be done by coating the disk largely with insulating material where contact is not desired, and striking an arc in an enclosing low pressure gas. The opinions of people more expert than I are sought, and that is the reason for raising this question once again after so many years at this topical conference.

RAILGUN ACCELERATORS FOR LAUNCHING 0.1-g PAYLOADS AT VELOCITIES GREATER THAN 150 km/s*

R. S. Hawke
Lawrence Livermore Laboratory, University of California
Livermore, California 94550

I. INTRODUCTION

The promise of an abundant energy supply has inspired many approaches to controlling thermal nuclear fusion. One approach to initiating fusion is to use a hypervelocity projectile to impact a deuterium-tritium (DT) pellet.[1-5] For this purpose, magnetic accelerators have been proposed for accelerating macroparticles to velocities greater than 100 km/s.[2-10]

This paper summarizes a portion of a study[11] that assesses the feasibility of accelerating a 0.1-g payload to a velocity of 150 km/s or more. In that study it was concluded that magnetic-gradient and railgun accelerators could achieve the goal. In this paper I discuss the critical factors that limit the design and operation of railgun accelerators and combine these factors with a simulation code to assess potential railgun performance in this regime.

A. Principle of Operation

A railgun accelerator is actually a linear dc motor consisting of a pair of rigid, field-producing conductors and a movable conducting armature. The armature is accelerated as a result of the Lorentz force F produced by the

*This work was performed under the auspices of the U.S. Department of Energy by Lawrence Livermore Laboratory under contract No. W-7405-Eng-48.

magnetic field B of the rail currents interacting with the current I in the armature throughout its width w where,

$$F = \int_0^w \frac{\vec{I} \cdot d\vec{w} \times B}{m} = \frac{L_1 I^2}{2m} \quad , \tag{1}$$

and L_1 is the specific railgun inductance in H/m, and m is the mass of the projectile (see Fig. 1a). In the analysis that follows, the armature modeled is a thin plasma arc that impinges on the backside of a dielectric projectile and accelerates it. The arc is presumed to be confined behind the projectile by the conducting rails on two sides and dielectric rail spacers in between (see Fig. 1b).

A railgun uses a primary energy storage device (PESD), such as a capacitor bank or homopolar generator (HPG), and a pulse-forming or storage inductor L_0 to supply the current.

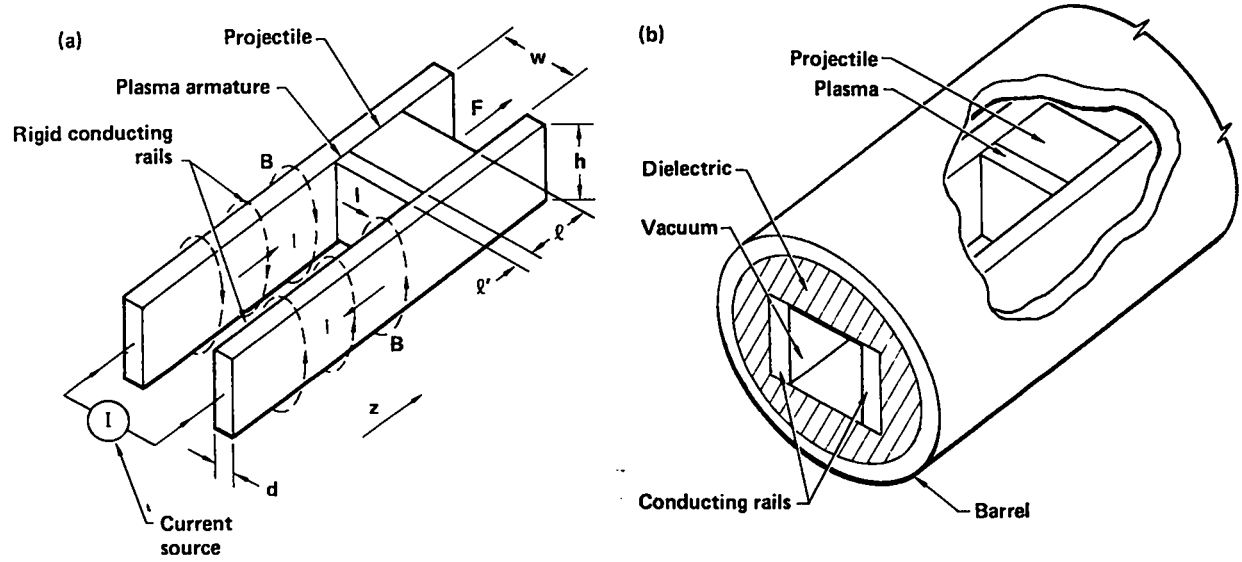

FIG. 1. Sketches of railgun. (a) Railgun accelerator. (b) Railgun assembly. The dielectric maintains the rail position and, along with the rails, confines the plasma behind the projectile.

B. Background

In 1964, researchers at MB Associates* used a 28-kJ capacitor bank as a PESD and accelerated 5- and 31-mg nylon cubes to about 5 to 6 km/s with a plasma arc.[12] They also used an explosively-imploded magnetic-flux compressor as a PESD and accelerated a copper sabot and a steel payload, with a total mass of 0.21 g, to a velocity of 9.5 km/s.[13]

Recently, researchers at the Australian National University at Canberra used a homopolar generator to accelerate a 3-g, 1/2-in. cube of Lexan dielectric to 5.9 km/s, again using a plasma arc.[14]

II. RAILGUN SIMULATION CODE

Railgun operation has been simulated with a computer code.[15] The code accurately reproduced the performance of the ANU railgun and is used here to predict operation at very high velocities.

III. FACTORS THAT INFLUENCE ACCELERATOR DESIGN AND OPERATION

The design and operation of a railgun is restricted by practical limits. These limits result from the properties of the rail and projectile materials, interior ballistics of the projectile, sustainable voltage without spurious arcing, and available energy.

A. Rail Melting

More[16] calculated the temperature rise and resistance of the rails as functions of time, rail dimensions, and current. The electrical resistivity was assumed to be linearly temperature dependent. The maximum temperature rise occurs on the surface of the rails, and it has been concluded[15] that to avoid rail melting of a copper rail system initially at room temperature, the

*Reference to a company or product name does not imply approval or recommendation of the product by the University of California or the U.S. Department of Energy to the exclusion of others that may be suitable.

perimeter current density should be limited to 43 kA/mm. The perimeter current density (see Fig. 1a) is the rail current divided by the rail perimeter p = 2(h + d).

Rapid repetitive launching would require heat removal during its operation. Use of Al_2O_3 ceramic dielectric with reasonable dimensions will allow the heat generated in the rails with each pulse to be conducted to the barrel in about one second without difficulty. Fluidic cooling and heat pipes are also capable of removing the heat at launch rates of up to one pulse per second or more.

B. Deformation of the Rails

The magnetic pressure P_R on the rails is

$$P_R = \frac{0.44\mu_0}{\pi}\left(\frac{I}{w}\right)^2 . \qquad (2)$$

To remain below the yield point of hardened steel, with an elastic strength of 0.7 GPa (100 ksi), the current must remain less than 75 kA/mm of rail spacing. Copper plating on the steel would maintain electrical efficiency while the steel would provide the needed strength. Careful design of the whole rail-support barrel structure will be required to operate at the limit established by the elastic strength of the rail material.[15]

C. Mechanical Integrity of the Projectile

The pressure P on the backside of the projectile with surface area A is given by

$$P_P = \frac{ma}{A} = \frac{L_1 I^2}{2A} . \qquad (3)$$

For a given elastic strength σ_y of a projectile, the maximum non-destructive acceleration a_{max} and current I_{max} are given by

$$a_{max} = \frac{\sigma_y A}{m} , \qquad (4)$$

and

$$I_{max} = \left[\frac{2\sigma_y A}{L_1}\right]^{1/2} . \qquad (5)$$

To retain the mechanical integrity of a square-bore projectile with an elastic strength of 1.4 GPa (200 ksi), the current must remain less than 81 kA/mm of rail spacing. High strength self-supporting projectiles have been designed and demonstrated.[17]

D. Projectile Stability

Because performance improves with current and because current per unit spacing and per unit perimeter have limits, it is desirable to maximize rail spacing and perimeter. The perimeter can be increased indefinitely on the outside portion of the rails, but the rail spacing governs the bore size (henceforth assumed to be square). It has been found experimentally that the aspect ratio A_R, defined as the ratio of the length to the width and height of the projectile, must remain greater than 0.5 to maintain dynamic in-bore stability. Hence, increasing the bore results in a longer, larger and more massive projectile, which in turn requires more input energy and a longer accelerator. Therefore, the choice of bore size is a compromise of competing factors that vary with the specific application.

E. Projectile-launcher Drag Considerations

Buckingham[18,19] calculated the drag and heating losses caused by sliding friction, solid deterioration at the surface, and by the liquid and gaseous boundary layers between the projectile and the launcher walls. He concluded that, in general, a tightly constrained projectile, particularly an all metal design, is unsuitable for hypervelocity launch because it will be almost completely consumed by frictional heating and melt. One possible exception would be a projectile banded by ablation material. In this case even if the projectile is initially tightly constrained, a surface recession gap and intervening ablation-erosion product layer is predicted to develop and lower the heating and drag sufficiently so that hypervelocity launch appears possible. Provision of even a modest (0.001 inch, 2.54×10^{-5} m) gap initially would

insure projectile survival under any of the launch circumstances modeled. The predictions suggest several projectile configurations and materials that are promising candidates for hypervelocity launch.

F. Voltage Gradient Between the Rails

An arc discharge in front of or behind the arc driving the projectile would divert some or all of the remaining energy and must be avoided.

G. Available Energy

In addition to all the above considerations, the performance of a railgun launcher is determined by the amount of energy delivered to it. The maximum delivered energy is equal to the energy stored in the PESD less the energy loss incurred in the transfers from the PESD to the storage inductor and then to the railgun.

IV. SINGLE-STAGE RAILGUN

The railgun simulation code was used with the limitations described above to determine the type of system needed to achieve the stated goal.

A. Bore Size

The above discussion points out that a higher current leads to a shorter accelerator and lower energy loss. The limit on current per unit rail spacing (75 kA/mm) requires a larger bore for higher currents. The limit on aspect

TABLE 1. Limiting factors and limits used in calculations.

Limiting factor	Limit	Value used
Rail melting (copper)	1083 C ⟶ I/P = 43 kA/mm	16 kA/mm
Rail yielding (steel)	1 GP_a ⟶ I/W = 75 kA/mm	75 kA/mm
Sabot failure (graphite composite)	1.4 GP_a ⟶ I/W = 81 kA/mm	75 kA/mm
Projectile stability	A_R = 0.5	0.5
Voltage breakdown (w = 10 mm)	120 kV	80 kV

ratio (0.5) requires a larger mass sabot for a larger bore. The larger mass requires more energy. Even though a larger bore permits higher current and hence acceleration force, a small bore is superior because of the smaller sabot mass and resulting higher payload velocity. A limit on how small the bore can be results from spurious arc breakdown. An inductive voltage appears across the rails immediately behind the arc. A resistive voltage occurs along the rails from the arc towards the breach of the accelerator where the total voltage appears. The breakdown voltage[20] establishes the smallest bore that could be used in this example is 6.7 mm. In the calculations that follow, 10 mm was used to provide a conservative safety margin.

B. Railgun Performance with a 10-mm Bore

Table 1 summarizes the limiting factors and the limits used in calculations that follow. Table 2 lists the geometrical and physical parameters common to all of these calculations.

Figure 2 shows, for several gun lengths, the calculated exit velocity versus the initial energy stored in the storage inductor. To achieve 150 km/s, we need a minimum initial energy in the storage inductor of 52 MJ. The PESD energy must be greater by the amount lost in charging the storage inductor. Typically, 85% efficiency could be expected; hence the PESD energy required would be about 60 MJ.

Figure 3 shows the launch velocity versus accelerator length for various initial energies in the storage inductor. The maximum exit velocity v_{max}

TABLE 2. Geometrical and physical parameters used for calculations.

Parameter	Value used
Rail bore width (w)	10 mm
Rail bore height (h)	10 mm
Rail perimeter (p)	40 mm
Sabot length (ℓ)	5 mm
Sabot mass	1.13 g
Payload mass (m_{pl})	0.1 g
Projectile mass (m_T)	1.23 g
Initial current (I_0)	750 kA
Circuit resistance (R_0)	10 L_0

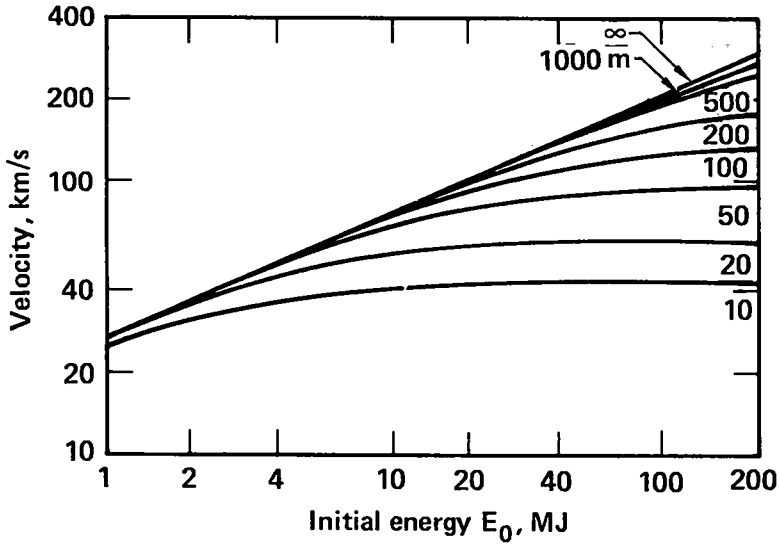

FIG. 2. Launch velocity versus initial energy stored in the inductor (for various accelerator lengths). Here, p = 40 mm, w = h = 2ℓ = 10 mm, m_T = 1.23 g (0.1-g payload), I_0 = 750 kA (see Table 2).

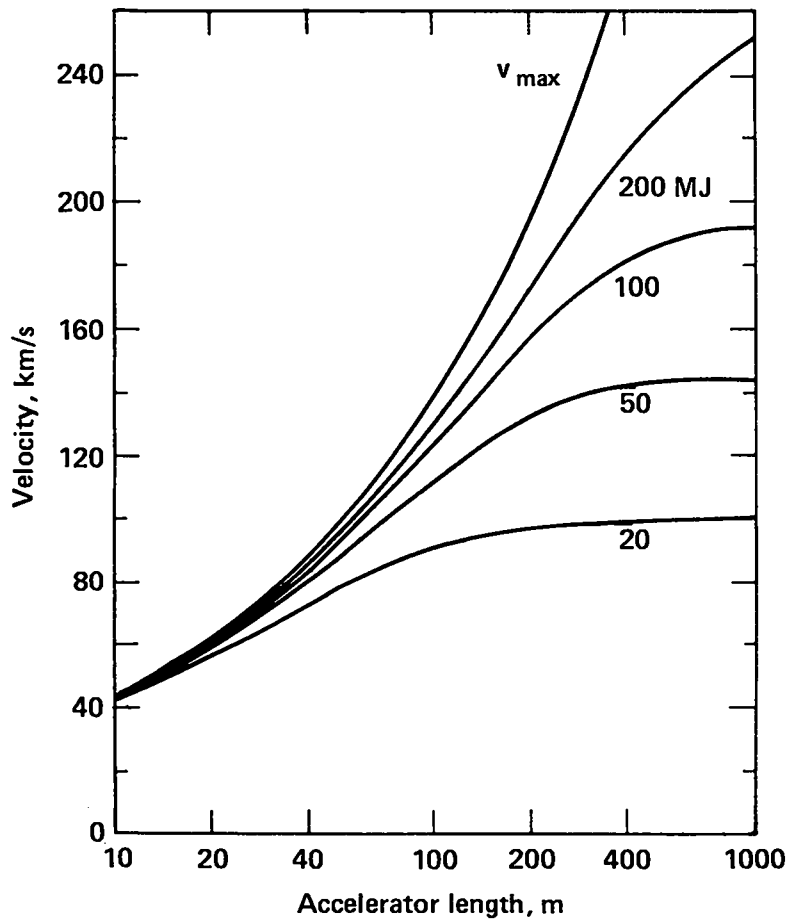

FIG. 3. Launch velocity versus accelerator length for various initial energies stored in the inductor. Same conditions as in Table 2; v_{max} corresponds to I = I_0 = constant (750 kA).

would result if there were enough stored energy to maintain a constant current of 750 kA. Consequently, the v_{max} curve also indicates the minimum-length accelerator needed to achieve a given velocity without exceeding the limits in Table 1. A velocity of 150 km/s would require an accelerator length of at least 115 m. In the case where the stored energy is not adequate to maintain constant current, a longer accelerator would be required.

C. Efficiency

Figure 4 is a plot of the energy-transfer efficiencies of the projectile ξ_p and payload ξ_{pl} versus velocity, where

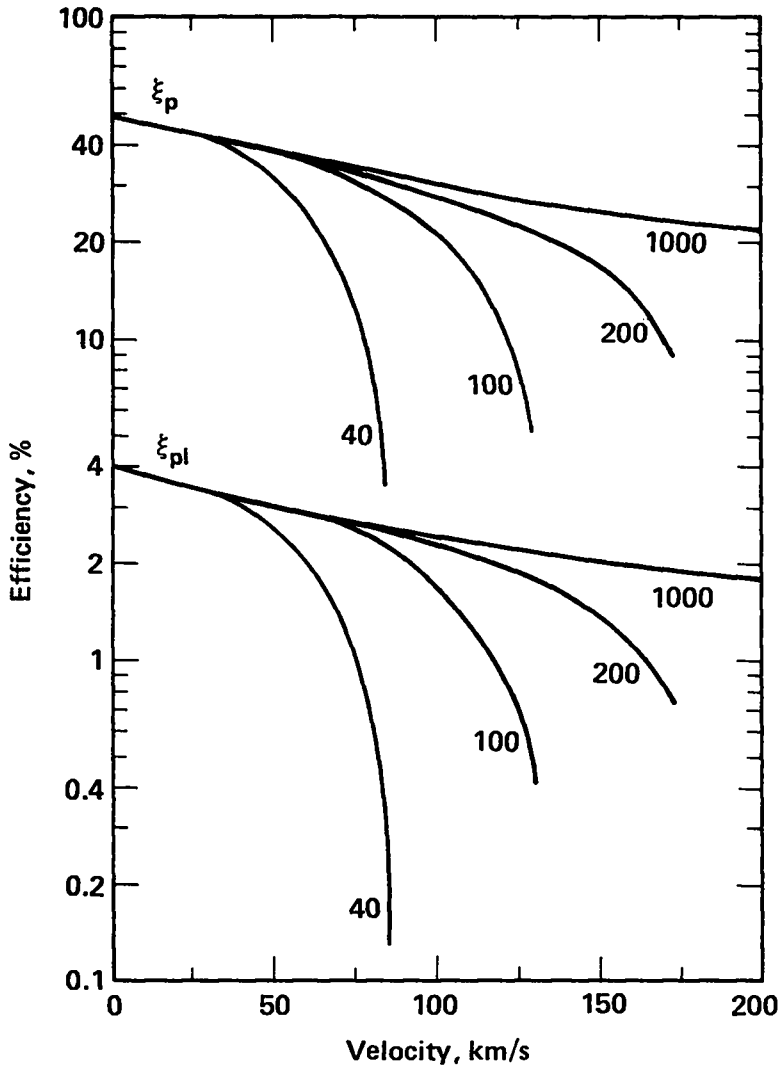

FIG. 4. Electrical to kinetic energy conversion efficiency versus launch velocity for various length accelerators. Conditions same as in Table 2.

$$\xi_p = \frac{m_T v^2}{L_0 I_0^2} , \tag{6}$$

and

$$\xi_{pl} = \frac{m_{pl} v^2}{L_0 I_0^2} . \tag{7}$$

The efficiency of converting the initial energy stored in the inductor into kinetic energy of the payload can be about 2% at 150 km/s. Note that if the kinetic energy of the sabot mass could be used as a payload, the efficiency would be about 20%.

V. MULTISTAGE RAILGUN

The discussion has been limited to a single pair of rails, i.e., a single stage railgun. Approximately 50% of the energy stored in the inductor is lost in resistive heating of the rails. Dividing the accelerator into several, shorter, modular stages would (1) reduce the amount of energy loss in heating the rails, (2) allow the current to be reestablished at the highest usable value in each stage, (3) reduce the resistive voltage drop, (4) provide a convenient division of the total amount of required energy into smaller units, and (5) lead to an accelerator that could be built by adding a few stages at a time. The total energy loss in the rails is approximately proportional to $1/\sqrt{N}$, where N is the number of stages.

The combined effect of the energy savings and operation at near maximum current throughout the acceleration is illustrated in Fig. 5, which shows the required energy E_{rq} versus velocity for 1-, 10-, and 100-section accelerators. The required energy is the sum of the kinetic energy E_p of the projectile, the stored inductive energy E_I in the railgun, and the lost energy E_L. An accelerator using 100 sections requires little more energy than a lossless accelerator. Furthermore, the inductive energy could be recovered in which case the energy expended would be the sum of the lost energy and the kinetic energy.

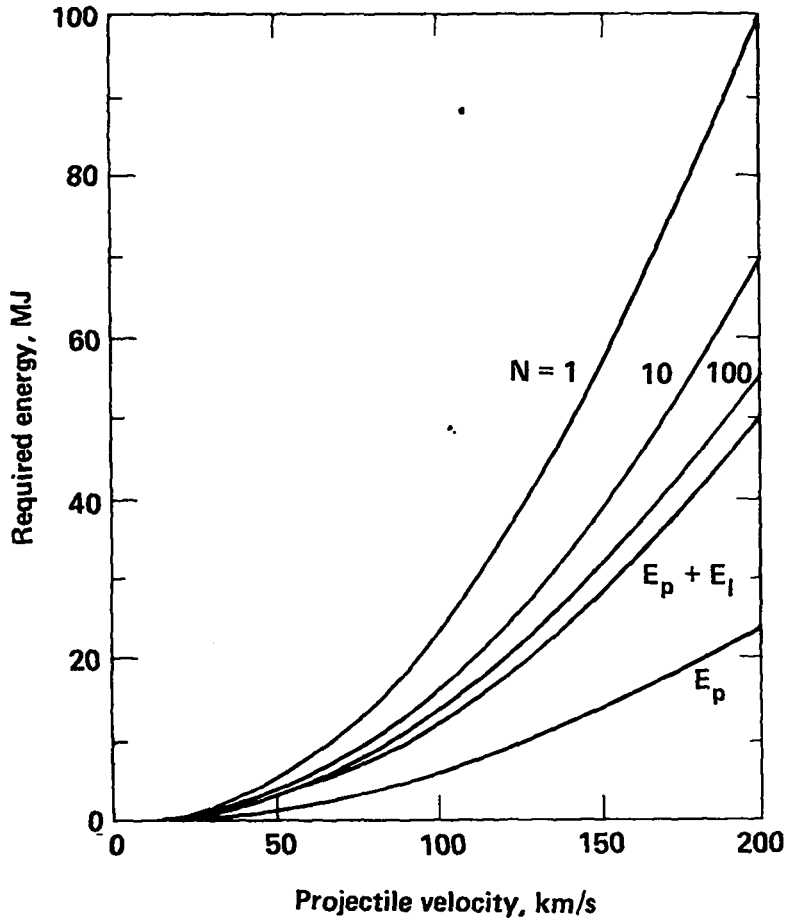

FIG. 5. Required energy versus projectile velocity for 1-, 10-, and 100-section railguns (projectile mass 1.23 g, initial current of each section 750 kA, p = 40 mm).

In summary, multisection accelerators offer flexibility in design and improved performance, which results in shorter accelerators, higher efficiency, and a lower total energy requirement.

VI. SUMMARY AND CONCLUSIONS

This report has summarized the results of a study to determine if a railgun accelerator might be used to launch a 0.1-g payload at a velocity of

150 km/s or more. A first-order design was analyzed. The analysis resulted in the following conclusions:

- Properties of launcher and projectile materials impose limits on railgun operation.
- Within these limits, a railgun appears capable of launching a 1.13-g sabot with a 0.1-g payload at a velocity greater than 150 km/s.
- The launcher needs to be at least 150 m long.
- A single-stage accelerator would require an ~60-MJ primary-energy storage device and could have an energy-conversion efficiency of about 1.9% for the payload and about 23% for the combined mass of the payload and sabot.
- A multistage (100) accelerator would require a total energy of about 35 MJ and could have an energy-conversion efficiency of about 3.2% for the payload and about 38% for the combined mass of the payload and sabot.

ACKNOWLEDGMENTS

The author is very pleased to express thanks to those persons who participated in this study. Specifically, he acknowledges the program support and guidance of Don Meeker, John Nuckolls, and Andy Poggio. John Kury's support of a 10- to 40-km/s railgun program provided valuable tools for this study. Jon Scudder's efforts have been instrumental in the evolution of railgun design and performance. The invaluable technical assistance of Alfred Buckingham, Fred Deadrick, Richard More, and Susan Weaver is appreciated. Much insight was gained from discussions with Jim Brittingham, Tom Burgess, Bruce Carder, Steve Moxon, Bill Nellis, Harry Sahlin, and Jim Shearer.

REFERENCES

1. E. R. Harrison, Phys. Rev. Lett., 11, 535, (1963).
2. F. Winterberg, Bull. Am. Phys. Soc., 9, 309 (1964).
3. F. Winterberg, Z. Naturforsch., 19a, 231 (1964).
4. C. Maisonnier, Nuovo Cimento, 42B, 332 (1966).
5. J. G. Linhart, Proceedings of International School Enrico Fermi (Academic Press, New York, 1971), p. 151.
6. F. Winterberg, Nuclear Fusion, 6, 152, (1966).
7. F. Winterberg, J. Nucl. Energy, 8, 541 (1966).
8. J. P. Barber, The Acceleration of Macroparticles and a Hypervelocity Electromagnetic Accelerator, Ph.D. thesis, Australian National University, Canberra, Australia (1972).
9. R. L. Garwin, R. A. Muller and B. Richter, Magnetic-Gun Ignition for Controlled Thermonuclear Fusion, SRI International, 1611 No. Kent St., Arlington, Virginia, Tech. Rept. JSN-77-20 (1978).
10. H. H. Kolm, "Basic Coaxial Mass Driver Reference Design," in Proceedings of Third Princeton/AIAA Conference on Space Manufacturing Facilities (May 1977).
11. J. N. Brittingham and R. S. Hawke, Magnetic Gradient and Railgun Accelerators for Launching 0.1 g-Payloads at Velocities Greater Than 150 km/s, Lawrence Livermore Laboratory, Livermore, Calif., Report UCRL-52778 (1979).
12. D. E. Brast and D. R. Sawle, "Study of a Rail-type MHD Hypervelocity Projectile Accelerator," in Proceedings of Seventh Hypervelocity Impact Symposium, Vol. 1 (1964), p. 187.
13. R. L. Chapman, D. E. Harens, and G. P. Sorenson, "The Magnetohydrodynamic Hypervelocity Gun," in Proceedings of Sixth Symposium on Hypervelocity Impact, Vol. 1 (1963), pp. 317-330.
14. S. C. Rashleigh and R. A. Marshall, J. Appl. Phys., 49, 2540 (1978).
15. R. S. Hawke and J. K. Scudder, "Magnetic Propulsion Railguns: Their Design and Capabilities," presented at the Second International Conference on Megagauss Magnetic Field Generation and Related Topics, May 29-June 1, 1979, Washington, D.C., to be published. (Also Lawrence Livermore Laboratory, Report UCRL-82677 (1979).
16. R. More, Lawrence Livermore Laboratory, private communication (1979).

17. Roger Werne, Lawrence Livermore Laboratory, private communication (1979).

18. Buckingham, A. C., "Railgun Accelerator Projectile Drag Estimates During Launch," to be published (LLL Report, UCRL-82856).

19. A. C. Buckingham, Appendix entitled "Theoretical Prediction of Erosive Drag" in Ref. 11.

20. R. Hackam, J. Appl. Phys., 46, 3789 (1975).

DC ELECTROMAGNETIC LAUNCH SYSTEMS - COMPONENTS AND TECHNOLOGY

by

I.R. McNab, D.W. Deis, and C.J. Mole
Westinghouse R&D Center
Pittsburgh, PA 15235

1. INTRODUCTION

During recent years, interest in the use of pulsed dc electromagnetic techniques to launch macroparticles to high velocities has grown considerably. This has largely occurred as a result of the work of Barber[1] and Marshall[2] and their colleagues at the Australian National University in Canberra, and Westinghouse work on advanced current collection,[3-5] homopolar generators[6-8] and superconducting energy storage coils.[9] Earlier attempts to accelerate solid objects to high velocities by electromagnetic techniques had taken place in the 1950's and 1960's but had proved to be of limited success,[10] although the acceleration of highly ionized plasmas to velocities in excess of 100 km/s had been demonstrated by Bostick and others in many cases for a space propulsion application.[11-14] In this case, plasma masses were in the microgram range whereas Barber and Marshall demonstrated that objects of up to a few grams could be accelerated to velocities near to 6 km/s.

The success of these experiments has led to several developments in this field. One is the consideration of whether such a launch system could be a practical alternative to conventional powder guns for the armed forces. Numerous Department of Defense applications for such systems may be envisioned, involving land, sea, air, or space basing. Present effort in this area is led by the DARPA/ARRADCOM program currently being undertaken at Westinghouse. The objective is to design and build a system to launch a 0.3 kg mass to 3 km/s, the primary application in this case being anti-armor.

The system under development for DARPA/ARRADCOM utilizes the basic components of a pulsed direct current launcher modeled on the ANU system. These comprise:

- a pulsed homopolar energy source
- an inductive energy storage coil
- one or more transfer switches
- a launcher barrel with associated projectile (and sabot, if necessary) and
- a muzzle arc suppression system

For the laboratory system presently being designed, a ballistic range with appropriate diagnostic instrumentation and a catcher/target assembly is also incorporated. Field applications would obviously not include these latter components.

At present, only tentative ratings have been ascribed to the system components, pending the result of optimization studies that are now in progress. As much as possible, the program philosophy is to utilize "low risk" technology for this demonstration system, consistent with the requirement that all components should be designed with the ultimate application in mind. Present estimates of the major parameters for this system are shown in Table 1. These values build upon technology of the type used at ANU, although with significant advances brought about as a result of modern technology programs and as a result of the ultimate desire to weaponize this system. The technology does not assume radical advances in barrel or switch technology, which may prove to be possible, although increased sliding speeds are assumed for (1) the homopolar generator (250 m/s) and (2) solid-on-solid sliding of the projectile in the

TABLE 1. Tentative Design Data for DARPA/ARRADCOM Launcher

Homopolar generator stored energy	: 15 MJ
Launcher input energy	: 11.25 MJ
Homopolar generator open circuit voltage	: 120 V
Homopolar generator peak current rating	: 1.5 MA
Inductive storage coil inductance	: 6 μH
Firing circuit resistance	: 30 μΩ
Time to peak current	: 175 ms
Firing circuit switching time	: 500 μs
Projectile mass	: 300 g
Acceleration period	: 2 ms
Projectile peak acceleration	: 1.4×10^6 m/s^2
Barrel length	: 5 m
Muzzle velocity	: 3 km/s
Overall efficiency	: 0.12

barrel (3 km/s). Commensurate with the required projectile mass (300 gm), the barrel cross-section will be approximately 20 cm^2.

Completion of the Westinghouse components with commissioning and test of the system during 1981 is presently planned. Note, however, that the use of the phrase "low risk" to describe the transfer of 1.5 MA currents across sliding surfaces at up to 3 km/s is a relative term!

2. LAUNCH SYSTEM AND COMPONENT CONSIDERATIONS

2.1 Technology Requirements

The conditions necessary to achieve impact fusion have not yet been clearly delineated (or, at least, published), indeed that may turn out to be the chief achievement of this workshop. However, the work of Winterberg[15] and Harrison[16] shows that ultra-high velocities are likely to prove necessary for success. Our present evaluation is that velocities in excess of 100 km/s, and masses in excess of 10 grams, will be required.[17] The kinetic energy of motion of such a projectile is 50 MJ, so that a single stage launcher circuit having an efficiency of 12.5% (approximately the same as predicted for the DARPA/ARRADCOM system) would require an energy input of 400 MJ. In itself, this is not a large amount of energy, but the requirement to deliver this energy electromagnetically to a small projectile in a small fraction of a second, necessitates an enormous power input. On the other hand, of course, the liberation of this total energy in a short period of time and in a small mass may yield exceptionally high temperatures. Thus, 50 MJ liberated in a target mass of 0.1 gm in 5 μs (corresponding to a target depth of 0.5 cm at the quoted speed of 0.1 cm/μ sec) would yield an ideal temperature of 250×10^6 K for the adiabatic compression of helium, neglecting the energy required for ionization, fusion, conduction, and radiation losses. This is a sufficiently high temperature to encourage research into techniques for achieving these goals.

2.2 Launcher Circuit

A number of technical issues have to be addressed in discussing which pulsed dc launcher circuit will prove to be most appropriate to enable the above target velocities to be achieved. At this time, it is not clear which arrangement will ultimately be chosen but a multi-stage segmented barrel system which could be staged fed from a series of fast energy stores may prove best. The staged power inputs may either be independent or could derive their energy from a primary energy storage device. Present launcher concepts are relatively wasteful of stored inductive energy and it is anticipated that inductive energy recovery arrangements will ultimately be incorporated in such systems.

Ultimate fusion applications, and even experimental facilities, will require reasonable pulse repetition rates, which will have a significant impact on the system and component design, including heat removal systems. Considerations that have to be addressed for each of the system components are outlined below.

2.3 Pulsed Energy Source

The requirement to provide pulsed powers up to, or even exceeding, 400 MJ presents a challenging although not necessarily insuperable problem. Several routes are available for investigation. The most rewarding (and lowest cost) at present appears to be that of inertial energy storage in a homopolar generator, or "electrified flywheel". For the present purposes, the simplest machine configuration has been selected for discussion. This is a two coil, single stage, single rotor, iron-cored, normally-excited drum machine. In practice, several considerations, including

factors such as torque reaction, would almost certainly require a more sophisticated design. Table 2 shows the approximate parameters.

TABLE 2. 400 MJ Homopolar Generator Characteristics

Peripheral speed	:	400 m/s
Rotor diameter (= length)	:	1.18 m
Rotational speed	:	6475 revs/min
Open circuit voltage	:	755 volts
Equivalent capacitance	:	1403 farads
Machine current	:	3.33 MA
Discharge time	:	0.5 secs
Brush packing factor	:	0.36
Brush current density	:	15.5 MA/m^2 (10 kA/in^2)
Current collection area	:	0.15 m per collector (2)
Rotor mass	:	10,000 kg

Probably the most critical assumption in this evaluation is that a surface speed of 400 m/s can be achieved. This is significantly greater (11% and 45%, respectively, than has been achieved in brush tests to date at Westinghouse[18] and at ANU[19] (note, however, that in the case of reference 18 these were undertaken at current densities 14% larger than assumed in Table 2). Current R&D programs at Westinghouse directed at steady state current collector improvements have raised current densities to 8 MA/m^2 from 0.16 MA/m^2, using improved monolithic and fiber brush technology.[20-22] The utilization of this technology for pulse duty may yield further significant improvements in current transfer capability.

Although high, the peripheral speed assumed in Table 2 is significantly (20%) lower than is presently employed in bladed gas compressors. The major differences are the rapid deceleration required for inertial pulsed power supplies and, in the long term, the component fatigue caused by cyclic stress variations. The eventual use of homopolar machines for very efficient energy applications will require such machines to have superconducting windings. Detailed designs of superconducting homopolar machines for fusion systems have already been completed.[23,24]

2.4 Intermediate Storage Coils

For a simple capacitive charging LCR circuit, the ratio of the energy transferred from the homopolar generator to the inductive storage coil is a function of the transfer time given by:

$$\frac{E_{coil}}{E_{HPG}} = \frac{\pi^2 + (t/\tau)^2}{\pi^2 \, e^{(t/\tau)} - (t/\tau)^2}$$

where $\tau = L/R$ is the characteristic frequency of the circuit. A minimum efficient energy transfer ratio is probably set by $t/\tau \lesssim 1$, for which $E_{coil} = 0.42 \, E_{HPG}$. Hence, the energy stored in the coil can be expressed as

$$\frac{1}{2} \, L \, I^2 = 0.42 \, E_{HPG}$$

Although multiple staged coils are most likely to be used, inserting the current and energy values of Table 2 shows that not-unreasonable values of 30 μH and 60 μΩ would be required for a single large coil. Even the requirement to store 400 x 0.42 = 168 MJ in a single coil, although a formidable task, does not appear impossible, The magnetic energy stored per unit volume in the coil is

$$E_{coil} = \frac{B^2}{2\,\mu_o}$$

For example, at B = 8 and 10 T, the energy stored is 25 and 40 MJ/m^3, respectively. That is, for the required stored energy, coil volumes of 6.7 m^3 and 4.2 m^3 are required. While large, these values are comparable with those already achieved in several fusion reactor experiments.

Major decisions that have to be made regarding the coil include whether it should be normal, cryogenically cooled, or superconducting, and whether it should have a solenoidal or toroidal configuration. Although cryogenic coils have proved capable of outstanding pulsed duty operation,[9] it is probable that a normally excited coil could be most easily built at this time for experimental purposes where only intermittent operation is required. Ultimately, however, efficiency requirements may require the development of superconducting coil technology for this application. Although a major concern in a coil of this type is the hoop stress generated in the conductors as a result of magnetic forces, it is generally likely that the mechanical coil design will be dominated by the resistance requirements for these applications.

2.5 Switching Considerations

In any LCR circuit where energy is being transferred from one component to another, switching is likely to play a major role. The difference for the applications being considered here is the size of the current being considered; i.e., megamps.

Up to four separate switching functions may be required even in a simple LCR circuit. These functions are:

(1) A make switch to initiate current flow from the homopolar generator to the inductive storage coil.

(2) A shorting or clamp switch to isolate the homopolar generator from the inductor once the latter has been charged up.

(3) An opening switch to transfer the inductively stored energy into the main projectile.

(4) A muzzle shorting or clamping switch to reduce the arcing damage caused by release of stored energy as the projectile leaves the barrel.

Depending on the method of operation of the system components, the required system efficiency, and technology advances one or more of these switches may prove to be unnecessary. Thus, the duties of switch 1 could possibly be incorporated in the brush operation, switch 2 may become redundant if the generator design is such that the unused energy in the storage coil can swing back into the generator after the projectile is fired, and switch 4 may be merely a short circuit across the muzzle of the gun.

Undoubtedly, the most difficult task has to be performed by the opening switch 3. Evaluation of present technology for solid state switches and circuit breakers indicates that these will be unsuitable to interrupt megamp currents without significant development. Explosive switches may ultimately prove to be feasible but, at present, the most suitable concept may simply be a rail switch.[25]

For ultra fast launcher concepts, the overall switching system is dominated by the high current to be switched, and the multiple staged barrel concept which requires very precise sequencing of pulse delivery. Considerable effort will be required to successfully develop a reliable high repetition rate switching system.

2.6 Launcher Barrel

The launcher barrel/rail assembly and the associated projectile comprise the essential portion of the pulsed direct current electromagnetic launcher. They also probably represent the most difficult technical challenge of the entire system. For ultra high velocity, the launcher barrel would be excited in stages in sequence in order to minimize the losses and maintain a steady projectile acceleration. The transient acceleration and bursting forces would be extremely large, requiring sophisticated structural systems.

The projectile sabot in such a barrel would be arc driven, and substantial research work will be required to develop the arc plasma characteristics and the conductor and insulation materials for the barrel and the projectile.

2.6.1 Accelerating Force and Rail Inductance

The accelerating force on the armature for the simple dc rail system is generally expressed as

$$F = \frac{L' I^2}{2}$$

(where L' is the rail inductance per unit length and I is the current), showing that there is relatively little scope in this case for adjusting the factors that provide the accelerating force on the projectile. For a flat parallel rail configuration, L' may be up to about 0.6 μH/m, although the presence of external materials (e.g., a metal barrel) may reduce this. Barber[1] and Marshall[2] found L' ∿ 0.42 μH/m for their experiments. The magnetic field strength in the gap between the rails can be increased by using one or more sets of augmenting rails placed outside the main rails. Large numbers of such rails are not effective, but calculations show that one or two sets of augmenting rails can offer some benefit in increasing B, and hence allowing I to be reduced.

2.6.2 Rail Heating

The transfer of very high currents gives rise to high local temperatures on the surface of the rails as a result of the electrical skin effects. Barber[1] showed that the temperature rise per pulse can be expressed approximately as

$$\Delta T \simeq 0.3 \mu_o^2 \left(\frac{I}{h}\right)^2$$

for copper and most similar metals. Typically, for I/h = 40 MA/m, ΔT ∿ 760°K, indicating that it is difficult to achieve values much greater than this without melting of the rail surface taking place. The more recent calculations reported by Hawke and Scudder[26] confirm Barber's estimates. Although forced cooling may not significantly reduce peak temperatures during each pulse, it will permit repetitive operation to be achieved.

2.6.3 Forces on Rail

The electromagnetic forces exerted on the projectile are also reflected in comparable forces which tend to spread the rails apart. The extent to which these may be tolerated depends not only on the material of the rails but also on the mechanical support structure, as described recently by Hawke and Scudder.[26] Additional forces arise as a result of friction effects, mechanical irregularities in the rail, and mechanical misalignment, but these are generally of a smaller magnitude.

The magnetic forces on the rails are given ideally by

$$\sigma_M = \text{magnetic stress} = \frac{B^2}{2\mu_o} = \frac{\mu_o}{2}\left(\frac{I}{h}\right)^2$$

showing that for $I/h \sim 40$ MA/m^2, $\sigma_M \sim 1$ GPa (= 145 Kpsi). Despite the fact that this substantial force may be reduced by up to 50% in real geometries, it is apparent that both mechanical, electrical, and thermal effects are critical design considerations.

2.7 Current Transfer - Plasma Drive

Despite, or perhaps because of, the use of electromagnetic forces to increase the contact force between a metallic projectile armature and the launcher rails, Barber[27] found that mechanical rail damage (gouging) occurred at sliding speeds above about 600 m/s and that ultimately lack of adequate electrical contact occurred. As a result, it became necessary to introduce a plasma arc drive technique to accelerate the projectiles to higher velocities. The conditions in this 300 kA copper vapor plasma have been inferred by McNab[28] and indicate that temperatures of 4 to 5 eV were achieved at plasma pressures of $\gtrsim$ 1000 atm. Since

earlier small-scale experiments carried out by John Marshall[29] at LASL and others in the 1960's showed that plasma velocities greater than 100 km/s could be achieved in plasma guns, it is clear that this technique offers the greatest promise for the high velocities required here. The main problems appear to be sealing of the projectile in the launcher bore, to prevent leakage of the high pressure plasma past the projectile without introducing high frictional dissipation. There appears to be scope for considerable ingenuity in this area. As yet, unresolved problems may relate to the speed at which the arc may be able to travel on the rail, especially in the presence of a very strong magnetic field. To replenish the arc, it is probable that rail material will have to be vaporized in transit. While there has been shown to be possible in plasma guns, it should be recalled that the plasma masses in those cases were much lower (i.e., micrograms) than those probably required for macroparticle acceleration.

It seems likely that the major advantage to be gained by the use of the plasma drive may be that the driving current does not have to pass through the projectile. With suitable design, possibly involving an ablation shield to minimize or eliminate heat transfer, heating of the projectile could be kept to an acceptable level. This is in contrast with the severe internal electrical heating which occurs when current transfer is through a metallic armature where softening, and ultimately melting, of the projectile becomes the factor limiting the stress than can be tolerated. An additional benefit of reducing, or eliminating, the metallic armature is that the system efficiency will be increased as a result of a reduction in the mass of the package to be launched.

3. MODEL ELECTROMAGNETIC LAUNCHER FACILITY

3.1 Purpose

A small electromagnetic launcher facility is under construction at Westinghouse for the experimental investigation of launcher performance. The system will be powered by a 36 kJ capacitor bank which will delivery currents up to 120 kA. With a 2 m barrel, it is estimated that this is sufficient to launch 3 to 5 gm projectiles to velocities above 1 km/sec. The principal areas to be investigated with this system include:

1. Ultra high velocity sliding contact properties such as friction, wear, current transfer, and load requirements for various combinations of materials,
2. plasma arc driven projectiles,
3. high current pulsed switchgear, and
4. muzzle arc suppression devices.

Details of the component designs are given below.

3.2 Power Supply

The capacitor bank comprises 12, dual 120 μF, 5 kV capacitors for a total of 2880 μF and a maximum stored energy of 36 kJ. The bank is discharged through six SCR switches in parallel, each switch containing two 2.8 kV SCR's in series.[30] The SCR's have a steady-state current rating of 800 A and a half cycle (8.3 msec) surge rating of 13 kA (the bank output pulse can be conservatively approximated by a 60 Hz, half cycle pulse). For non-repetitive discharge and without voltage reapplication the surge rating can be increased to $\sim$ 19 kA. The SCR's will be fired through a transformer coupled power supply to handle the

5 kV standoff requirement. To ensure equal current distribution in the switches, the bank is divided into six sections, each discharging through an individual switch. The six sections are then joined together at the output terminals of the SCR switches.

A diode crowbar network is used to avoid ringing. The diodes are attached directly to the terminals of each capacitor can to maximize the energy delivered to the barrel. Each diode crowbar is a series set of two 3 kV diodes, with a steady state rating of 600 A and a half cycle surge rating of 7 kA.[31]

The capacitor bank control system includes voltage and firing controls, interlocks, and a safety dump circuit. In addition, each capacitor is individually fused to limit the energy which would be dissipated internally in a failed (shorted) capacitor can.

3.3 Inductor

The capacitor bank discharges into an inductor which is connected in series with the barrel. The inductor, together with the bus bar stray inductance determines the peak current in the system. A total inductance of 5 μH (corresponding to a peak current of ∿ 120 kA) was selected, requiring the inductor to be 4.5 μH. The physical characteristics of the design used are given in Table 3.

TABLE 3. Inductor Characteristics

Inductance	:	4.5 μH
Resistance	:	375 μΩ
Turns	:	6.5
Conductor (4 in parallel)	:	6.4 mm x 4.2 mm
Mean Diameter	:	369 mm
Length	:	493 mm

A four start winding is used for ease of fabrication. The conductors are insulated, wound on a solid wooden form, and then banded with fiberglass tape. The four leads are brought radially inward to the center of the form on each end and joined to the primary bus bars. The calculated temperature rise during a single pulse is $\sim$ 3°C.

3.4 Barrel

A cross section of the first barrel built is shown in Figure 1. Micarta plates are used to restrain the rails against the magnetic pressure ($\sim$ 3.6 x 10^5 Pa maximum) and to maintain their alignment. These plates are each 413 mm long and assembled such that top and bottom axial joints overlap. Shorter pieces are used on the ends of the barrel. This type of design was used to facilitate rail changes and also to minimize the repair work necessary if a projectile fails in the bore. The copper rails are 19.05 mm high and 4.76 mm thick. The bore is 12.7 mm x 12.7 mm and is 2 m long. A 200 mm fiberglass I-beam is used to support the barrel. Fiberglass was chosen to minimize the interaction of the barrel magnetic field with surrounding materials. The fully assembled barrel is shown in Figure 2.

For this rail geometry, the high frequency inductance was calculated to be 0.494 μH/m. Meausrements at 1 kHz on the actual barrel system yielded a value of 0.487 μH/m, in excellent agreement with the calculated value. During operation, the peak rail temperature is estimated to be $\sim$ 78°C.

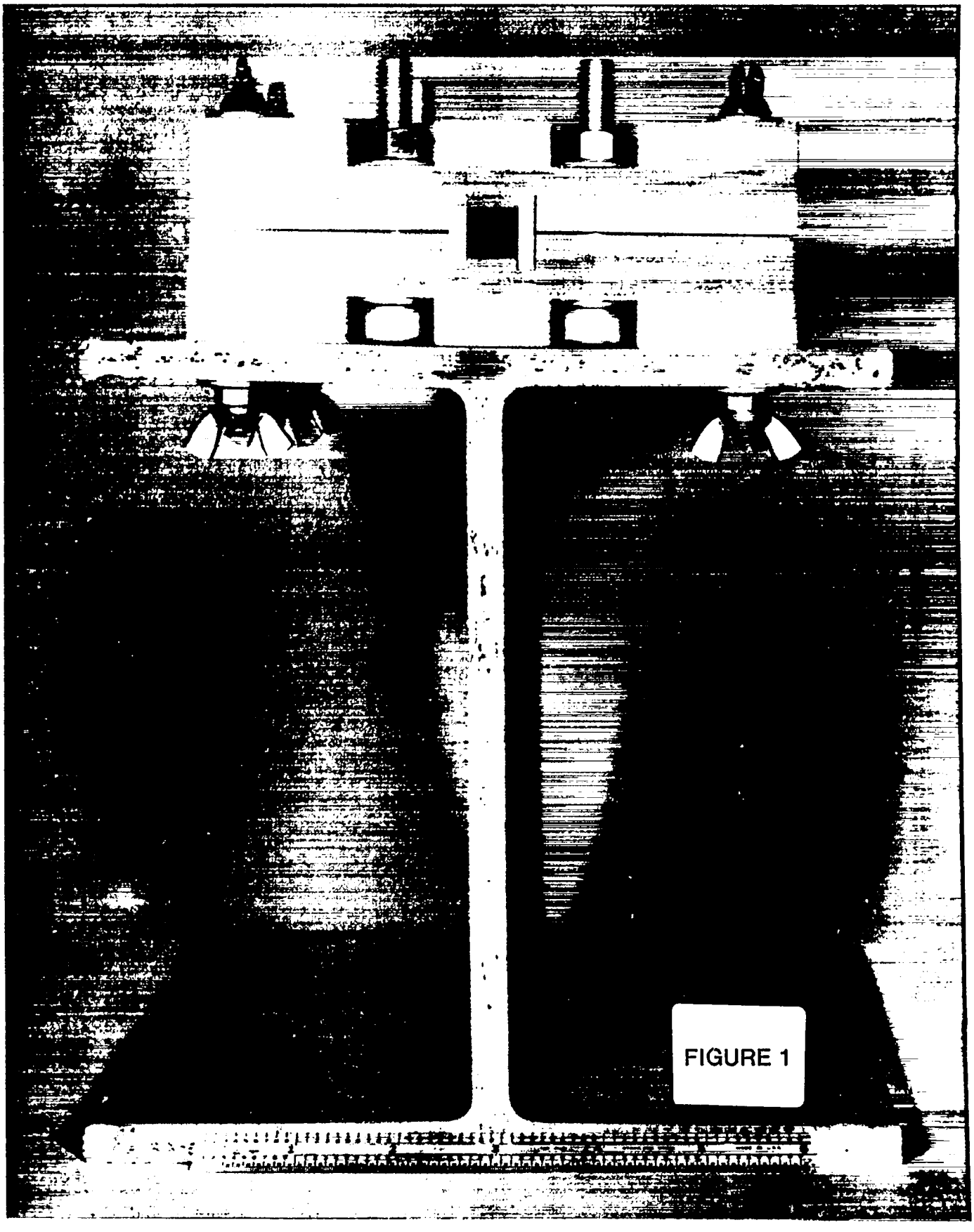

FIGURE 1

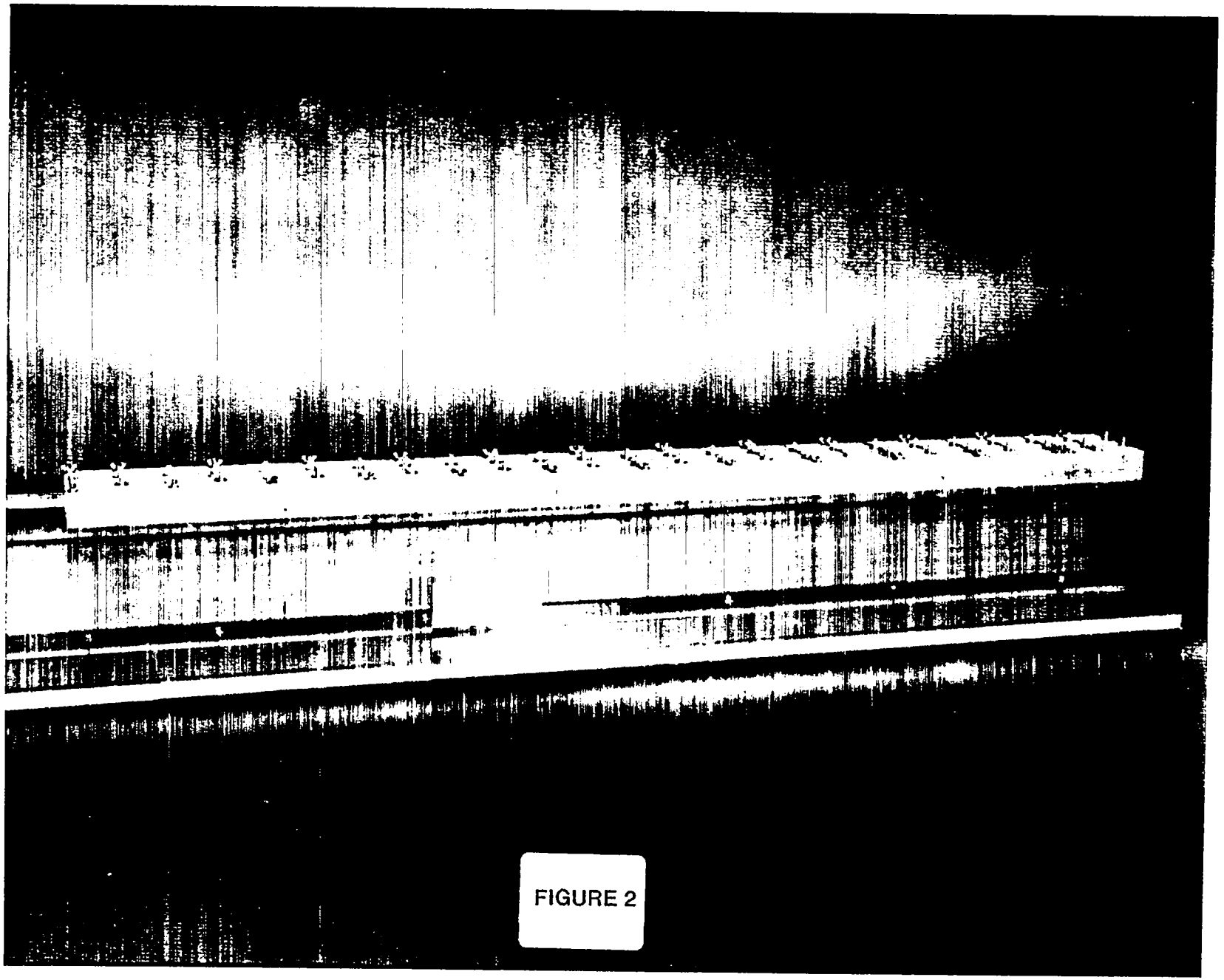

FIGURE 2

3.5 Projectile

For the initial experiments, an aluminum armature will be used to accelerate a polycarbonate projectile. The armature is made by stacking 15 chevron-shaped aluminum conductors to give multiple armature-rail contacts. The ends of the aluminum pieces facing the polycarbonate are flattened and the angle of contact with the rails is such that the Lorentz Force provides $\sim 10^{-2}$ N/A contact force. The armature mass is 1.34 gm and it is estimated that it will reach a peak temperature of about 410°C.

3.6 Performance Calculations

A computer program which simulates launcher operation has been used for sizing the components described here and for predicting performance under various conditions. Table 4 gives the performance data for a typical set of initial conditions.

TABLE 4. Calculated Launcher Performance Data

Initial Conditions

Circuit Inductance	:	5 μH
Circuit Resistance	:	500 μΩ
Capacitor Bank	:	2800 μF @ 5 kV
Rail Inductance	:	0.5 μH/m
Rail Resistance	:	690 μΩ/m
Rail Length	:	2 m
Armature Area	:	32.3 mm^2
Armature Length	:	14 mm
Launched Mass	:	5.0 gm

TABLE 4 (Continued)

Performance

Terminal Velocity	:	1.2 km/sec
Maximum Current	:	111 kA
Maximum Acceleration	:	0.71×10^6 m/sec^2

3.7 Range and Instrumentation

After leaving the barrel muzzle, the projectile will pass through a 1.2 m instrumentation section where its velocity will be determined from the time interval between two laser triggered photodiodes. After this section, the projectile will be stopped nondestructively in 1.2 m catcher. This will allow wear data to be obtained on the armature and its general condition to be determined. A flash x-ray system will be added in the future for inbore projectile photographs.

The barrel will contain pick-up coils for position versus time measurements during acceleration. Current and voltage data for the rails will also be recorded.

4. CONCLUSIONS

Major advances in the technology of electromagnetic launchers can be expected during the next few years, particularly as the result of the DARPA/ARRADCOM program to demonstrate technology for Department of Defense applications. The requirements for impact fusion will necessitate further significant improvements in system and component technology. A sufficient base of information on advanced current collection, homopolar generators and inductors exists that improvement can be foreseen in those areas.

However, it is apparent that major emphasis will have to be applied to barrel/rail and projectile technology improvements, and to switching, especially if multi-shot repetitive operation is required.

ACKNOWLEDGMENTS

The contributions of all the Westinghouse scientists, engineers, and consultants involved in the DARPA/ARRADCOM project are gratefully acknowledged. The inputs of Dr. J. P. Barber of International Applied Physics, and Dr. S. J. Bless of the University of Dayton Research Institute, and their colleagues form an integral and important part of the program

REFERENCES

1. J. P. Barber, "The acceleration of Macroparticles and a Hypervelocity Electromagnetic Accelerator", Ph.D. Thesis, Australian National Unviersity, March 1972.
2. S. C. Rashleigh and R. A. Marshall, "Electromagnetic Acceleration of Macroparticles to High Velocities", J. App. Phys. 49, 2540, 1978.
3. L. E. Moberly and J. L. Johnson, "High Current Brushes. I. Effects of Brush and Ring Materials", IEEE Trans., CHMT-1, 36, 1978.
4. P. K. Lee and J. L. Johnson, "High Current Brushes. II. Effects of Gases and Hydrocarbon Vapors", IEEE Trans., CHMT-1, 1978.
5. I. R. McNab and J. L. Johnson, "High Current Brushes. III. Performance Evaluation for Sintered Silver-Graphite Grades", IEEE Trans., CHMT-2, 1979.
6. J. L. Johnson and O. S. Taylor, "High Current Brushes. IV. Machine Environment Tests", 25th Holm Conference, Sept. 10-12, 1979.
7. C. J. Mole and E. Mullan, "Design Trends in Homopolar Machines Since the Mid-1960's", Seminar on Energy Storage, Compression, and Switching, Canberra, Australia, November 15-21, 1977.
8. C. J. Mole and E. Mullan, "Design of a 10 MJ Fast Discharging Homopolar Machine", Seminar on Energy Storage, Compression, and Switching", Canberra, Australia, November 15-21, 1977.
9. E. Mullan, M. A. Janocko, and D. C. Litz, "A Superconducting 0.54 MJ Pulsed Energy Storage Coil", Seventh Symposium on Engineering Problems of Fusion Research, Knoxville, Tenn., October 25-28, 1977.

10. D. E. Brast and D. R. Sawle, "Feasibility Study for Development of a Hypervelocity Gun", MB Associates, Report MB-R-65/40, 1965.

11. W. Bostick, Phys. Rev., 104, 242, 1956.

12. P. Mostov, J. H. Neursinger, and D. S. Rigney, "Electromagnetic Acceleration of a Plasma Slug", Phys. Fluids 4, 1097, 1961.

13. E. L. Shriver, "Analytical and Experimental Investigation of the Coaxial Plasma Gun for Use as a Particle Accelerator", NASA-TN-D-6687, April 1972.

14. C. J. Michaels, "Coaxial Plasma Gun Research at Lewis Research Center", NASA-TM-X-1600, March 1968.

15. F. Winterberg, "On the Attainability of Fusion Temperatures Under High Densities by Impact Shock Waves of Small Solid Particles Accelerated to Hypervelocities", Z. Naturforschg. 19a, 231, 1964.

16. E. R. Harrison, "Alternative Approach to the Problem of Producing Controlled Thermonuclear Fusion", Phys. Rev. Letts. 11, 535, 1963.

17. F. Winterberg, "Implosion of a Dense Plasma by Hypervelocity Impact", 1967.

18. R. A. Marshall and R. M. Slepian, "Pulsed High Power Brush Research. III. Experiments at 15.5 MA/m^2 and 277 m/s", IEEE Trans., CHMT-2, 100, 1979.

19. R. A. Marshall, "Design of Brush Gear for High Current Pulses and High Rubbing Velocities", IEEE Trans., PAS, 1177, 1966.

20. R. M. Slepian, "High Current Brushes. V. Subdivided Monolithic Brushes at Very High Current Levels", 25th Holm Conference, Sept. 10-12, 1979.

21. P. Reichner, "Metallic Brushes for Extreme High Current Applications", 25th Holm Conference, September 10-12, 1979.

22. I. R. McNab and W. R. Gass, "High Current Density Carbon Fiber Brush Experiments in Humidified Air and Helium", 25th Holm Conference, Sept. 10-12, 1979.

23. K. I. Thomassen et al., "Conceptual Engineering Design of a One-GJ Fast Discharging Homopolar Machine for the Reference Theta-Pinch Fusion Reactor, EPRI Report.

24. C. J. Mole, et al., "Design and Fabrication of a 20 MJ Fast Discharging Homopolar Machine for Tokamak Ohmic Heating", Final Report to LASL, Subcontract XN47-66667-1, April 1978.

25. J. P. Barber, "A Rapid Switching High Current Switch", Aeroballistic Range Association Meeting, AEDC, Tennessee, 1973.

26. R. S. Hawke and J. K. Scudder, "Magnetic Propulsion Rail Guns: Their Design and Capabilities", Second Megagauss Conference, May 1979, UCRL Preprint 82677.

27. J. P. Barber, "Experimental Observations on Rail Gun Acceleration", Aeroballistic Range Association Meeting, AEDC, Tennessee, 1973.

28. I. R. McNab, "Electromagnetic Macroparticle Acceleration by a High Pressure Plasma", Comments made at Gun and Launch Applications of EM Pulse Power, December 5 & 6, 1978, Annapolis, to be published.

29. J. Marshall, Phys. Fluids 3, 1960.

30. Westinghouse Model T960-2808-03-DH

31. Westinghouse Model R720-3006.

ELECTROMAGNETIC ACCELERATOR CONCEPTS

Henry H. Kolm

Massachusetts Institute of Technology
Francis Bitter National Magnet Laboratory
Cambridge, Massachusetts, 02139.

Abstract

Recent advances in energy storage, switching and magnet technology make electromagnetic acceleration applicable to guns, launchers and reaction engines. Some of the available accelerating mechanisms seem applicable to the achievement of impact fusion. These range from the dc railgun driven by energy stored inertially and transferred through a storage inductor, to the opposite extreme, the synchronous mass driver energized by a line of oscillating coil-capacitor circuits. A number of hybrid variants are also promising. These include railguns with augmenting fields, segmented railguns, helical railguns, superconducting slingshots, and a superconducting quench-propagation gun. A novel system described here is the momentum transformer, which transfers momentum from a massive chemically or magnetically driven armature to a much lighter projectile by magnetic flux compression.

The Railgun Family

The Classic Railgun consists of two parallel rails connected to a source of direct current, the projectile consisting of a short-circuit slide propelled between the rails by the Lorentz force $F = BLI/2$, where B is the magnetic field intensity between the rails in Tesla, L is the length of the current path through the slide, or the gap between rails in meters, and I is the current through the slide in amperes. Thefactor of 1/2 accounts for the fact that the field is B behind the slide, but zero in front of it, making the average B/2. The thrust force can also be expressed as $F = L'I^2/2$, where L' is the inductance per unit length of the rails. L' has a typical value of 0.3 microhenry/meter for a gap width to rail height ratio of 1/3; it is relatively insensitive to this ratio, and is independent of scale size. Railguns have been studied extensively by Brast and Sawle of MB Associates in the mid-sixties under NASA contract[1] and more recently by Marshall and Barber[2,3] using the World's largest homopolar generator at the Australian National University in Canberra, which stores 500 MJ. Railguns can operate in two distinct modes: by conduction through the sliding projectile, and by conduction through an arc confined so as not to bypass the projectile. Using a

non-conducting lexan projectile of about 3 gram mass, Marshall and Barber achieved 5.9 m/s with a 5 m long barrel, at an acceleration of 250,000 g. The distinction between brush conduction and arc conduction is likely to vanish in the sense that brush conduction will be supplemented by an arc as the limit of brush conduction current density is exceeded. The practical limit of railgun performance in terms of projectile size, acceleration, length and final velocity will have to be explored by progressive refinement of materials and engineering details. An effort at Westinghouse to explore the 300 gram mass range is described elsewhere in this report.

The advantages of the railgun are its simplicity and demonstrated acceleration capability. In relation to the velocities required for impact fusion, it has three fundamental limitations. As a railgun is lengthened, the resistance and inductance of the rails eventually absorb a dominant fraction of the energy. The effect results in a velocity saturation which is seen to begin at about five meters length in the Canberra tests. A third fundamental length limitation is the increasing back-emf with velocity. The intermedieate energy storage inductor will ensure continued current flow even when the back-emf exceeds the output voltage of the homopolar generator or compulsator, but there is a practical limit to the voltage which can be withstood by the gap between rails, which implies a practical velocity limit depending on scale size. There are several schemes for circumventing the limitations of the classic railgun.

The Augmented Railgun provides a supplementary magnetic field by means of current which does not flow through the sliding brushes. This supplementary current can be carried by separate conductors flanking the rails, or it can be added to the rail current itself by simply terminating the rails with a load resistor or inductor at the muzzle to carry a fraction of the current. The rails themselves will obviously contribute more field than auziliary rails located farther away, but the use of superconducting auxiliary rails might be expedient. It should be noted that railgun fields are much higher than superconductor critical fields. Augmentation has the additional effect of reducing the amount of current flowing through the brushes and the projectile, and thereby reducing the necessary conductor mass which must be accelerated. It should also

be noted that the augmenting field is twice as effective as the rail field itself. The augmenting field prevails in front of the projectile as well as behind it, and therefore the factor of one half in the Lorentz force expression is eliminated as far as the augmenting field is concerned. This fact is important inasmuch as it reduces to one half the rail bursting forces which must be contained for a given acceleration. Augmentation thus ameliorates both the brush current density limitation and the bursting force containment limitation of the classic railgun.

The Segmented Railgun eliminates the two length limitations imposed by rail resistance and inductance, but not the speed limitation of back-emf. Each of a number of segments is fed by an independent energy source. Certain commutation problems will have to be solved as the projectile transits between segments. On the other hand, it should be possible to store and re-use the energy remaining in each segment as the projectile leaves, which dissipates as a muzzle flash in the classic railgun.

The Mass Driver.

Linear synchronous motors based on a passive vehicle with superconducting coils, levitated and guided by induced repulsion forces, were first proposed for high speed ground transportation by J.Powell and G. Danby of Brookhaven[4] in 1966, and reduced to practice by H.Kolm and R. Thornton at MIT in 1972[5] in a system called the MIT "Magneplane". The vehicle rides the crest of a travelling magnetic wave much like a surfboard, synchronization being achieved on the basis of position information transmitted from the vehicle to wayside power conditioning units. In 1977 G.K.O'Neill and H.Kolm and collaborators[6] applied the technique to a device originally intended for launching payloads at a high repetition rate from the lunar surface to construction sites in space. This "mass driver" uses re-circulating buckets which release their payloads into precisely controlled trajectories and are decelerated and re-loaded, and periodically re-cooled and re-charged with current. The mass driver represents an electromagnetic launcher proposed many years ago by Arthur C. Clarke[7] and Robert Heinlein[8]. A primitive version of such a device was actually constructed in the twenties by Northrup[9] at Princeton University.

Mass drivers may be planar (flat, square bucket coils travelling between two planes of flat, square drive coils which look like two parallel ladders), or axial (cylindrical buckets travelling inside a coaxial line of circular drive coils), as described elsewhere[6]. In either configuration the instantaneous thrust is the product of three quantities: $F = I_d I_b (dM/dx)$, the instantaneous drive coil current, the instantaneous bucket coil current, and the local space derivative of the mutual inductance M between the interacting bucket and drive coils, taken in the direction of motion. The nature and limitations of the mass driver can be understood entirely in terms of this mutual inductance gradient, which behaves as shown in Fig. 1.

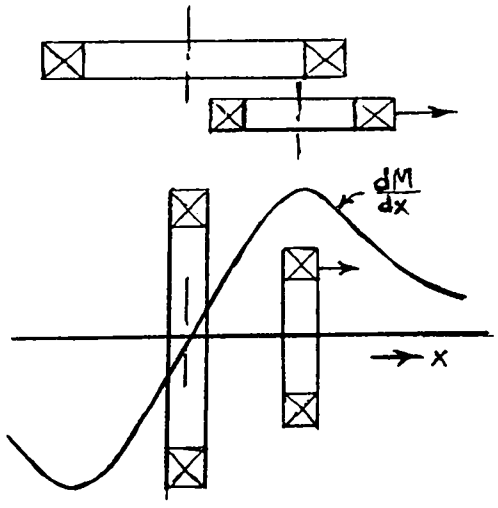

Fig. 1: The mutual inductance gradient as a function of drive coil position for planar and axial mass drivers; ref. 6.

The mutual inductance gradient is zero when a bucket coil is centered at the drive coil, the point at which the mutual inductance itself is maximum; it has positive and negative peaks at a certain distance on either side of the drive coil, called the "inductance length". This length depends on the ratio of bucket to drive coil radii in the manner shown in Fig. 2; it is typically equal to the drive coil radius in the case of mass drivers designed previously, which were of about four inch caliber. For optimized performance, the oscillating current in the drive coil must resemble the quasi-sinusoidal variation of dM/dx as a bucket passes a drive coil. It is this requirement which imposes the only velocity limitation on a mass driver. In a four inch caliber mass driver accelerating to 20 km/s for instance, the final drive coils would have to oscillate at a period of 20 microseconds, which is quite reasonable. Substantially higher velocities will require very high capacitor voltages, and ultimately single-turn drive coils.

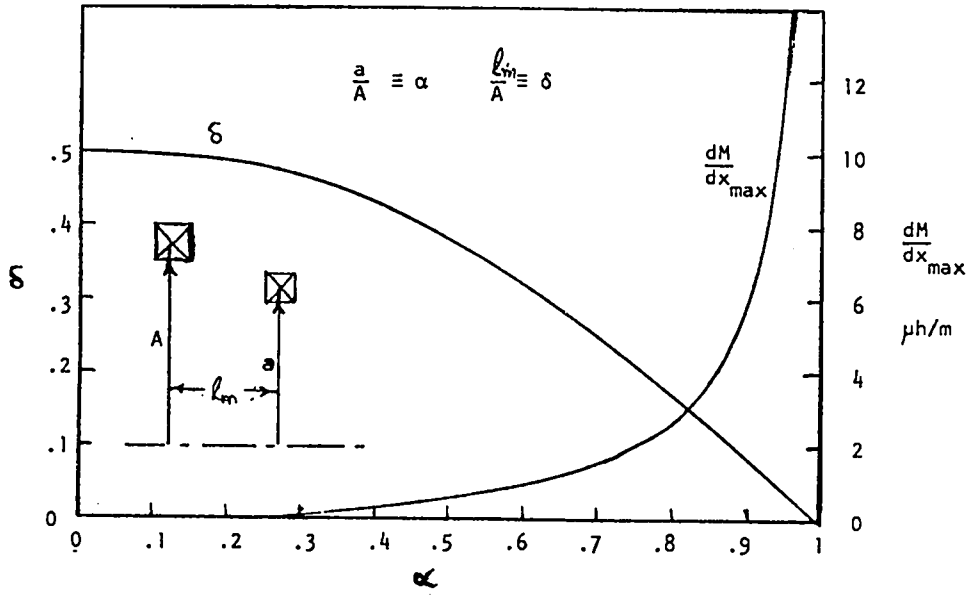

Fig. 2: Maximum inductance gradient $(dM/dx)_{max}$ and normalized inductance length δ (maximum thrust position / drive coil radius) as a function of the diameter ratio a/A = α.

The magnitude of the mutual inductance gradient, or the amplitude of its variation in Fig. 1, represents the coupling coefficient, or the degree of inductive coupling between bucket and drive coils. It depends on the effective bucket to drive coil diameter ratio, which is generally denoted by alpha in mass driver literature. The effective diameter of each coil is not its inside or outside diameter, but the diameter of the equivalent current filament, or the diameter of the center of mass of the current distribution in each coil. This dependence is shown in Fig. 2.

These circumstances explain certain scaling limits. Mass drivers designed previously[6] in the four inch caliber range had alphas slightly better than 0.5. Values as high as 0.75 can probably be achieved in the twelve inch caliber range, due to fixed clearance requirements. On the other hand, diameter ratios become worse if one attempts to increase the acceleration by making the drive or bucket coils fatter, because the current centroids are then separated by a greater distance.

There is a lower limit to the scale-down of mass drivers; a one inch diameter bucket, for instance, is unthinkable. It would have too small a volume-to-surface ratio to permit reasonable thermal inertia, a problem further aggravated by the lack of sufficient space to adequately insulate

the superconducting coils from their surrounding radiation shields and from the payload. Mechanical supports would simply be too short to reduce conduction losses by the available techniques of cryogenic design. The practical lower limit to size might lie in the vicinity of two inch caliber.

The fact that four inch caliber mass drivers with poor coupling coefficients corresponding to an alpha ratio of 0.5 have electrical-to-mechanical energy conversion efficiencies as high as 90% reflects a unique and very important characteristic of mass drivers. Most of the magnetic energy in a drive coil which is not used as mechanical energy due to poor coupling is returned to the capacitor, and only a small fraction of it is lost resistively in the drive coil. The poor coupling coefficient therefore affects only this relatively small loss. In the case of commutating dc motors discussed later, this is not the case, and the alpha ratio becomes very much more crucial.

A related property of mass drivers is their ability to use the energy storage capacitors over and over again to charge hundreds or even thousands of drive coils during a single launch cycle. The number of times a given capacitor can be used is limited in practice only by the length of the feeder line required to connect it to even more drive coils. Eventually it becomes more expedient to distribute a number of additional capacitors along the mass driver and to connect each to only a small number of nearby drive coils.

Limitations of the mass driver are inherent in its complexity. Calibers much below four inches are not practical for reasons stated above, and the structural complexity of cryogenic buckets limits acceleration to the order of 1,000 g, imposing length requirements in the kilometer range.

A question of interest here is whether a mass driver could be used to accelerated cheerio-sized, expendable superconducting rings to the range of several hundred km/s. Two circumstances conspire against such a scale-down. As mentioned above, alpha values become very much worse, probably below 0.1. The resultant poor coupling coefficient then imposes prohibitive drive coil current requirements to achieve a given thrust. This will of course also increase the resistive dissipation to the point

where efficiency may be unacceptable. The second scale-down problem involves the time domain and is even more serious. The small inductance length of about 0.125 inch (which will also be the optimum coil spacing) requires a drive coil discharge period of about 0.13 microsecond at the 100 km/s velocity point. Generating such fast-rising pulses of sufficient power content requires unrealistic capacitor voltages, particularly considering the very small drive coils into which these capacitors must discharge.

The essence of the scale-down problem can be understood by realizing that the projectile in a linear synchronous motor is a magnetic dipole, and the force on a dipole is proportional to the magnetic field *gradient in the direction of motion, in relation to the size of the dipole.* It is difficult to increase the gradient as the dipole size is decreased. Perhaps the synchronous accelerator will prove useful only as the first stage in a multi-stage process. It might serve to accelerate a relatively massive carrier from which smaller particles are then ejected with reasonable momentum conservation by the momentum transformer to be described below.

The Helical Railgun

The classical railgun is a single-turn motor. A multi-turn railgun would reduce the rail current and the brush current by a factor equal to the number of turns and thereby circumvent two of the most stringent limitations. It therefore seems worth-while to investigate a hybrid between the railgun and the mass driver, the "helical railgun".

In the helical railgun, shown in Fig. 3, the two rails are surrounded by a simple helical barrel which is logically constructed in the manner of a Bitter solenoid, a structue used to contain the world's highest continuous magnetic fields at the MIT National Magnet Laboratory. The projectile or re-useable bucket is also helical, and is energized continuously by two brushes sliding along the rails. Four additional brushes on the bucket serve to energize and commutate several windings of the helical barrel immediately in front of and behind the helical bucket, at a distance of about one inductance length. The barrel windings behind the projectile must be energized in the direction opposite the bucket

coil (bucking direction) so as to generate a repulsive force, while the windings in front of the bucket must be energized in the same direction to generate an attractive force. The number of barrel turns which can be energized effectively at one time are limited to the region within which the mutual inductance gradient has an appreciable value, and this circumstance again precludes very small calibers.

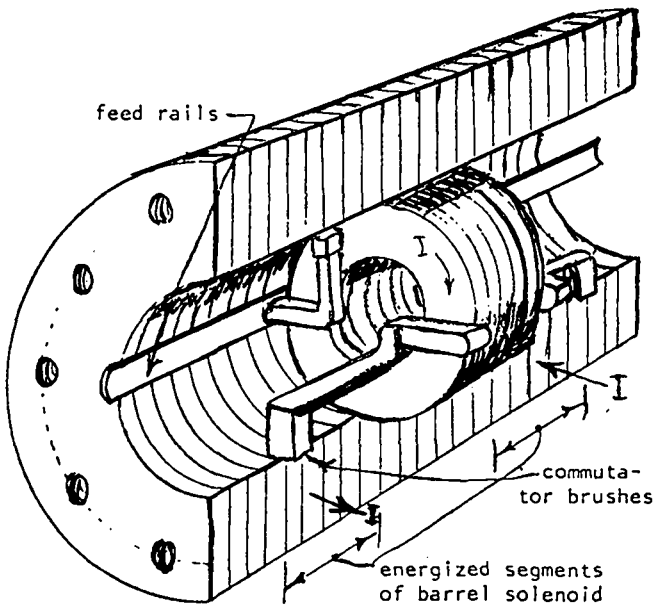

Fig. 3: The helical railgun.

The dominant limitation of the helical railgun will clearly be the as yet unexplored brush problems at very high speed, and the heat input to the bucket coil. In comparing the helical railgun with the mass driver, the crucial question is whether the railgun can develop sufficient acceleration to achieve the required velocity before its bucket melts.

To develop an intuitive feel for the comparison, it is useful to consider that for periods less than about one tenth second one can pass higher current densities through normal metal conductors than through presently available superconductors, which can carry conservatively 25 kA/cm^2, and probably as much as 100 kA/cm^2 if one pushes the limits. At an acceleration of 250,000 g, the Canberra record for 3 gram payloads, one tenth second would suffice to reach 250 km/s, if the railgun could be made 12.5 km long by using several sections in series.

The Superconducting Slingshot.

There is a family of accelerators which permit utilization of superconducting energy storage without the need for direct physical connection to the superconductor. Consider a short superconducting solenoid which is free to slide inside a long one. The travelling solenoid will be eith-

er attracted toward or repelled from the center of the long solenoid, depending on the relative current directions in the two solenoids. Either configuration can serve as an electromagnetic slingshot. In the attractive configuration the travelling solenoid would serve as the payload-carrier. Released at the breach end of the barrel coil, it will accelerate to the center where the payload will be released at the maximum velocity, come to rest at the muzzle end of the barrel, and then return empty to a position short of its release point, from where it can be returned to the release point by mechanical or electrical means. The oscillation is inherently loss-less. In the repulsive configuration, the travelling solenoid will be moved by mechanical force to a point just beyond the center of the barrel. When released, it will be expelled from the muzzle end as part of the payload.

Magnetic slingshots will only attain velocities of several hundred m/s, but they can serve as the input stage of a momentum transformer, to be described below. Slingshots can operate as simple heat engines, using thermal energy without the need for storage in electrical form.

The Superconducting Quench-Gun

By successively quenching a line of adjacent coaxial superconducting coils forming a gun barrel it is possible to generate a wave of magnetic field gradient travelling at any desired speed. A travelling superconducting coil can be made to ride this wave like a surfboard. The device in fact represents a mass driver in which the propulsion energy is stored directly in the drive coils. It should also be possible to make the quench-gun self-synchronizing by using the field of the travelling coil to trigger a quench when it reaches the proper position with respect to each individual drive coil. As in the case of the mass driver, the travelling coil is exposed to a constant field and field gradient. It is subject to an abrupt field change only at the instant the first drive coil is quenched.

The quench gun shares various attributes with the mass driver: it can be guided without contact by induced repulsion forces, it has no fundamental limit of length or speed. It can also be realized in planar rather than axial configuration.

The Momentum Transformer.

The momentum transformer makes use of a so-called "flux concentrator, first investigated by Howland[10] at the MIT Lincoln Laboratory in 1960. It is simply a conducting cylinder with a funnelled bore and one or more radial slots extending from the inside to the outside surface, as shown in Fig. 4. The cylinder is surrounded by a pulsed field winding, preferably imbedded in a helical groove to minimize hoop stresses on the winding. A fast pulse current in the winding induces an opposite image current in the outer surface of the cylinder. Due to the radial slot, this induced current is forced to return along the inner surface of the cylinder, thereby generating a magnetic field in the bore. All of the flux which would have passed through the coil in the absence of the concentrator is thus compressed into the bore, resulting in a field intensity higher than it would have been without the concentrator by about the outside-to-inside area ratio. The device was used at MIT for high field research and also for metal forming. In 1956 Chapman[11] used a flux concentrator with a tapered bore for accelerating milligram metal spheres to hypervelocities. Using a first stage explosive flux compressor, Chapman managed to reach 7 Mgauss with an initial field of only 40 kgauss.

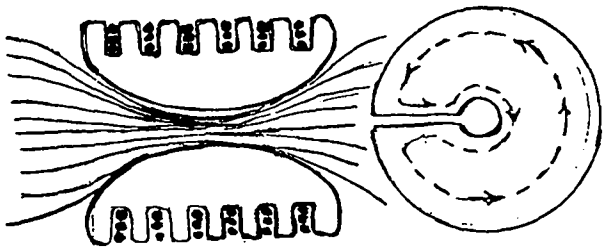

Fig. 4: The Flux Concentrator.

The momentum transformer proposed here uses a non-destructive flux concentrator as the armature of a first stage accelerator. It can be driven to moderate velocity by any means. As shown in Fig. 5, the travelling concentrator carries a much smaller projectile. When the concentrator enters a region of stationary field, it compresses the prevailing flux into its interior

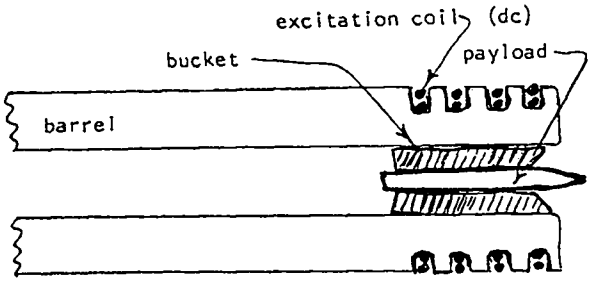

Fig. 5: The Momentum Transformer.

and thereby expels the payload cylinder at a much higher velocity. A large fraction of the total kinetic energy is transferred to the payload. Of course the effective pulse duration must be short enough to make the skin depth small compared to the dimensions of both the flux concentrator and the outer confining barrel. The flux concentrator could operate like a primary piston, oscillating back and forth through the action of a superconducting slingshot or a synchronous mass driver. Both payload an launch energy could be supplied to the piston at the breach end of the barrel at the beginning of each cycle.

Impulse Accelerators.

An ordinary induction motor is characterized by a slip frequency, or a slip velocity between the moving rotor (slidor) and a rotating (translating) magnetic field structure generated by the stator. For example, a snowmobile with magnets attached to its treads would be propelled along a frictionless metal surface by induced drag in a manner analogous to a paddle-wheeler or a canoe paddle: in both cases propulsion requires a slip velocity which involves energy dissipation.

There exists a second family of induction motors, however, which operate in a synchronous manner analogous to a surf-board rather than a paddle-wheeler, and which differ in a fundamental way from ordinary induction motors. Synchronous induction motors involve no slip and require no dissipation: they will work with superconducting rotors or slidors, while ordinary induction motors will not. The fundamental process is exemplified by a brass washer placed at the mouth of a pulsed field coil: it will be propelled by an impulse when the coil is pulsed. The process can be repeated periodically. A line of pulse coils such as a mass driver will propel a bucket consisting of a short-circuited ring if each coil is pulsed at the proper instant. The device is a synchronous induction motor, or an impulse accelerator.

If the bucket of a mass driver has normal conductor coils which are short-circuited, the decay time of the induced current is governed by the resistance-to-inductance ratio R/L, which depends only on the conductor cross section of the bucket coils and is independent of the number of turns into which the conductor is subdivided. This time constant is typi-

cally of the order of 0.01 second, a period which is long compared to the transit time between drive coils. It is therefore possible to sustain the induced current with relatively little effort by means of suitably synchronized asymmetric pulses superimposed on the sinusoidal pull-push oscillation of the drive coils. The asymmetry is needed to insure uni-directional induction. The impulse accelerator is interesting because it is able to accelerate cheerio rings made of conducting material, or for that matter any pelletized conductor, without physical contact, at high repetition rate, though at low efficiency compared to the mass driver. The device is inherently very simple and has infinite service life.

References.

1. D.Brast and D.Sawle, Feasibility study for development of a hypervelocity gun, Final Report, NASA Contract NAS 8-11204, May 1965.
2. S.Rashleigh and R.Marshall, Electromag. Accel. of macroparticles to high velocities, J.Appl.Phys. Vol. 49(4), 1978, p. 2540.
3. J.Barger, The accl. of macroparticles and a hypervelocity electromag. accel., Diss. 1972, Dept. Engr. Phys., Australian Natl. Univ.
4. J.R.Powell and G.T.Danby, The Lin. Synch. Motor and High Speed Ground Transp., 6th Intersoc. En. Conv. Conf., Boston, 1971.
5. H.Kolm and R.Thornton, The Magneplane: Guided Electromagnetic Flight, Proc. 1972 Appl. Supercon. Conf., Annapolis.
   H.Kolm et al.: The Magneplane System, Cryogenics, July 1975.
6. Proc. of the 1976 NASA-AMES Study on Space Manufacturing; Progress in Astronautics and Aeronautics, Series Vol. 57.

   Proc. of the 1977 NASA-AMES Study on Space Manufacturing, being published as a NASA technical report.

   H.Kolm, Basic Mass Driver Reference Design, Proceedings of the Third Princeton Symposium on Space Manufacturing, 1977, published by AIAA.

   G.K.O'Neill, The Colonization of Space, Phys. Today, Vol. 27, No. 9, Sep. 1974.
7. A.C.Clarke, Electromagnetic Launching as a Major Contribution to Space Flight, JBIS, Vol. 9, No. 6, Nov. 1950.
8. R.A.Heinlein, The Man who Sold the Moon, Signet NY 1951.
9. Edwin Fitch Northrup, Zero to Eighty, Science Pub. Co., Princeton 1937.
10. B.Howland and S.Foner, Flux Concentrators, High Magnetic Fields, H.Kolm, editor, Wiley 1962.
11. R.Chapman, Field Compression Accelerators, Proc. Conf. Megagauss Fields, Frascati, 1965.

GASDYNAMIC ACCELERATION OF MACROPARTICLES TO VERY HIGH VELOCITIES*

F. Winterberg
Desert Research Institute, University of Nevada System, Reno, Nevada 89507

ABSTRACT

It is shown that large macroparticles may be accelerated up to several 100 km/sec by ultrahigh pressures generated locally through coalescing Riemann waves focused both in time and space. Focusing in time can be done by a piston with a specified programmed time dependent velocity and focusing in space by reflection from a curved concave wall. The macroparticle is accelerated by the stagnation pressure of the coalescing waves acting on its backside. The piston can be propelled by a recoilless gun driven by an intense charged particle beam. In this way the beam power can be reduced by about $\sim$ three orders of magnitude compared to more conventional target implosion schemes.

INTRODUCTION

It has been known for a long time that if a way could be found to accelerate macroscopic objects, called macroparticles, to very high velocities this would then open a way for the controlled release of thermonuclear energy. One easily calculates that a velocity of $\sim 10^3$ km/sec would upon impact produce a temperature of $\sim$ 10 keV and which would be sufficient to ignite a thermonuclear DT-microexplosion. If however the high velocity impact sets in motion a spherical implosion, the required minimum velocity can be reduced to

*Presented at the DOE workshop on Impact Fusion, Los Alamos, July 10 - 13, 1979.

$\sim$ 100 km/sec[1]. Even a further reduction down to $\sim$ 50 km/sec may be possible using a nonspherical conical implosion[2]. The principal reason why a reduction in the required velocity is desirable is explained by the fact that the acceleration of macroparticles becomes increasingly difficult with increasing velocities. The reduction in required velocity however, must be compensated by a larger mass of the macroparticle.

Assuming conservatively that the energy required for thermonuclear ignition is $E \simeq 10^7$ J $= 10^{14}$ erg and assuming less conservatively that the conversion efficiency from kinetic projectile energy into implosion energy is 100%, one finds that the required macroparticle mass varies from $m = 2 \times 10^{-2}$ g for $v = 10^8$ cm/sec to $m = 8$ g for $v = 5 \times 10^6$ cm/sec. For $v = 2 \times 10^7$ cm/sec, which appears to be a reasonable compromise, one finds that $m = 0.5$ g.

The principal difficulty which one encounters in the problem of accelerating macroparticles can be appreciated in the following way. Let us consider a cylindrical macroparticle of radius r, height h and density ρ which shall be accelerated along its axis by a constant force σ, acting per unit area on its backside, which leads to a uniform acceleration $a = \sigma/h\rho$. The accelerator length ℓ to reach the velocity v will thus be

$$\ell = \frac{h\rho}{2\sigma} v^2 \qquad (1)$$

To make the length of the accelerator as small as possible one must choose σ as large as possible and h as small as possible. If it is desired to keep during the process of acceleration the macroparticle physically intact one has to make sure that $\sigma \leq \sigma_{max}$, where σ_{max} is the tensile strength of the material of which the macroparticle is composed. A value of $\sigma_{max} \simeq 10^{10}$ dyn/cm^2 is here realistic. The thickness h of the macroparticle has likewise a lower limit. The reason for this is that the force acting on the macroparticle always results from a pressure gradient ∇p and it is required that $\nabla p >> \sigma/h$, otherwise there will be equally strong pressure forces acting on the front of the macroparticle compensating the forces on its backside. Since the macroparticle is likely to consist of some metal the value of ρ cannot be made arbitrarily small. We will assume a light metal with $\rho \simeq 2$ g/cm^3.

In one scheme for example the proposal was made to accelerate a macroparticle having the characteristics of a small magnetic solenoid and composed of a type II superconductor by a travelling magnetic wave[3]. In this

case one finds that $\nabla p_{max} \simeq 5 \times 10^9$ dyn/cm^3, because ∇p_{max} is equal to the Lorentz force density $(1/c)(jxH)$ of type II superconductors. But since $\nabla p_{max} \geq \sigma_{max}/h \simeq 10^{10}/h$ it follows that $h \geq 2$ cm. In case of electrostatic acceleration the attainable field gradients are limited by electric breakdown. However, by utilizing the powerful concept of magnetic insulation much larger field gradients seem to be attainable, at least in principle, and thus much larger velocities than with the magnetic acceleration method may eventually be possible. This prospect is discussed somewhere else[4].

II. ACCELERATION BY A SHOCKWAVE

The requirement to preserve during its acceleration the physical integrity of the macroparticle can be given up if the length of the accelerator becomes so short that the projectile is kept together by inertial forces. Here then σ can be made as large as is possible. This suggest, in combination with the requirement that $\nabla p >> \sigma/h$, to accelerate the macroparticle with shock waves by placing the macroparticle exactly in front of the wave. If the stagnation pressure in the shock wave is p the pressure gradient is there of the order $\nabla p \simeq p/\lambda$, where λ is the mean free path of the gas into which the shock wave propagates. Because of the smallness of λ the condition that $\nabla p \sim p/\lambda >> \sigma/h \simeq p/h$ is here always satisfied, since for all practical purposes $h >> \lambda$. More difficulty poses the problem that the velocity of the shock wave must be exactly equal to the velocity of the macroparticle.

With condensed explosives the maximum shock wave velocities are about $\sim$ 10 km/sec[5]. The direct acceleration of macroparticles by detonation waves can thus not lead to velocities in excess of $\sim$ 10 km/sec. Larger velocities of course would be possible if the shock wave is driven by some other more powerful energy source, for example an intense laser or particle beam, or by letting the wave converge, like in a cylindrical or spherical implosion.

III. ACCELERATION BY COALESCING LARGE AMPLITUDE RIEMANN WAVES

The use of shock waves for macroparticle acceleration has the disadvantage that it is always accompanied by a large increase in entropy. Because of

this fact a large fraction of the energy initially supplied is uselessly dissipated into heat rather than converted into kinetic energy of the macroparticle.

To avoid this problem we suggest here an entirely different approach. In it large amplitude Riemann waves are launched into a medium an are focused in time and space to coalesce onto the backside of the macroparticle. The focusing in time can be done by a piston moving with a programmed velocity into a cylinder and the focusing in space can be done by reflecting the Riemann waves from the concave curved wall of a convergent nozzle (see Fig. 1). The piston could be propelled, like in a recoiless gun, by hydrogen heated with an intense electron or ion beam. A shock is then formed only at the common center of convergence and where the macroparticle to be accelerated has to be placed. The focusing in time and space depends on the Mach number. Therefore, if the gas into which the waves are launched has an axial gradient ∇A in the average atomic number, the focal spot of all the waves can be moved in a programmed manner to stay always behind the accelerated projectile. Furthermore, because of the conical wave pattern the macroparticle is during its acceleration radially confined by pressure forces retarding its disintegration.

We now study the coalescence process in further detail. First we consider the coalescence in time as shown in Fig. 2. From the piston P moving with the velocity $v_p(t)$ simple waves are projected along the characteristics into the gas in front of the piston. The initial conditions at $t = 0$, $z = 0$ shall be assumed $v_p(0) = 0$ and $c = c_o$, where z is the axial coordinate and c_o the initial sound velocity. To make all thusly launched waves coalesce at the moment $t = t_o$ at the position $z = z_o$ one must obviously have

$$v_p + c = \frac{z_o - z}{t_o - t} \quad . \qquad (2)$$

The value $z = z_o$ must be chosen to be positioned in the "virtual" focus of the concave wave reflector (see Fig. 1). From the initial conditions one furthermore has

$$c_o = z_o/t_o \quad . \qquad (3)$$

At the piston surface the local gas velocity v is equal to the piston velocity v_p. Since shock waves occur only for intersecting characteristics the coales-

cence of the waves up to the convergence position $z = z_o$ is completely isentropic. Therefore c and v are related by the Riemann invariant

$$v = \frac{2}{\gamma - 1}(c - c_o) = v_p \quad ; \qquad (4)$$

where γ is the specific heat ratio. The advantage of isentropic coalescing waves becomes clear from the Riemann invariant. Because for $c >> c_o$ and $\gamma = 5/3$, the latter valid for a monatomic gas, one has $v = 3c$, or $v^2 = 9c^2$. This implies that the isentropic wave remains relative cool and that about 9 times more energy in it goes into kinetic flow energy rather than heat.

Introducing the dimensionless variables $\xi = z/z_o$, $\tau = t/t_o$ one has $v_p = dz/dt = c_o d\xi/d\tau$. Then, eliminating c from eq. (2) and (4) one finds

$$\frac{d\xi}{d\tau} = \frac{2}{\gamma + 1}\left[\frac{1 - \xi}{1 - \tau} - 1\right] \quad . \qquad (5)$$

Integration of (5) yields

$$\xi = 1 - \frac{2}{\gamma - 1}(1 - \tau)\left[\frac{\gamma + 1}{2}(1 - \tau)^{-\frac{\gamma-1}{\gamma+1}} - 1\right] \quad . \qquad (6)$$

As $\tau \to 1$ one finds

$$z/z_o \to 1 - \frac{\gamma + 1}{\gamma - 1}(1 - t/t_o)^{\frac{2}{\gamma+1}} \quad . \qquad (7)$$

Because the gas density ρ is inverse proportional to $z_o - z$ one finds

$$\rho/\rho_o \to (1 - t/t_o)^{-\frac{2}{\gamma+1}} \quad . \qquad (8)$$

Using the adiabatic relations for an ideal gas one furthermore finds

$$p/p_o \to (1 - t/t_o)^{-\frac{2\gamma}{\gamma+1}} \quad , \qquad (9)$$

$$T/T_o \to (1 - t/t_o)^{-2\frac{\gamma-1}{\gamma+1}} \quad , \qquad (10)$$

where ρ_o, p_o and T_o are the initial values of the gas at $t = 0$.

Next we discuss the coalescence of the waves in space. This problem is explained in Fig. 3. In entering the tapered section at position $z = z_1$, the flow is assumed to have an initial Mach-number M_1. In the case of time focussing $v_p = v_p(t)$ did have to possess a particular functional dependence on time to make the waves coalesce at $t = t_o$. Likewise here the wall has to be shaped in a particular way to make all waves meet on the axis at the focal position $z = z_f$. The exact treatment of this problem has been given by Busemann[6], but we will present here an approximate much simpler method which has the advantage to be physically more transparent. This is explained in Fig. 3. In entering the tapered section at $z = z_1$ a simple wave is emitted under the angle

$$\mu_1 = \text{arc sin}(1/M_1) \quad . \qquad (11)$$

For flow lines intersecting the walls for $z > z_1$ and where $M < M_1$ one has

$$\mu = \text{arc sin}(1/M) \quad . \qquad (12)$$

A further relation is obtained from the integrated Prandtl-Meyer expression

$$\theta = \nu(M_1) - \nu(M) \quad , \qquad (13)$$

with

$$\nu(M) \equiv \sqrt{\frac{\gamma+1}{\gamma-1}}\ \text{arc tan}\sqrt{\frac{\gamma-1}{\gamma+1}(M^2-1)} - \text{arc tan}\sqrt{M^2-1} \quad , \qquad (14)$$

where θ is defined as shown in Fig. 3. If we introduce a polar coordinate system with the origin at the focus F one has for the condition that all Mach lines meet in F:

$$\phi = \pi - (\mu + \theta) \quad , \qquad (15)$$

and hence

$$\phi = \pi + \nu(M) - \arcsin(1/M) - \nu(M_1) \quad . \qquad (16)$$

To determine from this the wall shape, $r_s = r_s(\phi)$ more relations are needed. The first of these is the well known relation between M and ρ

$$\rho/\rho_1 = \left[(1 + \frac{1}{2}(\gamma - 1)M_1^2)/(1 + \frac{1}{2}(\gamma - 1)M^2)\right]^{\frac{1}{\gamma-1}} \quad . \qquad (17)$$

where ρ_1 is the gas density at $z = z_1$. The second relation is obtained from the wave focusing in time and space. Focusing in time increases the density by the factor $(z - z_f)^{-1} \simeq r_s^{-1}$ and focusing in space by the factor r_s^{-2}. Along the curved wall, having the equation $r_s = r_s(\phi)$, one thus has for the energy flux density

$$\frac{1}{2}\rho v^3 = \frac{1}{2}\rho_1 v_1^3 \left(\frac{r_1}{r_s}\right)^3 \quad , \qquad (18)$$

where $r_s = r_1$ is the radius at the wall position $z = z_1$. Instead of (18) one can write

$$\frac{\rho}{\rho_1}\left(\frac{v}{v_1}\right)^3 = \left(\frac{r_1}{r_s}\right)^3 \quad . \qquad (19)$$

One further has

$$\frac{v}{v_1} = \frac{M}{M_1}\frac{c}{c_1} = \frac{M}{M_1}\left(\frac{T}{T_1}\right)^{1/2} \quad . \qquad (20)$$

For large values of M_1 and M one obtains from (17)

$$\frac{\rho}{\rho_1} \simeq \left(\frac{M_1}{M}\right)^{\frac{2}{\gamma-1}} \quad , \qquad (21)$$

and because of the adiabatic relation between T and ρ

$$\frac{T}{T_1} = \left(\frac{M_1}{M}\right)^2 \quad . \qquad (22)$$

Combining (20) with (22) thus yields $v/v_1 = 1$, and it therefore follows from (19)

$$\rho/\rho_1 = (r_1/r_s)^3 \quad , \qquad (23)$$

or because of (21)

$$M/M_1 = r_s/r_1 \quad . \qquad (24)$$

After inserting relation (24) into (16) one obtains the equation for the wall shape in the form $\phi = \phi(r_s)$.

To make the focus to follow the accelerated projectile a slight gradient in the average value of the atomic number A of the gas directed towards the piston is sufficient. If the gas is hydrogen, which may be preferable because it has low radiation losses, this can be done by a small admixture of helium as can be seen as follows. The focal length is equal to $z_f - z_1$ and therefore approximately

$$z_f - z_1 \simeq 1/\mu_1 \quad . \qquad (25)$$

From this follows that for the change

$$\frac{\Delta(z_f - z_1)}{z_f - z_1} \simeq - \frac{\Delta\mu_1}{\mu_1} \quad . \qquad (26)$$

But because of (11) one has for large values of M_1

$$\mu_1 \simeq 1/M_1 \propto A^{-1/2} \quad , \qquad (27)$$

and hence

$$\frac{\Delta\mu_1}{\mu_1} \simeq - \frac{1}{2} \frac{\Delta A}{A} \quad , \qquad (28)$$

which yields upon substituting into (26)

$$\frac{\Delta(z_f - z_1)}{z_f - z_1} = \frac{1}{2}\frac{\Delta A}{A} \quad . \qquad (29)$$

Assuming that $\Delta(z_f - z_1) \simeq (1/10)(z_f - z_1)$ this would require $\Delta A/A \simeq 0.2$. To compute the pressure forces acting on the projectile is straightforward if we assume that the Riemann invariant (4) holds for each reflected wave. For $c >> c_o$ this implies that $M \to 2/(\gamma - 1) = \text{const.}$ The energy flux density in the reflected convergent conical wave, using the same arguments as before for the energy flux density along the wall, is given by

$$\frac{1}{2}\rho v^3 = \frac{1}{2}\rho_1 v_1^3 \left(\frac{r_1}{r}\right)^3 \quad . \qquad (30)$$

Eq. (30) however is different from eq. (18) because it applies for all values $r < r_s$ along the convergent conical wave. Then, because of the Riemann invariant M = const., which according to (17) for large Mach numbers implies that $\rho/\rho_1 \simeq$ const. along the convergent wave, it follows from (30) that

$$v/v_1 \simeq \quad . \qquad (31)$$

The stagnation pressure at position r is thus given by

$$p = (1/2)\rho v^2 \simeq (1/2)\rho_1 v_1^2 (r_1/r)^2 \quad . \qquad (32)$$

If instead of polar coordinates we introduce a cylindrical coordinate system r', z, with the channel radius at $z = z_1$, $r' = R_1$ and the projectile radius $r' = R_o$, assuming a cylindrical projectile, the stagnation pressure acting on the backside of the projectile is

$$p_o/p_1 = (R_1/R_o)^2 \quad , \qquad (33)$$

where $p_1 = (1/2)\rho_1 v_1^2$ is the stagnation pressure at $z = z_1$. The total pressure force acting on the rear end of the projectile is therefore

$$F = p_o \pi R_o^2 = p_1 \pi R_1^2 \quad . \qquad (34)$$

From (34) it follows that the total wave stagnation force which would act

accross the entire channel at $z = z_1$ will be concentrated onto the projectile. If this pressure focus is synchronized with the position of the projectile, it can be accelerated to very high velocities, depending on the values of p_1 and R_1. To reach projectile velocities of $\sim 10^7$ cm/sec however, the wave velocity must be larger than the projectile velocity to produce a large stagnation pressure.

IV. PROPULSION OF THE PISTON BY A BEAM DRIVEN RECOILLESS GUN

We proposed here as one promising method to propel the piston by a recoilless gun using as propellant dense hydrogen and for the energy source a pulsed intense charged particle beam. In comparison to more conventional concepts of microexplosion ignition by charged particle beams this concept has the advantage that it permits to lower the beam power considerably.

The concept is explained in Fig. 4. An intense charged particle beam enters from the left into the barrel of a recoilless gun filled with the liquid hydrogen propellant. The rear end of the gun has a Laval nozzle to increase the exhaust velocity of the propellant to its maximum isentropic value. To be consistent with temperatures which have been continuously sustained in vortex confined electric arcs we will assume that the maximum temperature in the gun barrel shall not exceed 5×10^4 °K. If m_p is the piston mass and m_H the mass of the hydrogen propellant the final piston velocity can be obtained from the rocket equation

$$v_p^{(max)} = \sqrt{c_p T}\, \ell n\left(1 + \frac{m_H}{m_p}\right) \quad . \qquad (35)$$

Here c_p is the specific heat of hydrogen at constant pressure. For a temperature of $T \simeq 5 \times 10^4$ °K the hydrogen is completely dissociated and one has $c_p = \gamma c_v = (5/2)R$, where $R = 8.31 \times 10^7$ erg °K^{-1}. The rocket has its maximum efficiency for $m_H/m_p \simeq 4$. Assuming this value and $T = 5 \times 10^4$ °K one finds from (35) $v_p^{(max)} \simeq 50$ km/sec. To impart a kinetic energy of $\simeq 10^{14}$ erg onto the piston its mass has then to be $\simeq 8$ g. The mass of the hydrogen is 32 g, and since its liquid density is $\simeq 0.08$ g/cm^3 it must occupy a volume of $\simeq 400$ cm^3. If we assume that the gun barrel has a cross section of ~ 10 cm^2, hence a ra-

dius of $\simeq 3.2$ cm, it would have to be filled up with liquid hydrogen to a length of 40 cm. The maximum pressure in the gun barrel is $p = \rho RT \simeq 3.24 \times 10^{11}$ dyn/cm^2. Such a large pressure could be sustained for a short moment using well developed high pressure techniques, for example by a gun barrel tamped with shrink fitted rings. The pressure could be also lowered somewhat by lowering the hydrogen density, but this would increase the dimension of the gun barrel.

To accelerate the piston in accordance with the requirement of isentropic compression, by which its position $z = z(t)$ must follow eq. (6), the power of the beam has to be varied accordingly. The thrust F and power P of a rocket are related to each other by

$$F = 2P/c \quad . \qquad (36)$$

But the power is also given by

$$P = (1/2)\rho c^3 S \quad , \qquad (37)$$

where S is the cross section of the gun barrel. From (36) and (37) follows

$$F = (2P)^{2/3}(S\rho)^{1/3} \quad . \qquad (38)$$

Since $F = F(t) = m_p dv_p/dt$ is a given function of t according to eq. (6), $P = P(t)$ can from there on be computed. If the acceleration of the piston to $v_p^{(max)} \simeq 50$ km/sec takes place over the distance of 250 cm, the acceleration time would be $\tau_a = 10^{-4}$ sec. Since at the optimal mass ratio $m_H/m_p \simeq 4$, 65% of the energy deposited goes into kinetic energy of the piston, the total beam energy must be $\simeq 1.5 \times 10^{14}$ erg. The average beam power is thus $\simeq 1.5 \times 10^{11}$ Watt. This is about three orders of magnitude less than what is required in more conventional target implosion schemes and it could be done by a $\sim 10^6$ V, $\sim 10^5$ A relativistic electron beam.

The initial radius of the waves coalescing on the projectile is equal to the radius of the piston $R_1 \simeq 3.2$ cm. The maximum stagnation pressure at this radius is $p_s(R_1) \simeq (1/2)\rho v_p^2$, where ρ is here the density of the gas placed in front of the piston and into which the Riemann waves are launched. Let us assume that this gas has an initial density equal to $\sim 10^{-3}$ g/cm^3, and by the

motion of the accelerated piston is isentropically compressed $\sim 10^2$ fold. The pressure in the coalescing waves according $p \propto \rho^{\gamma}$ would then rise $\sim 10^3$ fold, up to $\simeq 10^{13}$ dyn/cm^3. But by the radial focusing of the Riemann waves from a radius $R_1 = 3.2$ cm down to the projectile radius of $R_o \simeq R_1/3 \simeq 0.3$ cm, the pressure would be further amplified up to $\simeq 10^{14}$ dyn/cm^2. A cylindrical projectile with radius $R_o = 0.3$ cm, density ~ 5 g/cm^3 and mass 0.5 g would have to possess a length of ~ 0.35 cm. The force acting on the rearside of this projectile would be $F \simeq 4 \times 10^{13}$ dyn and hence its acceleration $a \simeq 10^{14}$ cm/sec^2. To accelerate it to a velocity of 2×10^7 cm/sec would require a length equal to ~ 2 cm. This length is consistent with the estimate (29) for ∇A, required to synchronize the motion of the wave focus with the motion of the projectile.

REFERENCES.

1. F. Winterberg, Plasma Physics 10 55 (1968).
2. F. Winterberg, Journal of Plasma Physics 18 473 (1977).
3. F. Winterberg, Journal of Nuclear Energy, Part C, 8 541 (1966).
4. F. Winterberg, Lett. Al Nuovo Cimento 19 397 (1977).
5. R. Schall, in: Physics of High Energy Density, Academic Press N.Y. 1971 p. 230 ff.
6. A. Busemann, Luftfahrtforschung 19 137 (1942).

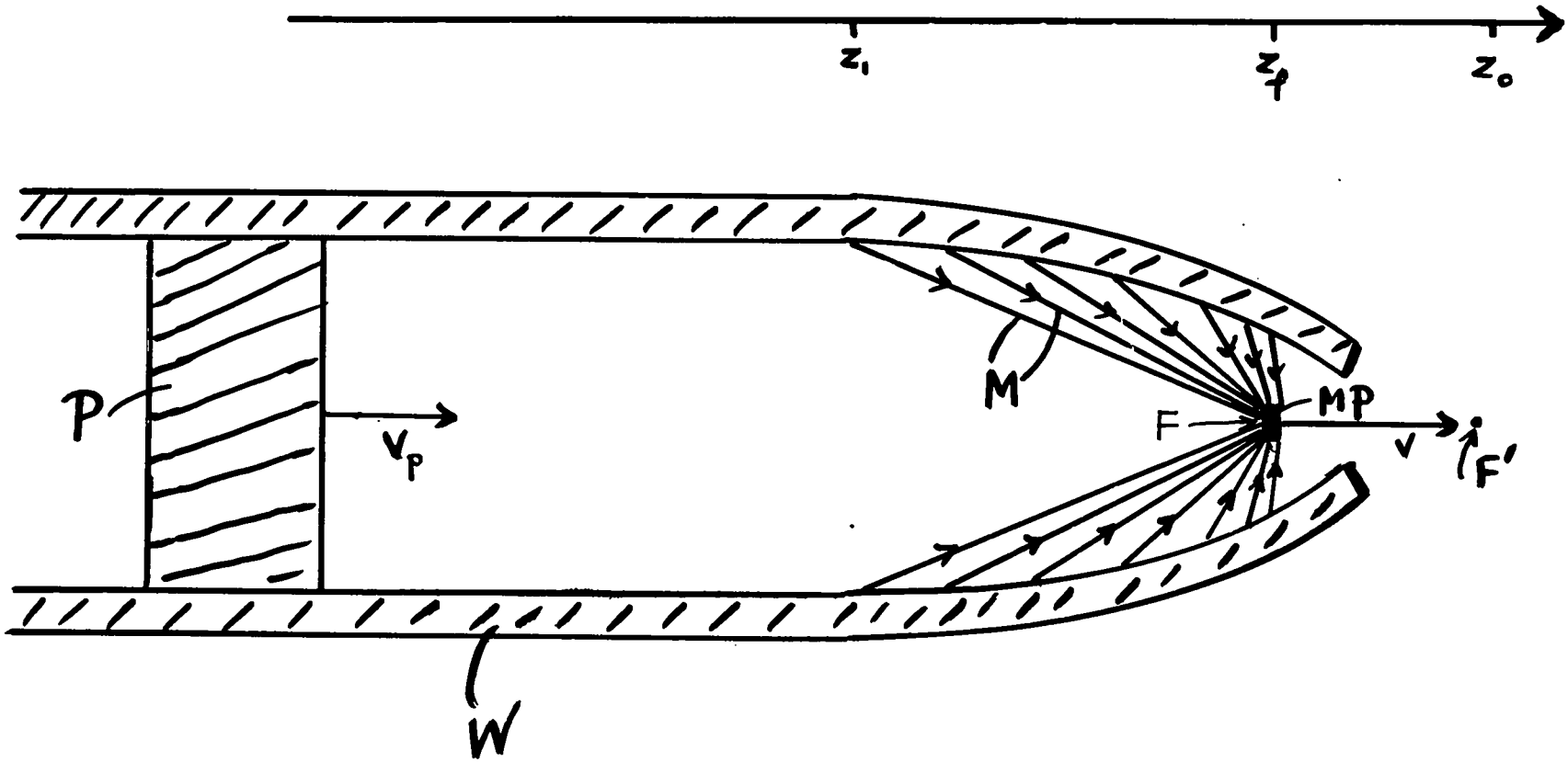

Fig. 1. P piston, W wall with concave curved end, M Mach lines in the r - z plane, MP macroparticle, F wave focus, F' virtual focus.

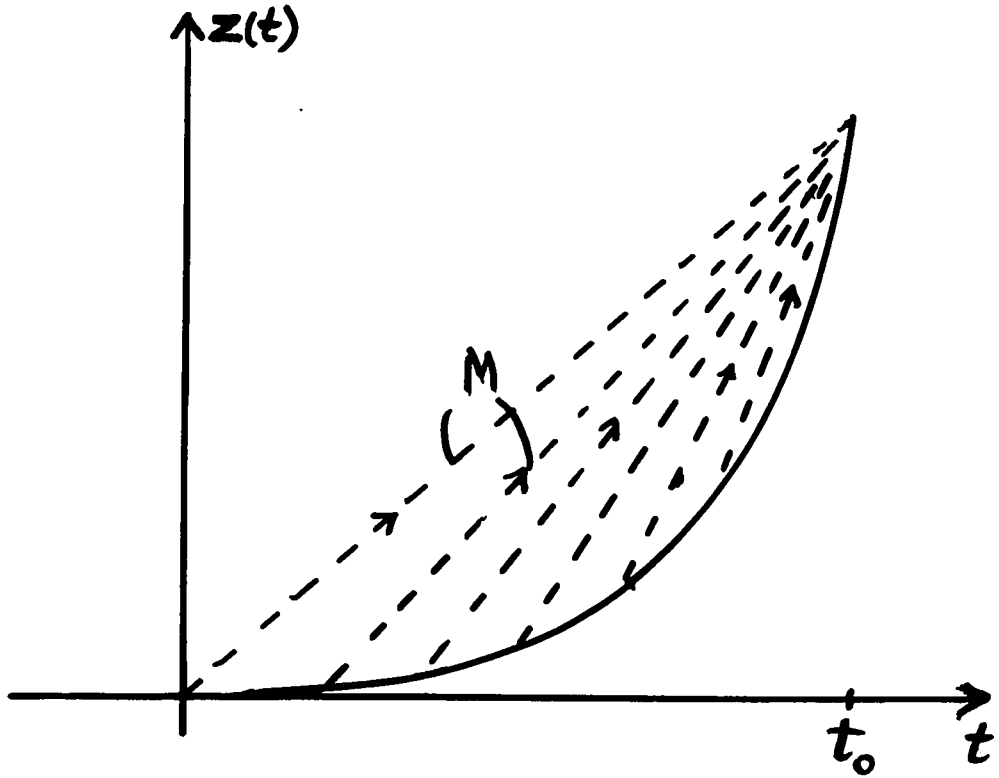

Fig. 2. Isentropic wave coalescence in time by accelerated piston: piston position z = z(t), M Mach lines in the z - t plane.

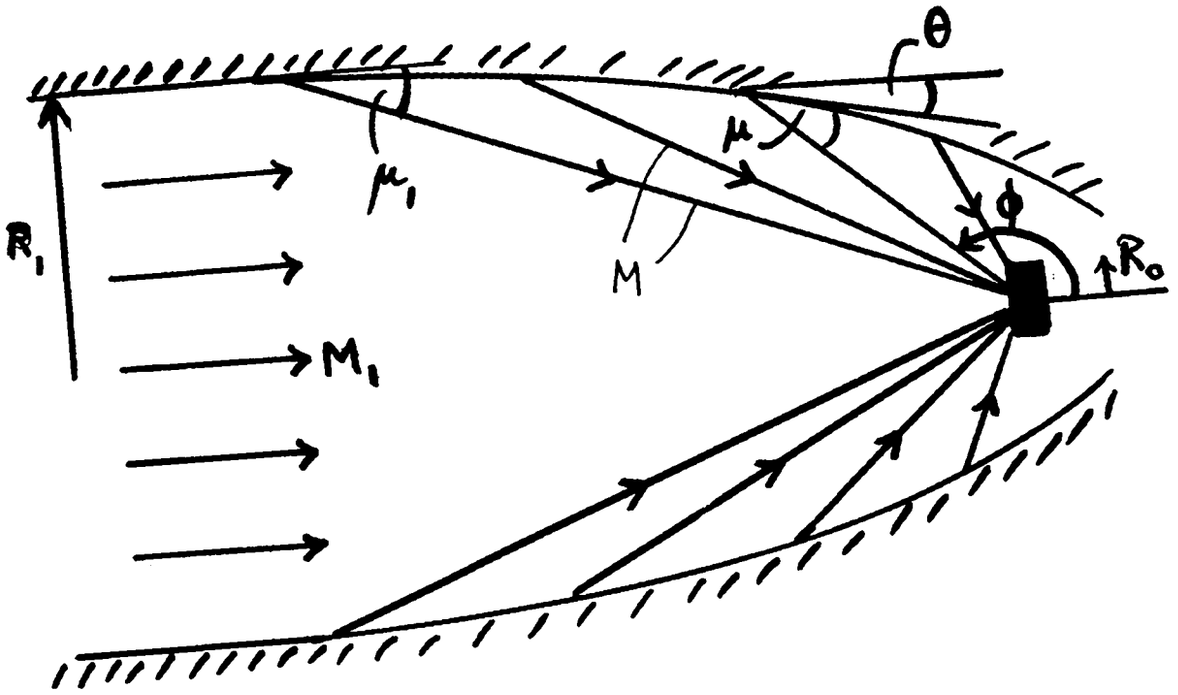

Fig. 3. Isentropic wave coalescence in space by reflection from a curved concave wall: M_1 Mach number of incoming wave, M Mach lines of reflected wave.

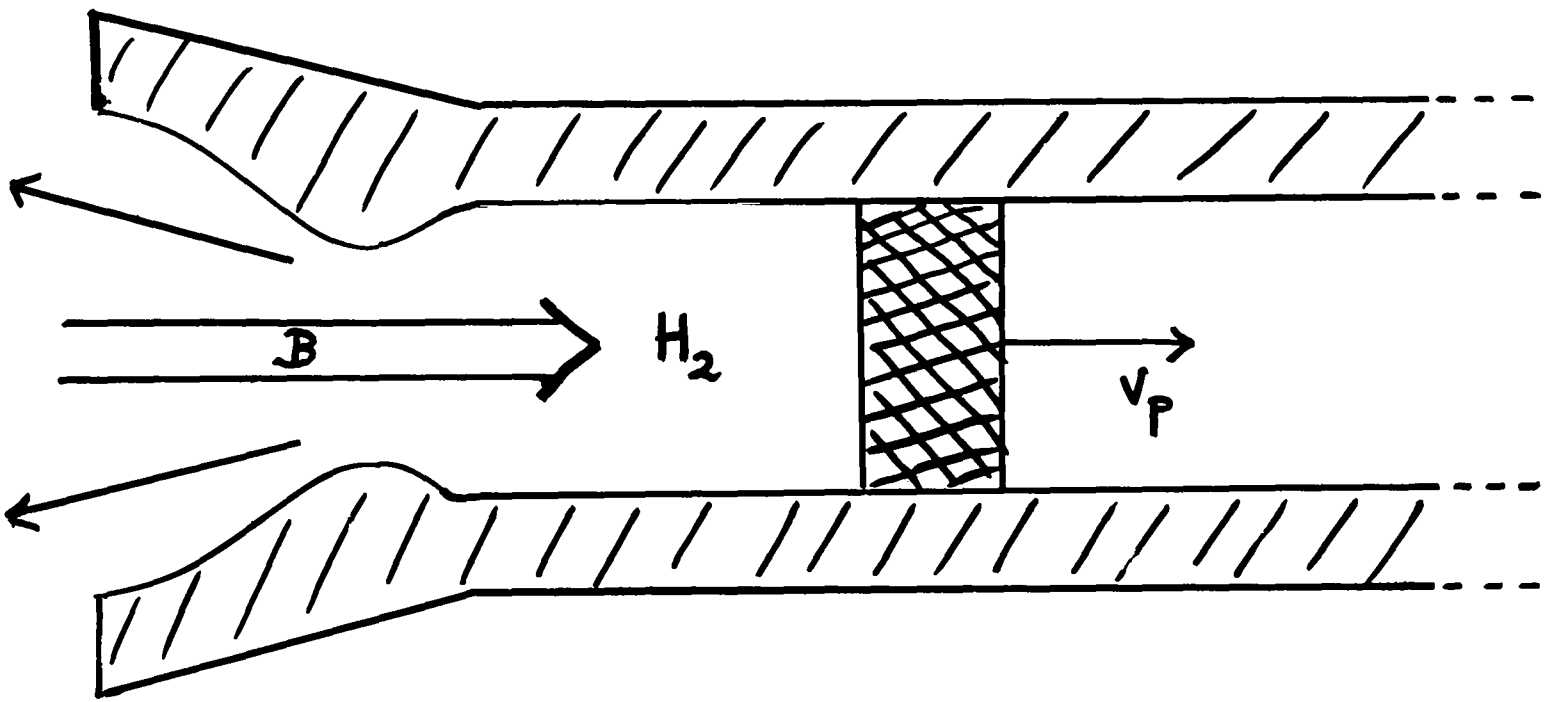

Fig. 4. Propulsion of piston by recoilless rifle using a hydrogen propellant and drawing its energy from an intense charged particle beam B.

RAIL GUN POWERED BY AN INTEGRAL EXPLOSIVE GENERATOR*

by
D. R. Peterson and C. M. Fowler
Los Alamos Scientific Laboratory
Los Alamos, NM 87545

ABSTRACT

We propose the use of a rail gun powered by an explosive magnetic flux compression generator built into the rail gun itself in which the rails of the gun are driven together behind the projectile by explosives. The magnetic field established between the rails by an initial current supplied by an external source at the breech of the gun is trapped and compressed by the collapsing rails to accelerate the projectile down the bore of the gun.

Whether used externally or integrally to power rail guns, the use of explosive magnetic flux compression generators appears promising.

I. INTRODUCTION

Kreisler[1] and Hawke and Scudder[2] list a number of applications that call for projectiles (macrons) that move at very high speeds. In particular, they note ranges of macron speeds required for various applications. As examples, equation-of-state measurements could be extended with suitable projectiles traveling at speeds in excess of 10 km/s, whereas impact fusion might be attainable at speeds greater than 100 km/s. Kreisler[1] gives a compact survey of various methods by which such particles might be accelerated. Some of the methods are by electrostatic acceleration, magnetic acceleration, and use of light gas guns.

The current interest in macron acceleration has been stimulated by the successes achieved in two recent experimental programs: the rail gun program of Marshall et al.[3] and the mass launcher program of Kolm et al.[4] The projectiles are accelerated magnetically in both programs, but the rail gun

* Many of the ideas presented in this paper were discussed at an informal session of the Second International Conference on Megagauss Magnetic Field Generation and Related Topics, May 29-June 1, 1979, Washington, DC.

uses direct-magnetic-field drive and the mass launcher employs magnetic-field gradients. The differences in the two techniques may be seen in Fig. 1, which shows schematically the systems employed by Fowler et al.[5] for direct drive and Chapman[6] for gradient drive. In the direct-acceleration arrangement (Fig. 1a), the projectile plate carries current and is accelerated down the rails away from the heavy base plate. Current was supplied by a capacitor bank. The accelerating force arises from the magnetic field that is confined to the region between the base plate and projectile. In case (b), a magnetic-field channel is constructed so that a magnetic-field gradient is developed opposite the direction of projectile motion. Here, the projectile does not carry current directly. To a first approximation, the projectile is accelerated by forces proportional to the local average field and the field gradient across the sample. Joule heating, from eddy currents in case (b), was a serious factor in both schemes, leading to vaporization of the projectiles at high speeds.

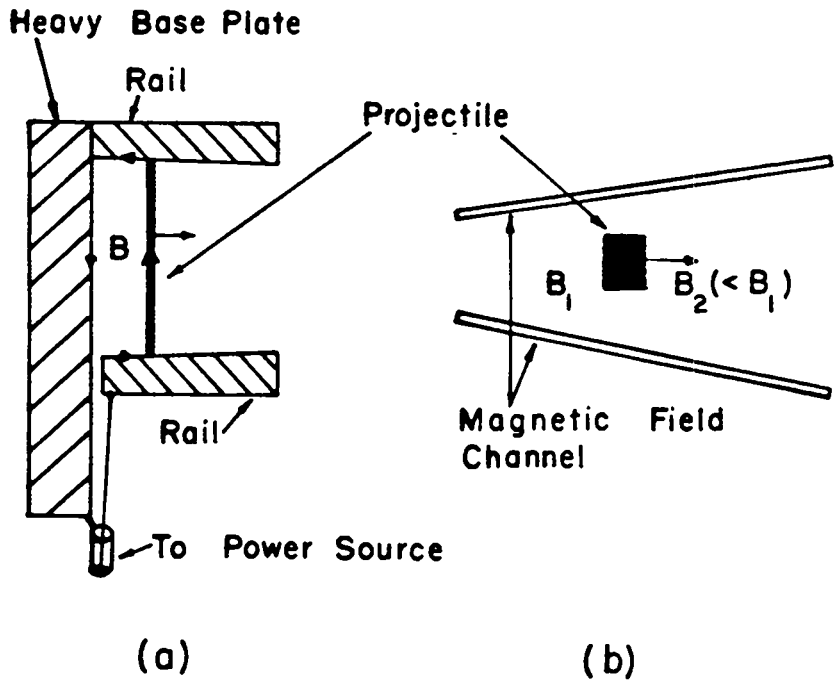

Fig. 1. Schematic drawings of projectiles accelerated by (a) magnetic fields and (b) magnetic field gradients.

In the direct-feed case, thin plates were successfully accelerated to about 3 km/s, but were completely vaporized when attempts were made to accelerate them to 8 km/s. As noted in Ref. 5, for this situation, there is a one-to-one correspondence of plate temperature with the ratio of plate velocity to its thickness, provided the current density throughout the plate is uniform and plate-edge effects are negligible. These thin plate results were consistent with this theory. It was felt then that efforts to increase plate thickness to obtain higher velocities before vaporization would not be too successful because the current would concentrate near the plate surface, leading to harmful ablation of projectile material. However, experiments with the rail gun seem to imply that such ablation would not be particularly harmful. This implication is consistent with recent work by Sherwood et al.[7] in which electromagnetic implosion of a cylindrical liner yielded inner radial velocities of about 10 km/s, even though calculations indicated that the temperature exceeded the melting point on the outer liner diameter. It might be profitable to repeat some of this earlier work with thicker plates and larger energy sources. Somewhat later, Guenther et al.[8] used the vaporization products obtained by deliberately exploding thin plates to drive thin plastic materials placed ahead of the plates. Speeds of these plastic projectiles reached several kilometers per second. In all of these experiments, acceleration was to be accomplished over short distances with single, intense magnetic pulses.

In the mass launcher, Kolm et al.[4] avoided the very large stresses needed to accelerate in a single short pulse by using a series of staged field coils, each giving an acceleration pulse as the projectile passed through the coil. The eddy current heating that would eventually melt and vaporize the projectile would be eliminated by using a superconducting coil as the projectile driver.

In the rail gun, Marshall et al.[3] avoided the large stresses by controlling the magnitude of the projectile driving current and greatly increasing the length of the rails. Figure 2a shows this basic rail gun assembly. Power was supplied from an inductive store that was energized by the Canberra homopolar generator. Much attention was devoted to the design of the armature to carry the current between the rails. Initially, metal armatures were used. Later, plasma-arc armatures were used.

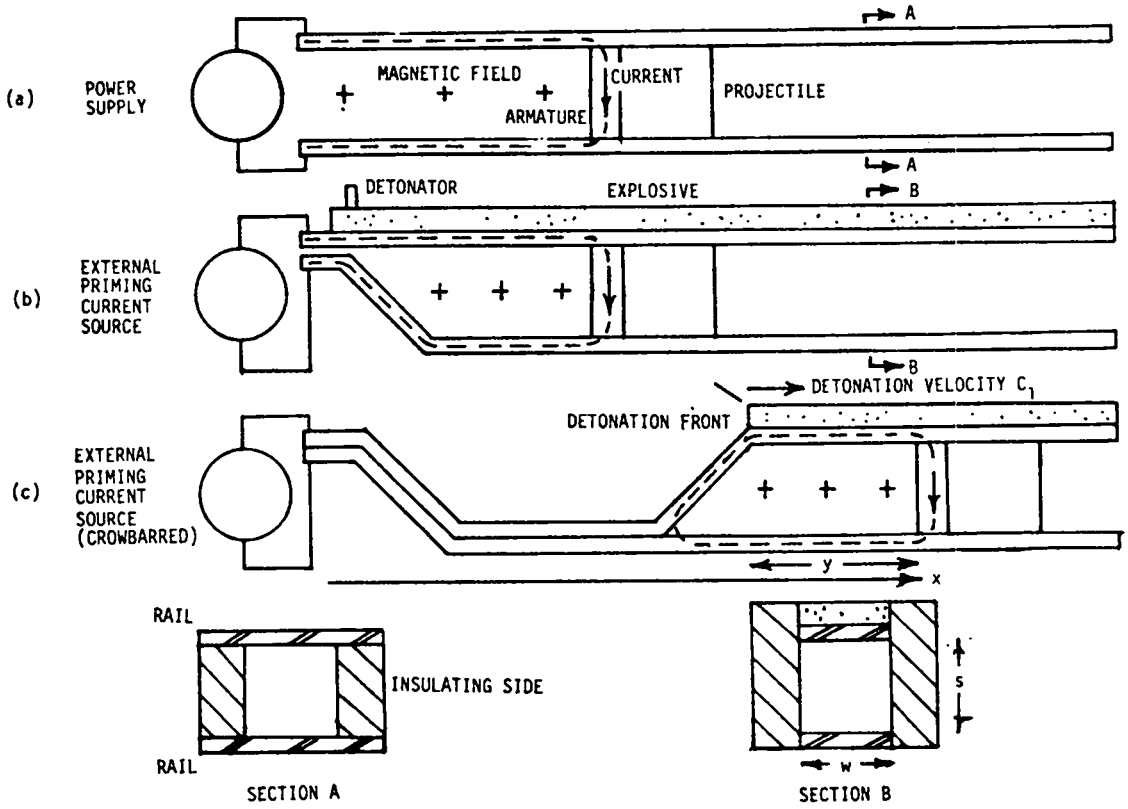

Fig. 2. Schematic drawings of externally powered (a) and hybrid (b) and (c) rail runs.

II. FLUX COMPRESSION GENERATOR POWER SUPPLY

Among the power supplies that have been used to power rails guns are the inductive store of Marshall et al.[3], capacitor banks by a number of workers, and flux compression generators.[9]

We propose the use of a rail gun powered by an explosive magnetic flux compression generator built into the rail gun itself, as in Figs. 2b and 2c, in which the rails of the gun are driven together behind the projectile by explosives. The magnetic field established between the rails by an initial current supplied by an external current source at the breech of the gun is trapped and compressed by the collapsing rails to accelerate the projectile down the bore of the gun. A rail gun powered by such an integral explosive generator is referred to as a hybrid rail gun.

Whether used externally to supply power to a conventionally fixed-rail gun or integrally to power a hybrid rail gun, the use of explosive magnetic flux compression generators appears promising, based on preliminary, idealized calculations. Plans are in progress to pursue both of these approaches.

External generators will be used to power the guns in a cooperative program with R. S. Hawke and J. K. Scudder of Lawrence Livermore Laboratory, and the hybrid approach is now being planned as a Los Alamos Scientific Laboratory (LASL) experiment. As planned, strip generators such as those described by Fowler et al.[10] will be used for both systems. They have the advantage of very long burn times (hundreds of microseconds) that are thought to be necessary for successful rail gun application.

III. ANALYSIS OF EXPLOSIVE-GENERATOR-POWERED RAIL GUN

In Fig. 2c, at time t, the position of the projectile is x; the distance between the explosive detonation front and the projectile is y; and the current is I. The detonation front moves with constant velocity C_1. The boundary conditions are that, at some particular time, t_0, the projectile position is x_0; the distance between the detonation front and the projectile is y_0; the current is I_0; and the projectile speed is C_0 ($C_0 < C_1$).

At any instant of time, the inductance L of the rail run is (in SI units)

$$L = \alpha \mu_0 \, sy/w, \tag{1}$$

where α is a dimensionless constant depending on the ratio s/w, $\mu_0 = 4\pi \times 10^{-7}$, the magnetic permeability, and s and w are the separation and width of the rails. Values of α are available in Ref. 11.

If there is no magnetic flux lost from the trapped magnetic field, the magnetic flux $\phi = LI$ is constant, and equal to the flux at time t_0,

$$\alpha \mu_0 \, sy \, I/w = \alpha \mu_0 \, sy_0 \, I_0/w,$$

so that the current is

$$I = I_0 \, y_0/y. \tag{2}$$

The average magnetic field B between the rails is

$$B = \phi/sy, \tag{3}$$

and the magnetic pressure P acting to accelerate the projectile down the rails (and, incidentally, acting to drive the rails apart) is

$$P = B^2/2\mu_0. \tag{4}$$

Using the above equations, the equation of motion of a projectile of mass m may be written

$$d^2x/dt^2 = D_1\, y_0/2y^2 - f/m, \tag{5}$$

where

$$D_1 = \alpha^2 \mu_0\, sy_0\, I_0^2/mw, \tag{6}$$

and f is the force caused by mechanical friction between the projectile and the bore of the rail gun, gas ahead of the projectile, etc., acting to resist the projectile acceleration.

For the case f = 0, Eq. (5) may be integrated twice using the relation

$$x = x_0 + y - y_0 + C_1(t - t_0), \tag{7}$$

with the initial conditions stated above to obtain the projectile velocity and the time in terms of y.

Solutions are expressed in terms of auxiliary y dependent parameters G and H, together with constants x_1, t_1, E_1, F_1, and the previously defined parameter D_1 determined from initial values. These new parameters are defined below. Velocities and times are then given by

$$dx/dt = \begin{cases} C_1 - G/y, & t_0 \leqslant t \leqslant t_1 \\ C_1 + G/y, & t > t_1 \end{cases} \tag{8}$$

and

$$t = \begin{cases} t_1 - H, & t_0 \leqslant t \leqslant t_1 \\ t_1 + H, & t > t_1 \end{cases} . \qquad (9)$$

The constant parameters are defined as follows:

$$E_1 = D_1 + (C_1 - C_0)^2. \qquad (10)$$

$$F_1 = D_1/2E_1^{1/2}. \qquad (11)$$

$$t_1 = t_0 + y_0 \left\{C_1 - C_0 + F_1 \ln[(C_1 - C_0 + E_1^{1/2} - F_1)/F_1]\right\}/E_1. \qquad (12)$$

$$x_1 = x_0 - y_0 (C_1 - C_0)^2/E_1 + C_1 (t_1 - t_0). \qquad (13)$$

The y dependent parameters are given by

$$G = (E_1 y^2 - D_1 y_0 y)^{1/2}, \text{ and} \qquad (14)$$

$$H = \left\{G + F_1 y_0 \ln [(G + y E_1^{1/2} - F_1 y_0)/F_1 y_0]\right\}/E_1. \qquad (15)$$

Equations (7) through (9) prescribe x, dx/dt, and t for the projectile in terms of y, the separation between the detonation front and the projectile.

At time t_1, the projectile velocity is equal to the explosive detonation speed C_1, and the separation between the detonation front and the projectile is minimum. Previous to t_1, the projectile is traveling slower than the explosive detonation front, the separation between the detonation front and the projectile is decreasing, the trapped magnetic field is being compressed, and the magnetic pressure accelerating the projectile is increasing. After t_1, the projectile is traveling faster than the explosive detonation front, the separation between the detonation front and the projectile is increasing, the trapped magnetic field is expanding, and the magnetic pressure accelerating the projectile is decreasing. If there are no mechanical losses and no flux losses from the trapped magnetic field, the projectile velocity will approach asymptotically the velocity

$$(dx/dt)_{max} = C_1 + E_1^{1/2}.$$

In a real rail gun, the projectile will, at some point, begin to decelerate after initially outrunning the explosive detonation wave.

It is useful to have the explosive detonation speed start out at a relatively slow speed and increase as the detonation front proceeds along the rail. One way of accomplishing this is to use segments of explosives of different detonation speeds, as in Fig. 3b. The equations obtained above may be used in this case, but must be written separately for each segment of explosive using the appropriate constants. The initial conditions for each segment are obtained from the final conditions of the preceding segment.

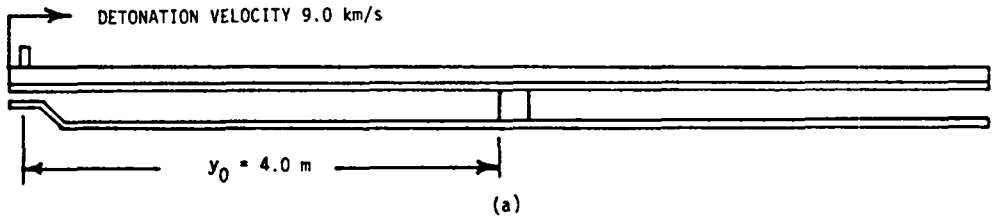

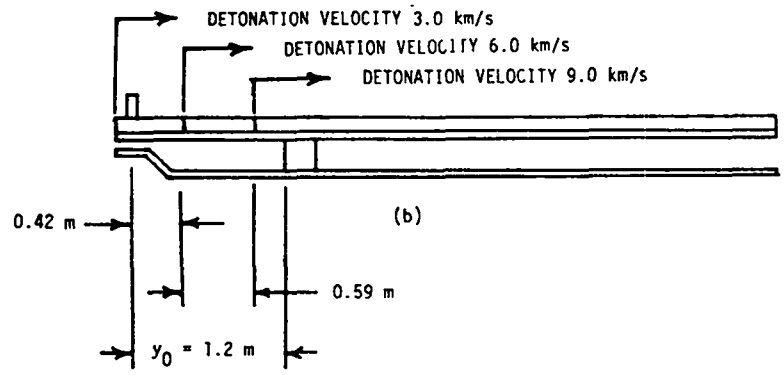

PROJECTILE MASS	2.5 g
INITIAL ENERGY OF MAGNETIC FIELD	100 kJ
RAIL GUN BORE	1.3 cm square
PROJECTILE INITIAL VELOCITY	0

Fig. 3. Parameters for example performance curves in Fig. 4.

Performance curves for the rail gun arrangements shown in Figs. 3a and 3b are given in Fig. 4. The use of staged explosives results in a shorter gun.

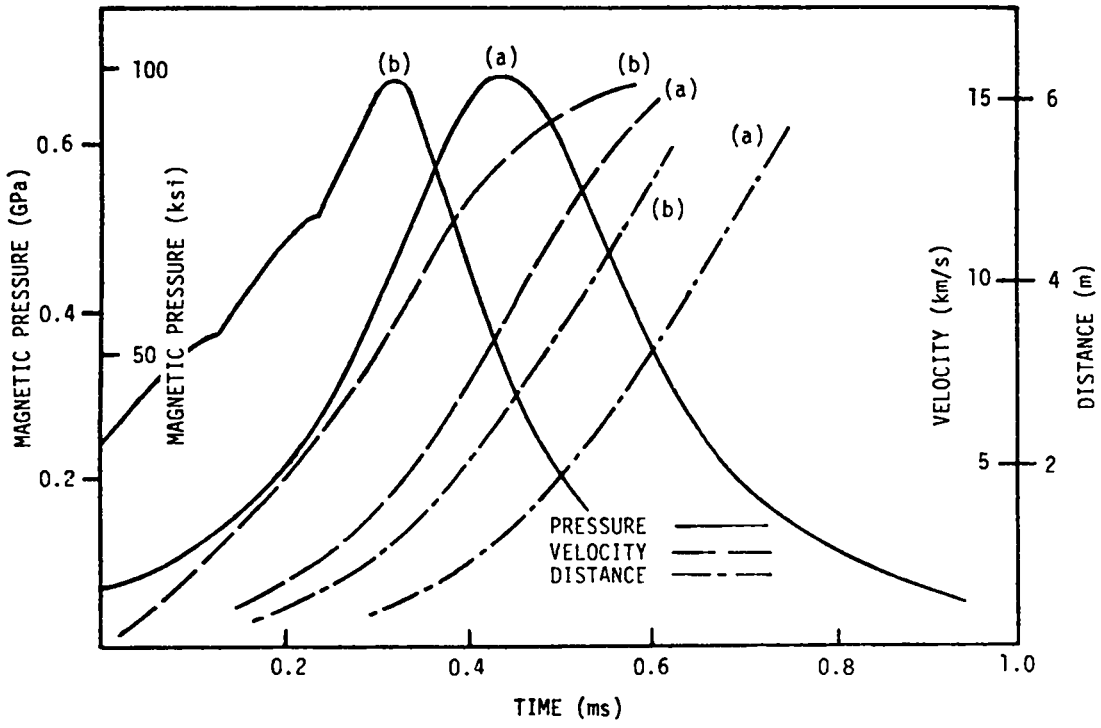

Fig. 4. Calculated performance curves for rail guns shown in Fig. 3.

IV. DISCUSSION

Both the externally driven and hybrid-type rail guns using the flux compression generators show considerable promise. Some of the favorable aspects and potential problems of this approach are discussed.

Ideally, projectile velocities exceed the detonation velocity of the explosives. Explosive strips can be detonated at arbitrary phase velocities greater than their normal detonation velocity. Thus, in principle, arbitrarily large effective detonation velocities and, thus, projectile velocities can be achieved.

The continuous collapse of the rails behind the projectile has several advantages. The active inductance of the rail gun is never very large. Therefore, relatively little magnetic energy must be stored inductively. Similarly, no part of the rails is exposed to current for a very long time. Heating effects, as well as integrated forces that displace the rails, are greatly reduced.

Aside from the obvious disadvantage of destroying the rails, there are some potential difficulties with the hybrid gun. These include the possible formation of harmful jets at the rail collision juncture and the loss of flux trapped in the rails. Jets could actually overtake the projectile, particularly when it is moving slowly, and would lead to undesirable flux losses. Flux losses from any cause result in projectile speeds slower than those calculated ideally, and therefore lead to the possibility of the detonation front overtaking the projectile.

We now lean toward the following approach. External flux compression generators will first be used to accelerate the pellet to several kilometers per second, after which the rail generator will be started. The rail explosive will be staged, starting with low detonation velocity explosives and finishing with fast detonating explosives. H. L. Flaugh, LASL Design Engineering Division, has undertaken the design and production of the staged explosives to drive the rail gun, and J. M. Christian, LASL Dynamic Testing Division, is developing the technique to assess the performance of the explosive-rail assemblies.

Strip generator systems can be built that require a millisecond or more to complete detonation, but it is likely that flux losses would be prohibitive for much longer times. Therefore, the ultimate speeds obtainable by this method are directly related to the stresses that the projectiles are able to withstand during acceleration.

REFERENCES

1. M. N. Kreisler, "Some Approaches to Macron Acceleration," presented at the Second International Conference on Energy Storage, Compression, and Switching, December 5-8, 1978, Venice, Italy, paper 6-1 (to be published in the conference proceedings).

2. R. S. Hawke and J. K. Scudder, "Magnetic Propulsion Railguns: Their Design and Capabilities," presented at the Second International Conference on Megagauss Field Generation and Related Topics, May 29-June 1, 1979, Washington, DC (to be published in the conference proceedings; available as Lawrence Livermore Laboratory report UCRL-82677).

3. R. A. Marshall. See the following, 1975-1977:
Department of Engineering Physics, Research School of Physical Sciences, the Australian National University, Canberra, A.C.T., 2600 Australia, "The Single Leaf Projectile in A.N.U. Rail Gun;" "The Flying Fuse in A.N.U. Rail Gun;" "The Flap-Back Fuse in A.N.U. Rail Gun;" "Moving Contacts in Macro-Particle Accelerators."

Also, S. C. Rashleigh and R. A. Marshall, "Electromagnetic Acceleration of Macroparticles to High Velocities," J. Appl. Phys. 49(4), (1978), pp. 2540-2542.

4. Henry Kolm, Kevin Fine, Peter Mongeau, and Fred Williams, "Electromagnetic Propulsion Alternatives," and Kevin Fine, Fred Williams, Peter Mongeau, and Henry Kolm, "Mass Driver Two: Cryogenic Module," presented at Symposium on Space Manufacturing by the Massachusetts Institute of Technology (MIT) E. M. and C. Group at Princeton, 1979; available from the Francis Bitter National Magnet Laboratory, MIT.

5. C. M. Fowler and W. B. Garn, "Magnetic Acceleration of Metal Plates," Los Alamos Scientific Laboratory internal report (May 1958), and C. M. Fowler, R. S. Caird, W. B. Garn, D. B. Thomson, and K. J. Ewing, "Magnetic Acceleration of Plates for Simulation Studies and to Achieve High Velocities," Los Alamos Scientific Laboratory internal report (March 27, 1968).

6. R. L. Chapman, "Development of Magnetic Field Compression Techniques for Metallic Particle Acceleration," Proceedings of the Conference on Megagauss Magnetic Field Generation by Explosives and Related Experiments; H. Knoepfel and F. Herlach, Eds., Euratom (1966), p. 107.

7. A. R. Sherwood, E. L. Cantrell, C. A. Ekdahl, R. A. Gerwin, I. Henins, H. W. Hoida, T. R. Jarboe, P. L. Klingner, R. C. Malone, J. Marshall, and G. A. Sawyer, "Results from the Los Alamos Fast Liner Experiment," presented at the Second International Conference on Megagauss Field Generation and Related Topics, May 29-June 1, 1979, Washington, DC (to be published in the conference proceedings). (In very recent experiments since this abstract was written, radial liner velocities of about 10 km/s were obtained.)

8. A. H. Guenther, D. C. Wunsch, and T. D. Soapes, "Acceleration of Thin Plates by Exploding Foil Techniques," Exploding Wires, Vol. 2, W. G. Chace and H. K. Moore, Eds. (Plenum Press, 1962), p. 279.

9. R. L. Chapman, D. E. Harms, and G. P. Sorenson, "The Magnetohydrodynamic Hypervelocity Gun," Proceedings of the Sixth Symposium on Hypervelocity Impact, Vol. 1 (1963), p. 317.

10. C. M. Fowler, R. S. Caird, W. B. Garn, and D. B. Thomson, "The Los Alamos Flux Compression Program from its Origin," Proceedings of the Conference on Megagauss Magnetic Field Generation by Explosives and Related Experiments; H. Knoepfel and F. Herlach, Eds., Euratom (1966), p. 1.

11. H. Knoepfel, Pulsed High Magnetic Fields (North-Holland Publishing Co., Amsterdam-London, 1970), p. 323.

Talk given at the Workshop on Impact Fusion at Los Alamos, NM
July 11, 1979

IMPACT FUSION OF THE SECOND KIND: DT FUELLED SPHERES INCIDENT UPON A PASSIVE TARGET

Bogdan Maglich
Fusion Energy Corporation
P. O. Box 2005
Princeton, New Jersey 08540

In all the impact fusion concepts presented at this meeting an 'active' target, DT ice, is bombarded by a 'passive', non-fuelled, projectile.

I will discuss a different case, that in which a 'passive' target, say a steel plate, is bombarded by an 'active' projectile, a DT fuelled sphere. This idea first occurred to us as a means of delivering neutrons to remote objects.[1,2]

Gratton has subsequently shown[3] that, under certain conditions, the impact-produced shock wave is more intense in the projectile than in the target. He assumed an impact velocity such that the average ion kinetic energy in the projectile, or the 'macron,' will be of the order of 5 KeV, which corresponds to v = 565 Km/s. Gratton derived some basic relations for the ion and electron temperature in the macron; the shock wave compression in the macron; confinement time; shock dynamics in the target, shock reflection, bremsstrahlung and electron heat conductivity losses. He concluded that a shock wave will be formed in the macron, which will convert its kinetic energy into the ion and electron

temperature, if the macron radius, r, is greater than the mean freepath for the multiple scattering $\lambda \approx 2 - 8 \times 10^{-4}$ cm; λ scales like $\lambda \propto \theta^2/n$, where θ is the temperature. Therefore, one can expect two entirely different physical regimes depending on whether $r \lesssim \lambda_i$, or $r > \lambda_i$. The features of these two regimes are summarized in Table 1.

I will now speculate on the physical processes within the macron beyond the earlier work[1,2,3]

<u>α - Ablation?</u> Let us consider a hyper fast spherical, shell, made of plutonium, filled with solid DT, incident upon a steel plate.

From the theoretical studies of the inertial fusion by the light ions, one can expect ablation if 10^{18} protons of 5 - 10 MeV are incident onto a $\sim$1 mm sphere in $\sim 10^{-8}$s. Let us denote with N_A the surface density of ions needed for ablation.

At a certain macron velocity v, the impact DT fusion will produce a sufficient number of the 3.52 MeV α particles within the macron to ablate the metalic sphere, <u>if</u> the α's can reach the shell. Range of the α particles is of the order of 10^{-3} g/cm^2. In the cold DT matter, only those α's produced in the outermost layers next to the sphere, could deposit their energy into the shell. However, a certain time τ after the impact, the entire macron will become ionized and both the electrons and ions will be hot. If the inertial confinement time is longer than τ, say $\tau_c \approx 2\ \tau$, the α particles will travel

TABLE 1

MACRON-TARGET IMPACT

(from Reference 3)

The mean free path in a hot plasma (multiple Coulomb scattering), $\lambda_{e,i}$

$\theta_{e,i} = 5$ KeV

$n = 4 \times 10^{22} - 1.6 \times 10^{23}$ cm^{-3} $\quad \langle A \rangle = 2.5$

$\lambda_{e,i} \sim 2 - 8 \times 10^{-4}$ cm $\quad \lambda \propto \theta^2/n$

Two Physical Regimes:

Regime 1	Regime 2
$r \lesssim \lambda_i$	$r > \lambda_i$
Free-ion flow; weak shock in the target only; stopping by excitation-ionization the target; beam-target interact	2 - fluid model (hydrodynamics); plasma heating by strong shock wave in macron; less intense shock in the target

Main Stopping Processes:

(a) Excitation-ionization in cold target
(b) Double-layer of electric charge
(c) Shock-wave interaction

Main Physical Effects to be considered:

Regime 1	Regime 2
Deposition of α particles in target only	Deposition of α particles both in target and macron
Cooling by electron conductivity and gas expansion	Cooling by gas expansion (if $t \lesssim 10^{-8}$ sec and $Z = 1$)
Damping of Double layer	Shock-Waves and Rarefaction
Oscillations	Wave dynamics

through a plasma rather than the solid matter. Let us assume that 10% of them will reach the metallic shell. Then the condition for ablation from within the projectile is given by

$$\tfrac{1}{2}\langle\sigma v\rangle\, n_s^2\, V_s\, \tau \geqslant 10\, N_A \times 2\pi\, r^2, \qquad (1)$$

where n_s and V_s are the shocked density and volume respectively $n_s = 4\, n_o$, $n_o = 4 \times 10^{22}\ cm^{-3}$; $V_s = V_o/4$, $V_o \approx 4r^3$. τ is the confinement time of the hot matter <u>without</u> the help of the inertial confinement sphere, and is given by[3]:

$$\tau = 3r/4v. \qquad (2)$$

Plugging into (1) all the values in terms of r and v we get the minimum radius of the macron to have ablation

$$r \geqslant \frac{12.65}{n_s} \left(N_A \frac{v}{\langle\sigma v\rangle}\right)^{1/2}. \qquad (3)$$

With $N_A = 2 \times 10^{19}\ \alpha/cm$, $v = 5.65 \times 10^7$ cm/s, $\langle\sigma v\rangle = 2 \times 10^{-17}$, Eq. (3) gives

$$r \geqslant 0.4 \text{ cm} \qquad (4)$$

<u>α - heating</u>. The ablation condition (3) assumes only the heating within the macron caused by the conversion of the kinetic energy into heat. In addition, the α heating will take place within the macron, this will lower the requirement on the projectile velocity.

<u>R E F E R E N C E S</u>

1. B. C. Maglich, U.S. Patent and Trademark Office Disclosure Document No. 065616 (November 3, 1977).

2. S. Channon and B. C. Maglich, U.S. Pat. and Trademark Office, Discl. Doc. No. 065654 (November 4, 1977).

3. Fausto T. Gratton, Notes on the physics of impacts produced by macroparticles with velocities in the range of 10^8 cm/sec, Maglich Energy Group Report MEG-1-78 (January, 1978).

Electrostatic Accelerators Revisited

J.F.Friichtenicht
TRW Space & Defense Systems Center

Recent technological developments in pellet fabrication in support of laser ICF raise interesting possibilities for electrostatic particle accelerators in impact fusion. It appears that hollow shells of arbitrary geometrical configuration and material composition can be constructed.

The use of thin walled structures, such as spheres and cylinders that have already been considered, markedly changes the charge-to-mass ratio limitation that has previously restricted the practical operating range of electrostatic accelerators to micron sized particles. Calculations show that final velocities of 200 kilometers per second can be achieved with accelerating voltages in the few gigavolt range for thin walled spheres (wall thickness equal to from 1 to 10% of the particle radius) in the 0.1 to 1 millimeter range. Particle kinetic energies in the 10's of kilojoules can be achieved.

Thin walled cyclinders may be even more interesting. Even though the specific charge is lower for cyclinders than for spheres, the charge-to-mass ratio is independent of length. Therefore, mass and kinetic energy can be increased without penalty in terms of required accelerating voltage. In an illustrative calculation, a particle kinetic energy of 240 kilojoules is achieved by a 2 millimeter diameter by 1 centimeter long cylinder with a wall thickness of 0.1 millimeter. The accelerating voltage required to reach 200 kilometers per second for this pellet is 40 gigavolts.

MODELS OF LASER ABLATIVE ACCELERATION FOR IMPACT FUSION

F. S. Felber*

General Atomic Company, P.O. Box 81608, San Diego, California 92138

Impact fusion, produced by impact of projectiles on fusion fuel pellets, may require projectile energies of 1 MJ and velocities exceeding 10^7 cm/s. One well-known means of accelerating a projectile to high velocities is irradiating one side with a laser, causing the projectile to accelerate in response to the ablation of material from its heated surface. This report presents analytic models of laser ablative acceleration that may prove useful in considering acceleration of projectiles for impact fusion.

1. Laser Acceleration - Background

Ths history of laser acceleration is almost as long as the history of lasers. Perhaps the first to suggest acceleration of projectiles by lasers were Askar'yan and Moroz in 1962.[1] They also suggested the application that motivated much of the work for the next few years, simulation of micrometeorite effects. Consequently, early measurements of momentum transfer to targets were sponsored by NASA.[2] In 1966 Gregg and Thomas[3] systematically measured momentum transfer to different materials in the interesting range 10^8 - 4×10^{10} W/cm^2.

In 1967, Askar'yan et al.[4] claimed to have routinely accelerated particles to the order of 10^6 cm/s, and further, that under optimal conditions, a particle velocity up to 10^7 cm/s and higher can be attained. The record for velocity by laser acceleration at that time, however, was claimed by Asmus at General Atomic. He accelerated a mass of 10^{-7} g to 2.9×10^6 cm/s with a gigawatt ruby laser at 2×10^{11} W/cm^2.[5]

Not all laser acceleration is by ablation. In fact, it is convenient to identify three modes of acceleration that depend on laser intensity and wavelength, target material, and perhaps on initial conditions. CO_2 laser light at 10^6 - 10^8 W/cm^2 accelerates targets by detonating a blast wave in the gas above the target surface. Cylindrical-detonation-wave theory[6]

*Now at Maxwell Laboratories, 8835 Balboa Ave., San Diego, CA 92123

seems to explain the results of long-pulse-laser experiments[7] in this intensity regime, while spherical-blast-wave theory[8] explains short-pulse-laser experiments.[9,10] This mode of acceleration is probably not useful for impact fusion, but may be useful for long, slow acceleration of heavy masses such as air or space vehicles.[11]

The second mode of acceleration is produced by ablation of solid or liquid targets at 10^8 - 10^{12} W/cm^2. The ablatant may be fully or only partially ionized in this moderate intensity range, but the target can be cold. Ablative acceleration at moderate intensities may be important for injecting fuel pellets into fusion reactors[12,13] and for impact fusion. Experiments have been performed on metal foils[14] and D_2[15] at moderate intensities with a view to fusion fuelling applications, and on thin films[16] to find scaling laws for momentum transfer, but there has been little analytic work. Results of Lasnex calculations have been compared with a simple analytic model of acceleration of infinite solid slabs at moderate intensities.[17] The first analytic model of pellets accelerated by partially-ionized ablation[18] is presented in the next section.

In the third mode of acceleration, at about 10^{12} - 10^{14} W/cm^2, the target itself becomes an ionized plasma, and the ablatant may be fully ionized. This mode may also be applicable to impact fusion, but is useful now for shock studies, x-ray production studies, and laser fusion scaling studies. Many analytic models treat planar ablation[19,20] and ablative acceleration of pellets[21-23] at high intensities. Section 3 describes one of these[23] that determines the ablation consistent with laser and target parameters and target acceleration. Preliminary analyses of the hydrodynamic stability of the ablation of laser-driven targets have been performed.[24-25] Much exciting experimental work on ablative acceleration at 10^{12} - 10^{14} W/cm^2 is being done at the Naval Research Laboratory,[26] Sandia Laboratories,[27] and laboratories in other countries. NRL and Sandia both report ablative acceleration at 1.06 μm of thin targets to velocities of 10^7 cm/s and higher, and both have numerical programs[28,29] in support of their experiments.

2. Ablative Acceleration at Moderate Intensities

This section presents an analytic steady-ablation model, drawn from Ref. 18, describing targets accelerated by lasers of moderate intensity. By moderate intensity is meant one high enough to cause ablation by steady Chapman-Jouguet deflagration, but low enough that high-flux effects such as density profile modification, radiation, parametric instabilities in the underdense ablatant, hot electrons, fast ions, saturation of heat flux, and reduced absorption do not significantly affect the ablation. The range of moderate intensities is approximately 10^8 to $\gtrsim 10^{12}$ W/cm^2. Laser intensities less than 10^{10} W/cm^2 generate temperatures in ablated hydrogen below 100 eV. At these temperatures atomic processes such as dissociation and ionization can strongly affect the ablation. The model presented here accounts for such energy sinks, and treats a simplified model of laser absorption consistently with partial ionization. In a partially-ionized ablation, laser light can penetrate to higher densities, and couple its energy more efficiently into the target, yielding high hydrodynamic efficiencies.

The target may be accelerated as a solid as long as its yield strength exceeds the ablation pressure. If a low-Z target or rapid acceleration is desired, frozen hydrogen may be used. It will be fluidized below 1 MPa, but if contained by lateral ablation pressure, will expand adiabatically and refreeze when the laser pressure is removed. Whether solid or liquid, the pellets must be accelerated "acoustically slowly" over a few sound-signal transit times to avoid disassembly by shocks or shock heating.[12]

Inverse bremsstrahlung causes absorption of laser light of moderate intensity in the ablatant. To obtain analytic solutions, we regard all the absorbed laser flux to be absorbed at the critical surface, where laser frequency equals plasma frequency, and to be conducted inwards by electron flux. The critical surface is located self-consistently in the ablation by using the Saha equation to calculate the fraction of ionization.

In a one-dimensional, planar, steady-ablation model, the integrated equations expressing conservation of mass, momentum, and energy inside the critical surface are

$$\rho v = \rho_c v_c \quad , \tag{1}$$

$$\rho_c v_c v + p = \rho_c v_c^2 + p_c \quad , \tag{2}$$

$$\frac{1}{2} v^2 + \frac{\gamma}{\gamma-1} \frac{p}{\rho} + s(p,\rho) + \frac{q}{\rho_c v_c} = \frac{1}{2} v_c^2 + \frac{\gamma_c}{\gamma_c - 1} \frac{p_c}{\rho_c} + s_c - \frac{\Phi}{\rho_c v_c} \quad . \tag{3}$$

Here, v is the velocity of a volume element of mass density ρ and pressure p. The laser flux is Φ, electron heat flux is q, and ratio of specific heats is γ. The quantity $s(\rho,p)$ is an energy sink term that denotes the average specific energy expended per particle in such processes as sublimation, dissociation, and ionization. Quantities evaluated at the critical surface are denoted by a subscript c.

If we assume the critical surface is a Chapman-Jouguet deflagration front,[30] then

$$v_c^2 = \gamma_c p_c / \rho_c \quad . \tag{4}$$

Because the correction to the ideal gas law from particle correlations is small unless the fraction of ionized atoms, f, is small under conditions existing at the critical surface, the pressure there is approximately

$$p_c = \rho_c T_c (1 + f_c)/m \quad .$$

The critical surface is located self consistently as that surface at which the free electron density equals the critical density.

The solutions, illustrated in Fig. 1 for 10.6 μm light on hydrogen, are double-valued. The physically realized branch may be determined by the rise of the laser pulse to its steady flux value or by a prepulse. Below a certain laser flux there are no steady Chapman-Jouguet deflagration solutions. The detonation-wave theory may pertain in the low-flux regime.

A simple rocket model gives the velocity of the pellet as

$$V_p = - \alpha v_{ex} \ell n(M_o/M_p) \quad ,$$

in which M_o is the original pellet mass, M_p is the final pellet mass, and α is the fraction of the momentum transferred to the pellet in the forward direction by the ablation flux, chosen to be 0.6.[22] Eqs. (1,2,4) imply the asymptotic exhaust velocity is $v_{ex} \approx 8v_c/5$.

We define the hydrodynamic efficiency as the ratio of kinetic energy to absorbed energy per particle ablated,

$$\varepsilon_H \approx (v_{ex}^2/2)/(\Phi/\rho_c v_c) \approx 1.3\ \rho_c v_c^3/\Phi \quad .$$

We further define the propulsion efficiency as the ratio of energy imparted to the pellet to the kinetic energy of the ablation, which is given by the rocket model as

$$\varepsilon_P \approx [\alpha\ \ell n(M_o/M_p)]^2 / (M_o/M_p - 1) \quad .$$

Finally, to account for light passing the target and some reflection, the efficiency of laser absorption is assumed to be $\varepsilon_A \approx 80\%$. The efficiency of conversion of laser pulse energy to pellet kinetic energy is $\varepsilon = \varepsilon_A \varepsilon_H \varepsilon_P$. The most efficient acceleration is not always possible because of the constraint imposed by shockless acceleration. The maximum pellet velocity for a given ratio of laser energy to final pellet mass is illustrated in Fig. 2 for 10.6 μm light on hydrogen, as is the maximum efficiency ε. Figure 2 illustrates the high efficiency of laser acceleration owing to hydrodynamic efficiencies in excess of 40%. The actual hydrodynamic efficiency will be somewhat lower, because some of the laser energy is absorbed outside the critical surface.

The solutions may be extended to fluxes higher than those shown in Fig. 1. At temperatures sufficiently high that s_c can be neglected, analytic solutions exist. Under such conditions, $T_c \approx (3m_H/10)(\Phi/2\rho_c)^{2/3} \approx (\Phi/19\ \text{MW cm}^{-2})^{2/3}$. This scaling of T_c as $\Phi^{2/3}$ is a feature of other models of fully-ionized ablation as well.[19,20] At optimal propulsion efficiency (ε_p = 23%) the momentum conversion coefficient is

$$M_p V_p / E_L \approx (\Phi/13\ \text{MW cm}^{-2})^{-1/3}\ \text{dyne-sec/J}, \quad (\Phi \gtrsim 2\ \text{GW/cm}^2)$$

at these higher temperatures. This scaling of conversion coefficient agrees well with experimental results[3] for momentum transfer to a variety of materials at laser fluxes $\gtrsim$ 1 GW/cm^2.

3. Ablative Acceleration at High Intensities

This section presents a steady-state model of a laser-driven plasma slab treated by 1-D, steady-flow hydrodynamic equations. The model, drawn from Ref. 23, is applicable to laser acceleration at high intensities ($\gtrsim 10^{12}$ W/cm^2) for which the target near the ablation surface is fully ionized. It differs from the model of the preceding section in several respects: the ablatant is fully ionized; the model allows for radiation pressure, flux-limiting, and density profile steepening at the critical surface; it accounts not only for the effects of the acceleration on the ablation, but, self-consistently, for the slow increase in acceleration of the target as a result of its diminishing mass. The ablation is analyzed in greater detail. The cold unablated fluid, the ablation layer, both classical and flux-limited hot conduction regions, the critical surface, and the underdense blowoff are all considered. A global description determines the temperature, density, velocity, and boundaries as well.

The model is formulated in terms of time-independent solutions of the continuity, momentum, and energy equations,

$$0 = \frac{\partial \rho}{\partial t} = - \frac{\partial}{\partial x} (\rho v),$$

$$0 = \frac{\partial}{\partial t} (\rho v) = - \frac{\partial}{\partial x} (\rho v^2 + P) + \rho g - \left(\frac{\Phi_a + 2\Phi_r}{c} \right) \delta(x - x_c), \quad (5)$$

$$0 = \frac{\partial E}{\partial t} = - \frac{\partial}{\partial x} (Pv + Ev + q) + \rho g v + \Phi_a \delta(x - x_c).$$

Here $E = \frac{1}{2} (3P + \rho v^2)$ is the local energy density, and Φ_a (Φ_r) is the absorbed (reflected) laser flux. The laser energy and momentum are regarded as deposited at the critical surface $x = x_c$. The momentum-deposition term causes gradient steepening and density shelves at the critical surface. The effective gravity g can not be neglected at high acceleration. The heat flux q at any point in the hot conduction region is considered to be the

lesser in magnitude of the classical flux $q_{class} = - KT^{5/2}T'$ and limited flux $q_{lim} = -\ell\rho(T/m)^{3/2}T'|T'|^{-1}$. A prime denotes d/dx, $KT^{5/2}$ is the conductivity, and the flux-limit parameter ℓ lies in the range $0.5 \lesssim \ell \lesssim 60$.[23] An upper bound, $\ell \lesssim 3$, is found to be required for a flux-limited region to exist in steady state.

The solutions of Eqs. (5) near the ablation layer are shown in Fig. 3. Characteristic of ablation surfaces are the steep density and temperature gradients and the outward displacement of the pressure peak from the density peak. The solutions allow for a sonic surface inside the cold plasma slab.

Jump conditions at the critical surface determine the height of the density plateaus on either side caused by radiation pressure and require that the critical surface be the sonic surface at which the ablatant exceeds the local sound speed. All energy deposited at the critical surface is assumed to be conducted into the much more massive and colder overdense region, so that q = 0 in the underdense region, and an adiabatic equation of state applies there. In this model the momentum equation is averaged over many wavelengths to iron out the effects of the ponderomotive force, $\langle \rho d|E|^2/dx \rangle_x = 0$, and leave only the gross profiles of the steady flow of an ideal, adiabatic gas in the underdense region. The exact solutions of (5) for the underdense, adiabatic gas are

$$v^2 - 5(T_c/m)[1 - (v_+/v)^{2/3}] = v_+^2 + 2g(x - x_c),$$

$$\rho = \rho_+ v_+/v, \qquad T = T_c(v_+/v)^{2/3}.$$

The gravity determines the boundaries self-consistently. Let the total plasma mass per area, M, be specified. Since momentum density is uniform, during a time δt a thin layer of mass $\delta M = \rho_L v_L \delta t = \rho_- v_- \delta t$ is effectively transferred from the left boundary x_L to the right boundary x_R at higher velocity v_R. The change in momentum, $\delta p = \delta M\,(v_R - v_L)$, must be compensated by an acceleration of the whole plasma to the left, since the hydrodynamic forces are internal, causing an effective gravity

$$g = \rho_- v_-(v_R - v_L)/M \quad . \tag{6}$$

Since the jump conditions are not satisfied at the slab boundaries, the steady-state assumption breaks down near the boundaries. Equation (6) is good, however, as long as the widths of the unsteady slab ends are much less than the overall width of the slab. The gravity increases,

$$dg/dt = \rho_- v_- (dv_R^2/dx - dv_L^2/dx)/2M \quad ,$$

with a characteristic time scale for growth of v_R/g. The dynamical development of a slab can be followed over longer time periods by respecifying gravity and intensity if desired, and repeating the integration of (5).

Equation (6) determines the approximate slab boundaries, and completes the global description of the laser-plasma interaction. Figure 4 shows the self-consistent profiles and boundaries found by specifying I_a, I_r, M, g, ρ_c, and T_c only. Reference 23 derives approximate analytic solutions for each of the plasma regions, including the ionized target, ablation layer, classical and flux-limited conduction regions, critical surface, and underdense region.

4. Application to Impact Fusion

This section presents some preliminary considerations of the use of laser-driven projectiles for impact fusion. For a baseline case we suppose that projectiles must be accelerated to 1 MJ and $V_p = 2 \times 10^7$ cm/s (implying $M_p = 0.05$ g) to produce impact fusion. Then there seems to be at least three kinds of laser-driven targets that may achieve the baseline case: solids, liquids, or plasmas. Each of these possibilities is considered below.

A solid sphere of density ρ_s can not be accelerated with a pressure greater than about its yield strength Y, implying

$$Y \gtrsim \left(\frac{16\, M_o}{9\,\pi}\, \rho_s^2\right)^{1/3} a \quad .$$

Therefore, a solid of mass $M_o = 0.25$ g with $Y \approx 10^{10}$ dyne/cm^2, and $\rho_s \approx 8$ g/cm^3 (such as stainless steel) can not be accelerated faster than 5×10^9 cm/s^2. This limitation implies an acceleration time greater than a few

milliseconds and an acceleration distance greater than a few hundred meters. Absence of fluid instabilities in a solid target may compensate for the long accelerators required.

Fluid targets can be accelerated much faster, but must be contained laterally during acceleration by lateral ablation pressure or other means. Perhaps the higher efficiency that might result from accelerating fluidized hydrogen will compensate for having to deal with fluid instabilities at the target surface. The higher ionization branch of solutions to the model of Section 2 is more efficient at the high velocities of interest for impact fusion, and stripping hydrogen requires only 13.6 eV per atom. The efficiency of laser acceleration of hydrogen in the velocity range of interest for impact fusion is shown in Fig. 5. The efficiency is the product of ε_A, ε_H, and ε_p optimized as a function of M_o/M_p. The laser flux Φ is found as the product of laser energy $\frac{1}{2} M_p V_p^2/\varepsilon$ with total particle flux $\rho_c V_c (M_o - M_p)^{-1}$. To achieve 2×10^7 cm/s with fluid targets requires an acceleration distance of only several tens of meters.

It may be possible to reduce the acceleration distance to the order of centimeters, and accelerate the projectiles completely within the reactor close up to the DT pellet, if the projectiles are accelerated as plasmas. Plasma targets are being accelerated to the order of 10^7 cm/s at intensities of 10^{12} to 10^{14} W/cm^2,[28,29] although the targets are five or six orders of magnitude less massive than required for impact fusion. At $10^{13} - 10^{14}$ W/cm^2, a laser can dump 10 MJ of energy onto an area the size of a 0.25-g sphere in $10^{-7} - 10^{-5}$ s, depending on target material. The laser must not dump energy into the target so quickly, however, that it explodes the target rather than accelerating it ablatively. This condition may limit target materials that can be used, as sound signal transit times across 0.25-g pellets are comparable to laser pulse widths in the range $10^{-7} - 10^{-6}$ s. For this range of acceleration time, acceleration distances are 1 - 10 cm.

Table 1 summarizes some of the considerations concerning the three kinds of targets that may be accelerated for the baseline case of impact fusion defined in this section.

TABLE 1
LASER ABLATIVE ACCELERATION FOR IMPACT FUSION

	Solid	Fluid	Plasma
Acceleration Characterized by	Below yield strength	Above yield strength, but no shocks or shock heating	Shocks + shock heating, but no exploding pusher behavior
Material	High yield strength (tungsten, steel,..)	Low Z (H_2, DT)	?
Laser Intensity (W/cm^2)	$10^9 - 10^{10}$	$\sim 10^{10}$	$10^{12} - 10^{14}$
Degree of Ionization	Ablatant partially ionized	Ablatant fully ionized, cold target	Target and ablatant ionized
Acceleration Distance (m)	Several hundreds	Several tens	Within reactor
Acceleration Time (s)	Few 10^{-3}	Few 10^{-4}	$10^{-7} - 10^{-5}$
Efficiency (Kinetic Energy/Laser Energy)	$\lesssim 5\%$	10%	?
Advantages	No fluid instabilities, high-Z for absorption of bremsstrahlung	Reasonable acceleration distance, good efficiency	Short acceleration distance, no external accelerator
Disadvantages	Long accelerator, long distance for focussing and stabilizing trajectory	Fluid instabilities, lateral containment needed	Fluid instabilities, lateral containment needed, heat conduction to back surface, targeting needed

References

1. G. A. Askar'yan and E. M. Moroz, "Pressure on Evaporation of Matter in a Radiation Beam," JETP Lett. 16, 1638 (1962).
2. F. Neuman, "Momentum Transfer and Cratering Effects Produced by Giant Pulse Lasers," Appl. Phys. Lett. 4, 167 (1964).
3. D. W. Gregg and S. J. Thomas, "Momentum Transfer Produced by Focused Laser Giant Pulses," Jour. Appl. Phys. 37, 2787 (1966).
4. G. A. Askar'yan et al., "Light-Reaction Acceleration of Macroparticles of Matter," Sov. Phys. JETP 28, 208 (1967).
5. J. F. Asmus, "Micrometeorite Generation with a High-Power Laser," IEEE Jour. Quantum Electr. 3, 265 (1967).
6. A. N. Pirri, "Theory for Momentum Transfer to a Surface with a High-Power Laser," Phys. Fluids 16, 1435 (1973).
7. A. N. Pirri, R. Schlier, and D. Northam, "Momentum Transfer and Plasma Formation Above a Surface with a High-Power CO_2 Laser," Appl. Phys. Lett. 21, 79 (1972).
8. Ya. B. Zel'dovich and Yu. P. Raizer, Physics of Shock Waves and High-Temperature Hydrodynamic Phenomena (Academic, New York, 1967), Vol. I.
9. J. F. Ready, "Impulse Produced by the Interaction of CO_2 TEA Laser Pulses," Appl. Phys. Lett. 25, 558 (1974).
10. K. Kuriki and Y. Kitora, "Momentum Transfer to Target from Laser-Produced Plasma," Appl. Phys. Lett. 30, 443 (1977).
11. A. R. Kantrowitz, "Propulsion to Orbit by Ground-Based Lasers," Aeronautics and Astronautics 10, 74 (1972).
12. F. S. Felber, "Laser Acceleration of Reactor Fuel Pellets," Nucl. Fusion 18, 1469 (1978).
13. F. S. Felber, "Fueling Moving Ring Field-Reversed Mirror Reactor Plasmas," General Atomic Report GA-A15177 (1979).
14. P. T. Rumsby, M. M. Michaelis, and M. Burgess, "Laser Induced Acceleration of Metal Foils," Optics Comm. 15, 422 (1975).
15. M.D.J. Burgess, H. Motz, I. J. Spalding, and A. C. Walker, "Acceleration of Macroparticles by Laser Light," Seventh International Conference on Plasma Physics and Controlled Nuclear Fusion Research, Innsbruck, IAEA/CN/37 R-5-1 (1978).

16. Annual Progress Report on Laser Fusion Program, Inst. of Laser Engineering, Osaka Univ. ILE-APR-77 (1977), p. 79.
17. T. E. McCann and J. S. DeGroot, "Acceleration of Solid Macro-Particles by Laser Produced Ablation," University of California UCRL-79732 (1977).
18. F. S. Felber, "Model of Ablative Acceleration at Moderate Laser Intensities," General Atomic Report GA-A14944 (1979).
19. J. L. Bobin et al., "Temperature in Laser-Created Deuterium Plasmas," Nucl. Fusion 9, 115 (1969).
20. H. Puell, "Heating of Laser Produced Plasmas Generated at Plane Solid Targets," Z. Naturforsch. 25a, 1807 (1970).
21. R. S. Cooper, "Motion of Solid D_2 under Laser Irradiation," AIAA Jour. 11, 831 (1973).
22. T. R. Jarboe, W. B. Kunkel, and A. F. Lietzke, "Study of Plasma Density Distribution Produced by Irradiating a 50 μ Deuterium Pellet on One Side with a Ruby Laser," Phys. Fluids 19, 1501 (1976).
23. F. S. Felber, "Steady-State Model of a Flat Laser-Driven Target," Phys. Rev. Lett. 39, 84 (1977); Phys. Rev. Lett. 40, 824 (1978).
24. K. A. Brueckner, S. Jorna, and R. Janda, "Hydrodynamic Stability of a Laser-Driven Target," Phys. Fluids 17, 1554 (1974).
25. F. S. Felber and S. E. Bodner, "Some Rayleigh-Taylor Stabilizing Mechanisms in Thin Laser Targets," Naval Research Laboratory Memorandum Report 3574 (1977).
26. R. Decoste et al., "Ablative Acceleration of Laser-Irradiated Thin Foil Targets," Phys. Rev. Lett. 42, 1673 (1979).
27. J. P. Anthes et al., "Ablative Response of Mass-Limited Targets at 1.064 μm," IEEE International Conference on Plasma Science, Montreal, 6Q4 (1979).
28. P. J. Moffa, J. H. Orens, and J. P. Boris, "Modelling of Laser Foil Interactions," IEEE International Conference on Plasma Science, Montreal, 1A11 (1979).
29. J. P. Anthes, M. A. Gusinow, and M. K. Matzen, "Experimental Observation and Numerical Simulations of Laser-Driven Ablation," Phys. Rev. Lett. 41, 1300 (1978).
30. R. Courant and K. O. Friedrichs, Supersonic Flow and Shock Waves, Vol. I (Interscience, N.Y., 1948).

Figure Captions

Fig. 1 Hydrogen ablation velocity v_c, temperature T_c, and degree of ionization f_c at critical surface, and energy absorbed per particle ablated $\Phi/N_c v_c$ versus absorbed laser flux. Solid curves are lower-ionization-branch solutions; dashed are higher-ionization-branch solutions.

Fig. 2. Final hydrogen pellet velocity V_p and optimized efficiency of conversion of laser pulse energy to pellet kinetic energy ε versus ratio of laser pulse energy to final pellet mass. Dashed curves represent less efficient acceleration at lower laser flux required to avoid pellet disassembly by shocks.

Fig. 3. Temperature, density, and pressure profiles at the ablation layer with $T/m_i = 10^{13}$ cm^2/s^2, $v = 2.2 \times 10^5$ cm/s, and $\rho = 0.3$ g/cm^3 specified at the surface of peak density, and acceleration $g = 3 \times 10^{15}$ cm/s^2. Dashed curve is analytic temperature approximation.

Fig. 4. Density, temperature, and Mach-number profiles of global slab model. Specified were the absorbed flux $I_a = 10.2$ TW/cm^2, reflected flux $I_r = 10.2$ TW/cm^2, total mass $M = 0.733$ mg/cm^2, acceleration $g = 3 \times 10^{15}$ cm/sec^2, critical density $\rho_c = 4 \times 10^{-3}$ g/cm^3, and critical temperature $T_c/m_i = 4.50 \times 10^{14}$ cm^2/sec^2; the coefficient of conductivity was $K = 10^{-33} m_i^{-7/2}$(cgs). Self-consistency of the global model required a critical surface at x_c, left and right boundaries at x_L and x_R, and upper and lower shelf densities ρ_- and ρ_+ as shown. No saturation of heat flux occurs here for the flux-limit parameter $\ell > 1.79$.

Fig. 5. Acceleration of hydrogen pellets by CO_2 lasers to velocity V_p at optimal efficiency. Curves show laser flux Φ, temperature at critical surface T_c, efficiency ε, and ratio of initial to final pellet mass M_o/M_p for any M_p. For $M_p = 0.05$ g and compressed pellet density 0.1 g/cm^3, curves show acceleration length L and time τ.

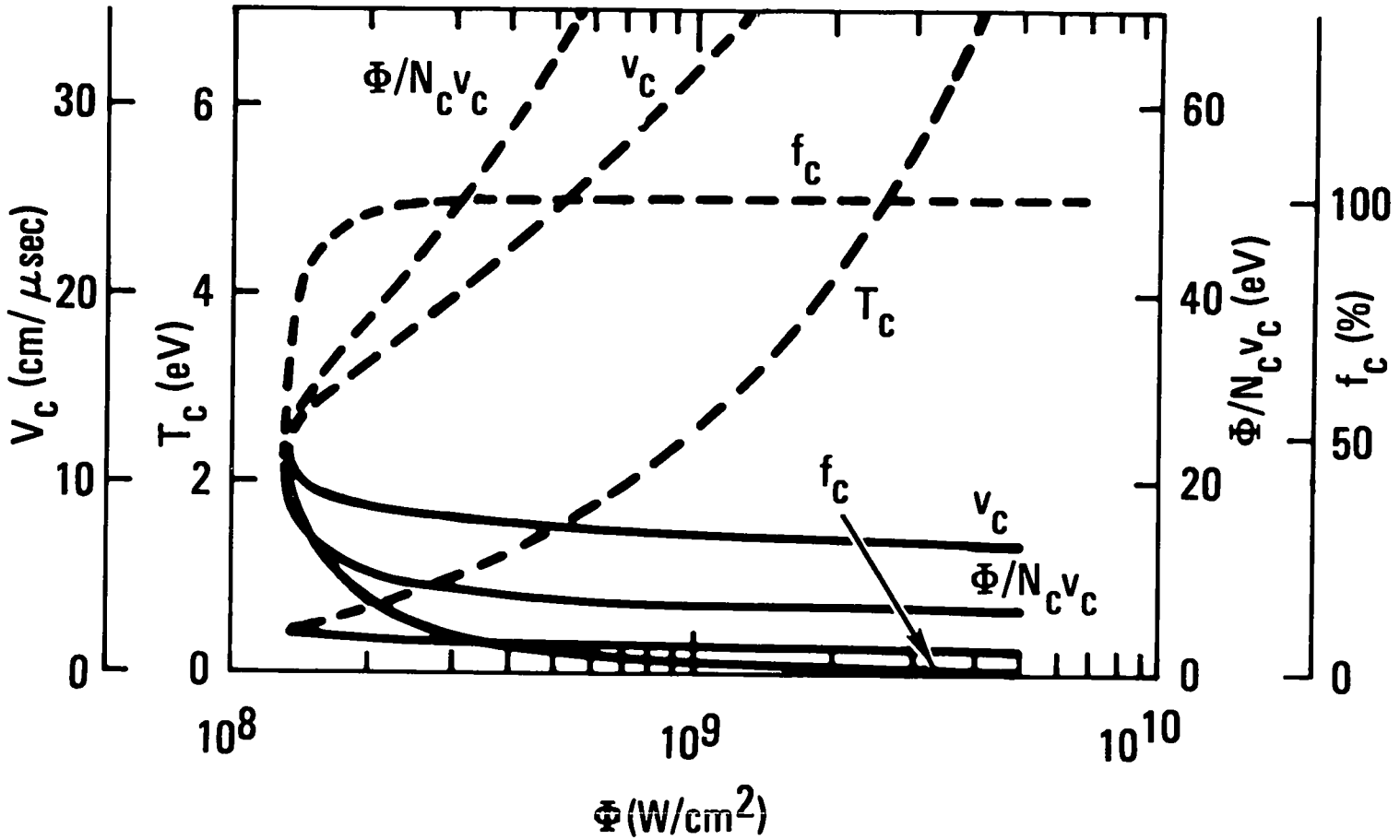

Fig. 1 Hydrogen ablation velocity v_c, temperature T_c, and degree of ionization f_c at critical surface, and energy absorbed per particle ablated $\Phi/N_c v_c$ versus absorbed laser flux. Solid curves are lower-ionization-branch solutions; dashed are higher-ionization-branch solutions.

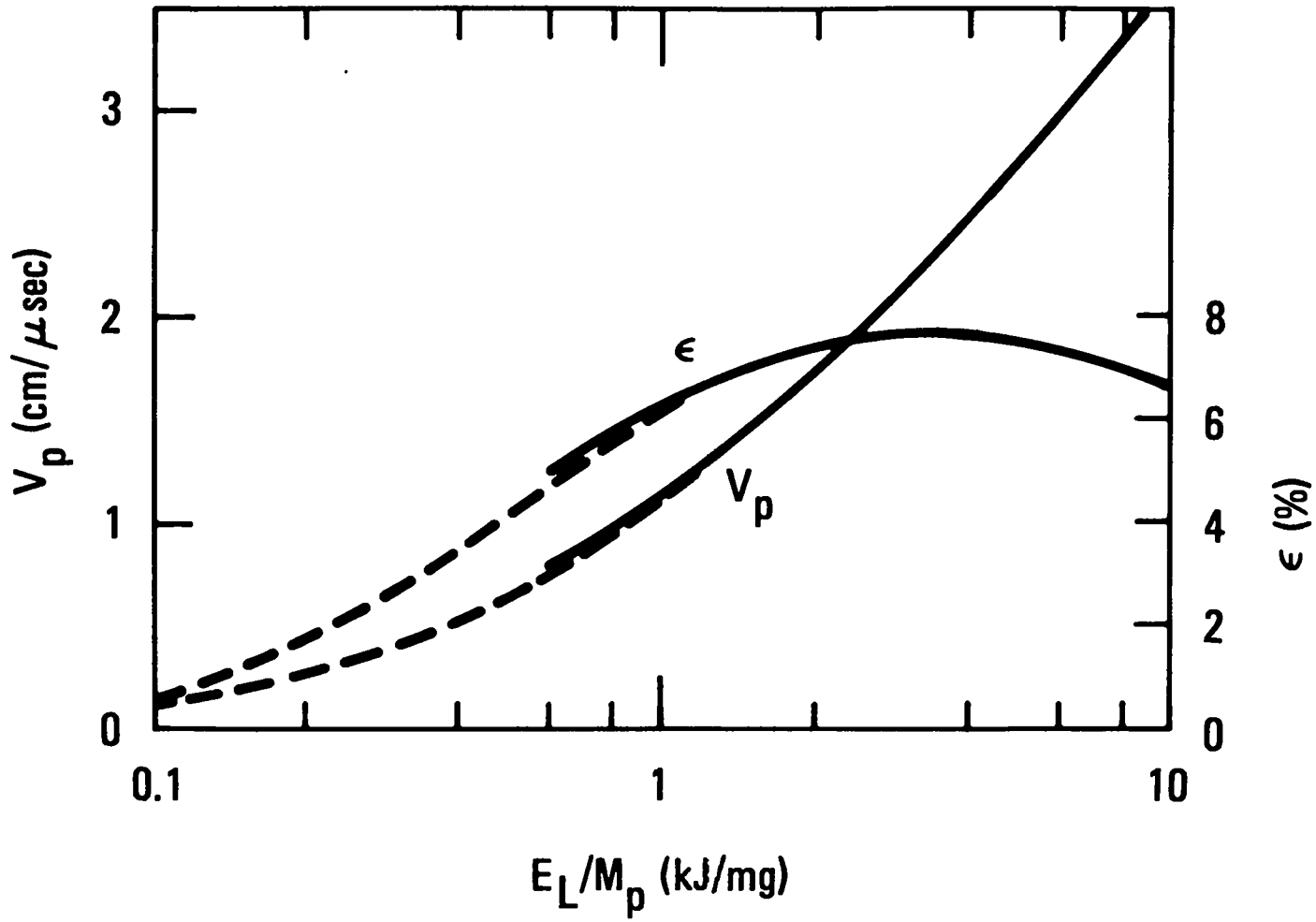

Fig. 2 Final hydrogen pellet velocity V_p and optimized efficiency of conversion of laser pulse energy to pellet kinetic energy ϵ versus ratio of laser pulse energy to final pellet mass. Dashed curves represent less efficient acceleration at lower laser flux required to avoid pellet disassembly by shocks.

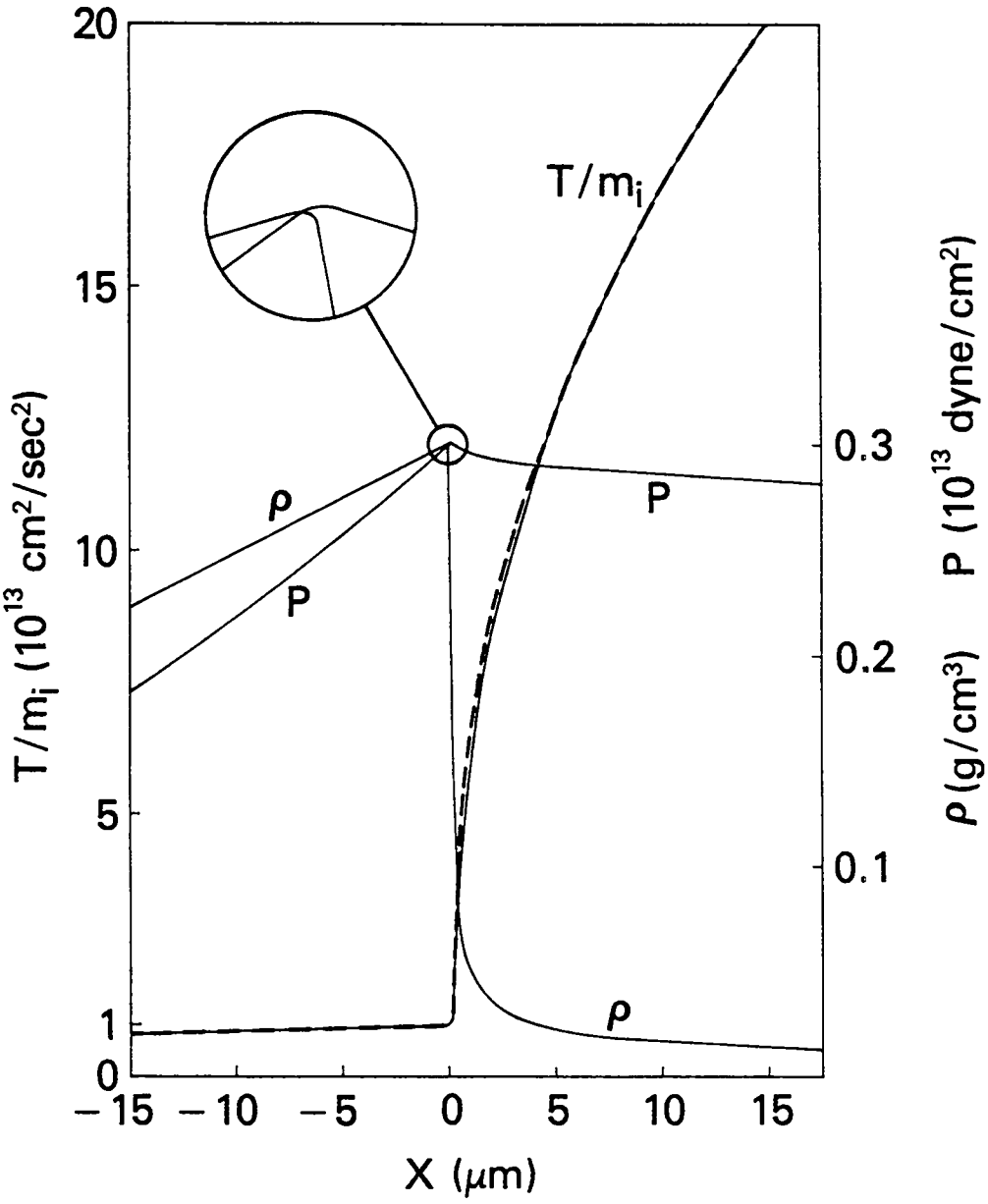

Fig. 3. Temperature, density, and pressure profiles at the ablation layer with $T/m_i = 10^{13}$ cm^2/s^2, $v = 2.2 \times 10^5$ cm/s, and $\rho = 0.3$ g/cm^3 specified at the surface of peak density, and acceleration $g = 3 \times 10^{15}$ cm/s^2. Dashed curve is analytic temperature approximation.

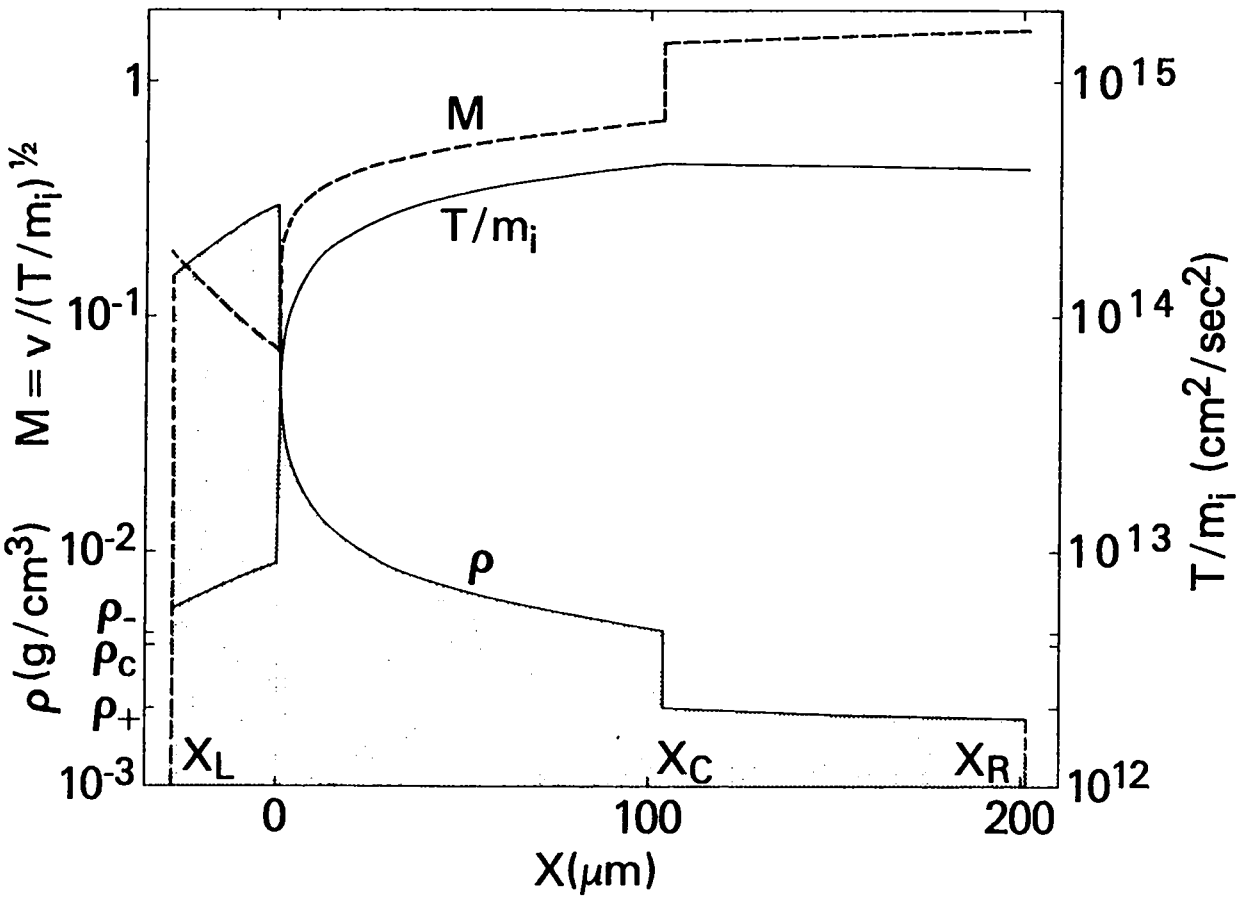

Fig. 4. Density, temperature, and Mach-number profiles of global slab model. Specified were the absorbed flux I_a = 10.2 TW/cm^2, reflected flux I_r = 10.2 TW/cm^2, total mass m = 0.733 mg/cm^2, acceleration g = 3 × 10^{15} cm/sec^2, critical density ρ_c = 4 × 10^{-3} g/cm^3, and critical temperature T_c/m_i = 4.50 × 10^{14} cm^2/sec^2; the coefficient of conductivity was K = $10^{-33} m_i^{-7/2}$(cgs). Self-consistency of the global model required a critical surface at x_c, left and right boundaries at x_L and x_R, and upper and lower shelf densities ρ_- and ρ_+ as shown. No saturation of heat flux occurs here for the flux-limit parameter $\ell > 1.79$.

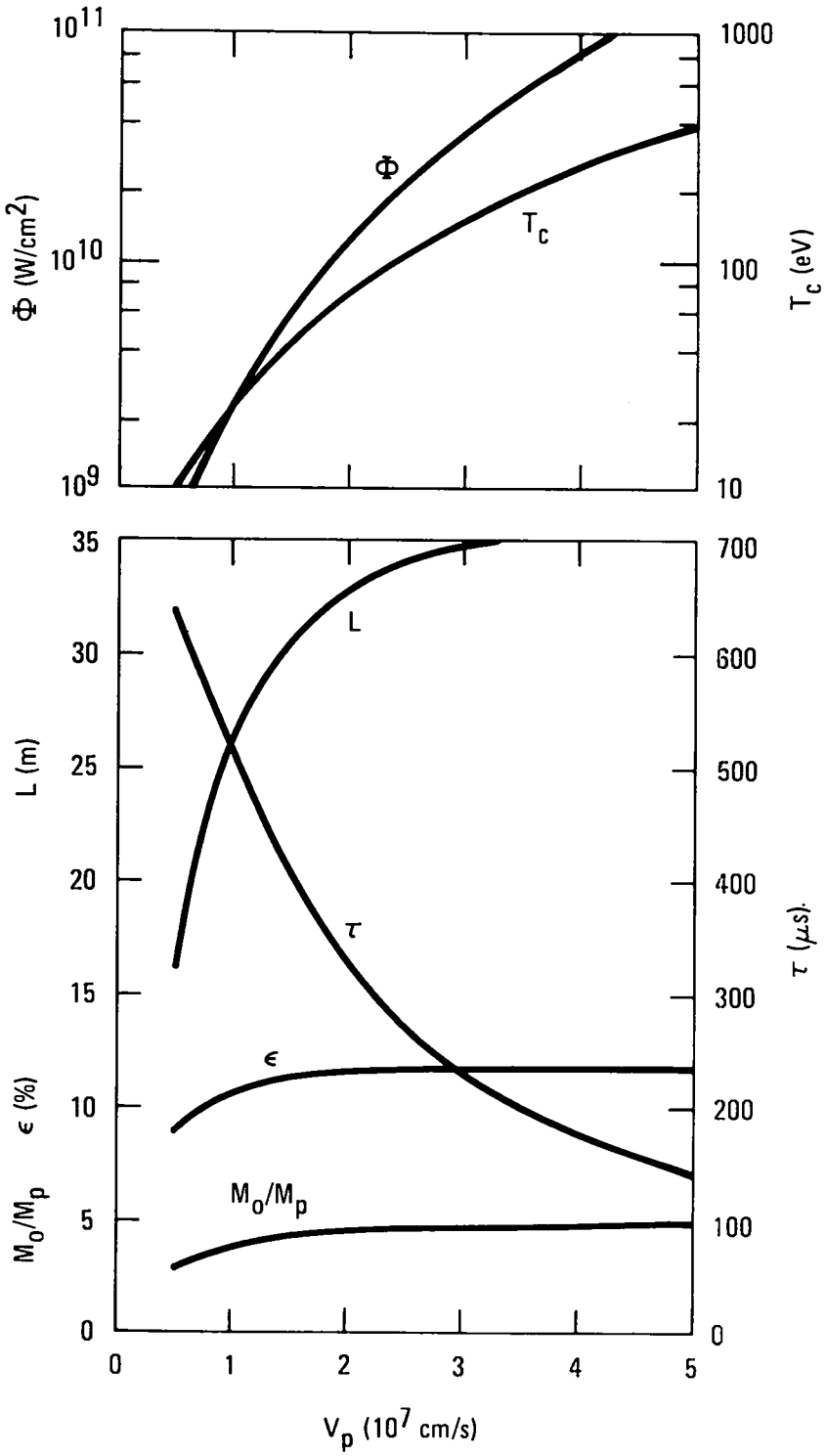

Fig. 5. Acceleration of hydrogen pellets by CO_2 lasers to velocity V_p at optimal efficiency. Curves show laser flux Φ, temperature at critical surface T_c, efficiency ϵ, and ratio of initial to final pellet mass M_o/M_p for any M_p. For M_p = 0.05 g and compressed pellet density 0.1 g/cm^3, curves show acceleration length L and time τ.

LASER DRIVEN MACROPARTICLES

J. S. DeGroot
Department of Applied Science
University of California, Davis;
Lawrence Livermore Laboratory

and

T. E. McCann
Air Force Academy;
Lawrence Livermore Laboratory

LASER DRIVEN MACROPARTICLES*

J. S. DeGroot
Department of Applied Science
University of California, Davis
and
Lawrence Livermore Laboratory
and
T. E. McCann
Air Force Academy
and
Lawrence Livermore Laboratory

ABSTRACT

The feasibility of using laser driven ablation to accelerate small (~ 0.1 gm) macroparticles (BB's) to high velocities (10^7 to 10^8 cm/sec) is investigated. It is shown that a solid accelerated BB could be produced with an efficiency of about 15%. Laser fluxes in the range $3 \times 10^8 \lesssim I \lesssim 10^{11}$ (W/cm^2) could be used. The lower limit is set by the condition that evaporation is the dominant heat removal mechanism. The upper limit is set by material yield strength.

I. INTRODUCTION

Recently, there has been renewed interest in the acceleration of small (10^{-3} to 10^{-1} gm) macroparticles (BB's) to high velocities (10^{7} to 10^{8} cm/sec). Several techniques have been suggested[1], e.g., ablative, magnetic, and electrostatic. We are studying[2] the feasibility of using lasers to ablatively accelerate a BB in such a way that a solid density high velocity BB is produced. The idea is not new. Since the first suggestion by Askar'yan[3] in 1962, several theoretical[1,4,5,6] and experimental[7,8,9,10,11] studies have been published. Our purpose is to study the complete process using theory and detailed hydrodynamic computer calculations.

The important physical phenomena which occur are shown in Fig. 1. Initially, the laser heats the back surface of the BB. If the laser flux, I, is large enough[12], i.e., if

$$I > I_{Min}$$

where

$$I_{Min} = \frac{\rho_o a^{1/2} U}{\tau^{1/2}}$$

ρ_o = solid density

a = thermal diffusivity

τ = laser pulse length

U = heat of sublimination,

then thermal conduction can not remove the heat fast enough, and evaporation is the dominant heat removal mechanism. (For a glass BB (SiO_2), $I_{Min} \leq 3 \times 10^{8}$ W/cm^2 for $\tau \geq 10^{-9}$ sec.)

For higher intensities, the material is evaporated, dissociated, and ionized in the ablation and conduction regions. The reaction to the ablation accelerates the BB. A thermal wave travels into the solid BB. However, the strong nonlinearity of the thermal conductivity maintains the thermal wave close to the ablation surface. A shock overtakes the thermal wave and travels through the BB. This shock must be weak enough so that the BB is not melted. Thus, the rise time of the laser pulse must be slow enough. Since a solid BB is required, the ablation pressure must be less than the yield strength of the material. Taking a low value for the yield strength of 5 kbar to be safe, we shall see that this requirement results in an upper intensity limit of $I_{max} \approx 10^{11}$ W/cm^2. Thus, the laser flux must be in the range $3 \times 10^8 \lesssim I \lesssim 10^{11}$, W/cm^2 . After a short time, a quasi-steady state is set up in the BB rest frame. The laser travels through the exhaust region and is absorbed. Electron conduction carries some of this energy through the conduction region to the ablation surface. The plasma plume expands in the exhaust region, and this hot plasma radiates a fraction of the laser energy.

A schematic of the quasi-steady state acceleration of a BB is shown in Fig. 2. The laser flux is lower in the center of the beam so that the BB tends to remain in the laser beam. Other lasers may be required to fully stabilize the BB within the beam.

2. HYDRODYNAMIC CALCULATIONS

We have used[2] a Lagrangian magnetohydrodynamics computer code to study the ablative acceleration of BB's. One-dimensional (slab) geometry was used in most of the calculations. Some two-dimensional (r,z) calculations were performed to study the effects due to the finite BB diameter.

Initial conditions for the 1-D calculations consist of a semi-infinite, solid material slab with a thickness of 16.3 μm. Most calculations were performed with a glass (SiO_2) BB. The initial mass/area was $m_o = 3.75 \times 10^{-3}$ gm/cm^2 ($\rho_o = 2.3$ gm/cm^3). The initial temperature of the glass was 0.1 eV (or 1160 °K, below the melting point of glass). The one-dimensional calculations must be corrected for the finite diameter ($\approx$ 0.5 cm) of the BB--a two-dimensional effect. During the laser pulse, the plasma expands beyond the BB diameter. To correct for this effect, the zone size is initialized so that during the calculations the distance from the absorption surface to the ablation surface was never greater than the BB diameter. In addition, the laser is propagated through the exhaust without attenuation until a computational zone is reached in which the density, ρ, is equal to or greater than the critical density (the density at which the plasma frequency equals the laser frequency), ρ_c, i.e., $\rho \geq \rho_c$. The laser energy is deposited into the electron thermal energy in that zone.

Spatial profiles of the electron temperature and plasma density are shown in Fig. 3 at times of t = 0.2, 0.3, 0.4, 0.5, 0.6, and 0.7 μsec after the laser was switched on. The various regions are visible (solid--high density width not resolvable; ablation--T_e rapidly increases and ρ rapidly decreases; conduction--T_e slowly increases and ρ slowly decreases; absorption--T_e is a maximum; and exhaust--T_e is approximately constant). The BB is accelerating to the left (the slab was initially at z = 0). The profiles are approximately constant in the frame of the accelerating BB. The ablation pressure, which supplies the force that accelerates the BB, is also closely constant. The variables which are required to calculate the BB acceleration are the ablation pressure and the rate of mass vaporization. The ablation pressure, P_A, and electron temperature in the critical zone, T_c, were obtained from several calculations where the laser intensity was varied from 4×10^9 W/cm^2 to 4×10^{10} W/cm^2, and the results are shown in Fig. 4 (solid circles). These values were averaged over 0.5 μsec to remove small spurious oscillations due to the discreteness of the calculations. The points are extremely well represented by $P_A = 3.0[I/(4 \times 10^9)]^{0.52}$ kbar (solid line) and $T_c = 21[I/(4 \times 10^9)]^{0.52}$ eV (dashed line). The rate of vaporization, $\dot{m}_v$, and the fraction of the laser energy which is not radiated, f_R, were also obtained from the calculations. These points are extremely well represented by

$\dot{m}_v = 0.56[I/(4\times10^9)]^{0.21}$ gm/cm^2-sec and $f_R = 0.5[I/(4\times10^9)]^{-0.14}$.

Results from the 2-D (r,z) calculations are similar to the 1-D results except that the density decreases rapidly with distance from the ablation surface. In the 2-D calculations, the laser energy is absorbed by inverse bremsstrahlung locally in the plasma as the laser light propagates toward the critical surface. We find that the density at the absorption surface, n_a, for a CO_2 laser is about $n_c = 10^{19}$ cm^{-3}, the critical density for a CO_2 laser. However, ρ_a is close to the critical density for a CO_2 laser even for a Nd (1μ) laser. This is because the electron temperature is rather cold so that inverse bremsstrahlung is very efficient in absorbing laser light.

3. ANALYTICAL RESULTS

We can use the results from the hydrodynamic calculations to construct analytical models of BB acceleration.

Since the exhaust region is closely isothermal, we can calculate[4] the energy/area contained in the exhaust as

$$E_e = 5m_v C_s^2, \text{ erg/cm}^2 \qquad (1)$$

where $C_s = \sqrt{\bar{Z}kT_e/M}$, the isothermal sound speed. We neglect the energy of the plasma in the conduction zone (the pressure (energy density) is almost constant throughout the plasma) and set the rate of exhaust energy change, $\dot{E}_e$, to the fraction

of the laser flux deposited in the plasma which is not radiated, i.e., $\dot{E}_e = f_R I$. This gives

$$I = 5\dot{m}_v C_s^2 / f_R \ . \tag{2}$$

The ablation pressure which accelerates the solid is the sum of a momentum flux, $\dot{m}_v C_s$, and a thermal term from the hot plasma, $n_a k T_a$ (where n_a and T_a are the electron density and temperature at the absorption surface, respectively), or $P_A = \dot{m}_v C_s + n_a k T_a$. The continuity equation gives $\dot{m}_v = \rho u = \text{constant}$, where u is the plasma flow velocity. We find that[13] $u \approx C_s$ at the absorption surface so that $\dot{m}_v = \rho_a C_s$. Thus, we see that

$$P_A \approx 2\dot{m}_v C_s . \tag{3}$$

Solving Eq. (2) for $\dot{m}_v$, substituting this into Eq. (3), and using Eq. (2) to eliminate C_s, we obtain

$$P_A = 0.68 (\rho_a)^{1/3} (f_R I)^{2/3} . \tag{4}$$

This result is within a few percent of the result obtained from the 1-D calculations (instead of 0.68, we get 0.64 from the 1-D results; we used $\rho_a \equiv \rho_c = n_{ec} \bar{M}/\bar{Z}$, where $n_{ec} = 4 \times 10^{19}$, $\bar{M} = 20\ M_p$ for SiO_2, and $\bar{Z}$ comes from the coronal model). In addition, we find that $\dot{m}_v = \rho_a C_s$ within a few percent. Thus, our analytical results agree quite well with the results from the detailed hydrodynamic calculations.

4. EFFICIENCY OF BB ACCELERATION

The equation of motion of the BB is just

$$m\dot{V} = P_A \ , \tag{5}$$

where

m = mass/area of the BB

V = BB velocity.

However, we found that $P_A = 2\dot{m}_v C_s$ so that

$$\dot{V} = -2C_s \frac{\dot{m}}{m} \ . \tag{6}$$

Here we used $m = m_o - m_v$, or $\dot{m} = -\dot{m}_v$, where m_o is the initial mass/area of the BB. If C_s is constant, then we can integrate Eq. (6) to obtain

$$V(t) = 2C_s \, \ell n\left(\frac{m_o}{m(t)}\right) \ . \tag{7}$$

Eq. (7) agrees with the well known equation for rockets, except here the effective exhaust velocity is $2C_s$.

The efficiency of the acceleration process, η_c, is just

$$\eta_c = \tfrac{1}{2} m_f V_f^2 / \int_0^{t_f} I \, dt \ , \tag{8}$$

where m_f and V_f are the mass and velocity of the accelerated BB (at time t_f). We assume that the laser flux is constant, which is consistent with C_s being constant. Using Eq. (2) to eliminate I, Eq. (7) (with $t = t_f$) to eliminate V_f, and the definition of t_f, i.e., $t_f \equiv (m_o - m_f)/\dot{m}_v$ (t_f is the time to vaporize a mass of $m_o - m_f$) we obtain

$$\eta_c = \eta_h \eta_p \ , \tag{9}$$

where $\eta_h = \frac{2}{5} f_R$ is the the efficiency of the production of exhaust velocity by the laser, $\eta_p = \ell n^2 x_f/(x_f-1)$ is the propulsion efficiency, and $x_f = m_o/m_f$. This expression for η_p is exactly the expression obtained for rockets. As is well known, η_p has a maximum value of $\eta_p \simeq 0.65$ at $x_f \simeq 5$. Cooper[4] has derived the efficiency using a similar argument, and Eq. (9) agrees with his result within a few percent (Fig. 3 in Ref. 4; $(x_f-1)/x_f \to z$, $\eta_c \to \varepsilon_a$, and $f_R = 1$). In Cooper's calculation, the laser was deposited according to the inverse bremsstrahlung formula. However, this should not affect the result substantially, because η is independent of the density at the absorption surface (Eq. (9)).

Thus, we find that the maximum efficiency is about $\eta_{c_{max}} \simeq (.4)(.65)(.4) \simeq 0.1$ (we used $f_R = 0.4$ consistent with the 1-D results). This efficiency may be too low for many applications.

How can this efficiency be increased? Notice that η_p is maximum near $V_f = 1.6V_{ex}$, where V_{ex} is the effective exhaust velocity. Also, if the rocket always moves at $V \simeq V_{ex}$, then the exhaust stands still (ignoring thermal energy) so that the driver energy is used very efficiently. This suggests letting the exhaust velocity change so that $C_s = aV$. We are assuming that the exhaust at a given time does not heat up the exhaust from earlier times. This ideal condition could be obtained by pulsing the laser. In this case the equation

of motion becomes

$$\frac{dV}{V} = -2a\frac{dm}{m} \quad , \tag{10}$$

or, integrating Eq. (10), we obtain

$$V = V_o\left(\frac{m_o}{m}\right)^{2a} \quad . \tag{11}$$

The acceleration efficiency with variable exhaust velocity is

$$\eta_v \equiv \frac{m_f V_f^2/2}{m_o V_o^2/2 + \int_0^{t_f} I\, dt} \quad . \tag{12}$$

This gives for $a \neq \frac{1}{4}$, (13)

$$\eta_v = \frac{1}{[(V_o/V_f)^{(4a-1)/2a} + (10a^2/f_R(4a-1))(1-(V_o/V_f)^{(4a-1)/2a})]},$$

and for $a = \frac{1}{4}$,

$$\eta_v = \frac{1}{1 + \frac{5}{4}\,\ell n(V_f/V_o)/f_R} \quad . \tag{14}$$

The first term in the demonimator of Eq. (13) is just the ratio of the initial kinetic energy of the BB to the final kinetic energy. For a = 1/4, the BB kinetic energy is constant during the motion. For the interesting case of $V_f \simeq 10V_o$, we get η_v = 12% (a = 1/4)--not much of an improvement. However, for a = 1/2 ($V = V_{ex}$), we get η_v = 17%, a 60% improvement over the constant intensity case.

5. PROBLEMS

We have shown that an accelerated solid BB can be produced with efficiencies in the neighborhood of 15%. This

estimate can be improved by chosing a material with a lower Z than glass (to reduce radiation). The problems which need to be investigated to obtain such an accelerator are:

1. Rayleigh-Taylor instability--The ablation interface is unstable to the Rayleigh-Taylor instability. However, we keep the ablation pressure below the yield strength, which should reduce the growth rate of this instability. The Rayleigh-Taylor instability of a solid interface needs to be investigated.
2. Stability of the BB in the laser beam--A laser beam profile which is lower in the center of the beam could be used to stabilize the BB in the laser beam. Small steering lasers would also be used to help keep the BB in the laser beam.

* Work performed under the auspices of the U. S. Department of Energy by the Lawrence Livermore Laboratory under contract W-7405-ENG-48 and partially supported by Lawrence Livermore Laboratory under Intramural Order 2435809.

REFERENCES

1. J. G. Linhart, Nuclear Fusion 10, 211 (1970).
2. T. E. McCann and J. S. DeGroot, "Acceleration of Solid Macro-Particles by Laser Produced Ablation", UCRL-79732 (1977); T. E. McCann, "Acceleration of Solid Macro-Particles by Laser Produced Ablation", Ph.D. dissertation (unpublished) (1978).
3. G. A. Askar'yan and E. M. Moroy, JETP Letter 16, 1638 (1962).
4. R. S. Cooper, AIAA Jour. 11, 831 (1973).
5. F. V. Burkin and A. M. Prokhorov, Sov. Phys. Usp. 19, 261 (1976).
6. F. S. Felber, General Atomic Co. Report GA-A14781 (1977).
7. John F. Asmus, IEEE Jour. Quantum Elec. 3, 265 (1967).
8. G. A. Askar'yan, M. S. Rabinovich, M. M. Savehcnko, V. K. Stepanov and V. B. Studenov, Soviet Phys. JETP 28, 208 (1967).
9. Ralph W. Woniek and Paul J. Jarmuy, App. Phys. Let. 12, 52 (1968).
10. A. N. Pirri, M. J. Monsler and P. E. Nebolsine, AIAA Journal 12, 1254 (1974).
11. P. T. Rumsby, M. M. Michaelis and M. Burgess, Optics Communications 15, 422 (1975).
12. O. M. Krokhin, in Physics of High Energy Density, Edited by P. Caldirola and H. Knoepfel, Academic Press, New York (1971), pg. 275.
13. F. S. Felber, Phys. Rev. Letters 39, 84 (1977).

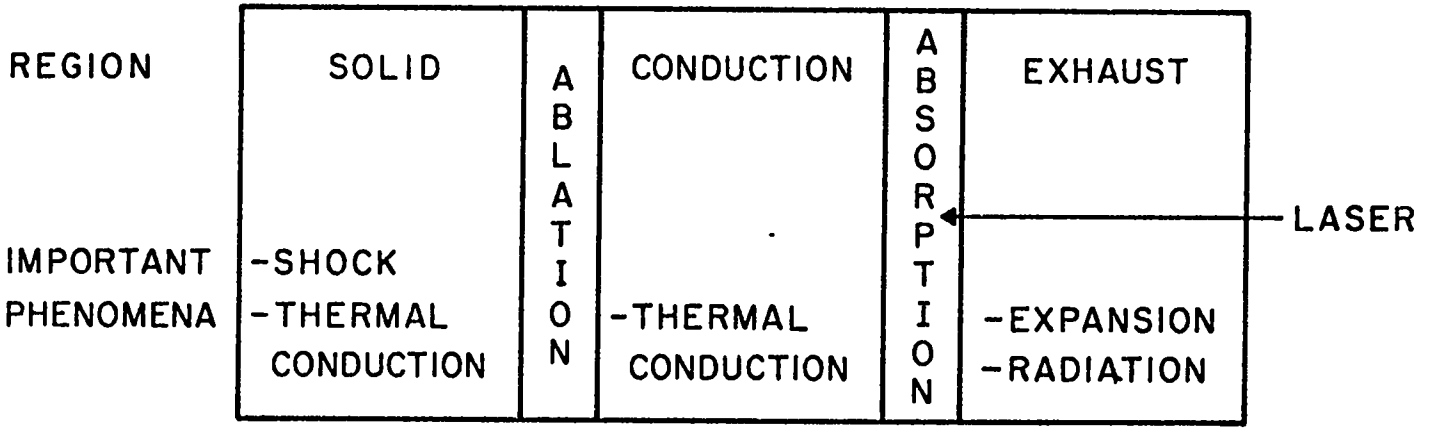

Fig. 1 The regions of the BB and the plasma plume and the important physical processes that occur in each region are shown.

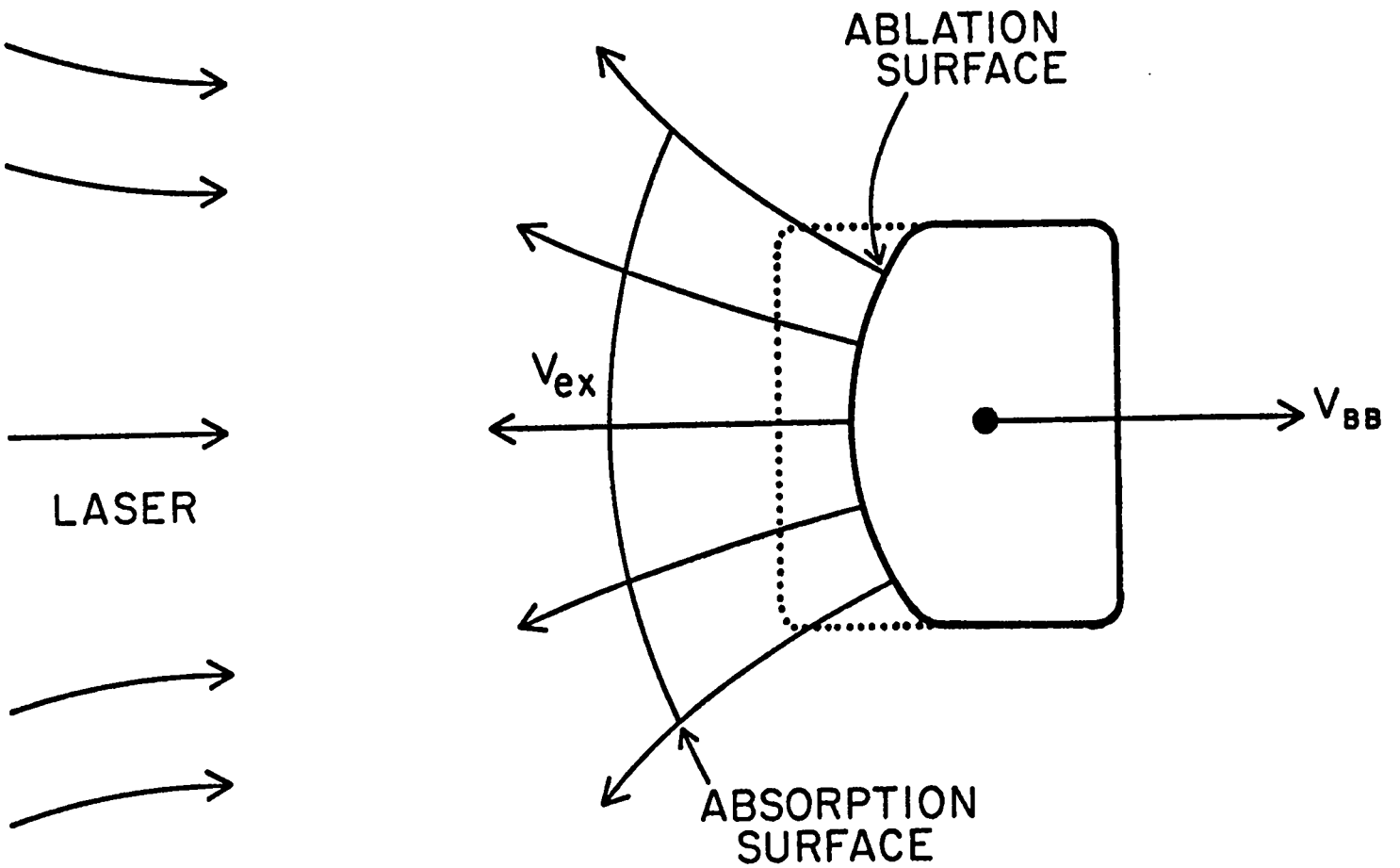

Fig. 2 Schematic of the quasi-steady state acceleration of a BB.

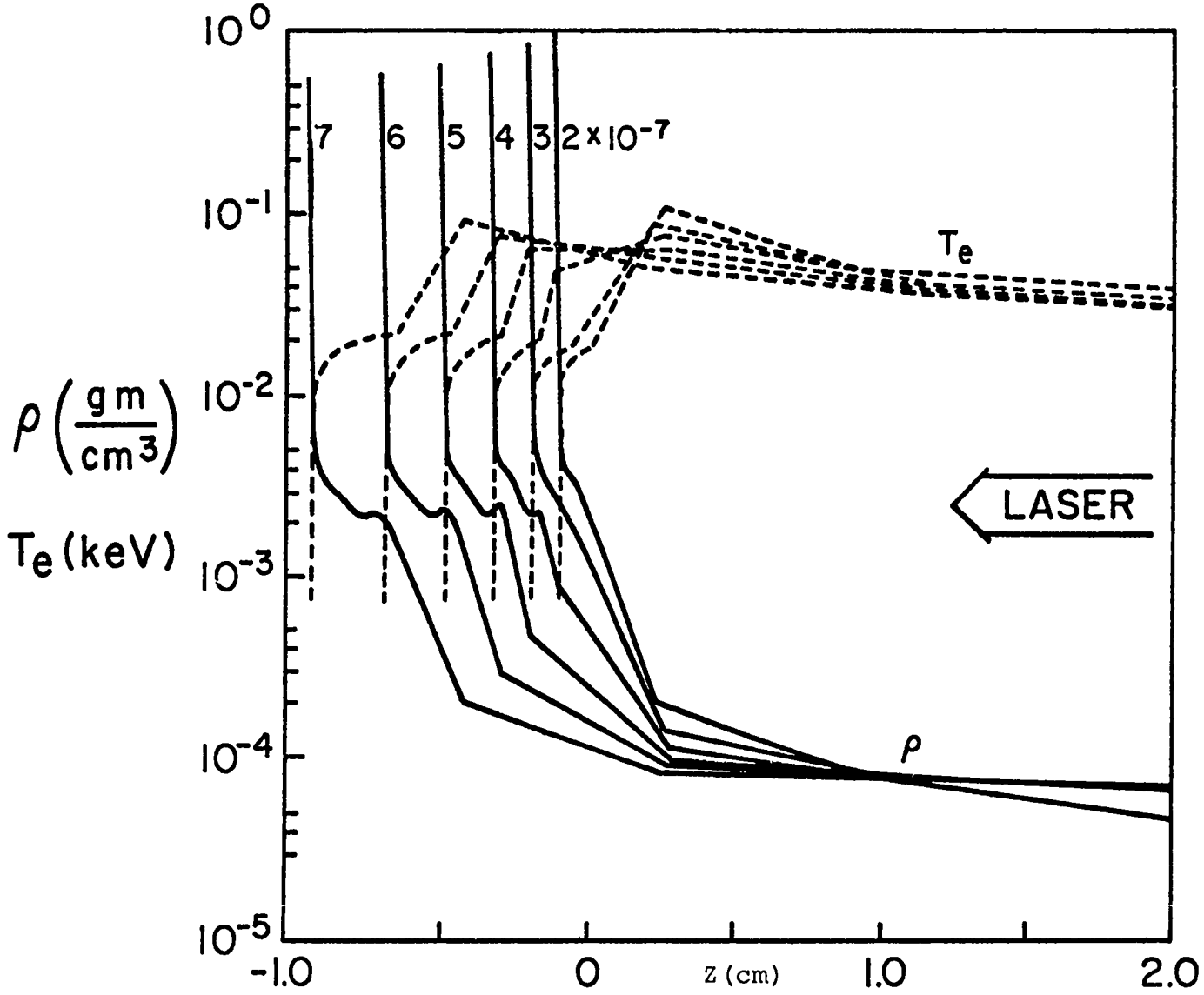

Fig. 3 Spatial profiles of electron temperature and plasma density at times of t = 0.2, 0.3, 0.4, 0.5, 0.6, and 0.7 μsec after the laser is switched on. Results from a 1-D calculation with I = 4 x 10^{10} W/cm^2, laser wavelength, λ = 5 μ, and a glass (SiO_2) BB.

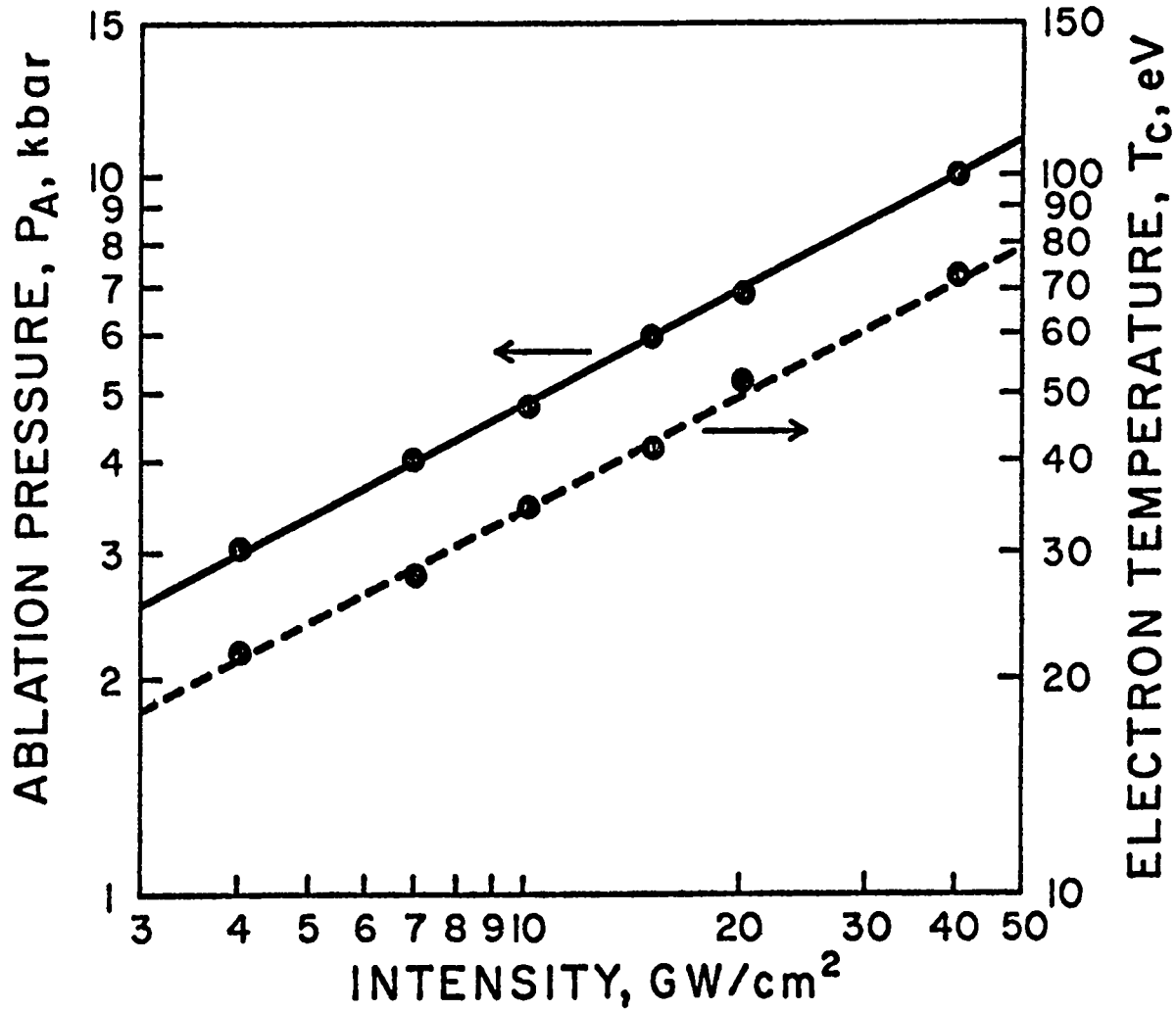

Fig 4 Ablation pressure and electron temperature at the absorption surface as a function of laser intensity. The laser wavelength, $\lambda = 5\mu$. The solid circles are time (0.5 μsec) averaged results from the 1-D calculations.

MASS ACCELERATOR FOR PRODUCING HYPER-VELOCITY PROJECTILES USING A SERIES OF IMPLODED ANNULAR DISCHARGES

Derek A. Tidman and Shyke A. Goldstein

JAYCOR Tech Note 350-79-004

May 1979

The implosion dynamics of self pinched annular discharges is a subject that has been well studied in the context of such devices as the plasma focus[1], or dynamically imploded annular foils[2] or gas puffs for radiation sources. In this note we briefly describe a mass accelerator system in which a series of axially aligned z-pinched annular discharges[3] are imploded sequentially on to the surface of a suitably tapered projectile. The system appears capable of accelerating projectiles of mass ranging from grams to kilograms up to velocities well above 10^6 cm/sec and possibly as high as 10^7 cm/sec. It also has good projectile survival and stability properties, and the attainable accelerations appear to be limited principally by the requirement that the projectile should not undergo material damage such as crushing or spalling.

The basic accelerator module is shown in Figure 1. It consists of an anode and cathode which for example could be discs with a hole at the center of sufficient radius to allow passage of the projectile. At a suitable time interval before arrival of the projectile in the anode-cathode gap from the left in Figure 1, a high voltage pulse is switched on across the electrodes which is sufficient to initiate a discharge through flashover in the low density gas along the inner surface of the insulator which separates the electrodes. This high current annular discharge is then driven by its azimuthal magnetic field radially inward away from the insulator surface and accelerates towards the axis of the module. As the discharge advances radially inward, it accumulates more plasma by sweeping up some of the background gas via the snow plow effect, so that the mass and density of gas colliding with the projectile surface depends on the initial background gas pressure (for example a few torr). The inner edge of the insulator between the anode and cathode could also be slightly tapered as shown, so that the

imploding annular plasma becomes itself more tapered during its implosion so as to match the projectile surface, although this tapering is not necessary and the insulator could also be a simple straight cylindrical section separating the anode and cathode. The discharge is timed so that it collides with the projectile surface when its front edge is approximately aligned with the cathode.

The projectiles could be constructed out of various materials. For cases in which high currents are used, it is important to minimize heating inside the projectile (if they are conducting) which can arise from eddy currents in its outer layers due to penetration of the surface magnetic fields through the discharge plasma into the solid projectile, since this would cause premature melting of the projectile before a high velocity had been reached. This problem is alleviated for metalic projectiles by arranging that the plasma pressure on the projectile derive mainly from the implosion momentum of the discharge so that the magnetic fields remain small at the inner plasma edge during impact with the projectile surface. This problem of eddy current heating can also be solved for cases in which lower accelerations (weaker projectiles) are acceptable by constructing the projectile of insulator material. In this situation, current is then able to flow only through the surface plasma layer pinched against the projectile, so that Joule dissipation is zero inside the projectile except for the thin-conducting skin layer that has been converted to plasma at its outer edge. This plasma layer advances into the projectile relatively slowly via thermal conduction and ablation during the acceleration, i.e., more slowly than would be the case for the more deeply penetrating skin current layer that occurs for metalic projectiles in devices in which magnetic fields provide the primary propulsion instead of plasma momentum and pressure as in this device.

The implosion velocity of the annular discharge as it approaches the projectile surface must be at least about twice as large as the projectile velocity. Under these circumstances the timing can be arranged so that contact is not made between the discharge and any part of the tapered projectile prior to arrival of the projectile in the gap, and further, the discharge can be timed to collide with the projectile surface before the projectile has had time to move ahead of the electrode gap. We also note that the implosion time

$$\tau_{impl} = \int_{r_m}^{R} \frac{dr}{V_r(r)} , \qquad (1)$$

for the plasma to implode radially from the insulator surface to the projectile surface, can be larger than the transit time of approximately ℓ/U taken for the projectile to cross the electrode gap, i.e., the condition

$$\tau_{impl} > \frac{\ell}{U} \qquad (2)$$

can be satisfied where U is the projectile velocity, and $V_r(r)$ is the inwardly directed radial velocity of the annular discharge as a function of radial position r, R is the mid-point radius of the insulator surface, r_m the radius of the projectile at a point located at a distance $\ell/2$ back from the leading edge of the tapered section of the projectile, and ℓ the axial length of the discharge as shown in Figure 1. For cases in which this condition is satisfied some power multiplication can be obtained in that the driving voltage and current can be applied so that the discharge plasma accumulates implosion momentum for a time longer than the characteristic encounter time ℓ/U which is available to communicate this accumulated momemtum to the projectile. It is also important that the gas density in which the discharge is initiated be

sufficiently low that the final implosion velocity exceeds the projectile velocity, while at the same time sufficiently high for the implosion radius involved that the discharge momentum provides a high surface pressure on impact with the projectile.

The generator voltage pulse, V(t), which is used to drive the discharge is related to the current, I, which flows through the discharge by

$$V = \frac{d}{dt}(LI) + IR \tag{3}$$

and

$$L = L_p + L_g,\ R = R_p + R_g \ , \tag{4}$$

where the lumped circuit inductance L and resistance R are made up of contributions from the system consisting of electrode modules containing the discharge plus the projectile, L_p and R_p, together with external contributions L_g and R_g associated with the electrical generator system. Solution of these equations involves solving hydrodynamic equations for magnetically imploded plasma shells and is a well studied subject. For a simple model see reference 2.

As an example, consider a module for which the circuit current rise time, L/R, is longer than the generator electrical pulse time, and the time dependent discharge inductance L_p is slightly less than the generator inductance, so that a rough average value will be assumed for L. The current thus rises approximately as I = Vt/L for an applied square wave voltage. If the discharge implosion time is 15 μsec and L≈30 nanohenries, a voltage of 2 kilovolts would give a final current of about 10^6 amps. Assuming an overall efficiency of 10%, the projectile would gain an energy of approximately 1.5 kilojoules in traversing this module.

Figure 2 shows a mass accelerator consisting of a series of axially aligned discharge modules. The voltages of each module are typically kilovolts to several tens of kilovolts depending on the application. As the projectile is propelled forward from one anode-cathode gap into the next module, a sensing device (for example the interruption of a light beam) is used to determine when to trigger the next diode modules. This is timed so that the next discharge arrives at the projectile surface when it is appropriately positioned in the anode-cathode gap for further acceleration, and the sequence is repeated as the projectile advances axially along the accelerator. In the second arrangement shown in Figure 3, the polarity of the electrodes is reversed (for high voltage packing reasons) in adjacent modules so that the surface plasma of the projectile experiences a reversal of the magnetic field and discharge current. Note that for devices that take full advantage of the power compression that results if the radius to the inner edge of the insulator is much larger than the projectile radius, several discharges ahead of the projectile could be initiated and be in different stages of implosion.

As an example of the approximate scaling involved, assume that the projectile has a mass of M grams and is accelerated up to a velocity of U cm/sec with an average acceleration of g cm/sec^2. The average total power in the electrical energy pulse that is required to generate this acceleration is then

$$P = nP_{mod} = 10^{-7}\ MUg/\varepsilon \text{ watts}, \qquad (5)$$

where ε is the efficiency with which electrical energy is transferred from the electrical storage system to projectile kinetic energy. In this formula

we distinguish between P and the power P_{mod} of each module, where n is the average number of discharge modules that are operating at any one time with their plasmas in various stages of implosion timed to impact the projectile surface as it passes through. This power would produce a projectile with kinetic energy

$$W = 5.10^4 M \left(\frac{U}{10^6}\right)^2 \text{ Joules} \qquad (6)$$

if applied for an acceleration length $L = U^2/2g$.

For example, assuming $g = 5.10^8$ cm/sec^2, $\varepsilon = 10^{-1}$, $U = 3.10^6$ cm/sec gives for the final maximum power $P_{mod} = 1.5.10^9$ M/n watts per module, and a projectile energy of $4.5\ 10^5$ M Joules acquired in an accelerator length of 100 meters. It will be obvious to the reader that a wide range of accelerator sizes will be involved depending on the projectile mass, acceleration, and the application for which the device is built. Note also that if the total mass of low density gas in the accelerator is about the same as the projectile mass, then the projectile can be accelerated up to a velocity comparable with the plasma implosion speed (see caption to Figure 2).

Various tapered projectile shapes (see Figure 4) can be chosen subject to the requirements that a forward force results when the discharge implodes against its surface, and that a stable progression of the projectile occurs as it advances from module to module along the accelerator. For example, a tail section could be added to the apex end of a conical projectile to ensure that the pinched discharge is provided with a hard core so that kink instability cannot occur as the main tapered section advances into the next electrode gap. Such a tail section, or hollowing of the projectile nose, also serves to move the center of mass of the projectile back behind the center of action of the

propelling force which is necessary for the mechanical stability of the projectile. Small thick fins or grooves in the trailing section might also be used to give the projectile spin.

Finally, we note that the plasma discharge which propels the projectile can be initiated in various ways, such as in low density background gas between an anode and cathode, or in low density gas along the surface of an insulator between the electrodes as shown in Figure 1, from which radius it is imploded radially inward against the projectile surface by its self-magnetic field. Alternatively, for some materials sufficient gas can be expected to continually ablate from the projectile surface during the time it takes to advance from a given driving discharge module into the next module electrode gap to initiate the discharge in each module, and in this case the arrival of the projectile in the gap may itself be utilized as the switch that triggers the discharge. In this case an injected gas puff could be injected into the first module to get the sequence of discharges started and a plurality of sharpened needle electron emitters could be distributed azimuthally around the inner edge of the cathode to ensure an azimuthally uniform discharge. However, the particular implosion approach we have emphasized here has the advantage of power compression over these others.

The results of more detailed analysis of the components of this scheme will be reported later.

References:

1. Principles of Plasma Physics, N. A. Krall and A. W. Trivelpiece, McGraww-Hill, 1973.

2. Coupling of Imploding-Plasma Loads to High-Power Generators, David Mosher, Naval Research Laboratory Memorandum Report 3687, January 1978.

3. Diode-Driven Mass Accelerators, Proposal submitted to DOE, March 1979. This proposal contains a description of the multiple z-pinch module concept (without the discharge initiation details given here), together with an e-beam ablator system, for their potential application to impact fusion.

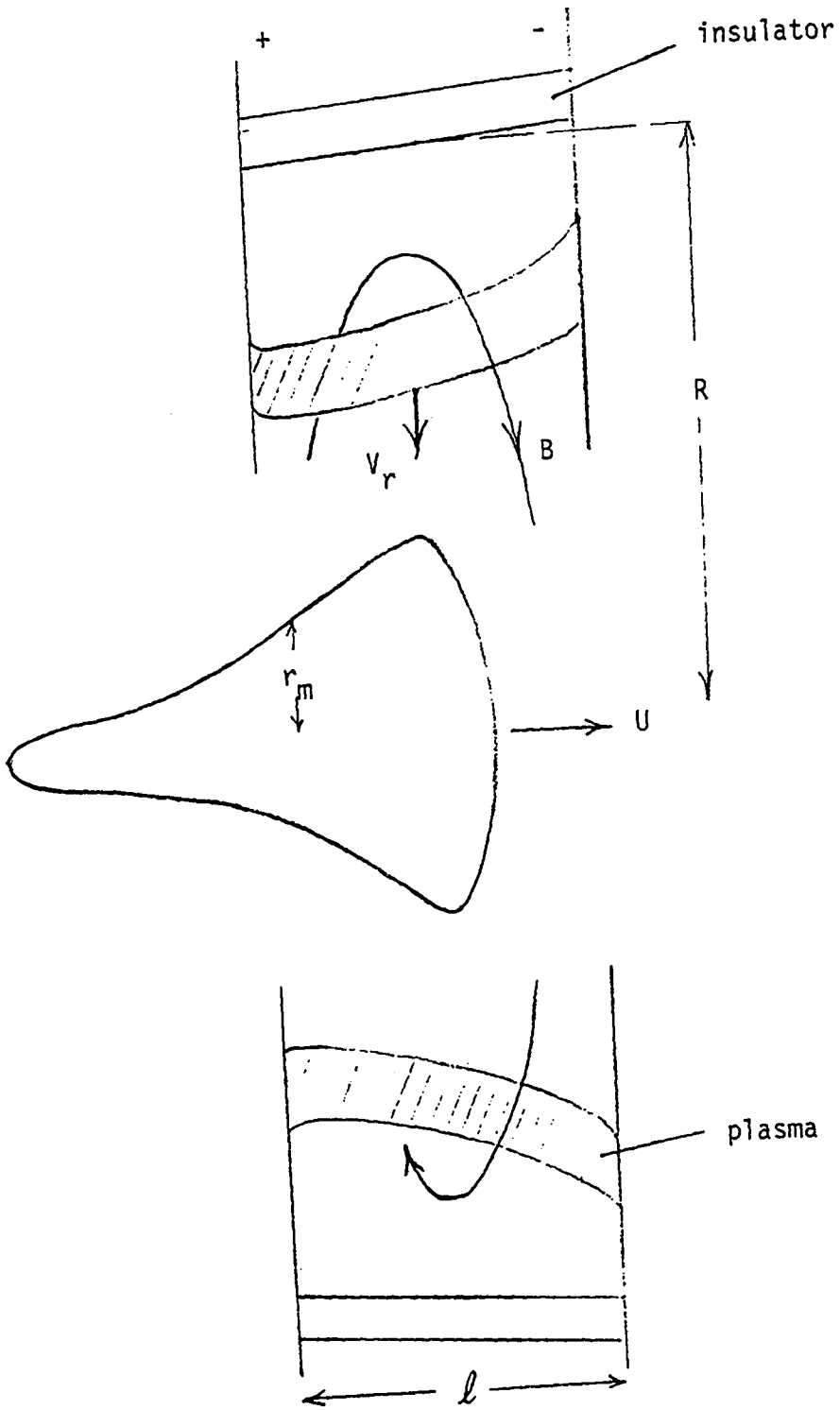

Figure 1

Annular discharge module with a driving voltage in the few-to-tens of kilovolts range. Power compression occurs when the plasma implosion time is longer than the projectile transit time through the module.

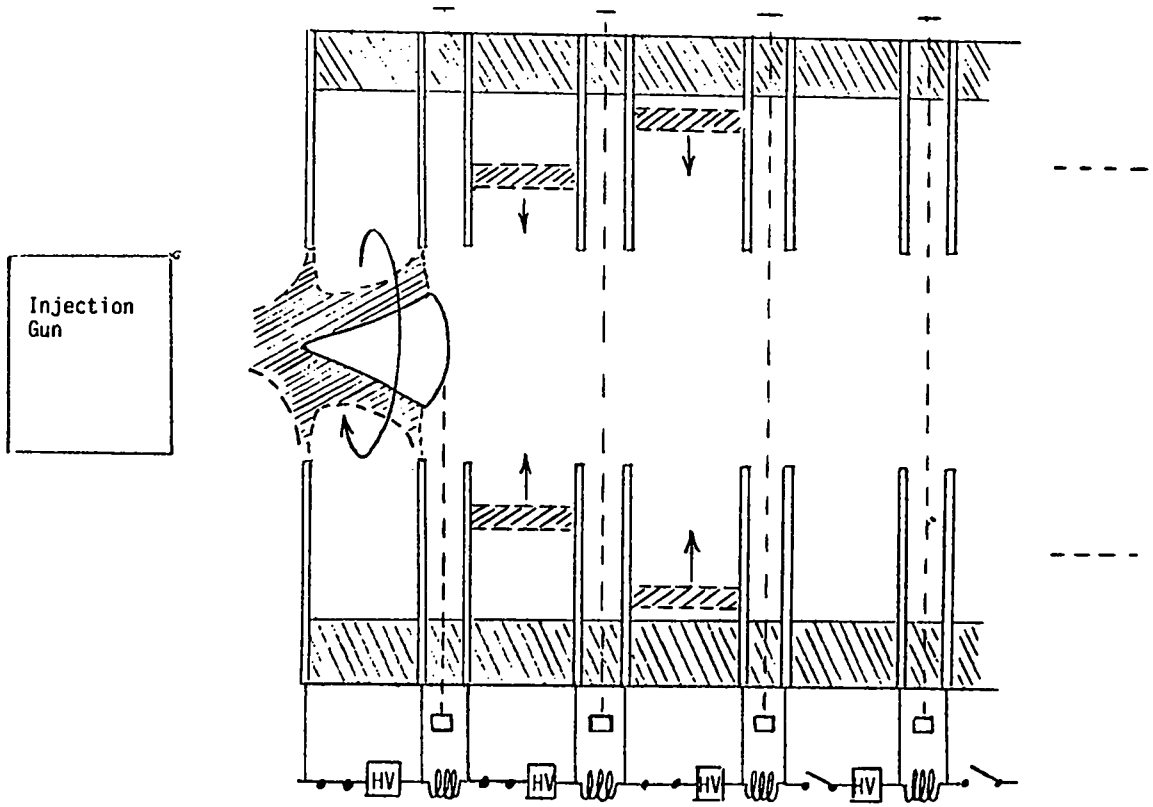

Figure 2

Multiple module accelerator in which the projectile is subjected to a series of imploding pinched plasma shells. Assuming a fraction α of the gas mass m_g is swept up and imploded with a velocity V_r against a projectile of cone half angle θ and mass M, a simple momentum conservation view gives $U \sim m_g V_r \alpha \sin 2\theta / M$ for the final projectile velocity. The initial gas pressure could be in the 1 to 10 torr range.

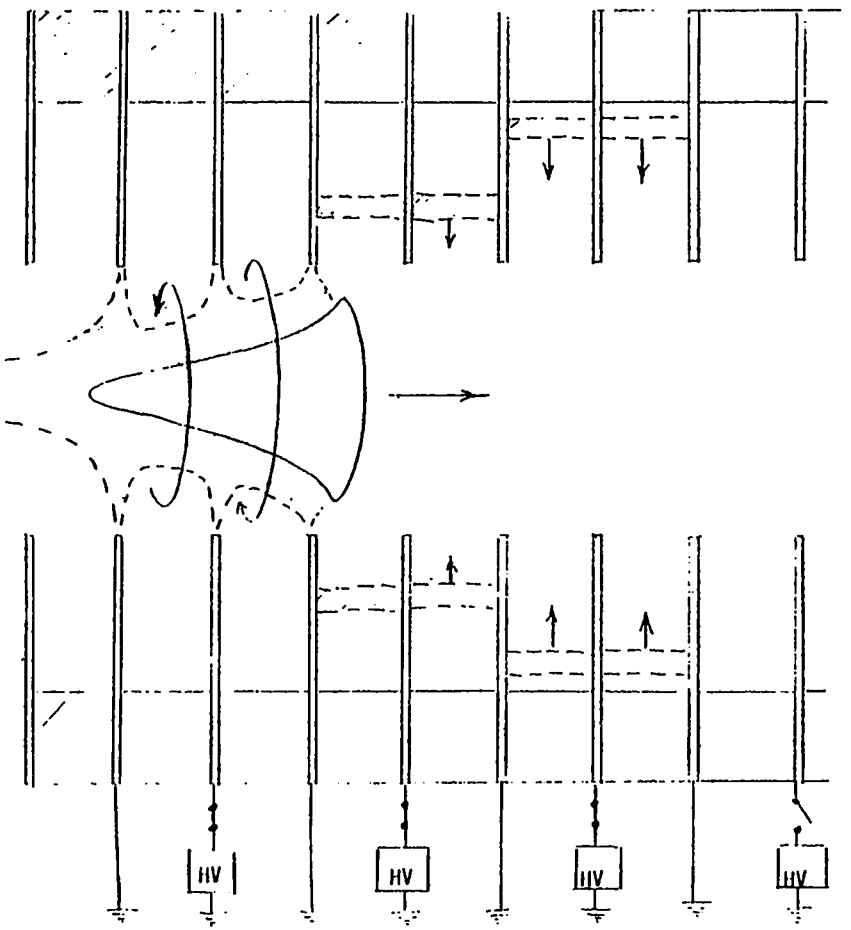

Figure 3

Example of a closer module packing for which the implosions are fired in pairs and the projectile length is at least two electrode gap lengths.

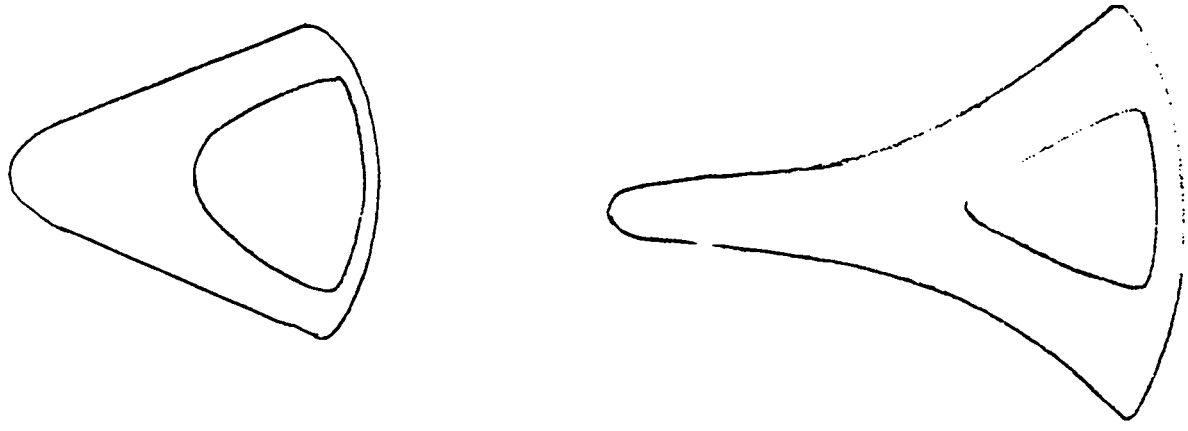

Figure 4

Projectiles of either metal or insulator with nose cavities which serve to move the center of mass back behind the center of thrust in the accelerator. for stability. Small thick oblique tail fins or grooves could also be used to spin the projectile if needed.

MAGNETIC LINEAR ACCELERATOR (MAGLAC) AS DRIVER FOR IMPACT FUSION (IF)

K. W. CHEN†

Michigan State University
East Lansing, Michigan 48824

ABSTRACT

This paper presents considerations on the design of a magnetic linear accelerator suitable as driver for impact fusion. We argue that the proposed approach offers an attractive option to accelerate macroscopic matter to centiluminal velocity suitable to fusion applications. Design and practical engineering considerations are treated. Future work are outlined.

I INTRODUCTION

We advance here a concept and a design of another promising driver which provides a simple match to the inertial target. The ignition is caused by a macroscopic particle (0.1 - 1.0 g) travelling at hypervelocity (sub-relativistic) speeds ($\leq 10^6$ m/s). We shall call this method of fusion by the generic name Impact Fusion (IF), and the driver, Magnetic Linear Accelerator (MAGLAC).

The impact of a fast moving object onto dense matter causes a shock wave accompanied by a severe rise in pressure and temperature. The high pressure, that lasts for a short period of time ($\sim$ 10 ns), is analogous to the high pressure that exists in the core of celestial bodies, where thermonuclear burn is the primary energy source.

This well known process of achieving controlled fusion through direct impact of a projectile has considerable advantages. One of the advantages of this inertial confinement scheme, apart from being of modest cost, is the very simplicity of ignition processes. During impact, a large amount of momentum is delivered onto the target, without a plethora of esoteric processes in which kinetic energy is converted to momentum.

---

†Other MAGLAC Group members include: B. L. Dougherty, M. Ghods, R. W. Hartung, J. G. Lee, E. S. Lehman, S. D. Mahanti, G. H. Plamp, J. E. Siebert and E. R. Salberta

The basic processes leading to compression are governed by classical hydrodynamics. The fusion target design should then be relatively simple, removing the need for classified complex target designs. Simplicity is also gained in reactor vessel design as its pressure can be maintained at high level. There are no space charge forces which usually limit the high intensities required in e-beam or ion-beam drivers. Since no focussing is required for the hypervelocity projectile, the coupling between the accelerator and the reactor chamber can be isolated except for a small hole (a few mm) for projectile entry. Thus the subsequent shock waves generated by the microexplosion are not expected to cause extensive pertubation to the alignment of accelerator elements. As we shall show in the following, the projectile will be only a few mm in length and diameter. The required input power, 10^{14} W, can be achieved by accelerating the projectile to over 10^5 m/s.

II ACCELERATION OF MACROSCOPIC OBJECTS

The magnetic linear accelerator is the only viable method to accelerate a macroscopic dipole to hypervelocities. Previously methods for accelerating macroscopic projetiles have been proposed or tried. These methods include light gas gun ($< 10^3$ m/s), electrostatic accelerator ($< 10^4$ m/s) and magnetic acceleration of conductive projectiles by a magnetic travelling wave. In the latter scheme, large eddy currents are induced in a highly conductive projectile, conceivably shaped as a torus, thus forming a magnetic moment. The rapidly changing magnetic field of the travelling wave accelerated the magnetic moment along the principal axis. It is shown however that the generation of eddy current will be accomodated by a disastrous joule heating which eventually will evaporate the conductor in flight.

Magnetic acceleration of ferromagnets or ferrites remains a possibly viable scheme. However, as we shall show below it is more difficult to accelerate the projectiles to the required velocity due to the relatively low saturation field strengths of the ferromagnetic materials. A simple approach to avoid the heating problem is the use of superconducting projectiles. A large intrinsic magnetic moment can be acquired by a superconducting solenoid and thereby accelerated by a travelling wave[1,2] Such a device can be shown to have a stable longitudinal acceleration, but it suffers from transverse instabilities which could destroy

the trajectory of the projectile due to inevitable transverse drifts during the injection cycle.

Our proposal[3] here is to accelerate a superconducting solenoid or a multiple film cylinder by a scheme similar to magnetic levitation[4]. In our case the transverse stability is guaranteed while the longitudinal stability is feedback controlled by tracking of the projectile during the acceleration process. We have performed a numerical analysis of our model accelerator based on a realistic mode of operation. We demonstrate trajectory stability in all directions and an acceleration in excess of 10^5 times gravity. An accelerator based on our design will be approximately 1-2 km in length. (See Figure 1), providing a 0.1 g projectile in excess of 1 MJ at the end of our accelerator. We also show the design of the accelerator element, the superconducting solenoid projectile and engineering factors in a realistic construction of the device.

III THE MAGNETIC LINEAR ACCELERATOR (MAGLAC)

To approach the problems of actual accelerator design it's useful to review magnetic levitation. Suppose we want to keep a dipole μ, on the axis of a circular current loop. Let the loop have radius a and carry current I. Let z be the vertical coordinate with z = 0 in the plane of the loop. We use a scalar potential

$$\phi = \frac{\mu_0 I z}{\sqrt{a^2+z^2}} . \tag{3.1}$$

If the dipole is on the z axis with μ vertical, it feels a force

$$F_z = -\mu \frac{\partial B_z}{\partial z} = \mu \frac{\partial^2 \phi}{\partial z^2} = \frac{3\mu \mu_0 I a^2 z}{\sqrt{a^2 + z^2}^5} \tag{3.2}$$

The first requirement for levitation is to balance gravity. If the dipole mass is m,

$$F_z + mg = 0 \tag{3.3}$$

The second requirement for levitation is stability: if the dipole wanders away from the equilibrium point, there must be a force to push it back. Consider first vertical stability. There are two regions of vertical stability: $a/2 < z < 0$, and $z > a/2$. The force itself has opposite sign in the two regions; they are qualitatively different. For example, a superconductor levitated by Meissner effect ("flux exculsion") would be vertically stable for $z > a/2$; an iron

object levitated by induced ferromagnetism would be vertically stable at $-a/2 < z < 0$.

But radial stability is also required. In any region not enclosing currents, ϕ must satisfy Laplace's equation. In cylindrical coordinates ($r^2 = x^2 + y^2$)

$$\frac{\partial \phi}{\partial r} + r\left(\frac{\partial^2 \phi}{\partial r^2} + \frac{\partial^2 \phi}{\partial z^2}\right) = 0. \tag{3.4}$$

Then at $r = 0$, $\frac{\partial \phi}{\partial r} = 0$, and by symmetry

$$\frac{\partial^2 \phi}{\partial r^2} = \frac{\partial^2 \phi}{\partial x^2} = -\frac{1}{2}\frac{\partial^2 \phi}{\partial z^2} \tag{3.5}$$

Then, if μ is directed along z.

$$\frac{\partial F_r}{\partial r} = \frac{\mu\, \partial^3 \phi}{\partial r^2 \partial z} = -\frac{\mu}{2}\frac{\partial^3 \phi}{\partial z^3} = -\frac{1}{2}\frac{\partial F_z}{\partial z}\,. \tag{3.6}$$

The negative sign means radial and vertical stability are mutually exclusive. This is a special case of Earnshaw's theorem. Thus magnetic levitation can be stable either radially or vertically, never both at once. The usual choice is to select radial stability and get vertical stability by feedback from a sensor.

IV ACCELERATOR STRUCTURE (R. Hartung)

By the principle of equivalence, a levitation scheme is an accelerator. But it's not yet useful; the current loop must move with the dipole. No acceleration persists unless we provide a way to accelerate the current loop. If we switch current from loop to loop, we can simulate a loop moving in an arbitrary manner.

For this initial evaluation, we neglect (a) resistance, R, of the loop, (b) reaction from the accelerated object, (c) radiative effects, including "retardation), and (d) mutual inductance between the loops. To avoid having to switch large currents, we drive each loop from a capacitor C, through a diode and a switch. When the switch is turned on, the LC circuit executes ½ period of an oscillation before being quenched by the diode.

In a loop turned on at $t - t_o$, the current is

$$I = 0, \qquad t < t_o \text{ and } t > t_o + \pi\sqrt{CL}$$

$$I = I_{max} \sin \frac{t - t_o}{\sqrt{CL}}, \quad t_o < t < t_o + \pi\sqrt{CL} \tag{4.1}$$

Here C is the capacitance, L is the self inductance of the loop, and the maximum current, $I_{max} = V_o \sqrt{C/L}$, depends on the initial voltage, V_o. Before presenting results of simulation of this model, we discuss some qualitative features. The dipole tends to line up so as to be sucked into the region of highest field. The opposite case, using Meissner effect, is not considered here.

Then the radial motion will be stable, if and only if the dipole is farther than -a/2 behind the peak current. Then z stability (longitudinal) must come from feedback, i.e. the switching on of the current loops must be synchronized with the dipole motion. We assume that an arbitrary trigger function of position and velocity is possible. As a first order proof-of-principle, a crude model has been simulated by numerically integration of a hypothetical accelerator. The simulation parameters are given in Table I. The trigger scheme used was as follows: The loop at position z_o is turned on when the solenoid position, z, and velocity, v, satisfy $z + v \cdot \pi \sqrt{LC} = z_o$. This trigger, which was picked arbitratily, is such that the extrapolated time when the solenoid will cross the plane of the loop, will be the end of the current cycle for that loop. Acceleration functions A_d, are shown in Figure 2a. The focussing function, k/m, of the accelerator is shown in Figure 2b. For $d \leq 1.0$ cm, k/m is always negative, thereby providing continuous radial focussing.

V PROJECTILE CONSIDERATIONS (E. Lehman, S. Mahanti)

For any projectile the equation describing magnetic acceleration is

$$\vec{F} = \vec{\nabla} \int \vec{M} \cdot \vec{B} \, dv \qquad (5.1)$$

where $\vec{M}$ is the magnetic dipole moment density and $\vec{B}$ is the external field, the integration is over the projectile volume. The magnetization is related to the internal current density $\vec{j}$ by $\vec{\nabla} \times \vec{M} = -\vec{j}$.

Requirements for the projectile choice include; (i) Interaction with the external field should be large enough to achieve velocities of about 10^5m/sec in a distance of a few km. (ii) Each projectile must have almost exactly the same behavior as every other projectile under the accelerating fields. (iii) A. C. fields are certain to be encountered by the projectile. The projectile must not have its moment destroyed by them. (iv) Other effects, such as collisional heating from residual gas in the accelerator or radiational heating, must not destroy the projectiles moment. (v) The projectile must be easy and cheap to build.

We now discuss different projectile choices. A piece of ferromagnetic material will be drawn into a magnetic field which is stronger than its satura-

tion moment density $\vec{M}_{sat}$ with a force,

$$F = \vec{\nabla}\int_v \vec{B}\cdot\vec{M}_{sat} \qquad (5.2)$$

In principle, there appears to be no limit to the acceleration possible. However, for iron the saturation moment corresponds to a field of about 2T. For an external field of 10T and a projectile radius of about 1mm it is found that a projectile energy of 10^6J will require about 10km. Increasing B would shorten this but is difficult.

The inevitable relative motion between the accelerating fields and the projectile will cause eddy currents in the projectile. Let the change of the magnetic field at the projectile be dB/dt, we can define dB/dt = ζvdB/dz. In the case of a radially constant magnetic field and a cylindrically symmetric projectile with velocity v the ohmic power is given by, (for resistivity ρ)

$$P_{ohm} = \zeta^2(dB/dz)^2V/8\rho \times r^2v^2 \qquad (5.3)$$

r is the projectile radius and V is its volume. This leads to a limiting velocity $v_f = 10^5$ m/sec. Even if v_1 the, limiting velocity, is equal to v_f, we find ζ is less than 10^{-2}. The total ohmic heat delivered is given by W_{ohm};

$$W_{ohm} = mv_f^2/2 \times 2/3\ v_f/v_1 \qquad (5.4)$$

For a final energy of 10^6J and $v_f/v_1 = 10^{-1}$, we find that an iron projectile will heat by about 10^4 ^{0}K! The temporal uniformity required at the projectile to avoid this, $\zeta<10^{-4}$, appears prohibitive. For ferrite projectiles ρ is much higher than for iron but the saturation moment density is at least ten times lower. This means that the accelerator would have to be much too long.

Another possible choice is a superconducting projectile. A type I superconductor excludes the applied magnetic field and thus has a magnetization density $\vec{M} = \mu_o\vec{B}$. However, critical fields of order 10^{-2}T rule out these materials.

A type II (hard) superconductor has a much higher critical field. However, the supercurrent density that can be carried is highly sample dependent. For example, if the sample has few lattice defects then only a small supercurrent can be carried in the presence of a large field H ($H_{c1} < H < H_{c2}$). The reason for this is that a type II superconductor is permeated by flux tubes each carrying a unit of flux Φ_o, a fluxon. The fluxons feel a Lorentz force j x Φ_o for current density j. This causes the fluxons to migrate and viscous resistance to their motion leads to losses. The flux migration is opposed by pinning forces P_v. In a defect free material P_v is very small so that small j's will cause losses. Defects greatly increase P_v and allow much greater supercurrents. In

order to overcome this one purposely makes the lattice poor. In spite of this the maximum j in a bulk sample is only about $10^9 amp/m^2$. This implies too small a magnetic moment for a 1 km accelerator. In addition, the actual magnetic moment will be strongly sample dependent which presents standardization problems.

Thin superconducting foils wound around a core and supporting a permanent dipole moment seem a promising choice of projectile. The superconducting foils will have very strong pinning forces and thus be able to sustain large supercurrents. Their A. C. properties will also be reasonably good. The A. C. fields will be shielded by the outer layer of superconductor. If ν is the frequency of the a.c. field, h its amplitude, P_v the pinning force and H the D. C. field, the power output of the outer layer is per unit area:

$$4\mu_o H h^3 \nu / 3P_v \ (W/m^2) \cdot \qquad (5.5)$$

We can estimate this by taking the D. C. field as 10T, the A. C. field as 0.1T and a pinning force corresponding to a maximum current density of 10^{10} amp/m^2. For a projectile flight time of 10^{-2} sec and $\nu = 10^4$Hz the projectile will heat by about 1^0K. We have made the assumption that the heat in the outer layer is dissapated rapidly in the projectile. Simple consideration based on a diffusion equation for heat flow into the projectile give a relaxation time for a temperature gradient across 1 mm of about 10^{-3} sec. The projectile gains little heat during this time so that it can be regarded in thermal equilibrium during its flight.

A foil projectile can be prepared by winding N layers of foil of thickness T and lenght 1 around a suitable core. The projectile is then placed in a magnetic field and cooled to below its transition temperature. The initial flux is trapped by setting up a magnetization current density j and the magnetic moment μ is given by;

$$\mu = j\pi R^2 N l T \left[1 + (NT/R) + 1/3\ (NT/R)^2\right] \qquad (5.6)$$

Recently large scale production of an Nb_3Sn foil was reported. T is 0.03 mm and experiments in trapping flux gave $j \simeq 10^9$ amp/m^2, limited by the 6T field of the magnetizing magnet.

If we assume that we can achieve current densities of 10^{10} amp/m^2, for N=30 (1mm of windings), R = 1mm and 1 = 3mm, we find μ = .64 amp·m. This should be suitable for a 1km. accelerator (1 is really not relevant as the magnetic field gradient is limited to $2B_c/l$ for B_c the critical field so that the energy gain is independent of 1). It appears that a foil wound projectile with a heat shield (see below) will provide a suitable choice of projectile.

Our final topic in this section is the heating the projectile undergoes

during flight. We have already discussed the effects from a.c. fields; two other sources of heating are absorption of radiation from the accelerator walls and inelastic collisions with the residual gas in the accelerator tube. To estimate the radiational heating we take the accelerator walls at a temperature T_a and the projectile at T = 0. For a projectile of surface area A energy is absorbed at a rate;

$$dE/dt = \frac{8\pi}{3} A\pi^4 h/15c^2 \quad (k_B T_a^4/h) \tag{5.8}$$

For our projectile with a specific heat of about $1 J/kg^{\circ}K$, we find a heating rate of 1 ^{0}K/sec with $T_a = 10^2$ ^{0}K. Radiational heating can thus be ignored for our flight time of 10^{-2} sec.

Collisional heating will be much more severe. If we assume that the air molecules are at rest relative to the projectile, that they have a density ρ and that the cross-sectional area of the projectile is A, we find a heating Q given by

$$Q = 1/8\ \rho A v_f^2 t \tag{5.9}$$

In the above v_f is the final projectile velocity and t is the transit time. We have also assumed perfectly inelastic collisions between the projectile and the gas. For $v_f = 10^5 m/sec$ and $t = 10^{-2}$ sec we find that a temperature rise of $10^{\circ}K$ occurs if ρ is as big as $10^{-14}\rho_{STP}$. This vacuum requirement seems impossible to meet, however, we can avoid it by using a heat shield (which can be molded with the core). With a heat shield we only need about $\rho = 10^{-8}\rho_{STP}$. We are confident, then, that the heating problem is tractable.

VI ACCELERATOR ENGINEERING FOR MAGLAC (G. Plamp)

A preliminary design of the MAGLAC enclosure has been made. Main feature include considerations in cooling vacuum chamber, cryogenic feed through and power delivery. Figure 4 shows a typical section ($\sim$ 1/100) of the accelerator. The power input calculations for this design has been made in Section VII. A cross section of the accelerator element is shown in Figure 5.

Most of the elements are commercially available. Since we expect to have large voltage between individual plates, considerable amount of care would be needed to construct these sections. We do not believe these designs are optimized as yet. Much work is still needed.

VII. POWER INPUT CONSIDERATIONS (B. Dougherty)

In order that the projectile support current desities over $j = 10^9$ A/m^2, and that dissipative losses be reduced in both the projectile and accelerator coils, cryogenic conditions must exist. To achieve this, cooled super (preferably inert) gas circulates around the coils and dielectrics in every accelerator section. Coaxial return lines (see cross-section) provide economical, uniform, additional cooling. Studies of comparable transmission lines[5] indicate that, with far-end expansion and return, one refrigeration/pumping station is adequate to maintain minimal temperature gain along the two kilometer accelerator. Also, three cooling lines, bored through the dielectric with regular disk-shaped adjoining spaces seem sufficient, resulting in a slight parabolic temperature rise ($\leq$ 1°K) near the center of the accelerator.

Heat loss via radiant transfer and gas convection is significantly reduced by using evacuated multi-layer insulation (such as aluminum coated mylar). Conduction through the accelerator sides is then on the same order as that lost through the metallic vacuum leads.

Ohmic heating within the cryogenic envelope is significant only in the electrical power terminators ending each section. Here, losses on the order of one percent of the diverted power, or around 10^4 watts, are encountered for the entire system.

Gas leaks and vibrations are negligible, as are the storage/supply requirements for the refrigerant. Altogether, total losses of nearly 1.5×10^4 Joules are expected for each pulse.

Cool down costs are harder to approximate, since it is difficult to predict the frequency with which this machine will require repair. Conservative estimates , however, indicate a crude value of around 10^{10} Joules necessary for every cool down, resulting in an equivalent operational loss of nearly 2×10^4 watts, comparable to cryogenic losses.

The refrigerant is gaseous helium at 6 - 10° K and 15 atmospheres feeding pressure. Higher temperatures jeopardize the projectile superconductivity, leading to possible disastrous heating due to increased resistivity.

As an additional benifit received when operating at low temperatures, material strength characteristics of the projectile and coils are altered enabling them to withstand the high outward magnetic pressure accompanying each current pulse. Also, temperatures below 77°K may improve the vacuum encountered in the flight path by transforming the two kilometer inner tube into an effective cold trap.

Vacuum loss itself is trivial, requiring only about 10^4 watts input for each one percent loss per minute along the entire length of the machine. Individual pumping stations at every accelerator section are used. Vacuum on the order of $< 10^{-8}$ Torr is expected.

Electrical input, on the other hand, is relatively large. Various spark-gap switches have quoted loss rates from 2 to 15 percent of the input power. Terminations for each LC accelerator section loose this same order of energy, provided a 90% recovery rate is maintained through use of storage capacitor banks. Other switches and recycling mechanisms are available, however, and it is expected that the full scale system will be appropriately engineered. Nevertheless, total losses of approximately 10^7 Joules per pulse may be realistic.

Other costs (true costs, converted through typical price estimates and present consumer markets) include downtime and repair. This, again, is hard to predict. However, downtimes from one hour to ten days at an average cost of 10^5 dollars, once a month, for switch repair of LC section replacement lend a total equivalent loss rate of around 5×10^4 watts operational cost.

Even harder to estimate is the projectile production and delivery costs. Assuming a conservative one percent efficiency and ten cents per pellet, we find an equivalent "loss" of nearly 5×10^4 watts. This is comparatively small, and represents double counting anyway, in that this cost is taken out of ultimate fusion delivery rates, and so will be ignored here for the sake of overall efficiency predictions.

All input sources and magnitudes are tabulated in Table II. It is evident that electrical losses constitute the majority of input, so much depends upon actual recovery rates and switch efficiency. Cryogenic and other losses are quite tolerable and sensitive, again, to operational frequency of repair. (We might note that by removing cryogenic needs, i.e. operating at room temperature, total power input remains about the same due to increased resistivities, but useful lifetimes of materials are dramatically reduced because of the accompanying heating.)

Assuming that 10^6 Joules of usable energy are got in every pulse, then, we find an overall efficiency of Q = 5 - 11%.

VIII. MAGLAC ACCELERATOR CONTROL AND POWER CONDITIONING

(J. E. Siebert)

Essential to the operation of MAGLAC is the maintenance of the dipole projectile within the transversely stable region of the propagating magnetic wave. This can be accomplished by achieving proximate longitudinal regulation through feedback-controlled sequential excitation of the accelerator sections. Hence, the dipole can be radially focussed to controllable degree along its trajectory. Clearly, optimization of the tradeoff between projectile acceleration and the strength of transverse focussing is necessary to minimize accelerator length for a given final velocity. The accelerator control system design must support the evolution and tuning of control strategies and accomodate system refinements.

Projectile arrival at discrete locations along the accelerator can be detected optically by fast PIN photodiode response to a laser light obscuration. These indications along with the elapsed time can serve as principle input parameters to a real-time numerical model. Since control actions need only occur at $\sim$ 100 μs intervals, implementation may take the form of a real-time computer-based controller. The attendant advantages of programmable control include the desired adaptability mentioned above along with the facilitation of development, implementation, operation, diagnosis, and maintenance.

As shown above, projectile acceleration will result from large $|dI/dt|$ on the pulse trailing edge. The required line excitation is then the delivery of a pulse of sufficient energy and fall-time to strongly accelerate the projectile. The scheme depicted in Figure 6 employs a capacitive store, a fast triggered switch(s), and a subsystem to recover the remaining wave energy at the end of that accelerator section. Alternative implementations of these subsystems are currently being explored. Especially interesting are the prospects of implementing the capacitive store in charged parallel-connected transmission lines whose lengths are half the desired pulse width, and employing fast opening switches recently reported[7;8] to achieve large dI/dt. The inefficiency of crowbar circuits prohibits their use here.

The capacitive store and switch combination must provide the following:

Pulse Voltage	:	25-75 kV
Peak Current	:	160-400 kA
$\|dI/dt\|$	:	$>10^{12}$ A/sec
Jitter	:	<10 nsec
Repetition Rate	:	1-3 pps
Pulse Energy	:	~10 kJ/pulse
Life	:	$>10^{8}$ pulses without maintenance

Of all the requirements, the component lifetime will be the most difficult to achieve. This requirement arises from reliability and practicality considerations for a useful fusion reactor.

IX. CONCLUSIONS AND RECOMMENDATIONS

Concepts and design parameters for a magnetic linear accelerator capable of accelerating a 0.1-1.0 gm superconducting projectile (multiple film layer or solenoid) to a velocity exceeding 10^5 m/s are presented. Such a device could conceivably serve as an ignitor for inertial confinement fusion. In contrast to other options for macroscopic particle acceleration, we propose a magnetic linac in which the longitudinal acceleration elements are individually controlled while transverse and rotational motions are inherently stable. This approach is an extension of the well-known method of magnetic levitation. Accelerator and projectile elements are described. Longitudinal and radial stability analysis indicate no obvious obstacles within the current technological state-of-the-art.

None of the considerations of this work indicate any intrinsic limitations. A superconducting linac certainly can be constructed with a modest cost.

We are now entering a situation in which some future substantive theoretical and experimental work should now be supported. These include, for example,

1. Further material research on superconductors under high magnetic field and high frequencies.
2. Theoretical and experimental designs of MAGLAC. Optimization of accelerator designs.
3. Construction of elementary section of MAGLAC.
4. Properties of projectile under traveling wave acceleration.
5. Engineering design of projectiles.
6. Projectile-target interactions.

Perhaps in the near future we could see generation of fusion power in this promising approach as shown in Figure 7.

REFERENCES

1. D. Anderson, S. Claflin, and F. Winterberg,"On the Acceleration of a Superconducting Macroparticle in a Magnetic Travelling Wave Accelerator, "Zeitschrift für Naturforschung 26a, 1415 (1971) and references therein.

2. R. Garwin, R.A. Muller and B. Richter (private communication).

3. K. W. Chen and E. Lehman, "Inducing Controlled Thermonuclear Fusion with a Macroparticle Accelerator" MSU-CSL-66, Sept. 1978 (unpublished); K.W. Chen, R.W. Hartung, E. Lehman, and S.D. Mahanti Proceedings of 1979 Particle Accelerator Conference, IEEE Transaction on Nuclear Science, p. 3318, March (1979).

4. The magnetic levitation idea has been used extensively in magnetic monopole search experiments. e.g. J. Beams, et at. J. Appl. Phys. 17, 886 (1946).

5. G.H. Morgan and J.E. Jense, "Counter-flow Cooling of a Transmission Line by Supercritical Helium", Cryogenics, 259, May 1977.

6. A.M. Baron, V.M. Eroshenko, and L.A. Yaskin, "Studies on Cooldown of Cryogenic Cables", Cryogenics, 161, March 1977.

7. C.W. Mendel, S.A. Goldstein and P.A. Miller, "The Plasma Erosion Switch," in Proc. IEEE Pulsed Power Conf., Nov., 1976.

8. R.O. Hunter, "Electron Beam Controlled Switching", in Proc. IEEE Pulsco Power Conf., Nov., 1976.

TABLE I. Typical Accelerator Parameters

a	radius of loop	0.01 m
d	separation	0.015, 0.01, & 0.004m (see graphs)
L	inductance of loop	10^{-8} H
C	capacitance per loop	0.7 μF
V_0	applied voltage	20 kV
$\tau = \sqrt{LC}$		84 ns
I_{max}	peak current	170 kA
v	initial velocity of dipole	1 km/s
m	mass of dipole	0.1 g
μ	moment of dipole	1 $A \cdot m^2$

TABLE II. Overall Input

Source (entire system)	Est.'d Magnitude (Joules/projectile)
Cryogenics	∿ 1% efficiency
Elec. heating	
capacitors	20
leads	50
noise	10
terminations	$\lesssim 10^4$
Heat transfer	
conduction	3×10^3
radiation	nil
convection	10
Miscellaneous	
cool down	$\sim 2 \times 10^4$ (equivalency)
absorption	nil
gas leaks	20
vibration	nil
refrigerant production & storage	nil
Vacuum	∿ 1% efficiency
Maintainence	$\lesssim 10^2$
Initial evacuation	nil
Electrical	$\gtrsim$ 80% efficiency
Switches	$\sim 5 \times 10^6$
Leads	$\sim 3 \times 10^3$
Terminations (90% recovery)	$\gtrsim 4 \times 10^6$
Other	$\sim 10^2$
Other	(equivalency)
Downtime	$\sim 4 \times 10^5$
Repair	$\gtrsim 5 \times 10^3$
Total input	$\sim (1.4 \pm 0.5) \times 10^7$ J

CONCEPT OF MAGNETIC ACCELERATOR

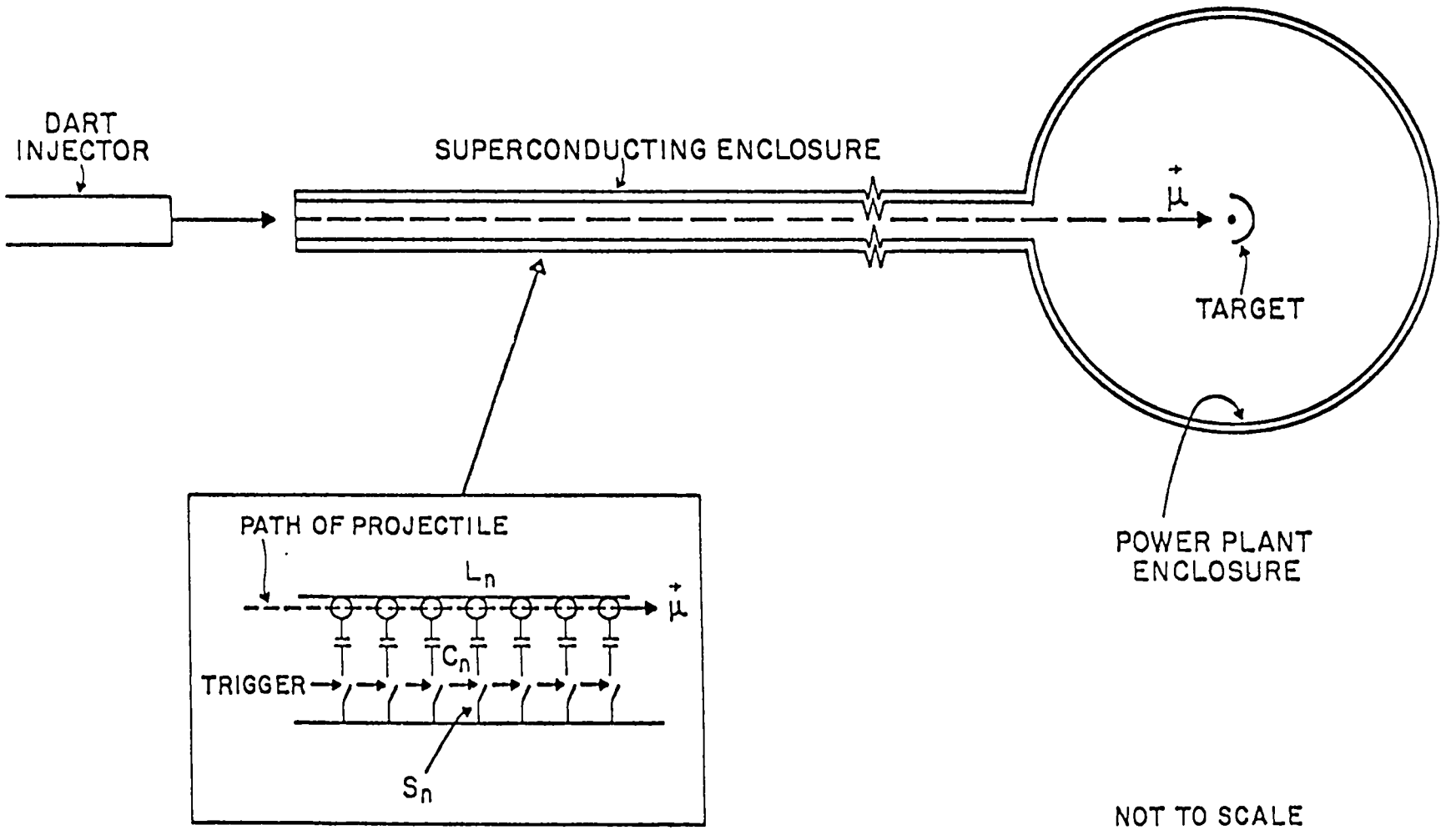

FIGURE 1.

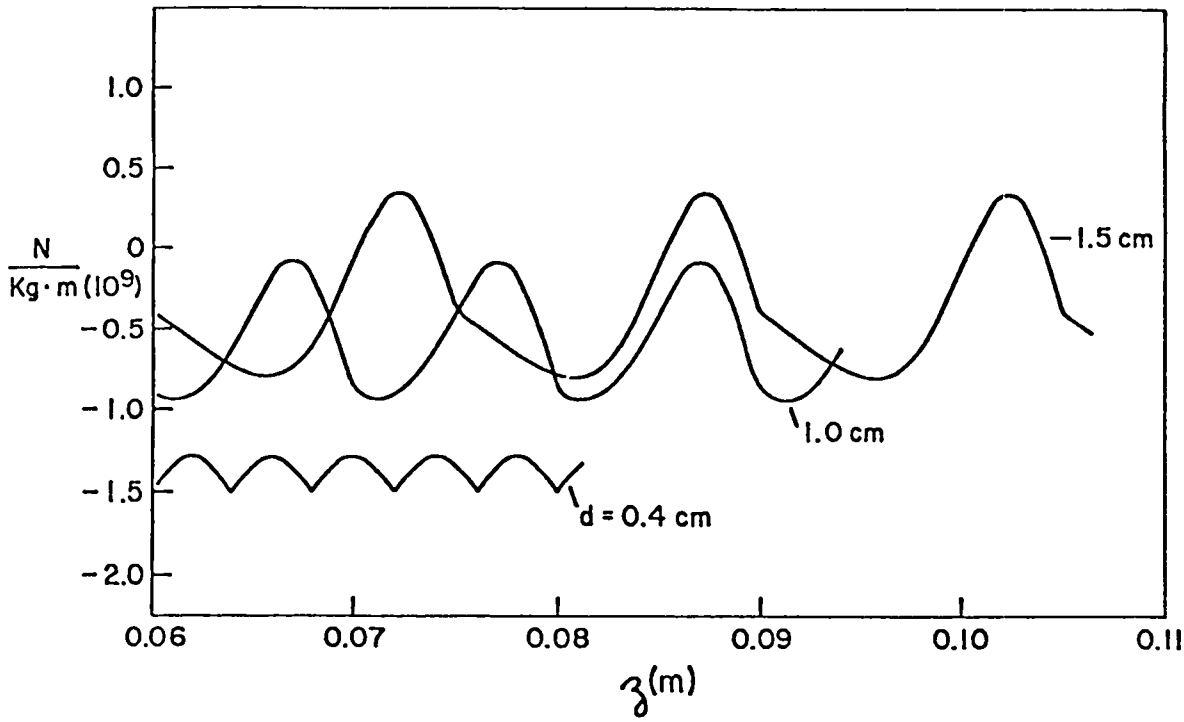

(b)

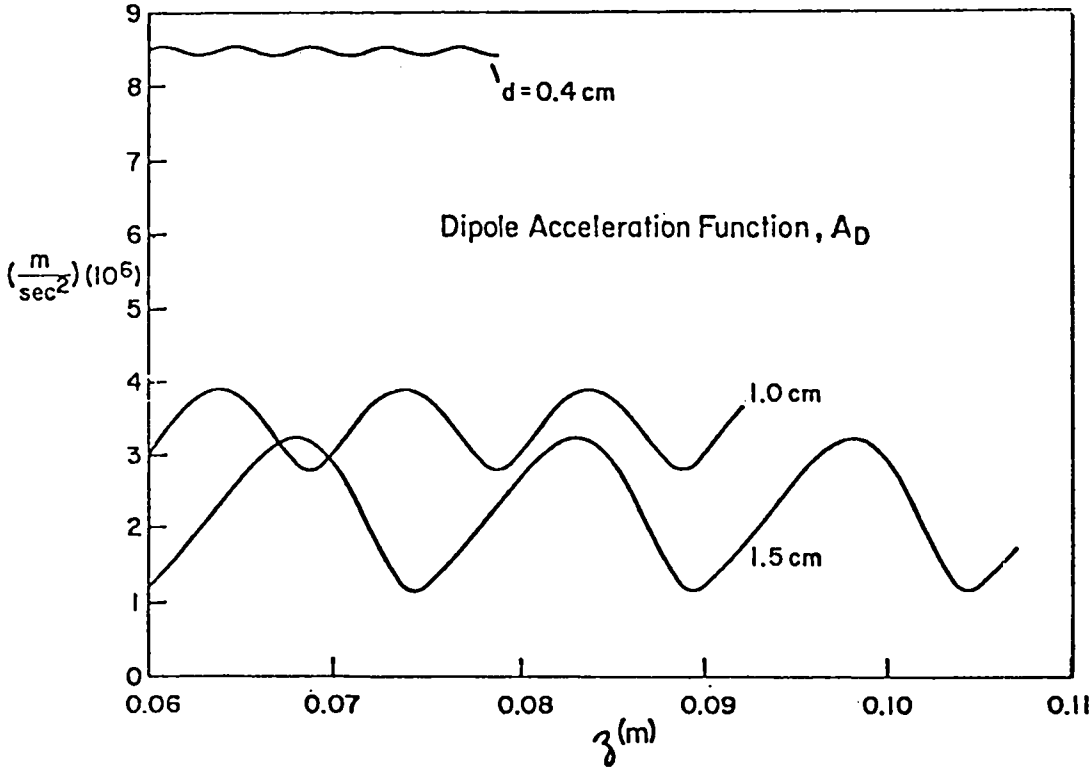

(a)

FIGURE 2(a,b).

PROJECTILE (THIN FOIL DESIGN)

PROJECTILE

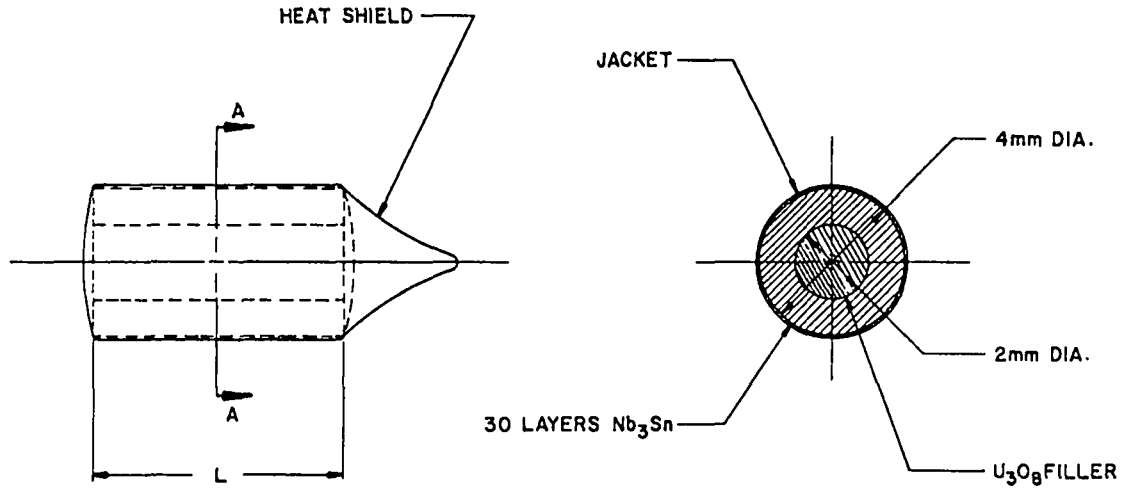

L – INDICATES THE LENGTH OF THE PROJECTILE
WHICH IS SEVERAL MILLIMETERS LONG

FIGURE 3.

LABORATORY FOR IMPACT FUSION		
13/1	Dr. K. W. CHEN	G.H.P.
6/10/79		
MICHIGAN STATE UNIVERSITY		

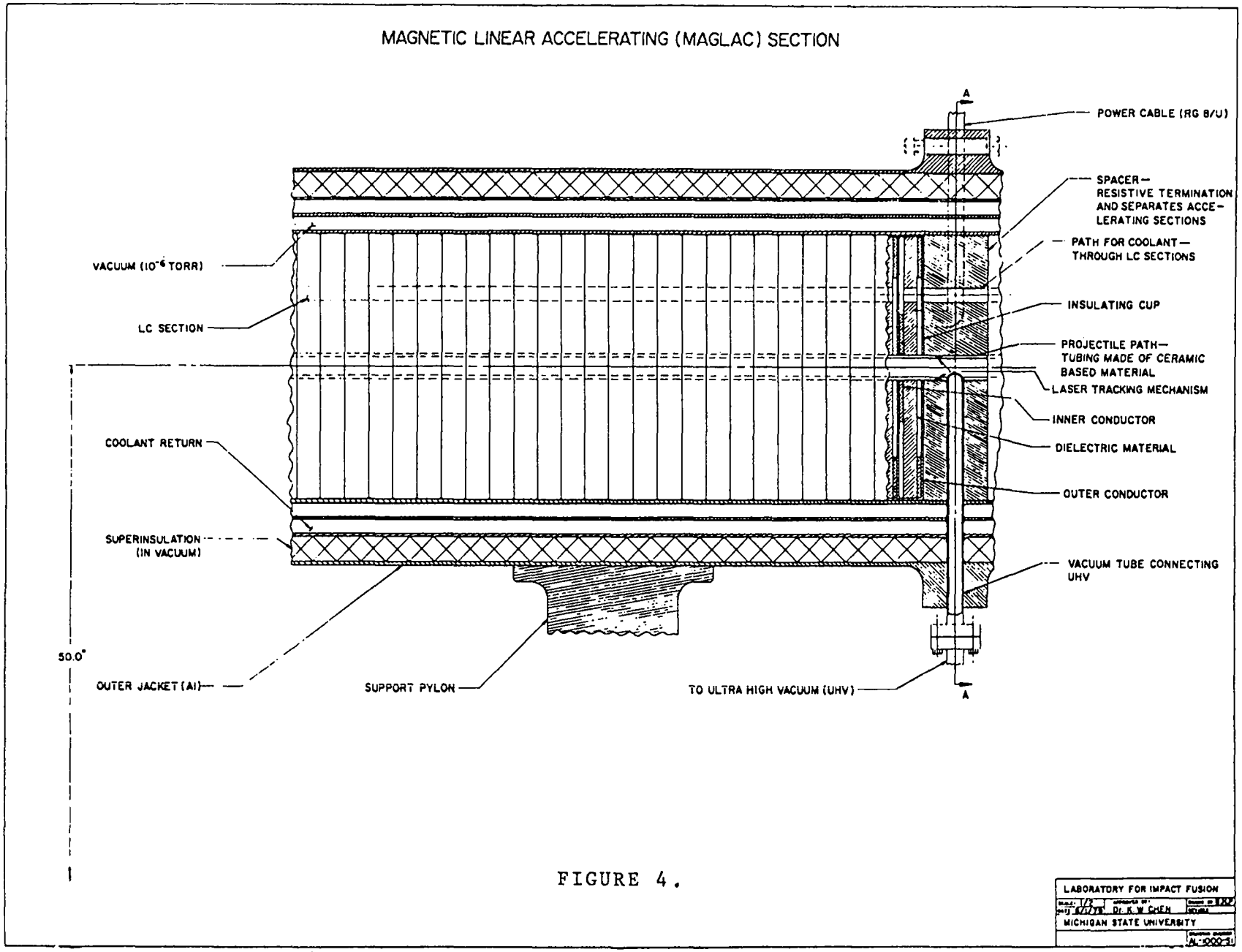
MAGNETIC LINEAR ACCELERATING (MAGLAC) SECTION
A
POWER CABLE (RG 8/U)
SPACER— RESISTIVE TERMINATION AND SEPARATES ACCE- LERATING SECTIONS
PATH FOR COOLANT— THROUGH LC SECTIONS
INSULATING CUP
PROJECTILE PATH— TUBING MADE OF CERAMIC BASED MATERIAL
LASER TRACKING MECHANISM
INNER CONDUCTOR
DIELECTRIC MATERIAL
OUTER CONDUCTOR
VACUUM TUBE CONNECTING UHV
VACUUM (10^{-6} TORR)
LC SECTION
COOLANT RETURN
SUPERINSULATION (IN VACUUM)
50.0'
OUTER JACKET (Al)
SUPPORT PYLON
TO ULTRA HIGH VACUUM (UHV)
A
LABORATORY FOR IMPACT FUSION
DR. K.W. CHEN
MICHIGAN STATE UNIVERSITY

FIGURE 4.

MAGNETIC LINEAR ACCELERATING (MAGLAC) SECTION

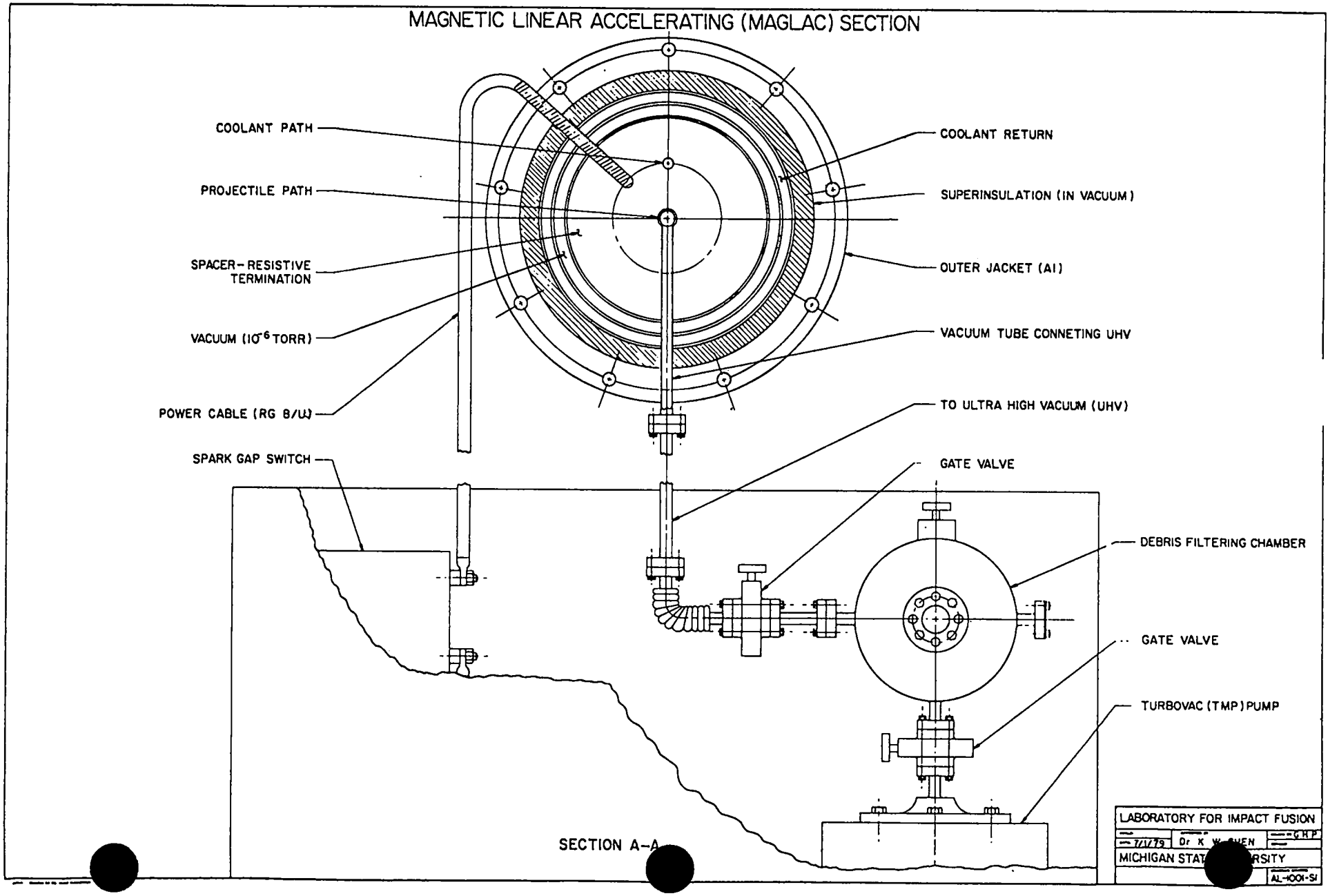

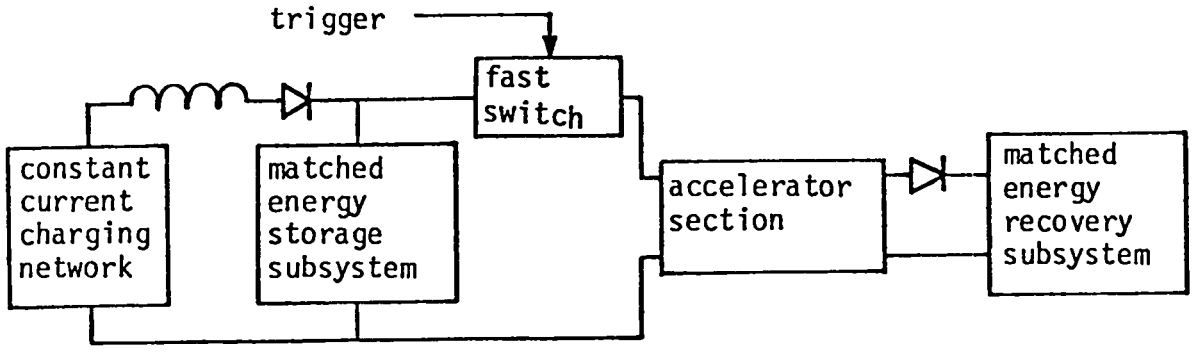

FIGURE 6.

Power Conditioning For A Single Accelerator Section

INJECTOR AND ACCELERATOR LINE

POWER STATION (ENLARGED VIEW)

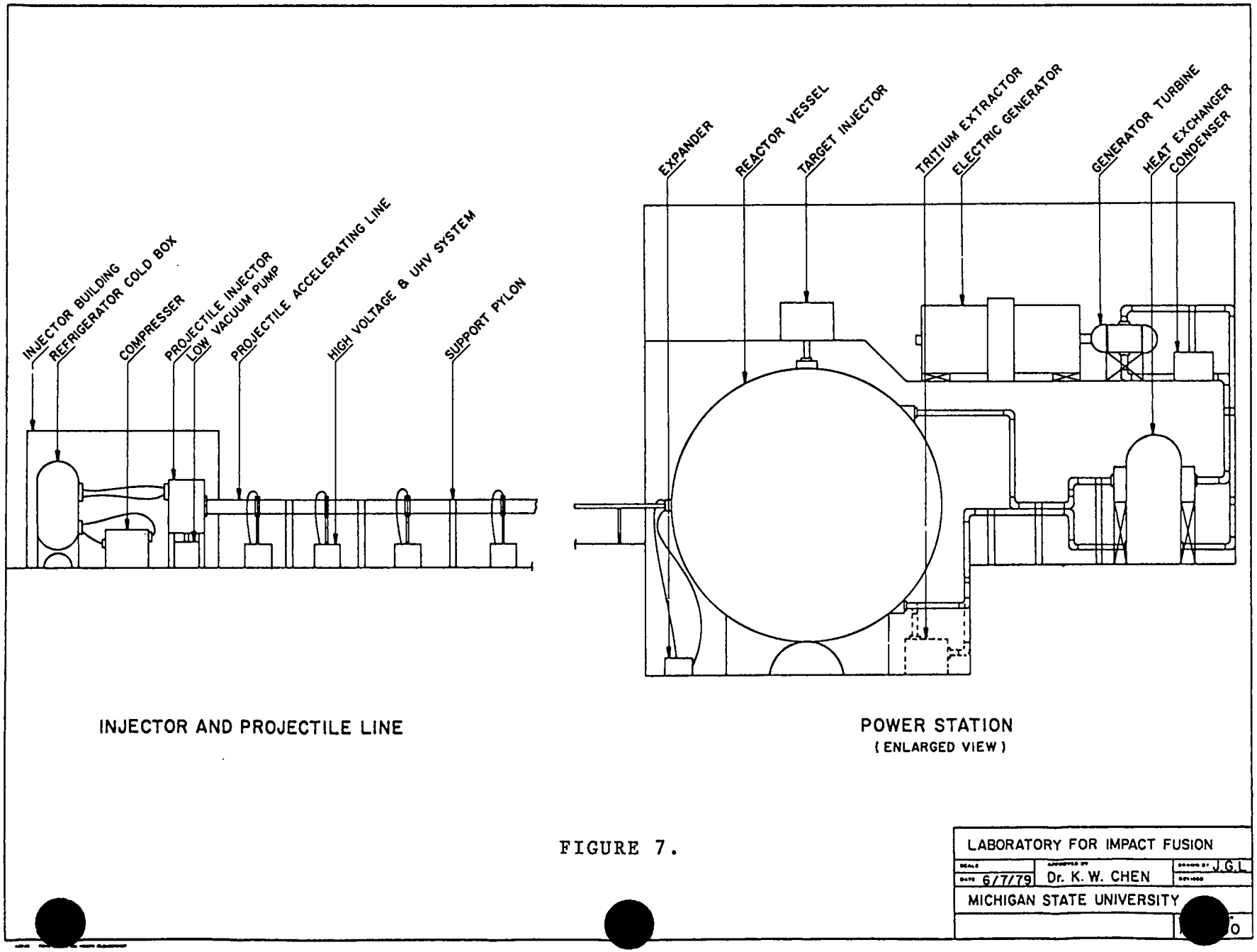

FIGURE 7.

LABORATORY FOR IMPACT FUSION		
SCALE	APPROVED BY Dr. K. W. CHEN	DRAWN BY J.G.L
DATE 6/7/79		
MICHIGAN STATE UNIVERSITY		

Some Approaches to Macron Acceleration†

Michael N. Kreisler
Department of Physics, University of Massachusetts,
Amherst, Massachusetts 01003, USA*

Abstract

Several recent proposals and attempts to achieve hypervelocities with macroscopic particles are reviewed. Some new approaches are discussed.

I. Introduction

In this paper, I would like to discuss some recent thoughts on the problem of achieving hypervelocity of macroscopic particles -- presenting conventional approaches as well as some, perhaps, unconventional ideas. The subject of macron acceleration or "fast dust" is not a new one. Much of the early work and theoretical treatment is due to Harrison [1], Winterberg [2], and many others.

Aside from the fact that making things go very fast is interesting and enjoyable in its own right, it is a legitimate question to ask why this particular type of research is worth pursuing and how it relates to the topic of energy production, in general, and to the subject of this conference, in particular.

---

* Permanent address

† Invited paper presented at the Second International Conference on Energy Storage, Compression, and Switching, December 5-8, 1978, Venezia, Italy. and at Impact Fusion Workshop, Los Alamos, July 1979

Both questions can be answered by referring to Figure 1 in which we plot the effects of increasing macron velocities. As the velocity is increased from 10^5 cm/sec to 10^8 cm/sec and beyond, the average energy per nucleon increases from a fraction of an electron volt to energies approaching an MeV (million electron volts). When such macrons are stopped by stationary targets, the resulting interactions are rather interesting. At the lower end of the velocity scale, the process is non-explosive and relatively cool. However, the collisions become increasingly more violent and generate much higher temperatures as the velocity is increased. At velocities of approximately 10^8 cm/sec, it appears likely that the collision could initiate a fusion reaction, thereby allowing the development of CTR.

In addition to having an alternative approach to the problem of obtaining CTR, the subject of macron acceleration is useful in the study of the equation of state of matter at high densities and pressures. It is also a means of producing dense states of matter which are interesting in a variety of fields including high energy elementary particle physics [3]. As an aside, we note that velocities in excess of 10^9 cm/sec would allow some tests of special relativity.

As we hope to show, the use of macron acceleration to achieve the goal of CTR seems promising and appears to merit greatly increased attention and support. There is really an exciting opportunity for some very interesting research here.

However, the problem of accelerating macrons to velocities approaching 10^8 cm/sec is quite difficult. To demonstrate the problem in a naive fashion, we consider the case of a simple rocket. The well-known relation for the final velocity given a rocket with a constant thrust is

$$v_f = v_{exhaust} \ln \frac{m_i}{m_f}$$

where $v_{exhaust}$ is the exhaust velocity and m_i and m_f are the initial and final masses respectively. It therefore appears that one can achieve any final velocity given a large enough mass ratio. Some numbers are perhaps instructive. If we assume that $v_{exhaust}$ is 3000 m/sec (approximately 10 times the speed of sound), we require that the logarithm of the mass ratio be 300 in order to have a final velocity of 10^8 cm/sec. This implies that

$$m_i = e^{300}\, m_f.$$

But e^{300} is a huge number -- approximately 2×10^{130} !! The mass of the earth is only 6×10^{27} grams so that clearly another approach is necessary. In what follows, we consider several different methods.

II. Electrostatic Acceleration

As an example of a technique which deserves further effort, let us consider the use of an electrostatic field. In the simplest case, one takes a macron, places as large a charge on it as possible and then allows it to fall through a large potential difference. The expressions for the acceleration and the final velocity are :

$$\dot{v} = \frac{Q}{M} E \qquad \text{and} \quad v_f^2 = 2\, L\, \frac{Q}{M} E$$

where Q/M is the charge to mass ratio for the macron, E is the magnitude of the electric field, and L is the length of the accelerator.

There are several problems and limitations of this technique. 1) There is a natural limit to the magnitude of Q/M. For negative charges, the magnitude is limited by field emission and for positive charges by the tensile strength of the material. 2) Q/M may vary during the acceleration. This might present some problems in the use of travelling wave accelerators. 3) The accelerator lengths necessary to achieve hypervelocities seem somewhat long. One calculation [1] indicates that in a travelling wave accelerator

with $\sim 10^4$ Volts/cm, velocities of 10^8 cm/sec can be obtained for small particles ($r \sim 10^{-4}$ cm) with a 10 km accelerator.

In the past, these large lengths have been regarded as great impediments to this technique. However with today's technology, we realize that 10 km is big but it is not outrageous. In particular, there are several elementary particle accelerators which rival that dimension (S.L.A.C. is 3.2 km long, S.P.S. is 7.5 km in circumference, and the proposed L.E.P. is 22.2 km in circumference). Certainly the dimension of the accelerator should not discourage active effort.

III. Magnetostatic Acceleration

Other acceleration schemes have been proposed which also should be investigated actively. One of the more interesting of these is a scheme proposed by Winterberg [2] to use a travelling magnetic wave to accelerate a superconducting solenoid. The choice of the superconducting material is dictated by the need to prevent Joule Heating of the projectile, which would vaporize it long before interesting velocities were reached. The shape of the magnetic field and a sketch of a proposed system [4] are shown in Figures 2 and 3.

It is interesting to note that this method has been recently proposed by Shaner [5] as a possible fuel injection scheme for Tokomak devices. Thus, this technique would be very useful even if there are problems reaching 10^8 cm/sec.

In Figure 4, the relationship between the accelerator length, the projectile velocity, the magnetic field, and parameters of the solenoid is presented. As an incentive to spur further work on the subject, we have indicated the lengths of the elementary particle accelerators on the Figure. Clearly, if the length of the accelerator were the only limitation, we could easily achieve very high velocities. Given the fact that the accelerator components are relatively simple and repetitive, there is every reason to attempt a large scale version of the device. Why not try ?

IV. Gas Guns

An obvious naive choice for a device to accelerate a projectile is a gun. Unfortunately, even so-called "high speed bullets" are barely moving compared to the velocities under discussion here. The limitation on the velocity of such bullets can be understood from a simple analysis [5]. In order to get high velocity projectiles, one wants to maintain a very high pressure on the particle for as long a time as possible. The magnitude of the pressure is limited by the strength of the gun barrel itself. The time during which the pressure acts is limited also, independent of the length of the barrel. As the particle moves, the driving gas expands to fill the space behind the particle. This expansion is, of course, limited by the local speed of sound in the gas. When the velocity of the projectile exceeds the local sound velocity, the driving pressure drops rapidly and further increases in projectile velocity are very small.

There are many ways to parametrize this phenomenon, one of the simplest being the following expression [5]:

$$p/p_o = \bar{e}^{\gamma v/a} ,$$

where p is the driving pressure, p_o is the initial pressure, γ is the ratio of specific heats for the driving gas, v is the projectile velocity and a is the sound velocity. For the case of an ideal gas

$$a \simeq (\frac{kT}{m}\gamma)^{\frac{1}{2}}.$$

Therefore, in order to get the local speed of sound high thereby increasing the particle velocity, it is desireable to go to high temperatures and low atomic number gases. This approach has been followed quite intensely in the past few years culminating in the two-stage light gas gun.

In the two stage gun, the first stage is used to compress and heat the gas in the second stage. This high temperature allows final velocities of the projectile to reach several times sonic velocities of the ambient gas. In fact, velocities approaching 0.5 cm/μsec (5×10^5 cm/sec) have been obtained regularly, thereby allowing accurate equation of state measurements [5,6]. There are several ideas to improve the velocities obtained ranging from the use of shaped charges to superheat the driving gas to the acceleration of the entire second stage in addition to the heating and compression.

Unfortunately, although small increases might be obtained, it is hard to see any improvement which would result in velocities approaching 10^8 cm/sec. For that reason, coupled with the fact that this method is intrinsically messy and has a very low repetition rate, it does not seem to be a promising approach for CTR through macron acceleration.

V. Laser Ablation Acceleration

The acceleration of small particles using high power lasers seems to hold great promise. The idea, of course, is quite simple. One hits the end of a target projectile with a high power laser pulse. A large amount of material is ablated off at supersonic velocities and the remaining mass is accelerated to large velocities.

In order to calculate the velocity, the simple rocket equation suffices (with some problems to be mentioned below). The advantage of this method is that the ablated material is ejected supersonically. Recently, Mc Cann and Degroot [7] performed a calculation in which they showed that it is possible to achieve very high velocities. Using a 1 gram target, the laser ablated 90 % of the mass in 1 ms yielding a projectile of 0.1 gram with a kinetic energy of a megajoule and a velocity of 1.4×10^7 cm/sec. The laser power required is, of course, quite large (typical efficiencies of conversion of laser power to kinetic energy are about 10 %). Fortunately there have been great strides made in the development of large laser facilities.

There is, however, a serious problem with this technique. In particular, the cloud of ablated material gets in the way of the incident laser light. Since one desires a target material which will absorb a large fraction of the incident laser energy, it is entirely reasonable that the cloud will absorb the energy as well. (This phenomenon has been variously discussed as the opacity of the cloud [1] or the size of the inverse bremsstrahlung cross section [7]). In the extreme case, the incident energy is primarily absorbed by the cloud and the target vaporizes, acquiring little or no velocity in the process.

It seems as though there are at least two possible solutions to this problem.

1) Pulse along the trajectory -- If the laser pulses are directed onto the projectile at widely spaced intervals along its path, the particle can outrun the cloud. Of course, this requires very careful monitoring of the particle position. However such systems should be rather simple to develop.

2) Multilayered targets -- Although it is somewhat speculative, it may prove convenient to utilize targets constructed of layers of different materials and driving lasers at different wavelengths. It may then be possible for the ablated cloud from the outer layer of the target to be somewhat transparent to the light from the second laser. Obviously, such a scheme is merely a variation on the pulsing technique mentioned above.

In general, it appears that this technique may be very promising and is worth a reasonable effort. Apparently, it is not particularly easy to obtain time with the large laser facilities for this technique for several reasons. First, this method is somewhat messy, and second there is strong competition for the use of the lasers. Specifically, the lasers are involved in accelerating mass inwards (laser ablation implosions). That method may be a more promising one to reach CTR than the one just described. But ... unless we investigate the macron accelerator more carefully, who can be sure ?

VI. The Rail Gun

The rail gun is an ingenious device which uses the Lorentz force to push a current carrying element. A sketch of such a gun from the recent work of Rashleigh and Marshall [8] is shown in Figure 5. When the driving slug crosses the rail gun, the current carrying elements on the projectile are switched into the circuit. The current in the circuit is approximately 300 kAmps. The magnetic field created by that current results in a sizeable pressure on the projectile. The observed accelerations are satisfactorily explained by a simple theory in which the driving force is :

$$F = \frac{1}{2} L' I^2$$

where I is the current and L' is the inductance per unit length of the rails. In their paper, the authors report being able to accelerate 12.7 mm cubes of LEXAN to velocities of 6×10^5 cm/sec.

One is, of course, impressed by these results. But are orders of magnitude improvement in the final velocity possible through optimization of the system (lower mass targets, higher currents etc.) ? It is clearly worth the research effort.

VII. Other Possibilities

Before discussing some new and perhaps unconventional approaches, I have attempted to list in Table 1 other acceleration schemes which may be of interest.

VIII. New Approaches - 1 : Orbital Collisions

If we consider an object orbiting the Earth in a near-Earth orbit, elementary physics shows us that the velocity is :

$$v^2 = \frac{GM}{R^2}$$

where G is the gravitational constant, M is the mass of the Earth, and R is the Earth's radius. This corresponds to a velocity of

Table 1

Other Possible Acceleration Techniques

Type of Acceleration	Comments	Reference
Acceleration by a charged beam	Projectile is charged Velocities of 10^6-10^7 cm/sec possible in 1-5 km long accelerators	1
Transport Linear Accelerator	Large induction motor ; average acceleration $\sim$300 m/sec^2	9,10
Rotary Pellet Accelerator	2300 RPM motor, 10 m radius blades Velocity 2.4 x 10^5 cm/sec	9
Velocity Multiplication	In an elastic collision, a stationary object recoils with a velocity which is the velocity of the incident object times an appropriate ratio of masses -- problems of strength of materials, speed of sonic shock waves.	-
Possibilities : Use of Steep Wave Fronts Use of Plasma Focus Machines	?	13 -

7.9×10^5 cm/sec. Head-on collisions between two objects in opposite orbits would thus yield a relative velocity upon impact of 1.6×10^6 cm/sec. Although this is still far from 10^8 cm/sec, it is not enough to discourage further thought.

Since the velocity is proportional to $M^{\frac{1}{2}}$, it is appropriate to search for larger masses. The obvious choice is the sun. The dependence on the radius also indicates that we want to conduct our experiments close to the sun. At the radius of Mercury, we find that the orbital velocity is $\sim 4.7 \times 10^6$ cm/sec, yielding head-on collisions with relative impact velocities of 10^7 cm/sec.

In order to get 10^8 cm/sec, it is necessary to reduce the radius to $\sim$ 1/100 $R_{Mercury}$, which unfortunately is inside the sun ! Undaunted by this dilemna, we note that in previous discussions of energy sources, the use of black holes was freely discussed [11]. We shall leave the problem of finding such objects to others. But, when they find them ... with a black hole with a mass approximately equal to the mass of the sun, very interesting orbital velocities would exist at radii of 10^6 km. (To be sure, other interesting phenomena would exist as well !!).

IX. New Approaches - 2 : Electrostatic Acceleration Revisited

Recently Harrison and I [12] have been reexamining the use of electrostatic fields as accelerators. There are several ways to accelerate particles using such fields.

A) Acceleration of Charged Bodies

As we mentioned earlier, it is quite straightforward to accelerate charged objects. One of the major problems is that the constancy of Q/M is hard to guarantee and therefore the use of travelling waves may prove difficult. There are also problems of matching the speed of the travelling wave with that of the particle.

B) Acceleration of Induced Dipoles

When a dielectric is placed in an electric field, a dipole moment is induced. The particle then feels a force given by

$$F = m\dot{v} = \alpha E \nabla E = \alpha E^2/\lambda$$

where E is the electric field strength and λ sets the scale of the gradient ($\frac{\partial E}{\partial x} \sim E/\lambda$).

At first glance, this particular scheme seems very promising as (i) the acceleration is proportional to the square of the electric field strength ; (ii) the dipole moment is induced so that the use of a travelling wave is facilitated ; and (iii) the accelerating force is always pulling the object so that questions of phase stability are reduced.

However, when some calculations are done, it becomes apparent that very high fields are necessary to get velocities approaching 10^8 cm/sec. In particular, if the electric field is roughly ϕ/λ, where λ is as defined above, we find that to get the required velocities in a 10 km long accelerator implies that ϕ is about 10^7 volts ! Therefore, this approach seems somewhat hopeless.

C) Acceleration of uncharged dielectrics in static fields

Let us consider the behavior of a dielectric body which is placed into a region of electrostatic field. (1) If the potential on the boundaries are fixed and the surface charges are free to move, the dielectric body experiences a force towards the region of <u>weaker</u> fields. But (2) if the surface charges are fixed and the potentials on the boundaries are free to vary, the body experiences a force towards the region of <u>stronger</u> fields.

Thus if we were clever enough to arrange an electrostatic field as sketched in Figure 6a, we would have an ideal accelerator. The particle starts from a field-free region, enters one in

which the surface charges are fixed, passes to a region where the potentials on the boundaries are constant, and ends in a field-free region. In passing through this accelerator section, the particle is constantly accelerated and experiences a strong focussing toward the axis of the accelerator. Such sections could be repeated many-fold resulting in very large velocities.

This seems promising but there is a fundamental problem in constructing such a field configuration. In one region the electric field is constant and in the other the displacement field is constant. It is hard to arrange these two regions to be adjacent without discontinuities in the fields. Such discontinuities would yield retarding forces so that no net acceleration results.

Therefore, we have changed the design of the accelerator section slightly (see Figure 6b). The fields are arranged so that the projectile is pulled into the accelerator section by one type of field configuration. Once inside the region, the field is switched to the other configuration and the particle is expelled. With simple monitoring, it is easy to match the speed of this "travelling wave" to the speed of the particle. One finds that the velocity is

$$v \sim E\sqrt{\frac{N\varepsilon_0}{\rho}}$$

where N is the number of accelerating sections, ε_0 the permittivity of free space and ρ is the density of the projectile. This scheme is independent of the size of the macron. For reasonable values of the parameters, it may be possible to obtain velocities in the 10^5-10^7 cm/sec range. Obviously this idea is at a very preliminary and speculative stage and needs further work. There are some serious questions about heating and about frequency and temperature dependent dielectric properties.

X. Conclusions

There exist a large number of possible acceleration techniques. Many of them deserve to be investigated actively now. There are problems with all of the methods ranging from questions of heating of the projectile to questions regarding fundamental strengths of materials. Nevertheless, this research is exciting and it could be the way to achieve CTR. It should be worked on now !

XI. Acknowlegdements

I would like to thank T. Harrison, H. Sahlin and J. Shaner for many informative discussions. I would like to thank John Anderson for his continued enthusiasm and support. This work was supported in part by a University of Massachusetts Faculty Research Grant.

References

1. E.R. Harrison, Phys. Rev. Letters 11, 535 (1963) ; Plasma Physics 9, 183 (1967)
2. F. Winterberg, Plasma Physics 8, 541 (1966) ; Z. Naturf. 19a, 231 (1964)
3. W. Willis, private communication. Extremely dense materials make excellent anti-proton production targets.
4. At the conference, it was noted that H. Koln at N.M.L. has a small working model of this device.
5. J. Shaner, Internal Livermore Note (1977) ; private communication
6. See for example, J. Shaner et al., UCRL 79586 (1977).
7. T.E. McCann and J.S. De Groot, "Acceleration of Solid Macro-Particles by Laser Produced Ablation", UCRL-79732, (1977) ; 19th Meeting of APS, Div. Plasma Physics, Atlanta (1977)
8. S.C. Rashleigh and R.A. Marshall, J. Appl. Phys. 49, 2540 (1978)
9. G.K. O'Neill, Physics Today, Sept. 1974, p. 32
10. Westinghouse Engineer, 6, 160 (Sept. 1946)
11. Lowell Wood, Berkeley Conference on Energy Compression
12. E.R. Harrison and M.N. Kreisler, to be published
13. See for example, G.A. Askar'yan and N.M. Tarasova, ZhETF Pis. Red. 18, No. 1,8 (1973).

Figure Captions

1. Effect of increasing macron velocity
2. Shape of magnetic field for magnetostatic acceleration (from Reference 2)
3. Sketch of proposed accelerator (from Reference 2)
4. Relationship between accelerator parameters and projectile velocity (from Reference 2). The lengths of existing or proposed elementary particle accelerators is shown.
5. Sketch of rail gun (from Reference 8)
6. a) Ideal field configuration desired
   b) Possible accelerator design.

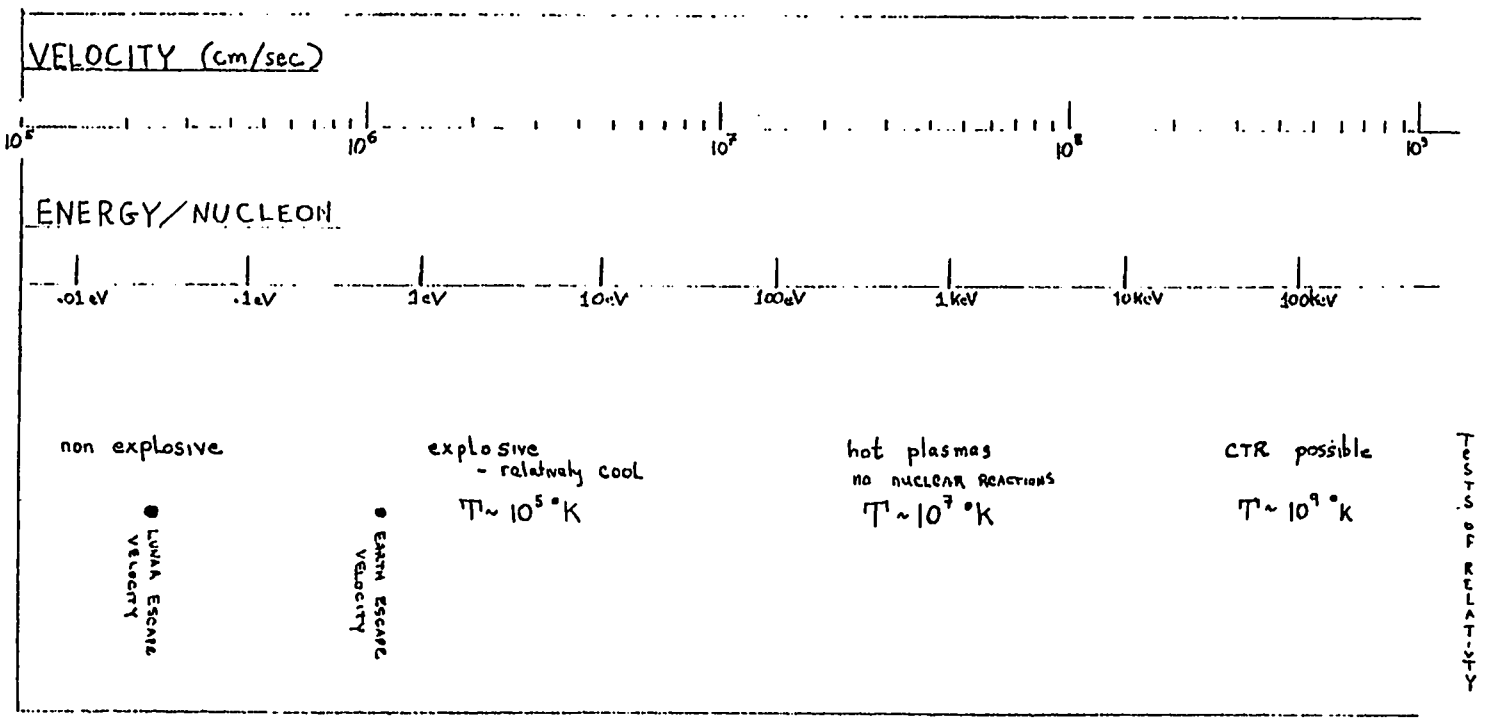
VELOCITY (cm/sec)
10^5
10^6
10^7
10^8
10^9
ENERGY/NUCLEON
.01 eV
.1 eV
1 eV
10 eV
100 eV
1 keV
10 keV
100 keV
non explosive
explosive
- relatively cool
$T \sim 10^5$ °K
hot plasmas
no nuclear reactions
$T \sim 10^7$ °K
CTR possible
$T \sim 10^9$ °K
LUNAR ESCAPE VELOCITY
EARTH ESCAPE VELOCITY
TESTS OF RELATIVITY

FIGURE 1

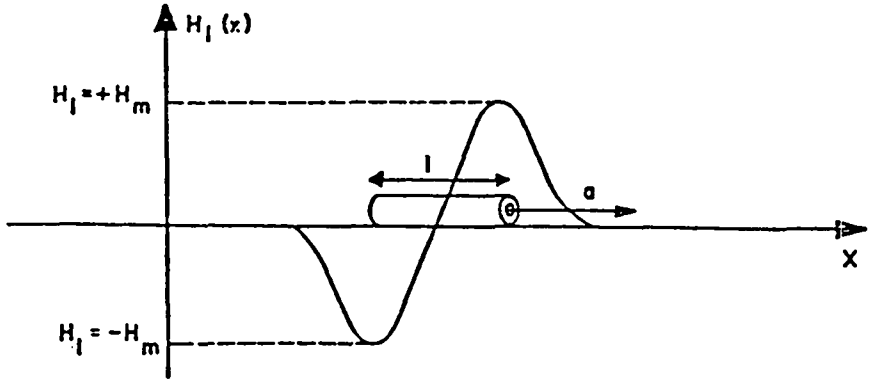

FIG. 2.—Schematic diagram showing the shape of the magnetic field and position of the solenoid in it (paramagnetic case).

FIGURE 2

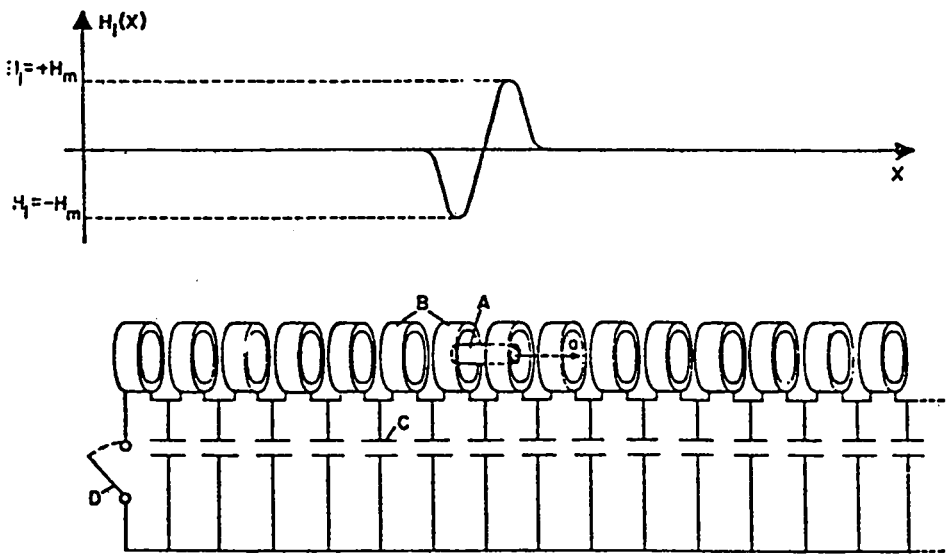

FIG. 5.—Transmission line accelerator. A: accelerated solenoid; B: field coils; C: capacitors; D: switch to be closed to start travelling magnetic wave. $H_1(x)$: magnetic field on transmission line relative to the frame of the solenoid. $n(x)$: windings per unit length in field coils (arbitrary units).

FIGURE 3

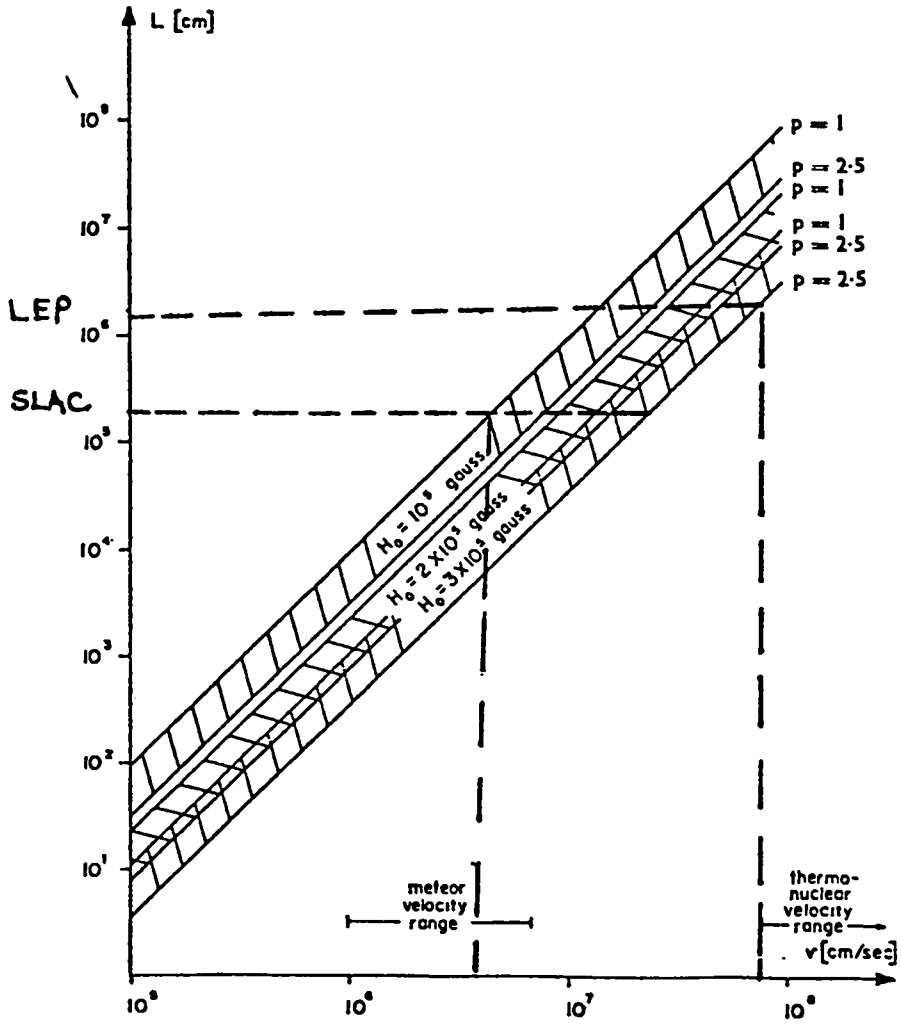

FIG. 4.—Accelerator length L as a function of v, H_0 and p.

FIGURE 4

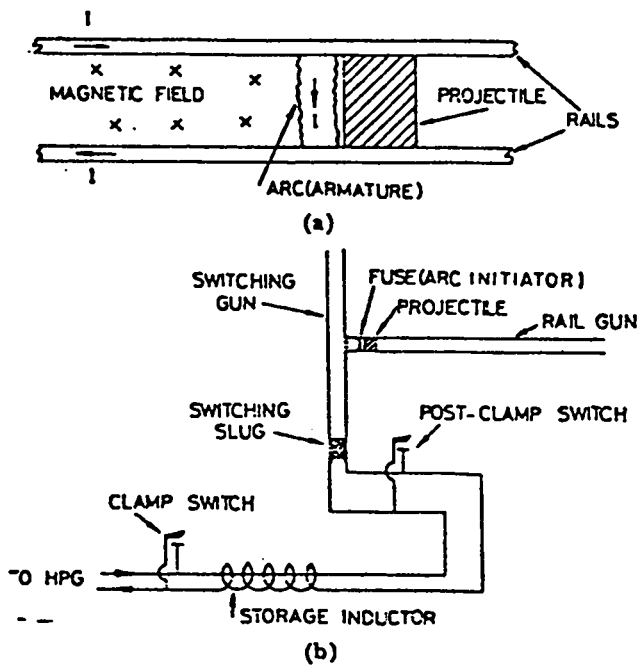

FIG. 1. (a) Principle of the rail gun. (b) Schematic circuit of the ANU rail gun.

FIGURE 5

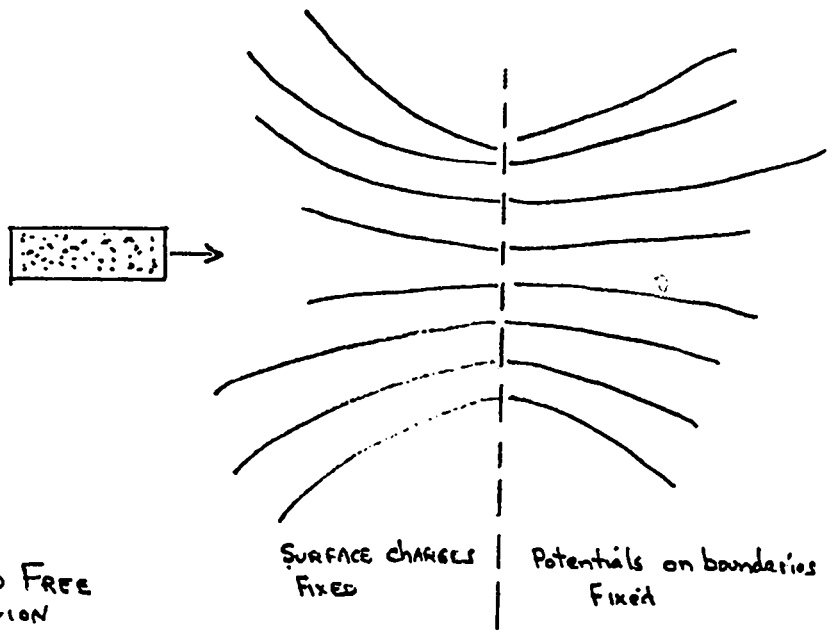
FIELD FREE REGION
SURFACE CHARGES FIXED
Potentials on boundaries Fixed
FIELD FREE REGION

(a)

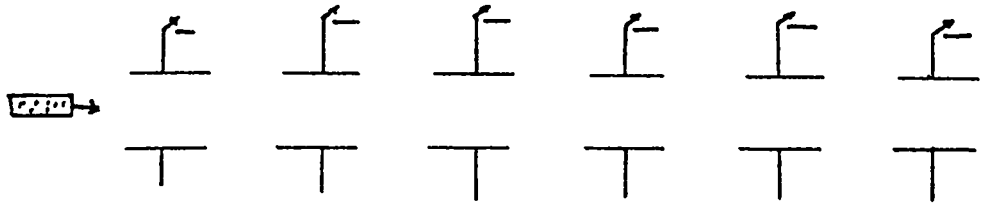

(b)

FIGURE 6

Driver Efficiency Requirements for Inertial Confinement Fusion

Roger O. Bangerter

University of California, Lawrence Livermore Laboratory
Livermore, CA 94550

Although target gains (output energy/input energy) of about 1000 are theoretically possible, [1] more conservative computer simulations typically give significantly less gain. Figure 1 shows the results of recent calculations done at Livermore. The gain band is applicable to short wavelength lasers or ion beams of an appropriate energy. There doesn't appear to be any reason why impact fusion targets should exhibit higher gains than laser or ion beam targets, and in fact the gain may be less. For example, achievement of the gain shown is dependent on a specified input pulse shape. A driver capable of providing the prescribed pulse shape may well be incapable of driving targets to even this level of gain.

If we assume that the laser and ion curves also apply to impact fusion and assume total projectile energy of 10 MJ, a driver efficiency of 0.5 to 1 % is required for net energy gain. For the production of electricity an appropriate conversion efficiency might be about 1/3 so that the driver efficiency would have to be greater than 1.5 to 3 % for net energy gain. For economical power production it is commonly assumed that the product of driver efficiency and target gain must be greater than about 10. In this case a driver efficiency of 5 - 10 % is required. For total projectile energies less than 10 MJ the efficiency must be even higher. This criterion eliminates some proposed acceleration schemes as power plant drivers. Other important criteria are adequate pulse repetition rate, reliability and driver longevity. Of course purely scientific and military applications are not subject to such criteria.

Reference

[1] J.H.Nuckolls, R.O.Bangerter, J.D.Lindl, W.C.Mead, Y.L.Pan, Lawrence Livermore Laboratory Report UCRL-79373, Rev. 1 (1978).

Fig. 1--Target gain as a function of input energy for short wavelength lasers and ion beams.

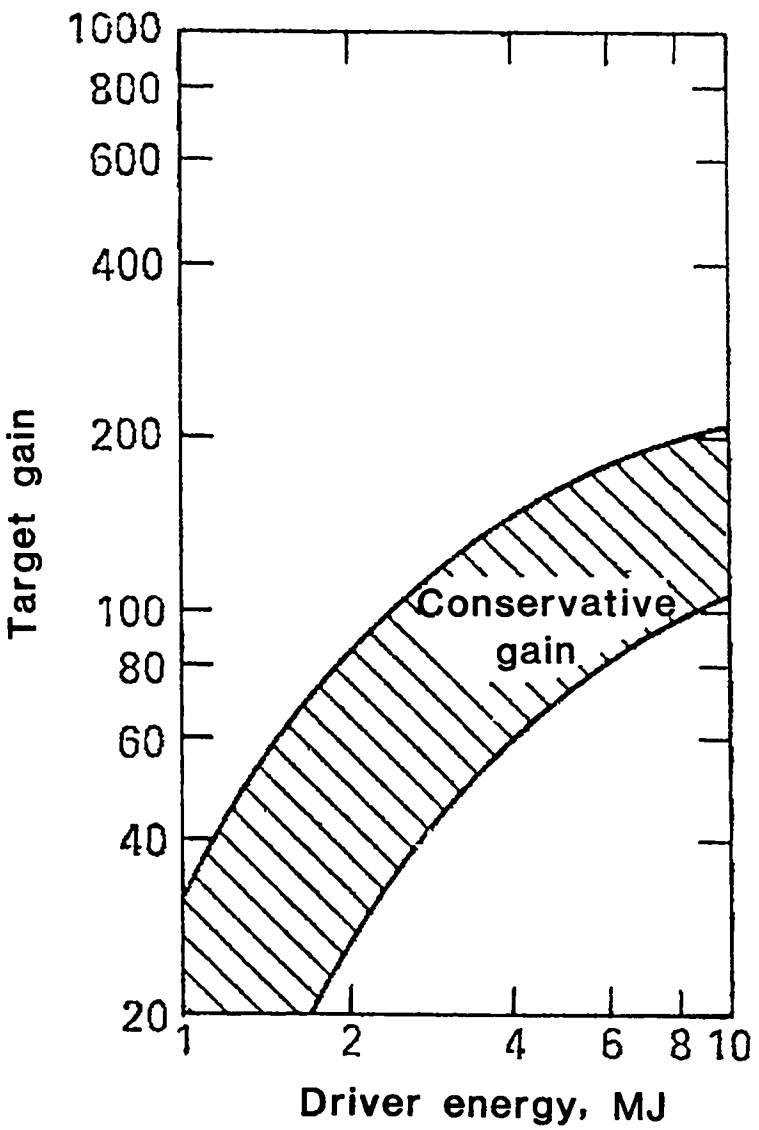

FOUNDATION
85 E. GERANIUM AVENUE
ST. PAUL, MINN. 55117
PHONE: (612) 370-0990

IMPACT FUSION METHODS AND THEIR APPLICATION TO ROCKET PROPULSION

GARY C. HUDSON
(Foundation, Inc.)

IMPACT FUSION WORKSHOP, LASL, JULY 10-13, 1979

THE GOALS

- HIGH CHARACTERISTIC EXHAUST VELOCITY (C^*) (OR SPECIFIC IMPULSE, $ISP = C^*/g_o$)
- HIGH ENGINE THRUST-TO-WEIGHT (T/W) ($>5:1$)
- HIGH POWER LEVELS ($>1000\ MW_T$)
- LOW COST PROPELLANT & FUELS
- REUSE, LOW ACTIVATION, COMMERCIAL APPLICABILITY
- "MINI-ORION"

IMPACT FUSION WORKSHOP, LASL, JULY 10-13, 1979

THE PROBLEMS

- ■ *INITIATION OF A NUCLEAR EVENT(S) OF SUFFICIENT YIELD TO GENERATE REQUIRED PWR LEVELS*
- ■ *PACKAGING TRIGGER SYSTEM IN PORTABLE, REUSABLE FORM (INCLUDING ENERGY SOURCE)*
- ◪ *RELIABILITY, REUSE, ECONOMICS*
- □ *ENVIRONMENTAL IMPACTS*

■ *=IMPACT FUSION TECHNOLOGY/SCIENCE OFFERS POSSIBLE BENEFITS.*

IMPACT FUSION WORKSHOP, LASL, JULY 10-13, 1979

IMPACT FUSION HYBRIDS

- *PURE FUSION EVENTS DO NOT OFFER ADEQUATE PWR LEVELS IN ENGINE IN MOST CASES (ΔV'S > 60,000 fps, > 20 km/sec; F > 100,000 lbs, > 50 tons)*
- *USE OF HYBRID SCHEMES IS INDICATED*
- *USE RAILGUNS?, GAS GUN HYBRIDS? MOMENTUM CONCENTRATORS? (REF. 1)*

FUSION-FISSION HYBRIDS

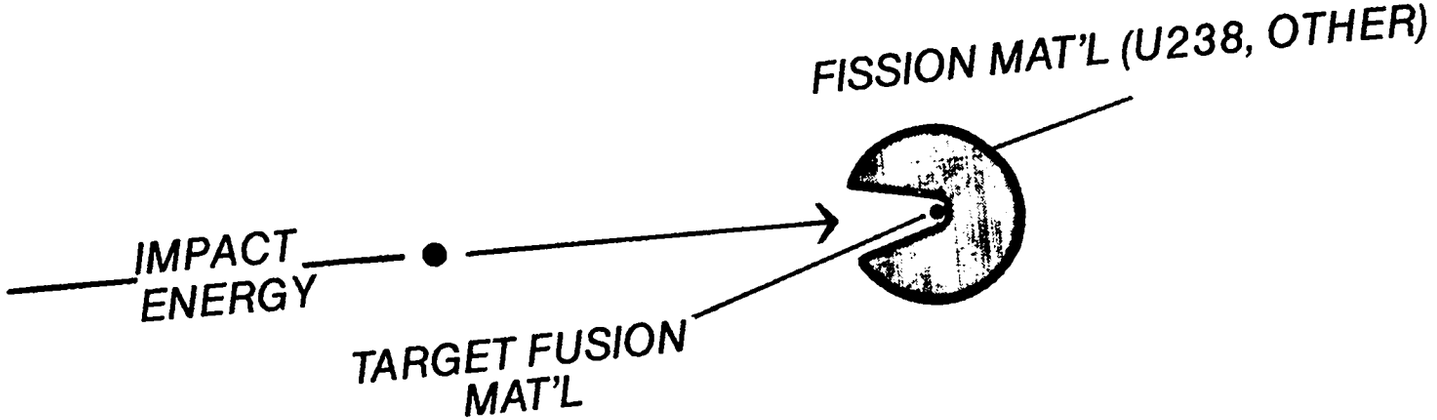

- FUSION EVENT SHOULD PRODUCE $\approx 10^{22}$ NEUTRONS
- FISSION MAT'L ABSORBS FUSION NEUTRONS; GAIN MAY BE 10 - 1000 TIMES FUSION YIELD DEPENDING ON CONFIGURATION

IMPACT FUSION WORKSHOP, LASL, JULY 10-13, 1979

FISSION-FUSION HYBRIDS

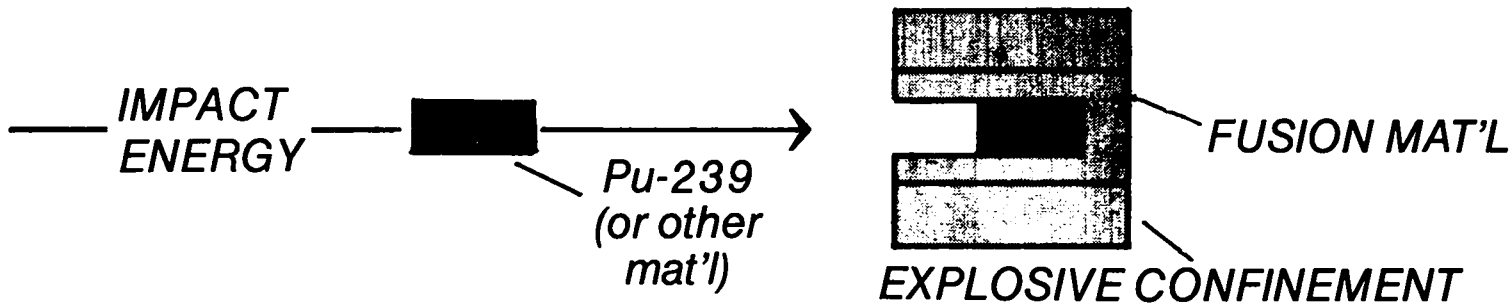

- HIGH COMPRESSION OF FISSILE MAT'L MEANS VERY HIGH BURNUP OF TARGET (>50% - 70%)
- ENERGY OUTPUT FROM FISSION PROCESS OCCURS DURING VERY SHORT TIME SPAN (<0.7 nanosec)
- FUSION BURN GIVES GOOD YIELD EVEN IF FISSION EVENT "FIZZLES"

IMPACT FUSION WORKSHOP, LASL, JULY 10-13, 1979

BARE 239 Pu IMPACT EVENT

MASS (gm)	WORK (MJ)	(M Bar) PRESSURE	(gm/cm³) DENSITY	(cm/sec) VELOCITY	YIELD (MJ)/ T TNT EQUIV.
1000	≈20.0	10^2	70.0	6.3×10^5 *	$\approx 10^7$ / 2400
100	≈35.0	2×10^3	300.0	2.6×10^6 **	$\approx 10^6$ / 240
10	≈30.0	4×10^4	≈1,000	7.7×10^6 ***	$\approx 10^5$ / 24
1	≈20.0	10^6	≈5,000	2.0×10^7 ***	$\approx 10^4$ / 2.4
.1	≈ 8.0	2×10^7	≈20,000	4.0×10^7 ***	$\approx 10^3$ / .2
.01	≈ 3.0	3×10^8	≈90,000	7.7×10^7 ***	$\approx 10^2$ / .02

*attainable w/light gas gun

**factor of two higher than present light gas guns

***railguns or similar electromagnetic launchers should be capable of these velocities

assumes 10% yield

INCREASING COST OF OPERATION

IMPACT FUSION WORKSHOP, LASL, JULY 10-13, 1979

SUMMARY

- *HIGH THRUST/HIGH Isp ENGINES MAY USE PULSED NUCLEAR DEVICES*
- *POWER REQUIREMENTS MAY FORCE USE OF FISSILE OR FISSIONABLE MATERIALS*
- *VELOCITY REQUIREMENTS MAY PERMIT TEST OF CONCEPT IN NEAR FUTURE*
- *OTHER METHODS OF ACHIEVING SIMILAR RESULTS ARE UNDER STUDY. NEW IDEAS ARE SOLICITED.*

REFERENCES

1) Kolm, H., Fine, K., Mongeau, P., and Williams, F., **Electromagnetic Propulsion Alternatives,** Fourth Princeton/AIAA Conference on Space Manufacturing Facilities, AIAA Paper 79-1400, May 14-17, 1979.

2) Cole, Jr., R.K., Renken, J.H., (1975) **Analysis of the Microfission Reactor Concept.** Nuclear Science and Engineering, **58,** 345-353.

3) Everett, C.J., Ulam, S.M., (1955) **On a Method of Propulsion of Projectiles by Means of External Nuclear Explosions.** LASL Report LAMS-1955.

4) Winterberg, F., (1973), **The Possibility of Microfission Explosions by Laser or Relativistic Electron-Beam High Density Compression.** Lettere Al Nuovo Cimento **6:**11, 407-411.

5) Seifritz, W., Ligou, J., (1975) **Laser Induced Thermonuclear Micro-Explosions Using Fissionable Triggers.** Nuclear Science and Engineering **56,** 301-319.

DESIGN ISSUES AND MATERIAL PROBLEMS IN INERTIALLY-CONFINED FUSION REACTORS*

Jack Hovingh

Lawrence Livermore Laboratory
University of California
Livermore, California 94550

Introduction

The reactor design for inertially confined fusion (ICF) power plants will have different design constraints than magnetically confined fusion (MCF) reactors. The ICF reactors will have more geometric flexibility and easier maintenance because they are unencumbered by the large magnet systems of MCF reactors. The ICF reactors will have more freedom in material options such as the use of flowing conducting fluids and ferritic steels because of the absence of large magnetic fields. In addition, since plasma contamination is not a problem in ICF reactors, the fusion cavity can operate at pressures limited only by the requirements of driver beam transmission. However, the energy from the microexplosion in the ICF reactors is deposited as a sequence of intense pulses while the fusion energy from an MCF reactor is deposited at a relatively constant rate.

This paper discusses the effects of the deposition of energy from D-T microexplosion in intense pulses, as well as some general material selection criteria. In addition, the effects of the cavity environment on the microexplosion spectra and the implications on the first wall design are discussed. Finally, the applications of the above effects are applied to a reactor, the LLL HYLIFE converter concept.

Methods of Analysis

Surface conditions in a conceptual laser fusion reactor are dependent on the first-wall materials, the energy flux, and the partition of the

* Work performed under the auspices of the U.S. Department of Energy by Lawrence Livermore Laboratory under contract number W-7405-ENG-48.

energy from laser-pellet interaction and burn. The materials are important in terms of energy attenuation coefficient, strength, fatigue lifetime, equation of state and thermal properties. The partition of energy from the pellet irradiation and burn is a function of the pellet design, pellet mass and the pellet compression. An example of the effect of pellet compression on the fraction of the microexplosion energy released in neutrons is shown in Figure 1.[1]

The first wall design in an inertially confined fusion reactor will be determined from the allowable surface conditions at the first wall, which in turn are determined by the design lifetime of the first wall material as well as the vacuum pumping power required to evacuate the microexplosion cavity to its required pressure prior to each explosion.

The physics of the laser induced implosion and thermonuclear burn of the pellet is very complex. Large computer codes have been developed to calculate the transport and interaction of the laser photons, electrons, ions, x-rays and fusion reaction products, together with the magnetic and electric fields and hydrodynamic behavior of the pellet.[2]

Theoretical energy-release forms from a 10 MJ bare DT pellet microexplosion are shown in Table I.[3] The x-ray energy spectrum is peaked at about 3 keV and the neutron energy spectrum closely resembles a 14 MeV monoenergetic source. Most of the alpha energy is assumed to be deposited within the pellet. About 30% of the alpha energy escapes from the pellet with an average particle energy of 2 MeV. The pellet debris is assumed to have a Maxwellian energy distribution with an average energy of 53 keV/amu. The arrival time of the various energy forms at a first wall located 3.5 m from the 10 MJ microexplosion is shown in Figure 2.

The microexplosion energy deposition in, and the response of the first wall can be found by inserting spectra of the various forms of energy from the pellet into special deposition computer codes.[4-7] Other institutions may use different codes to assist in their analyses of the energy deposition and first wall response.[8]

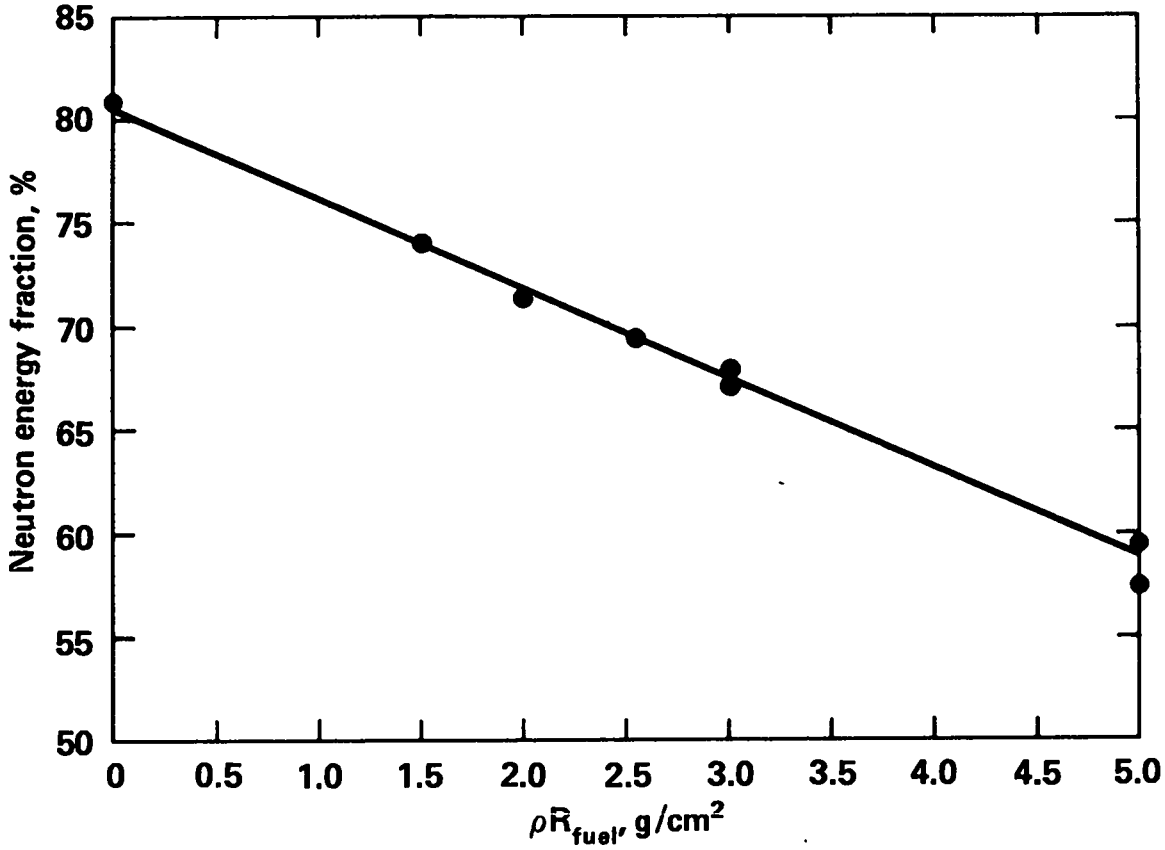

Fig.1 Effect of pellet compression on the fraction of microexplosion energy released in neutrons.

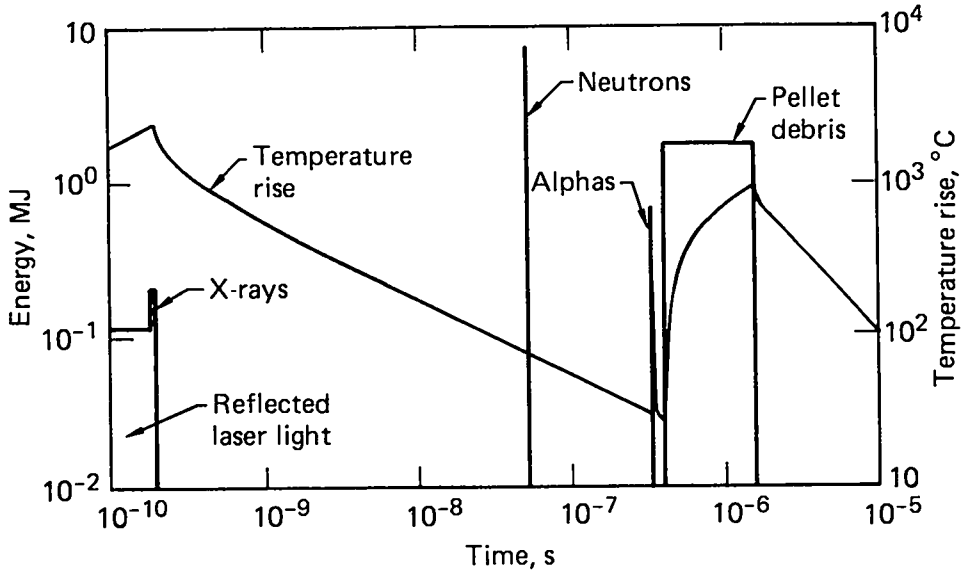

Fig.2 Arrival Time of Various Energy Forms and Surface Temperature Response of Graphite Located 3.5 m From a 10 MJ Microexplosion.

Table I: Energy Partition From Laser-pellet Interaction and Microexplosion

Energy Form	Energy, MJ
Reflected Laser Light	0.16
X-rays	0.10
14 MeV Neutrons	7.7
Energetic Alpha Particle (2 MeV Average)	0.7
Pellet Debris	1.8

Effects of Energy Deposition Time on Temperature and Stress

The sudden deposition of the burn product energy in the first wall results in stress due to the thermal gradients in the material from non-uniform heating and conduction, as well as inertial effects. The boundary value problem is of considerable mathematical difficulty as it combines the theories of elasticity and viscoelasticity as well as head conduction. Usual engineering solutions are obtained by omission of the mechanical coupling term in the energy equation and the inertia terms in the equation of motion. The basis for the omission of the mechanical coupling term and the inertial term is a consideration of the characteristic times of the system. These time considerations will be discussed below.

The response of a continuum to internal energy deposition is dependent on temporal-spatial deposition profiles, and the thermal-physical properties of the continuum. We consider first the effects of the temporal-spatial deposition profiles by assuming that a pulse of energy is deposited in the continuum in a time τ and spatially in the form

$$q_0'''(x) = q_0''' \exp[-\mu x] , \qquad (1)$$

where q_0''' is the energy deposition from a given source in the surface layer of the continuum and μ is the energy attenuation coefficient through the continuum. We define the characteristic thermal time of the

energy deposition in the continuum as the ratio of the energy storage in the distance μ^{-1}, to the rate of heat conducted across the distance μ^{-1}, or

$$\tau_T = [u^2\alpha]^{-1} \quad , \tag{2}$$

where α is the thermal diffusivity of the continuum material. We also define the characteristic mechanical response time of the continuum due to the energy deposition as time required for a disturbance to propagate the distance μ^{-1} or

$$\tau_m = [\mu c]^{-1} \quad , \tag{3}$$

where c is the wave velocity in the continuum.

Two cases are of special importance for inertial fusion. These cases are:

Case I $\quad \tau < \tau_m << \tau_T$

Case II $\quad \tau_m << \tau_T \approx \tau$

For Case I the time variation effects produced by heat conduction are small compared to those produced by the pressure wave. Because the energy is deposited in a short time the initial temperature rise and pressure rise can be estimated by simple models,

$$\Delta T(x) = \frac{q'''(x)}{\rho C_v} \tag{4}$$

$$\Delta p(X) = \Gamma\, q'''(x) \tag{5}$$

where $q'''(x)$ is the energy deposition at position x in the continuum, ρ, C_v and Γ are the density, specific heat at constant volume, and Gruneisen constant, respectively, of the continuum. Approximate theories

of uncoupled dynamic thermoelasticity and viscoelasticity can then be used to determine the moving stress pulse produced by the energy deposition.

For energy deposition in times that are long compared to the thermal characteristic time, which is long compared to mechanical characteristic time (Case II), the stress can be determined by quasi-static thermoelastic or viscoelastic theory while the temperature history can be determined using classical diffusion theory.

If the fusion energy is deposited in such a short time that the pressure cannot relieve itself during the deposition time, a relief wave moves into the continuum from the surface. If the continuum is a solid, and if the tensile strength is exceeded, the surface will spall.

The results of a bare D-T 10 MJ microexplosion in a 3.5 m radius microexplosion chamber with a graphite first wall are shown in Table II. The surface temperature history is shown in Fig.2. The lifetime of the graphite liner is about one year for a fusion power of 200 MW.[3] Note that the peak surface temperature increases are from the reflected laser light and the pellet debris. The peak stresses are from the reflected laser light and the high energy alphas.

Radiation Damage and Effects

If a high-energy particle enters a crystalline lattice, there is a certain probability that the neutrons will be scattered by the lattice nuclei. A target atom (or ion) involved in such a collision will usually be displaced from its normal (stable) position in the lattice leaving behind a vacancy. The scattered neutron can then proceed to collide with other nuclei and produce more displaced atoms. If a normal site is not readily available, a displaced atom may occupy an intermediate, less stable location, called an interstitial position. The result of the particle collisions is thus the formation of more or less permanent defects in the solid. Since it requires only about 25 ev of energy to move an atom from its normal position in a metal lattice, it is evident that a 14 MeV neutron, for example, might produce many defects. If these defects are sufficiently common, there may be a marked change in the physical and mechanical properties of the material.

Table II Graphite first wall energy deposition and response characteristics.

Source	Fluence kJ/m^2	Surface deposition kJ/g	Deposition depth μm	Deposition time ns	Surface temperature rise C	Peak tensile stress MPa**
Reflected laser light	1.0	28.6	0.02*	0.20	2900.0	>100***
X-rays	0.65	0.006	7.2*	0.01	2.0	0.2
14-MeV neutrons	50.0	—	—	0.01	—	—
High energy alphas	4.5	0.40	6.9	0.01	200.0	33.0
Pellet debris	12.0	4.7	1.6*	1200.0	950.0	<0.1

*Depth at which energy deposition is e^{-1} of the surface deposition
**Spall strength of graphite is 10^2 MPa
***Spalls at a depth of 0.1 μm. Reflected laser light surface deposition for no spall is 20 kJ/g

Fast neutrons may be captured by the lattice material in (n,p) and (n,α) reactions. The gas produced in the lattice as well as the solid transmutations from these reactions will result in changes of the mechanical properties of the lattice material. In addition to the effects of fast neutrons described above, the capture of thermal neutrons in (n,γ) reactions may produce significant changes in some materials. Since momentum must be conserved in these reactions, the emission of a gamma-ray photon is accompanied by the recoil of the residual nucleus. The recoil energies may be as large as hundreds of electron volts and so are sufficient to produce a significant number of atomic displacements.

Radiation damage effects in a fusion reactor can be categorized into surface effects, and bulk effects. Surface effects include physical and chemical sputtering from the plasma debris and neutrons, and blistering from the implantation of the helium as from the fusion reaction in the reactor first wall. Bulk damage effects include swelling and material property changes. The magnitude of the radiation damage effects of a given material are dependent on such conditions as the particle energy and mass, the particle number flux and the material temperature and temperature history.

Radiation damage effects in an inertially confined fusion reactor will be different from those in a magnetically confined fusion reactor. This is primarily due to the pulsed nature of the energy from an ICFR microexplosion vis-a-vis the steady nature of the energy from a MCFR plasma. For example, an ICFR operating at 1 Hz may have the same time averaged first wall flux as a MCFR. Thus the peak energy deposition in an ICFR may be 10^7 to 10^8 times that of the MCFR with the same first wall flux. A comparison of the peak damage rates of various radiation sources is shown in Fig.3.[9] Also, the radiation damage occurs in an ICFR during a period of large temperature transients which results in significant alteration of both point and cluster defect behavior. The relation between surface temperature excursion and displacement production as a function of time for copper located 7 m from a 100 MJ microexplosion is shown in Fig.4.[10] The displacements from the debris energy deposition occur about 1 μs after the x-ray pulse. The synergism

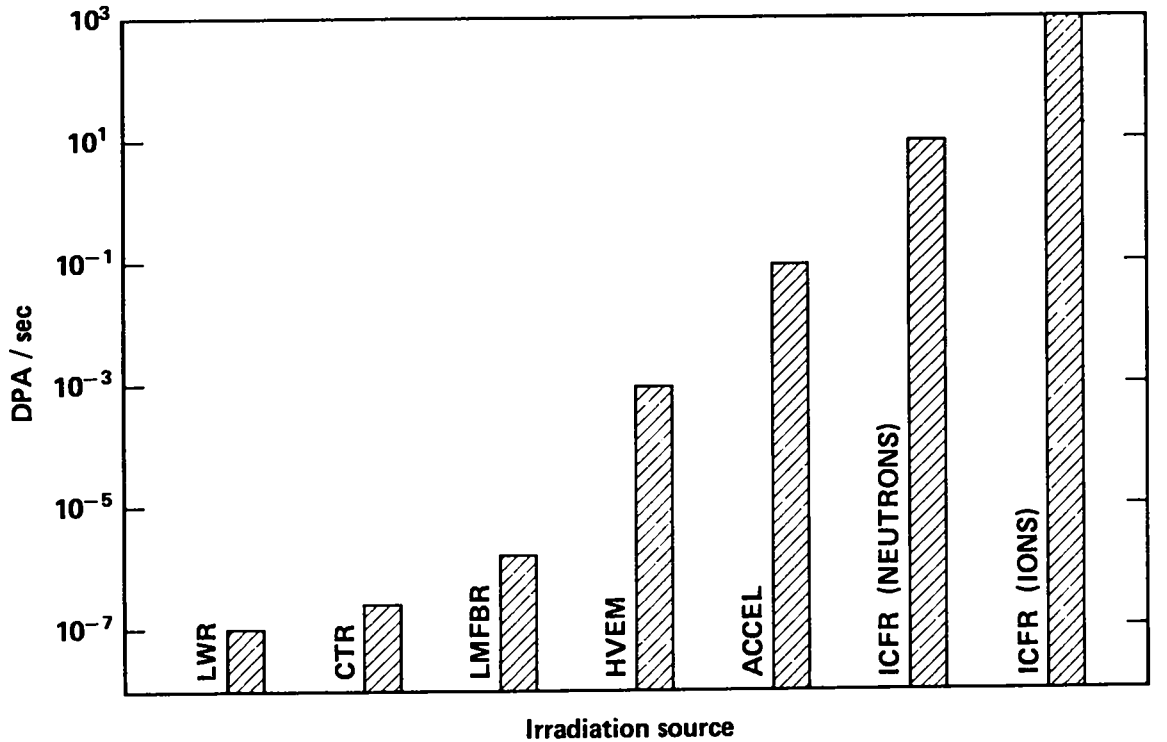

Source: G. Kulcinski

Fig.3 Comparison of peak damage rates for various irradiation sources.

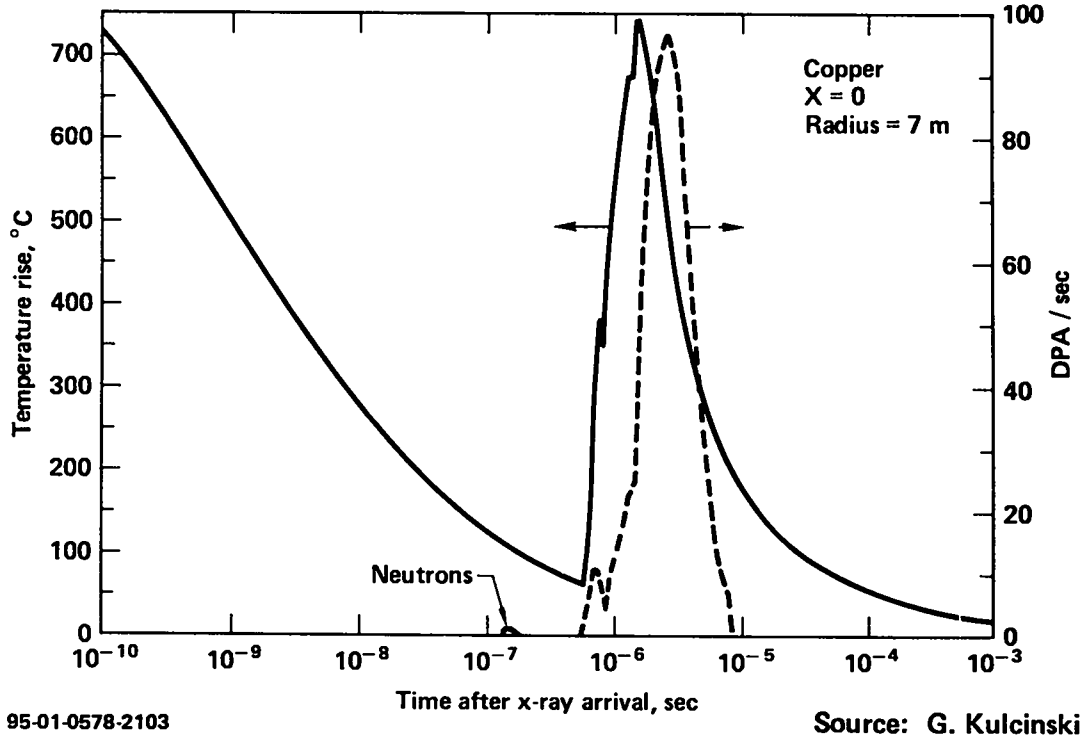

Fig.4 Thermal Response and Displacement Rate of Copper Located 7 m from a 100 MJ Microexplosion.

of high damage rates and high temperature transients will cause a higher surface recession rate due to sputtering and evaporation in an ICFR than in a MCFR.

The effects of the radiation damage on fatigue properties of various material is important for ICFR design because of the cyclic nature of the structural stresses. This complex problem of synergistic temperature, displacement production and stress excursion is very difficult to analyze.

Material Selection Considerations for Inertially-Confined Fusion Reactors

Fusion represents a potential, inexhaustible, environmentally acceptable energy source. Thus, materials selected for fusion reactors must be available in the United States in abundant quantities at reasonable cost. These materials must have low extraction and production hazards. They must also have low activation cross-sections to neutrons and they must be capable of performing their functions for a long period of time to minimize waste disposal problems.

The first wall of an ICFR must absorb the short-ranged microexplosion energy and transmit the neutrons to the reactor blanket. Thus, the first wall must cope with high energy densities, cyclic stresses and the surface and bulk effects of radiation damage.

For first wall materials, there are several parameters that should be minimized to reduce the temperature rise and stress per shot from the microexplosion energy deposited within the first wall. From Eqs. (1) and (5), the product of the Gruneisen constant and energy attenuation coefficient, $\Gamma\mu$, should be minimized to reduce the amplitude of the stress pulse. From Eqs. (1) and (4), the ratio of the energy attenuation coefficient to the specific heat at constant volume μ/C_v, should be minimized to reduce the amplitude of the temperature pulse. Generally, for x-rays and pellet debris, this involves using materials of low atomic number.

The blanket of a fusion reactor must moderate and transfer the fusion neutron energy and breed tritium. The blanket materials must cope with bulk radiation damage effects, corrosion of structural material by the blanket coolant, and cyclic stresses.

For blanket materials, lithium metal, alloys and compounds must be used to furnish the tritium breeding for the fuel cycle. Most inertially confined fusion reactors use a liquid lithium breeding blanket and circulate the lithium through heat exchangers such that the energy is transferred to a secondary fluid. Two disadvantages of using liquid lithium are the large pressure pulses produced in the blanket structures due to the rapid deposition of the neutron energy in the lithium, and lithium corrosion of blanket structural materials.

The SOLASE concept uses Li_2O pellets as both the tritium breeding material and the neutron energy transport medium.[11] Thus, the pressure pulses produced in the pellets by the neutron energy deposition are not transmitted to the graphite structure, and the corrosion problem is mitigated.

For structural materials, ferritic steels can be used in an ICFR because of the lack of high magnetic fields. These steels are more radiation damage resistant than the austenitic stainless steel, and have good resistance to corrosion from lithium up to temperatures of 750 K. The use of ferritic steels that contain only small amounts of chromium should be less costly and dependent on foreign sources than the austenitic stainless steels or refractory metals.

Other considerations in the selection of materials for ICFRs are discussed in the literature.[12,13]

Cavity Environment Effects on the First Wall and Blanket

The cavity of an ICF reactor can operate at pressures limited only by the requirements of the driver beam transmission. Thus, the ambient cavity conditions can be used to modify the microexplosion energy release forms and spectra prior to the energy deposition in the first wall. The effects of the ambient cavity on the energy release forms are shown in Table III.[14]

These various cavity environments have been proposed to decrease the deleterious effects of the microexplosion on the reactor structure to increase the first wall energy flux for higher power density fusion plants, or to increase the wall lifetime for a given first wall flux.

Table III Effects of ambient cavity conditions on fusion-pellet energy release mechanisms.[14]

Cavity "atmosphere"	X-rays	Neutrons	High-energy alpha particles	Plasma debris
Vacuum	No effect	No effect	No effect	No effect
Ambient gas	Some attenuation	No effect	Attenuation	Energy transfer
Vapor	Attenuation	Little effect	Attenuation	Energy transfer
Liquid	Absorption	Attenuation and absorption	Absorption	Energy transfer
Magnetic fields	No effect	No effect	Diversion possible	Diversion possible

Source: T.G. Frank

Reactor concepts based on the various cavity environments will be discussed by Booth.[14-17]

The HYLIFE converter concept[18] is described below to illustrate the use of cavity environmental effects to mitigate the radiation damage problems to achieve high reactor power densities and long component lifetimes.

The High Yield Lithium Injected Fusion Energy (HYLIFE) Converter

The HYLIFE concept, shown in Fig.5, is a continuously renewable first wall. It features a thick blanket of liquid lithium jets that protects the first structural wall, allowing it to last for the useful life of the plant. Besides moderating neutrons, the jets also absorb the photons (x-rays and reflects laser light) and pellet debris (alpha particles, unburnt fuel, and other pellet material). The majority of the fusion energy is deposited in the liquid lithium, which serves as the primary coolant, fertile material for tritium breeding, and first wall.

The 1.0 m-thick lithium blanket produces a softer and less intense neutron spectrum on the structure. This softer spectrum results in less radiation damage to the structural material. The absence of structure in the blanket allows a tritium breeding ratio greater than unity for a blanket thickness of 0.6 m.

The primary neutron damage mechanisms are atomic displacements and gas production (primarily helium). The damage limits for 316-SS at an operating temperature of 500°C are estimated to be 150 displacements per atom (dpa) and 500 atomic parts per million (appm) helium. For an unprotected first wall of 316-SS, the displacement damage rate is $\sim$ 10 dpa per full power year, and the helium production rate is $\sim$ 220 appm per full power year at a neutronic wall loading of 1 MW/m^2. The damage limits for He production would thus be reached in only 2.3 years at this wall loading. The allowable first-wall fluence increases exponentially with lithium thickness. A 0.4 m thickness of lithium is required to reduce neutron damage to the point where the first structural wall could last for 30 years at 1 MW/m^2 (at 70% capacity factor).

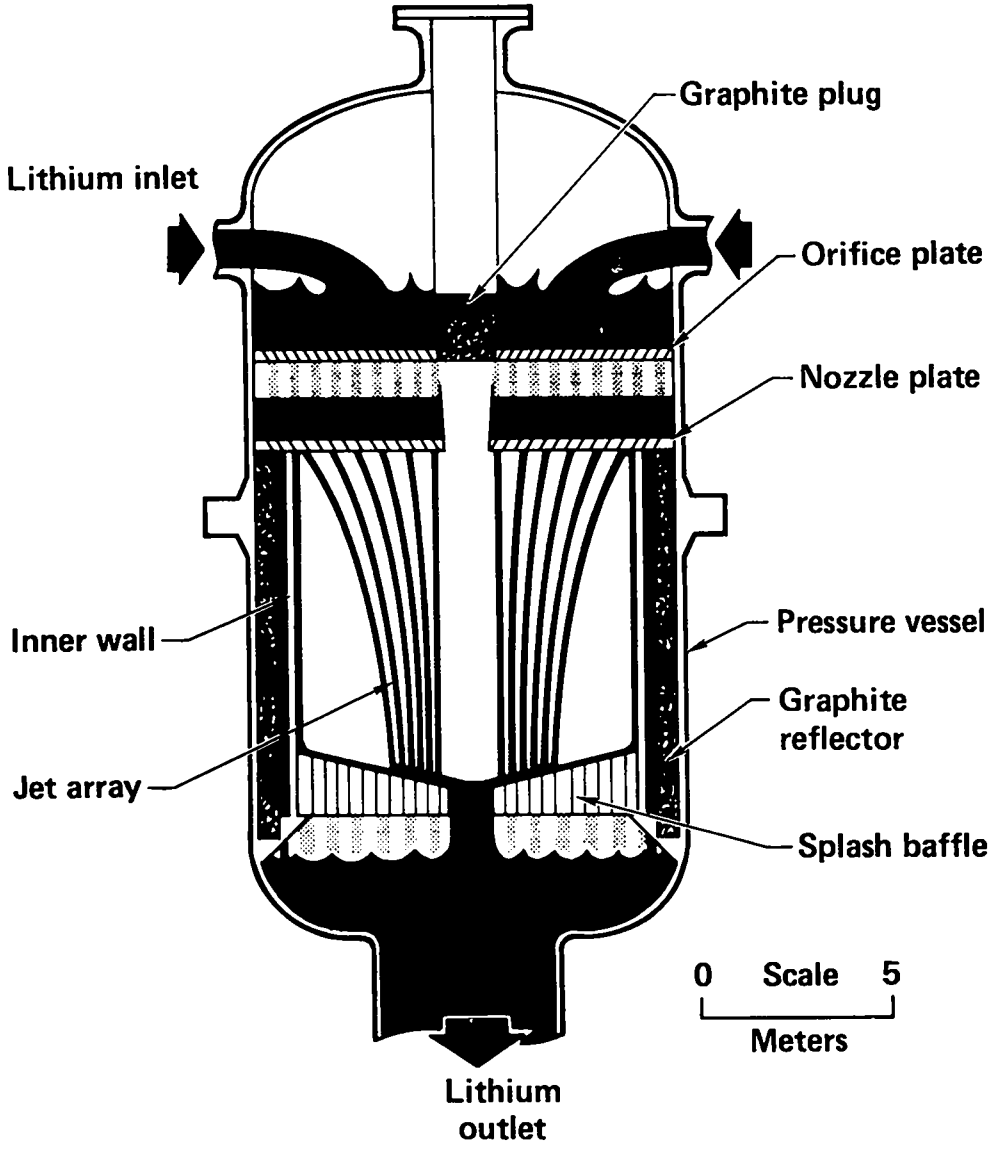

Fig.5 The HYLIFE Converter Concept.

A conceptual HYLIFE converter is being designed by a team including LLL, Energy Technology Engineering Center, Rockwell International-Energy Systems Group, and Bechtel National. A preliminary configuration includes a 1-m-thick blanket with an inner radius of about 0.5 m. The first structural wall, of ASTM-A-387-67 Group II, Grade D ferritic steel, is located 5 m from the 2700 MJ microexplosion. This reactor, operating at 1.1 hertz will have a power density of about 3 MW/m^3 compared to a power density within a BWR vessel which is about 8 MW/m^3.

The results of the design study to date show that:

- The HYLIFE concept can be operated with pulsed thermonuclear yields of several thousand megajoules and power densities approaching those of an LWR.
- No replacement of the first-wall or blanket structure is required.
- The power to circulate the lithium is less than 1% of the gross power.
- The radioactive waste and biological hazard potential reduced by more than 10 fold over concepts without fluid walls.
- Common stainless or ferritic steels can be used for the reactor structure.

More detailed description of the HYLIFE converter concept design and analysis can be found in the literature.[18]

Conclusion

The materials problems in an inertially confined fusion reactor are different from those in a magnetically confined fusion reactor with the same time-averaged first-wall neutron energy flux. These differences are due to the arrival of the charged particles, x-rays, and neutrons in extremely short-time pulses in the low-duty cycle, inertially confined, laser-fusion reactor as opposed to the long-time pulse in the high duty cycle typical of the magnetically confined fusion reactors. However, the ICF reactors have more freedom in materials options than MCF reactors because of the absence of magnetic fields. In addition, since plasma contamination is not a problem in inertially confined fusion reactors, the fusion cavity can operate at pressures limited only by the require-

ments of driver beam transmission. Therefore, the fusion product energy release forms on the first structural wall can be altered in timing, intensity, and spectra. Judicious selection of the cavity environment and structural materials tailored to the specific laser-pellet system design and fuel cycle may result in reactor structural component lifetime on the order of the plant lifetime with reactor power densities near that of current fission reactors.

References

1. J.A. Blink, P.E. Walker, and H.W. Meldner, "Energy Partition and Neutron Spectra From Laser Fusion Reactor Targets," Trans. ANS 1977 Winter Meeting, 70, San Francisco (1977).
2. G.B. Zimmerman, Numerical Simulation of the High Density Approach to Laser-Fusion, Lawrence Livermore Laboratory Report UCRL-74811, (17 October, 1973).
3. J. Hovingh, "First Wall Studies of a Laser-Fusion Hybrid Reactor Design," Proc. 2nd Topical Meeting on the Technology of Controlled Nuclear Fusion, Vol.II, 765, Richland, Washington (1976).
4. R.K. Cole, Jr. BUCKL: A Program for Rapid Calculation of X-ray Deposition, Sandia Corporation Report SC-RR-69-855, (1970).
5. J. Hovingh and S.L. Thomson, "Energy Deposition from Microexplosion Particle Debris in the First Wall of an Inertially-Confined Fusion Reactor," Proc. 7th Symposium on Engineering Problems of Fusion Research, Vol.I, 162, Knoxville, TN, (October, 1977).
6. W.W. Engle, Jr., Users Manual for ANISN, Union Carbide Report K1963, (March, 1967).
7. S.L. Thompson, Improvements in the CHART D Energy Flow Hydrodynamic Code V: 1972/73 Modifications. Sandia Laboratories Report SLA-73-0477, (1973). See also S.L. Thompson and H.S. Lauson, Improvements in the CHART D Radiation Hydrodynamic Code II; A Revised Program, Sandia Laboratories Report SC-RR-71-0713 (1972).
8. T.O. Hunter, S.I. Abdel-Khalik, and G.L. Kulcinski, "Response of First Walls in Inertial Confinement Reactors to Thermonuclear Radiation," Proc. of IAEA Workshop on Fusion Reactor Design, Madison, Wisconsin (October, 1977).

9. G.L. Kulcinski, "Unique Materials Requirements for Laser Fusion Reactors," Proc. of the Third Topical Meeting on the Technology of Controlled Nuclear Fusion, 598, Santa Fe, NM (May, 1978).
10. T.O. Hunter and G.L. Kulcinski, "Surface Damage and Thermal Effects From Transient Thermonuclear Radiation in Inertial Confinement Fusion Reactors," Proc. of the Third International Conference on Plasma Surface Interaction in Controlled Fusion Devices, UKAEA Culham Laboratory, Abingdon, Oxfordshire, UK (April, 1978).
11. G.A. Moses, R.W. Conn and S.I. Abdel-Khalik, "The SOLASE Conceptual Laser Fusion Reactor Study," Proc. 3rd Topical Meeting on the Technology of Controlled Nuclear Fusion, 448, Santa Fe, NM (1978).
12. J.M. Williams and T.G. Frank, "Laser-Controlled Thermonuclear-Reactor Materials Requirements," Nucl. Technol., 22, 360, (June, 1974).
13. T.G. Frank and L.A. Booth, "Laser-Fusion Reactor Materials Problems Resulting from Fusion Microexplosion Emissions," J. Nuclear Materials, 63, 31 (1976).
14. L.A. Booth, D.A. Freiwald, T.G. Frank and F.T. Finch, "Prospects of Generating Power with Laser-Driven Fusion," Proc. IEEE, 64, 10, p.1460 (October, 1976).
15. I.O. Bohachevsky, J.J. Devaney, J.F. Hafer, and J.H. Pendergrass, "Inertial Confinement Fusion Reactor Cavity Phenomena," Proc. of the Third Topical Meeting on the Technology of Controlled Nuclear Fusion, 1167, Santa Fe, NM (May, 1978).
16. S.I. Abdel-Khalik, R.W. Conn, and G.A. Moses, "Engineering Problems of Laser-Driven Fusion Reactors," Nuclear Technology, 43, 7, (April, 1979).
17. J. Hovingh, "Overview of Inertial Confinement Fusion Reactor Designs," Proc. 13th Intersociety Energy Conversion Engineering Conference, 1353, San Diego, CA (August, 1978).
18. M. Monsler, J. Maniscalco, J. Blink, J. Hovingh, W. Meier, and P. Walker, "Electric Power From Laser Fusion: The HYLIFE Concept," Proc. 13th Intersociety Energy Conversion Engineering Conference, 2164, San Diego, CA (August 1978).

Presented at the First Workshop on Impact Fusion, Los Alamos, NM, July 10-13, 1979

Fluid Wall Reactor Systems for Impact Fusion

James R. Powell
Department of Nuclear Energy
Brookhaven National Laboratory
Upton, NY 11973

There has been considerable examination of blankets and power systems for magnetic and inertial fusion reactors, so that an assessment of similar systems for impact fusion reactors should emphasize the similarities and differences that can be expected, and in particular what advantages and disadvantages may be encountered.

Table 1 lists the functions required of (or by) impact fusion reactor vessels. As with other inertial fusion concepts, entry and guidance for the driver (hypervelocity pellets in the case of impact fusion) is necessary. The driver entrance requirements will probably be somewhat simpler than those for laser or particle beam drivers, since smaller entrance ports should be necessary, and final focusing elements (mirrors for lasers, magnets for particle beams) will not be needed. (Control over the pellet trajectory will probably be required, but this can be done by devices at some distance from the reactor vessel, with the final part of the trajectory in an empty, long transport tube.)

Pellet velocity requirements have not been defined, nor has the nature of the impact process. For example, one might have a relatively slow moving, massive target block (either following a trajectory determined by gravity or shot in by a separate, low velocity accelerator) that would be hit by one

or more ultra high velocity pellets. Alternatively, one might have two or more high velocity pellets impacting together. Tolerances on final pellet velocity and spatial position have not been defined, and may or may not be difficult to achieve.

The problem of absorption of very short, high intensity bursts of released energy is shared by all inertial fusion concepts. The principal differences between impact fusion and the laser and particle beam concepts will probably be in the amount of energy release. Even if impact fusion pellet explosions would be practical at the same minimum yield level as laser or particle beam pellet explosions (which does not appear to be the case so far--it seems likely that impact fusion will inherently require larger yields), pellet fabrication costs will probably dictate as large a yield as possible. It should be simpler and cheaper to obtain large yields with impact fusion, since, if the concept works, the accelerator should be cheaper than laser or particle beam systems. The question of an upper limit to yield in an impact fusion reactor vessel will be addressed later, but handling a yield of $\sim$ 100 GJ appears possible.

A significant difference between impact fusion and other inertial fusion concepts will be the response of the vessel to a miss (where the driver misses the target), misfire (where the driver hits the pellet, but no fusion yield occurs), or a fizzle (where a yield occurs, but much lower than expected). In each case, impact fusion appears to present a more difficult safety/containment problem than other drivers. Laser and particle beams will defocus to a considerable extent if they miss the target and should not damage the reactor vessel to the same degree as a 200 km/sec pellet. In the case of a misfire, with relatively massive target blocks hit by a non-fusioning pellet, the

problem of high velocity shrapnel will be a severe one. A misfire with laser/particle beams would be less serious because of the much smaller masses involved. A similar situation would hold for low yield fizzles.

Blanket options for impact fusion reactors are summarized in Table 2. The following concepts have been investigated as part of the U. S. inertial fusion program: 1. conventional and wetted-wall blankets for laser fusion reactors, 2. thick liquid-wall blankets for laser fusion (Hylife concept) and heavy-ion drivers (BAM concept), and 3. a no-leak blanket (NOEL) for magnetic fusion reactors, which appears desirable also for inertial fusion reactors. A combination of a liquid wall blanket backed by a no-leak outer blanket would appear to offer a high reliability blanket system.

Energy conversion to electricity and/or chemical products (e.g., synthetic fuels) is another required function for impact fusion reactors. The final function relates to the use of neutrons generated in the pellet explosions. If DT fuel pellets are used, then the burnt tritium must be replenished by absorbing neutrons in some lithium-bearing material with a tritium-producing neutron reaction (either Li^6 [n, α]T or Li^7 [n, $n^1\alpha$]T produce tritium). If DD is the primary fuel for the bulk of the pellets, then tritium requirements for a central ignition core can probably be met by processing the plasma "ash", and a tritium breeding blanket would not be necessary. In either case, excess fusion neutrons could be simply parasitically absorbed, releasing additional energy, or they could generate fissile material (U^{233} or Pu^{239}) by absorption in a fertile blanket (Th^{232} or U^{238}).

The remaining portion of this paper concentrates on the analyses of the fluid wall reactor systems for impact fusion.

Figure 1 shows the fluid wall BAM Concept initially proposed for heavy ion fusion reactors [1]. The pellet explodes in the center of a cylinder and is enclosed by a thick falling curtain of liquid metal or salt. The liquid wall is detached from the surrounding solid structural wall to prevent transmission of shock waves after the pellet explosion. The liquid wall at the cylinder ends is shown in contact with the solid structure. Shock effects should be much less at the ends; however, if they are still excessive, the liquid wall could be detached from its surrounding structure prior to the pellet explosion. For example, a pulsed magnetic field could drive the top and bottom sections inwards at an appropriate time before the pellet explosion so that the liquid would form a thick complete continuous shell around the pellet. Alternatively, a suitably timed discontinuous liquid flow could be used from the upper surface of the cylinder. The flow from the top of the cylinder would be interrupted for a short period and then resumed. Pellet(s) would then be injected into the resultant clear zone.

A pellet entrance tube will be necessary to prevent obstruction of the pellet trajectory by the liquid wall. The ends of such tubes will experience blast effects and may have to be periodically replaced. Since they are simple, non-cooled tubes of relatively small diameter (e.g., a few cm), their replacement should be relatively quick and cheap.

The deposition channels for the fusion energy release are schematically illustrated in Figure 2. Plasma debris and x-rays from the exploding pellet are stopped in a thin discontinuous inner spray zone of liquid metal. The discontinuity prevents a shock wave from propagating into the relatively thick liquid wall behind. Neutrons from the pellet explosion are attenuated and

degraded in energy by their passage through the liquid wall. As Hovingh [2] has shown, neutron shock heating effects in thick liquid curtains may cause spallation of high velocity drops from the outer liquid surface, which would then be driven into the surrounding structure. This effect can be eliminated by making the liquid curtain a set of discontinuous jets, as in the Hylife fluid wall concept.

In these analyses the effect of neutron shock heating is not considered. Bulk momentum and kinetic energy acquired by the liquid wall are calculated with three momentum components considered:

1. momentum transferred from the impacting plasma debris,
2. momentum acquired by evaporation of liquid from the inner zone of the liquid wall when pellet debris and x-ray energy is absorbed, and
3. momentum acquired by expansion of a thick liquid wall due to the pressure of the enclosed vapor resulting from mechanism (2).

The time scales for making these velocity components is very different, with $t\ (V_1) << t\ (V_2)$ as shown schematically in Figure 3. Generally, the magnitude of the velocity components is $V_3 >> V_1$.

The calculated liquid wall expansion velocities are upper limits to the the expansion velocity in an actual reactor system. To reduce neutron shock heating effects, as discussed above, the liquid wall will probably involve a set of discontinuous jets or sheets which will allow some vapor to move to velocity component (V_3) of the liquid wall.

Three candidates have been considered for the liquid curtain--lithium, flibe ($LiF \cdot BeF_2$), and lead (with a small amount of dissolved lithium for tritium breeding). The vapor pressures of these liquids are shown in Figure

4 as a function of temperature. The liquid temperatures that correspond to an operating pressure of $\sim 10^{-3}$ torr are 650°C for lead, 550° for flibe, and 460°C for lithium. An upper limit to pressure level in the reactor chamber for satisfactory entry of the hypervelocity pellets has not been determined; however, it should be substantially higher than 10^{-3} torr. The total weight of lead vapor impacted on a hypervelocity pellet traveling in 10^{-3} torr of lead vapor is 3×10^{-4} g/cm^2 of pellet per meter of travel, and impacts in flibe and lithium vapors will be an order of magnitude smaller. The kinetic energy delivered by impacting vapor will be $\sim$ 10,000 Joules/cm^2 at 200 km/sec. If the pellet is carrying frozen DT, some sort of thin heat shield will probably be required for protection. Substantially higher background pressures than 10^{-3} torr would probably be allowable from the standpoint of pellet integrity; however, the corresponding temperature of the liquid curtain probably would be too high from the standpoint of materials for piping and heat exchanger systems. Thus, practical operating temperatures for liquid lead, flibe, and lithium will probably be on the order of 500°C.

The intermittent energy release of the pellet explosions will produce a temperature rise on the order of 30°K in the liquid wall. The liquid then will flow to a thermal smoothing reservior (Figure 5) with sufficient capacity to smooth out the temperature fluctuations that result from the non-steady energy release. A continuous side stream will be drawn from the tank and circulated through a steam generator to produce steam for the power cycle. The outlet to inlet temperature differential for this stream will be on the order of 100°K. Additional small side streams will be withdrawn for recovery of the in-situ

tritium generated by neutron capture in the flowing liquid and for removal of corrosion products. In the lithium and flibe systems, the liquid wall will not be residually radioative, though dissolved corrosion products will be. Continual removal of such products (e.g., by cold trapping fused salt contacting, etc.) can reduce the radioactivity of the main liquid current to low levels. This will be advantageous for safety and maintenance purposes. Lead will have some non-removable residual activity due to formation of radioactive lead and thallium isotopes which will be difficult to separate. The amount of such activation will be small, however, on the order of a few thousand curies.

Table 3 compares design parameters for lead, lithium, and flibe liquid walls for the particular case of a 4 GJ pellet yield in a 5 meter diameter chamber, 10 meters long with a 0.5 meter thick liquid wall. The pressure of vapor generated by absorbed energy on the inner surface of the liquid wall is approximately 10 atm, for the three alternate liquid wall options. The response of the liquid wall in terms of outwards expansion velocity is quite different, however. A heavy liquid wall, e.g., lead, has a much smaller outward velocity (0.64 m/sec) than a light liquid wall, e.g., lithium (10.5 m/sec), because of the much higher mass to be accelerated. The vapor condensation time was taken to be 2 milliseconds in all cases. As will be seen later, this appears to be an upper limit to vapor condensation time, and condensation may be more rapid. In this case, the outward expansion velocity will be considerably less than the values shown in Table 3.

Figure 6 illustrates the kinetic energy carried by a unit volume of the expanding liquid wall for the three candidate liquids as a function of pellet yield (in these cases, $\sim$ 1/3 of the pellet yield is taken to be in the form

of x-rays and plasma debris; this appears to be representative of the energy partitioning when pellets are compressed to the requisite ρR for ignition). The kinetic energy per unit volume in heavy liquid walls, e.g., lead, is over an order of magnitude smaller than that for light liquid walls, e.g., lithium; and the impact pressures on surrounding structures will be correspondingly lower for heavy walls than for light walls. From the point of view of impact pressure, pellet yields well above 10 GJ appear feasible even with relatively small reactor vessels.

Figure 7 shows the effect of reactor vessel size on expansion velocity of a liquid lead wall for a range of pellet yields from 0 to 10 GJ. Increasing reactor vessel radius to 4 meters allows one to absorb 100 GJ of pellet yield with an outward velocity of $\sim$ 5 meters per sec in the liquid wall. This is likely though a somewhat larger vessel for yields over $\sim$ 50 GJ would probably be desirable.

The effect of pellet mass on expansion velocity of the liquid wall is shown in Figure 8 for an upper and lower extreme of pellet mass, i.e., 3 grams and 3 kilograms. There is only a minor difference in expansion velocity between the two cases. This results from the relatively small contribution to outwards wall velocity from the momentum of the pellet debris; evaporation and pressure effects account for virtually all of the expansion effects.

The time required to condense the vapor produced when pellet debris and x-rays are absorbed on the inner surface is an important factor in determining expansion velocity. Figure 9 illustrates how much condensation area is required as a function of pellet yield. Effects due to finite sound speed are neglected, with the vapor and drops of the condensing liquid assumed to be intimately mixed.

Heat transfer coefficients are very high for pure vapors condensing on clean surfaces. The principal factors determining condensation rate will be the thermal conductivity, diameter, and number of liquid drops available, with the rate determining process being thermal conduction in the drop. Based on analytical solutions for the time dependent temperature profile in the drops, an effective time for condensation can be derived, assuming no interfacial heat transfer resistance on the condensing surface. The condensation is assumed to be complete when the time dependent surface temperature drops to a value corresponding to 95 percent condensation of the vapor. For liquid lead, a relatively thin layer of drops is sufficient to condense vapor quite rapidly. A 2 cm (equivalent thickness) layer will condense the vapor resulting from a 6 GJ yield in $\sim$ 1 millisecond, for example. The parametric analyses in this paper typically assume a constant condensation time of 2 msec, which should be easy to achieve. In practice, it is likely that the effective condensation time would be substantially less than 2 msec for pellet yields in the range of 0 to 10 GJ. This would result in somewhat smaller expansion velocities than predicted in this paper. For very high pellet yields, on the order of 100 GJ, achieving condensation times of 2 msec will require condensing layers on the order of tens of centimeters in thickness, which is probably achievable. Fused salt liquid walls will have much longer condensation times because of the lower thermal conductivity of fused salt. This will tend to make expansion velocity for flibe walls considerably larger than indicated in these analyses. Liquid lithium walls should have comparable or somewhat faster condensation times than liquid lead walls.

Figure 10 illustrates the comparative breeding ratios for lead, lithium, and flibe as a function of liquid wall thickness. All breed satisfactorily, with lead having the highest breeding ratio. The liquid wall region is backed up by a graphite block structure, which is cooled by the same fluid as the liquid wall. (Uncanned graphite is chemically compatible with lead and flibe but must be canned with a suitable material, e.g., 316 stainless steel, if used with lithium.)

The liquid lead stream has a small concentration of lithium--6 for tritium breeding, by means of the (n, α) T reaction. The high tritium breeding ratios for lead result from the high (n, 2n) cross-section of lead and the relatively low cross-sections for parasitic neutron reactions like (n, p) and (n, α). Very low Li^6 concentrations, i.e., $\sim$ 1 part in 5000, are adequate for good tritium breeding (Figure 11). The ability to adjust tritium breeding is an important advantage for lead. If the impact fusion reactor is only a power producer, it is probably undesirable from an environmental and proliferation standpoint to produce large excess amounts of tritium. The tritium breeding ratio should be only slightly greater than one (e.g., $\sim$ 1.05) to allow for the necessary buildup of tritium inventory for additional reactors in an expanding fusion economy. In a steady state economy the tritium breeding ratio would approach 1.00 With lithium and flibe liquid walls, adjustment of T/n to 1.0 could only be done by using very thin liquid walls, which would seriously degrade their protective capability against blast and radiation damage. With lead walls, the tritium breeding ratio could be adjusted to any desired value by using the appropriate Li^6 concentration. Similar arguments apply to hybrid impact fusion reactors where one would capture the excess neutrons in a fertile material (e.g. U^{238}

or Th^{232}) to produce makeup fissile material for an LWR nuclear economy. Here one would want to avoid extra captures in Li so that production of fissile material could be maximized.

In practice, natural lithium would probably be dissolved in lead rather than Li^6. This would eliminate the cost of isotopic separation. The total lithium concentration would then be an order of magnitude higher than indicated in Figures 10 and 11. At the low concentrations of Li^6 (< 0.1 percent), use of natural lithium should not cause any significant alteration in the chemical or physical properties of the lead coolant. The activity coefficient of lithium lead is very low, and it is expected that the lead-lithium coolant will essentially behave like pure lead.

Tritium extraction studies with solid lithium lead alloys have shown that tritium holdup times are typically a few minutes for diffusion of tritium from solid particles at $\sim$ 500°C (characteristic particle sizes of $\sim$ 1 mm). The lithium concentration in the liquid walls will be much smaller than in the solid alloys (e.g., Li_7Pb_2 is a typical alloy), which will result in much lower lithium activity. This should substantially increase the tritium extraction rate. Extraction could be carried out either by spraying liquid lead into a low pressure cavity or by sparging the liquid with an inert gas, e.g. He, from which it could be trapped out.

The fraction of energy directly absorbed in the liquid wall and the liquid coolant in the graphite structure behind the liquid wall is shown in Figure 12 as a function of liquid wall thickness for lead, lithium, and flibe. Lead and flibe exhibit the highest capture fractions, on the order of 98 percent at a liquid wall thickness of 50 cm. The high attenuation of absorbed energy should greatly reduce the cyclical temperatures and stresses in the solid structures of the reactor vessel as well as the radiation damage (dpa, in-situ He generation).

Pumping power fractions for the liquid wall candidates are shown in Figure 13 as a function of pellet yield. An upper limit to pumping power fraction is probably on the order of 0.06, pumping power to reactor thermal power. (This is equivalent to a recirculating power of 15 percent for a power cycle efficiency of 40 percent. The mechanical pumping energy is recovered as heat after the liquid falls through the reactor vessel, and this recovery essentially compensates for mechanical inefficiencies in the liquid metal pumps.)

At low pellet yields, pumping power becomes unacceptably high. However, the lower limit for pellet yield for lithium and flibe of < 1 GJ will be very easy to contain. For a liquid lead wall, the lower limit is $\sim$ 4 GJ with full flow of the lead and a pulse repetition rate of 0.3 Hz. The effective limit can be reduced either by using a thinner lead wall (< 0.5 m), intermittent flow (in Figure 13, 50 percent flow indicates a flow shutoff after the pellet explosion and flow reestablishment 1.5 sec prior to the next explosion), a smaller reactor vessel (which appears acceptable for the lower yields), or a higher pulse repetition rate (e.g., $\sim$ 1 Hz instead of 0.3 Hz). For large pellet yields, $\geq$ 10 GJ, there appears to be no problem in keeping pumping power below the acceptable limit.

In summary, the liquid wall reactor approach appears to be very attractive for impact fusion reactors. It has the following significant advantages:

1. It can handle large pellet yields, probably up to $\sim$ 100 GJ,
2. It minimizes blast and radiation damage to solid structures by attenuation of neutrons and pellet debris through the liquid wall,
3. High tritium breeding ratios are possible if desired (with lead and lithium), and are adjustable to a range of desired values (with lead),

4. Power cycle efficiencies of ∿ 40 percent should be achievable, and
5. Shrapnel from pellet misfires can be safely caught in the liquid wall. Solid first walls would probably suffer unacceptable damage if a pellet misfire occurred.

Some type of solid blanket structure will still be required behind the liquid wall. While the blast and radiation damage to this solid structure will be far less than it would experience in the unprotected state, severe damage can still be anticipated. Effects of shock heating, thermal cycling, dpa, and in-situ helium generation will occur with the consequent possibility of local structural failure and coolant leakage. Such failure and leakage should not be as serious for impact fusion as magnetic fusion since much higher pressure levels can be tolerated in impact fusion reactors. However, it is still desirable to prevent local failure of the blanket and to minimize consequences if it occurs.

A blanket concept that cannot leak has been proposed for magnetic fusion reactors, the NOEL--No External Leak--Blanket. Analyses and tests of the blanket concept indicate that it is feasible and will prevent coolant leaks even when relatively large cracks and failures occur in the blanket first wall and structure. Figure 14 illustrates the basic principle of the NOEL blanket. A frozen layer of material "A" is produced behind the solid structural wall at the left. The frozen layer is maintained by a set of imbedded coolant tubes carrying a coolant "B" which is below the freezing point of "A". There is an energy flow into the frozen layer from the structural wall and from a liquid zone of "A" at the right. Neutron and gamma heating in the blanket interior provide the two energy flows (for those fusion reactors without an inner liquid wall, radiant and ion energy deposited on the first wall also contribute to energy flow # 1).

The frozen layer of "A" prevents leakage into the reactor chamber even if extensive through cracks and failures appear in the first wall. The pressure on the liquid "A" zone is maintained at a higher level than the coolant pressure "B" so that the coolant cannot leak even if cracks develop in the tubes that maintain the frozen layer.

Various blanket designs embodying the NOEL concept have been investigated. Figure 15 shows a design with lithium-lead (Li_7Pb_2) as material "A" and flibe as the coolant "B". The design in Figure 15 is for a magnetic fusion reactor with a first wall load of 2 MW(th)/m^2. Placement of the coolant tubes will determine the thickness of the liquid "A" zone; in the case of an MFE reactor with no liquid wall and a relatively high wall loading, two rows of coolant tubes will probably be required with the second some 10 to 15 cm behind the first. (The placement of the second row at 6.7 cm in Figure 15 causes a completely solid zone between the rows, while using only one row results in an excessively high temperature in the molten "A" zone.) For impact fusion reactors with a liquid wall, one row of tubes behind the module structural wall will probably be ample. There will be considerable attentuation of the pellet energy by the liquid wall; however, liquid wall systems generally will have quite high equivalent wall loads (e.g., $\sim$ 10 to 21 MW(th)/m^2), so the wall load in the structure behind the liquid wall will not be too much less than that in a standard MFE reactor. The materials for a NOEL blanket for an impact fusion reactor would probably be lead with a small amount of Li for material "A" and water as the coolant "B". The higher temperature performance of the design shown in Figure 15 would not be required since most of the fusion energy would be extracted by the liquid wall.

The NOEL concept has been successfully tested in a simulated blanket module using a low melting liquid metal alloy (Wood's metal) as material "A" and water as coolant "B". The module did not leak into the surrounding vacuum even when 1/8 inch diameter holes were drilled through the first wall of the module. The cracks that might occur in an actual NOEL blanket module will probably be longer but much narrower than the test holes, and satisfactory performance is expected for NOEL blankets in a fusion environment.

REFERENCES

1. Powell, J. R., et al., "A Liquid Wall Boiler and Moderator (BAM) for Heavy Ion-Pellet Fusion Reactors," Brookhaven National Laboratory, BNL-50744 (November 1977).

2. Hovingh, J., et al., "Response of a Lithium Fall to an Inertially Confined Fusion Microexplosion," Proc. 3rd Topical Meeting on the Technology of Controlled Nuclear Fusion, Vol. 1, P. 308, Santa Fe, NM (1978).

ACKNOWLEDGMENT

The author wishes to express his grateful appreciation to Miss Pamela Walton for preparation of the manuscript and to Mr. Don Mackenzie for his helpful comments.

TABLE 1

PRINCIPAL FUNCTIONS OF IMPACT FUSION REACTOR VESSELS

- PROVIDE ENTRY AND GUIDANCE FOR HYPERVELOCITY PELLETS
- ABSORB RELEASED ENERGY
- CONVERT ABSORBED ENERGY TO ELECTRICAL POWER AND/OR CHEMICAL PRODUCTS
- ABSORB NEUTRONS TO GENERATE USEFUL NUCLEAR MATERIALS
  - TRITIUM
  - FISSILE MATERIALS

TABLE 2

BLANKET OPTIONS

- CONVENTIONAL MODULAR BLANKET
- WETTED WALL BLANKET
- THICK (~ 50 TO 100 CM) FLUID WALL BLANKET
- NOEL - NO LEAK BLANKET
- MODERATELY THICK (~ 10 TO 20 CM) FLUID WALL BLANKET FOLLOWED BY CONVENTIONAL OR NOEL BLANKET

TABLE 3

TYPICAL BAM REACTOR PARAMETERS

CONDITIONS: $F_P = 1/3$
$R_W = 2.5$ M
$\Delta R_W = 0.5$ M
$E_P = 4$ GJ
$L_W = 10$ M
$\Delta T_W = 2$ MILLISEC

	LEAD	LITHIUM	FLIBE
DENSITY, KG/M^3	10,000	500	1900
M_{LW}, KG	1.1×10^6	5.51×10^4	2.09×10^5
λ_W, J/KG	9.4×10^5	22.7×10^6	3.1×10^6
KG VAPORIZED	1415	58.6	214.5
G MOLES VAPORIZED	6830	8470	5810
P_V (T = 0), ATM	8.65	11.4	7.37
V_{TH}, M/SEC	450	2600	1120
V_1, M/SEC	2.6×10^{-3}	0.051	0.0135
V_2, M/SEC	0.289	1.38	0.57
V_3, M/SEC	0.346	9.12	1.55
V_T, M/SEC	0.638	10.55	2.13

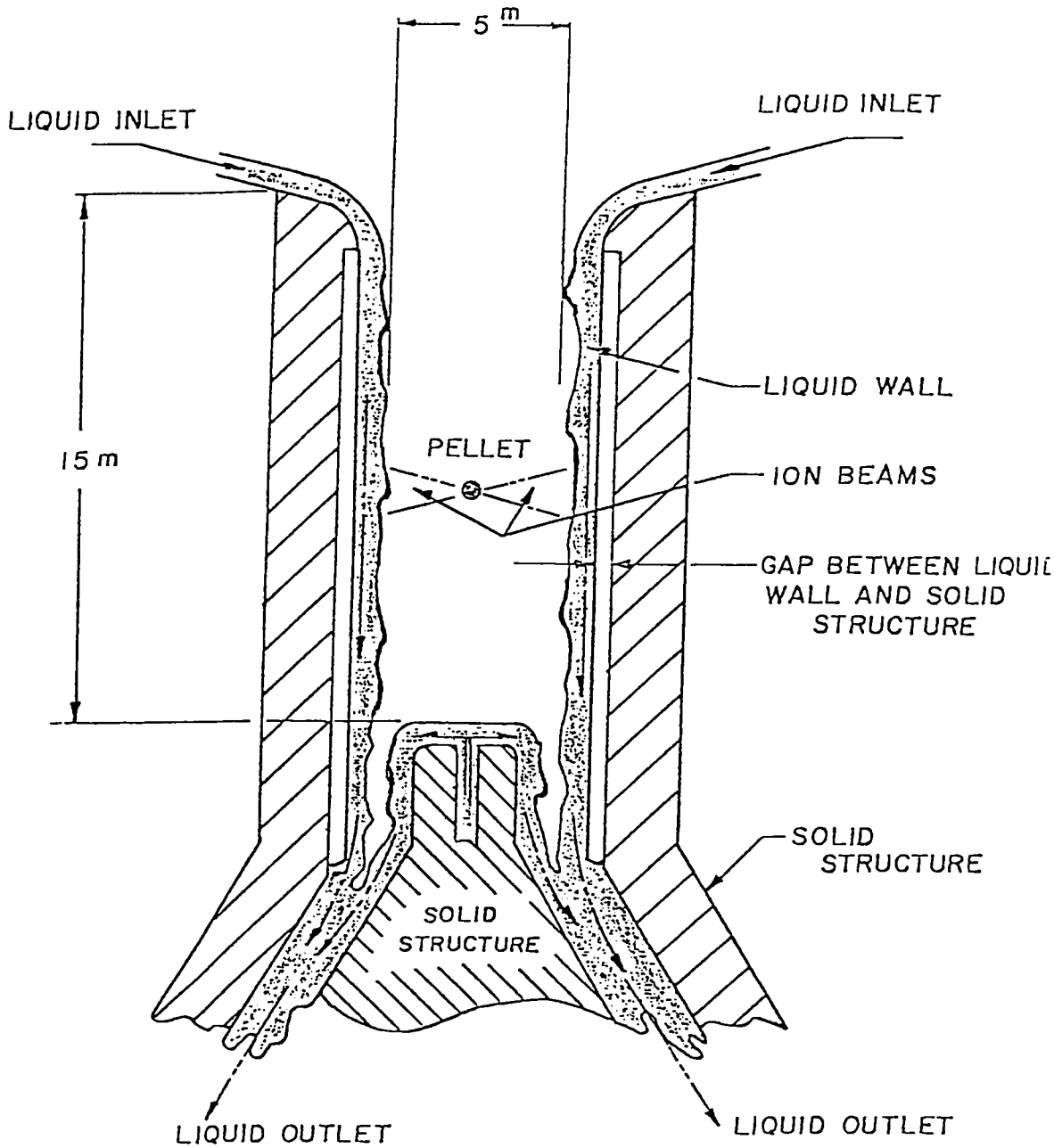

FIGURE 1

LIQUID WALL BOILER FOR PELLET FUSION SYSTEMS

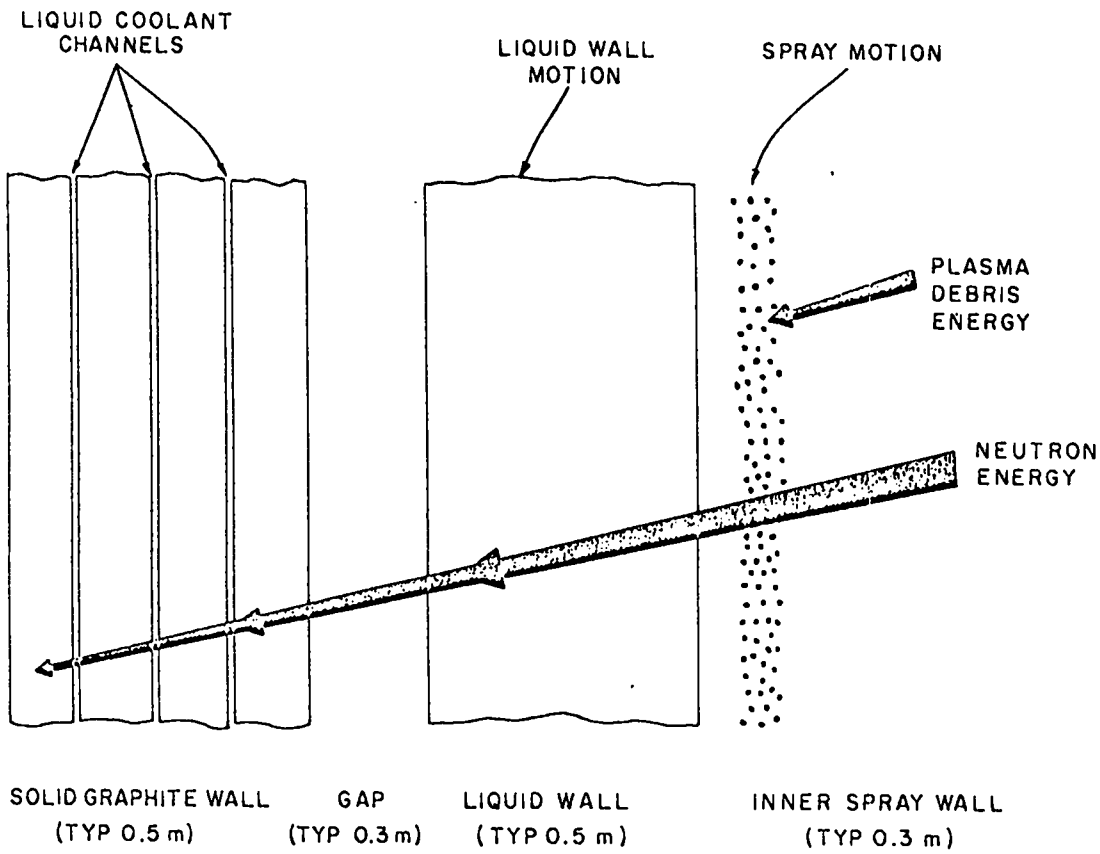

FIGURE 2

DETAIL VIEW OF LIQUID WALL

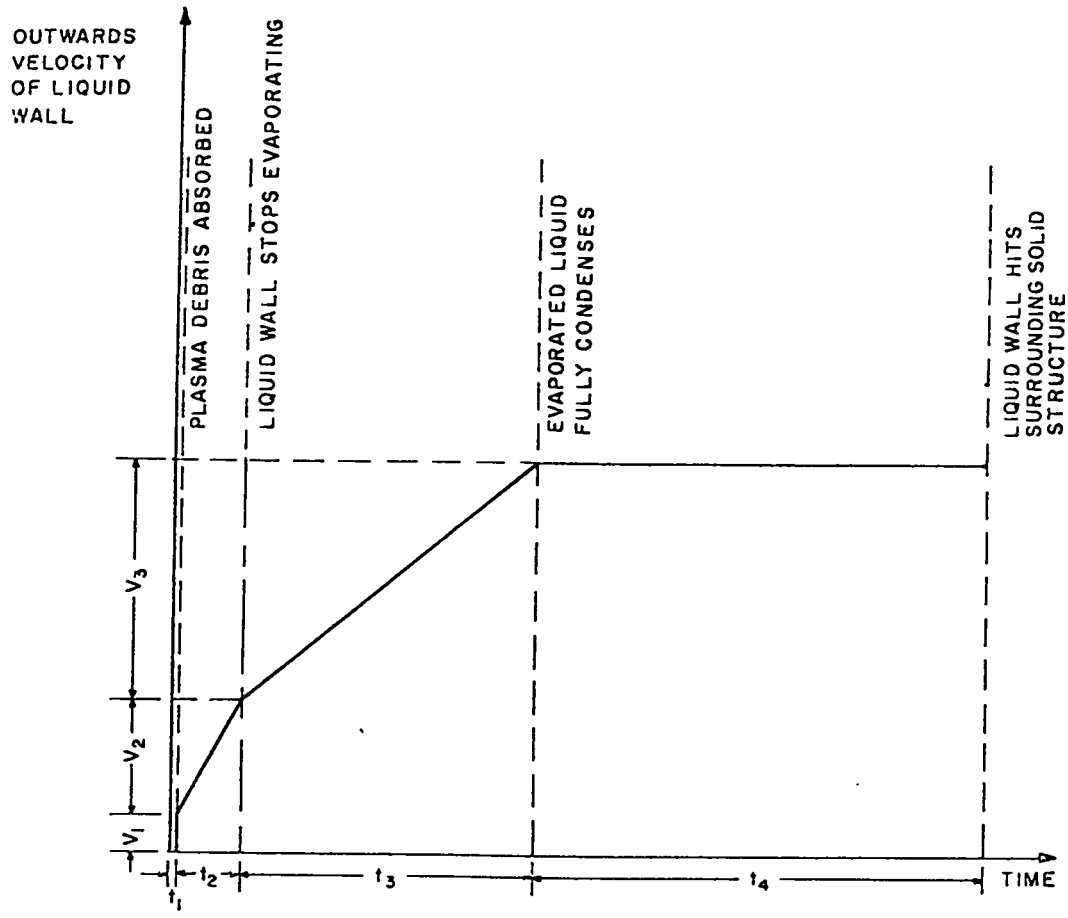

FIGURE 3

IDEALIZED EXPANSION OF LIQUID WALL
AFTER PELLET EXPLOSION

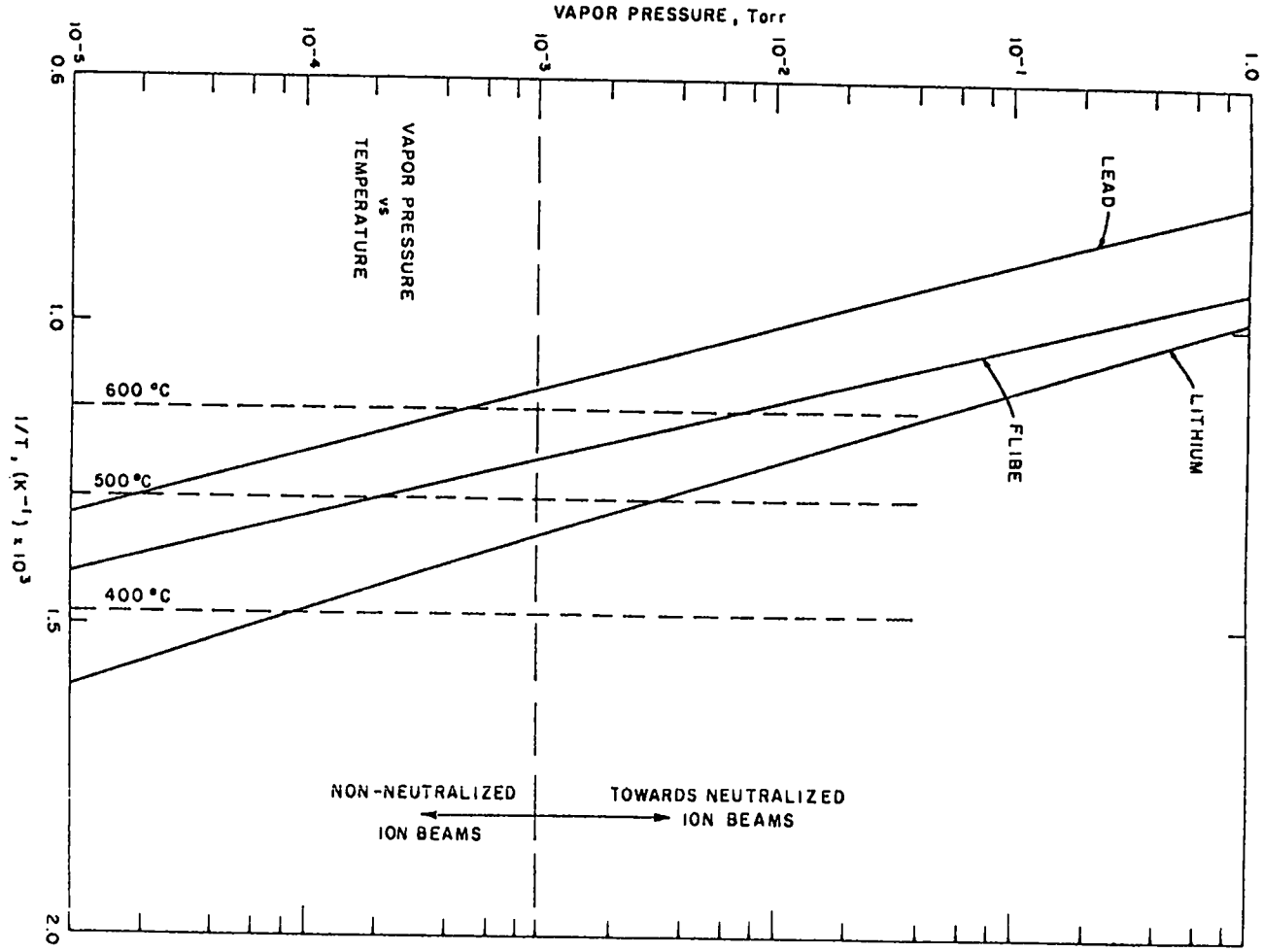
VAPOR PRESSURE, Torr
10⁻⁵
10⁻⁴
10⁻³
10⁻²
10⁻¹
1.0
0.6
1.0
1.5
2.0
1/T, (K⁻¹) x 10³
VAPOR PRESSURE vs TEMPERATURE
LEAD
FLIBE
LITHIUM
600 °C
500 °C
400 °C
NON-NEUTRALIZED ION BEAMS
TOWARDS NEUTRALIZED ION BEAMS

FIGURE 4

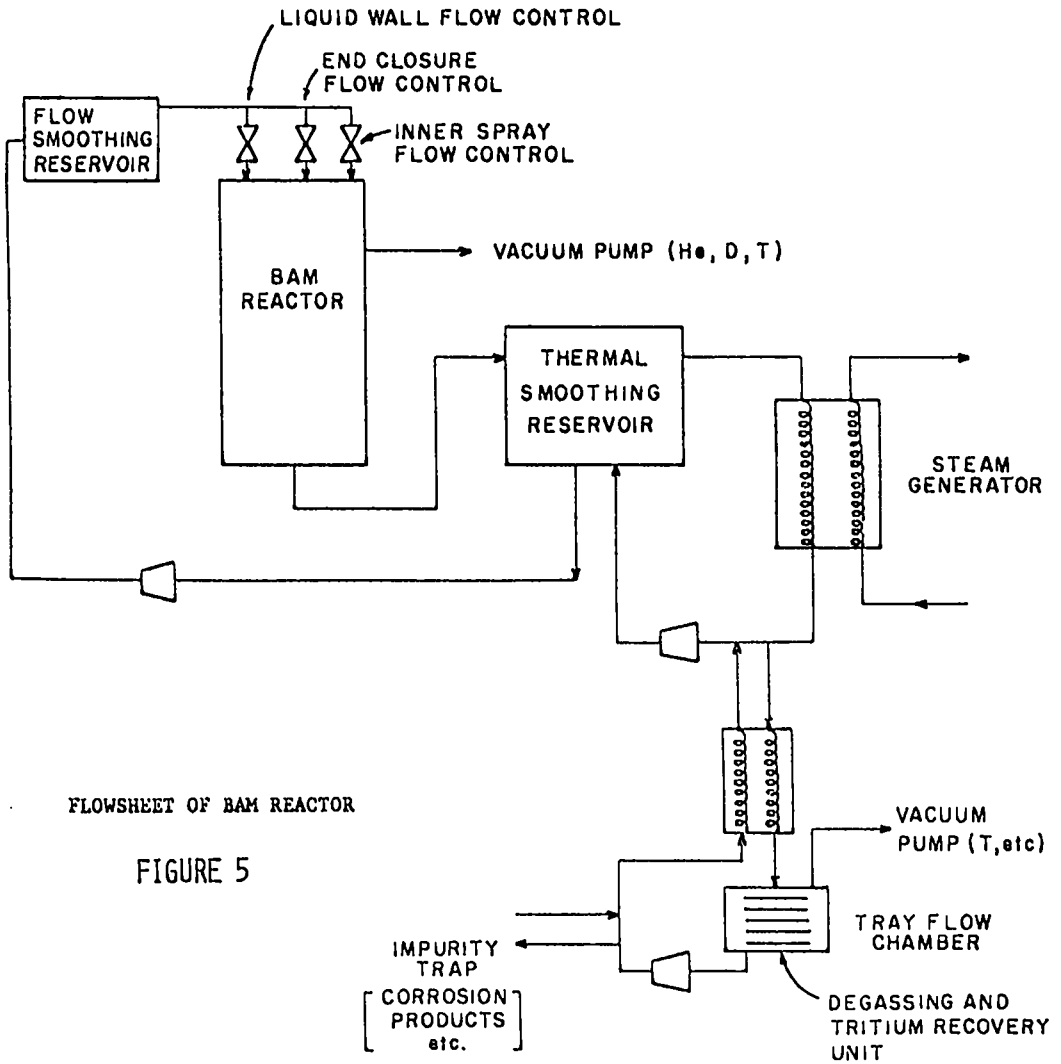

FLOWSHEET OF BAM REACTOR

FIGURE 5

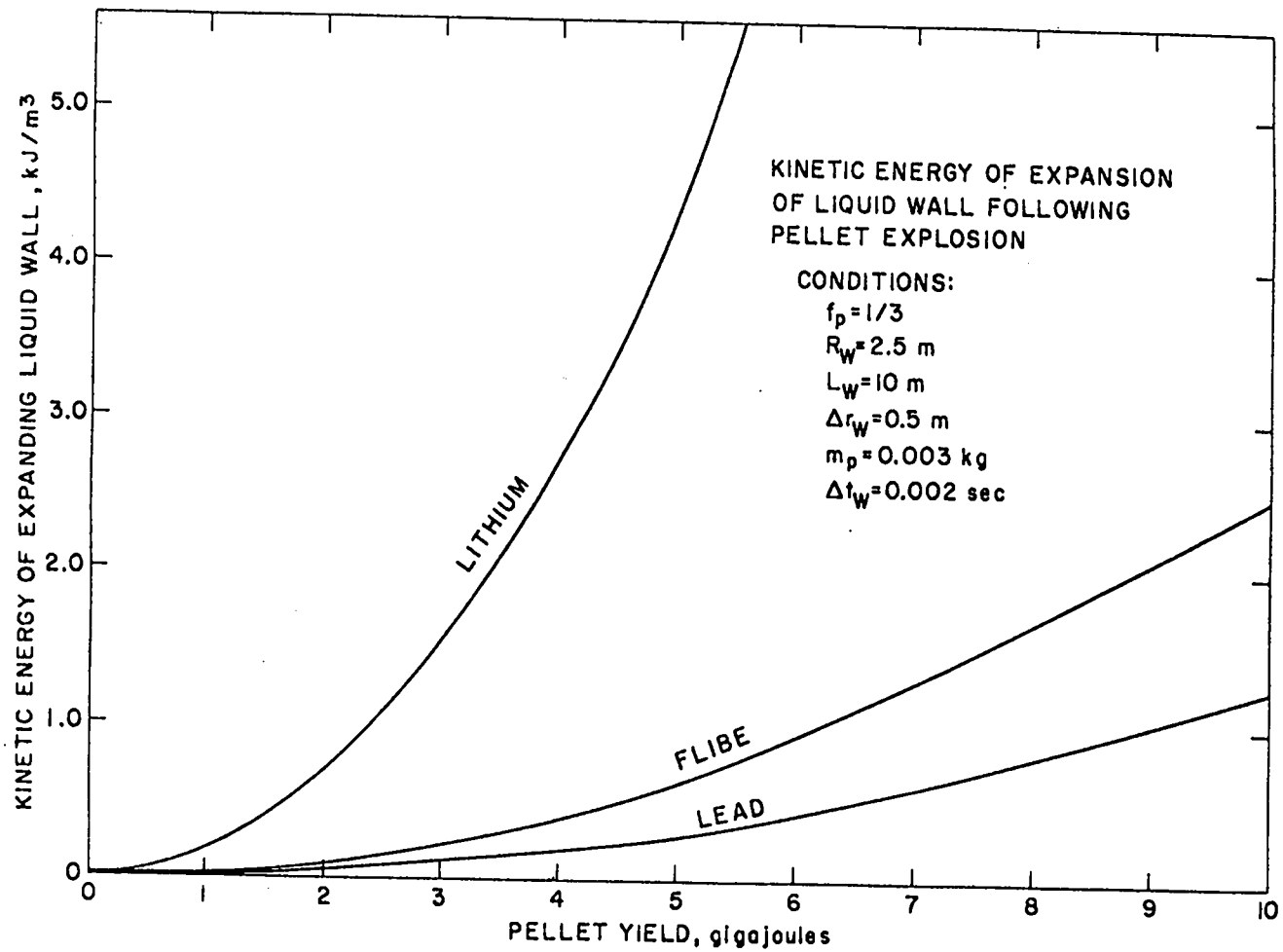
KINETIC ENERGY OF EXPANDING LIQUID WALL, kJ/m3
5.0
4.0
3.0
2.0
1.0
0
0
1
2
3
4
5
6
7
8
9
10
PELLET YIELD, gigajoules
LITHIUM
FLIBE
LEAD
KINETIC ENERGY OF EXPANSION
OF LIQUID WALL FOLLOWING
PELLET EXPLOSION
CONDITIONS:
$f_p = 1/3$
$R_W = 2.5$ m
$L_W = 10$ m
$\Delta r_W = 0.5$ m
$m_p = 0.003$ kg
$\Delta t_W = 0.002$ sec

FIGURE 6

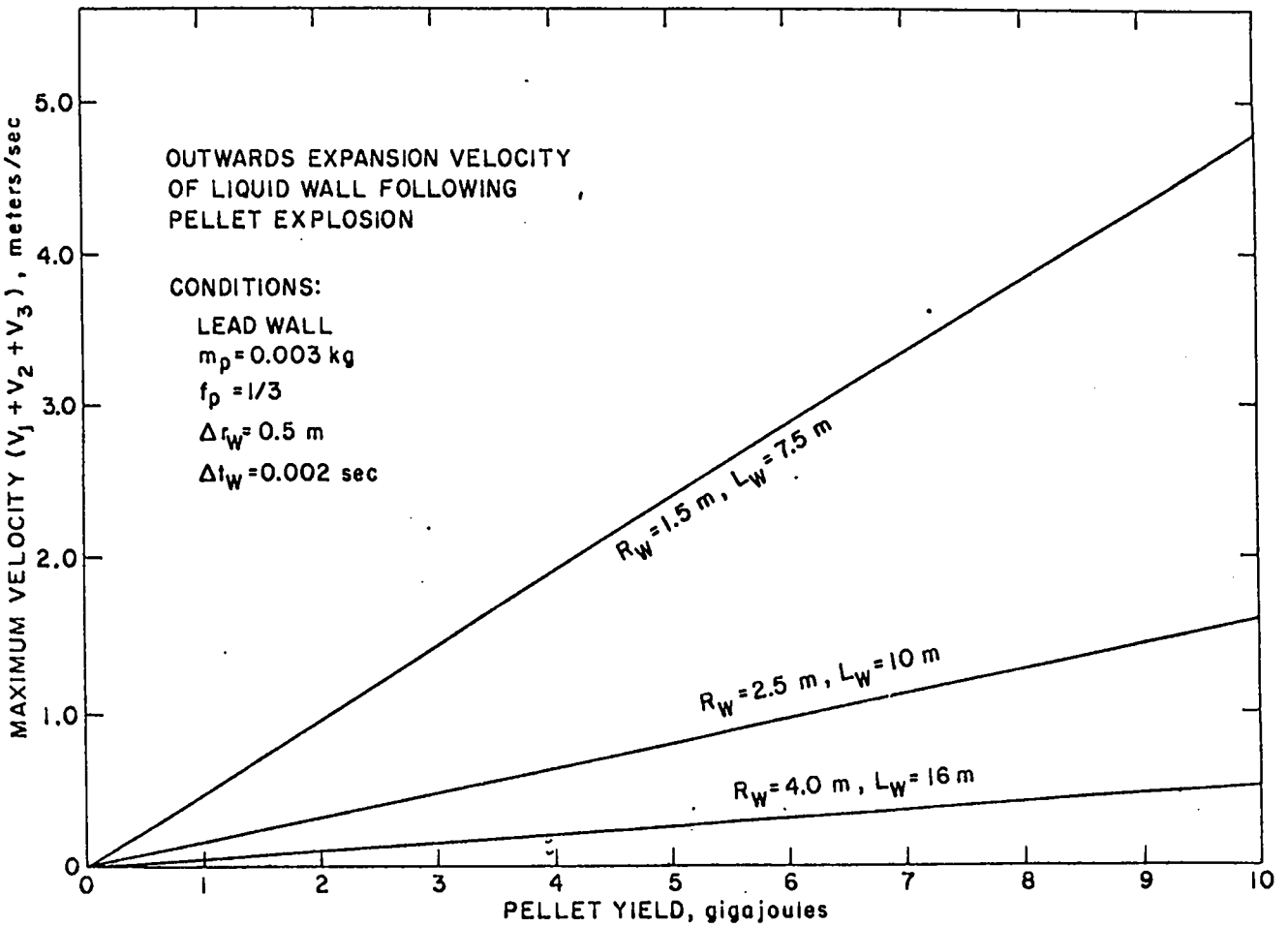
OUTWARDS EXPANSION VELOCITY
OF LIQUID WALL FOLLOWING
PELLET EXPLOSION
CONDITIONS:
LEAD WALL
m_p = 0.003 kg
f_p = 1/3
Δr_W = 0.5 m
Δt_W = 0.002 sec
R_W = 1.5 m, L_W = 7.5 m
R_W = 2.5 m, L_W = 10 m
R_W = 4.0 m, L_W = 16 m
MAXIMUM VELOCITY ($V_1 + V_2 + V_3$), meters/sec
PELLET YIELD, gigajoules
0
1.0
2.0
3.0
4.0
5.0
0
1
2
3
4
5
6
7
8
9
10

FIGURE 7

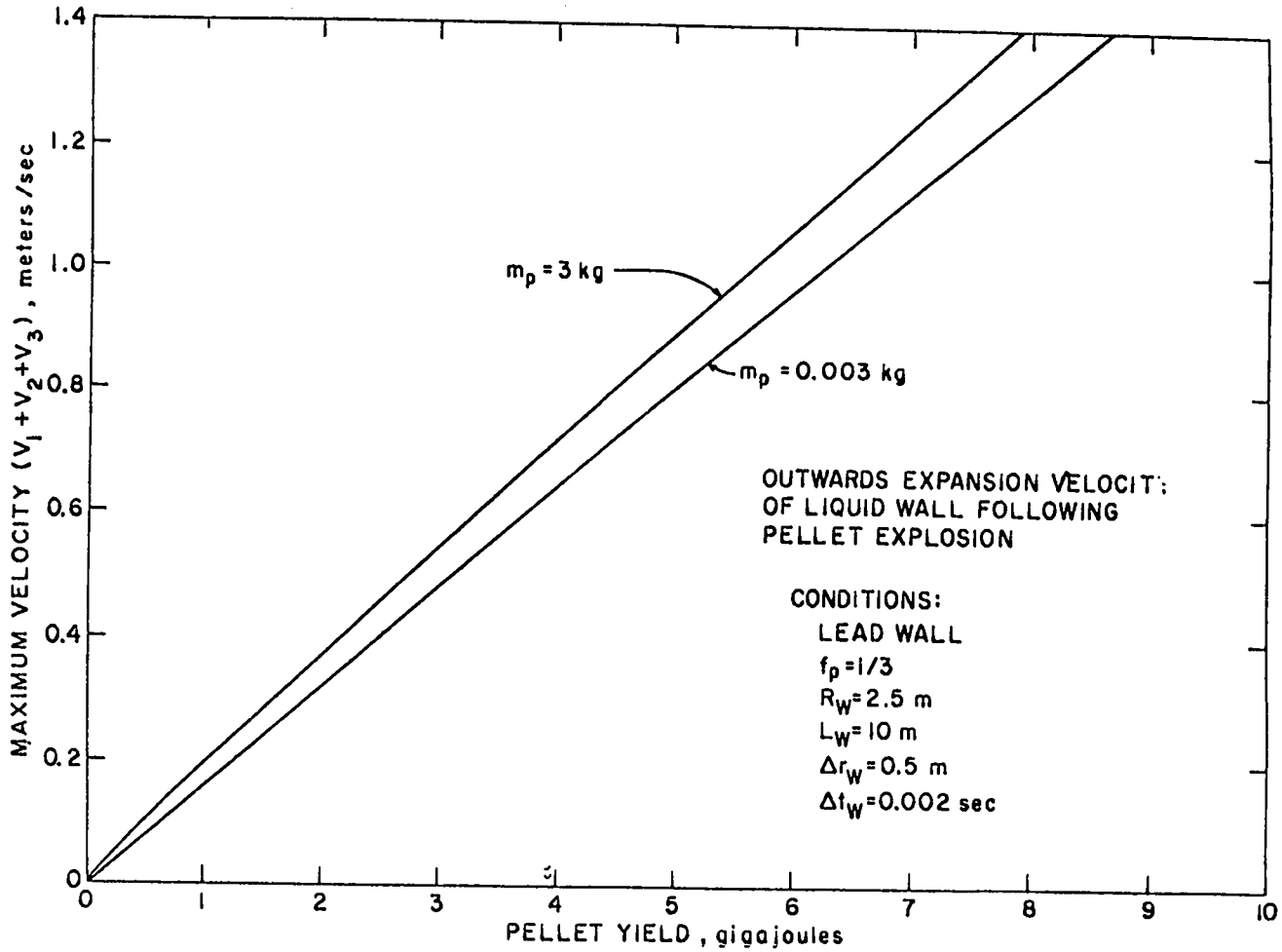
MAXIMUM VELOCITY ($V_1+V_2+V_3$), meters/sec
PELLET YIELD, gigajoules
m_p = 3 kg
m_p = 0.003 kg
OUTWARDS EXPANSION VELOCITY OF LIQUID WALL FOLLOWING PELLET EXPLOSION
CONDITIONS:
LEAD WALL
f_p = 1/3
R_W = 2.5 m
L_W = 10 m
Δr_W = 0.5 m
Δt_W = 0.002 sec
0
0.2
0.4
0.6
0.8
1.0
1.2
1.4
0
1
2
3
4
5
6
7
8
9
10

FIGURE 8

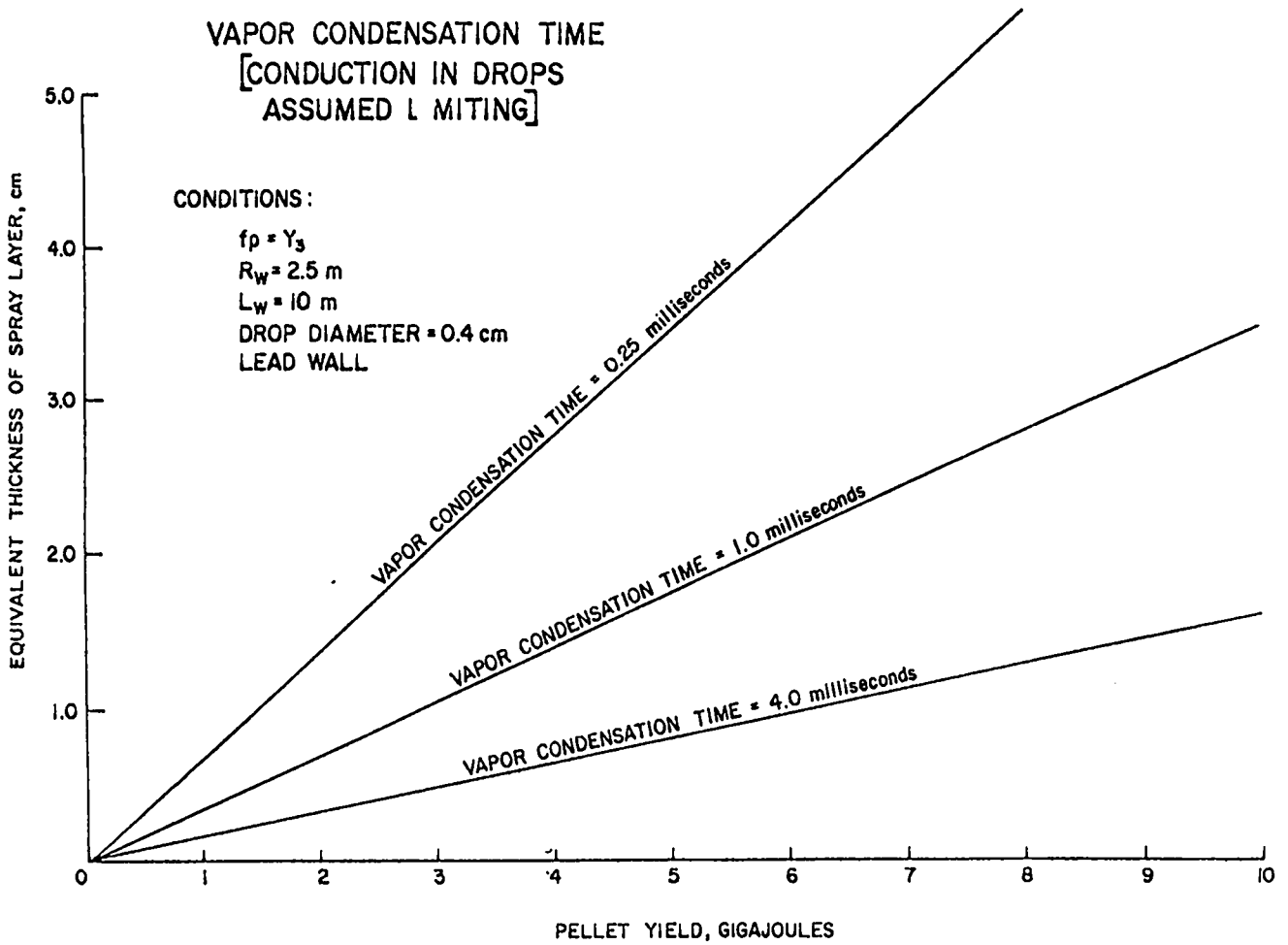
VAPOR CONDENSATION TIME
[CONDUCTION IN DROPS
ASSUMED L MITING]
CONDITIONS:
fρ = Y3
Rw = 2.5 m
Lw = 10 m
DROP DIAMETER = 0.4 cm
LEAD WALL
VAPOR CONDENSATION TIME = 0.25 milliseconds
VAPOR CONDENSATION TIME = 1.0 milliseconds
VAPOR CONDENSATION TIME = 4.0 milliseconds
EQUIVALENT THICKNESS OF SPRAY LAYER, cm
5.0
4.0
3.0
2.0
1.0
0
1
2
3
4
5
6
7
8
9
10
PELLET YIELD, GIGAJOULES

FIGURE 9

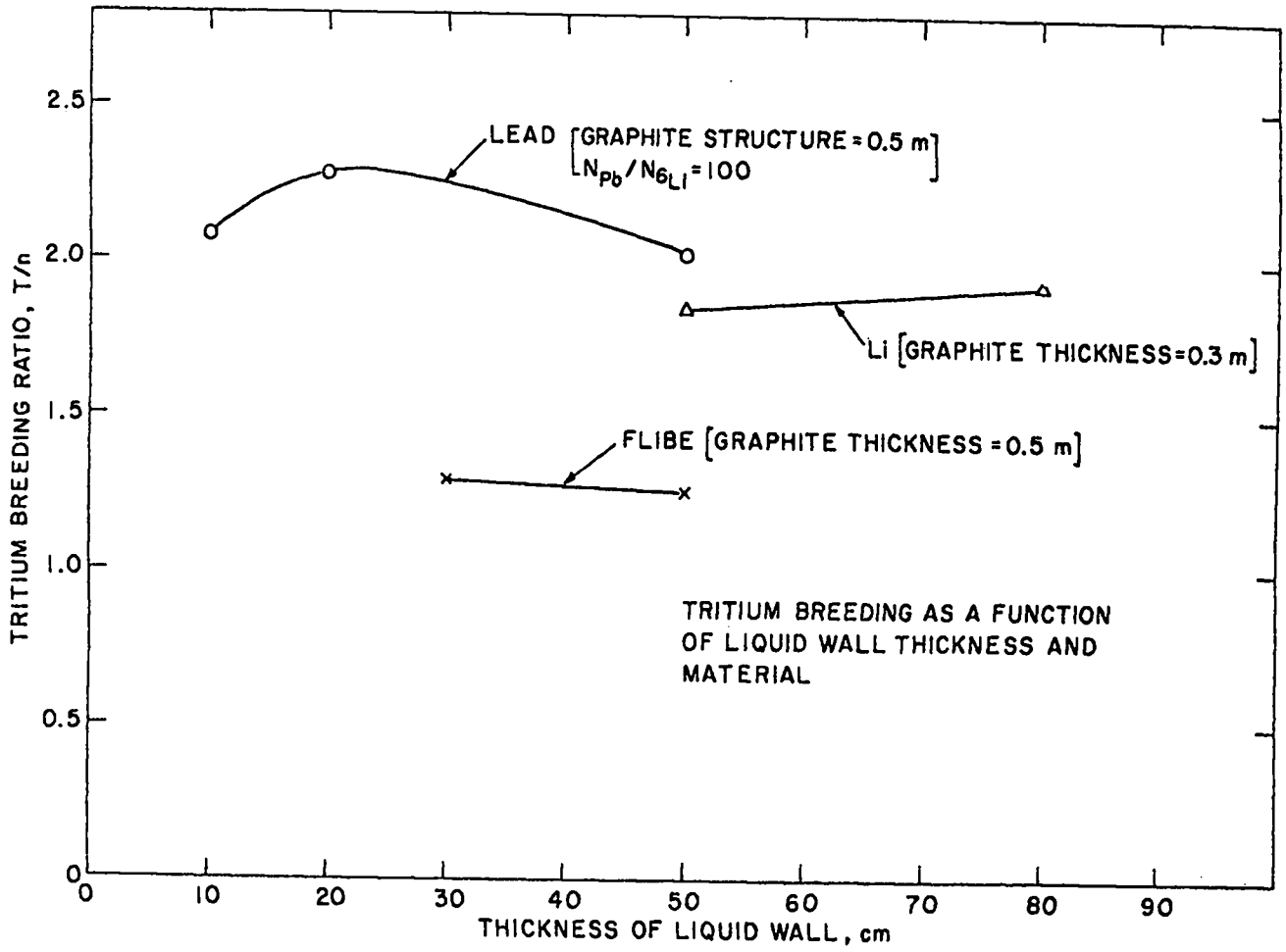
LEAD [GRAPHITE STRUCTURE = 0.5 m]
N_{Pb}/N_{6Li} = 100
Li [GRAPHITE THICKNESS = 0.3 m]
FLIBE [GRAPHITE THICKNESS = 0.5 m]
TRITIUM BREEDING AS A FUNCTION OF LIQUID WALL THICKNESS AND MATERIAL
TRITIUM BREEDING RATIO, T/n
THICKNESS OF LIQUID WALL, cm
0
0.5
1.0
1.5
2.0
2.5
10
20
30
40
50
60
70
80
90

FIGURE 10

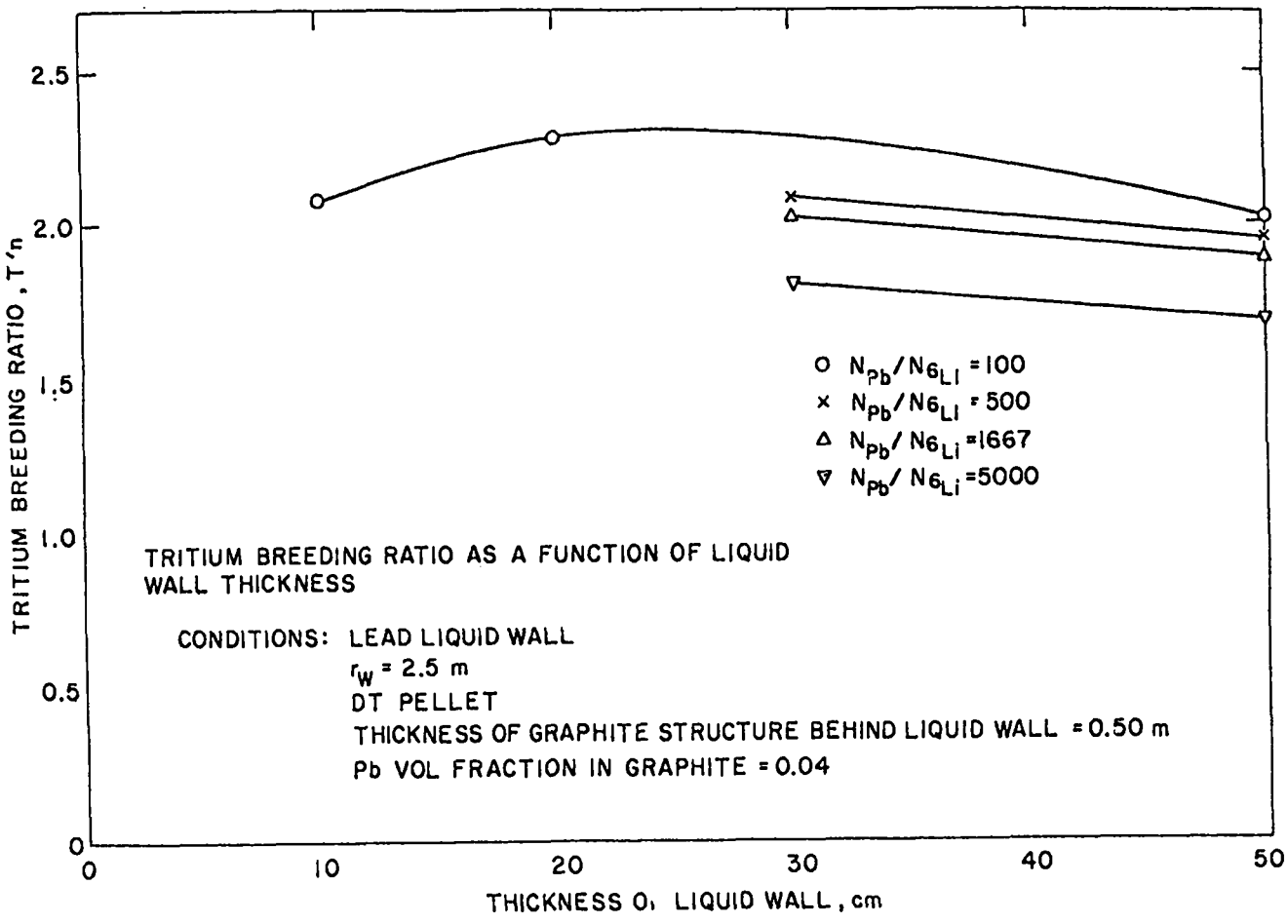
TRITIUM BREEDING RATIO , T'n
2.5
2.0
1.5
1.0
0.5
0
0
10
20
30
40
50
THICKNESS O, LIQUID WALL , cm
O $N_{Pb}/N_{6_{Li}}$ = 100
× $N_{Pb}/N_{6_{Li}}$ = 500
△ $N_{Pb}/N_{6_{Li}}$ = 1667
▽ $N_{Pb}/N_{6_{Li}}$ = 5000
TRITIUM BREEDING RATIO AS A FUNCTION OF LIQUID WALL THICKNESS
CONDITIONS: LEAD LIQUID WALL
r_W = 2.5 m
DT PELLET
THICKNESS OF GRAPHITE STRUCTURE BEHIND LIQUID WALL = 0.50 m
Pb VOL FRACTION IN GRAPHITE = 0.04

FIGURE 11

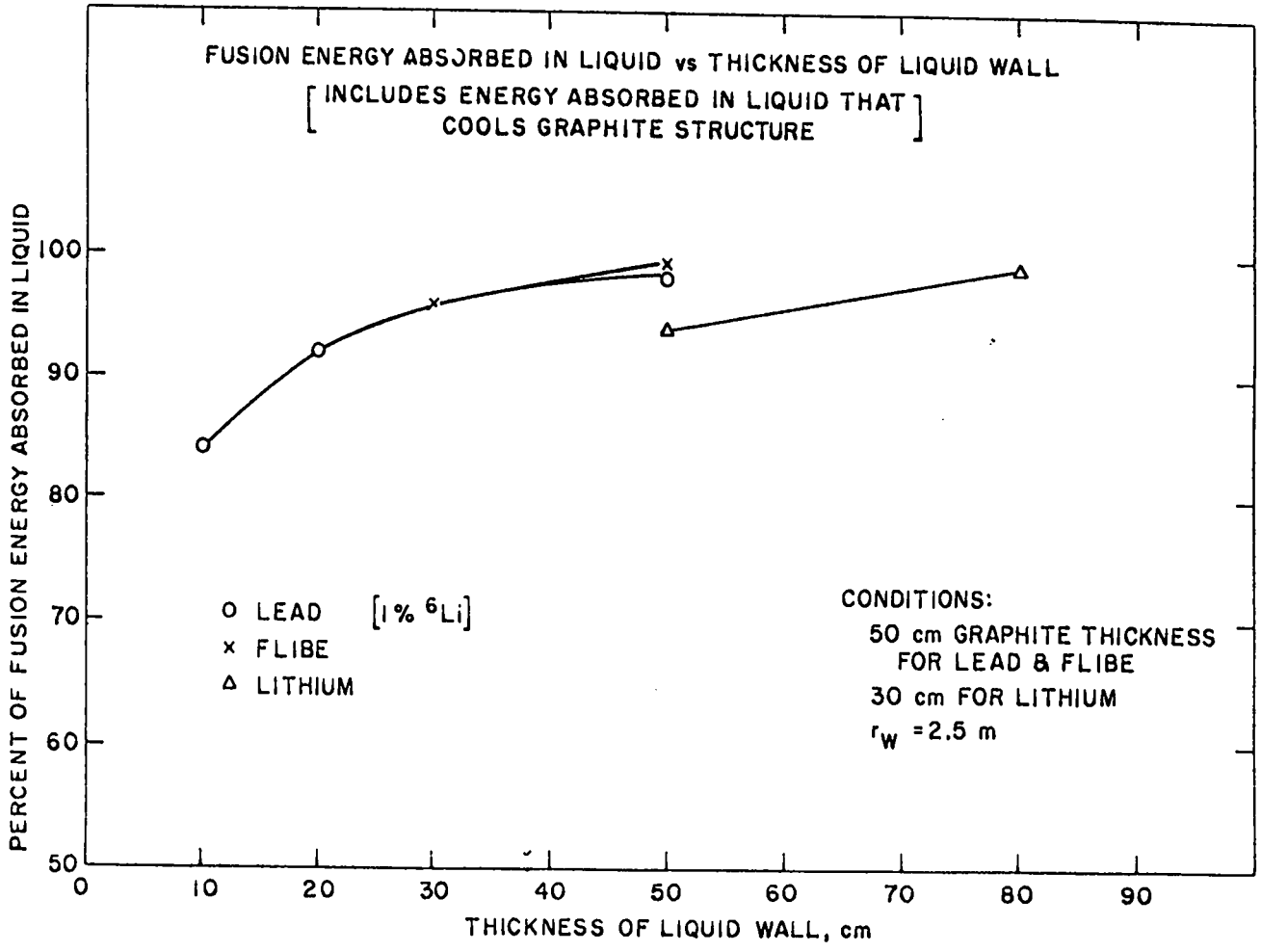
FUSION ENERGY ABSORBED IN LIQUID vs THICKNESS OF LIQUID WALL
[INCLUDES ENERGY ABSORBED IN LIQUID THAT COOLS GRAPHITE STRUCTURE]
PERCENT OF FUSION ENERGY ABSORBED IN LIQUID
100
90
80
70
60
50
0
10
20
30
40
50
60
70
80
90
THICKNESS OF LIQUID WALL, cm
o LEAD [1% 6Li]
x FLIBE
Δ LITHIUM
CONDITIONS:
50 cm GRAPHITE THICKNESS FOR LEAD & FLIBE
30 cm FOR LITHIUM
r_w = 2.5 m

FIGURE 12

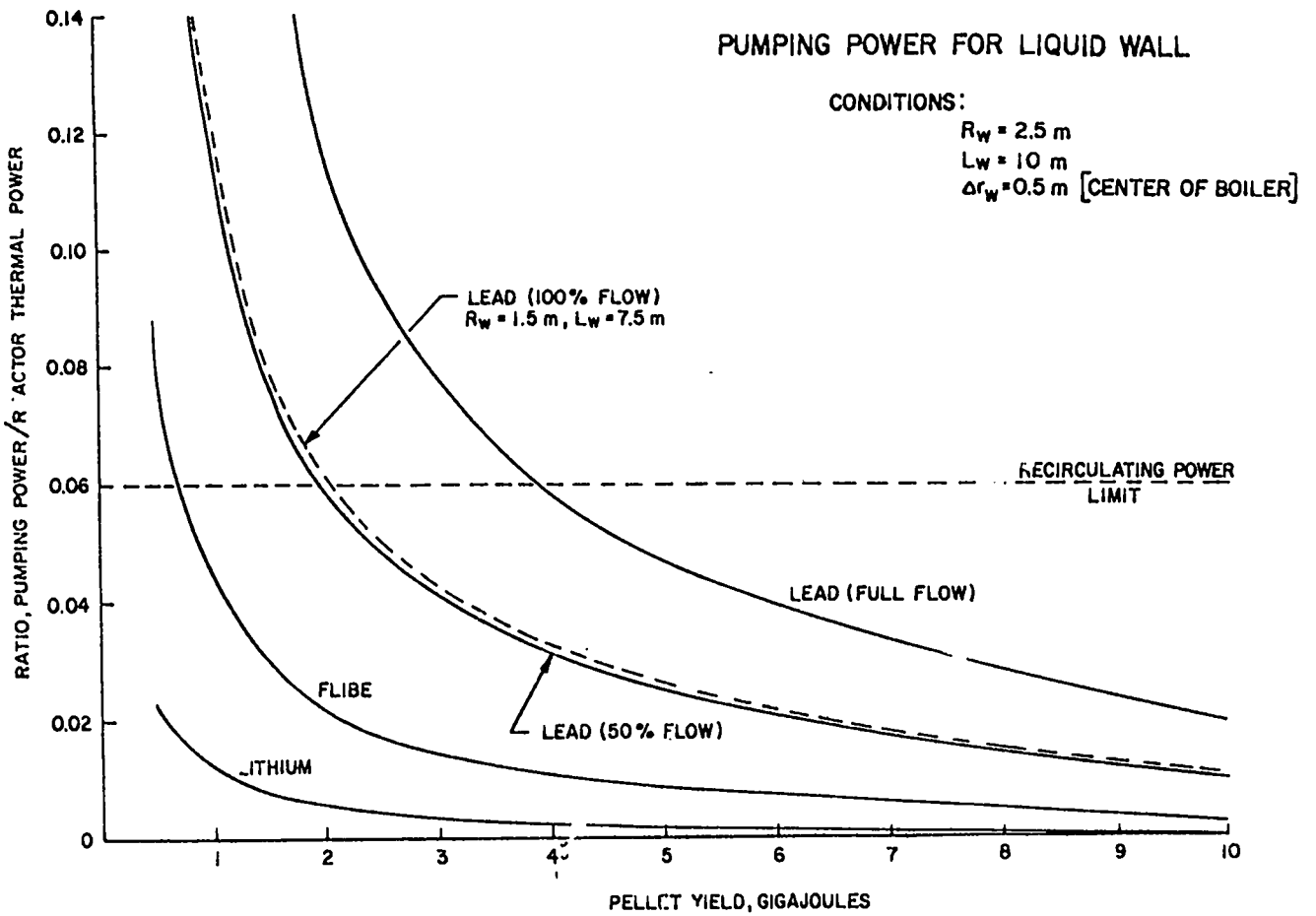
PUMPING POWER FOR LIQUID WALL
CONDITIONS:
R_W = 2.5 m
L_W = 10 m
Δr_W = 0.5 m [CENTER OF BOILER]
LEAD (100% FLOW)
R_W = 1.5 m, L_W = 7.5 m
RECIRCULATING POWER LIMIT
LEAD (FULL FLOW)
FLIBE
LEAD (50% FLOW)
LITHIUM
RATIO, PUMPING POWER/REACTOR THERMAL POWER
0.14
0.12
0.10
0.08
0.06
0.04
0.02
0
1
2
3
4
5
6
7
8
9
10
PELLET YIELD, GIGAJOULES

FIGURE 13

NOEL [A NO EXTERNAL LEAK]
ENERGY ABSORPTION SYSTEM FOR THERMAL POWER CYCLES

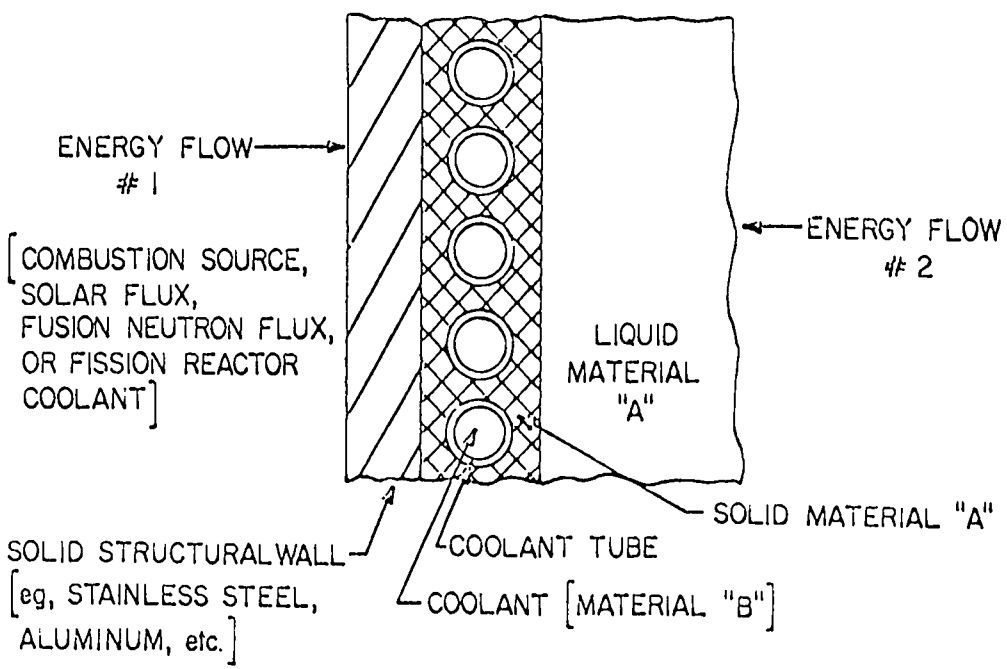

NOEL CONDITION: $P_B < P_A$

FIGURE 14

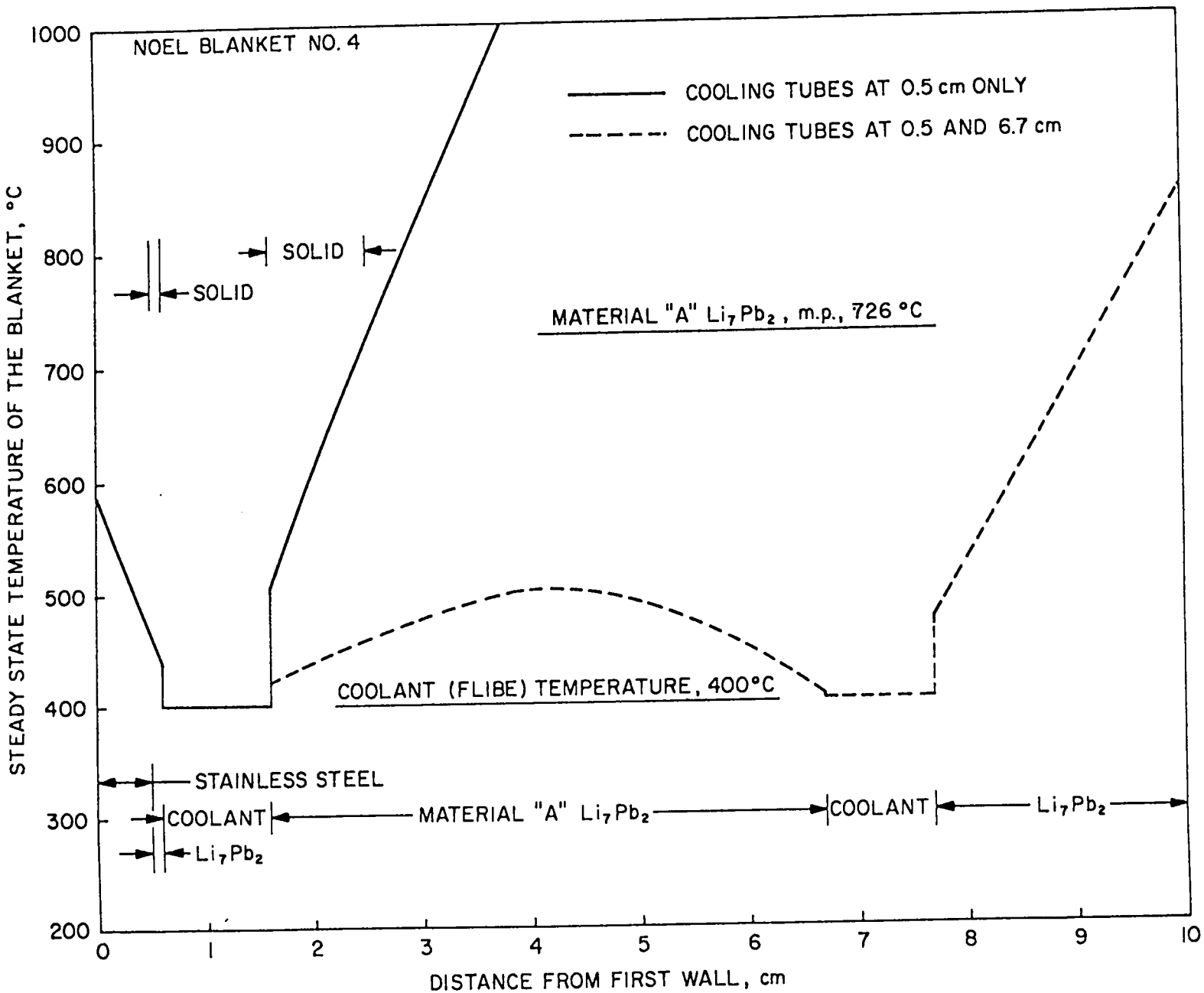
NOEL BLANKET NO. 4
COOLING TUBES AT 0.5 cm ONLY
COOLING TUBES AT 0.5 AND 6.7 cm
SOLID
SOLID
MATERIAL "A" Li7Pb2 , m.p., 726 °C
COOLANT (FLIBE) TEMPERATURE, 400°C
STAINLESS STEEL
COOLANT
Li7Pb2
MATERIAL "A" Li7Pb2
COOLANT
Li7Pb2
STEADY STATE TEMPERATURE OF THE BLANKET, °C
DISTANCE FROM FIRST WALL, cm
1000
900
800
700
600
500
400
300
200
0
1
2
3
4
5
6
7
8
9
10

SYSTEMS-DESIGN AND ENERGY-BALANCE CONSIDERATIONS FOR IMPACT FUSION

R.A. Krakowski and R.L. Miller
University of California
Los Alamos Scientific Laboratory
Los Alamos, New Mexico 87545

I. INTRODUCTION

The approach to thermonuclear fusion power embodied in the term "impact fusion" envisages the acceleration of a DT-bearing projectile to velocities in the range 10^5 - 10^6 m/s and a subsequent impact with a stationary target or a similarly accelerated projectile. Heating to and burn at thermonuclear temperatures would be achieved by means of a coupled shock-heating and adiabatic compression process. No magnetic fields would be present, and the dominant energy losses would occur through radiative and thermal conduction channels. "Bootstrap" heating by alpha-particle deposition into the DT plasma under certain conditions may be possible. Conceptual designs and rudimentary systems studies of power reactor embodiments based on the impact fusion approach are for all intents and purposes nonexistent. Furthermore, the relationship between projectile velocity and thermonuclear yield have been estimated only by approximate models and analyses. The focus of these analyses[1,2] has been the elucidation of the relationship between projectile velocity and temperature upon impact; accurate energy balances yielding useful projectile gain *versus* input energy simply do not exist.

In view of the durth of system design studies and fundamental calculations of projectile yield, a paper of this nature can only rely on the results, insight and indications generated by more comprehensive studies of other fusion concepts. Additionally, simple scoping calculations can be made of limiting and sometimes unrealistic situations in order to bracket the expected projectile gain and input energy requirements. Without even highly approximate estimates of the gain *versus* yield relationship, any prognosis of reactor viability will be almost meaningless.

Because of the absence of substantive experience, design studies, and theoretical physics analysis, the posture of this study is highly qualitative and approximate. The primary intent is to point out areas of concern and potential problems within an overall systems context, rather than to present a

polished and optimized Impact Fusion Reactor (IFR) design. After a parametric and qualitative description of the general energy-balance and systems considerations in Sec. II, Sec. III addresses a number of reactor design problems anticipated for the IFR. Section IV attempts to approximate and/or to define the operating regime for an IFR based on highly simplified but limiting projectile/target energy balances and thermonuclear burn models. Major conclusions and/or indications are summarized in Sec. V.

II. GENERAL ENERGY-BALANCE AND SYSTEMS CONSIDERATIONS

The essential elements of the IFR are depicted schematically on Fig. 1 in terms of a generalized energy balance. These elements include:

- A macroparticle accelerator with the capability of imparting a kinetic energy W_K with an overall efficiency η_{ACC} to a DT projectile.
- A projectile transport and guidance system that is capable of accurate and rapid injection of projectiles into a reactor or target chamber.
- An energy store and power supply for the projectile accelerator.
- A system for rapid replacement of targets and auxiliary equipment destroyed after each implosion.
- A reactor or target chamber that is surrounded by a medium for blast or shock attenuation and/or absorption. Generally, this chamber is defined by the boundaries of a blast cavity, outside of which all structures must function with an acceptably long life-time.
- A blanket system that provides a multifunction region where tritium is bred (only a DT fusion reaction is considered), and where moderation of the 14.1-MeV fusion neutron, heat removal, and radiation shielding occur. A portion of these functions may be performed by materals placed within the blast cavity.[3]
- A means to extract the thermal power received by and deposited into the blanket system. The thermal power must be steady state, must be delivered with less than ~ 5-10 K temperature fluctuation, and could be used to generate either electricity (as shown in Fig. 1) or process heat for synthetic fuel production.[4,5]
- A turbine-generator energy-storage and switch-yard system that as a minimum must be capable of generating and distributing all electrical energy used within the power plant without large power surges, while simultaneously assuring a source of constant and reliable electrical power to a user.
- An auxiliary support system needed to sustain and to maintain the operation of the IFR power station on an $\geq$ 80% basis. For example:

- tritium recovery, purification and processing from the breeding blanket.
- fabrication and recycle of projectile, target, and destroyed ancillary equipment within the blast cavity.
- remote maintenance and repair systems
- control and instrumentation systems, particulary as applied to the synchronous operation of projectile/target acceleration, guidance, and abort (if necessary) functions.

Each of these major subsystems must function at an acceptable level of reliability and cost, while simultaneously operating as an integrated system to render a favorable net energy balance that is compatible with as yet proven or resolved physics and engineering technology issues. The engineering energy balance depicted on Fig. 1 can be evaluated in terms of a projectile gain, $Q = (MW_N + W_\alpha)/W_K = W_F/W_K$, that is define in terms of the primary 14.1-MeV

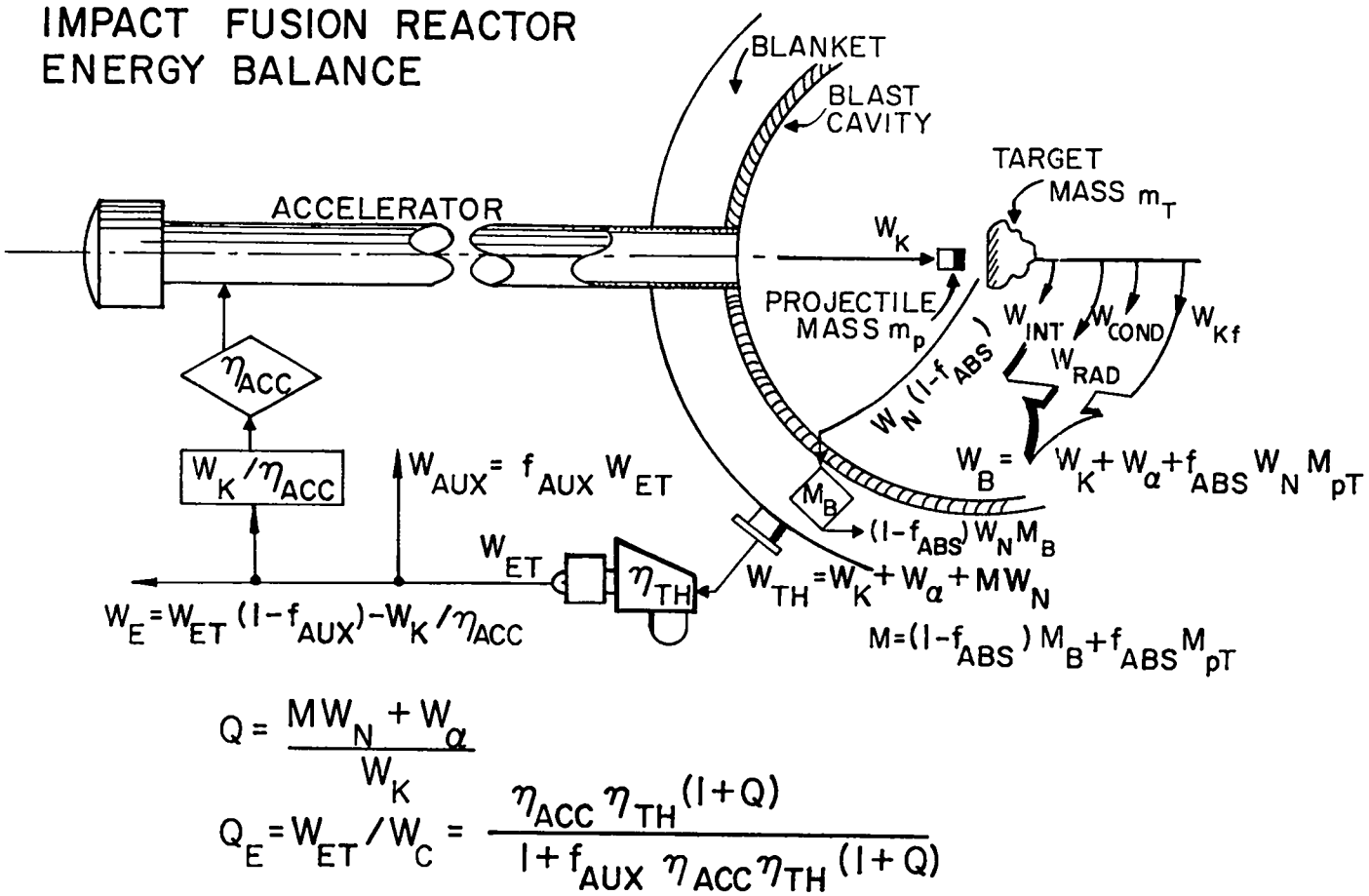

Fig. 1 Generalized energy-flow diagram for a conceptual Impact Fusion Reactor (IFR).

neutron yield, W_N, multiplied by M to reflect exoergic nuclear reactions occuring within the blanket, the alpha-particle yield, W_α, and the initial projectile energy, W_K. As a measure of overall plant performance, an engineering Q-value, $Q_E = W_{ET}/W_C$, is defined as the ratio of total electrical energy generated from each implosion, W_{ET}, relative to the total recirculating energy requirement, $W_C = f_{AUX}W_{ET} + W_K/\eta_{ACC}$, where f_{AUX} represents the fraction of W_{ET} needed to drive all auxiliary plant power requirements (feedwater pumps, "housekeeping" power, etc., $f_{AUX} \sim 0.05$, typically), and W_K/η_{ACC} is the energy demanded by the projectile accelerator. The following expression relates Q_E to Q:

$$Q_E = \frac{\eta_{ACC}\eta_{TH}(1+Q)}{1 + f_{AUX}\eta_{ACC}\eta_{TH}(1+Q)} \quad , \tag{1}$$

where $\eta_{TH} \simeq 0.3\text{-}0.4$ is the thermal to electric conversion efficiency. Equation (1) is displayed on Fig. 2 parametrically in η_{ACC}, the projectile accelerator efficiency. Since recirculating power fractions, $\varepsilon = 1/Q_E$, below $\sim 0.15\text{-}0.20$ are desirable for economic reasons,[6] a Q_E in the range 5-6 would require projectile gains, Q, in the range 40-50 if the accelerator efficiency can be maintained in the range 0.6-0.4. It is noted that a "coupling coefficient" that gives the fraction of the incident energy, W_K, which actually appears as increased internal energy of the DT is embedded in the parameter Q. The coupling coefficient is highly dependent on the projectile/target design and is not introduced at this level of analysis. The projectile velocity, u, and energy, W_K, needed to achieve desirable gains are simply not accurately known today for impact fusion. Section IV attempts to establish bounds on this crucial relationship between Q and W_K, (i.e., the so-called "gain curve"). This Q versus W_K relationship is vitally important for technological reasons, as well for the plant energy balance and system economics. As indicated on Fig. 1, the energy $W_B = W_K + W_\alpha + f_{ABS}W_N M_{pT}$ can potentially contribute to a significant blast or shock containment problem. In addition to W_α and W_K, the fraction f_{ABS} of the 14.1-MeV fusion neutrons can be absorbed by and multiplied in energy (M_{pT}) through nuclear interactions with the destroyed projectile and target/support structure; if the associated masses, m_p and m_T, are sufficient, f_{ABS} may be as large as 0.1-0.2.[3] Consequently, even for high-gain

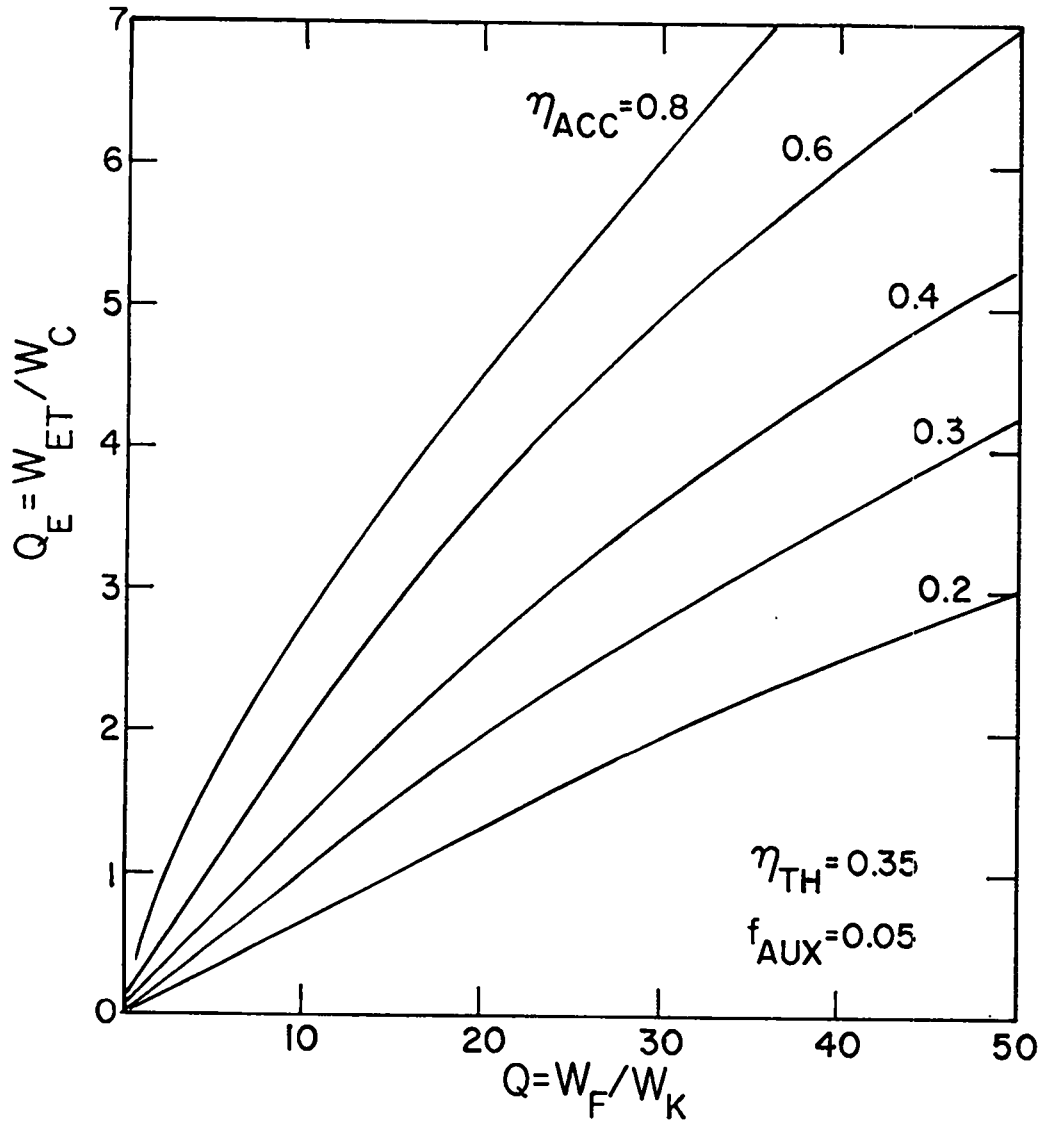

Fig. 2 Parametric systems design curves for an Impact Fusion Reactor (IFR).

projectile/target systems ($W_F = MW_N + W_\alpha >> W_K$), as much as 30-40% of the fusion yield can appear as structurally destructive blast energy, W_B. The severity of this problem depends crucially on the amount of mass ($m_p + m_T$) accelerated during an implosion, the magnitude of W_B, and, obviously, the Q versus W_K relationship.

III. REACTOR SYSTEMS DESIGN CONSIDERATIONS

The extrapolation of most fusion confinement schemes to reactors must be accompanied by a complex interaction between physics, engineering and electric utility constraints. Ultimately, a proposed power system should promise safe, reliable, and economic operation, as evaluated at the time of its

implementation. The accuracy of such projections depends sensitively upon the existing theoretical and experimental physics base. Figure 3 presents diagramatically the major physics/engineering/utility interfaces expected for a power system based on the impact fusion scheme. Within each discipline perceived issues and/or problems are grouped according to functional subsystems. For example, the complex interaction between projectile/target phenomena, the physics basis for a gain curve (Q versus W_K), and the technology implications of the magnitude and form of the blast energy, W_B, have been discussed in Sec. II. Additionally, the pellet/target mass and the extent of auxiliary support structure damage could be reflected as a significant operating cost.[3] For example, a 1-GJ thermonuclear yield with $\eta_{TH} = 0.35$ and $Q_E = 5$ (Fig. 1) corresponds to a net electrical energy of 78 kWeh, which at 50 mills/kWeh would yield a net revenue of \$3.90; given that at most 20% of this revenue can be appropriated towards projectile/target replacement costs, these costs cannot exceed \$0.78 per implosion. It remains to be seen if this cost constraint can be met or if economic considerations will dictate larger thermonuclear yields.

Similar to the scaling of projectile/target costs with thermonuclear yield, the cost of the blast cavity and containment vessel must be carefully analyzed. These latter cost will fall into the category of capital investment and, unlike the operational costs of projectile/target replacement, may show an optimum with thermonuclear yield.[7]

A number of key physics and technology "drivers" can be identified for impact fusion, in addition to the issues of projectile/target and blast cavity costs described above. Although more detailed studies of other inertial fusion schemes can lend valuable insight into these systems problems/uncertainties, eventually device-specific analysis of an impact-fusion reactor embodiment will have to be performed if an unambiguous physics/technology assessment is to result. This kind of in-depth analysis, however, should not be performed until a reasonable operating point(s) can be identified (i.e., a promise of economic fusion gain at an acceptable yield and energy input). Given that a favorable, realistic energy balance can be developed that is based on a credible estimate of fusion yield for a specific projectile/target configuration, the following systems issues should be subjected to detailed analyses:

- Identify type, size, efficiency and cost of a high pulse-rate, macroparticle accelerator. Clearly, this crucial component of the impact fusion system should be examined in parallel with the physics of the projectile/target interaction and the realistic estimate of the Q versus W_K gain curve.

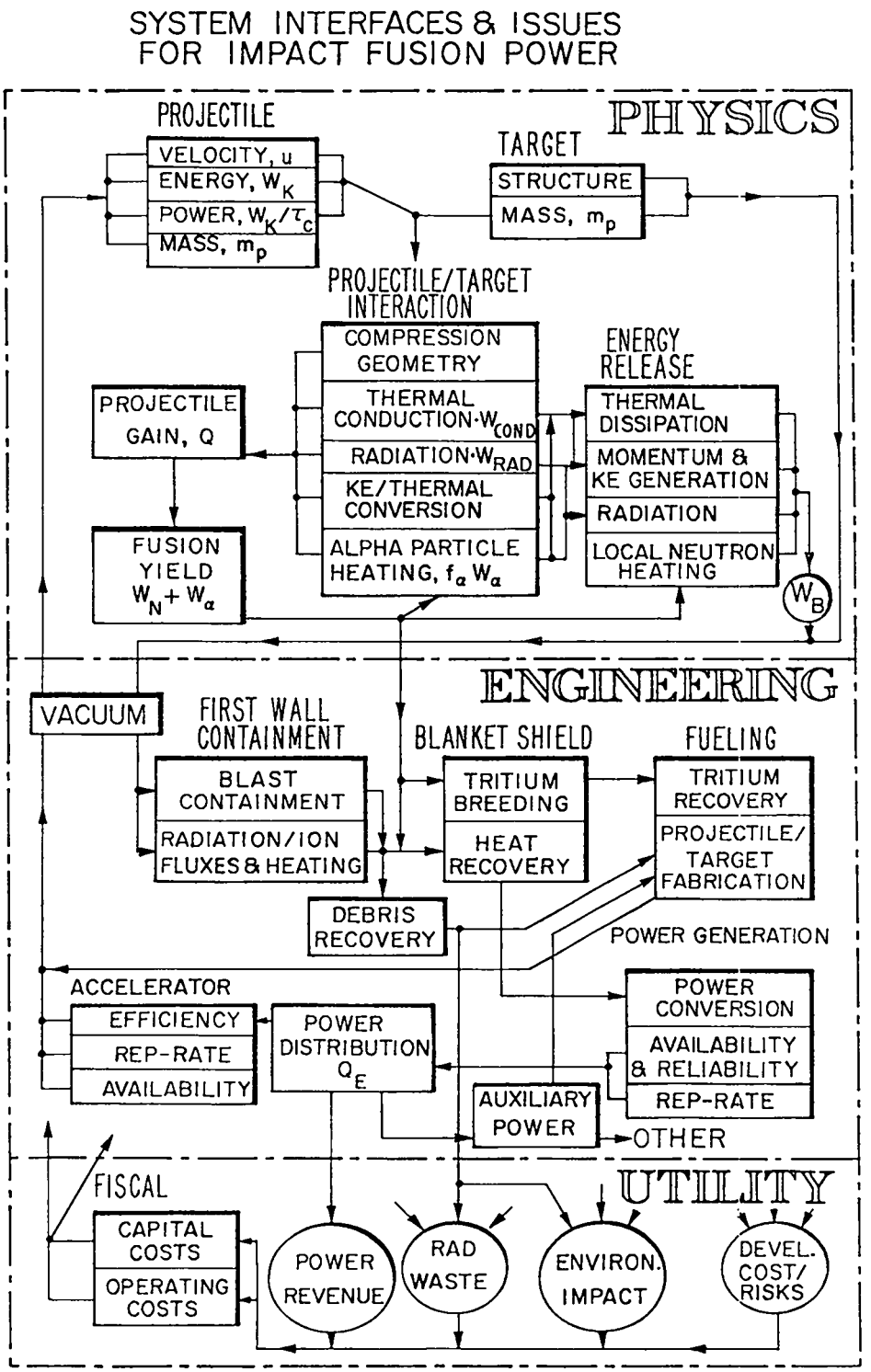

Fig. 3 Systems interfaces for an Impact Fusion Reactor (IFR).

- Systems design considerations for the reactor core and nuclear island include:

  - projectile transport, guidance, and entry system. A discardable, replacable vacuum barrier or a quick-acting "gate" situated at the accelerator/blast-cavity interface may be required.

  - the mechanism by which the target and destructible structure is inserted, replaced, and recycled must be resolved, unless a companion accelerator and projectile is used in place of a target.

  - the structural loads caused by blast-related momentum transfer and the means by which these loads can be attenuated (if necessary) must be resolved. Can a lithium spray be employed as a blast attenuator, tritium breeder, and coolant?[3]

  - the design of the first permanent structural wall represents a crucial issue for this pulsed power source. An appreciable fraction of the thermonuclear yield in all likelihood will pass through this structure as thermally conducted heat, and the lifetime of this cavity wall could represent a major technology/cost driver. What are the consequences and means to deal with a projectile/target or projectile/projectile trajectory mismatch?

  - Although an IFR will operate in a highly pulsed mode, the thermal-hydraulic systems (blanket, coolant, etc.) must function in a thermal steady state. Other blanket design considerations (i.e., tritium breeding, shielding, etc.) are expected to differ little from those proposed for other fusion concepts.

- A large number of ex-reactor issues can be identified, aside from the projectile accelerator and its system requirements.

  - What is the relationship between the projected yield curve, accelerator and blast cavity pulse rate, total power, blanket response, and system economics/costs? For instance, a 1-B$ accelerator that drives a 1-GJ yield with $\eta_{TH} = 0.35$ and $Q_E = 5$ will have to be pulsed at 5 Hz in order to maintain the accelerator capital cost for this 1400 MWe(net) plant below 700 $/kWe, or ~ 30% of the anticipated goal for total plant investment.

  - As noted previously, the operating cost associated with projectile/target fabrication and recycle could consume a measureable fraction of the plant revenue. The tradeoffs between this technology/economics issue and the physics-dictated projectile/target design must be resolved. The related issue of radwaste associated with projectile/target debris may also be important.

  - The degree of thermal cycling of the primary coolant exiting the reactor blanket must be minimized to 5-10 K.

  - The degree of cavity modularization needed to defray the cost of a potentially expensive accelerator, by more effectively using this investment, may play an important economic role.

- Protection of the capital investment against "stray" projectile trajectories in a high repetition-rate system may prove to be important.

- A majority of fusion power schemes tend to operate with large size, power output, and total capital outlay. Does the impact fusion scheme differ in this respect by offering a potentially small but economic system?

- The feasibility of designing and operating reliable and economic subsystems should be addressed.

- The issue of plant availability is directly related to the ease of remote maintenance and the facility for rapid changeout/replacement/repair of key system components.

As noted previously a detailed assessment of many of these issues is not warranted until a better understanding is developed of the relationship between accelerator requirements, projectile/target design, and the thermonuclear yield/gain relationship. The following section addresses these questions by means of a highly-simplified, analytic model.

IV. APPROXIMATE AND LIMITING ENERGY BALANCES

In order to assess, at a preliminary level, the reactor viability of the impact fusion approach, the relationship between initial projectile velocity, u, total thermonuclear yield $W_F = (MW_N + W_\alpha)$, and the ratio, $Q = W_F/W_K$, of the thermonuclear yield to the initial projectile energy is needed. An analytic or numerical determination of the inter-relationship between u, W_F, and Q is made difficult by the multidimensional and coupled nature of this hydrodynamic, shock- and radiation-transfer problem. Consequently, calculations and modelling of the kind represented by Refs. 1 and 2 have been primarily concerned with estimating the relationship between final temperature and initial projectile velocity in the presence of classical loss processes. A self-consistent resolution of the trade-offs and limitations of thermonuclear yield, as embodied in Q or W_F, is rarely given because of the approximate and simplified nature of the analytic models. Unfortunately, even the most approximate assessment of an IFR cannot be made without even a simplified yield curve (i.e., relationship between Q and u, W_K or W_F).

Any inhibition associated with avoiding the presentation of definite Q-values expected for an IFR because of the poorness and/or limitations of the phenonological model is cast aside here. The simple shock-heating model reported in Ref. 1 is used to estimate Q for a one-dimensional (planar) impact

without adiabatic compression. The constraints imposed by classical thermal conduction and bremsstrahlung radiation are examined. Although no claim is made as to the exactness of the results that emerge from this simple analysis, these results do serve as a reference from which the degree to which improvement in device performance from multidimensional effects, adiabatic compression and alpha-particle heating can be qualitatively estimated. Generally, the predictions of this simple shock model are expected to be pessimistically conservative. The improvement expected by compressional heating of a shocked planar DT medium is examined subsequently.

A. DESCRIPTION OF IDEAL SHOCK MODEL*

A cylindrical DT projectile of initial length L, density ρ_o, and radius $R \simeq L$ is assumed to impact axially a perfectly inelastic barrier at a velocity u. An ideally sharp shock is postulated to move in one dimension through the projectile at a velocity v_s relative to the projectile or velocity z relative to the barrier (laboratory frame). Dimensional changes in the radial direction are ignored. Figure 4 depicts this model schematically. The Hugoniot relationships are used to determine the shock conditions, which are then applied to estimate the thermonuclear yield and loss rates. Referring to Fig. 4, the Hugoniot relationships are

$$u = \frac{2}{\gamma+1} v_s \tag{2A}$$

$$\rho_s = \frac{\gamma+1}{\gamma-1} \rho_o \tag{2B}$$

---

* Except for plasma temperature, $T_e = T_i = T(keV)$, mks units are consistently used. The electronic charge, $e = 1.60(10)^{-19}$ J/eV is used to represent the Boltzmann constant k_B(i.e., $10^3 e\ T(keV) = k_B T(K)$). Other constants used are: fusion energy release, $E_N = 20$ MeV/fusion; mass of a proton, $m_p = 1.67(10)^{-27}$ kg; heat capacity ratio $\gamma = 5/3$; atomic mass unit for DT, $A = 2.5$; initial DT density, $\rho_o = 200$ kg/m^3; Coulomb logarithim, $\ell n\Lambda = 10$.

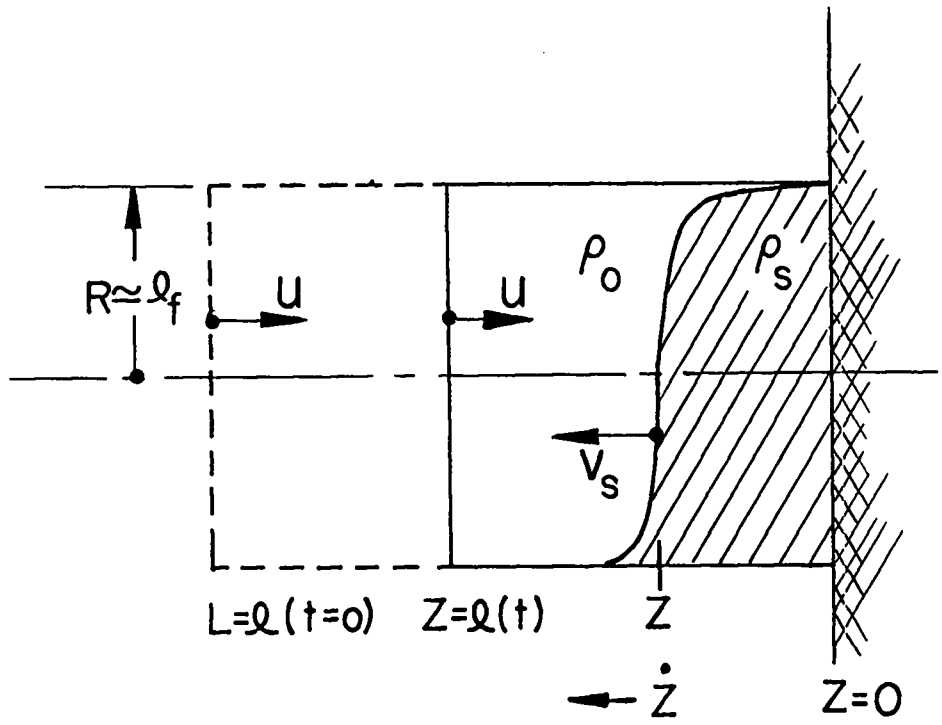

Fig. 4 Schematic diagram of one-dimensional shock-heated projectile model without adiabatic compression.

$$P_s = \frac{2}{\gamma+1}\rho_o v_s^2 = \left[\frac{2(10)^3 e}{Am_p}\right]\rho_s T \tag{2C}$$

$$\dot{z} = \frac{\gamma-1}{2}u = \frac{\gamma-1}{\gamma+1}v_s \tag{2D}$$

The thermonuclear fusion yield $W_F(J)$ is given by

$$W_F = \int_o^{\tau_B} E_N \left(\frac{1}{4}n_s^2 \langle\sigma v\rangle\right)\pi R^2 z\,dt \tag{3A}$$

$$W_F/\pi R^2 = \frac{E_N(10)^6 e}{8(Am_p)^2}\left(\frac{\gamma-1}{\gamma+1}\right)\left(\frac{\langle\sigma v\rangle}{v_s}\right)(\rho_s \ell)^2 , \tag{3B}$$

where the burn time τ_B has been taken as one shock transit time, L/v_s, $\rho_o L = \rho_s \ell$ by mass conservation and $n_s = \rho_s/Am_p$. Given that the initial kinetic energy of the projectile, $W_K/\pi R^2 = \rho_o L u^2/2$, the following expression for $Q = W_F/W_K$ results

$$Q = \frac{10^{3/2} E_N}{16(Am_p e)^{1/2}}(\gamma-1)^{1/2}\frac{\langle\sigma v\rangle}{T^{3/2}}(\rho_o L) \tag{4}$$

$$= 1.25(10)^{24}\frac{\langle\sigma v\rangle}{T^{3/2}}(\rho_o L)$$

For example, at T = 10 keV, Q equals $4.30(\rho_o L)$. The projectile energy, $W_K(J/m^2)$, and velocity, u(m/s), are given by

$$W_K/\pi R^2 = 1.15(10)^{11} T\ (\rho_o L) \tag{5}$$

$$u = 4.80(10)^5 T^{1/2} \tag{6}$$

If the classical electron thermal conductivity, k(W/m keV), is taken as[8]

$$k = \frac{9.8(10)^{14}}{\ell n \Lambda} T^{5/2} , \tag{7}$$

and with thermal conduction power loss per unit volume of an equivalent sphere

of radius $R \sim \ell$ equal to $3kT/\ell^2$, the thermal conduction time, $\tau_{COND} \cong 3(10^3 enT)/(3kT/\ell^2)$, equals

$$\tau_{COND} = \left[\frac{10^3 e \ell n \Lambda}{9.8(10)^{14} Am_p}\right] \frac{\rho_s \ell^2}{T^{5/2}}$$

$$= 3.84(10)^{-4} \rho_s \ell^2 / T^{5/2} \tag{8}$$

Equating τ_{COND} to the effective burn time, $\tau_B \simeq L/v_s$, gives the following expresion for $\rho_o L = \rho_s \ell$

$$(\rho_o L)_{COND} = \frac{0.15}{\ell n \Lambda} T^2 \tag{9}$$

The volumetric bremsstrahlung power loss is approximated by[9] $5.35(10)^{-37} n^2 T^{1/2}$ (W/m^3), which when divided into the plasma energy, $3(10)^3 enT$, gives the following expression for an effective time constant for radiation loss

$$\tau_{BR} = \left[\frac{3(10)^3 eAm_p}{5.35(10)^{-37}}\right] \frac{\gamma-1}{\gamma+1} \frac{T^{1/2}}{\rho_o}$$

$$= 9.37(10)^{-7} T^{1/2}/\rho_o \tag{10}$$

Again, equating τ_{BR} to $\tau_B \simeq L/v_s$ gives the following expression for a $\rho_o L = \rho_s \ell$ related to radiation losses

$$(\rho_o L)_{BR} = 2.40T \tag{11}$$

B. EVALUATION OF SIMPLE SHOCK MODEL

Equations (4), (9) and (11) for Q, $(\rho_o L)_{COND}$, and $(\rho_o L)_{BR}$, respectively, are plotted in Fig. 5 in the form of $\rho_o L$ versus T. Also shown for convenience is Eq. (6), giving the relationship between u and T. For $\rho_o L$ values below the $(\rho_o L)_{BR}$ curve on Fig. 5, τ_B is less than τ_{BR} and a proper kinetic analysis would predict a burn temperature that is relatively uneffected by radiation losses over a period equal approximately to the burn time. Similarly, for $\rho_o L$ values above the $(\rho_o L)_{COND}$ curve on Fig. 5, τ_B is less than τ_{COND}, and again a region is defined where conduction losses should not be serious. The wedge-shaped region on Fig. 5, where $(\rho_o L)_{COND} < \rho_o L < (\rho_o L)_{BR}$, indicates conditions where both radiation and conduction losses might occur without seriously degrading the

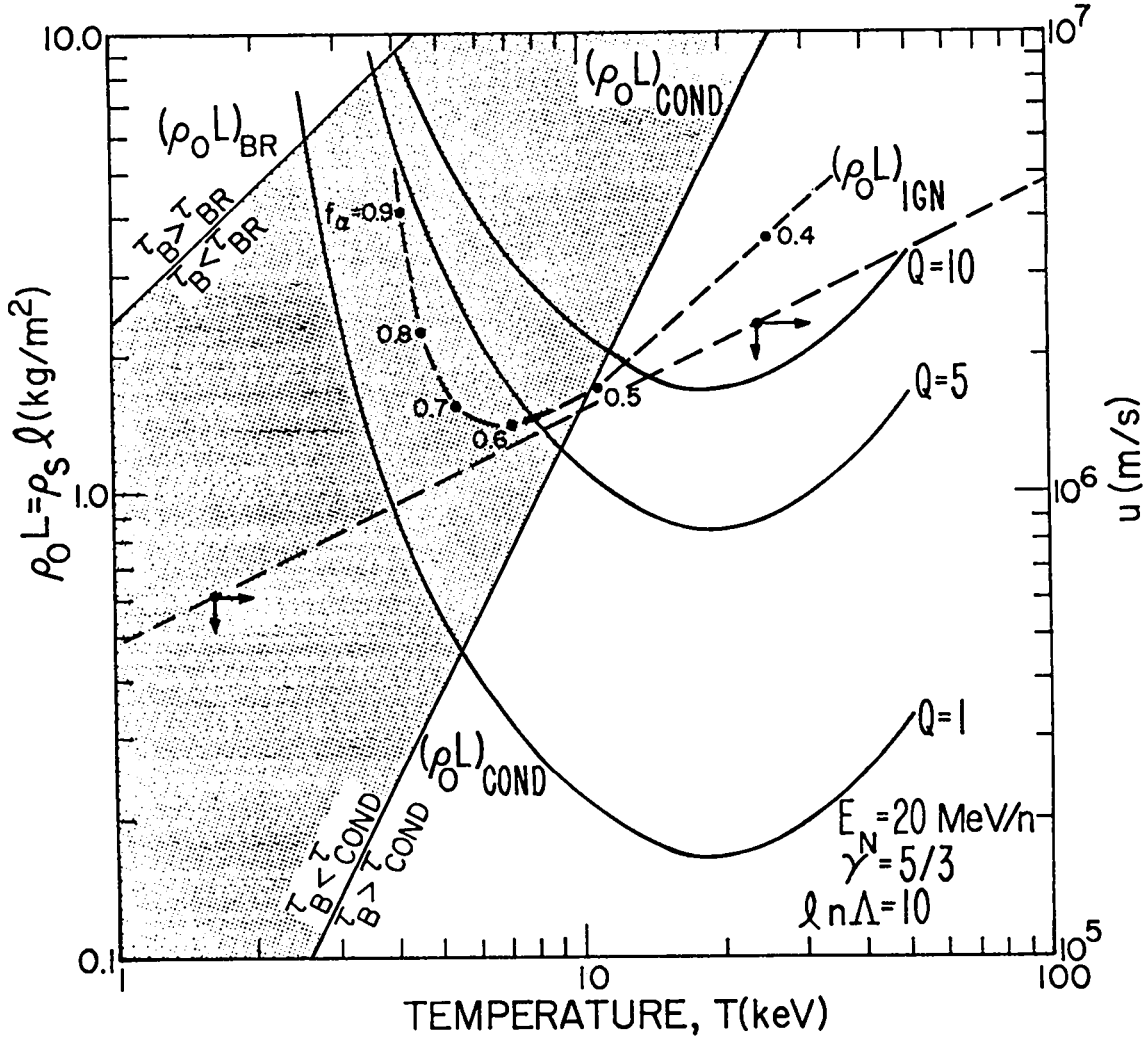

Figure 5. Temperature dependence of $\rho_o L$ for various constraints.

defined burn (shock) kinetics. The parametrically evaluated Q curves on Fig. 5 (Eq. (4)) indicate that radiation and/or conduction would limit Q to values below ~ 8 for this purely shock-heated example.

The results presented in Fig. 5 indicate regions where radiation and/or conduction losses may represent significant and voracious sinks for the ideally transformed projectile kinetic energy. Clearly, these energy sinks would most desirably be supplied by the fusion process itself, i.e., alpha-particle heating. Before the DT alpha-particle reaction product can deposit an appreciable fraction of the 3.5-MeV alpha-particle energy, the thermalization range λ_α must approach the heated projectile dimension, ℓ. The alpha-particle range, $\lambda_\alpha(m)$, is given by[10]

$$\lambda_\alpha = 1.38(10)^{26} \frac{T^{3/2} E_\alpha^{1/2}}{n\ell n(1/\delta)} \quad , \tag{12}$$

where

$$\delta = (1 + m_e/m_\alpha) e n^{1/2}/T^{3/2}$$

$$= 1.73(10)^{-18} n^{1/2}/T^{3/2} \quad , \tag{13}$$

and alpha-particle thermalization on electrons has been assumed to dominate. The quanitity f_α is defined as the fraction of the 3.5-MeV alpha-particle energy, E_α, deposited into a heated projectile of average dimension $\langle\ell\rangle$. This average dimension is defined as four times the volume-to-surface ratio (i.e., $\langle\ell\rangle$ is a "wetted perimeter" and equals 2ℓ for a slab of thickness ℓ or a cylinder of radius ℓ, or $4\ell/3$ for a sphere of radius ℓ). Following the usual transport approximation, f_α is given by

$$f_\alpha = 1 - 1/(1 + \langle\ell\rangle/\lambda_\alpha) \quad . \tag{14}$$

In the limit $\langle\ell\rangle/\lambda_\alpha \gg 1$, therefore, f_α approaches unity and good alpha-particle

confinement results. In the opposite extreme, $\langle \ell \rangle / \lambda_\alpha << a$, f_α approaches zero and the potential for "bootstrap" self-heating is nil. For a homogeneous projectile, perfect alpha-particle energy confinement ($f_\alpha = 1$) is not possible since some alphas will always be born within a mean free path length of the surface and will escape prior to thermalization. Substituting Eqs. (12) and (13) into Eq. (14) gives the following relationship between $\rho_o L$ and f_α for a homogeneous projectile

$$(\rho_o L)_\alpha = \frac{0.54\ T^{3/2}}{\ell n(1/\delta)} \left(\frac{f_\alpha}{1-f_\alpha}\right) \quad . \tag{15}$$

Figure 6 gives the dependence of $(\rho_o L)_\alpha$ on T for a range of specified alpha-particle energy trapping efficiencies, f_α. Shown also on Fig. 6 are the loci of points where the alpha-particle power deposited within the projectile, $f_\alpha P_\alpha$, equals the radiation power, as well as the radiation plus conduction powers. The latter curve represents the locus of ignition points, and the corresponding values of $(\rho_o L)_{IGN}$ are also included on Fig. 5. The achieveable Q-values, as predicted by this simple, one-dimensional shock-heated model, are unacceptably low from the viewpoint of an engineering power balance.

If longer burn times and, consequently, higher Q-values are to be achieved, the system must be designed for and operate with significant alpha-particle heating in order to maintain a thermonuclear plasma against classical radiation and conduction losses. The increase in Q accompaning a burn time that is sustained for considerably more than a single shock transit time, however, can be determined only by a kinetic model of the ignited system. The results of this analysis, as presented on Fig. 5, indicate a high potential for an ignited mode of operation. Furthermore, the density compression that accompanies a purely shock heating is very low ($\rho_s/\rho_o = 4$, Eq.(2B)), and the large dimensions required to give a $\rho_o L$ with a sufficient Q (Eq.(4)) translate into considerable input energies, W_K, and thermonuclear yields. This situation is best shown quantitatively by combining Eqs. (4) and (5) to give

$$Q = 1.09(10)^{13} \left(\frac{\langle \sigma v \rangle}{T^{5/2}}\right) \left(\frac{W_K}{\pi R^2}\right) \quad . \tag{16}$$

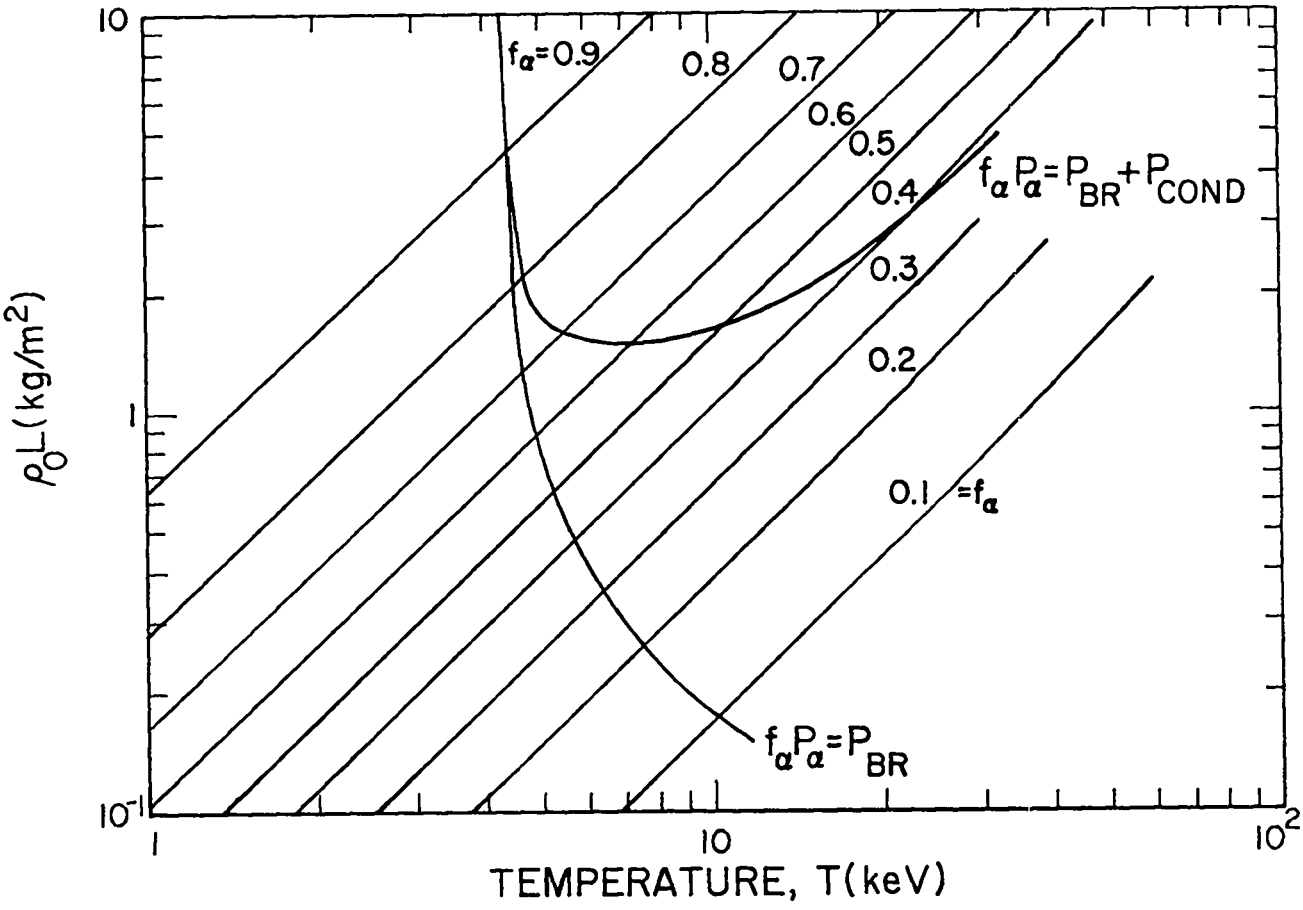

Figure 6. Temperature dependence of $\rho_o L$ required to trap a fraction f_α of the 3.5-MeV alpha-particle energy.

In order to obtain an explicit relationship between Q and W_K (i.e., the yield curve) for this shock-heated case, the projectile radius, R, is taken equal to the compressed length ℓ (near minimum surface-to-volume ratio at full compression), and ρ_o is equated to the density of cryogenic DT (~ 200 kg/m^3).

For $T = 10$ keV ($\langle\sigma v\rangle/T^{5/2}$ is fairly insensitive to temperature in this range), the yield curve for this shock-heated system becomes

$$Q = 0.0232\, W_K^{1/3} \quad , \tag{17}$$

where W_K is given in units of Joules. The parametric plot of Q_E versus Q and η_{ACC} given on Fig. 2 has been replotted on Fig. 7 in more convenient form, and Eq. (17) is also shown (curve 1). For any realistic value of η_{ACC} and with $Q_E > 5$, W_K and $W_F = QW_K$ will be considerable for the shock-heated yield curve [Eq. (17)]. A typical yield curve used for the design of laser/pellet fusion reactors[11] is also included as curve 5 on Fig. 7. Curves 2-4 show the results of a simple model based on adiabatic compression of a moderately shock-heated system. The adiabatic compression allows higher final DT densities to be achieved, and, for the same value of $\rho_o L$ and Q, a smaller projectile dimension and total energy requirement results. This adiabatic-compression model assumes no net energy losses and is described in the following section.

C. YIELD CURVES FOR IDEAL ADIABATIC COMPRESSION

In order to examine the potential improvement in the yield curve for a one-dimensional compression, a tamper of density ρ_T and length ℓ_T is added to the back of the DT cylinder depicted in Fig. 1. The tamper and DT projectile, again, is assumed to impact a perfectly rigid wall at an initial velocity u_o, and the DT mass is instantaneously shock-heated to an initial temperature T_o and length ℓ_o. A strong shock is assumed to move through the tamper, creating a pressure $(\gamma + 1)\, u_o^2 \rho_T/2$ at the tamper/DT interface. The DT would be compressed adiabatically over a period of time equal to the shock transit time within the tamper. Radiation and conduction losses are either assumed zero or equal to the alpha-particle "bootstrap" heating. This assumption is open to question, in view of the predictions given by Fig. 5. Nevertheless, this idealized, one-dimensional model provides an interesting limiting case that is amenable to analytic evaluation. The integrated adiabatic energy balance and the pressure balance enforced on the DT material gives the following relationships between the time-dependent temperature, T, and DT length, ℓ,

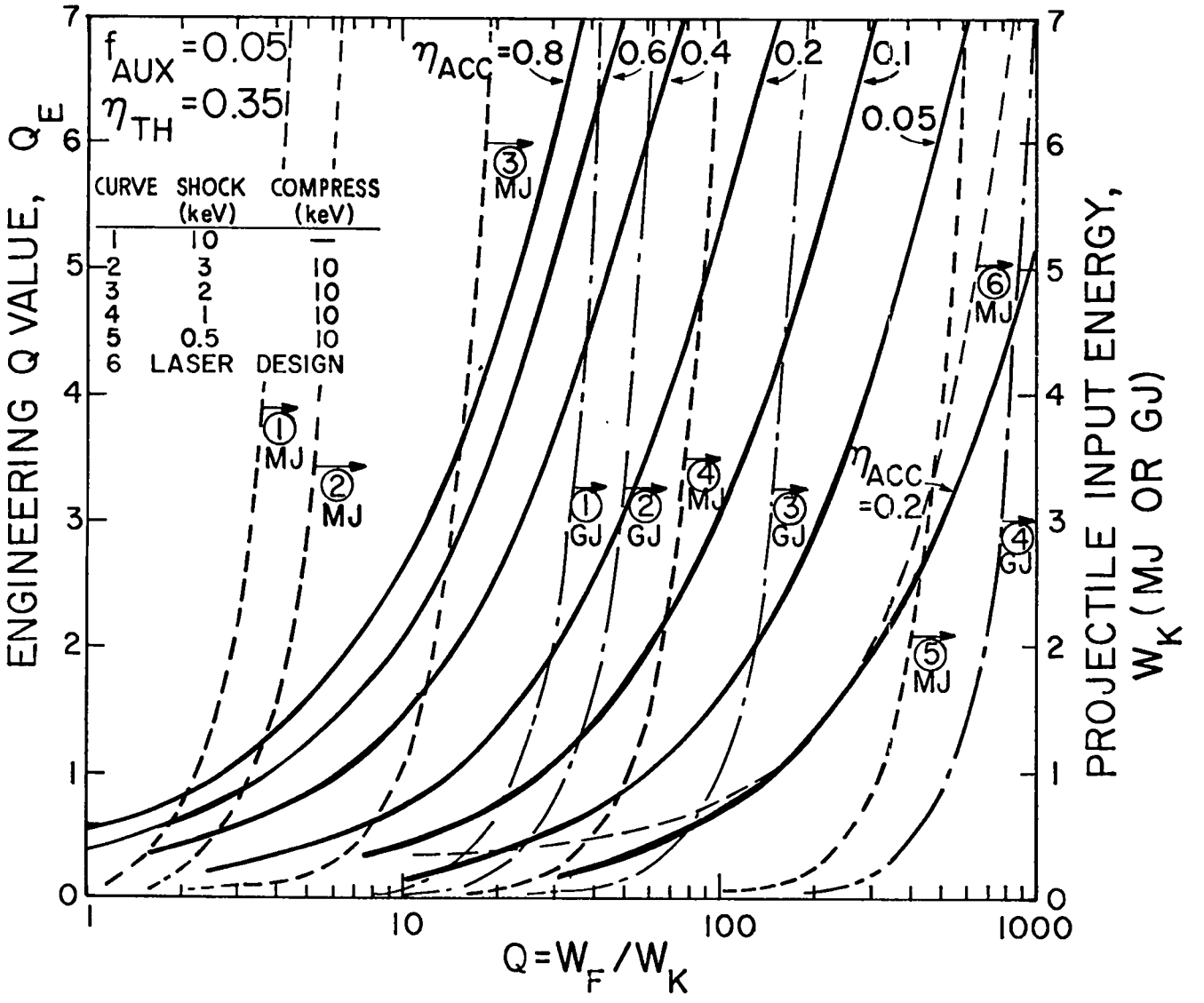

Fig.7 Parametric systems design curves for an Impact Fusion Reactor (IMF) showing limiting-case yield curves. Solid line curves represent Q_E versus Q and η_{ACC}, dashed-dot curves represent Q versus W_K(GJ) and the dashed curves represent Q Versus W_K(MJ).

$$T - T_o = \left[\frac{Am_p}{6(10)^3 e}\right] \xi \, (u_o^2 - u^2) \tag{18}$$

$$T/\ell = \left[\frac{(\gamma+1)Am_p}{4(10)^3 e}\right] \frac{u_o^2 \rho_T}{\rho_o \ell_o} \quad , \tag{19}$$

where mass conservation has been specified ($\rho\ell = \rho_o\ell_o$), the quantity ξ is defined as $\rho_T\ell_T/\rho_o\ell_o$, and the zero subscript refers to the shocked DT initial conditions. The time for a strong shock to traverse the tamper length is approximately given by

$$\tau = \left(\frac{2}{\gamma+1}\right)(\ell_T/u_o) \quad , \tag{20}$$

and is taken as approximately equal to the burn time. Defining $x = t/\tau$, the time dependence of u, T, and ℓ is easily shown to equal

$$u = u_o\left(1 - \frac{3}{2}\,x\right) \tag{21}$$

$$T - T_o = \frac{2T_o}{\gamma-1}\,\xi\,\left(x - \frac{3}{4}\,x^2\right) \tag{21}$$

$$\ell_o - \ell = u_o\tau\left(x - \frac{3}{4}\,x^2\right) \quad . \tag{21}$$

From these relationships, peak compression occurs at $x = 2/3$, and the final compression ratio ℓ_f/ℓ_o is given by

$$\ell_f/\ell_o = 1 - \frac{2}{3(\gamma+1)}\,(\ell_T/\ell_o) \tag{22}$$

$$= (T_o/T_f)^{1/\gamma-1} \quad , \tag{22}$$

where the last expression relates the final peak temperature, T_f, to the maximum compression ratio by means of the adiabatic relationship.

Substituting Eqs. (21) and (22) in Eqs. (3A) and (5) gives the following expression for $Q = W_F/W_K$

$$Q = \frac{E_N}{16e}\left(\frac{\langle\sigma v\rangle}{T^2}\right)\frac{\xi^2}{1+\xi}\,u_o\,(\rho_o \ell_o)\,I(\xi, \ell_T/\ell_o) \tag{23}$$

$$I(\xi, \ell_T/\ell_o) = \int_o^{4/3} \frac{\left[\frac{2(\gamma-1)}{3\xi} + \frac{4}{3}x - x^2\right]^2}{\frac{2(\gamma+1)}{3}(\ell_o/\ell_T) - \frac{4}{3}x + x^2}\,dx \quad . \tag{23}$$

In arriving at Eq. (23), $\langle\sigma v\rangle/T^2$ has been assumed constant ($\sim 1.09(10)^{-24}$ $m^3/s\ keV^2$), and the burn time is taken as one full cycle time for the compression, which equals 4/3 times the shock propagation time in the tamper, τ.

Designating the shock-heated Q-value given by Eq. (4) as Q_s, the ratio Q/Q_s is given by

$$Q/Q_s = \frac{2\xi^2}{(\gamma-1)(1+\xi)}\,I(\xi, \ell_T/\ell_o). \tag{24}$$

It is noted that Q represents an enhancement resulting from adiabatic compression, the total Q-value actually being $Q + Q_s$.

Finally, specifying, as in Sec. IV.B., the projectile radius, R, to equal ℓ_f gives the following expression for the yield curve

$$Q = 3.13(10)^{-3}\,T_o^{1/6}\left(\frac{T_f}{T_o}\right)\frac{\xi^2}{(1+\xi)^{4/3}}\,I\,(\xi, \ell_T/\ell_o)W_K^{1/3} \quad . \tag{25}$$

On the basis of Fig. 5, T_f is specified at 10 keV. Once T_o is selected, u_o, ℓ_T/ℓ_o, and ξ result. In this way $Q/W_K^{1/3}$ and Q/Q_s have been evaluated parametrically in T_o(or u_o) for T_f = 10 keV; this dependence is shown on Fig. 8. Curves 2-5 on Fig. 7 show the yield curves for T_o = 0.5-3 keV ($u_o = 3.4(10)^5$-$8.3(10)^5$ m/s). The beneficial effects of a lossless adiabatic compression in pushing the "edge" of the yield curve to higher gains is clearly shown. On the bases of these yield curves and the associated Q_E <u>versus</u> $Q_E(f_{AUX}, \eta_{TH}, \eta_{ACC})$ design curves, a range of "operating points" (i.e., Q_E, W_K, u_o, W_F) can be established from Fig. 7. Since these designs curves are based upon a lossless, one-dimension compression following an ideal shock heating,

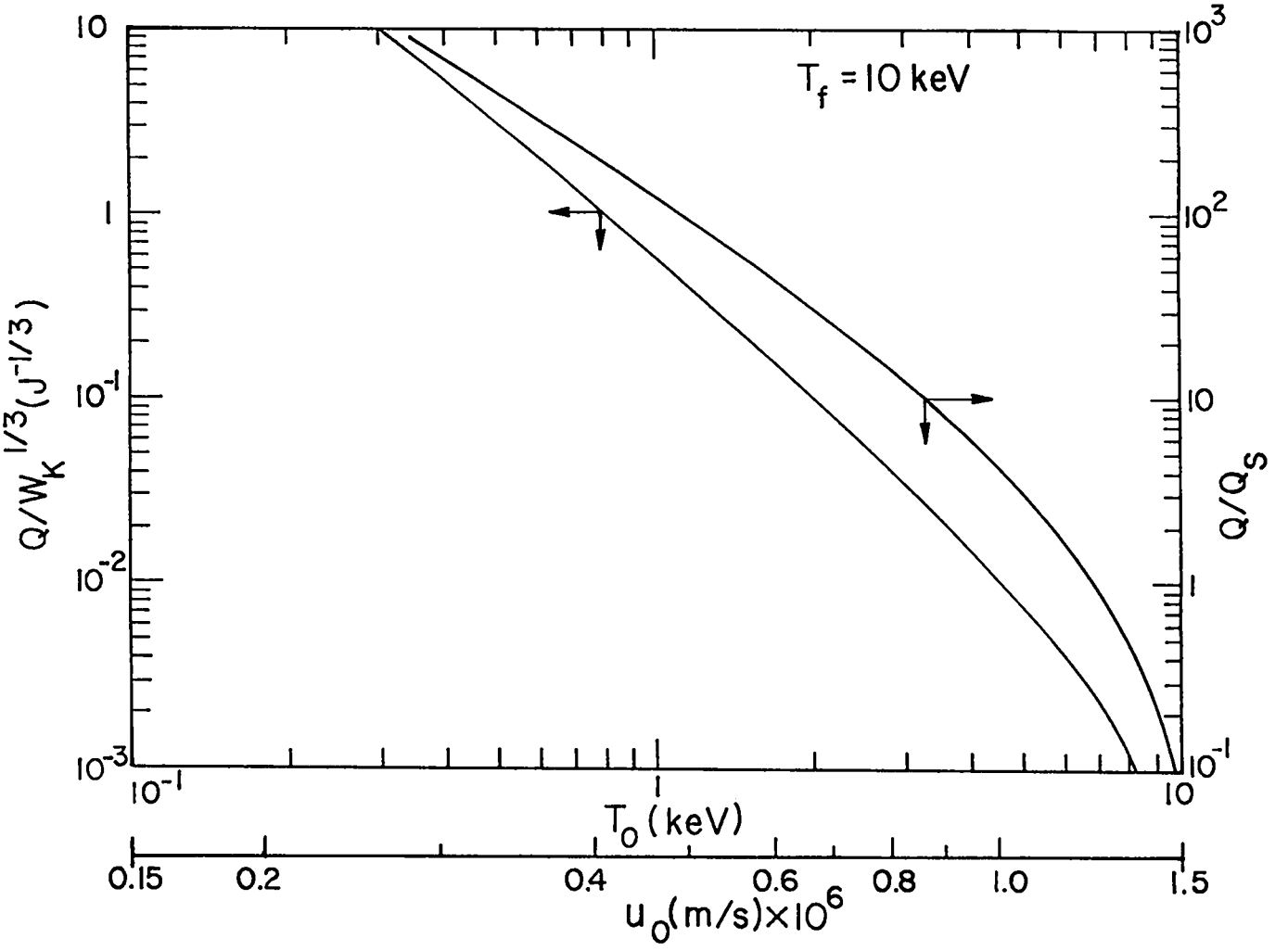

Fig. 8 Range of possible yield curves (Q versus $W_K^{1/3}$) for a lossless adiabatic compression as a function of initial projectile (DT/tamper) velocity or initial shock-preheat temperature. Dependence of associated Q-value relative to purely shock-heated case (Q_s) is also shown. Note that Q is an incremental value relative to Q_s.

predictions based on this model should obviously be used with caution. The indications are clear, however; adiabatic compression, to increase ρ for a given $\rho\ell$ and Q while reducing ℓ and W_K, is highly desirable.

V. CONCLUSIONS AND RECOMMENDATIONS

A number of wide ranging issues have been discussed in connection with the reactor promise portended by impact fusion. Because in-depth analyses of this specific fusion scheme are unavailable, much of this discussion has been presented in the form of questions that have been guided in part by system designs of other related fusion schemes. Depending upon the shape of the Q

versus W_K yield curve and the accelerator efficiency, the blast confinement and projectile/target materials requirement may present a critical path item towards the development of an IFR.

The economic and technical feasibility of an IFR depends crucially on the Q versus W_K yield curve, and an unambiguous resolution of this issue is required before serious system design studies can proceed. By means of simple analytic models, an attempt has been made to estimate these yield curves on the basis of a purely shock-heated system and an approach that envisages shock pre-heating followed by an inertial adiabatic compression. Although ignition may be possible with a purely shock-heated approach, the energy input requirements and energy releases for an acceptable value of Q_E will probably prove technologically unfeasible. The situation is considerably improved, however, when higher compressed densities are generated by adiabatic compression (smaller projectile dimensions and energies for the same $\rho\ell$ and Q values). The effect of radiation and/or conduction losses on achieving an appropriate adiabat, however, may be crucial, and other schemes to improve the performance that attempt to reduce radiation/conduction losses while improving compression efficiencies should be investigated by more realistic physics models.

REFERENCE

1. E. R. Harrison, "Alternative Approach to the Problem of Producing Thermonuclear Power," Phys. Rev. Lett. 12, 12, 535-537 (1963).

2. F. Winterberg, "Implosion of a Dense Plasma By Hypervelocity Impact," Plasma Physics, 10, 55-77 (1967).

3. R. W. Moses, R. A. Krakowski, and R. L. Miller, "A Conceptual Design of the Fast-Liner Reactor (FLR) for Fusion Power," Los Alamos Scientific Laboratory report LA-7686-MS (February, 1979).

4. L. A. Booth (Chairman), "Fusion Energy Applied to Synthetic Fuel Production," US Department of Energy report CONF-770593 (October, 1977).

5. R. A. Krakowski, K. E. Cox, J. H. Pendergrass, and L. A. Booth, "Synfuel (Hydrogen) Production from Fusion Power," 14th Intersociety Energy Conversion Engineering Conference, Boston, Mass., (August 5-10, 1979).

6. R. L. Hagenson, and R. A. Krakowski, "The Reversed Field Pinch Reactor (RFPR) Concept," Los Alamos Scientific Laboratory report, to be published (1979).

7. I. O. Bohachevsky, personal communication, Los Alamos Scientific Laboratory (1979).

8. L. Spitzer, Physics of Fully Ionized Gases, Interscience Inc., N.Y., (1956).

9. D. J. Rose, M. Clark, Jr., Plasmas and Controlled Fusion, The MIT Press, Cambridge, Mass., (1961).

10. T. Kammash, Fusion Reactor Physics; Principles and Technology, Ann Arbor Science Publishers, Inc., Ann Arbor, Mich., (1976).

11. L. Booth, personal communication, Los Alamos Scientific Laboratory, (1979).

VELOCITY REQUIREMENTS FOR ONE-DIMENSIONAL TARGETS

Thomas R. Jarboe
University of California
Los Alamos Scientific Laboratory
Los Alamos, New Mexico 87545

ABSTRACT

A simple zero dimensional model which includes thermal conduction, Bremsstrahlung, compressional heating, alpha heating, and wall movement losses is used to estimate the velocity necessary for a fusion reactor based on impact fusion. Simple 1D impact and spherical 3D shock heating and compression are considered. The results are that an absolute minimum of 6E7 cm/s is needed for the 1D case while 0.85E7 cm/s is needed in the 3D case. However 7E7 cm/s and 1.3E7 cm/s respectively look like good operating points.

INTRODUCTION

The purpose of this paper is to give an estimate of the minimum velocity needed for a projectile which is to shock heat and compressionally heat, in a simple one-dimensional manner, a column of DT gas to temperatures and densities necessary for a fusion reactor. The same model will also be applied to spherical implosions. The physical phenomena taken into account in the 1D estimates are thermal conduction, Bremsstrahlung, compressional heating, alpha heating, and losses due to motion of the containing back wall. In the 3D estimate the same effects are included, however there is no back wall but compression ratios and transfer efficiencies are discussed. These calculations are of the temperature at the center of the plasma and analytic equations are used to estimate the rate of change of this temperature due to each of the physical effects. Thus, there is no zoning of the plasma and its pressure is assumed uniform and acts on a slug (or spherical shell) which is assumed to have a mass per unit area but no thickness. Its velocity is determined by F = ma and the initial velocity.

DISCUSSION AND RESULTS

A. General

The basic equation for the normalized rate of change of the temperature is as follows:

$$\frac{1}{T}\frac{dT}{dt} = -\frac{[3](\gamma-1)v_p}{x} + 2.75E\text{-}4\ f_\alpha n T^{-5/3}\ \exp(-211.1/T^{1/3}) - 3.2E\text{-}14\ n/T^{1/2} - \left[\frac{3}{4}\right]\frac{1.4E21}{\ell n\Lambda}\frac{T^{5/2}}{nx^2} \quad (1)$$

The square bracket factors are needed when compression is 3D. The x which is the length of the plasma in 1D becomes the radius of the shell in 3D. T is in eV, n is in cm^{-3}, and v_p is the velocity of plasma compression. A γ of 5/3 is used in this calculation. The first term on the

right is the compressional heating term. The second term is the alpha heating term.[1] Where f_α is the fraction of alpha energy being absorbed

$$f_\alpha \equiv \frac{<\ell>/\lambda_\alpha}{1 + <\ell>/\lambda_\alpha}.$$

Where $<\ell>$ = 4x Volume/Area and λ_α is the range of α particles given by Spitzer[2] due to energy absorption by only the electrons. The equation is good only for temperatures up to about 20 keV. The third term on the right is for Bremsstrahlung and is derived from the equation of Boyd and Sanderson.[3] The last term is the thermal conduction loss term. The coefficient of thermal conductivity of an unmagnetized plasma is given by Spitzer.[2] The term is found by considering a system of contained plasma with thermal conduction in only one direction. To get this equation one uses the fact that the pressure and its time derivative are uniform over the plasma and the density profile is time independent.

In the calculation the plasma's initial temperature is found by assuming that it is equal to that of the DT in a one-dimensional shock where the piston has the velocity of the imploding wall. The energy which is needed for shock heating is subtracted from the plug energy and the remaining velocity is the initial velocity for the calculation and is used to find the initial temperature. This temperature for DT is:

$$T_i = v^2/2.4E12 \qquad \text{(eV, cm/s)}$$

The final approximation is that the mass of the plasma is ignored.

Before discussing the methods of optimization for minimum velocity and the calculational results a discussion of Eq. (1) is in order. Multiplying it by x and rearranging yields:

$$[3]\ (\gamma - 1)\left|v_p\right| \geq \frac{C(t)}{y} + [B(T) - A(T)]y \qquad (2)$$

when

$$\frac{1}{T}\frac{dT}{dt} \geq 0,\ f_\alpha = 1,\ \text{and}\ y \equiv nx.$$

A(T), B(t) and C(T) are the Alpha heating, Bremsstrahlung, and thermal conduction temperature dependent parts. Note that the velocity requirement for a given T depends only on y which can be chosen to minimize the v_p requirement. However in the 1D case Bremsstrahlung is worse early in time since $B(T) \alpha 1/T^{1/2}$. This gives another velocity requirement namely

$$(\gamma - 1)\ v_p \geq B(T_i)y. \tag{3}$$

Since both C(T) and A(T) have strong temperature dependence they are negligible early in time. Thus Eq. (2) and (3) give the velocity requirement for achieving any given T in 1D. Besides the obvious factor of 3 in Eq. (2) another advantage of 3D compression is that the velocity requirements for both Bremsstrahlung and thermal conduction are greater at higher compression because y is time dependent in 3D. Thus, an optimum y can be picked for Eq. (2) further reducing the velocity requirements in 3D. Figure 1 shows the 1D velocity requirement as a function of temperature. In Fig. 1 the mass per unit area is infinite and hence it does not give information about Q. Q is the ratio of thermonuclear energy divided by the initial kinetic energy.

B. 1D Q Calculations

The fact that the back wall motion is included in these calculations adds a loss mechanism which does not depend on the nl product but more on nT. In these calculations the back wall moves according to:

$$p = \rho_o v_w (v_s + 4/3\ v_w)$$

where v_w is the wall speed and p is the plasma pressure. ρ_o = 20 gm/cm^3 and v_s = 5.E5 cm/s. These are the density and sound speed of the wall material. The initial length of the system is set at 10 cm. The mass unit area and n are varied (20% stop size) to find the optimum Q for each velocity. The results are shown in Table I. Since fuel depletion is not calculated Q's over 100 are not accurate, but these calculations show when alpha heating dominates Eq. (1). Also shown in Table I is the minimum energy required to achieve the Q's shown. The table shows the initial Bremsstrahlung cooling time divided by the time needed to shock-heat the gas to its initial temperature. The fact that this ratio is about 1 shows that some cooling will occur during the shock heating process especially in the gas that is shocked first. Thus the actual initial temperature may be some lower than used in the calculation. However, if it is large enough to satisfy Eq. (3) then the plasma will heat and the same Q's will be achieved but with a larger compression ratio.

Figure 2 shows the plasma length, plasma temperature and Q versus time for the v = 7E7 cm/s case. It can be seen in Fig. 2 that the compresssional heating ignites the fuel and most of the energy is released during the expansion. The piston in this case has a mass of 0.86 gm/cm and an energy of 230 MJ/cm^2. The 1D system also has the other two undiscussed dimensions which can cause added thermal conduction losses. However, it appears that in the v = 7E7 case the diameter need only be about 1 cm so that radial thermal conduction losses even at L = 10 cm will be small compared to the compressional heating. The reason that the diameter can be this small is due to the strong temperature dependence of the thermal conduction. Thus, a copper slug for the 7E7 cm/s case could be 1 cm in diameter and 1 mm thick which is about the thickness of a penny and half as large in diameter.

In this example the total energy is rather large. However, the system can be made smaller provided that a) the values of y, the velocity, and mass per unit area are kept the same, b) the back wall movement doesn't rob significantly more energy, and c) the thickness of the slug does not exceed the final plasma length. The last condition is necessary for the model to be applicable and will be necessary for efficient transfer of liner energy into plasma energy in any case. This last condition puts the largest lower

bound on the system size. Thus if the plug were tungsten then it could be 0.5 mm thick and the system could be made half as large in all dimensions giving a peak compression length of 0.6 mm which is acceptable. The area of the plug would be about 0.2 cm^2 with an energy of about 50 MJ.

C. 3D Q Calculations

The optimization in this case is done by varying y and the mass per unit area divided by y. The maximum Q for a given velocity is shown in Table II. The energy in the model thus far can be arbitrarily small but what is shown is from the following considerations. In order for the shell to efficiently transfer its energy to the plasma it cannot have a thickness much greater than the radius of the plasma. If its thickness is too great, it will transfer too much of its kinetic energy into its own internal energy. This is a consequence of the fact that the speeds involved here are well above the speed of sound in the shell material. From this we have that at peak compression

$$f_o \, \varepsilon \, \frac{1}{2} \rho_o v_i^2 = 3 \, n_f \, kT_f .$$

Here f_o is the ratio of shell volume to plasma volume and ε is the efficiency of transfer of shell energy to plasma energy. From this the initial energy in the shell can be written as

$$E = f \, \frac{4}{3} \pi \left[\frac{3kT_f \, (n_f r_f)}{f \, \varepsilon \, \frac{1}{2} \rho_o \, v_i^2} \right]^3 \frac{1}{2} \rho_o \, v_i^2$$

$$= 35 \; E41/v_i^4 \quad \text{(ergs)} \tag{4}$$

where $n_f r_f$ is the final value of $3E22/cm^2$. T_f is 4000 eV, ρ_o is 20, and v_i is the initial shell velocity. Values from Eq. (4) are shown in Table II when $f_o = 7$ and $\varepsilon = 1/4$.

Another consideration is that radial compression ratio limitations also limit the minimum velocity. Figure 3 shows the velocity requirements necessary for each compression ratio. It seems that a good velocity would be 1.3E7 cm/s. It will give a high Q for a modest amount of shell energy while requiring a radial compression of about 20:1.

CONCLUSION

It appears that a projectile with an energy of 50 MJ and a velocity of about 7E7 cm/s will be required for simple 1D impact fusion and that an imploding shell of about 12 MJ at a speed of 1.3E7 cm/s could be used for a 3D implosion. In 1D the velocity is much higher but the geometry is simpler. The ability to achieve high velocities compared to the ability to produce symmetrical 3D implosions will determine which geometry is most desirable.

REFERENCES

1. R. Krakowski and R. Miller, Los Alamos Scientific Laboratory, personal communication, June 1979.

2. Lyman Spitzer, Jr., "Encounters between Charged Particles", in Physics of Fully Ionized Gases, (Interscience Publishers, New York, 1967), Chap. 5, pp. 120-153.

3. T. J. M. Boyd and J. J. Sanderson, Plasma Dynamics (Barnes Noble, Inc., New York, 1969), p. 230.

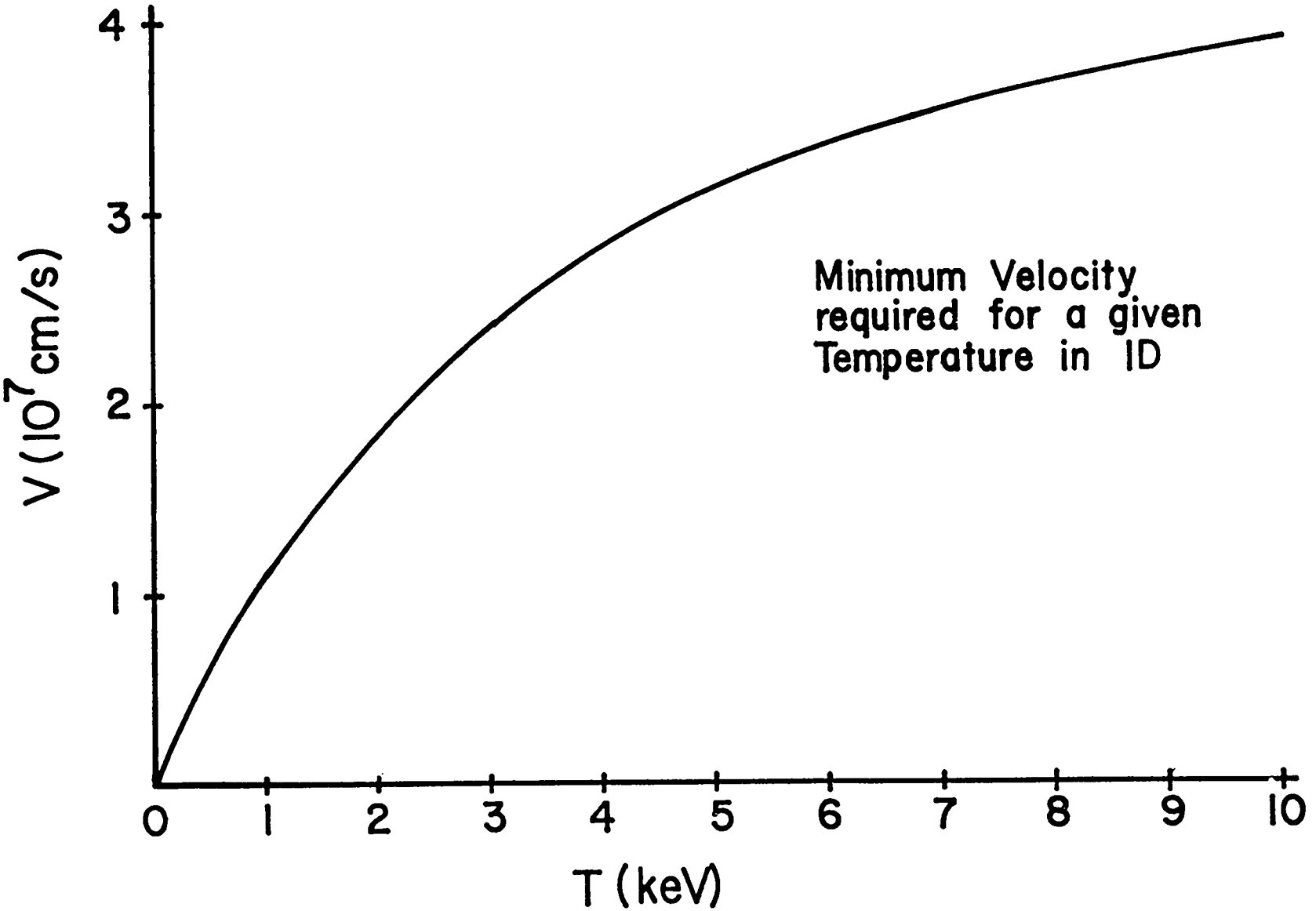

Fig. 1. Minimum impact velocity in 1D needed to achieve a given temperature.

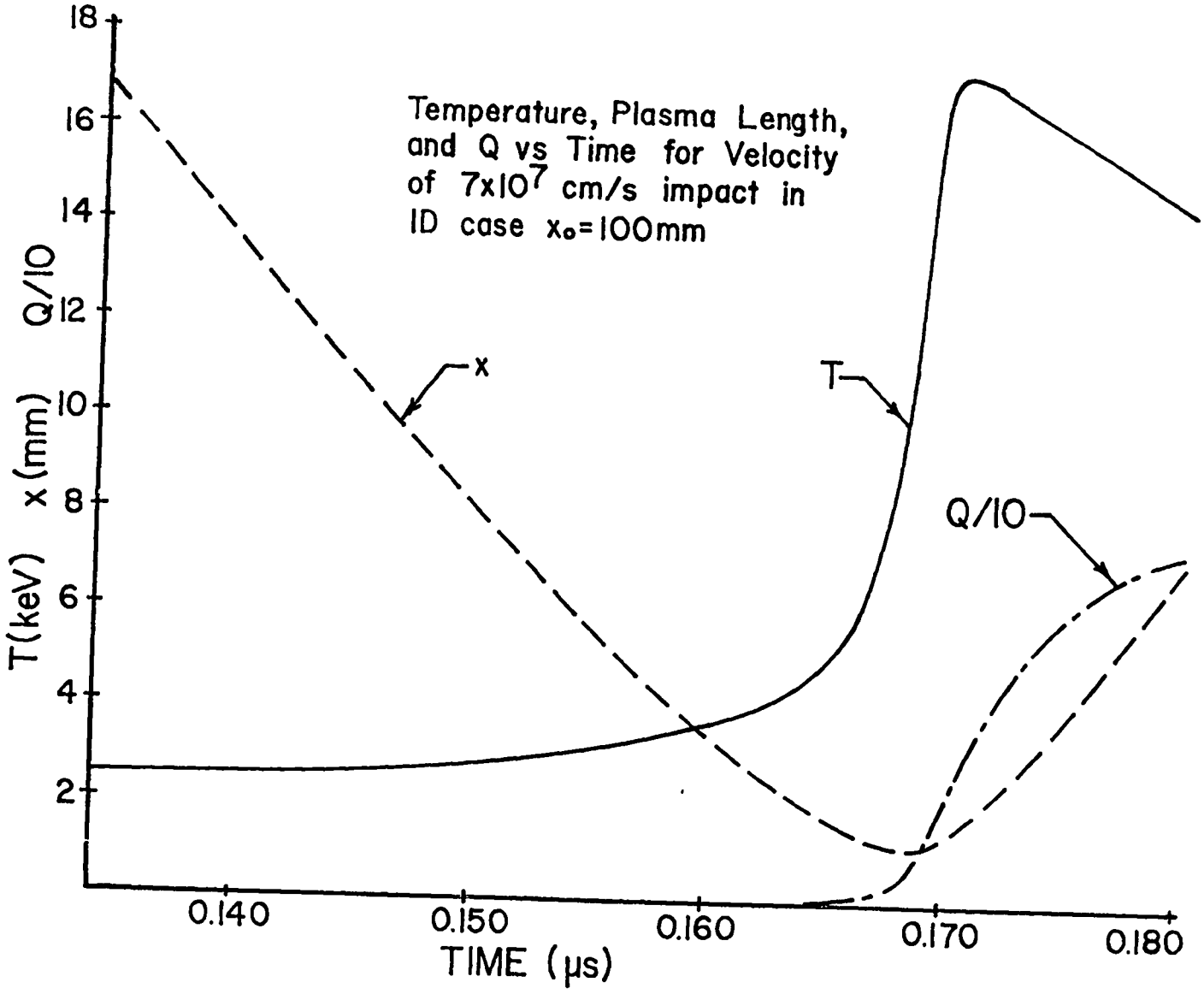

Fig. 2. Plasma length, temperature, and Q vs time for the 1D impact in the 7E7 cm/s velocity case of Table I.

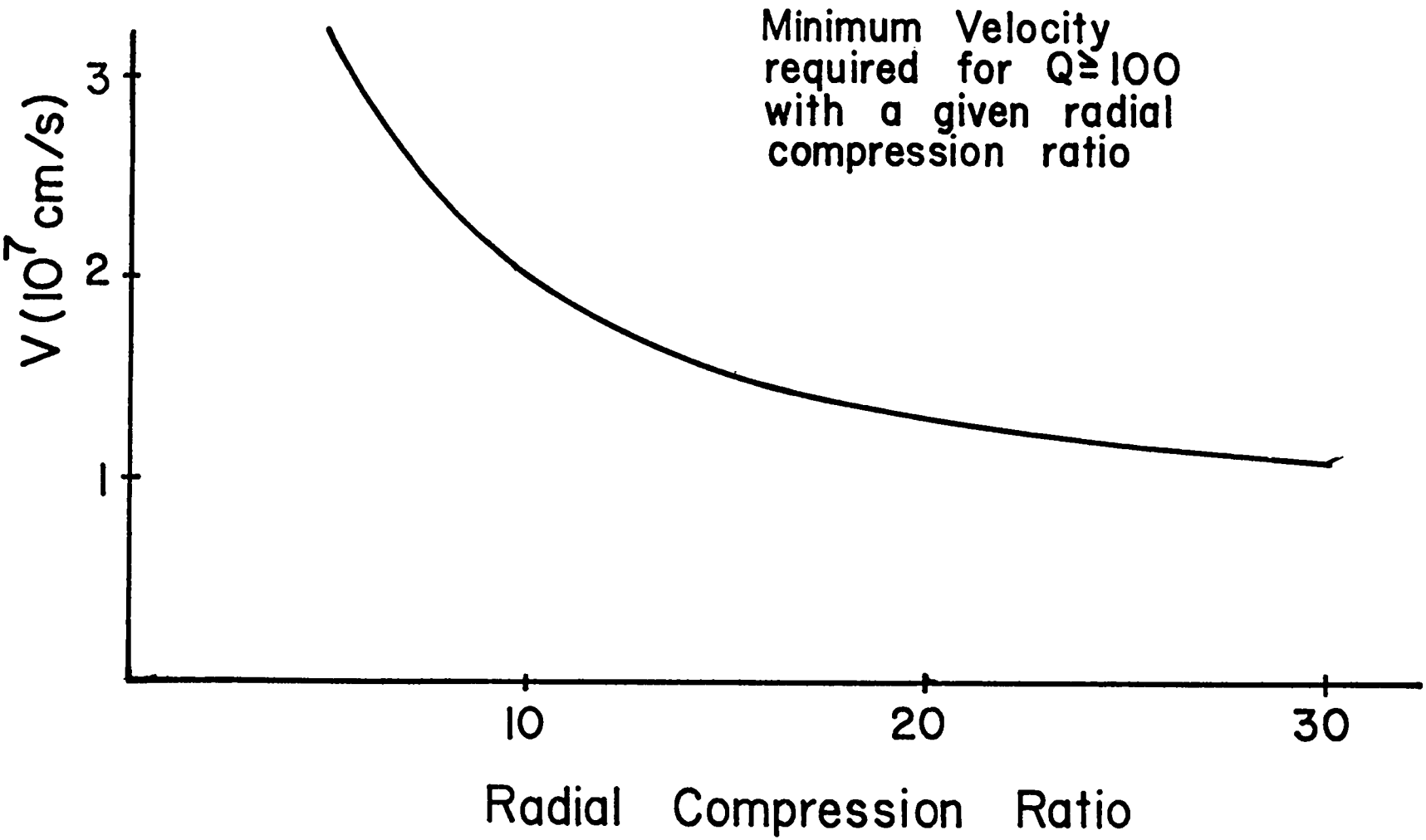

Fig. 3. Minimum velocity requirements as a function of the maximum allowable compression ratio to achieve $Q \geq 100$ in 3D compression.

TABLE I

Optimum parameters for 1-D impact

Velocity	$T_{INITIAL}$	Q	$\frac{MJ}{cm^2}$	$\frac{mass}{cm^2}$	nx	Initial $\frac{\tau_{BREM}}{\tau_{SHOCK\ HEAT}}$
1×10^7	41eV	.000007	1.1	.22gm	$6.7\times10^{20}cm^{-2}$	1.0
2×10^7	160	.0021	8.0	.40	2.6×10^{21}	1.0
3×10^7	360	.028	26	.58	5.0×10^{21}	1.2
4×10^7	640	.15	69	.84	8.7×10^{21}	1.1
5×10^7	1000	.64	150	1.2	1.5×10^{22}	1.1
5.5×10^7	1200	2.5	630	4.2	2.4×10^{22}	.82
6×10^7	1500	>100	1100	6.0	3.4×10^{22}	.71
6.5×10^7	1600	>100	360	1.7	3.6×10^{22}	.75
7×10^7	1800	>100	230	.96	3.6×10^{22}	.86
8×10^7	2100	>100	190	.60	4.1×10^{22}	.93
9×10^7	2400	>100	170	.43	4.5×10^{22}	1.0
10×10^7	2600	>100	150	.30	4.3×10^{22}	1.2

TABLE II

Optimum parameters for 3-D impact

Velocity	$T_{INITIAL}$	Q	Energy (MJ)
$.5 \times 10^7$	10eV	.010	--
.6	15	.029	--
.7	20	.068	--
.8	27	.15	--
.85	30	>100	67
.9	34	>100	54
1.1	50	>100	24
1.3	60	>100	12
1.5	81	>100	6.9
2.0	167	>100	2.2
3.0	375	>100	.43
4.0	667	>100	.014

KALISKI'S EXPLOSIVE DRIVEN FUSION EXPERIMENTS

J. Marshall
Los Alamos Scientific Laboratory*
Los Alamos, NM 87545

In this paper I report on an experiment performed by a group in Poland on the production of DD fusion neutrons by purely explosive means. Briefly, they have found means to produce a linear piston motion with a velocity of 5×10^6 cm/sec, and have used that motion to shock heat and compress D_2 gas to temperatures of 500 eV, with densities of $6 \times 10^{22}/cm^3$, and neutron yields of up to 3×10^7.

The group was headed by Sylvester Kaliski, unfortunately now deceased, who although he held a large number of political and administrative positions, was an exceptionally productive physicist. At the time of his death in September 1978 at the age of 54, Kaliski was a member of the Polish Academy of Science, a member of the Polish Parliament, a member of the Central Committee of the Polish United Workers Party, Minister of Science, Higher Education and Technology in the Polish government, and was Director of the Institute of Plasma Physics and Laser Microfusion in Warsaw. He had been Commander of the Military Academy of Technology from 1969 to 1974 and held the rank of Liuetenant General in the Army. He was founder and Editor in Chief of the Journal of Technical Physics, published entirely in English in Warsaw. In 1977 he published 12 theoretical papers in that journal and was co-author of nine additional papers, mostly experimental. He appears to have started his work in inertial fusion no earlier than 1976. His first papers on the subject appear in 1977.

*Work performed under the auspices of the U.S. Department of Energy.

The work I wish to discuss here was published in collaboration with others in Refs. 1 and 2. Presumably the experimental work was chiefly done by the others, Derentowicz, Wolski, and Ziolkowski. The first paper is theoretical, while the second is experimental. Derentowicz and Ziolkowski appear to be the principal experimental authors.

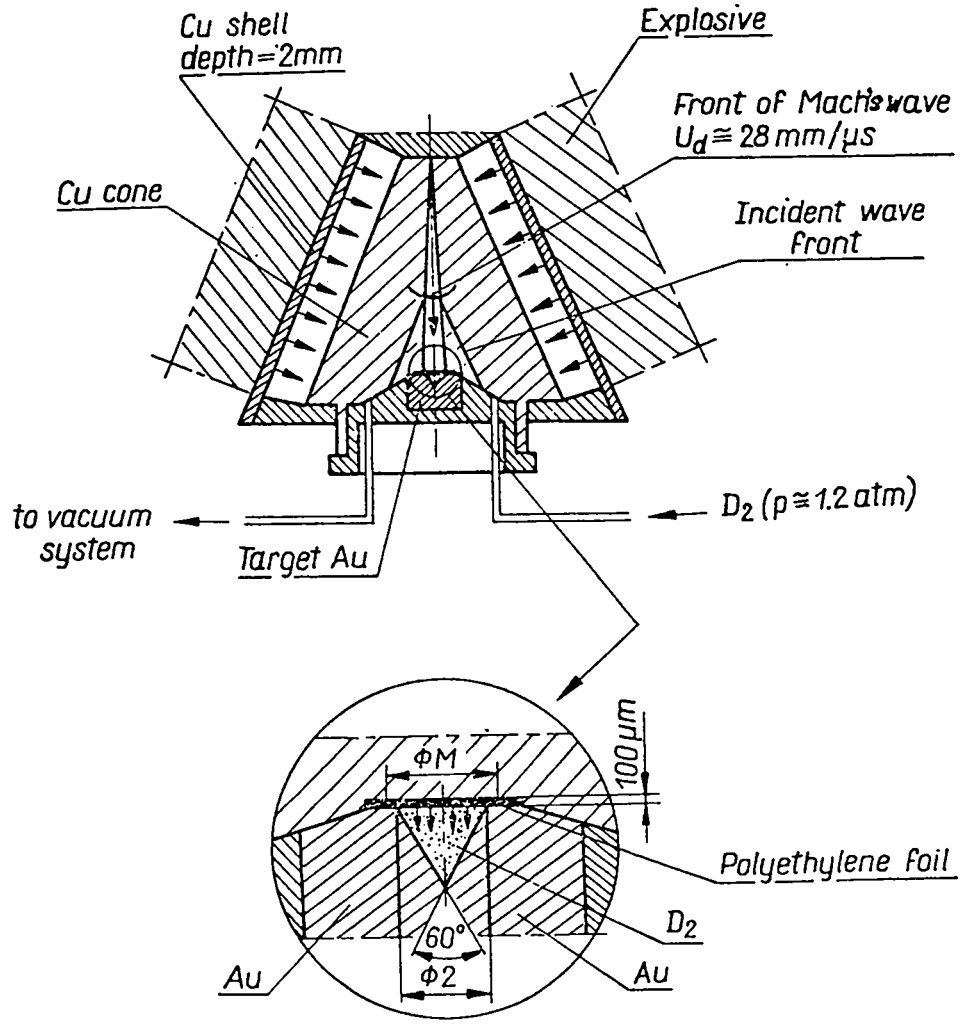

Fig. 1. Experimental Arrangement.

A schematic diagram of the system is given in Fig. 1. A solid copper truncated cone of half-angle is surrounded by a 2-mm thick conical copper liner having the same half-angle. The angle is varied in different shots from 15^{o} to 31^{o}. A vacuum space, several times as thick as the liner separates the liner from the solid copper cone. A hollow conical explosive charge fits closely around the liner. The explosive is fired in such a way that an inward moving detonation wave reaches its entire inner surface as simultaneously as possible. By means of a series of shock waves and rarefaction waves running back and forth through its thickness, the liner is accelerated to a speed of 4 to 5 x 10^{5} cm/sec by the time it has crossed the vacuum gap separating it from the surface of the solid cone. The impact of the liner against the cone produces in it a conical shock wave moving inward toward the axis at velocity v_s. The shock wave is stronger than it would have been if the explosive had been directly against the cylinder but sustains its pressure for a shorter time. The convergence of the conical shock toward the axis moves with a phase velocity v_m along the axis of the cone. The axial phase velocity is larger than the velocity of the conical shock by the factor

$$\frac{v_a}{v_m} = \frac{1}{\sin \alpha}$$

Thus, if the cone had a half angle of 30^{o}, the phase velocity along the axis would be twice the velocity of the conical shock.

Under certain conditions, viz. weak conical shock or small cone angle, α , the shock will simply reflect from the axis, so as to form an outward moving conical wave. With strong conical shocks of large enough α, the conical wave is refracted into an axial direction and produces enough pressure to support an axially propagating, nearly plane shock wave at phase velocity v_m. The result is the conical analog of Mach reflection, or a Mach wave. The pressure

behind the Mach wave front can be, because of cylindrical convergence, many times larger than pressures in ordinary explosive-driven shocks. In the present experiments, pressures of 30 to 50 megabars (Mb) are generated in a small diameter circular Mach wave. Small cone angles, α, result in larger pressures, see Fig. 2, but in smaller diameter Mach waves, greater sensitivity to small asymmetries in the explosive system, and poorer reproducibility from shot to shot. Characteristics of the Mach wave in cones of three different angles are given in the Fig. 2 and in Table I.

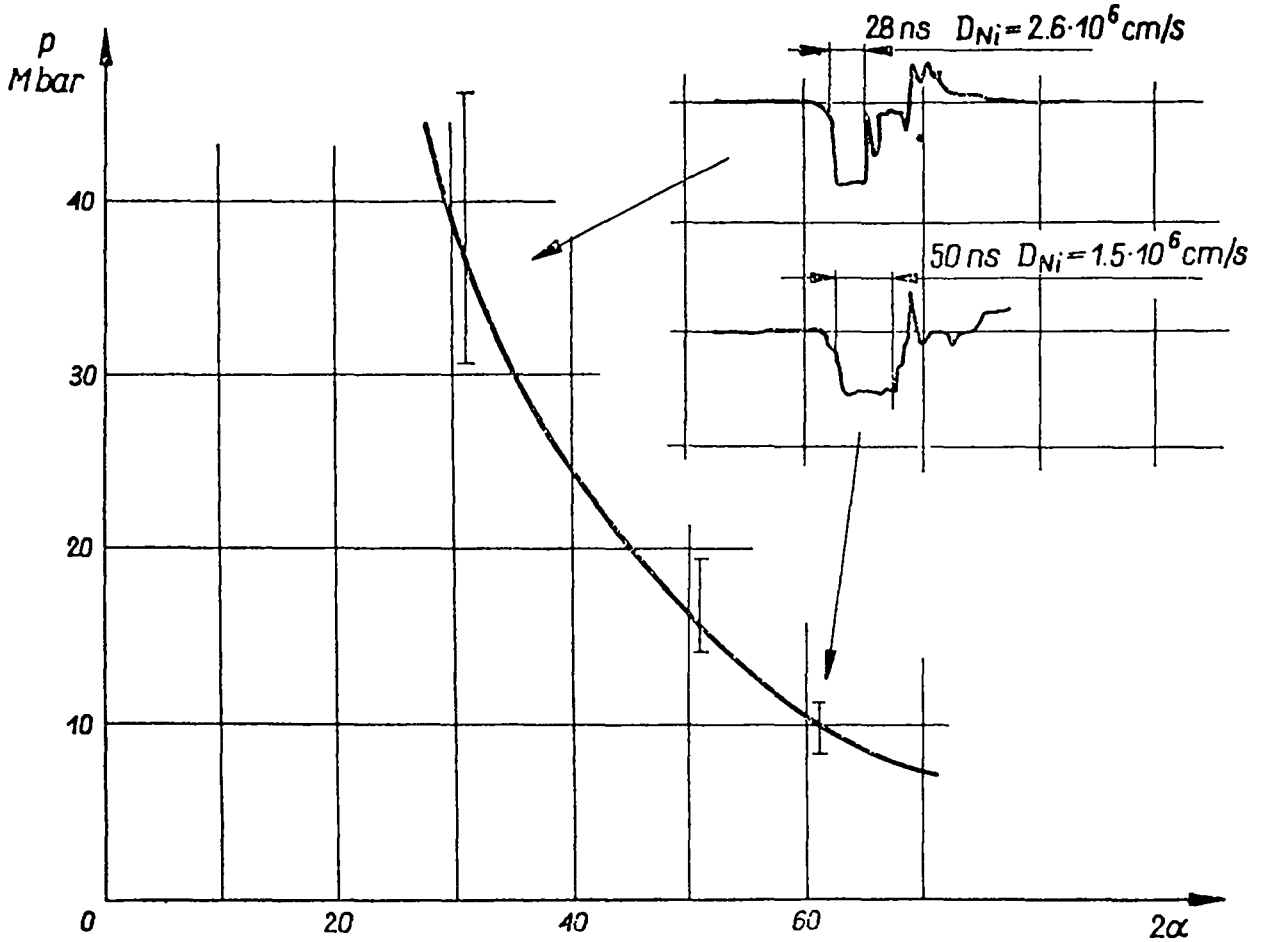

Fig. 2. Cu-Ni thermoelectric probe results and derived shock pressure as function of cone half-angle, α.

TABLE I

Mach Wave Characteristics as Function of Cone Half-Angle, α.

Angle 2α	Pressure on the Mach wave front [Mb]	Diameter of the Mach wave front [mm	Velocity of the wave front in plexiglass [cm/s]
62°	9.0	7.0	$1.8 \cdot 10^6$
30°	30÷35	2.4	$3.5 \cdot 10^6$
36°	30	2.5	—

When a shock wave reaches a free surface, in this case when the Mach wave reaches the base of the solid copper cone, a rarefaction wave is reflected back into the material with a particle velocity parallel to and approximately equal to the particle velocity in the shock. In the present system, the base of the copper cone is not precisely a free surface, but is covered by a thin layer of polyethylene as shown in Fig. 1. The polyethylene is sufficiently soft, relative to the copper that it allows near doubling of the particle velocity, thereby producing a shock in the polyethylene with double the particle velocity of the Mach wave in the copper. On the back side of the polyethylene is D_2 gas at 1.2 bar pressure. Again relative to the polyethylene, this looks like a vacuum, and a further near doubling of the particle velocity occurs.

The D_2 gas is contained in a 30^0 half-angle cone in a small block of gold. The cone is 2-mm in diameter at its base and is sealed against the polyethylene layer, which is 40- m thick. The free surface of the polyethylene compresses D_2 gas ahead of it toward the apex of the cone, with an initial piston velocity of nearly 5×10^6 cm/sec. The D_2 is shock heated and compressed by a factor of about 1000 in volume, achieving an estimated final temperature and density of 500 eV and $6 \times 10^{22}/cm^3$. Neutrons were recorded on nine shots altogether, with yields varying from 2.5×10^4 to 3×10^7. They ascribe the wide scatter of neutron yields to instabilities in the Mach wave generation process. For every shot with D_2 there was a blank shot without D_2. The blank shots produced no sign of neutrons.

What this group has done is to employ a set of standard (and not so standard) tricks in tandem to multiply the velocities, ordinarily available from high explosives, by a factor of 10 or so. The final piston has a linear motion resembling what we might associate with impact fusion. The linear motion is used to produce a quasi-spherical compression in a conical system.

The shock wave tricks, giving the high velocity, are mostly similar to procedures that have been developed over the years to extend equation of state shock wave measurements to extreme pressures. Direct application of explosive pressures to copper is capable of producing shock particle velocities of 1.5 km/sec, and pressures approaching 1 Mb. The accelerated copper liner reaches speeds of 4 to 5 km/s, producing an intensified conical shock in the solid copper cone with particle velocities of 2 to 2.5 km/sec and pressures of perhaps 1.5 Mb. Similar work has been done in equation-of-state measurements to extend them to 2 Mb. The conical shock waves combine pressure augmentation by cylindrical convergence with an appropriate Mach wave, resulting from the conical arrangement, to bring the pressure to the range of 50 Mb. Equation-of-state work in the USSR has been extended to nearly 10 Mb pressure by the use of plane Mach waves in the work of Al'tshuler, et al. Velocity multiplication by free surfaces follows well extablished techniques in equation-of-state work.

The use of a polyethylene free surface to compress the deuterium and a gold cone to give it quasi-spherical convergence is made practical in these experiments by the relatively low density of the deuterium that is compressed from atmospheric pressure gas rather than from solid or liquid densities. Bremsstrahlung and thermal conduction losses appear to be small enough not to interfere seriously with the compression heating.

The development of the explosive and shock wave techniques employed for velocity augumentation appear to have been the result of extensive experimentation with cylindrical shock waves and axial Mach waves. Some of the measurement techniques had to be developed specially because of the small dimensions involved. One technique (Fig. and Ref. 3) involves the use of a Cu-Ni-Cu thermoelectric gauge, which measures the velocity of the shock directly as it sweeps over a small nickel cylinder. A thermoelectric signal results when the shock sweeps over the Cu-Ni junction and then is canceled when it sweeps over the Ni-Cu junction. The time between the two events, together with the length of the cylinder, gives the shock velocity in nickel. This should be essentially the same as in copper because of the same density.

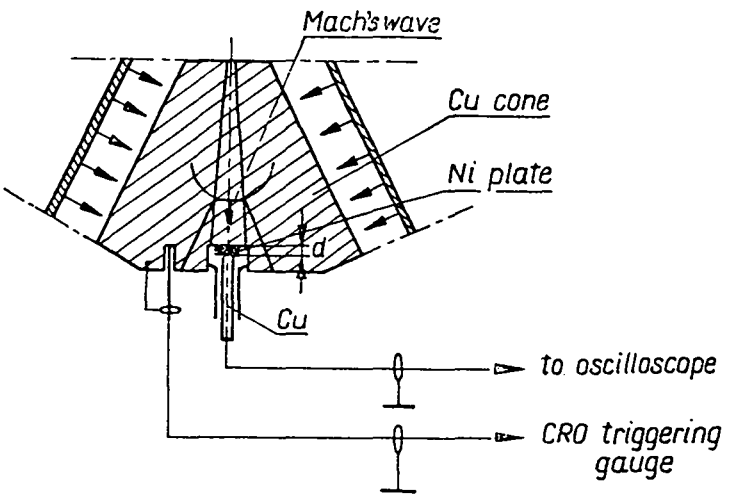

Fig. 3. Cu-Ni-CU Thermoelectric Probe.

Most of the measurement techniques were optical since these required very little change from standard techniques used in equation-of-state work. Typically, these involve light from shocked argon gas layers recorded by streak and framing cameras. Neutrons were measured using scintillators. Optical diagnostics are indicated in Fig. 4.

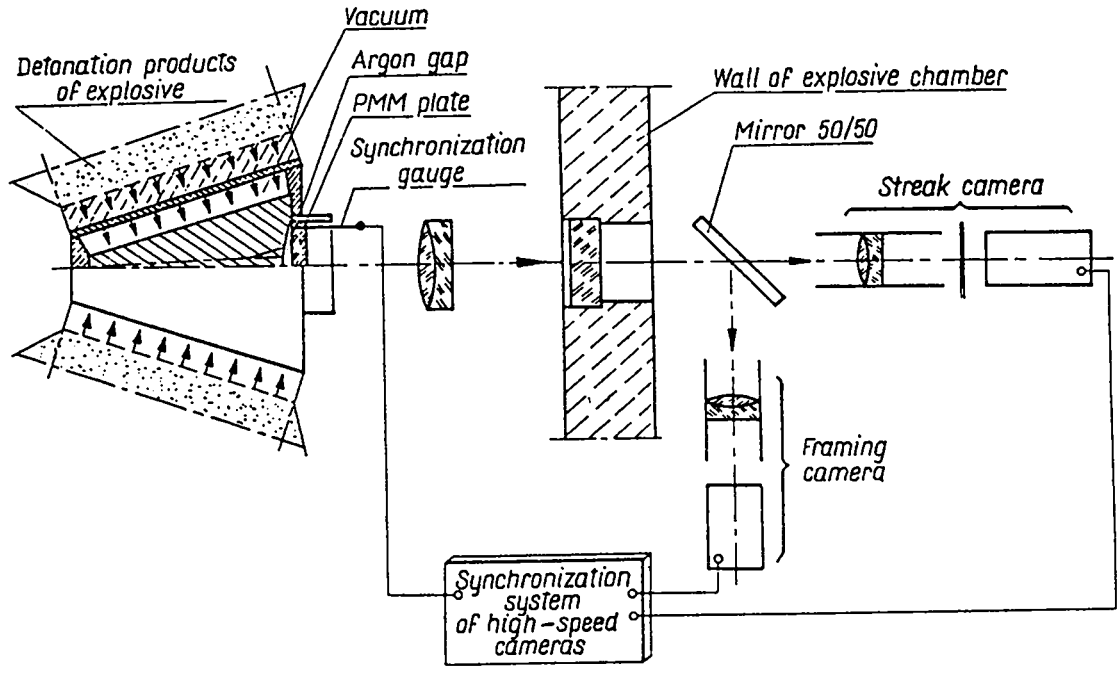

Fig. 4. Optical Diagnostics.

References

1. H. Derentowicz, S. Kaliski, and Z. Ziolkowski, "Generation of Fusion Neutrons in a Deuter Filled Cone by Means of Explosive Implosion of Polyethylene Shell, Part I, Theoretical Estimations," Journal of Technical Physics 18, 4, 465 (1977).
2. H. Derentowicz, S. Kaliski, J. Wolski, and Z. Ziolkowski, "Generation of Thermonuclear Fusion Neutrons by Means of a Pure Explosion. II. Experimental Results," Bull. de l'Academie Polanaise des Sciences, serie sciences techniques XXV #10, 135- 897 (1977).
3. H. Derentowicz and Z. Ziolkowski, "Measurement of Parameters of Convergent Cylindrical Shock Waves by Electrical Methods in Metal Samples," Journal of Technical Physics 19, 2, 201 (1978).

Power Multiplication Using Hydrodynamic Bunching for Ion Driven Impact Fusion

Jay Boris and John Gardner, Code 6020
U.S. Naval Research Laboratory
Washington, D.C. 20375

In recent analyses of ion deposition and ablative acceleration of thin foils performed at NRL efficiencies in excess of 25% were found for conversion of light ion beam energy to directed kinetic energy of a rather cold foil. The accelerated foils reached $2\text{-}5*10^6$ cm/sec in times of order 100-200 nsec. Light ion drivers seem limited in current technology to about 1 cm^2 spot size and do not yet have the total energy needed to accelerate the payload to 10^7 cm/sec directly as yet. Heavy ion and laser drivers allow smaller spot size in principle but do not yet have the total deliverable energy of existing pulsed power machines. In Figure 1 we show a schematic diagram for a device which hydrodynamically bunches the delivered energy in both spot size and time. In effect we are proposing a two-stage gas gun which the input velocity of $2\text{-}5*10^6$ cm/sec is about equal to the output velocity of conventional hypervelocity technology.

Rough calculations indicate that enough energy is available to accelerate small plugs at the convergence of the chamber to velocities well in excess of 10^7 cm/sec but the resultant accelerations must be very large, 10^{14} to 10^{15} cm/sec^2. Figure 2 shows the configuration in which the plug is driven down a short "barrel" by the quasi-spherical compression of the buffer gas. The efficiency of conversion of the foil kinetic energy to the compressed gas buffer has been calculated to be approximately 20%, the remainder of the energy residing in internal energy of the thickening compressing driver foil material. Calculations are planned in which the convergent geometry and non-ideal effects are treated during the plug acceleration to determine how much of the buffer energy can be transferred to the accelerating plug.

The hydrodynamic stability of the driver foil and the plug appears to be very good. The foil is, in effect, an exploding pusher and its inner edge in contact with the buffer accelerates continuously until just before peak compression so Rayleigh-Taylor instability (as opposed to assymetry) is not expected to be important until the driver material starts to decelerate strongly. Recent analyses of ablation accelerated foils such as the plug indicate Rayleigh-Taylor stability in the parameter regime of interest here on the back of the plug. Care must be taken to ensure that the buffer plasma losses to the wall are acceptable (an axial discharge for magnetic insulation might be indicated). Care must also be taken to ensure that the adiabat of the plug is kept low despite the fast acceleration at peak compression. Using existing pulsed power systems the questions raised here could be answered at least in part in the next year or two.

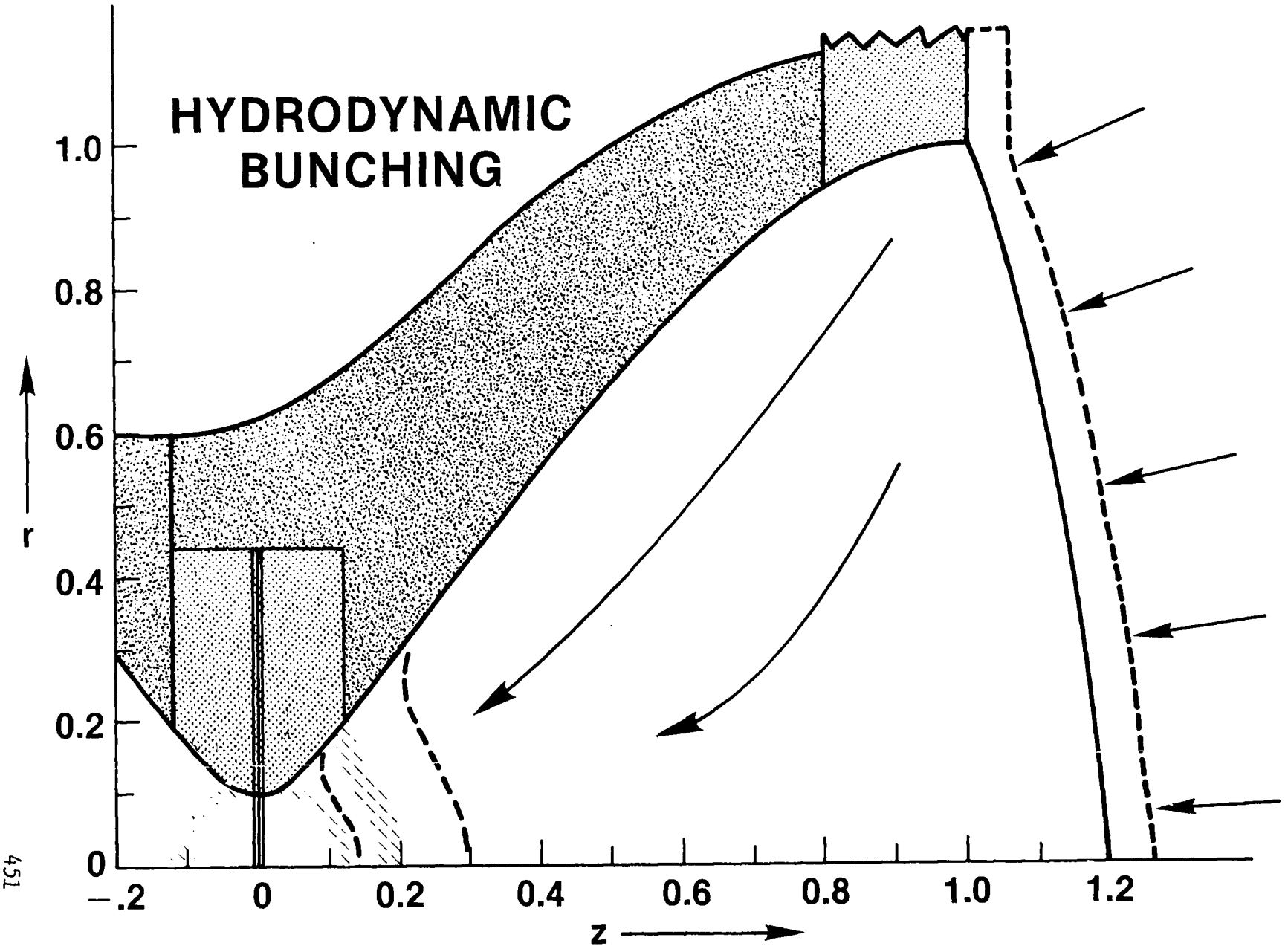

Figure 1.

PLASMA POWER MULTIPLIER

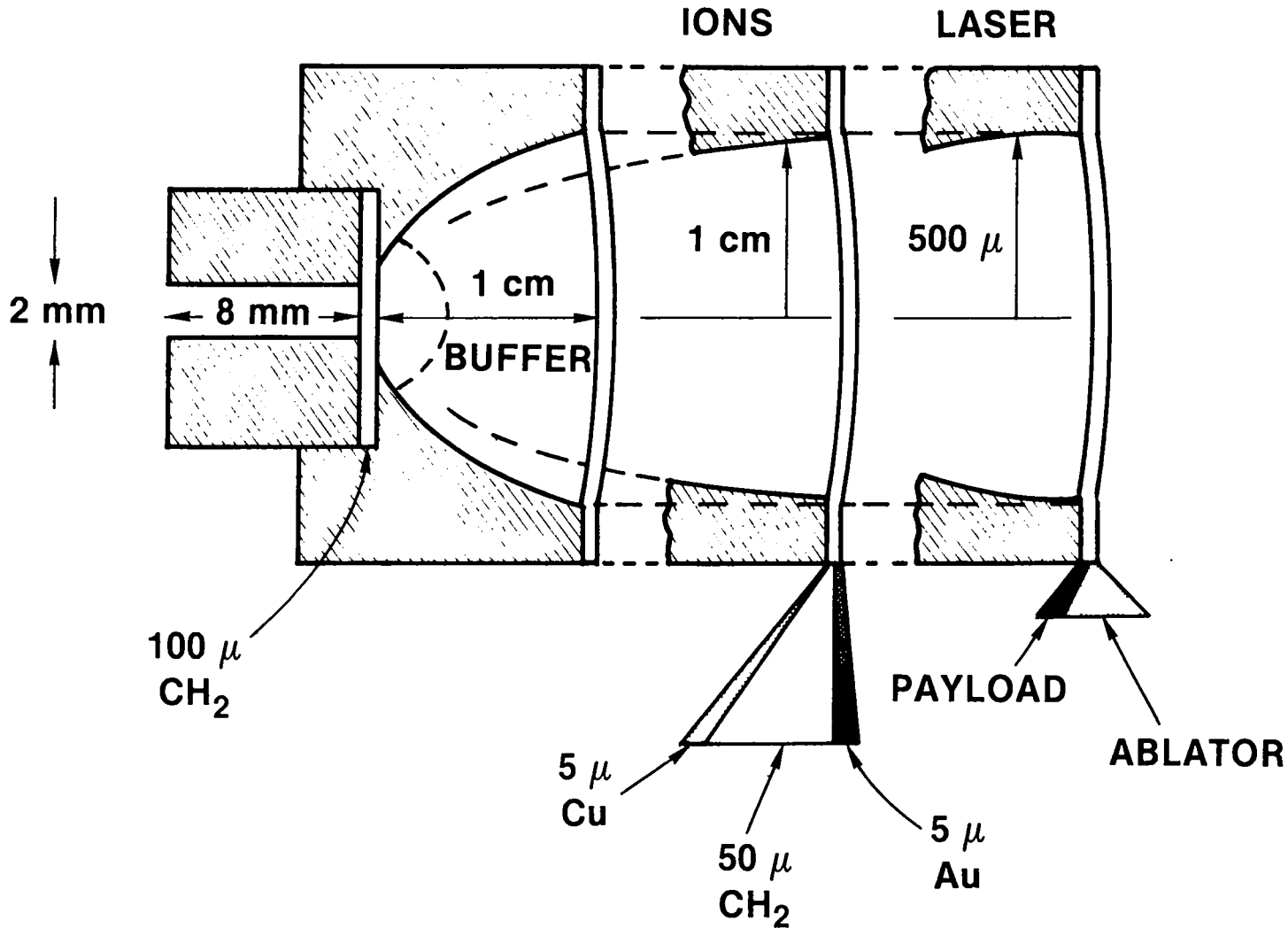

Figure 2.

ACCELERATION OF MACRO-PARTICLES TO HYPER-VELOCITIES BY COOPERATIVE PROCESSES.

F M Russell

Rutherford Laboratory, Chilton, Didcot, Oxfordshire OX11 0QX

SUMMARY

The possibility of applying the principle of magnetic levitation to the acceleration of condensed matter to obtain hyper-velocities is examined. Condensed matter is adopted to avoid space-charge effects at high particle densities and consequently necessitates the use of cooperative phenomenon such as superconductivity or ferromagnetism to achieve coupling to applied electromagnetic fields. Since cooperative processes are relatively weak a long flight path is inevitable which suggests use of an orbital path. Conditions for stable orbital motion are derived and related problems are examined from which it is concluded that projectile velocities of 2.10^7 cm sec^{-1} should be achievable with present technology. Tests with a small-scale model have verified the principles involved.

The potential for application to the inertial confinement approach to controlled thermonuclear reactions is considered briefly.

INTRODUCTION

The acceleration of macro-particles to hyper-velocities has been a persistent problem to which considerable attention has been given[1-6]. To achieve significant interaction with uncharged macro-particles a bulk cooperative effect is required. Since no substance with relative permittivity less than one exists only two possible classes of materials are available which exhibit both cooperative effects and satisfy the condition for levitational stability[7]. These are ferromagnetics and superconductors. The condition of levitational stability is necessary because the gravitational interaction with a macro-particle is comparable in magnitude with either of these cooperative effects.

Using cooperative processes hyper-velocities can be achieved only with very long flight paths which in practice necessitates an orbital path configuration. In this proposal it is suggested that macro-particles are injected into a superconducting guidance ring, in which they exhibit levitational stability, and are accelerated up to hyper-velocities by the repeated action of small impulses, eventually to be extracted from the ring and directed to a target.

The condition for levitational stability states that at least one component in the system must be a superconductor. Let the guidance ring be made from a superconductor to form a nearly closed toroidal ring, C-shaped in radial cross-section, with the gap facing the centre of the ring. Let the macro-particle be represented by a magnetic dipole which is located inside the horizontally mounted guidance ring. Under the action of both gravitational and inertial forces caused by orbital motion of the macro-particle it will follow an oscillatory path about an equilibrium orbit parallel to the outer wall of the guidance ring but displaced from that wall by the levitational force. A limiting condition of interest occurs when the combined inertial and gravitational forces equal the maximum levitational force achievable in the system.

MACRO-PARTICLE SIZE

To represent the macro-particle as a magnetic dipole there must be either an impressed longitudinal magnetic field parallel to the guidance wall or the macro-particle must be a permanent magnet. Let this longitudinal field be uniform to first order and of magnitude B_θ. Assume also that the dimensions of the dipole are small relative to the curvature of the guidance wall so the wall can be treated locally as a plane.

The principal factors determining the size of the macro-particle relate to simultaneously meeting the following conditions: the ratio of magnetic force from the dipole image-dipole interaction should be maximised; the peak magnetic field at the superconducting wall should not exceed a critical value B_c dependant upon the material used for the wall; the macro-particle should be orientation-stable in the longitudinal magnetic field against small departures from the equilibrium position. The geometry of the dipole image-dipole system is shown in figure 1 where all dimensions are normalised to the effective spacing between the dipole and image. It is assumed that the relative permeability of the dipole material is large so that leakage can be neglected.

It can be shown that for small spacings the ratio of magnetic to inertial forces is inversely proportional to the space d for given dipole geometry. To satisfy the third condition it is necessary for b> a and c>b in the presence of a longitudinal magnetic field.

MAGNETIC FORCE STRENGTH

The presence of the dipole near the wall changes the magnetic field distribution at the wall surface. The magnetic force acting on the wall can be found by integrating over the surface area the magnetic pressure change caused by the dipole and must equal the force acting on the dipole itself. It is useful to compare this force to that which would act if the field perturbation were confined to that area of the wall facing the dipole and at a constant field change equal to the maximum occuring in the actual distributed field case.

This procedure is illustrated in figure 2. The ratio of the integrals of the two pressure functions, where $B_w^2/2\mu_o$ is the magnetic pressure,

$$R = \frac{1}{2\mu_o} \int B_w^2 . ds / \frac{1}{2\mu_o} B_{w(max)}^2 \int ds$$

depends on the spacing d and the dipole geometry only, for constant u of the dipole material. For dipole configurations of interest here R is found numerically to be of order unity.

Equating the inertial and magnetic forces

$$\frac{m.v^2}{r} = \frac{1}{2\mu_o} \int B_w^2 . ds$$

Introducing R and the normalised dipole dimensions gives

$$\rho . d\ (abc) \frac{v^2}{r} = \frac{d^2 (bc)}{2\mu_o} B_{w(max)}^2 . R$$

so that

$$ad = B_{w(max)}^2 . Rr / 2\mu_o \rho v^2 .$$

Recalling the second condition that must be met by the macro-particle, namely B_w must not exceed the critical field strength of the superconductor, then to first order the thickness of the dipole is given by

$$ad = B_c^2 . Rr/2\mu_o \rho v^2 .$$

MACRO-PARTICLE ACCELERATION

By modulating the longitudinal magnetic field locally the dipole would experience the force

$$F = M.d^3(abc)\nabla B/\mu_o$$

giving for the equation of motion in the x-direction

$$d^3(abc)\rho . d^2x/dt^2 = M.d^3(abc)(1\mu_o)dB/dx$$

Hence, the rate of acceleration is independent of the size of the macro-particle to first order. Assuming the magnetic field strength in the acceleration sections also is limited to the critical value for the superconductor then for a ferromagnetic macro-particle the ratio of the magnetic to gravitational (g) force is approximately given by 10.dB/dx. If only a few percent of the guidance ring is occupied by acceleration sections then the rate of acceleration of the macro-particle will be of order (g).

ORBIT STABILITY

The equation for radial motion is

$$W.d^2r/dt^2 - W.v^2/r + 2\ M^2S^2/\mu_o . (r_w - r)^2 = 0$$

where W is the mass of the macro-particle and r_w is the radius of the guidance wall. Let x be the displacement from the assumed equilibrium orbit of radius r_e, $h = (r_w - r_e)$ and $v = \omega . r_e$.

Linearising by expanding to first order terms only gives the oscillatory solution

$$x = x_o . \sin \left[(1 + 2.r_e/h)^{\frac{1}{2}} \omega \right] t$$

The frequency of oscillation f_r in terms of the orbital frequency f_o is given by

$$f_r = (2.r_e/h)^{\frac{1}{2}} . f_o , \qquad 2r_e/h >> 1$$

To achieve stability of motion in the vertically transverse direction the guidance wall must provide some position dependent restoring force. This could be provided by adding walls above and below the equilibrium path giving the guidance wall a channel cross-section. A similar analysis then applies to the vertically transverse motion which also is oscillatory but of much lower frequency than the radial motion. The large difference in frequencies of the two motions should reduce the degree of coupling between the two modes.

DISSIPATIVE PROCESSES

During acceleration to full velocity and possible subsequent storage in the guidance ring energy will be coupled to the macro-particle through dissipative processes. Since the target velocity is about 10^3 greater than the most probable velocity of any residual gas atoms in the guidance ring system the only process by which the macro-particle could lose energy is by radiation.

The principal dissipative processes are impact heating from collisions with residual gas atoms and eddy currents induced by field variations near the macro-particle. The first process is proportional to gas pressure so is readily reduced to an acceptable level by high vacuum techniques. The eddy-currents are driven by field perturbations caused by location errors of the guidance wall, by harmonics in the field gradient acceleration sections and by damping of transverse oscillations. Calculations suggest that the temperature reached by the macro-particle most probably exceeds the critical temperature for superconductivity. Persistence of the cooperative phenomenon of ferromagnetism to the much higher Curie temperature is a clear advantage and suggests the preferred material for macro-particles.

PHASE-STABLE ACCELERATION

Suppose that in an acceleration section a magnetic field gradient is produced, by suitably phased time varying currents in a multi-element structure, which travels at the mean velocity of the macro-particles. Many macro-particles could be contained and accelerated within a single guidance channel by spacing them longitudinally at intervals of v/f_a, where f_a is the instantaneous frequency of the frequency modulated acceleration system. To ensure synchronism during acceleration of the macro-particles to full velocity f_a must satisfy the relation

$$n.v/f_a = 2\pi r_e$$

where n is the number of macro-particles per turn in a guidance channel. Defining the momentum compaction factor as

$$K = \frac{L}{p}\frac{dp}{dL} = \frac{r_e}{h} >> 1,$$

so that a velocity greater than that for synchronous motion has a shorter period of rotation.

With reference to figure 3 the motion is phase stable if the synchronous phase angle ϕ_s lies in the range

$$0 < \phi_s < \pi/2.$$

LIMITS ON SIZE

An upper limit on the size of the macro-particles is set by the critical field of Type I materials and the requirement of internal stability. Lower limits are set by the finite length associated with the cooperative phenomenon used, namely, λ_L for superconductors. Although ferromagnetics have a shorter characteristic distance than λ_L this limit again applies because of the involvement of superconductors in the guidance channel and acceleration sections. A second limit is set by the readily attainable smoothness of the superconducting surfaces.

For a terminal velocity of 2.10^7 cm/sec for macro-particles composed of iron, and Niobium for the superconductor, the probable size of the macro-particles is: ad = 2.10^{-5}cm, bd = 5.20^{-5}cm, cd = 5.10^{-4}cm giving in excess of 10^{12} nucleons per macro-particle.Arrays are possible in which each macro-particle satisfies the conditions derived above with the additional condition that the macro-particles are not free to move relative to each other. Such an array can be treated as a single entity in phase-energy space.

MODEL TEST

A small analogue model has been constructed and used to demonstrate the principles involved in the proposed macro-particle accelerator. To simulate the superconducting ring an aluminium guidance channel was rotated at high speed and a small permanent magnet, suspended so as to move freely in the radial direction, was rotated in the opposite direction. Stable motion was maintained upto a magnetic force to weight ratio close to the maximum possible for the system.

CTR APPLICATION

If velocities of the order 2.10^7 cm/sec can be obtained in the manner described then the possibility of controlled thermonuclear reactions using the inertial confinement principle can be considered[8]. Extraction of macro-particle arrays from the guidance channel appears feasible in principle as does their subsequent convergence upon a (D,T) fuel pellet. First order calculations indicate that gaseous contamination of the reactor chamber would not be a major difficulty for macro-particle penetration to a localised target.

Since the maximum energy per nucleon in a macro-particle is only 200eV it is impossible for there to be any induced radioactivity in the accelerator, a very important factor for maintenance and life expectancy of the machine.

ACKNOWLEDGEMENTS

I wish to thank T C Randle for helpful discussions and M W Russell for assistance in testing the analogue model.

REFERENCES

1. F Winterberg. J Nuc. Energy C 1966, Vol 8,541
2. C Maisonnier. Il Neuvo Cimento, XLII B,N2, 1966
3. E R Harrison. NIRL/M/60, 1964
4. J C Linhart. Lab.Gas Ionizzati, CNEN, Frascati
5. M Kreisler. 2nd. Int. Conf. on Energy Storage, Compression and Switching, 1978
6. K Wendell Chen, E Lehman. Inducing Controlled Thermonuclear Fusion with a Superconducting Macroparticle Accelerator, Submitted to Nuclear Fusion, 1978
7. W Braunbek. Zeitschrift fur Phvsik. Vol.112. 1939. pp 753-763
8. R C Arnold. Nature, Vol.276, p 19, 2 Nov. 1978

12th March 1979

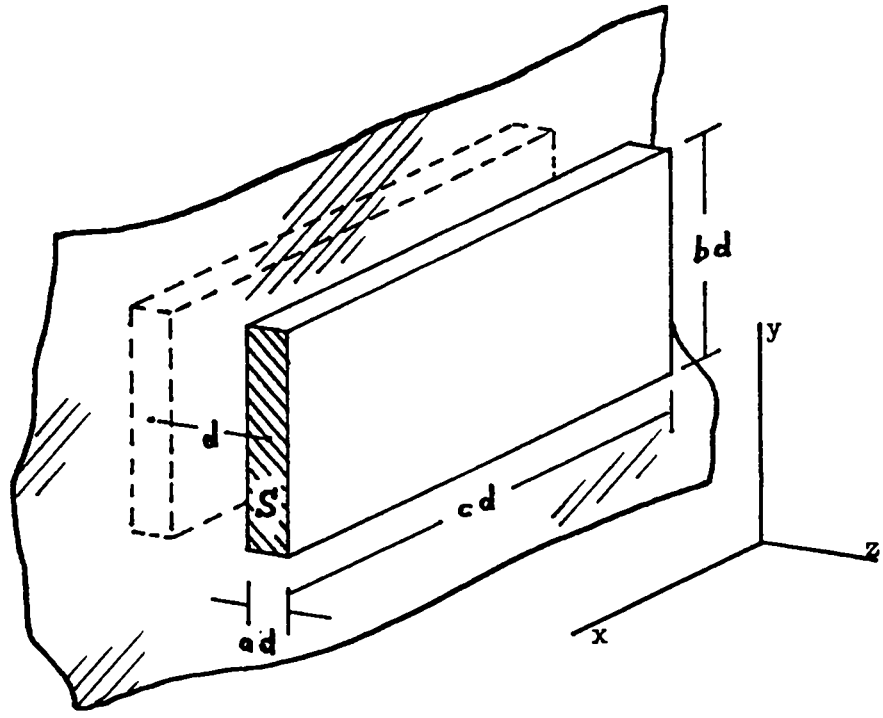

Geometry of the macro-particle and image in the superconducting wall of the guidance ring. All dimensions are normalised to the dipole image-dipole spacing.

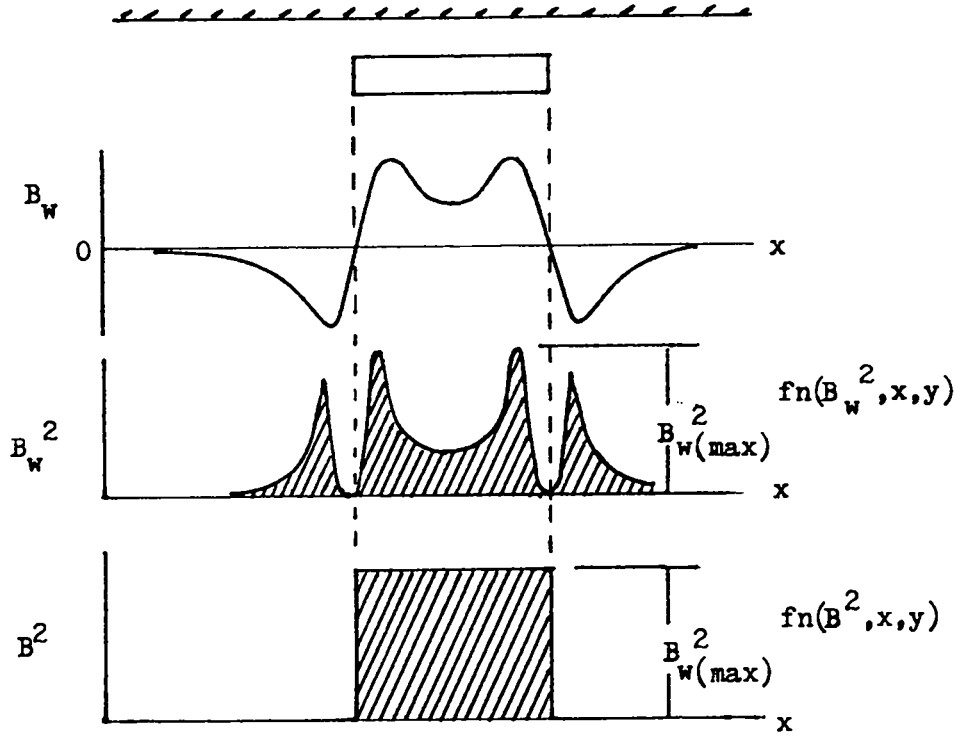

Magnetic field and energy density variations at the wall surface.

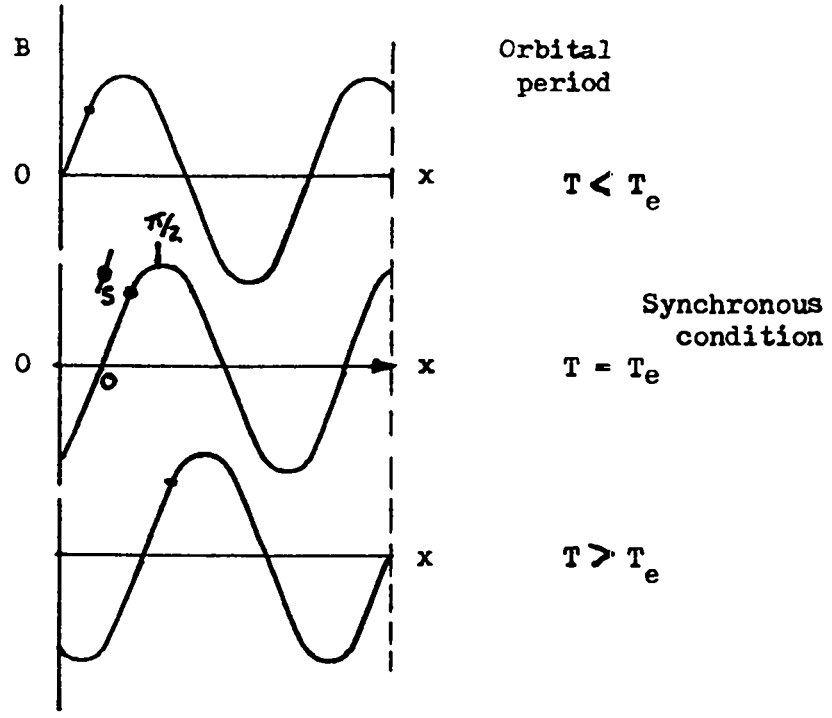

Diagram showing time and distance variations of magnetic field in acceleration section, indicating phase relations and the synchronous phase angle.

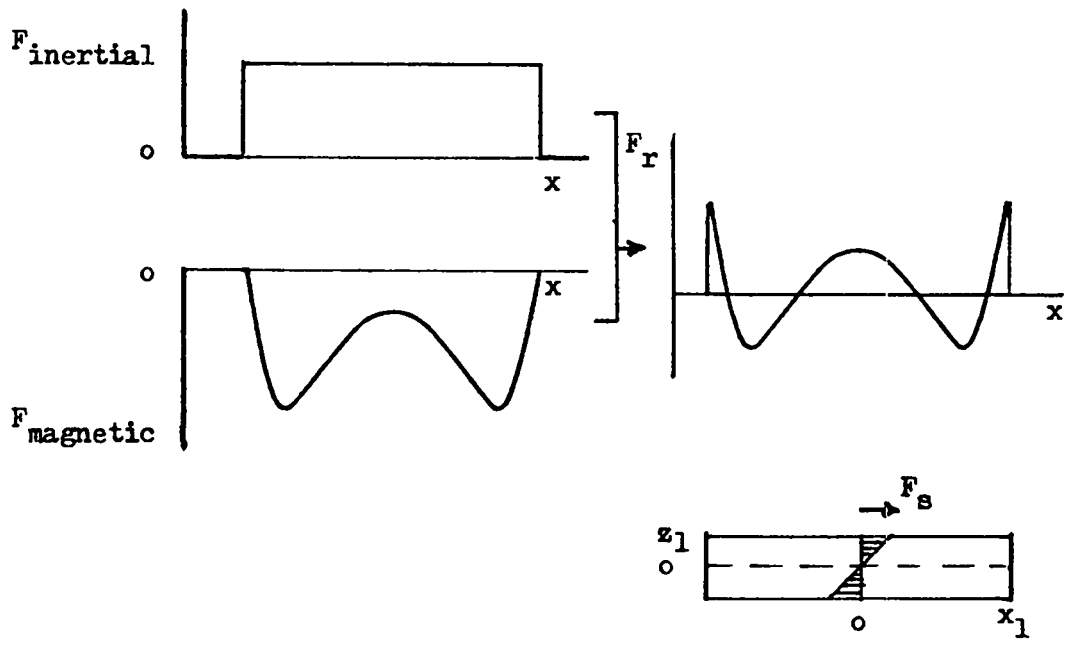

The inertial and magnetic force distributions on the macro-particle causing internal stresses.

Author Index

Printed in the United States of America. Available from
National Technical Information Service
US Department of Commerce
5285 Port Royal Road
Springfield, VA 22161

Microfiche $3.00

001-025	4.00	126-150	7.25	251-275	10.75	376-400	13.00	501-525	15.25
026-050	4.50	151-175	8.00	276-300	11.00	401-425	13.25	526-550	15.50
051-075	5.25	176-200	9.00	301-325	11.75	426-450	14.00	551-575	16.25
076-100	6.00	201-225	9.25	326-350	12.00	451-475	14.50	576-600	16.50
101-125	6.50	226-250	9.50	351-375	12.50	476-500	15.00	601-up	

Note: Add $2.50 for each additional 100-page increment from 601 pages up.